CRITICAL POINT BEHAVIOUR

IN BINARY AND TERNARY LIQUID MIXTURES

with particular reference to rheological and interfacial properties in model mixtures for microemulsions

Patricia J. Clements

A thesis submitted for the degree of Doctor of Philosophy.

Department of Chemistry, University of Sheffield.

October 1996

SUMMARY

The phase behaviour, rheological effects and interfacial properties of binary and ternary liquid mixtures have been studied near critical points. In particular, measurements have been made of the viscosity–at the bulk macroscopic level by capillary viscometry and at the microscopic level by fluorescence depolarisation–and of critical-point wetting and adsorption–at the solid-liquid interface using evanescent-wave-generated fluorescence spectroscopy and at the liquid-vapour interface using specular neutron reflection. The systems investigated have been mostly alkane + perfluoroalkane mixtures or 2-butoxyethanol + H_2O or D_2O mixtures, although in some cases hexamethyldisiloxane, propanenitrile and perfluorooctyloctane have also been the components of mixtures. The main outcomes of this study are:

- **Macroscopic viscosity:** The divergence to infinity in the shear viscosity of hexane + perfluorohexane at the critical endpoint for approach along the path of constant critical composition both from the single phase and along both limbs of the coexistence curve is described well using the Renormalisation Group Theory critical exponent y = 0.04. The correlation length amplitude obtained by fitting the shear-gradient dependence of the viscosity is $\xi_0 = (5.5 \pm 1.5)$ Å.
- **Microscopic viscosity:** The product of the rotational correlation time and the temperature $\tau_R \cdot T$, often taken as a measure of the microscopic viscosity, exhibits an anomaly as the critical point is approached as a function of temperature. This anomaly mirrors that in the macroscopic viscosity for some fluorescent dye probes, but for others the anomaly is in the opposite sense indicating that other effects such as solvent structure must play a part in the near-critical behaviour of $\tau_R \cdot T$.
- **Critical-point wetting at the solid-liquid interface:** The wetting transition temperature has been identified for heptane + perfluorohexane at the quartz-liquid interface from fluorescence lifetime measurements of a probe. The wetting layer is of the same composition as the bulk heptane-rich phase and the transition is tentatively identified as first-order.
- **Adsorption and wetting at the liquid-vapour interface:** The surface structure of several mixtures has been determined by neutron reflection. The results are in general agreement with the expectations of critical-point wetting and adsorption. The surface is complex and in some mixtures an oscillatory scattering length density profile through the interface is required to model the reflectivity data.
- **Ternary mixtures:** The phase behaviour of three mixtures exhibiting tunnel phase behaviour has been studied experimentally and various characteristics of the shape of the tunnel identified. A theoretical study on one of the mixtures predicts the drop in temperature for the locus of maximum phase separation temperatures which is observed experimentally.

PAPERS SUBMITTED FOR PUBLICATION

October 1996

Macroscopic viscosity of near-critical mixtures

McLure, I.A.; Clements, P.J. (1996) *Ber. Bunsenges. Phys. Chem.*, in press. 'Shear viscosity of hexane + tetradecafluorohexane near the upper critical endpoint.'

Microscopic viscosity of near-critical mixtures

Clements, P.J.; Bowers, J.; Brocklehurst, B.; McLure, I.A. (1995) *Mol. Phys.*, 86, 873-878. 'The near-critical microscopic viscosity of binary liquid mixtures: 2-butoxyethanol + water at the lower critical endpoint.'

Critical-point wetting at the solid-liquid interface

Bowers, J.; McLure, I.A.; Clements, P.J. (1996) *Physica A*, in press. 'Wetting near consolute points by evanescent-wave-generated fluorescence spectroscopy. 3. Fluorescence lifetimes: *n*-heptane + perfluoro-*n*-hexane at the upper critical endpoint.'

McLure, I.A.; Clements, P.J. (1996) Submitted for publication in *Surface Sci. Lett.* 'Wetting in narrow gaps and capillaries: Temperature- and surface-pressure-induced wetting transitions. A comment.'

Adsorption and wetting at the liquid-vapour interface

Bowers, J.; Clements, P.J.; McLure, I.A.; Burgess, A.N. (1996) Accepted for publication in *Mol. Phys.* 'The structure of the liquid/vapour interface of *n*-hexane + perfluoro-*n*-hexane along the path of critical composition through the critical endpoint by neutron reflectivity.'

Phase behaviour of binary and ternary mixtures

Arriaga-Colina, J.-L.; McLure, I.A.; Clements, P.J.; Hill, E. (1996) Accepted for publication in *Fluid Phase Equilibria.* 'Phase equilibria for binary *n*-alkanenitrile-*n*-alkane mixtures. IV. Liquid-liquid phase equilibria for propanenitrile with C_5-C_8 and C_{10} *n*-alkanes.'

Batchelor, H.K.; Clements, P.J.; McLure, I.A. (1996) *J. Chem. Soc. Faraday Trans.*, 92, 2255-2262. 'Thermodynamics of ternary mixtures exhibiting tunnel phase behaviour. Part 1. Cyclohexane-perdeuterocyclohexane-perfluorohexane.'

Clements, P.J.; Hill, E.; McLure, I.A. (1996) Submitted for publication in *J. Chem. Soc. Faraday Trans.* 'Thermodynamics of ternary mixtures exhibiting tunnel phase behaviour. Part 2. Hexane-decane-propanenitrile.'

Clements, P.J.; Zafar, S.; Galindo, A.; Jackson, G.; McLure, I.A. (1996) Submitted for publication in *J. Chem. Soc. Faraday Trans.* 'Thermodynamics of ternary mixtures exhibiting tunnel phase behaviour. Part 3. Hexane-hexamethyldisiloxane-perfluoro-hexane.'

ACKNOWLEDGEMENTS

This work was funded by a Hossein Farmy Scholarship awarded by the University of Sheffield for research into some aspect of mining and I am grateful to the University for their support. I would also like to acknowledge the financial support of the EPSRC through allocations of beamtime at the Daresbury and Rutherford Appleton Laboratories.

The work presented in this thesis would not have been possible without the assistance of many people. I would like to thank Ian McLure for his supervision over the course of the past three years. In particular I am thankful for the range of areas and techniques that he has allowed this project to cover and I feel lucky to have been a part of the 'McLure group' during such an active period. The work outside of Sheffield at the Daresbury and Rutherford Appleton Laboratories would not have been so enjoyable if I had not been part of a team. I would like to thank past and present members of the group for their assistance with these experiments, namely James Bowers, Emilio Manzanares, Marcos Vergara and Jon Howse. Other past and present members of the group–Amanda Archer, Richard Whitfield and Luis-Miguel Trejo–have also ensured that the lab has been a very pleasant place to work. Jean Stevenson in particular deserves a special mention for being ready to help with so many different things and ensuring the smooth running of the lab.

The fluorescence work at Daresbury would not have been possible without the collaboration of Brian Brocklehurst of the department and his skilful manipulation of the electronics. I am also indebted to Brian for providing ideas, for imparting to me some of his vast range of knowledge on fluorescence, and for his patience and assistance with the data analysis. Numerous Daresbury Laboratory staff have also been of service at various times and I would like to thank them, especially David Clarke, David Shaw, Celia Gregory and Moira Behan-Martin. Thanks are also due to the Daresbury workshop staff for making us a successful new cell holder.

I am grateful to Andrew Burgess of ICI C&P for his assistance with the neutron reflection work at the Rutherford Appleton Laboratory and with the data fitting. I am also grateful to Rob Richardson and Ali Zarbakhsh for the loan of the gas-tight cell. The staff at Rutherford deserve a special mention for their help, in particular Jeff Penfold, David Bucknall and John Webster at ISIS, and Mike Towrie and Pavel Matousek at the Central Laser Facility.

Many of the determinations of the experimental ternary phase diagrams were carried out by third year students during their final year project under my supervision. I was also responsible for the supervision of a project on the measurement of the viscosity of a ternary mixture. I would like to thank Emma Hill, Hannah Batchelor, Shazia Zafar and Suzanne Cooke for their hard work. In the theoretical predictions of the phase behaviour I used the existing 'Jackson' programs and I am grateful to George Jackson

and Amparo Galindo for their advice with this section of work. I would also like to thank them and the other members of 'G-floor' for their friendship and for their help with various computing aspects over the past three years.

This work has relied on the support of the departmental staff and I would like to thank them all. The electronic, central mechanical and glass workshops have made specific equipment, or have repaired or altered numerous existing items. Thanks are due to Mike Carr, Paul Turner, Alan Hall, John Murray and Ken Hough and their colleagues in workshop, and to D-floor technical staff in particular Chris Lumley, Richard Wilkinson and Paul Booth for all their help.

The list of people who have participated in this project is extensive. I am grateful to everyone and ask to be forgiven by anyone I have forgotten.

Finally, I reserve a special mention and thankyou for my husband Mike Quail and for all my family for many things, especially their love and encouragement. I would particularly like to thank my Dad for willingly proof reading much of this thesis and Mike for taking good care of me.

CONTENTS

LIST OF PLATES

CHAPTER 1: INTRODUCTION AND BACKGROUND

1.1 Introduction to critical behaviour

Critical point behaviour is widespread in nature, occurring in systems as diverse as fluids, ferromagnets, ferroelectrics and superconductors. It is associated with phase transitions between two states, one ordered and one disordered, and the critical point marks the limit of order. We shall be concerned chiefly with liquid-liquid critical points in binary liquid mixtures and will relate their behaviour to gas-liquid critical points in pure fluids. In a pure substance criticality is associated with the liquid-vapour transition and in a partially miscible binary liquid mixture criticality is associated both with the liquid-vapour *and* with liquid-liquid transitions.

In a pure substance the critical point represents the transition point from the two-phase equilibrium of the liquid and vapour to the single-phase fluid in which the distinction between liquid and gas is lost. The critical point for a pure substance is identified by a critical temperature T_c, the maximum temperature at which a liquid can coexist with its vapour, a critical pressure p_c and a critical molar volume $V_{m,c}$.

In a binary liquid mixture one or two lines of gas-liquid critical points exist. In addition, a liquid-liquid critical point defined by a critical composition x_c, in mole fraction terms, and a critical solution temperature T_{CS} may occur if the two components are partially miscible at a particular pressure. In partially miscible ternary and multicomponent systems, lines of liquid-liquid critical points may be observed.

The phase transition which occurs on passing through the critical point, e.g. of a pure substance, is second order. The first derivative of the chemical potential (the chemical potential of a species is defined as the derivative of the Gibbs free energy with respect to the number of moles) with respect to temperature or pressure is continuous, but the second derivative is discontinuous. Since the first derivatives of the chemical potential with respect to temperature and pressure are the partial molar entropy and partial molar volume, respectively, the entropy and volume of the system do not change during the transition. This is in contrast with a first-order phase transition at which the first derivative of the chemical potential is discontinuous.

In the following sections, 1.1.1 to 1.1.3, the liquid-vapour phase behaviour of a pure substance and the liquid-vapour and liquid-liquid phase behaviour of mixtures are discussed in more detail. Section 1.1.4 then looks at the anomalous behaviour that occurs in various properties near a critical point.

1.1.1 Liquid-vapour phase behaviour of pure substances

There are several ways of representing the phase behaviour of pure substances. The variables to be considered are pressure, temperature, and volume or density, and any two of these can be plotted against each other in a two-dimensional diagram. The most usual representations for the present work are those of pressure *versus* temperature to show the full phase diagram, and of pressure *versus* volume on which several isotherms can be displayed to represent the liquid-vapour states.

The pressure-temperature and pressure-molar volume diagrams for carbon dioxide are shown in Figures 1.1 and 1.2, respectively. In Figure 1.2, at 20°C (293.15 K), the point A represents the gas; as the volume is decreased or the pressure increased, this gas reaches point C. On further increasing the pressure, or decreasing the volume, phase separation occurs and a liquid phase is also formed. At the pressure corresponding to points C-E the liquid and gas can coexist and the pressure represents the vapour pressure. On further increasing the pressure, a single phase is again formed, this time of the liquid. At temperatures below the critical temperature T_c liquid and gas phases coexist as described; at T_c and higher temperatures the gas can effectively change into a liquid without the appearance of an interface. The critical point occurs at the point of inflection of the isotherm at the critical temperature and is defined by T_c, the critical pressure p_c and the critical molar volume $V_{m,c}$. The conditions for the critical point are:

$$(\partial^2 A_m/\partial V_m^2)_T = -(\partial p/\partial V_m)_T = 0$$

$$(\partial^3 A_m/\partial V_m^3)_T = -(\partial^2 p/\partial V_m^2)_T = 0$$

where A_m is the molar Helmholtz free energy. These equations define a single critical point.

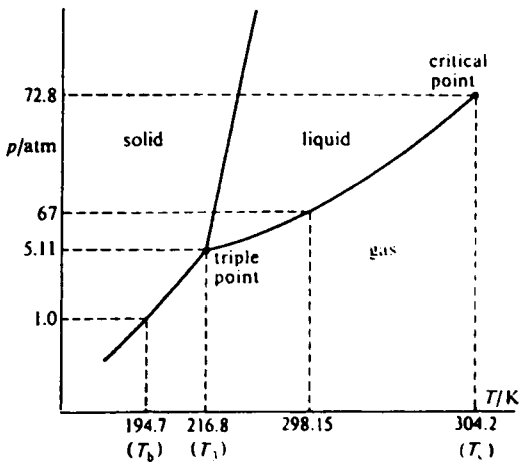

Figure 1.1: The phase diagram for carbon dioxide. (Reproduced from Atkins, 1982.)

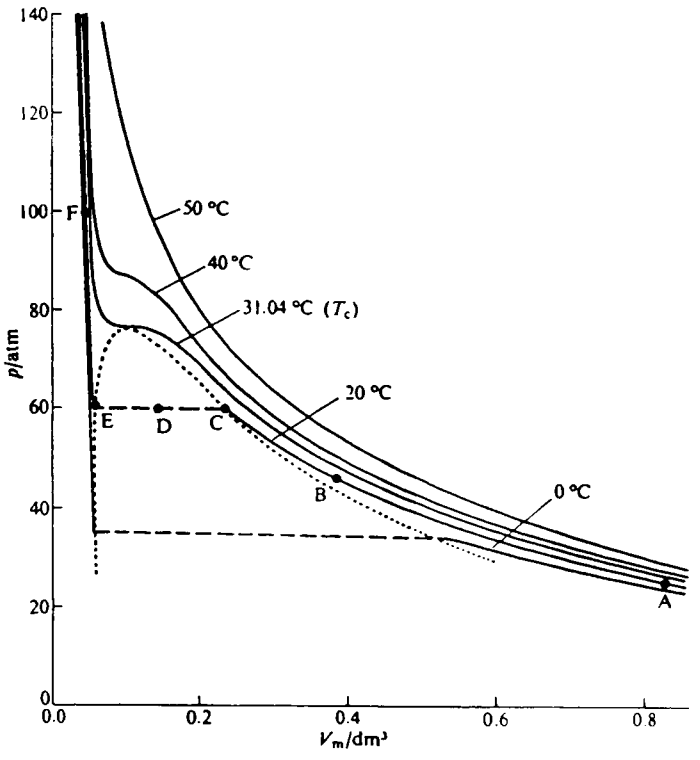

Figure 1.2: The experimental isotherms for carbon dioxide. (Reproduced from Atkins, 1982.)

The behaviour of perfect gases can be described by the equation of state, pV = nRT, where n is the amount of substance and R is the gas constant. However, this equation is not appropriate for most real gases. The van der Waals equation of state is commonly used to broadly describe the behaviour of imperfect gases. It takes into account the repulsive and attractive interactions between molecules. The repulsive interactions are accounted for by including a molecular volume. The volume in which the molecules can move is thus reduced from V to (V - nb), where nb represents the volume occupied by the molecules. Attractive forces between molecules are included by supposing that they reduce the pressure exerted by the gas. The term $-an^2/V^2$ represents the reductions in the number and impulse of molecular collisions with the walls, which are both proportional to the density of molecules (e.g. see Atkins, 1982). The 'a' and 'b' parameters are constants for a given substance. The van der Waals equation of state can thus be written:

$$p = nRT/(V - nb) - an^2/V^2 \qquad (1.1)$$

or as:

$$p = RT/(V_m - b) - a/V_m^2 \qquad (1.2)$$

since $V_m = V/n$.

Isotherms predicted by the van der Waals equation are shown in Figure 1.3 in two-dimensional and three-dimensional representations. The variables used are the reduced variables obtained by dividing by the critical pressure, temperature or volume. At high temperatures the van der Waals equation qualitatively predicts the observed experimental behaviour, see Figure 1.2. At lower temperatures, unrealistic oscillations are predicted but if the Maxwell construction is used and the oscillations replaced by a line at constant pressure, drawn so that the areas of the loops above and below the line are equal, the form of the experimental isotherms is reproduced.

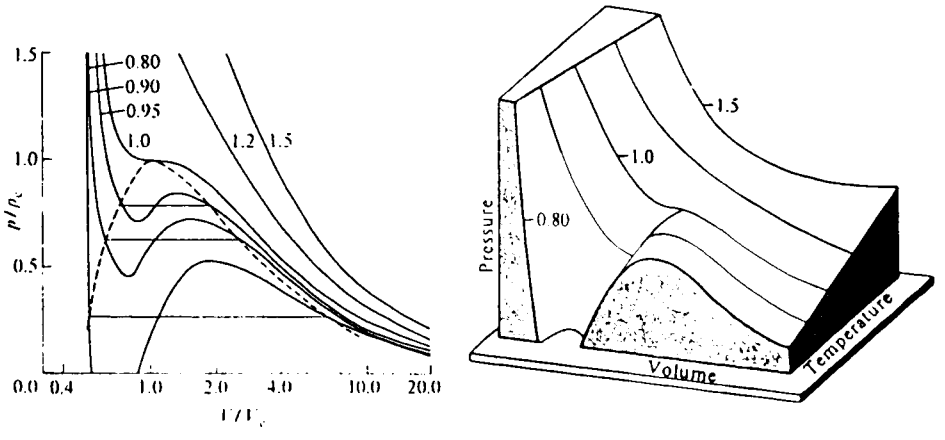

Figure 1.3: The van der Waals isotherms. The isotherms are labelled with the values of T/T_c. (Reproduced from Atkins, 1982.)

Various other equations of state, for example the virial equation, have been used to describe real gases. Some may describe the behaviour of a given gas more accurately; however, the continuing appeal of the van der Waals equation is its relative simplicity.

We turn now to the liquid-vapour phase behaviour of mixtures.

1.1.2 Liquid-vapour phase behaviour of mixtures

The liquid-vapour equilibria described in this section are of importance for the theoretical predictions of the phase behaviour to be presented in Chapter 6. In this section we shall discuss mainly binary liquid mixtures. For mixtures a composition variable needs to be considered in addition to the temperature and pressure.

Mixtures are often classified as ideal or nonideal according to their behaviour. For a real mixture:

$$\mu_i(p,T,x) - \mu_i^0(p,T) = RT \ln(x_i\gamma_i) \qquad (1.3)$$

where $\mu_i^0(p,T)$ is the chemical potential of pure component i at a given temperature and pressure, $\mu_i(p,T,x)$ is the chemical potential of component i in the liquid mixture at the same temperature and pressure, x_i is the mole fraction of component i in the mixture and γ_i is the activity coefficient of component i. This equation defines ideal mixtures when

the activity coefficients are all unity. In nonideal mixtures the activity coefficients are functions of pressure, temperature and composition.

An almost equivalent approach to mixtures is *via* Raoult's Law. For ideal mixtures a plot of the total vapour pressure p against mole fraction of one of the components in the liquid x_i at a given temperature is linear in accordance with Raoult's Law:

$$p = \sum_i x_i p_i^0 \qquad (1.4)$$

where p_i^0 is the vapour pressure of pure i and $x_i\, p_i^0$ is the partial vapour pressure p_i of component i. The total vapour pressure can also be plotted against the mole fraction of one of the components in the vapour y_i, where $y_i = x_i\, p_i^0/p$. The vapour and liquid curves can then be represented on the same diagram, as shown in Figure 1.4. The form of the temperature-composition curves for the liquid and vapour at constant pressure are also plotted. This type of diagram is used to explain the process of distillation.

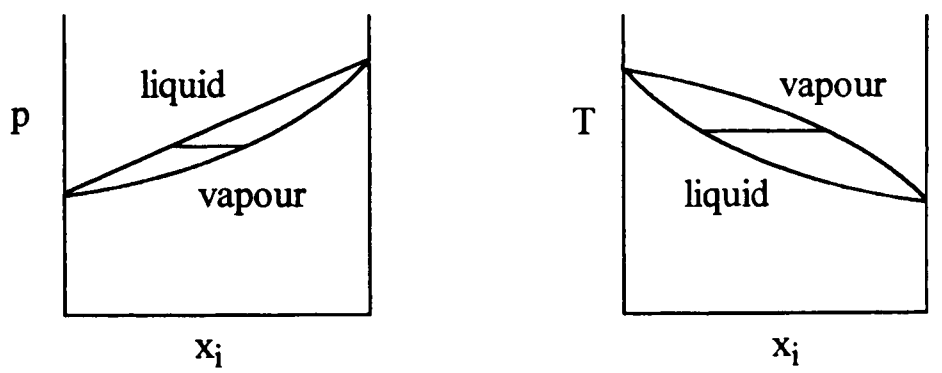

Figure 1.4: Vapour pressure-composition and temperature-composition curves for an ideal binary mixture.

In nonideal mixtures the vapour pressure dependence on the liquid composition is no longer linear. The total vapour pressure can then be expressed as:

$$p = \sum_i x_i \gamma_i p_i^0 . \qquad (1.5)$$

When $\gamma_i > 1$ positive deviations from Raoult's Law occur.

In some nonideal systems, a maximum or a minimum may be observed in the vapour pressure. This leads to a corresponding minimum or a maximum, respectively, in the temperature-composition curve with the formation of a minimum-boiling or maximum-boiling azeotrope, as shown in Figure 1.5. M represents the azeotropic composition at which the compositions of the liquid and vapour in equilibrium are equal. A liquid of this composition boils at a constant temperature and the two components cannot be separated by distillation.

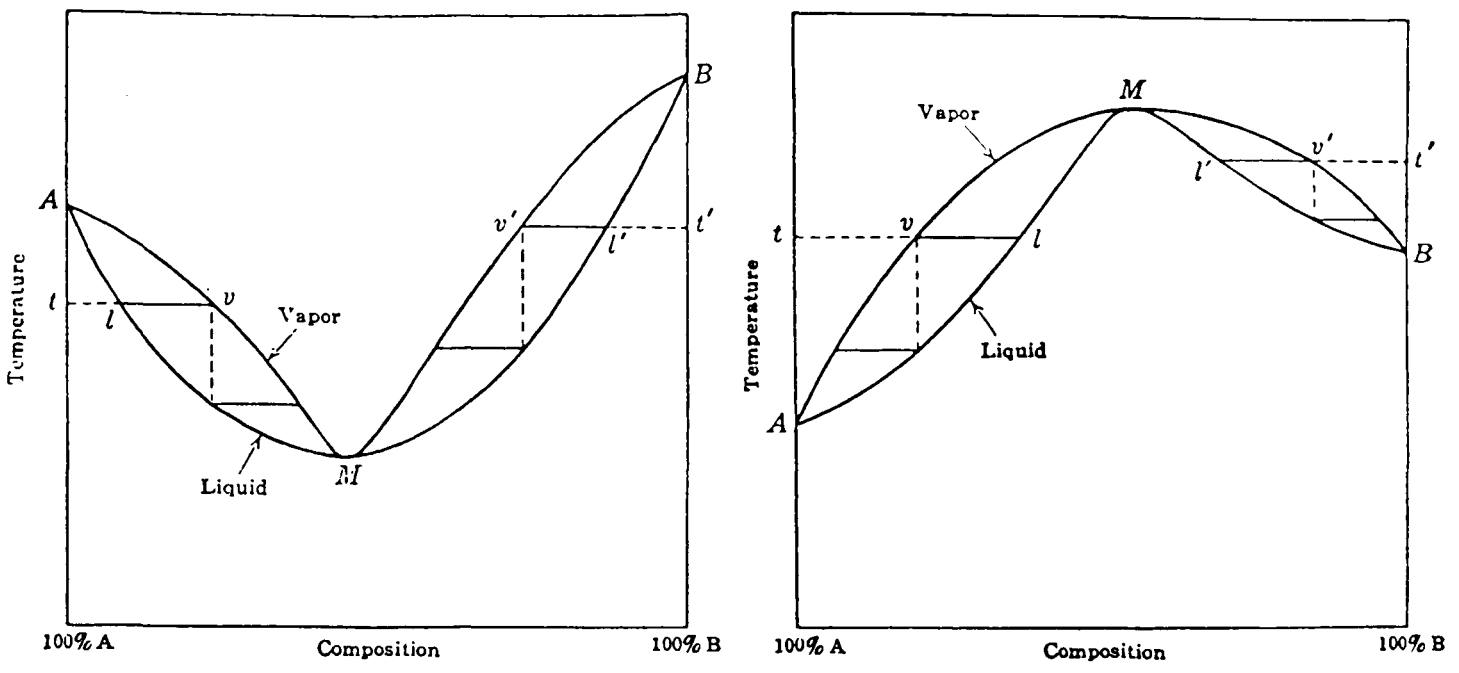

Figure 1.5: Binary mixtures forming minimum-boiling and maximum-boiling azeotropes. (Reproduced from Glasstone, 1940.)

We turn now to the gas-liquid critical behaviour of binary mixtures. A critical point occurs for each of the pure components and, for the cases we consider, for mixtures of any composition. The critical points of the pure substances are connected in the simple case by a line of critical points termed a gas-liquid critical line. The three-dimensional representation in p-T-x space is shown in Figure 1.6. CP I and CP II are the critical points of the pure components I and II. The dashed lines are the vapour pressure curves of the pure components and the hatched areas are pressure-composition slices at constant temperature. At temperatures below the critical temperatures of both pure components, for example at the temperature of the first slice, the pressure-composition slice resembles those discussed above for nonideal mixtures. In each slice the upper curve is for the liquid, and the lower curve for the vapour. Consider now the middle slice in Figure 1.6. The temperature of this slice is above the critical temperature of component I, but below that of component II. The region of liquid-vapour coexistence no longer extends across the whole composition range and a critical point occurs at the point of highest pressure of the p-x isotherm. T-x slices at constant pressure can be considered in a similar way. The behaviour discussed for continuous gas-liquid critical lines applies to mixtures of types I, II or VI in the Scott and van Konynenburg classification (van Konynenburg and Scott, 1980), which is mentioned in the following section. The p-T projections of Figure 1.6 can also be used in considering the critical behaviour, and the pure component critical points and binary critical lines are superimposed. This representation is used in the next section to display both gas-liquid and liquid-liquid critical points.

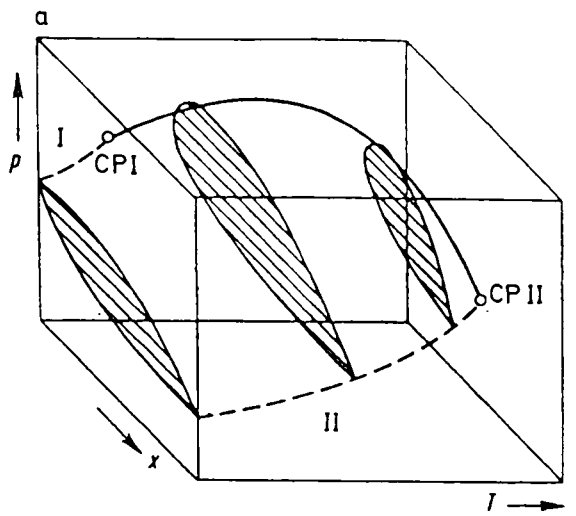

Figure 1.6: Three-dimensional representation in p-T-x space of gas-liquid equilibria in binary mixtures. (Reproduced from Schneider, 1978.)

Liquid-vapour equilibria in binary mixtures have been discussed by many authors including Prigogine and Defay (1954) and Schneider (1978). The liquid-liquid phase behaviour of binary and ternary mixtures forms an essential part of this work and is now discussed.

1.1.3 Liquid-liquid phase behaviour of mixtures

Liquid-liquid phase behaviour at low pressures, say near atmospheric pressure, is usually represented on a temperature-composition phase diagram. Critical solution points in a partially miscible binary mixture are points at which two liquid phases merge identity; such points are defined by a critical composition in terms of a mole fraction x_c, volume fraction ϕ_c or weight fraction w_c, and a critical solution temperature T_{CS}, usually at a given pressure. An upper critical solution temperature T_{UCS} is defined as the *maximum* temperature at which two liquid phases coexist and, similarly, a lower critical solution temperature T_{LCS} is the *minimum* temperature at which two liquid phases coexist. A critical *endpoint* CEP is that point at which the two coexisting liquid phases merge identity to form a single liquid phase in the presence of the *noncritical* coexisting vapour phase. If the CEP occurs at a T_{UCS} it is known as an upper critical endpoint UCEP and if at a T_{LCS} as a lower critical endpoint LCEP. The phase diagrams for binary mixtures exhibiting UCEPs and LCEPs are shown in Figure 1.7. At temperatures and compositions within the region bounded by the curved phase boundary the mixture forms two coexisting liquid phases, the compositions of which are given by the ends of the tie line drawn at a given temperature to link both limbs of the curve. In the region outside the phase boundary the components are fully miscible.

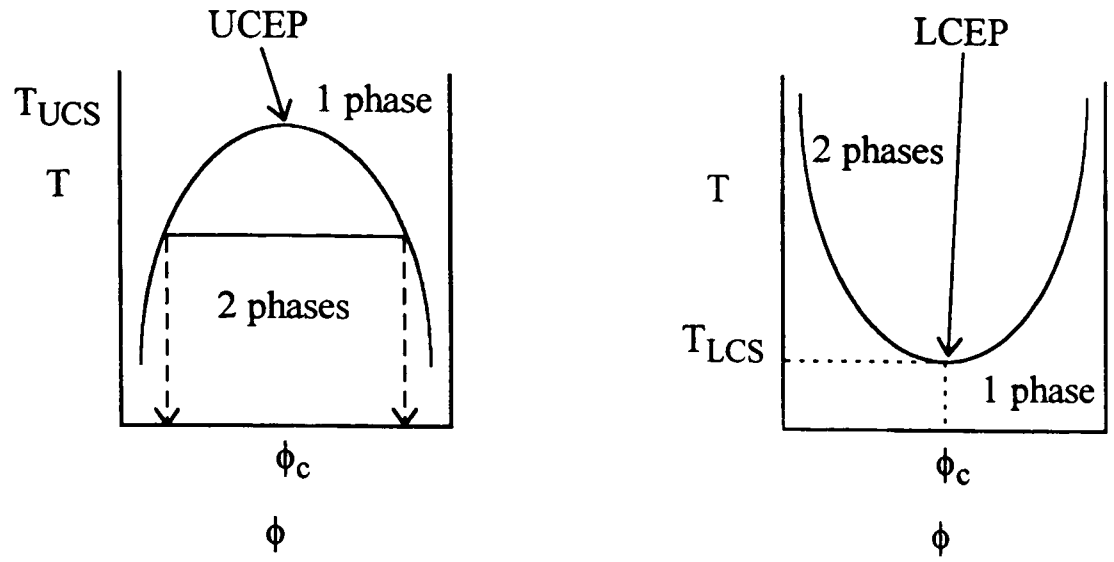

Figure 1.7: The phase behaviour of binary mixtures exhibiting upper critical endpoints UCEPs or lower critical endpoints LCEPs.

In summary, at low pressures binary mixtures exhibit five types of liquid-liquid phase behaviour. The components may be totally miscible in all proportions at all temperatures in the liquid range, or may be partially miscible and thus exhibit i) a UCEP, ii) an LCEP, iii) a UCEP at a temperature *above* an LCEP, termed a closed loop or miscibility gap, or, iv) a UCEP at a temperature *below* an LCEP. Of the four types of partial miscibility a UCEP of type i) is the most common. The mixtures studied here include those exhibiting i), ii) or iii). Examples of type i) mixtures are an alkane with an alkanenitrile, a perfluoroalkane or an alcohol. Examples of type ii) are found in aqueous nonionic surfactant solutions, e.g. water + 2-butoxyethanol; such mixtures also often exhibit type iii) behaviour with the formation of a closed loop unless the UCEP lies inaccessibly above the gas-liquid critical line of the mixture.

The equations defining a liquid-liquid critical point in a binary mixture are analogues of the equations given in section 1.1.1 that define a gas-liquid critical point in a pure substance. At a binary mixture critical point:

$$(\partial^2 G_m/\partial x_2^2)_{T,p} = (\partial \mu_{21}/\partial x_2)_{T,p} = 0$$

$$(\partial^3 G_m/\partial x_2^3)_{T,p} = (\partial^2 \mu_{21}/\partial x_2^2)_{T,p} = 0$$

where G_m is the molar Gibbs free energy and $\mu_{21} = \mu_2 - \mu_1$, the difference in the chemical potentials of the two components. These equations define a critical line in T-p-x space. There is thus a critical solution temperature for each fixed pressure.

Various effects in the intermolecular forces at upper and lower critical endpoints lead to the differences in behaviour. This is illustrated most easily for quadratic mixtures in which the excess Gibbs free energy (excess functions are defined as the difference between the value of the function in a given mixture and in an ideal mixture of the same composition) is given by $G^E = Ax(1 - x)$, where A is a constant for a given mixture at a given temperature. For such a mixture the principal condition for a critical endpoint is $G^E = RT_c/2$. A UCEP can occur if the excess enthalpy $H^E > 0$ and the excess entropy $S^E > (-R/2)$, and an LCEP can occur if $H^E < 0$ and $S^E < (-R/2)$ (Copp and Everett, 1953; Rowlinson and Swinton, 1982). A UCEP is enthalpy driven and an LCEP is entropy driven.

For most mixtures exhibiting an LCEP, the major class of exception being polymer solutions, a UCEP occurs at higher temperatures, thus forming a closed-loop kind of phase diagram, providing a gas-liquid critical line is not reached first. H^E necessarily changes from positive to negative on going from a UCEP down in temperature to an LCEP and the principal condition given above can be satisfied only by the large negative S^E.

Below an upper critical endpoint two liquid phases coexist. As the temperature is raised, the kinetic energy of the molecules increases sufficiently to disrupt the clustering of molecules of the same species, and mixing occurs. Lower critical endpoints generally occur in hydrogen-bonded systems. At temperatures below a lower critical endpoint the two components are fully miscible. As the temperature is raised, the extent of the hydrogen bonding between unlike species falls and the mixture phase separates.

At a CEP the interface between the liquid phases, known as the critical interface, disappears. Both the liquid-vapour interface and the interface between the liquid or liquids and the inner wall of the container or any other solid spectator phase at a CEP are known as *noncritical* interfaces. As a mixture of overall critical composition moves from the two-liquid-phase region into the one-liquid-phase region, by either raising or lowering the temperature, the liquid-liquid interface disappears from the centre of the total liquid volume. For mixtures of other compositions the relative volumes of the phases change and the liquid-liquid interface thus rises or falls and may even disappear from the top or bottom of the liquid.

Critical compositions in the past have often been determined either as the mixture composition yielding the limit of two-phase coexistence or, more quantitatively, by extrapolating the diameter of the coexistence curve to the phase boundary thereby identifying both T_{CS} and x_c. These procedures can sometimes be fairly arbitrary due to the flat nature of the coexistence curve near the critical endpoint.

Another method is to measure the volumes of coexisting liquid phases. For an upper critical endpoint, the composition for which the volumes are equal just below the critical temperature is the critical composition. An even more structured approach relies on fitting the full coexistence curve two of whose parameters are T_{CS} and x_c; this is discussed in more detail below.

The effect of pressure at low pressures on binary temperature-composition phase diagrams is small (Myers *et al.*, 1966). Experimentally, the phase diagram is often measured by determining the phase separation temperatures for mixtures of known composition in sealed tubes in the presence of the vapour. The mixture thus moves along the three-phase gas-liquid-liquid line to the coexistence curve where one liquid phase disappears.

The phase behaviour of systems exhibiting closed loops is particularly interesting, especially in relation to the influence of pressure. Increasing the pressure often causes the closed loop to shrink. The upper and lower critical endpoints may then merge at a double critical point (Walker and Vause, 1987).

The coexistence curve for a binary mixture can be described mathematically in terms of ε, the scaled distance in temperature from the critical temperature T_c, $\varepsilon = |T - T_c|/T_c$, by the equation:

$$\phi_{\pm} = \phi_c + [C\varepsilon + C_1\varepsilon^{\Psi} + C_2\varepsilon^{\Psi+\Delta_1} + ..] \pm {}^1/_2[B\varepsilon^{\beta} + B_1\varepsilon^{\beta+\Delta_1} + B_2\varepsilon^{\beta+2\Delta_1} + ..] \qquad (1.6)$$

where the $\phi_{\pm}$ are compositions on either side of the critical composition ϕ_c, the C_i are the diameter amplitudes, ψ is the critical index for the diameter $(\phi_+ + \phi_-)/2$, the B_i are the amplitudes for the order parameter $(\phi_+ - \phi_-)$, β is the order-parameter critical index and Δ_1 is the Wegner gap exponent for the order parameter (Wegner, 1972). In the early days of the development of the modern theory of criticality, the values of the critical exponents were treated as empirical to be determined by experiment. More recently, however, the values predicted by Renormalisation Group Theory, see section 1.1.4, have come to be regarded as correct and are widely used: $\beta = 0.325$, $\psi = 1 - \alpha = 0.89$ and $\Delta_1 = 0.5$. The first set of terms in equation (1.6) describes the diameter and the second set describes each limb of the coexistence curve. This equation has been used in later chapters to fit coexistence curve data. It should be noted that different exponents for the separate terms have various effects on the shape of the curve, particularly at the origin. The limiting values of the slope dy/dx for $y = x^{\beta}$ at $x \rightarrow 0$ are $+\infty$ for $\beta < 1$, 1 for $\beta = 1$, and 0 for $\beta > 1$ as illustrated in Figure 1.8. Further opportunities for altering the shape of the coexistence curve and the diameter arise from amplitudes of different sign.

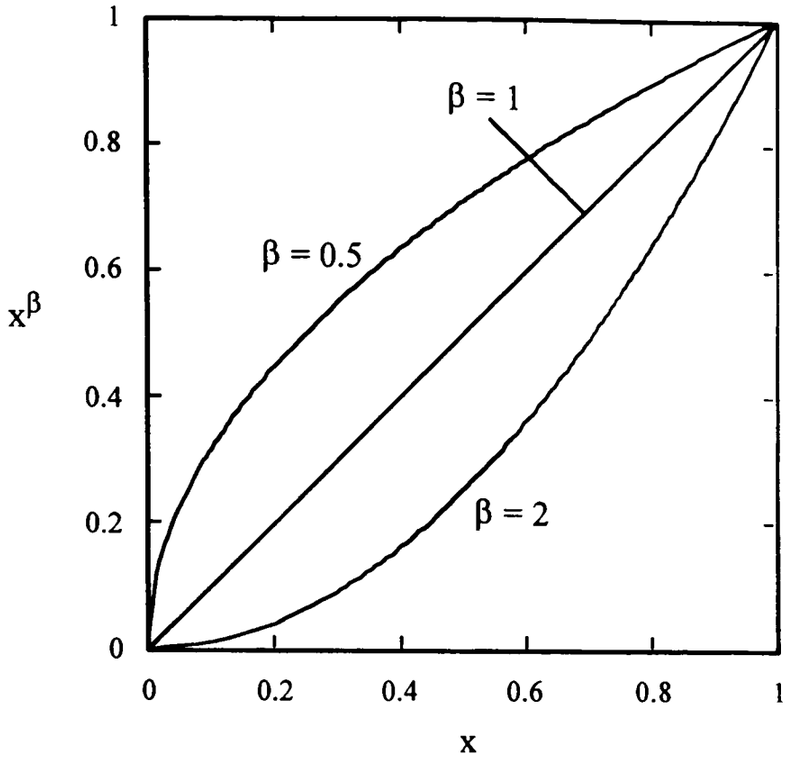

Figure 1.8: The effects of different exponents on the form of the curve.

The mixtures considered for the theoretical phase diagram predictions in Chapter 6, namely hexane or hexamethyldisiloxane + perfluorohexane, fall under the Scott and van Konynenburg classification of type II mixtures (van Konynenburg and Scott, 1980), i.e. they exhibit a continuous gas-liquid critical line *and* an upper liquid-liquid critical line. The projection of the pressure-temperature phase diagram showing both gas-liquid and liquid-liquid critical behaviour for type II mixtures is shown in Figure 1.9. In such projections points at all compositions are effectively collapsed onto one plane. The line lying between the vapour pressure curves of the pure components is the line of liquid-liquid-gas equilibrium, i.e. at temperatures below that of the upper critical endpoint UCEP, two liquid phases and the gas are in equilibrium at the mixture vapour pressure. At the UCEP the two liquid phases merge in the presence of the vapour. The dashed line starting at the UCEP is the liquid-liquid critical line; this line is nearly straight at low pressures and has a very large slope. At pressures which cut this line and at temperatures lower than those defining the line, two liquid phases coexist and there is no vapour present.

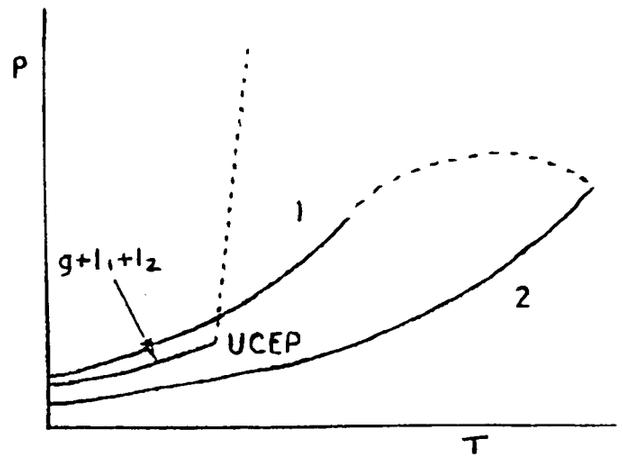

Figure 1.9: The pressure-temperature phase diagram for type II binary mixtures. (Reproduced from Green, 1992.)

A pressure-composition slice of Figure 1.9 for a temperature below the UCEP is shown in Figure 1.10. As mentioned above, experimentally for a sample in a closed tube the gas-liquid-liquid three-phase line is followed with increasing temperature. The vertical lines representing the liquid-liquid coexistence in Figure 1.10 move closer together with increasing temperature and at the UCEP they merge. Temperature-composition slices can also be extracted in a similar way.

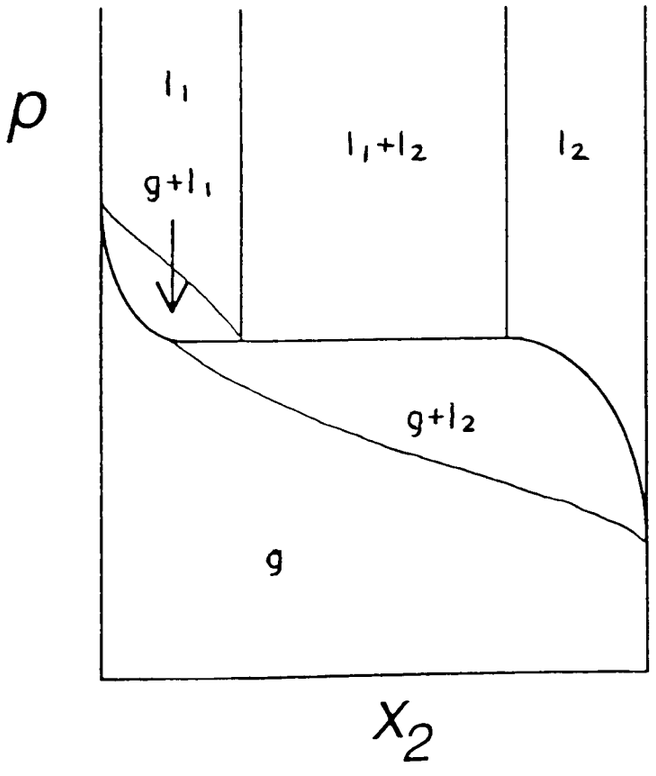

Figure 1.10: A pressure-composition slice from Figure 1.9 for a type II binary mixture below the UCEP. (Reproduced from Green, 1992.)

The liquid-liquid phase behaviour of partially miscible ternary mixtures is complex. Phase equilibria at constant pressure can be represented by a three-dimensional diagram

of an upright triangular prism to include both the compositions of all three components and the temperature. The detailed discussion of the phase behaviour of ternary mixtures is deferred to Chapter 6.

The liquid-vapour behaviour of a binary mixture near a critical endpoint, in particular the form of the vapour pressure and surface tension, is discussed in section 1.3.1.2.

The previous sections have considered the phase behaviour and the location of the critical points in pure substances and in mixtures. We turn now to the anomalous behaviour observed in fluids near critical points.

1.1.4 Near-critical anomalous behaviour in fluids

Close to a critical point anomalous behaviour is observed in many properties of a fluid. At the liquid-liquid critical point in a binary mixture there is a fine balance between the molecular attractive forces–which tend to produce aggregation of molecules of the same kind into groups, clusters and eventually separate phases–and the disruptive effect of collisions–which tend to disperse these clusters, and so mitigate against miscibility. Raising or lowering the temperature very slightly around the critical temperature T_{CS} upsets this balance and marked changes are then observed in the behaviour of the fluid.

Close to the critical point long-range fluctuations occur. In the case of a pure fluid near the liquid-vapour critical point, liquid-like fluctuations occur in the vapour phase and vapour-like fluctuations occur in the liquid phase. In a binary liquid mixture near the liquid-liquid critical point, fluctuations occur in the single-phase as it begins to form two separate phases, or in both coexisting phases as they begin to merge. As the critical point is approached, these fluctuations extend over greater distances. The characteristic size of the fluctuating regions, called the *correlation length* ξ, diverges to infinity at the critical point.

As the critical point of a pure or mixed fluid is approached from above or below the critical temperature, the fluid usually loses its transparency and turns milky or cloudy. This is known as *critical opalescence* and it persists over a narrow range of temperatures close to the critical temperature. Critical opalescence occurs due to the density and thus refractive index fluctuations in the near-critical fluid. Away from the critical region these fluctuations are insignificant, but in the critical region they give rise to domains of different densities within the fluid. When the size of the clusters grows to be comparable with the wavelengths of visible light, light is scattered from this optically non-homogeneous medium giving rise to the milky appearance of the liquid.

A useful distinction is often made in the consideration of critical phenomena between *field* and *density* variables. Field variables are those variables–such as temperature, pressure and chemical potential–which of necessity are equal in coexisting phases, while density variables, by contrast, are variables–such as density, entropy per

unit volume and composition–which need not be, and usually are not, equal in each of the coexisting phases. Refractive index is one density variable which in some mixtures at certain wavelengths of light takes the same value in coexisting liquid phases; this phenomenon is termed *isooptic* (Francis, 1951); mixtures whose coexisting phases have the same mass density are known as *isopycnic* (Francis, 1953).

The term *order parameter* is used for quantities which yield a measure of the dissimilarity of the phases, and in a two-phase system are usually differences in any suitable density variable in the two coexisting phases. For example, differences in refractive index or mass density are commonly chosen as order parameters, however, in isooptic or isopycnic mixtures, respectively, clearly neither choice is appropriate. As the system approaches a critical point, the order parameter tends to zero since the two phases become more similar and eventually merge identity.

As the critical point is approached, some properties tend to vanish and others tend to infinity . Power laws are used to describe both kinds of behaviour close to the critical point, they are generally of the form:

$$f(X) = AX^{\lambda} \tag{1.7}$$

where f(X) is the property described. In these expressions, A is the power law amplitude, X is a scaled distance away from the critical point and λ is the *critical exponent* or index. The scaled distance from the critical point is often expressed in terms of $\varepsilon = (T - T_c)/T_c$. where T_c is the critical temperature, or in terms of composition $(x - x_c)/x_c$, where x_c is the critical composition. The sign of λ determines whether f(X) vanishes–$\lambda > 0$–or diverges to infinity–$\lambda < 0$–at the critical point. The rate at which a property approaches zero or infinity depends on the size of the critical exponent. The value of the critical exponent is characteristic both of the property considered and of the path along which the critical point is approached. Critical exponents are universal, that is they are the same for all systems in a given universality class, see below, and do not depend on the nature of the components and the details of the intermolecular forces. The values of the critical exponents are generally defined to be positive.

The Ising model was first used by Lenz and Ising in 1926 to model the ferromagnetic phase transition and it is now an important model system used to study critical points. In the Ising model, magnetic spins are allowed to point 'up' or 'down' and are placed on regular lattice sites with any interactions limited to nearest neighbours only. This model can be used to describe a variety of phase transitions. For example, antiferromagnetism is described by allowing neighbouring spins to align antiparallel. For liquid-liquid phase transitions the 'up' and 'down' spins are replaced by particles A and B; for liquid-gas transitions the spins are replaced by particles and holes.

Phase transitions can be grouped into classes of systems which show similar behaviour. Each system in a particular universality class has the same spatial

dimensionality d and the same number of spin components n as all the other members. A universality class (d,n) is a set of systems which all have the same critical exponents. Fluids and ferromagnets both belong to class (3,1).

Renormalisation Group (RG) Theory is another approach to studying critical phenomena and was introduced by Wilson in 1971. The renormalisation group is a general method for constructing theories and can deal with problems that have multiple scales of length (Wilson, 1979). In RG theory the behaviour of a system depends only on the universality class to which it belongs. Values of critical exponents have been calculated using this method.

Critical exponents have also been calculated using classical theories. Classical 'mean-field' theories such as van der Waals-like theories assume that the Helmholtz free energy is analytic, e.g. that it can be expanded by a Taylor series around the critical point in powers of, for example, $(T - T_c)$ or $(V_m - V_{m,c})$. However, the Helmholtz free energy of real systems turns out not to be analytic and the exponents found for real systems and those predicted using RG theory thus both differ from the classical values obtained from mean-field theories. For example, the near-critical behaviour of the order parameter in terms of the difference in the mole fraction of one of the components in each phase $(x' - x'')$ is described by the scaled distance in temperature from the critical point ε raised to the power of the exponent β. The classical value of β is 1/2 and the RG value for class (3,1) fluids is 0.325 (Le Guillou and Zinn-Justin, 1977), close to values measured experimentally. The physical consequence of the smaller critical exponents found experimentally and from the RG theory is that the top of the coexistence curve is 'flatter' than is predicted by mean-field theories, and in practical terms this means that T_{UCS} is overestimated by such theories.

Different critical exponents are used to represent the near-critical behaviour of properties such as the heat capacity or correlation length. The correlation length is represented by a power law of the form $\xi = \xi_0 \varepsilon^{-\nu}$, where ξ_0 is a power law amplitude and the critical exponent ν is 0.630, calculated from RG theory. The critical exponents describing different properties are interrelated by scaling laws (Scott, 1978).

The anomalous critical behaviour of fluids has been extensively studied. Reviews of the literature were carried out by Scott in 1978 and by Greer and Moldover in 1981 and these appear to continue to represent essentially the current view of such matters.

Almost all of the discussion of critical-point behaviour so far in this chapter has been concerned with thermodynamic or bulk equilibrium properties. The sole exception has been the mention of the behaviour of the molecular correlation length. Much the same set of ideas, however, has been applied to the behaviour of transport properties and to the critical behaviour of one of these, the viscosity, we now turn. The principal features of the anomalous viscosity of near-critical binary mixtures are outlined in the following section and laid out in more detail in Chapter 2.

1.2 Macroscopic and microscopic viscosities near a critical endpoint

The macroscopic and microscopic viscosities of binary mixtures near critical endpoints have been studied and are discussed in Chapters 2 and 3, respectively. Here brief introductions to each type of viscosity, their differences, and reasons for their interest are given.

1.2.1 Macroscopic viscosity

Like most properties of near-critical mixtures, there are two main approaches to the critical point along which the anomalous behaviour of the viscosity is studied. The first is the constant critical composition path in the one-phase mixture leading into two limbs of the coexistence curve for two-phase mixtures. The second approach is along a path of constant critical temperature. The behaviour of the macroscopic shear viscosity of a binary mixture near an upper or a lower critical endpoint has been well characterised. Along both paths, the viscosity diverges to infinity at the critical endpoint. A different critical exponent is used to describe the form of the anomaly along each path.

The anomaly in the viscosity at a critical endpoint is a result of the density fluctuations occurring in the liquid and the divergence of the correlation length of these fluctuations as discussed in the previous section.

1.2.2 Microscopic viscosity

The microscopic viscosity of a liquid or a liquid mixture can be studied by a variety of spectroscopic techniques. In this investigation the principal technique employed is the measurement of the rotational correlation time of a fluorescent probe molecule in the liquid. This method is widely used to determine the microviscosity of the interior of micelles, or of interfacial films. In this study, it has been used to investigate the viscosity of near-critical binary mixtures at microscopic level.

The viscosity of the environment around the probe affects the rate at which the molecule can rotate. If the viscosity is high, the probe experiences high viscous drag and thus rotates relatively slowly. The temperature also plays a part through its effect on both the viscosity of the solvent and the kinetic energy of the probe.

1.2.3 Comparison of macroscopic and microscopic viscosities

The study of the microscopic viscosity of mixtures near critical endpoints is of interest to allow a comparison with the macroscopic viscosity, in particular to the form of any anomaly and the critical exponents characterising the anomaly. Critical anomalies previously observed in binary mixtures have generally been in macroscopic properties. In this study a molecular quantity is measured.

The macroscopic viscosity is a bulk property of the mixture and can be measured by capillary flow. The microscopic viscosity, however, is the local resistance to translation or rotation of a given probe molecule in solution. The issues are whether i) the method of measurement of the rotational correlation time provides a true measure of the microscopic viscosity, ii) the local viscosity of the liquid surrounding the probe has the same value as the bulk macroscopic viscosity, iii) the critical anomaly which occurs in the macroscopic viscosity is also observed at a microscopic level. These issues are addressed in Chapter 3.

1.3 Adsorption and wetting in mixtures near critical points

In sections 1.1.2 and 1.1.3 the liquid-vapour and liquid-liquid phase behaviour of mixtures has been discussed. In this section we turn to the interfacial behaviour of binary mixtures near critical endpoints. Both the liquid-vapour and the solid-liquid interfaces are considered. The issues of critical adsorption and critical-point wetting considered here form the general introductions for Chapters 4 and 5.

As mentioned in section 1.1.3, at a critical endpoint, CEP, two coexisting liquid phases merge identity in the presence of the coexisting vapour phase. This *noncritical* vapour phase is known also as a spectator phase as it is not involved in the phase separation process. The solid walls of the vessel play a similar spectator role since they are not directly involved in the critical event; however, since they do not share material with the critical phases in some senses the role is different. The liquid-vapour and solid-liquid interfaces are thus noncritical interfaces. The liquid-liquid interface is the critical interface and vanishes when a single-phase is formed.

Although the liquid-vapour and solid-liquid interfaces are noncritical, interesting effects are observed at these interfaces close to the critical endpoint. Preferential adsorption of one of the mixture components at the noncritical interface occurs when the mixture is in a single phase close to the critical endpoint, and is also expected just into the two-phase region. This is known as *critical adsorption*. Another effect, which is observed in two-liquid-phase mixtures, is the complete wetting of the noncritical interface by one of the liquid phases. This occurs for a range of temperatures close to the critical solution temperature and is known as *critical-point wetting*.

Critical-point wetting at the solid-liquid interface of a binary liquid mixture has been investigated by evanescent-wave-generated fluorescence spectroscopy and is discussed in Chapter 4. The detailed structure of the liquid-vapour interface of binary mixtures near critical endpoints with respect to critical adsorption and critical-point wetting has been investigated by neutron reflectivity and these results are presented in Chapter 5.

1.3.1 Adsorption

1.3.1.1 Theory

The Gibbs adsorption equation can be used as a starting point for a consideration of adsorption at an interface. For a two-component mixture at fixed temperature and pressure the Gibbs adsorption equation can be expressed as:

$$-d\sigma = \Gamma_1 d\mu_1 + \Gamma_2 d\mu_2 \tag{1.8}$$

where σ is the surface tension of the mixture and μ_i is the chemical potential of component i. Γ_i is the adsorption of component i at the interface and is defined as an amount per unit area of the surface:

$$\Gamma_i = n(s)_i/a \tag{1.9}$$

where a is the area of the surface and $n(s)_i$ is the number of moles of i adsorbed at the surface or the surface excess. This surface excess is defined by:

$$n(s)_i = n_i - n(g)_i - n(l)_i \tag{1.10}$$

where n_i is the total number of moles of component i and $n(g)_i$ and $n(l)_i$ are the number of moles of i in the gas and liquid phases, respectively.

The Gibbs-Duhem equation, relating the changes in the chemical potentials of the two components of a given phase of the mixture at constant temperature and pressure, is given by:

$$d\mu_1 = -(x_2/x_1)d\mu_2 \tag{1.11}$$

where x_i is the mole fraction of component i. Using this equation, the Gibbs adsorption equation above reduces to:

$$-(d\sigma/d\mu_2)_T = \Gamma_2 - (x_2/x_1)\Gamma_1. \tag{1.12}$$

The relative adsorption of component 2 with respect to component 1, $\Gamma_{2,1}$, is defined by the right-hand side of the above equation, thus:

$$\Gamma_{2,1} = \Gamma_2 - (x_2/x_1)\Gamma_1 = -(d\sigma/d\mu_2)_T. \tag{1.13}$$

The relative adsorption, $\Gamma_{2,1}$, has been the quantity generally used to represent the adsorption, but recently the quantity $\Gamma_{2,1}/x_2$ termed the Total Surface Segregation (TSS) has been suggested as an alternative and more suitable measure of adsorption (McLure *et al.*, 1993) and is thus defined by:

$$\Gamma_{2,1}/x_2 = \Gamma_2/x_2 - \Gamma_1/x_1 = -(1/x_2)\,(d\sigma/d\mu_2)_T. \tag{1.14}$$

The TSS can be evaluated (McLure *et al.*, 1993; Williamson, 1990) as:

$$\Gamma_{2,1}/x_2 = -(d\sigma/dx_2)_T/\{RT[1 + x_2(d\ \ln\gamma_2/dx_2)_T]\} \tag{1.15}$$

where γ_2 is the Raoultian activity coefficient of component 2. In equation (1.15) it is implicit that the experimental quantities are measured orthobarically, i.e. at the vapour pressure of the mixture. For condensed phase properties at temperatures well removed from the gas-liquid critical line, the vapour pressure is essentially constant and equal to zero thus maintaining thermodynamic propriety.

We turn now to adsorption close to a critical endpoint. This has been discussed by Rowlinson and Widom (1982). Equation (1.13) can be rewritten:

$$\Gamma_{2,1} = -(d\sigma/dx_2)_T/(d\mu_2/dx_2)_T. \tag{1.16}$$

The near-critical behaviour of $\Gamma_{2,1}$ can be deduced from the behaviour of the numerator and denominator of the above equation by the following arguments. Considering the approach to the critical endpoint as a function of composition with the temperature fixed at the critical temperature T_c, the expressions for the numerator and denominator near a critical endpoint are:

$$(d\sigma/dx_2)_T \sim |x_2 - x_{2,c}|^{(\mu/\beta-1)} \tag{1.17}$$

$$(d\mu_2/dx_2)_T \sim |x_2 - x_{2,c}|^{\gamma/\beta} \tag{1.18}$$

where $\mu = 1.26$ is the critical index for the temperature dependence of the surface tension, $\beta = 0.325$ is the order-parameter exponent associated with the temperature dependence of the compositions of coexisting phases of a mixture close to a critical endpoint and $\gamma = 1.24$ is associated with the chemical potentials in a mixture near a critical endpoint. Using the exponent relation $\mu + \nu = \gamma + 2\beta$, where $\nu = 0.63$ is the exponent for the temperature dependence of the correlation length, equation (1.16) can be rewritten:

$$\Gamma_{2,1} \sim |x_2 - x_{2,c}|^{(-\nu/\beta+1)} \sim |x_2 - x_{2,c}|^{-0.938}. \tag{1.19}$$

The temperature dependence of $\Gamma_{2,1}$ for fixed critical composition $x_{2,c}$ is obtained by replacing $|x_2 - x_{2,c}|$ in equation (1.19) with $|T - T_c|^{\beta}$ leading to:

$$\Gamma_{2,1} \sim |T - T_c|^{(-\nu+\beta)} \sim |T - T_c|^{-0.305}. \quad (1.20)$$

The total surface segregation (TSS), $\Gamma_{2,1}/x_2$, thus diverges at the critical endpoint along either path. This can be interpreted, using equation (1.14), as the formation of a macroscopically thick layer of essentially pure component 2 at the interface.

The preferential adsorption of one of the mixture components at the noncritical interface close to the critical endpoint is known as *critical adsorption*. This adsorption is considered as a local modification of the order parameter and should extend over the range of the correlation length ξ which describes the fluctuations of the bulk order parameter and diverges at the critical endpoint (Beysens, 1989).

Fisher and de Gennes (1978) have calculated the variation of the order parameter as a function of distance z through a noncritical solid interface in terms of a universal surface scaling function. The order parameter can be expressed in terms of, for example, volume fraction, density or, as in Chapter 5, the neutron scattering length density. Here it is expressed in terms of volume fraction ϕ as the difference between the value at a given distance $\phi(z)$ and the bulk value $\phi(bulk)$, effectively the value at infinite distance from the interface. Close to the interface, within approximately 10 Å, density oscillations are predicted due to packing effects. Further away, the order parameter decays according to a power law:

$$[\phi(z) - \phi(bulk)] \sim z^{-\beta/\nu} \sim z^{-1/2}. \quad (1.21)$$

This type of decay continues until z is of the same order as the correlation length ξ. For $z > \xi$ the adsorption decays exponentially as:

$$[\phi(z) - \phi(bulk)] \sim e^{-z/\xi}. \quad (1.22)$$

For sufficiently large values of z, $\phi(z)$ approaches $\phi(bulk)$ and the adsorption vanishes. Liu and Fisher (1989) have suggested functions for the order parameter profile such that the cross-over from the power law to the exponential form can be tuned by parameters. The interfacial structure due to critical adsorption is thus interesting and occurs in a binary mixture close to the critical endpoint at either the solid or the vapour interface. Various theoretical treatments of critical adsorption have been discussed by Dietrich (1988). The total amount of adsorption varies as $[(T - T_c)/T_c]^{-(\nu-\beta)}$ and so diverges at T_c (Beysens, 1989).

1.3.1.2 Behaviour of the liquid-vapour surface tension

At the liquid-vapour interface of a simple mixture, the component adsorbed is that with the lower liquid-vapour surface tension as this lowers the surface free energy. In this section the behaviour of the surface tension of a mixture near a critical endpoint is briefly discussed. In the previous section it was mentioned that $d\sigma/dx_2$ along the critical isotherm goes to zero at the critical composition. We show here that this takes the form of a horizontal inflection.

The surface tension σ is formally defined by:

$$dw = \sigma\, da \tag{1.23}$$

where dw is the work involved in forming a surface of area da. The surface tension as a function of temperature for the binary mixture 2-methylpentane + perfluorotributylamine of critical composition in the single-phase and along both limbs of the coexistence curve is shown in Figure 1.11a. The three curves meet at the critical temperature with a common tangent. The surface tension as a function of composition along the critical isotherm ($T = T_c$) for decamethyltetrasiloxane + perfluorohexane is shown in Figure 1.11b. A horizontal inflection occurs at the critical composition. This experimental observation is in agreement with predictions by Widom (1977).

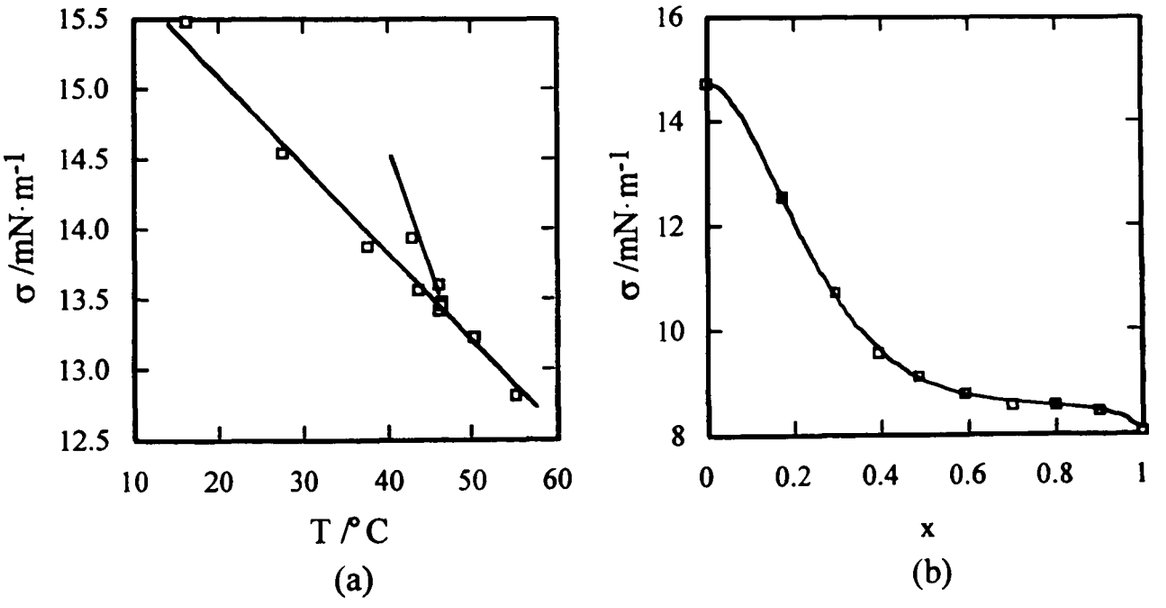

Figure 1.11: (a) The surface tension σ for (1-x) 2-methylpentane + x perfluorotributylamine as a function of temperature for a mixture of critical composition. (b) The surface tension σ for (1-x) decamethyltetrasiloxane + x perfluorohexane as a function of composition at the critical temperature. (Taken from Bowers, 1995.)

In 'usual' binary mixtures the component with the higher surface tension has the lower vapour pressure, i.e. is the less volatile. The form of the vapour pressure-composition curve at the critical temperature is effectively the inverse of the surface tension-composition curve, and thus also exhibits a horizontal inflection. Examples of usual mixtures include hexane or heptane + perfluorohexane, methylcyclohexane + perfluoromethylcyclohexane, hexamethyldisiloxane + perfluorohexane and decamethyl-tetrasiloxane + perfluorohexane. 'Unusual' mixtures also exist, in which the component with the higher surface tension has the *higher* vapour pressure. Examples of unusual mixtures include nearly all surfactant + solvent mixtures, of which 2-butoxyethanol + water is a well studied example, pentane + perfluoroheptane, and 2-methylpentane + perfluorotributylamine (Bowers, 1995).

In addition to a horizontal inflection, a maximum or minimum may be observed in the surface tension along the critical isotherm; this effect is termed surface azeotropy, or *aneotropy* (McLure *et al.*, 1973). At an azeotrope the vapour and liquid compositions are equal. At an aneotrope the bulk and surface compositions are equal, i.e. there is no net adsorption of either component at the liquid-vapour interface. A mixture which exhibits an aneotrope is hexamethyldisiloxane + perfluorohexane. The aneotropic composition occurs at a mole fraction of perfluorohexane close to 0.89, as shown in Figure 1.12. The surface structure of a mixture of the aneotropic composition has been studied by neutron reflectivity and is discussed in Chapter 5.

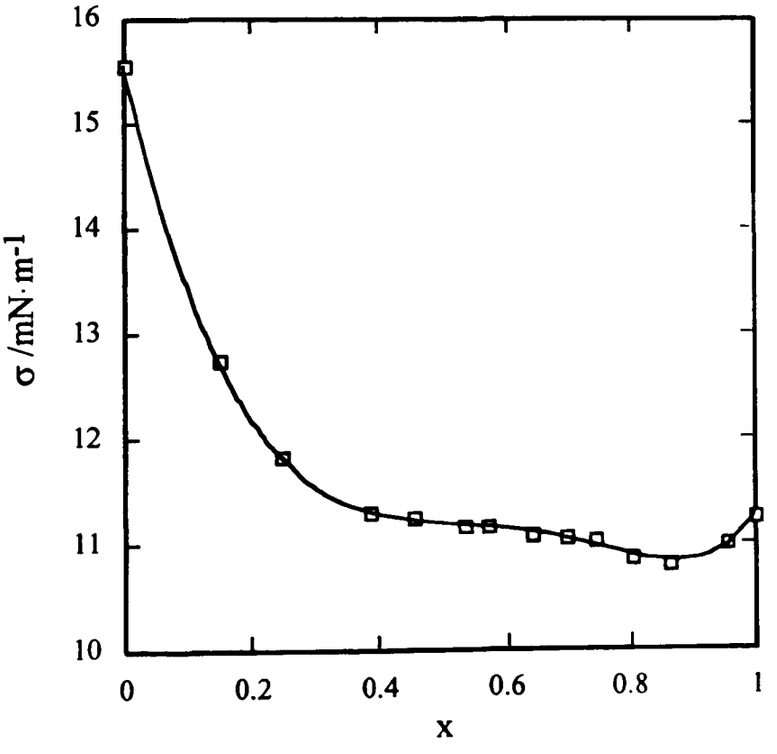

Figure 1.12: The surface tension σ for (1-x) hexamethyldisiloxane + x perfluorohexane at T = 25°C, close to T_{UCS} = 23.8°C, showing the horizontal inflection at the critical composition, x = 0.52, and the aneotrope at x = 0.89. (Taken from Bowers, 1995.)

1.3.1.3 Experimental investigations of critical adsorption

In this section some of the previous experimental studies of critical adsorption are briefly described. Ellipsometry is one of the most frequently used techniques in these studies. It involves the measurement of the depolarisation upon reflection of plane-polarised light incident at an interface. The ellipticity measures the ratio of the complex Fresnel reflection coefficients for p-polarised light, where the electric field vector is in the plane of incidence, and s-polarised light, where the electric field vector is perpendicular to the plane of incidence, and is defined by the ratio of the minor and major axes of the ellipse of polarisation (e.g. see Hirtz *et al.*, 1993). For light incident at the Brewster angle θ_B, where $\theta_B = \tan^{-1} n_2/n_1$ with n_2 and n_1 the refractive indices of the media at the interface, the reflected light is plane-polarised and the ellipticity can provide a measure of the interfacial structure normal to the interface. The analysis of ellipsometric data, like neutron reflectivity data, can be fairly involved. Further details of the use of ellipsometry in obtaining surface structural information are given by Greef (1990).

An experimental study of critical adsorption at the liquid-vapour interface of aniline + cyclohexane was undertaken by Beaglehole (1980) using ellipsometry. It was shown that the coefficient of ellipticity could be related directly to the relative adsorption at the interface, with the sign of the ellipticity indicating which component was preferentially adsorbed. The ellipticity was positive and increased close to the upper critical solution temperature T_{UCS}, indicating adsorption of cyclohexane at the interface as expected from the lower surface tension of cyclohexane relative to aniline. It should be noted that in some cases the ellipticity can be negative if the permittivity of the surface layer is greater than the permittivity of the bulk phase (Hirtz *et al.*, 1993). Incidentally, the permittivity is proportional to the square of the refractive index.

Other studies by ellipsometry, which have shown the increasing preferential adsorption of one of the components at the liquid-vapour interface as the critical temperature is approached, include those of Heidel and Findenegg (1984) for nitrobenzene + heptane, where the heptane was preferentially adsorbed, and Schmidt and Moldover (1985) for isopropanol + perfluoromethylcyclohexane, where the fluorocarbon was preferentially adsorbed. The methanol + cyclohexane system has been studied by Schmidt (1986) by adding deuterated cyclohexane, thus increasing the density of the cyclohexane-rich phase and inverting the coexisting phases below T_{UCS}. In the deuterated system a methanol-rich region was observed to build up from above and below T_{UCS}, however the ellipsometric data below T_{UCS} could not be fitted to the same model profile as those above T_{UCS}. In some studies (Heidel and Findenegg, 1987) a finite maximum in the ellipticity has been observed slightly above T_{UCS}, e.g. 0.4 K above for solutions of polystyrene in cyclohexane. The ellipticity of a sample of critical composition did not, however, exhibit the expected second maximum below T_{UCS}.

The studies mentioned above have investigated the liquid-vapour interface by ellipsometry. Hirtz *et al.* (1993) have described in detail the use of ellipsometry in investigating critical adsorption. Critical adsorption at a silica-liquid interface has been observed for nitrobenzene + hexane (Beysens and Leibler, 1982). A fluorescence technique was used to detect the preferential adsorption of the fluorescent nitrobenzene.

1.3.2 Critical-point wetting

1.3.2.1 Theory

Critical-point wetting can occur at the solid interface in a single-component fluid close to the gas-liquid critical point, or at the solid or vapour interfaces in a binary liquid mixture close to a critical endpoint. In the following discussion of critical-point wetting we consider two coexisting liquid phases α and β of a binary mixture in contact with a third noncritical phase γ which may be the solid or the vapour. The interface between the two liquid phases forms an angle θ, called the contact angle, at the noncritical interface, as shown in Figure 1.13.

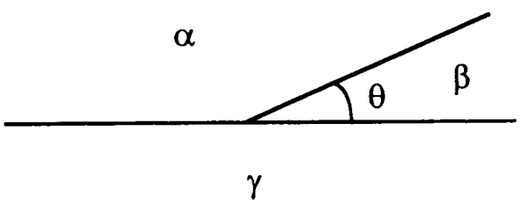

Figure 1.13: The contact angle θ made by the $\alpha\beta$ interface at the noncritical phase γ.

Resolving the forces along the noncritical interface leads to the Young-Dupré equation:

$$\sigma_{\alpha\beta}\cos\theta = \sigma_{\alpha\gamma} - \sigma_{\beta\gamma} \tag{1.24}$$

where σ_{ij} is the surface tension between phases i and j. For values of θ which satisfy this equation, i.e. for $\cos\theta$ between 0 and 1:

$$\sigma_{\alpha\beta} \geq |\sigma_{\alpha\gamma} - \sigma_{\beta\gamma}|. \tag{1.25}$$

For $\theta = 0$, i.e. $\cos\theta = 1$, the equation reduces to Antonow's rule:

$$\sigma_{\alpha\beta} = \sigma_{\alpha\gamma} - \sigma_{\beta\gamma}. \tag{1.26}$$

In this case phase β interposes itself between phase α and phase γ. Phase β is said to completely wet the noncritical interface. For $\theta > 0$ the interface is only partially wet.

As the critical endpoint is approached, $\sigma_{\alpha\beta}$ and $\sigma_{\alpha\gamma} - \sigma_{\beta\gamma}$ both vanish as the two liquid phases merge identity and the equation for the contact angle:

$$\cos\theta = (\sigma_{\alpha\gamma} - \sigma_{\beta\gamma})/ \sigma_{\alpha\beta} \tag{1.27}$$

becomes indeterminate.

The detailed behaviour near the critical point may be identified by considering the way in which the numerator and denominator approach zero. Since $\sigma_{\alpha\gamma} - \sigma_{\beta\gamma}$ is an order parameter which approaches zero as the scaled distance from the critical point $\varepsilon = |T - T_c|/T_c$, it has the same critical exponent β as that which describes the composition difference between the two phases. The value of β is approximately 0.3. Thus close to the critical point the form of the numerator is:

$$\sigma_{\alpha\gamma} - \sigma_{\beta\gamma} \sim \varepsilon^{\beta}. \tag{1.28}$$

The denominator $\sigma_{\alpha\beta}$ follows the form:

$$\sigma_{\alpha\beta} \sim \varepsilon^{\mu} \tag{1.29}$$

where μ is the characteristic exponent for the surface or interfacial tension near a critical point and is approximately 1.3. These considerations lead to the form of $\cos\theta$:

$$\cos\theta \sim \varepsilon^{\beta-\mu} \sim \varepsilon^{-1}. \tag{1.30}$$

$\cos\theta$ thus diverges as the critical point is approached and can reach a value of 1 at some temperature not quite at the critical temperature. The physical meaning of this, for example for a mixture with an upper critical endpoint, is that complete wetting occurs at some temperature T_w below the critical temperature T_c or T_{UCS}. T_w is called the wetting temperature and represents the temperature at which a transition from partial to complete wetting of the noncritical interface takes place. This phenomenon is known as *critical-point wetting* and was first predicted by Cahn (1977) following the above arguments. At partial wetting a microscopic film may be present, but at complete wetting a macroscopic film of the wetting phase forms at the interface with the solid or vapour. Wetting and adsorption phenomena in a binary mixture are illustrated in Figure 1.14.

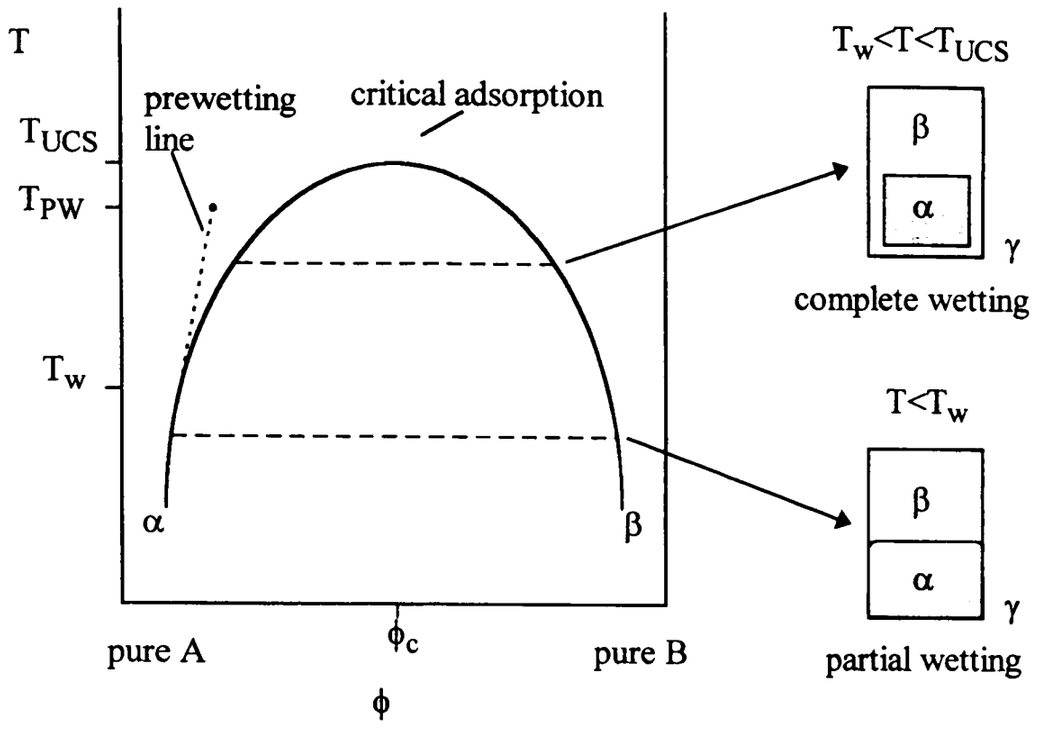

Figure 1.14: Schematic diagram illustrating wetting and adsorption phenomena in a binary liquid mixture close to the upper critical endpoint. The liquid phases are represented by α and β. T_{UCS}, T_w and T_{PW} are the upper critical solution temperature, the wetting transition temperature and the prewetting critical temperature, respectively.

The order of the wetting transition, which has been the subject of some controversy, is briefly discussed below. The transition may be of first or second order. If the transition is first order the thickness of the wetting film changes abruptly at T_w and if it is second order the film thickness increases gradually up to T_w.

For a first-order transition the existence of a prewetting line is predicted. This line starts tangential to the coexistence curve at T_w and terminates at a prewetting critical temperature T_{PW}, as shown in Figure 1.14. The prewetting line is a line of first-order surface transitions in the single-phase fluid at the noncritical interface from weak adsorption, to strong adsorption for compositions and temperatures close to two-phase coexistence. T_{PW} may occur above or below T_{UCS}. The prewetting transition across the prewetting line may be considered as a jump in wetting-film thickness from thin 'outside' the prewetting line to thick in the region bounded by the prewetting line and the coexistence curve. Close to T_w the jump in film thickness is large, but close to T_{PW} the differences in film thickness on either side of the prewetting line decrease and at T_{PW} the two films become indistinguishable (Evans and Chan, 1996).

Cahn's original approach to critical-point wetting, which was partly based on the analysis of a simple mean-field theory for the density profile at an interface, predicted

that the wetting transition was first order (Cahn, 1977). Independently Ebner and Saam (1977) using a more sophisticated density-functional theory for films on a solid substrate, which included packing effects due to short-range repulsive forces between atoms, reached the same general results. However, Sullivan (1981), using a slightly different approach for a liquid film on a solid substrate, found that the transition from partial to complete wetting was second order.

Further theoretical work led to increased controversy over the order of the wetting transition. Telo da Gama and Evans (1983) predicted a first-order wetting transition for a binary mixture of Lennard-Jones fluids, although as their calculations were based on an approximate numerical minimisation procedure they could not rule out the possibility that the transition might not be first order.

Tarazona, Telo da Gama and Evans (1983) resolved the dispute by showing explicitly that the transition from partial to complete wetting could be first *or* second order. They used a simple model free energy functional and showed that the order of the transition was dependent on the form assumed for the attractive part of the intermolecular pair-wise potentials. Teletzke, Scriven and Davis (1982, 1983) using a generalised version of Sullivan's theory found that the theory permitted either a first-order or a second-order transition depending on the parameters characterising the fluid-solid and fluid-fluid interactions.

Dietrich and Schick (1986) have formulated general analytic expressions which permit the determination of the order of wetting transitions in mean-field theory for one-component fluids near a solid wall and for binary liquid mixtures near a solid wall and at three-phase coexistence using long-range van der Waals forces.

1.3.2.2 Experimental investigations of critical-point wetting

In this section some of the experimental studies of critical-point wetting, carried out to determine the nature and thickness of the wetting film, the wetting transition temperature T_w, the order of the transition or the existence of prewetting, are discussed. This section is not intended to be a full review, but some of the main experiments are highlighted. Critical-point wetting is an active area of research and a fairly recent issue of *Ber. Bunsenges. Phys. Chem.* (1994, No. 3) was dedicated to the subject. Experimental and theoretical considerations of wetting phenomena have been discussed in detail by Dietrich (1988).

The phase which completely wets the liquid-vapour interface in a binary mixture close to its critical endpoint is generally the phase richer in the component with the lower surface tension. In some mixtures this may be the upper phase of a two-liquid-phase mixture, but in others it may be the lower phase. In the latter case, the lower more dense phase interposes itself between the upper phase and the vapour and the wetting transition from partial to complete wetting can be studied. The wetting layer is generally

assumed to be of the same composition as that of the bulk phase from which it originated. The thickness of the layer is determined by a competition between gravity–which tends to thin the layer–and dispersion forces–which tend to thicken the layer (Law, 1994).

At the solid-liquid interface, generally the phase with the lower solid-liquid interfacial tension wets. The phase which completely wets the solid-liquid or liquid-vapour interface close to the critical endpoint is called the *wetting* phase and the other phase is termed the *wetted* phase.

For a mixture in contact with a solid inner container wall and the vapour, the temperature at which complete wetting occurs is different at each interface. Different values of T_w may also be observed on changing the nature of the solid container, e.g. from one glass to another or from quartz to Teflon.

Many of the systems in which wetting has been studied in this work involve hydrocarbon + perfluorocarbon mixtures. In these mixtures the perfluorocarbon-rich phase is the more dense and also has the lower surface tension. The perfluorocarbon-rich phase is thus expected to wet the liquid-vapour interface. The hydrocarbon-rich phase is generally observed to wet the quartz-liquid interface. Different values of T_w are found for each interface, with T_w for the quartz-liquid interface generally lying closest to the upper critical solution temperature T_{UCS}. The wetting behaviour at the liquid-vapour and solid-liquid interfaces in a hydrocarbon + perfluorocarbon mixture is illustrated in Figure 1.15.

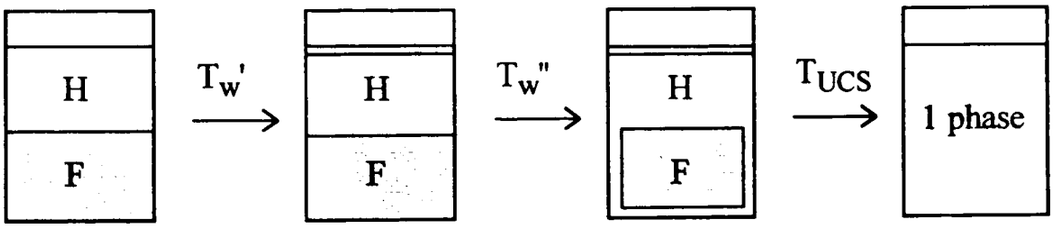

Figure 1.15: Critical-point wetting transitions at the liquid-vapour and solid-liquid interfaces for a hydrocarbon + perfluorocarbon mixture. T_w' and T_w'' represent the wetting transition temperatures for the liquid-vapour and solid-liquid interfaces, respectively. H and F represent the hydrocarbon-rich and perfluorocarbon-rich phases and the vapour is unmarked.

Various techniques can be used to study wetting at different interfaces. We have used evanescent-wave-generated fluorescence spectroscopy at the solid-liquid interface in Chapter 4 and neutron reflectivity at the liquid-vapour interface in Chapter 5. We turn now to previous investigations of critical-point wetting.

The methanol + cyclohexane mixture has been studied by Moldover and Cahn (1980) among others. Close to the critical point the lower methanol-rich phase was observed to completely wet the glass-liquid, quartz-liquid and liquid-vapour interfaces, and the cyclohexane-rich phase was observed to wet Teflon and other similar materials. On raising T_{UCS} by the addition of water, the methanol-rich phase ceased to wet the quartz completely.

A direct measurement of the transition from partial to complete wetting on changing the temperature through T_w was made by Pohl and Goldburg (1982) using capillary rise for the lower critical endpoint system 2,6-lutidine + water at the Pyrex-liquid interface. T_w - T_{LCS} was found to be approximately 15 K.

Kwon *et al.* (1982) measured the thickness of the wetting layers in methylcyclohexane (MCH) + perfluoromethylcyclohexane (PFMCH) and methanol + cyclohexane mixtures at the liquid-vapour interface, by ellipsometry, to be between 50 and 400 Å at ambient temperatures. The thickness of the wetting layer varied as $L^{-1/3}$ for small values of L where L was the height spanned by the upper liquid phase, in agreement with the prediction of de Gennes (1981), although it was noted that deviation from this behaviour could occur near the critical endpoint. In the MCH + PFMCH system, the upper MCH-rich phase wetted the quartz container walls and the lower PFMCH-rich phase wetted the vapour interface. In this system, equilibration of the thickness of the wetting film at the vapour interface must occur by diffusion of the PFMCH-rich phase through the upper phase. In contrast, in methanol + cyclohexane systems the methanol-rich lower phase wets both the quartz-liquid and liquid-vapour interfaces, and thus equilibration of the wetting layer at the vapour interface with the lower liquid phase should be facilitated by the connecting wetting film at the solid wall.

Schmidt and Moldover (1983a, 1983b) observed a first-order wetting transition at the liquid-vapour interface in isopropanol + PFMCH at a temperature 52 K below T_{UCS}. The ellipsometric data corresponded to an intruding layer of thickness less than 20 Å below T_w and a jump to about 350 Å in a narrow 0.03 K temperature interval. The thickness of the wetting layer changed by less than 30 Å with increasing temperature up to 12 K above T_w. The thickness dependence on the height of the upper phase L was not consistent with a -1/3 power law, instead depending only weakly on L.

Fattinger *et al.* (1987) pioneered the use of evanescent-wave-generated fluorescence spectroscopy to wetting problems. They observed a second-order wetting transition for 2,6-lutidine + water at different optical glass-liquid interfaces, with T_w - T_{LCS} equal to about 7 K. The maximum film thickness measured was 150 Å.

The existence of a first-order prewetting transition in methanol + cyclohexane has been observed experimentally by Bonn *et al.* (1994) using ellipsometry.

The foregoing survey, although not totally comprehensive, does list the significant investigations into critical-point wetting until now. The details of many important

aspects of wetting phenomena near critical points in mixtures have been revealed. However, neither the mixtures chosen for study nor the methods employed have been systematic. Furthermore, some of the techniques, e.g. ellipsometry, do not afford very detailed information at molecular level. As a consequence, some of the pressing issues remain unresolved. An experimental approach that does not appear until now to have been brought to bear on wetting problems at the liquid-vapour interface in near-critical systems–and rarely to problems in nonaqueous mixtures in general–is neutron reflectivity. This technique offers the opportunity to determine surface structure in great detail provided it is applied to mixtures of substances with useful reflectivity contrast, in practice differences in molecular scattering lengths. In this regard, the natural contrast between hydrocarbon and perfluorocarbon mixtures, and the potential available for different kinds of wetting, can be utilised to great advantage and forms the basis of much of the wetting research recorded later in this thesis. Turning to wetting at the solid-liquid interface, the most promising approach appears to be evanescent-wave-generated or total-internal-reflection fluorescence spectroscopy, particularly for the identification of wetting phases and determination of wetting layer composition and thickness. This technique can be regarded as the complement for solid-liquid wetting of neutron reflectivity for liquid-vapour wetting.

1.3.3 Summary of critical adsorption and critical-point wetting

Critical adsorption at the noncritical interface occurs in single-phase and also in two-phase mixtures close to the critical endpoint (Law, 1994). The component with the lower surface tension preferentially adsorbs at the interface. The composition of the adsorbed layer gradually decays to the bulk composition with increasing distance from the interface and the increase in the effective thickness of the layer is proportional to the bulk correlation length of composition fluctuations which diverges to infinity at the critical temperature. Single-phase mixtures have been frequently studied; however, the form of the critical-adsorption just into the two-phase region and the link with critical-point wetting appears not to have been fully characterised so far.

Critical-point wetting occurs in the two-phase region of the phase diagram at temperatures between the wetting temperature T_w, at which the transition from partial to complete wetting occurs, and the critical temperature T_c. The phase which wets the liquid-vapour interface is generally that with the lower surface tension. Similarly, at the solid-liquid interface the phase which wets is that with the lower solid-liquid interfacial tension. The wetting film and the order of the transition can be studied at the liquid-vapour interface, if the phase with the lower surface tension is the more dense, and at the solid-liquid interface by observing the phase at which a change in the wetting takes place. The composition of the wetting layer is usually assumed to have the same composition as that of the bulk phase from which it originated, but this had apparently

not been verified until the investigations reported later in this thesis. The wetting transition may be first order, i.e. the thickness of the film increases abruptly at T_w, and is in this case accompanied by a prewetting line believed to lie close to the coexistence curve, or second order, i.e. the thickness of the film increases gradually.

The thicknesses of the wetting films for different systems at solid-liquid and liquid-vapour interfaces, the values of T_w, the order of the transitions and the existence and location of prewetting transitions are all areas that are of interest in further investigations of critical-point wetting. Many experimental and theoretical studies have been carried out, but some of the factors governing these effects, such as the relative importance of long-range and short-range interactions and the differences in behaviour at various interfaces, are not fully understood.

1.4 Adsorption and wetting in surfactant solutions

Adsorption and wetting in binary mixtures near critical endpoints have been discussed in the previous section. We turn now to adsorption and wetting in surfactant solutions. Wetting behaviour of liquids and solutions is of importance in a variety of areas including lubrication, paints and detergency.

The behaviour discussed so far has been for any binary liquid mixture near a critical endpoint and each component has been present in roughly equal amounts at the critical composition. Surfactants are particular types of molecules and are usually considered in aqueous or hydrocarbon solutions in which they are present in small quantities. In aqueous solutions, surfactants generally adsorb at the air-water interface thereby modifying the surface tension and wetting properties of the solution. In bulk aqueous solution, surfactants can form aggregates called micelles, and this allows them to solubilise fairly large amounts of oil. In oil + water + surfactant systems microemulsions can form. Surfactants have a variety of applications including detergency and tertiary oil recovery.

In this section surfactants, micelles and microemulsions are discussed and the wetting behaviour of these solutions is considered. Microemulsions are multicomponent systems with complex phase behaviour. In order to fully understand the phase behaviour of these types of systems simpler mixtures must also be considered. In Chapter 6, the results of experimental and theoretical studies of the phase behaviour of simple ternary mixtures are presented. These will form the basis for further work on systems of increasing complexity, such as those described here. A range of studies is currently being carried out on microemulsions and an issue of *Ber. Bunsenges. Phys. Chem.* (1996, No. 3) highlights some of the most recent developments.

1.4.1 Surfactants, micelles and microemulsions

The name surfactant comes from *surf*ace *act*ive and surfactants are thus generally defined as substances that are active at the interface between two phases. The two phases are often air and water and the surfactant molecules accumulate at the surface thereby modifying the surface tension. Aqueous surfactants are usually long-chain molecules consisting of a hydrophilic head group and a hydrophobic, or lipophilic, tail. Surfactants, sometimes also termed detergents or amphiphiles, where this latter term is more general and can be applied to molecules containing two different functionalities, may be nonionic or ionic, depending on the nature of the head group. A surfactant molecule may also be composed of several chains of various lengths, which may be branched and may contain a variety of chemical groups, and these different factors can lead to variations, amongst other things, in chain flexibility, surface activity and bulk aggregation behaviour.

A more general definition of a surfactant is that of a molecule containing two different functionalities at each end of a chain, i.e. an amphiphile. In the most common case these functionalities are hydrophilic and hydrophobic groups, but the more general definition could also be applied, for example, to a molecule containing a hydrogenated chain and a perfluorinated chain, i.e. a perfluoroalkylalkane. These amphiphilic molecules have the potential to increase the mutual solubility of alkanes and perfluoroalkanes in a similar way that a traditional surfactant increases the solubility of oil and water, and are thus of interest in forming nonaqueous surfactant systems. Perfluoroalkylalkanes in alkane and perfluoroalkane solutions are discussed in detail in section 1.5.2.

In addition to their surface behaviour, surfactants can also form aggregates in bulk solution. Such *micelles* typically contain 20-100 surfactant molecules. The term micelle comes from the latin 'micella' meaning small bit. In aqueous solution, the hydrophobic tail parts of each molecule come together and form the inside of the roughly spherical micelle. This hydrophobic core is surrounded by a solvent-permeated layer containing the hydrophilic head groups. The driving force for aggregation is largely due to hydrophobic interactions between the lipophilic parts of the molecules (Kertes, 1977). Micelle formation is a cooperative process and the alkyl chains are located at such distances from each other that the core of the micelle can be assumed to be liquid-like (Birdi, 1977). Micelles form above a specific concentration, the *critical micelle concentration (cmc)*, which is typical of the system and depends upon the structure of the surfactant and the physicochemical conditions. Below the cmc the surfactant molecules tend to adsorb at the gas-liquid interface as the hydrophobic tails try to escape from the water environment and they thus decrease the surface tension of the water and affect its wetting properties. As the surfactant concentration is increased the interface becomes covered by a close-packed monolayer and then, on further increasing the concentration, micelles form in the bulk phase (Kahlweit and Busse, 1989). Examples of

critical micelle concentrations at 25°C are 8.3 x 10^{-3} mol dm^{-3} for sodium dodecyl sulphate and 3.3 x 10^{-2} mol dm^{-3} for sodium decyl sulphate (Lindman and Wennerström, 1980).

In some cases the equilibrium concentration of the surfactant in solution is reached below the cmc. However, on raising the temperature the solubility of the surfactant increases dramatically at a particular temperature, referred to as the *Krafft point*. This dramatic increase is due to the formation of micelles at higher temperatures which are more soluble than the monomers which exist at lower temperatures. The Krafft point for sodium dodecyl sulphate (SDS) is about 20°C (Lindman and Wennerström, 1980). Below this temperature the solubility of SDS in water is about 0.2%, but increases to 10-20% at about 4°C above the Krafft point (Hutchinson and Shinoda, 1967).

Aggregates of surfactant molecules which form in nonpolar organic solvents are called *inverse micelles*. The polar head groups form the core of the micelle leaving the hydrophobic tails in contact with the solvent. Both polar and nonpolar interactions are important in forming inverse, or reverse, micelles. The driving force for the aggregation process is essentially due to dipole-dipole interactions between the polar head groups. Micelle formation is promoted by the interaction of polar groups, especially in the presence of water, and is minimised by the interaction of the polar groups with the solvent (Fowkes, 1967).

The shape of a micelle is generally close to spherical, but varies slightly depending on the concentration of the surfactant, and may be distorted to ellipsoidal. For a given surfactant the size of a micelle depends on the temperature, the concentration of surfactant, and the concentration and nature of any added electrolytes or nonelectrolytes (Hutchinson and Shinoda, 1967). One dimension of a micelle is limited by the maximum possible extension of a hydrocarbon chain (Tanford, 1972). On increasing the surfactant concentration in water, various micelle-like structures are formed including cylindrical and lamellar micelles (Bansal and Shah, 1977).

Ionic micelles differ from nonionic micelles in that they have associated counterions. An ionic micelle is composed of three regions: the core of hydrophobic chains, the Stern layer containing the head groups and some of the counterions and the Gouy-Chapman double layer consisting of the excess counterions (Stigter, 1967). Nonionic micelles, which are often formed from alkyl polyethoxylates, or alkyl polyglycol ethers, have less well-defined regions. The hydrocarbon core is generally surrounded by a diffuse region grading off from polyether to water. The polyether head groups may be long and may have a definite, e.g. helical, structure, or may be randomly coiled (Tanford, 1977).

Nonionic surfactant micelles have different properties from those of ionic micelles. The critical micelle concentrations of most nonionic surfactants are much smaller, often by a factor of 100, than those of the corresponding ionic surfactants with the same alkyl

chain length (Shinoda, 1967). For nonionic systems intra-micellar and inter-micellar head group repulsions are generally reduced and often 1000 or more nonionic surfactants can cluster together (Atkins, 1982).

The mixtures described so far have been binary surfactant + water or oil mixtures. In ternary oil + water + surfactant mixtures different types of behaviour such as microemulsion formation can be observed. Emulsions are dispersions of liquids in liquids. *Microemulsions* are defined as thermodynamically stable apparently homogeneous dispersions of water in oil or oil in water, which form in the presence of surfactants (Nicholson *et al.*, 1982). Microemulsions can be formed in a mixture of a nonionic surfactant with oil and water and they can also be observed using an ionic surfactant in place of a nonionic surfactant, but generally a cosurfactant such as a short-chain alcohol is also required. The main features which distinguish microemulsions from other 'normal' emulsions are i) their transparency, ii) their low viscosity, iii) the high stability they exhibit towards separation into distinct phases (Hunter, 1987).

Microemulsions can be of three main structures, namely i) droplet-like dispersions of oil in water, ii) droplet-like dispersions of water in oil, or iii) bicontinuous. The first type of structure can be formed on adding a small amount of oil to an aqueous micellar solution. The oil is solubilised inside the micelle, forming an oil-in-water (o/w) microemulsion. The second type of structure, a water-in-oil (w/o) microemulsion, can be formed in a similar way by adding a small amount of water to an inverse micellar solution. The third structure is different from the first two types. It can exist when substantial amounts of both water and oil are present. Both oil and water form continuous interpenetrating domains with the surfactant assumed to lie between the separate regions. The bicontinuous structure for these mixtures, first proposed by Scriven (1977), is considered to be intermediate between (w/o) and (o/w) (Langevin, 1988).

The applications of microemulsions include catalysis and detergency. They are also of interest in tertiary oil recovery. In the primary and secondary oil recovery processes, oil is obtained from a reservoir under its own pressure and by pumping, followed by water flooding. In tertiary oil recovery as much as possible of the remaining oil is obtained by processes such as surfactant flooding. Aqueous solutions of surfactants and cosurfactants are injected and the low viscosities and interfacial tensions of the microemulsions formed aid the removal of the oil from the rock.

Microemulsion phases are often part of two-phase or three-phase liquid systems with most of the surfactant contained in the microemulsion phase. The three possible types of system are labelled in the Winsor nomenclature as shown in Figure 1.16. Winsor I (WI) systems are two-liquid-phase states with the microemulsion (o/w) in equilibrium with an upper organic phase. Winsor II (WII) systems are again two-phase states, but with the microemulsion (w/o) in equilibrium with a lower aqueous phase and Winsor III

(WIII) systems are formed from three phases, in which the middle bicontinuous microemulsion phase is in equilibrium with both an organic and an aqueous phase. Transitions from one Winsor state to another, e.g. WI-WIII-WII, can be observed in the case of a nonionic surfactant by increasing the temperature and in the case of an ionic surfactant by increasing the salinity or by modifying the surfactant-cosurfactant concentration ratio.

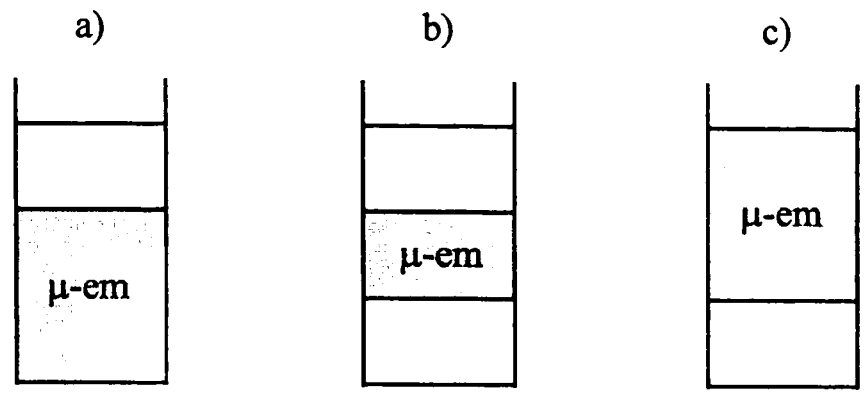

Figure 1.16: Winsor systems. a) WI, b) WIII, c) WII. The shaded phase is the microemulsion phase, denoted μ-em.

Microemulsions formed from nonionic surfactants probably exhibit the simplest type of phase behaviour for these systems. Three components, oil, water and surfactant, are required and differences in behaviour can be brought about by changing the temperature. The phase behaviour of microemulsions has been described in detail (Kahlweit and Strey, 1985; Kahlweit *et al.*, 1990), and is effectively built up from those of the constituent binary mixtures. The oil + water binary diagram has a lower miscibility gap with an upper critical endpoint which is well above the boiling points of oil and water, so the oil and water are almost completely immiscible at all temperatures considered. The oil + nonionic surfactant diagrams show lower miscibility gaps with critical points close to the melting point of the mixture. For water + nonionic surfactant mixtures a lower miscibility gap occurs below the melting point. Above the melting point, water and nonionic surfactants are miscible in all proportions but at higher temperatures a closed loop appears, with the upper critical endpoint generally above the boiling point of the mixture.

The phase behaviour of a ternary oil + water + nonionic surfactant mixture can be represented at constant pressure by an upright triangular prism, where the vertices represent each pure component and the vertical axis the temperature. A series of isothermal triangular slices can be used to display the phase behaviour in two dimensions. These types of phase diagram representations are discussed in Chapter 6. The exact locations of the binary critical points, in terms of temperature and

composition, change on going into the three-phase prism by adding the third component, but the behaviour of the ternary system can be determined by considering the miscibility gaps of the constituent binary mixtures. In oil + water + nonionic surfactant systems exhibiting the phase behaviour described, single-phase and two-phase regions exist in the phase prism at certain temperatures, but also a three-phase region evolves, as shown in Figure 1.17. This three-phase region is represented by a triangle, the vertices of which give the compositions of the coexisting phases. The three phase triangle first appears at a lower critical point T_l and on increasing temperature disappears at an upper critical point T_u. At T_l the aqueous surfactant phase of the two-phase ternary system separates into a water-rich phase and a surfactant-rich phase. At T_u, the surfactant-rich phase and the oil-rich phase of the three-phase system merge. These critical points occur at certain temperatures and compositions, which may be hard to identify, and the phase behaviour is fairly complex. Microemulsion systems may also exhibit tricritical points, at which a homogeneous mixture separates into three phases, if the appropriate temperature and pressure are chosen (Kahlweit, 1988).

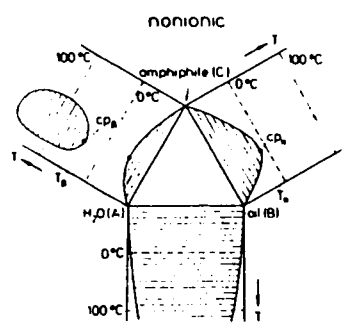

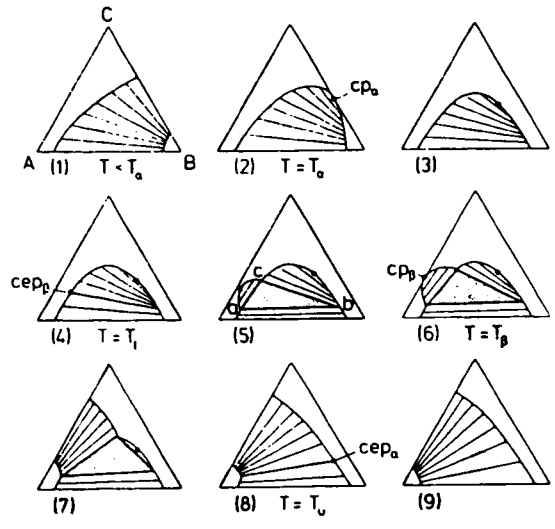

Figure 1.17: Schematic diagram of the evolution of the three-phase triangle with rising temperature in a mixture of oil + water + nonionic amphiphile. (Reproduced from Kahlweit *et al.*, 1990.)

Investigations have been carried out on various ternary, quaternary and quinary microemulsion systems formed from nonionic or ionic surfactants using a variety of techniques. The optical methods used to probe both bulk and surface properties have been discussed by Langevin (1996). The quinary systems studied are generally oil +

water + ionic surfactant systems, which require a cosurfactant such as a short-chain alcohol and the phase behaviour is studied by adding a salt (Langevin, 1987; Bellocq *et al.*, 1980). Phase behaviour and critical behaviour in these types of system have been investigated by optical and rheological techniques (Pouchelon *et al.*, 1980a, 1980b; Cazabat *et al.*, 1982a, 1982b, 1982c; Guest and Langevin, 1986). Systems with the ionic surfactant sodium di(2-ethylhexyl) sulphosuccinate, AOT, have also been extensively investigated as, unusually, no cosurfactant is required. Ternary oil + water + nonionic surfactant systems are generally simpler. The nonionic surfactant is often an alkylpolyglycol ether, $CH_3(CH_2)_a$-$(OCH_2CH_2)_b$-OH, or C_iE_j where i is the number of carbon atoms in the alkyl chain and j the number of -OCH_2CH_2- oxyethylene units. One of the simpler members of this series is 2-butoxyethanol, C_4E_1, which has been used in binary mixtures with water and heavy water in this thesis and is discussed in section 1.5.5. The study of hydrocarbon + water + short-chain C_iE_j systems can lead to an understanding of the phase behaviour of the more complicated systems encountered with typical detergents (Kahlweit, 1982). The phase diagrams for several systems of this type have been determined (e.g. Kahlweit, 1982; Kahlweit *et al.*, 1983; Kilpatrick *et al.*, 1986; Bonkhoff *et al.*, 1991). Measurements of properties such as the density, refractive index, viscosity and interfacial tension have been made of the coexisting phases in the three-phase system over a range of temperatures between the two critical points (Bonkhoff *et al.*, 1991).

Surfactants tend to adsorb at the liquid-air interface thus lowering the surface tension. In the following section the wetting of interfaces by surfactant-rich phases is considered.

1.4.2 Wetting at the liquid-vapour interface by surfactants

Binary water + C_iE_j mixtures generally exhibit closed loops and the lower and upper critical temperatures of the closed loop vary with the amphiphile chain lengths. With medium-chain and long-chain amphiphiles in phase-separated binary mixtures the upper amphiphile-rich phase, studied by adding a small drop to the water-rich phase, does not completely wet, i.e. spread across, the water-air interface (Kahlweit and Busse, 1989). This finding was unexpected as surfactants form monolayers at the air-water interface and this should facilitate the spreading of the amphiphile-rich phase. Studies of the surface of concentrated aqueous surfactant solutions by ellipsometry show that a water-enriched layer exists just below the monolayer of surfactant (Hirtz *et al.*, 1993). It has been conjectured that the surfactant-depleted layer is induced by the orientation of the surfactant molecules in the monolayer, which provide a strongly hydrophilic inner side thus favouring the accumulation of water. Another factor may also be the repulsion between micelles and the monolayer, due to the hydration layer of the micelles (Hirtz *et*

al., 1993). Neutron reflectivity studies also provide evidence for a layer of water below the surfactant monolayer (Lu *et al.*, 1993d).

Although the behaviour of binary surfactant mixtures is rich and varied, that of multicomponent surfactant mixtures is richer and even more varied. Confirmation of this, for example, lies in the formation of microemulsions, as discussed above. It is to these multicomponent mixtures that we now turn.

Computer simulation studies at the water-oil interface in oil + water + surfactant systems have shown that a monolayer of surfactant molecules is formed at the interface, with the hydrophilic head groups in the water, and that spontaneous micellisation takes place in the bulk aqueous phase (Smit *et al.*, 1990, 1991). In the water phase a surfactant depletion layer, i.e. a layer of water containing almost no surfactant, was indicated next to the monolayer.

In most experimental studies, mixtures formed from an alkane + water + a C_iE_j surfactant have been considered in the three-phase region. The middle microemulsion phase may wet or not wet the interface between the upper alkane-rich and the lower water-rich phases (Aratono and Kahlweit, 1991). The nonwetting behaviour is similar to that in two-phase binary water + surfactant mixtures, discussed above, in which the surfactant-rich phase does not wet the water-air interface. In microemulsion mixtures the wetting behaviour depends on the alkane chain length, the chain lengths of the hydrophilic and hydrophobic parts of the surfactant molecule and the temperature, which in turn affect the relative interfacial tensions of the three phases (Chen *et al.*, 1990). For systems in which nonwetting, or partial wetting, of the oil-water interface occurs at a temperature intermediate between the upper and lower critical points T_u and T_l, wetting transitions to complete wetting, as in a binary liquid mixture, are expected as T_u or T_l is approached.

In some systems, the middle microemulsion phase has been observed to completely wet the oil-water interface over the complete range of temperatures between T_l and T_u. Examples of these systems are octane + water + C_4E_1 and other *n*-alkane + water + C_4E_j mixtures investigated by Chen *et al.* (1990). Systems in which a wetting transition from partial to complete wetting has been observed on increasing the temperature towards T_u include tetradecane, hexadecane or octadecane + water + C_6E_2, in which the wetting transition occurred 4-15°C below T_u and was closest to T_u for the shortest alkane-chain-length system (Chen *et al.*, 1990). Some controversy exists over whether wetting transitions have been observed in different systems, particularly close to T_l, and seems to stem from the possible existence of impurities in some work and the different measurement techniques, which include contact-angle measurement from photographs and enhanced video microscopy. The wetting transitions observed close to T_u have been of first order (Chen *et al.*, 1990; Robert and Shukla, 1992).

Chen *et al.* (1994) have observed a different type of wetting transition in tetradecane + water + C_6E_2 on approaching T_l. Instead of a transition from partial to complete wetting of the oil-water interface by the microemulsion phase as observed close to T_u, the lower aqueous phase formed 'suspended beads' at the microemulsion-oil interface and then formed an intruding layer, i.e. completely wet this interface, on decreasing the temperature.

The investigations described above have focused mainly on nonionic surfactants of the polyoxyethylene type, C_iE_j. A simple member of this series, 2-butoxyethanol C_4E_1, and the binary mixture water + C_4E_1 will be discussed in section 1.5.5. Other amphiphiles may possibly act as surfactants in terms of their surface behaviour and aggregation in bulk solution. An example is perfluoroalkylalkanes in alkanes or perfluoroalkanes and these mixtures are considered in section 1.5.2 and have formed a part of our neutron reflectivity studies in Chapter 5.

The previous sections have described the behaviour of mixtures in general. We now consider the particular properties of the mixtures that have been studied using various techniques.

1.5 Mixtures of interest in this work

The binary and ternary mixtures we have studied exhibit partial miscibility within an accessible temperature range. Many of the mixtures investigated fall under the class of perfluoroalkanes + alkanes and these mixtures are considered first in some detail. This discussion is then extended to include binary and ternary mixtures of perfluoroalkylalkanes with alkanes and perfluoroalkanes. Perfluoroalkanes with siloxanes show upper critical endpoints in a similar way to perfluoroalkanes with alkanes. In particular, hexamethyldisiloxane shows strikingly similar behaviour to hexane and the mixtures of each of these with perfluorohexane are compared. Mixtures of alkanenitriles with alkanes are a very different class of mixture from perfluoroalkanes with alkanes, in that the nitrile group introduces a dipole into the molecule, and these mixtures are briefly discussed. Finally, 2-butoxyethanol + water or heavy water mixtures are considered, in particular in the vicinity of the lower critical endpoint of the closed loop and in relation to the effects of the hydrogen-bonding on the bulk structure.

1.5.1 Perfluoroalkanes + alkanes

Perfluoroalkane + alkane mixtures have been extensively studied because, although both perfluoroalkanes and alkanes are nonpolar, their mixtures display large positive deviations from ideality, including characteristic partial miscibility, that is much more reminiscent of mixtures containing highly polar substances. The differences between the two types of molecules which lead to this behaviour are discussed below.

The electrical properties of alkanes and perfluoroalkanes are the cause of many of their distinguishing properties. Fluorine has many more electrons and is more electronegative than hydrogen thus the C-F bond dipole is greater than the C-H dipole; as a further contrast, the carbon in a C-H bond has a slight negative charge whereas in a C-F bond it has a rather larger positive charge. Despite the charge separation, the high molecular symmetry denies either alkanes or perfluoroalkanes a net permanent dipole or quadrupole. However, the octupole moment of perfluoromethane, and presumably of higher homologues, is nonzero and appears to contribute to the thermodynamics in a significant fashion (Parsonage and Scott, 1962; Benavides, 1996).

The intermolecular energies of perfluoroalkanes differ from those of alkanes. In particular, the former are the more peripheral or non-central and hence are much better represented by a non-central Kihara potential energy function than by a central Lennard-Jones potential. Strangely, given the much greater number of electrons in perfluoro-alkanes it appears for simple molecules such as CH_4 and CF_4 that the actual depth of the potential energy functions is similar; this contradicts the commonly expressed view that the intermolecular forces in perfluoroalkanes are weaker than those in corresponding alkanes. In reality, as emphasised by Hildebrand, Prausnitz and Scott (1970), it is the *density* of cohesion that is smaller in perfluoroalkanes, not the *depth* of the interaction well.

Several pieces of evidence confirm that the chain flexibility of *n*-alkanes is generally greater than that of perfluoro-*n*-alkanes. This arises largely from the steric hindrance occasioned by the greater size of fluorine atoms compared to hydrogen atoms and the effect is heightened by the increased repulsion arising from the partial negative charges on neighbouring fluorine atoms. The energy barrier for $-CF_3$ internal rotation in perfluoroethane is greater than that for $-CH_3$ in ethane, again due to the relatively large size of the fluorine atoms and the greater polarity of the C-F bond (Bates and Stockmayer, 1968).

The bulk properties of several perfluoroalkanes have been comprehensively studied: for example, tetrafluoromethane (Lobo and Staveley, 1981) perfluorobutane (Simons and Mausteller, 1952), perfluoropentane (Simons and Dunlap, 1950) and perfluorohexane (Dunlap *et al.*, 1958). These and other studies confirm that alkanes and perfluoroalkanes of the same chain length possess significantly different physical

properties. Thus perfluoroalkanes generally have higher melting points and are more volatile, they are more dense, have lower refractive indices and are less polarisable than alkanes. The surface tensions of perfluoroalkanes are markedly lower than those of the *n*-alkanes, and indeed, are among the lowest observed for substances of moderate complexity. These observations are all consistent with lower cohesive energy density. Strikingly, however, the enthalpies of vaporisation are similar (Majer and Svoboda, 1985).

1.5.1.1 Perfluoroalkane + alkane cohesion

Alkane + perfluoroalkane binary mixtures characteristically display partial miscibility with an upper critical endpoint UCEP at an upper critical solution temperature T_{UCS}. When this was first observed, attempts were made to account for it using the Regular Solution theory (Scott, 1948; Hildebrand and Scott, 1950). Despite the advent of more modern theories of liquid mixtures, this treatment is still useful and the solvent properties of liquids are still most simply and hence perhaps best described within it by the solubility parameter δ, see section 1.5.4, whose value reflects the density of cohesive energy. This theory attributes the major cause of nonideality to the square of the difference in the δ of the components $(\delta_2 - \delta_1)^2$. Since solids tend have high δ and gases low δ, this implies that liquids with relatively high δ, such as polar liquids, are in general good solvents for solids and those with low δ, such as perfluorocarbons, are good solvents for gases. Mixtures of liquids of sufficiently greatly differing δ thus exhibit partial miscibility at relatively low temperatures and mix completely only above a critical solution point. The large difference, 33 $J^{0.5}\cdot cm^{-1.5}$, between δ(water) = 48 $J^{0.5}\cdot cm^{-1.5}$ and δ(hexane) = 15 $J^{0.5}\cdot cm^{-1.5}$ therefore quantifies the mutual insolubility of these liquids; the UCEPs for such mixtures thus occur at very high temperatures. In the homologous *n*-alkanes the solubility parameter increases with chain length but insufficiently at a given temperature to disturb this argument; the same is true for perfluoroalkanes.

The difference between the solubility parameters of alkanes, e.g. δ(hexane) = 15 $J^{0.5}\cdot cm^{-1.5}$, and of perfluoroalkanes, e.g. δ(perfluorohexane) = 12 $J^{0.5}\cdot cm^{-1.5}$, is about 3 $J^{0.5}\cdot cm^{-1.5}$, much smaller than that between alkanes and water. Within the Regular Solution framework in the original Scott and Hildebrand formulation this difference in δ is insufficient to account for the widespread partial miscibility at ambient temperatures of many alkane + perfluoroalkane mixtures. More recent developments have led to an understanding of the nature of this only apparent deficiency in the primitive theory.

1.5.1.2 Experimental studies of perfluoroalkane + alkane partial miscibility

Many hydrocarbon + perfluorocarbon mixtures have been studied in detail. In particular, the upper critical solution temperatures and parts of the liquid-liquid coexistence curves have been reported for many mixtures (for example, Munson, 1964; Hurle *et al.*, 1977; Hicks *et al.*, 1978; Waterson *et al.*, 1980; McLure and Mokhtari, 1982; Gross *et al.*, 1993; Archer *et al.*, 1996). For fewer mixtures the liquid-vapour equilibria have also been reported; for example, *n*-hexane + perfluoro-*n*-hexane (Bedford and Dunlap, 1958; Dunlap *et al.*, 1959) and methylcyclohexane + perfluoromethylcyclohexane (Dyke *et al.*, 1959; Heady and Cahn, 1973). The liquid-vapour properties of some simple alkane + perfluoroalkane mixtures such as CH_4 + CF_4 have also been studied (Gilmour *et al.*, 1967 and previous papers; Simon and Knobler, 1971; Simon *et al.*, 1972).

From these studies it appears that alkane + perfluoroalkane binary mixtures show large positive deviations from ideality and partial miscibility below an upper critical solution temperature T_{UCS}. The only apparent exception is ethane + perfluoroethane in which the immiscibility is masked due to the high melting temperature of perfluoroethane. The liquid-liquid temperature-composition phase diagrams are characteristically much more symmetrical when plotted *versus* volume fraction ϕ rather than mole fraction x (Hildebrand *et al.*, 1950). The critical volume fraction ϕ_c is close to 0.5 for most mixtures and the diameter of the curve is almost parallel with the temperature axis. This symmetry in most mixtures has also been demonstrated by plotting the coexistence curves in terms of the reduced temperature, i.e. T/T_{UCS} (Munson, 1964). The shapes of different alkane + perfluoroalkane coexistence curves superimpose almost exactly.

The differences in T_{UCS} with chain-length for mixtures of perfluoroalkanes with linear alkanes and the effect of branched chains or cyclic and aromatic hydrocarbons have been determined for many mixtures. In general, T_{UCS} increases with chain length of either perfluoroalkane or alkane. The effect of chain branching in the alkane is to lower T_{UCS} (Hickman, 1955). For a given fluorocarbon a cyclic or aromatic hydrocarbon gives rise to a higher T_{UCS} than with a linear alkane with the same number of carbon atoms. Conversely, cyclisation of the perfluoroalkane with a given alkane reduces T_{UCS} (Fernández and McLure, 1996). An extensive account of hydrocarbon + perfluorocarbon mixtures has been given in a recent review article by Lo Nostro (1995).

Not only was the Regular Solution theory originally believed inadequate to explain alkane + perfluoroalkane immiscibility, but a further and continuing theoretical problem is the somewhat unexpected large nonideal behaviour between two essentially nonpolar species such as alkanes and perfluoroalkanes (Lo Nostro, 1995). Currently there are two contending explanations for the immiscibility of alkane + perfluoroalkane mixtures.

One explanation offered for this behaviour is the difference in chain conformations. In alkanes the chain is considered to form a 'zig-zag' with carbon-carbon bonds in a trans-trans arrangement with a cross-section of approximately 18.5 $Å^2$ per molecule, whereas in perfluoroalkanes a helix structure with a cross-sectional area of 28.3 $Å^2$ per molecule is formed due to the greater size of fluorine causing steric constraints (Lo Nostro *et al.*, 1995). This difference is expected to make mixing in the liquids difficult resulting in partial miscibility.

The explanation described by Lo Nostro *et al.*, though cogent, is inapplicable to the simplest mixture CH_4 + CF_4 and to mixtures of larger cyclic molecules such as methylcyclohexane + perfluoromethylcyclohexane since here the issue of chain flexibility does not arise. The flexibility argument, although important in explaining some aspects of alkane + perfluoroalkane behaviour is greatly overshadowed in mixture thermodynamics, partly by the size difference, but overwhelmingly by the apparent 10% weakness of the interaction energy ε_{FH} of the unlike alkane-perfluoroalkane molecular pair relative to the prediction of the Berthelot rule. This rule states that ε_{FH} is the geometric mean of the characteristic energies of the like alkane-alkane and perfluoro-alkane-perfluoroalkane molecular pairs, i.e. $\varepsilon_{FH} = (\varepsilon_{FF}\varepsilon_{HH})^{0.5}$. In reality, the Berthelot rule is not exact and departures from it are usually corrected using a factor ξ, i.e. $\varepsilon_{FH} = \xi(\varepsilon_{FF}\varepsilon_{HH})^{0.5}$. For alkane + perfluoroalkane mixtures the weakness is described by $\xi = 0.9$ approximately. The origin of this value is essentially unexplained, but since it can be invoked directly in all theories of mixtures to predict mutual insolubility there is no doubt about its existence (Rowlinson and Swinton, 1982).

The apportioning of the two approaches in a complete account of the immiscibility of alkane + perfluoroalkane mixtures remains rather uncertain but, on balance, the energy-based explanation appears more comprehensive.

The wetting behaviour of alkanes and perfluoroalkanes is also different, as discussed in section 1.3. Although the perfluoroalkane-rich phase of a two-phase mixture formed from an alkane + a perfluoroalkane is generally the more dense phase, at temperatures below T_{UCS} a perfluoroalkane-rich wetting phase exists at the liquid-vapour interface. At temperatures below T_{UCS} wetting can also occur at the solid wall of the container. For example, in a mixture of heptane + perfluorohexane, the heptane-rich phase wets the quartz-liquid interface.

The macroscopic viscosity of a perfluoroalkane + alkane mixture has been studied and is described in Chapter 2. Adsorption and wetting in perfluoroalkane + alkane mixtures have been investigated by evanescent-wave-generated fluorescence spectroscopy at the quartz-liquid interface and by neutron reflectivity at the liquid-vapour interface and are discussed in Chapters 4 and 5. Ternary mixtures involving perfluorocarbons and hydrocarbons are considered in Chapter 6.

1.5.2 Perfluoroalkylalkanes + perfluoroalkanes and alkanes

Perfluoroalkylalkanes PFAAs, also termed semifluorinated *n*-alkanes, are composed of an *n*-alkyl chain covalently bonded to a perfluorinated *n*-alkyl chain. They are abbreviated F_nH_m where n is the number of fluorinated carbons and m is the number of hydrogenated carbons in the chain. PFAAs thus possess a hydrogenated part and a perfluorinated part.

A full account of the present state of knowledge of PFAAs has been given by Lo Nostro (1995). As a preface to a description of the PFAA series, it is useful to note that PFAA molecules, although formed from two essentially nondipolar constituents, are likely to be significantly polar, at least in the vicinity of the junction between the differently substituted chains. In this sense it is interesting to compare with the more common kind of dipolarity which is usually located near the periphery of the molecule and if several polar groups are present the net dipole moment can sometimes be calculated by straightforward vector addition. PFAA molecules with an increasingly deeply buried dipole may be regarded safely as nonpolar at high chain lengths of *both* sections of the molecules but must be regarded as polar in substances of short chain length in either one section or both.

1.5.2.1 Synthesis of perfluoroalkylalkanes

PFAAs can be synthesised by free-radical-initiated addition of a perfluoroalkyl iodide to a terminal alkene. Experimental details of this process are given in detail by Rabolt *et al.* (1984). The process described is carried out in two steps. First the perfluoroalkyl iodide is added to the alkene; the reaction is catalysed by an initiator such as Bu_3SnH or AIBN. The iodide formed is isolated and then reduced to form the semifluorinated alkane by the action of Bu_3SnH or Zn/HCl. The synthesis has also been carried out in one step from the starting materials using Bu_3SnH under nitrogen at room temperature in ethanenitrile solvent (Bowers, 1995).

1.5.2.2 Solid state structure of perfluoroalkylalkanes

Most early work on PFAAs has been carried out in the solid state and that work is still continuing. The melting point and crystal structures have been the focus of attention and solid-solid phase transitions have been observed as different crystal structures form. The melting points and melting entropies of F_nH_m have been found to vary only slightly with the length of the hydrocarbon chain, but to be more sensitive to changes in the length of the fluorocarbon chain (Höpken and Möller, 1992; Rabolt *et al.*, 1984). In contrast, at the solid-solid transition the temperature and entropy of transition increase strongly with the length of the hydrocarbon chain. This suggests that disordering of the perfluorinated part of the chain occurs at the melting transition, but disordering of the hydrogenated segment occurs at the solid-solid transition. Various structures have been proposed for

the packing in the solid phases (Höpken and Möller, 1992). Melting points have been determined for a series of semifluorinated *n*-alkanes (Rabolt *et al.*, 1984). The melting point of F_8H_8 = 27.0°C. This is slightly higher than the melting point of 18°C for hexadecane with the same total number of carbon atoms, but much lower than the melting point of perfluorohexadecane of approximately 127°C. The data plotted of melting point *versus* number of carbon atoms for F_nH_m fall onto three curves, i) F_nH_m with n = m, ii) $F_{12}H_m$ with m < 12, iii) $F_{12}H_m$ with m > 12. For this last series the curve is parallel to that for the *n*-alkanes. Rabolt *et al.* state that these curves suggest the existence of at least three different modes of molecular packing in the crystal lattice. They have identified a solid-solid phase transition in addition to a crystalline melting point. Triblock semifluorinated alkanes such as $F_{12}H_{10}F_{12}$ have also been investigated and the phase transitions in the solid state studied at low temperatures (Song *et al.*, 1990).

1.5.2.3 Binary mixtures of perfluoroalkylalkanes in perfluoroalkanes or alkanes

Although PFAAs are generally soluble in hydrocarbon solvents, some of these solutions have been found to form a 'gel' phase on cooling to room temperature. This behaviour has been observed for solutions of $F_{10}H_{12}$ in alkanes with even numbers of carbons in the chain C_8-C_{16} (Twieg *et al.*, 1985). Due to their amphiphilic nature PFAAs are also soluble in fluorocarbons. Gel phases have been observed for F_8H_{16} and $F_{12}H_{16}$ in perfluorooctane or isooctane on cooling a warm solution down to room temperature (Lo Nostro and Chen, 1993). In the gel the solvent is entrapped in cavities in the extensive structure of long intersecting copolymer fibres. Solubility measurements have been reported for F_8H_{16} in various hydrocarbon and fluorocarbon solvents (Binks *et al.*, 1996).

We consider first the bulk structure of PFAA solutions. The presence of micelles has been reported in PFAA + perfluoroalkane solutions, with the hydrocarbon segment of the PFAA forming the core of the micelle. This is a novel type of phase behaviour for uncharged low molecular weight molecules and was first discovered for F_8H_{12} in perfluorotributylamine and F_8H_{16} in perfluorooctane by Turberg and Brady (1988) who claim that this demonstrates that PFAAs may be regarded as a new class of simple uncharged nonpolar surfactants. This claim, as explained above, must be modified for small PFAA molecules or for PFAAs in which the chain junction is close to one end of the molecule. The formation of micelle-like aggregates is suppressed in alkane solvents relative to conventional aqueous surfactant mixtures as the fluorocarbon segments of the PFAA required to form the core are more rigid due to the large size of fluorine atoms in the molecule and thus the micelle structure is likely to be less favourable (Binks *et al.*, 1995).

Turning now to the surface activity of PFAAs we seek indications of the likely behaviour of PFAAs in alkane, perfluoroalkanes, and their mixtures. It is important first to note that since in general the surface tensions of perfluoroalkanes are smaller than those of alkanes of similar chain length it is unsurprising that in alkane + perfluoroalkane mixtures the latter is usually positively adsorbed. Due to the lower cohesive energy of perfluoroalkanes compared to alkanes this can be regarded as the outcome of achieving lower surface energy. A resonance of this behaviour emerges from the results of molecular dynamics simulations of the surface behaviour of short PFAA diblock chains (Hariharan and Harris, 1994). The simulations were carried out for pure PFAAs modelled as block copolymers of fluorocarbons and hydrocarbons and the results showed that the fluorinated parts are oriented towards the surface, i.e. lowering the surface energy, as would be predicted from the alkane and perfluoroalkane surface tensions.

We now extend the analysis to include systems containing PFAAs. The surface tensions σ of alkanes, PFAAs and perfluoroalkanes might generally be expected to decrease in the order σ(alkane) > σ(PFAA) > σ(perfluoroalkane), with exceptions likely only when comparing substances of greatly disparate chain length which might locally invert the order just quoted, for example a long chain perfluoroalkane compared with a short chain PFAA containing few CH_2 segments. In the general case one would expect surfactancy in PFAA solutions in alkanes but *not* in PFAA solutions in perfluoroalkanes.

Surface tension measurements on various PFAAs in alkanes offer a partial confirmation at the alkane-air interface (Binks *et al.*, 1995). The adsorption of a PFAA at this interface was established and found to be favoured by i) long fluorocarbon segments of the PFAA, ii) long chain lengths of the alkane solvent and iii) low temperatures.

Solutions in perfluoroalkanes are likely to be more complex at first sight. Although ordinarily from the consideration of the surface tensions of pure substances given above PFAA adsorption on perfluoroalkanes would seem unlikely, a mechanism for its occurrence can readily be developed provided that the emphasis on *monolayer* formation is tempered. There are two competing effects, both caused by the need to achieve minimum interfacial energy. One effect is the tendency for a perfluoroalkyl section to be oriented towards the perfluoroalkane-rich solvent and the other is the tendency for a perfluoroalkyl section to be oriented towards the outermost layer at the liquid-air interface. The simplest resolution of these effects is the presence of a PFAA bilayer with an interpenetrating layer of hydrocarbon tails.

The surface activity of PFAAs has been studied at the air-water interface by Gaines (1991). Stable monolayers were formed after spreading a PFAA solution in hexane on the surface. X-ray reflectivity measurements on an $F_{12}H_{18}$ monolayer at the air-water

interface were consistent with a model with the fluorocarbon part oriented up at the surface and the hydrogenated end down (Huang *et al.*, 1995, 1996).

1.5.2.4 Ternary mixtures of perfluoroalkylalkanes in perfluoroalkanes + alkanes

Due to the amphiphilic nature of PFAAs they may be expected to increase the mutual solubility of alkanes and perfluoroalkanes thus acting as surfactants. Lo Nostro *et al.* (1995) have reported the first observation of mixing between perfluorooctane and isooctane on adding F_8H_{16}. The addition of F_8H_{16} to perfluorooctane and isooctane lowered T_{UCS} and thus increased the mutual solubility between the alkane and the perfluoroalkane. For large amounts of PFAA the mixture did not form two liquid phases on cooling, but formed a white gel below the liquid-gel transition temperature T_g. As the temperature was decreased approaching T_g some of the PFAA molecules aggregated to form a basic micelle unit. The structure proposed is with the alkane chains interdigitated, but with the perfluorinated blocks packed side-by-side. It is expected that in the mixed alkane + perfluoroalkane solvent the alkane chains of the PFAA molecules will form the inside of the aggregate structure due to the size and rigidity of the perfluorinated segment causing the reverse structure to be unfavourable. As the gel formed below T_g the micelle structure of packed chains grew to form lamellar layers. The lowering of T_{UCS} in alkane + perfluoroalkane mixtures on addition of a PFAA indicates that they may act as emulsifiers and the existence of a new nonpolar class of microemulsions is postulated (Lo Nostro, 1995). Fluorocarbons are known to be able to solubilise large amounts of gases–oxygen in particular–and PFAA microemulsions may have a possible future use as blood substitutes (Lo Nostro and Chen, 1993).

The surface of alkane + perfluoroalkane + PFAA mixtures may show some ordering of PFAA molecules. The ratio of the chain lengths of the hydrogenated and fluorinated parts of the PFAA affects the surface structure and the structure of any aggregates in solutions of alkanes and perfluoroalkanes due to the different surface tensions and solubilities of the two ends of the molecule. The liquid-liquid interface in an alkane + perfluoroalkane + PFAA mixture is also of interest.

A comparison can be made between (alkane + perfluoroalkane + PFAA) and (oil + water + surfactant) mixtures known to show microemulsion phase behaviour. The perfluoroalkane is the analogue of the water and the PFAA forms the equivalent of the surfactant. The differences between the two types of system are that the latter involves hydrogen-bonding and that the nature of the intermolecular forces between the different species are more different than in the PFAA system. This difference is apparent from the lower T_{UCS} for alkane + perfluoroalkane mixtures compared with oil + water mixtures. The (alkane + perfluoroalkane + PFAA) mixtures are easier to model than the conventional microemulsion mixtures as only two types of species are present, CH_2 and

CF_2 groups, and the interactions of each end of the PFAA with the alkane or the perfluoroalkane can be simply described as the species are nonpolar.

In addition to PFAAs other partially fluorinated surfactant molecules have been studied. Infrared reflectance spectroscopy has been used to study the structure of the air-water interface for a semifluorinated alcohol, $CF_3(CF_2)_9(CH_2)_2OH$, spread on water from *n*-hexane solution and to study water-soluble polymers of poly(ethylene oxide), PEO, endcapped with perfluoroalkane chains linked to the PEO chain by a CO group (Ren *et al.*, 1995). In these molecules, invoking the logic employed in the discussion of PFAAs at the liquid-air interface, the fluorinated endgroups are expected to accumulate preferentially at the air-water interface. The hydrophobic fluorinated part of the molecules was indeed found to be highly ordered and aligned with the long axis normal to the water surface; unexpectedly some ordering was also found in the attached PEO part of the polymer. Results for the endcapped PEOs were consistent with the formation of a monolayer at the interface.

Perfluoropolyether (PFPE) surfactants have been studied at the perfluoro-polyether-water interface (Chittofrati *et al.*, 1989a). Microemulsions were formed from a perfluoropolyether surfactant (ammonium salt of PFPE carboxylate) + water + oil (a perfluoropolyether). The phase behaviour of these ternary mixtures and the pseudoternary systems formed by adding a short chain alcohol such as isopropylalcohol or a fluorinated alcohol as a cosurfactant has been determined (Chittofrati *et al.*, 1989b).

Nonionic microemulsion formation has also been observed in the ternary mixture water + fluorocarbon + perfluoroalkylpoly(oxyethylene) surfactant, $C_mF_{2m+1}(CH_2)_p$-$(OC_2H_4)_nOH$ (Mathis *et al.*, 1984). This type of mixture may have applications as a blood substitute.

The surface activity of perfluoroalkanes in alkane and deuterated alkane solutions has been investigated by neutron reflectivity and is discussed in Chapter 5.

1.5.3 Perfluoroalkanes + hexamethyldisiloxane or hexane

Hexamethyldisiloxane $(CH_3)_3Si\text{-}O\text{-}Si(CH_3)_3$ is a member of the series of linear dimethylsiloxanes of general formula $(CH_3)_3Si\text{-}[O\text{-}Si(CH_3)_2]_{n-1}\text{-}(CH_3)$. Tetramethyl-silane TMS is formally the first member of the series. The higher members are often denoted M_2, M_2D, M_2D_2, M_2D_x, where M = $(CH_3)_3Si\text{-}O_{1/2}$ and D = $O_{1/2}\text{-}Si(CH_3)_2\text{-}O_{1/2}$. The number of Si atoms in the molecule n is given by $n = (x + 2)$ and thus hexamethyldisiloxane M_2 is called the siloxane dimer. We are concerned with linear dimethylsiloxanes and hexamethyldisiloxane in particular but other branched and cyclic siloxanes are available and the longer chain liquids can possess very high viscosities.

Hexamethyldisiloxane is very similar to hexane in many respects, both in pure component properties such as the critical temperature and in mixtures with, for example, perfluoroalkanes, despite the greater chain flexibility of hexamethyldisiloxane. The nonideality of dimethylsiloxane + perfluoroalkane mixtures arises, as in alkane + perfluoroalkane mixtures, from the weakness of the unlike interaction energies. This leads to partial miscibility in dimethylsiloxane + perfluoroalkane mixtures, and the upper critical solution temperatures T_{UCS} for mixtures with perfluorohexane increase with increasing siloxane chain length (McLure *et al.*, 1996).

Generally, linear dimethylsiloxanes and *n*-alkanes are completely miscible over a wide range of temperature and pressure, particularly if the components are of similar size. The gas-liquid critical properties of several pure dimethylsiloxanes have been determined and compared with those for the *n*-alkanes (McLure and Neville, 1977). The gas-liquid critical temperatures and pressures for dimethylsiloxane + alkane mixtures have been determined and the Berthelot rule correction factors ξ, in $\varepsilon_{12} = \xi(\varepsilon_{11}\varepsilon_{22})^{0.5}$ where ε_{11} and ε_{22} are the like interaction energies and ε_{12} the unlike interaction energy, have been found to be close to 1.0, for example $\xi = 0.993$ for hexamethyldisiloxane + hexane (Dickinson and McLure, 1974a). The vapour pressures, excess enthalpies and excess volumes of mixing for hexamethyldisiloxane + hexane have also been measured (Dickinson *et al.*, 1974; Dickinson and McLure, 1974b). The surface tensions of dimethylsiloxane + alkane mixtures also show only slight deviations from ideality (Edmonds and McLure, 1982).

As mentioned above, hexamethyldisiloxane can generally be considered as the dimethylsiloxane equivalent of hexane. For binary mixtures formed from perfluorohexane + hexamethyldisiloxane or hexane the T_{UCS} are 296.95 K and 295.8 K, respectively, a difference of just 1.15 K (McLure *et al.*, 1996), see Chapter 6 also. Both mixtures show fairly symmetrical coexistence curves, with the critical composition close to 0.5 and the diameter almost parallel with the temperature axis, when plotted in terms of the volume fraction, and the hexamethyldisiloxane + perfluorohexane mixture is also close to symmetrical in the mole fraction representation due to the similarity of the molar volumes of these two components.

Binary perfluorohexane + hexamethyldisiloxane mixtures have been studied by neutron reflectivity to investigate critical-point wetting and the surface structure of mixtures of the aneotropic composition at which a minimum in the surface tension critical isotherm occurs, as discussed in section 1.3.1.2. The phase behaviour of the ternary mixture hexane + hexamethyldisiloxane + perfluorohexane has been studied both experimentally and theoretically and the outcomes are discussed in Chapter 6.

1.5.4 Alkanenitriles + alkanes

Alkanenitriles are polar molecules, that is they have permanent dipole moments, due to the terminal -CN group. Here we consider aliphatic nitriles, where the first two members of the series are ethanenitrile or acetonitrile CH_3CN, and propanenitrile CH_3CH_2CN. The effective polarity of polar molecules is best expressed in terms of reduced multipole moments, i.e. in terms of reduced dipole moments $\mu^{*2} = \mu^2/\varepsilon\sigma^3$, reduced quadrupole moments $Q^{*2} = Q^2/\varepsilon\sigma^5$, and reduced octupole moments $\Omega^{*2} = \Omega^2/\varepsilon\sigma^7$, where ε is the depth of the energy well and σ is the collision diameter (Rowlinson and Swinton, 1982). Since ε and σ are often much more inaccessible than μ, Q and Ω, these reduced quantities, at least for quasi-spherical molecules, can be written explicitly using $\varepsilon \propto kT_c$ and $\sigma^3 \propto V_c$, where T_c and V_c are the critical temperature and critical molar volume, respectively, i.e. $(\mu^{*\prime})^2 = \mu^2/kT_cV_c$, and similarly for the quadrupole and octupole moments. At a given temperature, the polarity of molecules can be compared on the basis, at least for dipoles, by $(\mu^{*\prime\prime})^2 = \mu^2/V_c$ (McLure *et al.*, 1982).

Large positive deviations from ideality can be observed in alkane + alkanenitrile mixtures. This stems from an overall interaction energy in the mixture which is less negative than the mean of the like interactions (McLure, 1979). In alkanenitriles the like interactions are dipole-dipole and dipole-induced dipole and in alkanes + alkanenitriles the main unlike interactions are dipole-induced dipole. Generally, the polar alkanenitriles are only partially miscible with the nonpolar alkanes, forming upper critical endpoints UCEPs at upper critical solution temperatures T_{UCS}. The chain lengths of both the alkane and the alkanenitrile can be varied and a systematic change in T_{UCS} is observed. For a given *n*-alkane T_{UCS} decreases with increasing alkanenitrile chain length, and for a given alkanenitrile T_{UCS} increases with increasing alkane chain length (McLure *et al.*, 1982). Most alkanenitrile + *n*-alkane mixtures have large positive excess functions, such as excess volumes (McLure and Trejo Rodriguez, 1980; Eustaquio-Rincón and Trejo, 1994), and excess enthalpies (McLure and Trejo Rodriguez, 1982), particularly for mixtures with a small polar molecule and a large nonpolar molecule.

The behaviour of alkane + alkanenitrile mixtures is consistent with the decrease in the effective polarity of the nitrile with increasing chain length. This effect can also be demonstrated on considering the solubility parameters for alkanes and alkanenitriles. The solubility parameter δ, approximated by $[(\Delta H^{vap} - RT)/V]^{1/2}$ where ΔH^{vap} and V are the molar enthalpy of vaporisation and the molar volume, respectively, at a given temperature T, increases with increasing number of carbon atoms for the alkane series but decreases with increasing number of carbon atoms for the alkanenitriles (McLure, 1979). At long chain lengths the two series converge. The experimental trend for the alkanenitriles is correctly predicted from this as the mixtures tend towards smaller deviations from ideality with increasing alkanenitrile chain length. In general, the positive deviations from ideality decrease with increasing alkanenitrile chain length and with

decreasing alkane chain length and thus T_{UCS} and the excess volumes and enthalpies fall to lower values.

Other investigations on alkane + alkanenitrile mixtures include the determination of the pressure-temperature-composition gas-liquid critical lines (Trejo Rodriguez and McLure, 1983) and vapour-liquid equilibria (McLure *et al.*, 1994) for ethanenitrile or propanenitrile with a series of alkanes of increasing chain length.

Propanenitrile has been used to form a simple ternary mixture with hexane and decane and the phase diagrams which have been determined experimentally are shown in Chapter 6.

1.5.5 2-Butoxyethanol + water or heavy water

1.5.5.1 Phase behaviour

The binary liquid mixture 2-butoxyethanol + water shows closed loop behaviour with a lower critical endpoint LCEP characterised by a lower critical solution temperature T_{LCS} at about 49°C and an upper critical endpoint UCEP with an upper critical solution temperature T_{UCS} at about 130°C (Cox and Cretcher, 1926; Ellis, 1967). The phase diagram has been measured in several studies, particularly at the LCEP (see for example Pegg, 1982) and slight variations in values for T_{LCS} and the critical composition are reported due to differing purities of the materials. The critical composition for both the LCEP and UCEP corresponds to a mole fraction of 2-butoxyethanol x_{BXE} of about 0.06. The shape of the coexistence curve close to the LCEP has been carefully determined and analysed in terms of extended scaling equations (Pegg, 1982; Aizpiri *et al.*, 1992). The effect of increasing pressure is to shrink the closed loop (Schneider, 1963).

Mixtures exhibiting closed-loop behaviour are generally those formed from species in which both like and unlike hydrogen bonding can occur, for example 2-butoxyethanol + water. At low temperatures below T_{LCS} hydrogen bonding between both like and unlike species is widespread thus contributing to miscibility. As the temperature is raised past T_{LCS}, the extent of the weaker hydrogen bonding between the unlike species falls and the mixture phase separates into water-rich and 2-butoxyethanol-rich phases. As the temperature is increased further to T_{UCS} the molecules gain kinetic energy and the extent of the stronger hydrogen bonding between like species diminishes and the mixture again forms a single phase.

1.5.5.2 Properties

Many physical properties of the 2-butoxyethanol + water binary mixture have been studied. The shear viscosity in particular has received much attention in relation to the anomaly observed in binary liquid mixture viscosities close to a critical point. The viscosity has been measured in single-phase mixtures on the approach to both the lower and upper critical endpoints (Izumi *et al.*, 1981) and in the single phase and each of the two coexisting phases on approach to the LCEP (Pegg and McLure, 1984). The temperature dependence of the viscosity for a range of compositions including the critical composition has been determined from low temperatures up to the phase separation temperature of each mixture (Mallamace *et al.*, 1991).

Static and dynamic light scattering measurements have been used in addition to viscosity measurements to determine the correlation length of the critical fluctuations in 2-butoxyethanol + water mixtures (Fusenig and Woermann, 1993; Lombardo *et al.*, 1994; Schmitz *et al.*, 1995). The value of the critical amplitude of the correlation length ξ_0 has been determined from these and other studies to be 4.5±0.5 Å. This value of ξ_0 is relatively large compared with values for other binary mixtures of molecules of low molar mass which are usually less than 3 Å (Baaken *et al.*, 1990).

The composition and temperature dependence of the surface tension close to the LCEP in 2-butoxyethanol + water mixtures has been studied (Pegg, 1982; Knecht and Woermann, 1995). The surface tension, foam stability and heat capacity have also been measured by Elizalde *et al.* (1988).

The form of the anomaly in the specific heat capacity of 2-butoxyethanol + water mixtures of critical composition close to the LCEP has been determined as a function of temperature (Wurz *et al.*, 1992).

1.5.5.3 Intermolecular forces and their effect on the bulk structure

The intermolecular hydrogen bonding in 2-butoxyethanol + water mixtures in relation to the phase behaviour has been discussed above. Hydrogen bonding is very directional. A water molecule can form hydrogen bonds to two other water molecules by attraction of the two lone pairs of electrons on the oxygen atom to hydrogen atoms on different molecules. In this way a tetrahedral network of molecules is built up. In ice the structure is extensive, but does not have such a long range in liquid water. A 2-butoxyethanol molecule can form hydrogen bonds at the two oxygen atoms and at the hydroxyl hydrogen atom. An extensive structure is not so easily built up as in water due to the lack of symmetry of the molecule and the presence of the bulky alkyl chains.

In 2-butoxyethanol + water mixtures hydrogen bonding can occur between like and unlike species and for low concentrations of 2-butoxyethanol the hydrogen-bonding network of water is likely to remain largely intact with the 2-butoxyethanol molecules

being incorporated into the structure. For larger concentrations the water structure is more disrupted and microscopic aggregates have been observed in solutions with ratios of water:2-butoxyethanol molecules corresponding to the ratio of water:2-butoxyethanol in the two coexisting phases above T_{LCS}. The microscopic structure thus reflects the stable macroscopic compositions. The nature of these aggregates is discussed below.

The effect of aggregates in other systems such as aqueous alcohol mixtures can also give information about the structure of 2-butoxyethanol + water mixtures. In particular, mixtures that do not show any phase separation can be studied to investigate whether the observed aggregates in 2-butoxyethanol + water are due to the nature of the bonding leading to phase separation or whether they also apply to miscible hydrogen-bonding mixtures.

1.5.5.4 Aggregation in solution

The presence of local aggregates in 2-butoxyethanol + water mixtures has been inferred from measurements of the mutual diffusion coefficients obtained from Rayleigh scattering spectra (Ito *et al.*, 1981). Concentration fluctuations in single-phase solutions below T_{LCS} as a function of composition at various temperatures were found to exhibit a maximum at the same concentration as the critical concentration and to be greatest for temperatures close to T_{LCS} (Ito *et al.*, 1983). This effective mapping of the concentration fluctuations onto the shape of the coexistence curve around the LCEP suggests that the microscopic aggregate structures formed in different concentration regimes even 30°C below T_{LCS} correspond to the ratio of H_2O:2-butoxyethanol in the stable macroscopic phases formed close to the LCEP. For example, in the concentration regime close to the critical concentration, $x_{BXE} = 0.07$, bounded by the compositions of the coexisting phases above T_{LCS}, approximately $x_{BXE} = 0.02$ and $x_{BXE} = 0.2$, local structures of the clathrate hydrate-like type $g[(H_2O)_{50}BXE]$ and micelle-like type $h[(H_2O)_4BXE]$ are expected with the relative amounts of each structure changing as the concentration changes (Ito *et al.*, 1983). The values of g and h depend on the temperature and may range from ten to several hundred. At high concentrations of water the 2-butoxyethanol-modified water structure is described by a clathrate-hydrate model in which the 2-butoxyethanol molecules are incorporated into a water cage (D'Arrigo *et al.*, 1991a).

Small-angle neutron scattering studies (SANS) on 2-butoxyethanol + D_2O and other short-chain alcohol + D_2O mixtures at 25°C show the existence of alcohol aggregates (D'Arrigo and Teixeira, 1990). The two proposed structures for the aggregates are (i) micelle-like aggregates with the alkyl groups of the alcohol inside and the polar groups hydrogen-bonded to surrounding water molecules or (ii) mixed alcohol + water aggregates with no obvious distinction between separate regions as in the micelle model. Further SANS studies on 2-butoxyethanol + D_2O mixtures show that

alcohol aggregation occurs for concentrations greater than x_{BXE} = 0.015-0.02 and that the aggregate size increases with temperature with a maximum value for concentrations close to the critical concentration (D'Arrigo *et al.*, 1991b).

A mixing scheme boundary was determined for 2-butoxyethanol + water mixtures from the loci of the maxima of quantities proportional to the third derivatives of the Gibbs free energy such as the composition derivative of the excess partial molar enthalpy (Koga *et al.*, 1990). This pseudo-phase boundary separates water-rich and intermediate regions and the transition is associated with a change from short-range to medium-range order. At low concentrations of 2-butoxyethanol the hydrogen-bonding network of water is enhanced, but at higher concentrations no more 2-butoxyethanol molecules can be incorporated into this structure and so the complete network throughout the liquid is lost as a transition to a new mixing scheme takes place (Koga, 1992; Westh and Koga, 1996).

Ultrasonic relaxation studies of binary 2-butoxyethanol + water and ternary 2-butoxyethanol + water + cetyltrimethylammonium bromide solutions indicate the formation of aggregates whose structure is dependent on the relative amounts of alcohol and water (Kato *et al.*, 1986). The microstructure of the 2-butoxyethanol + water + cetyltrimethylammonium bromide mixture has been studied using fluorescent probes and at low concentrations of 2-butoxyethanol the 2-butoxyethanol molecules penetrate the surface of the cetyltrimethylammonium bromide micelles (Jobe and Verrall, 1990). Like other short-chain alcohols 2-butoxyethanol can act as a cosurfactant in aqueous surfactant and microemulsion systems and the presence of a surfactant in aqueous 2-butoxyethanol solutions stabilises the micro-aggregates (Perron *et al.*, 1981).

Of the series C_iE_1, it seems that 2-butoxyethanol may have the minimum hydrophobic chain length required to form aggregates in aqueous solution. This suggests that 2-butoxyethanol + water mixtures may be considered as reference systems for more complicated aqueous surfactant solutions (D'Arrigo *et al.*, 1991b).

1.5.5.5 Substitution of water by heavy water

In some experiments it is useful to be able to deuterate one of the species. In a neutron scattering experiment heavy water, deuterium oxide, D_2O can be used in place of H_2O to provide a contrast between 2-butoxyethanol and water. The critical composition expressed in terms of the mole fraction of 2-butoxyethanol is the same for 2-butoxyethanol + H_2O and for 2-butoxyethanol + D_2O (Baaken *et al.*, 1990). In 2-butoxyethanol + D_2O mixtures the critical composition, determined by the equal volume criterion, is, however, not the same as the lower temperature of phase separation due to isotope exchange reactions (Schön *et al.*, 1986). Another effect of substituting D_2O for H_2O is to decrease the miscibility of the two components due to the stronger nature of the D_2O-D_2O hydrogen bond. This is illustrated by the lower value of T_{LCS} =

42.7°C for 2-butoxyethanol + D_2O compared with T_{LCS} = 49.4°C for 2-butoxyethanol + H_2O (Schmitz *et al.*, 1994).

The microscopic viscosity of both 2-butoxyethanol + H_2O and 2-butoxyethanol + D_2O mixtures has been investigated and the results are presented in Chapter 3. The surface structure of 2-butoxyethanol + D_2O mixtures has been studied by neutron reflectivity and is discussed in Chapter 5.

Some physical properties of H_2O and D_2O are given by Némethy and Scheraga (1964). The effects of substituting D_2O for H_2O in other binary mixtures has been studied by many authors (for example, Fenby *et al.*, 1981; Szydlowski, 1994) and is discussed in Chapter 6 in relation to our studies on a nonaqueous ternary mixture incorporating isotopomers.

Some background to this thesis and the details of the particular mixtures used in this work have been given in this chapter. To conclude, an overview is given of the results chapters.

1.6 Overview of chapters

In Chapter 1, the following areas have been highlighted: i) phase behaviour, in general and for specific binary and ternary mixtures, ii) critical behaviour in binary mixture properties, particularly in the viscosity, and iii) adsorption and wetting behaviour in near-critical binary mixtures and in surfactant solutions. These are all issues of importance in later chapters.

Chapters 2 and 3 are concerned with the macroscopic and microscopic rheology, i.e. flow behaviour, of near-critical mixtures. The macroscopic viscosity has been studied by capillary viscometry and the microscopic viscosity by measurement of the rotational correlation time of a fluorescent probe.

A different fluorescence technique, evanescent-wave-generated fluorescence spectroscopy, has been used to investigate another aspect of critical behaviour, that of critical-point wetting at the solid-liquid interface, and is discussed in Chapter 4.

Critical-point wetting and critical adsorption in mixtures have also been studied at the liquid-vapour interface, by neutron reflectivity, and the results are presented in Chapter 5. In addition, neutron reflectivity has been used to investigate the surface activity of perfluoroalkylalkanes in alkanes.

Chapters 2-5 are mainly concerned with binary mixtures. Chapter 6 forms the start of an extension of this work to multicomponent mixtures, and the phase behaviour of simple ternary mixtures studied both experimentally and theoretically is described.

Finally in Chapter 7 general conclusions are drawn and considerations are given for future work.

CHAPTER 2: MACROSCOPIC VISCOSITY OF NEAR-CRITICAL MIXTURES

2.1 Macroscopic shear viscosity

Near a critical point many equilibrium properties of a fluid, such as the heat capacity, show an anomalous divergence to infinity of the kind discussed in section 1.1.4. The non-equilibrium transport properties exhibit similar behaviour and in the present chapter the characteristic form of the *macroscopic* viscosity, i.e. the flow behaviour of the bulk fluid, is discussed in detail. In the following chapter this topic is extended to the *microscopic* viscosity, i.e. the *local* resistance to translation or rotation of a given molecule.

The transport properties–diffusivity, viscosity and thermal conductivity–are properties in which some quantity is transferred from one part of a system to another due to the presence of a physical gradient. The diffusivity is the transfer of matter or mass m across a concentration gradient; the viscosity is the transfer of momentum mv across a velocity v gradient; and the thermal conductivity is the transfer of heat energy, effectively mv^2, across a temperature gradient.

The coefficient of viscosity, often just termed the shear viscosity, is defined as the ratio of the rate of applied shearing stress to the rate of shear. The rate of shear, or shear gradient, is the change in velocity of flow with distance measured perpendicular to the direction of flow. For simple fluids the shear viscosity is assumed to be independent of the shear gradient, however for binary mixtures near a critical point the shear viscosity can become dependent on the shear gradient, and this is discussed in more detail later.

The shear viscosity η, discussed here, describes the flow behaviour of the bulk fluid; a high viscosity fluid, often called a *viscous* fluid, has a high resistance to flow. The usual units for viscosity, or more strictly dynamic viscosity, are centipoise (cP); 1 Poise is equivalent to 1 g cm^{-1} s^{-1}. The kinematic viscosity is sometimes quoted and is the ratio of the dynamic viscosity and the density, i.e. η/ρ. In capillary-flow viscometry–the method used in this work to study viscosity–the measured flow times of a liquid through a capillary are used to calculate the kinematic viscosities, which can then be converted to dynamic viscosities if the densities are known.

Close to a critical point, for example a critical endpoint (CEP) in a binary mixture, the viscosity diverges to infinity. This follows from the simultaneous divergence of the correlation length, see section 1.1.4, which effectively means that close to the CEP the mixture is correlated throughout its bulk and thus tends to move as one viscous mass. The viscosities of noncritical pure fluids and mixtures, discussed below, are more easily described mathematically than those of near-critical mixtures and can yield information about the 'background' part of the viscosity of a near-critical mixture, i.e. the form of the viscosity expected in the absence of a critical point.

The viscosities of noncritical fluids have received a large amount of attention, but less work has been carried out on near-critical mixtures. The viscosity is of importance in a number of applications particularly in the engineering industry since the flow behaviour

of fluids can have a large effect on mechanical processes. Taking one particular example, in tertiary oil recovery, in which as much as possible of the remaining oil is removed from the well by injecting aqueous surfactant mixtures, the low viscosities of the microemulsions formed are crucial for the successful extraction of the oil.

The viscosity of fluids can be measured by a variety of techniques including capillary flow, oscillating or rotating discs, falling balls, and observation of Brownian motion of particles immersed in the fluid. The oscillating disc method has generally been used for fluids close to a gas-liquid critical point. Many studies on liquid mixtures, particularly close to a CEP, have used the capillary-flow method in which the time of flow of a given volume of liquid through a capillary is measured. There are several different types of capillary viscometers of which those of the Ostwald and Ubbelohde types are the most common for measuring the viscosity of liquids at atmospheric pressure. In Ostwald viscometers the liquid flows from a bulb into a capillary and then into a widened U-shaped tube and a second bulb. The design of Ubbelohde viscometers (Ubbelohde, 1936), also known as suspended-level viscometers, is such that the liquid in the capillary is 'suspended'. One advantage of Ubbelohde viscometers over Ostwald viscometers is that the hydrostatic driving head does not depend on the volume of liquid in an Ubbelohde viscometer and so this does not have to be adjusted during a series of measurements. Capillary-flow viscometry with an Ubbelohde-type viscometer was used in the present investigation of the viscosity of hexane + perfluorohexane near the CEP; the details are given in the following section.

2.1.1 Capillary-flow viscometry

Capillary-flow viscometry is one of the most popular methods for measuring the viscosity of liquid mixtures. Its main advantages are that the apparatus is relatively simple and cheap to build and that the flow of a fluid through a capillary can be treated using well-established mathematical equations. The basic Hagen-Poiseuille equation for fluid flow was first obtained from experimental results by Hagen in 1839 and Poiseuille between 1840 and 1846, and was later derived theoretically by Wiedemann in 1856 and Hagenbach in 1860. In this equation the viscosity η of a fluid flowing through a circular tube or capillary is given in terms of the radius r and length l of the tube, the pressure drop along the tube Δp, and the volume of fluid flowing through the capillary per second Q, by:

$$\eta = \frac{\pi r^4 \Delta p}{8Ql}. \qquad (2.1)$$

This equation is modified to include the kinetic energy correction–since Δp balances not only the viscous resistance but also transfers kinetic energy to the fluid–and the Couette, or end, correction–to allow for the energy loss of the fluid on entering the capillary from a bulb or reservoir. The equation generally used for capillary-flow viscometers is thus:

$$\eta = \frac{\pi r^4 \Delta p}{8Q(l + nr)} - \frac{m\rho Q}{8\pi (l + nr)} \tag{2.2}$$

where ρ is the density, and m and n are the kinetic-energy and Couette correction factors, respectively. The Couette correction is negligible if the length of the capillary is sufficiently long, i.e. if the ratio l:r exceeds 200. The effects of these factors, studied both experimentally and theoretically, have been discussed by several authors (for example, Barr, 1931; Cannon *et al.*, 1960; Van Wazer *et al.*, 1963; Kestin *et al.*, 1973).

In the derivation of equation (2.2) several assumptions are made including i) the flow is streamline or laminar, ii) the fluid in contact with the capillary wall is stationary, i.e. there is no slip, iii) the capillary is straight and of uniform circular cross-section, iv) the fluid is incompressible and of constant density, v) the fluid is Newtonian and the variation in viscosity due to the pressure drop along the tube is negligible, and vi) the temperature is constant and no heat is generated due to the viscous flow (Wakeham *et al.*, 1991). The best viscometer designs are those which meet these requirements. Factor i) in particular can cause problems since if Δp, and hence the mean velocity, is greatly increased, a change from streamline to turbulent flow is observed. This was studied by Reynolds (1883) and a factor now known as the Reynolds number Re can be calculated for a given viscometer from:

$$\mathrm{Re} = \frac{2r\rho\bar{v}}{\eta} \tag{2.3}$$

where $\bar{v}$ is the average flow velocity, and ρ and η the density and viscosity of water, respectively. If $\mathrm{Re} < 2000$ then laminar flow occurs, but if $\mathrm{Re} > 2000$ turbulent flow is observed and equation (2.2) is no longer valid. In our calibrations with water Re was much less than 200, well within the limits of streamline flow.

Other factors that require consideration when commissioning a new viscometer include the exact design of the entrance and exit of the capillary. Generally the fluid flows from a bulb into the capillary and at the bottom of the capillary enters either another bulb or a widened tube. A trumpet-shaped *entrance* to the capillary reduces turbulent flow, whereas an *exit* with a sudden enlargement, rather than with a gradual or trumpet-shaped opening, reduces surface tension effects. Since the driving force for flow in a gravity-flow viscometer derives from the difference in liquid levels, capillary rise of the liquid in the bulb at the top of the capillary, or at the bottom of the capillary, affects the flow and thus if the viscometer is calibrated with a liquid of different surface tension

from that under investigation a correction is required (Hardy, 1963). In practice, surface tension effects are minimised by using a viscometer with a suitable exit shape of the capillary and ensuring that the working volume and the driving head are sufficiently large (Gonçalves *et al.*, 1991).

The advantages of the capillary-flow method for measuring viscosity are discussed above; however it does have some potential disadvantages close to a critical point. For example, it may be difficult to ensure uniformity in the temperature and composition along the length of the capillary, and it is also generally assumed that the compressibility of the fluid is small which may not be valid close to a critical point (Sengers, 1973). A uniform constant temperature throughout the water bath should be achieved by adequate thermostatting. Another issue is whether the composition changes during the course of the measurements, particularly close to the critical point, due to continuous pressurising and releasing of the mixture (Leister *et al.*, 1969). Brunet and Gubbins (1969) noted that close to the critical point the measured flow times depended on the previous shear history of the mixture. This problem can be overcome by allowing long equilibration times and ensuring that the liquid is not forced up the capillary too rapidly.

A general working equation for a capillary viscometer is obtained from equation (2.2) using $\Delta p = \bar{h}\rho g$, where g is the acceleration due to gravity and $\bar{h}$ is the mean effective height of the liquid column. It turns out that $\bar{h}$ is the height at which the actual flow rate becomes equal to the mean flow rate, i.e. $Q = V/t$, where V is the volume of timing bulb and t is the time taken for a liquid volume V to flow through the capillary. Thus substituting for Δp and Q in equation (2.2) leads to:

$$\eta = \frac{\pi r^4 \bar{h} \rho g t}{8V(l + nr)} - \frac{m\rho V}{8\pi t(l + nr)}. \tag{2.4}$$

This equation can be more simply expressed as:

$$\frac{\eta}{\rho} = At - \frac{B}{t} \tag{2.5}$$

where $A = \dfrac{\pi r^4 \bar{h} g}{8V(l + nr)}$ and $B = \dfrac{mV}{8\pi(l + nr)}$.

If nr is small compared with l, as is usually the case, then A is a constant of the apparatus. The parameter B, however, is not an apparatus constant since the kinetic energy factor m varies with Reynolds number (Cannon *et al.*, 1960). It has been found that m varies inversely with t so the equation becomes:

$$\frac{\eta}{\rho} = At - \frac{E}{t^2} \tag{2.6}$$

where E is a constant for Reynolds number < 200, as in the present work. For many viscometers the second term is negligibly small compared with At and the equation is further simplified to:

$$\frac{\eta}{\rho} = At. \tag{2.7}$$

The constants are generally obtained for a given viscometer by calibration with a liquid of known viscosity and density over a range of temperatures.

2.1.2 Viscosity of pure fluids

The viscosities of pure gases usually increase roughly in proportion to the temperature. In contrast, the viscosities η of noncritical pure liquids of relatively low viscosity decrease with increasing temperature T and generally obey a simple Arrhenius-type equation of the form:

$$\eta = A \exp\left(\frac{B}{T}\right) \tag{2.8}$$

where A and B are constants. More viscous substances, in particular glasses, have also been the subject of much investigation (Van Wazer *et al.*, 1963). A distinguishing feature of such substances is the occurrence of a sharp change in viscosity exhibited over a relatively narrow range of temperature. Other substances which show different behaviour from low viscosity liquids are high molecular weight polymers such as polyethylene, usually termed pseudoplastic fluids. The pure liquids used in this work have low viscosities and thus are expected to obey equation (2.8).

As mentioned earlier, fluids near a critical point display an anomaly in the viscosity. The simple Arrhenius equation is no longer obeyed and the viscosity diverges to infinity at the critical point. This occurs both for pure fluids near a gas-liquid critical point and for binary mixtures near a critical endpoint (CEP). Early measurements revealing the anomaly at a gas-liquid critical point were made on carbon dioxide using an oscillating disc viscometer by Naldrett and Maass (1940) and Kestin *et al.* (1964), and on xenon and ethane using a tortionally oscillating quartz cylinder by Strumpf *et al.* (1974) who attempted to describe the anomalous behaviour mathematically.

2.1.3 Viscosity of liquid mixtures

The main parts of this section are devoted to the near-critical viscosity of binary mixtures; however, we begin by considering the form of the viscosity for noncritical mixtures as a function of temperature or composition.

The viscosities of noncritical pure and mixed liquids as a function of temperature usually obey equations of the form of (2.8). As a function of composition, the viscosities of binary mixtures do not generally follow a linear form and at the extremes of the composition range the mixture viscosity is, of course, constrained to the viscosities of the pure components. One form of equation that has been employed for the noncritical viscosity of binary mixtures is: $\ln \eta_{mix} = (1-x_2) \ln \eta_1 + x_2 \ln \eta_2$, where x_2 is the mole fraction of component 2, η_{mix} is the viscosity of the mixture and η_1 and η_2 the pure component viscosities (Grunberg and Nissan, 1949; Reed and Taylor, 1959). The mixture viscosity described by this equation is linear when the viscosities of the two pure components are equal, i.e. $\eta_1 = \eta_2$. When $\eta_1 \neq \eta_2$ the form of the equation is a 'concave downwards' dependence for η_{mix} on x_2. Although this form describes the behaviour of 'ideal' mixtures, positive or negative deviations occur for most real mixtures and the expression has no adjustable parameters to allow fitting to measured viscosities. Expressions for deviations from the ideal behaviour have been discussed by Mertsch and Wolf (1994).

The general behaviour of noncritical mixtures is of interest in establishing the form of the viscosity expected away from a critical point and to allow the true critical part of the viscosity of near-critical mixtures to be extracted from the background noncritical viscosity. We turn now to experimental and theoretical studies of near-critical mixtures and the methods used for fitting the background and anomalous parts of the observed viscosity.

2.1.3.1 Experimental studies of near-critical mixtures

In binary mixtures near a CEP, evidence for an anomalous increase in the viscosity was first found at the beginning of the century by Friedländer (1901) and Scarpa (1903). More recent studies, cited by Sengers (1973, 1985), show that the anomaly occurs at both upper and lower critical endpoints.

The CEP can be approached along three main paths: i) the path of constant critical composition x_c in the single phase for the region of total miscibility, ii) the coexistence path along both limbs of the coexistence curve in the region of partial miscibility, or iii) the isothermal path at constant critical temperature T_c, as shown in Figure 2.1 for a mixture exhibiting an upper critical endpoint (UCEP). Paths i) and ii) are often considered together, and have been studied for mixtures exhibiting UCEPs, for example nitroethane + 3-methylpentane, hexadecane + acetone (Pegg, 1982; Pegg and McLure, 1984) and methylcyclohexane + perfluoromethylcyclohexane (Davies, 1988; Maczek *et*

al., 1990), and LCEPs, for example 2-butoxyethanol + water (Pegg, 1982; Pegg and McLure, 1984). Other studies along path i) for various mixtures, particularly for 2-butoxyethanol + water, include those of Izumi *et al.* (1981), Berg and Moldover (1988), Mallamace *et al.* (1991) and Zielesny *et al.* (1994).

Path iii) has been less well studied but recent measurements have been obtained for methylcyclohexane + perfluoromethylcyclohexane (Archer, 1995). Earlier investigations, in which the viscosities of mixtures were measured as a function of composition for several temperatures both close to and further away from the critical temperature, provide indications of the range of temperatures over which the signature of the critical point is apparent but not enough data are available close to the critical point to allow the critical exponent to be fully characterised (for example, Reed and Taylor, 1959; Brunet and Gubbins, 1969; Tsai and McIntyre, 1974). A more rigorous analysis of experimental results including many more data points has been undertaken by D'Arrigo *et al.* (1977).

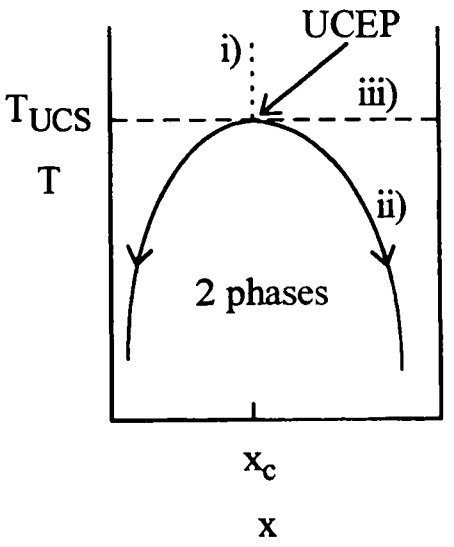

Figure 2.1: Paths of approach to the UCEP. i) Path of constant critical composition x_c, ii) coexistence path, and iii) isothermal path at the upper critical solution temperature T_{UCS}.

2.1.3.2 Theoretical predictions for the anomalous viscosity of near-critical mixtures

Early mean-field theory predictions for the viscosity near a critical point–first formulated by Fixman (1962) and based on the existence of long-wavelength composition fluctuations in the critical region–suggested that the viscosity should diverge in proportion to the correlation length, i.e. $\eta \sim \xi \sim \varepsilon^{-\nu}$, where from mean-field theory $\nu = {}^1/_2$. Although some experimental studies were in agreement with this prediction, most later studies showed that the viscosity diverged much more weakly, i.e. the actual index y was less than ${}^1/_2$ (Sengers, 1971, 1973). Kawasaki (1966) later extended and generalised Fixman's theory.

Fixman also predicted a strong dependence of the viscosity on the magnitude of the shear gradient in the critical region. Nieuwoudt and Sengers (1989) reanalysed several published data sets to include the effects of the shear gradient close to the critical point, using the predictions of Oxtoby (1975). The effect of the shear gradient was to round-off the measured near-critical viscosity. The corrected results thus showed higher critical exponents than the uncorrected data sets.

The ideas of Fixman were further developed by Kawasaki (1969, 1970a, 1970b) and formulated into what is now known as mode-mode-coupling theory. Similar results were also obtained by Perl and Ferrell (1972a, 1972b) using decoupled-mode theory. These theories have been reviewed and compared by Swinney and Henry (1973) and Hohenburg and Halperin (1977).

More recently dynamic renormalisation group (RG) theory has been applied to transport properties near a critical point (Siggia *et al.*, 1976) and yields similar results to those obtained by mode-mode-coupling theory (Garisto and Kapral, 1976). The theory predicts a divergence of the anomalous viscosity $\Delta\eta$ according to the power law:

$$\Delta\eta = A\xi^{\chi_\eta} \tag{2.9}$$

where ξ is the correlation length, A is an amplitude, and χ_η is the critical exponent with a value close to 0.065. Since the correlation length can be expressed by the power law $\xi = \xi_0\,\varepsilon^{-\nu}$, where $\varepsilon = |T - T_c|/T_c$, and the correlation length critical exponent $\nu = 0.630$, see section 1.1.4, equation (2.9) can be expressed as:

$$\Delta\eta = B\varepsilon^{-\nu\chi_\eta} = B\varepsilon^{-y} \tag{2.10}$$

where $y = \nu\chi_\eta = 0.04$. Experimental results (Pegg, 1982; Davies, 1988) have shown good agreement with this prediction. The value $y = 0.04$ was predicted by Siggia *et al.* (1976). Since then the theoretical value of y has received further attention. Bhattacharjee and Ferrell (1983) found $y = 0.032$. Later, work by Hao and Ferrell revised the value to $y = 0.040$ ($\chi_\eta = 0.063$) (Hao, 1991) and this is currently the best theoretical estimate (Luettmer-Strathmann *et al.*, 1995). The value $y = 0.040$ has therefore been used in the treatment of our data.

A similar RG approach has been suggested for the anomalous viscosity as a function of composition along the isothermal path to the critical point (Sengers, 1993). The critical exponent proposed is $\nu\chi\eta/\beta$, i.e. the constant composition path exponent renormalised by the order parameter critical exponent. The power law can be written:

$$\Delta\eta = C(|x - x_c|/x_c)^{-\nu\chi\eta/\beta} = C(|x - x_c|/x_c)^{-\lambda} \qquad (2.11)$$

where the critical exponent $\lambda = \nu\chi\eta/\beta = 0.126$, with $\beta = 0.325$.

The RG theory approach is now generally accepted as the best available theoretical treatment of the anomalous critical viscosity, as careful experimental results are in agreement with the predictions of the theory. In the following section the separation of the anomalous viscosity from the total measured viscosity is discussed.

2.1.3.3 Analysis of near-critical viscosity data

In most analyses of viscosity data near a CEP, the measured viscosity η is separated into a background viscosity η_B, expected in the absence of any critical fluctuations, and an anomalous part $\Delta\eta$. The procedure for separating these contributions is complex. The starting issue is the decision whether the background and the anomalous contributions are linked additively (Sengers, 1971, 1973) or multiplicatively (Calmettes, 1977; Ohta, 1977). This issue is crucial and is further complicated since the critical exponent depends on the exact form chosen for the background viscosity. Along the constant composition path the critical exponent $y = 0.040$ is very small and the temperature range for which $\Delta\eta > \eta_B$ is inaccessible (Sengers, 1985), as it is within micro-Kelvins of T_c. The background contribution is thus not negligible compared to the anomalous part, even in the close vicinity of the critical point, and cannot be ignored. In practice η_B is often obtained by extrapolating data away from the critical point (Burstyn and Sengers, 1982), although this approach is open to error since it is not known how far from the critical point the anomaly is no longer present. Brunet and Gubbins (1969) observed the signature of the critical point more than 20 K away from the critical point, and it is likely that the critical fluctuations may extend over even greater temperature ranges.

Along the path of constant critical composition, for which most studies have been carried out, the total viscosity is generally fitted to a multiplicative equation of the form:

$$\eta = \eta_B \cdot \Delta\eta. \tag{2.12}$$

The background contribution η_B is usually fitted to an Arrhenius-type equation. Thus, using equation (2.10), equation (2.12) becomes:

$$\eta = A \exp\left(\frac{B}{T}\right) \varepsilon^{-y} \tag{2.13}$$

where A and B are constants, and the critical exponent y = 0.040. From this equation and for T_c = 300 K it can readily be shown that 1 K away from T_c the anomaly amounts to almost 26% of the background, and even 100 K away from T_c the anomaly amounts to 4% of the background.

Along the isothermal path the form of the equation for the viscosity is not known because of the uncertainty in a) the nature of the background term and b) in the link between the background and anomalous terms, i.e. whether they should be linked multiplicatively or additively. There are some limitations and the requirements to be fulfilled are i) the viscosities at the extremes of the composition range must be equal to those of the pure components at T_c, and ii) the background viscosity at the critical point must be the same irrespective of the approach along either the isothermal or the constant composition paths.

The thermal conductivities of binary gaseous mixtures have been successfully described by the Wassiljewa equation (Gray *et al.*, 1970):

$$\lambda_{mix} = \frac{\lambda_1}{1 + A_{12} x_2 / x_1} + \frac{\lambda_2}{1 + A_{21} x_1 / x_2} \tag{2.14}$$

where λ_{mix} is the thermal conductivity of the mixture, λ_1 and λ_2 the thermal conductivities of the pure components, x_1 and x_2 are the mole fractions of each component in the mixture, and A_{12} and A_{21} are adjustable parameters. Equation (2.14) ensures that for $x_1 = 1$ and $x_2 = 1$ the thermal conductivity of the mixture is equal to that of the respective pure component. The equation is flexible and with appropriately chosen values for A_{12} and A_{21} can represent maxima and minima, and also a point of inflection and an S-shaped conductivity-composition curve.

A similar type of equation to describe the background viscosity, but also incorporating the anomalous viscosity term has been proposed (Archer, 1995):

$$\eta = \frac{\eta_1 x_1}{(1-x_2)+A_{12}x_2} + \frac{\eta_2 x_2}{x_2 + A_{21}(1-x_2)} + Ax_2(1-x_2)\left(\frac{|x-x_c|}{x_c}\right)^{-\lambda} \qquad (2.15)$$

where A_{12} and A_{21} are variable parameters, A is the critical amplitude and λ is the critical exponent. The background viscosity is represented with $\lambda = 0$ and varying A_{12} and A_{21}, and the total viscosity is described with $\lambda \neq 0$ and varying A_{12}, A_{21} and A. In this equation the background and anomalous terms are linked additively. A multiplicative relation may, however, be preferred since the form generally used along the constant composition path is multiplicative. A suitable form for the anomalous viscosity in a multiplicative equation may be: $\Delta\eta = 1 + Ax_2(1 - x_2)(|x - x_c|/x_c)^{-\lambda}$ (Archer, 1995). If the viscosities along the two paths are represented in similar forms, agreement at the critical point may more easily be achieved.

2.2 Experimental details

We turn now to the specific details of our work. In this section the capillary viscometer used in the measurements and the details of the materials used are described. The results of the calibration with distilled water are also presented.

2.2.1 Apparatus

The viscosities presented in this chapter were measured using a sealed capillary-flow viscometer of the Ubbelohde suspended-level type. The Pyrex viscometer, shown in Figure 2.2 and Plate 1, has two separate tubes leading into the main reservoir at different levels to allow the measurement of the flow times and hence viscosities of two coexisting liquid phases. Pressure is applied through a two-syringe system attached to the viscometer by Teflon tubing, with the Youngs taps correctly adjusted, to force the liquid sample up the Veridia capillary. Table 2.1 shows the dimensions of the viscometer.

Table 2.1: Viscometer dimensions.

parameter	value
capillary radius r /cm	0.025
length of capillary l /cm	23.7
maximum height of liquid above bottom of capillary h /cm i.e. distance between upper timer level and bottom of capillary	26.6
approximate volume of bulb V /cm^3	1.5

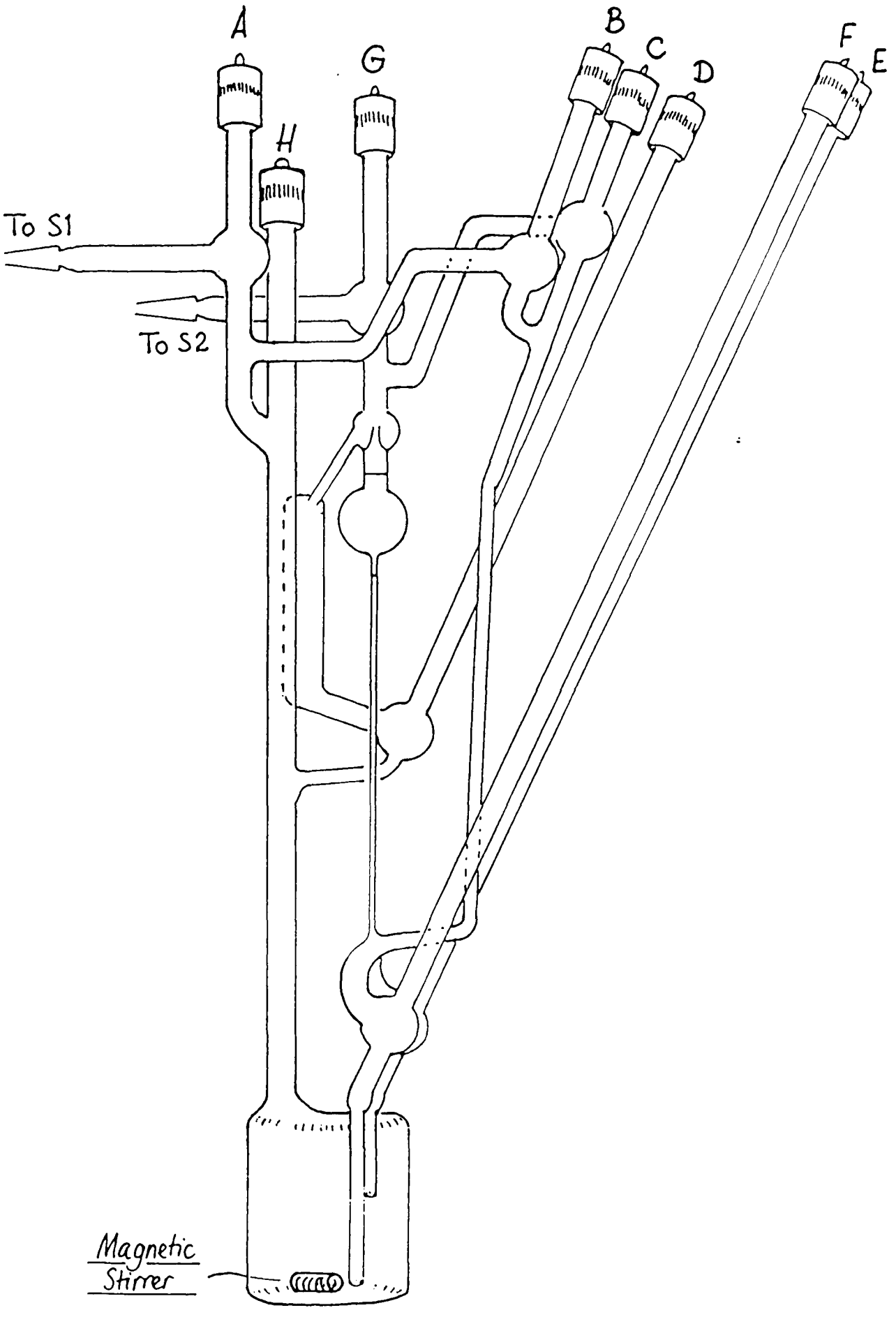

Figure 2.2: The suspended-level viscometer used in this work. (Reproduced from Haslam, 1992.)

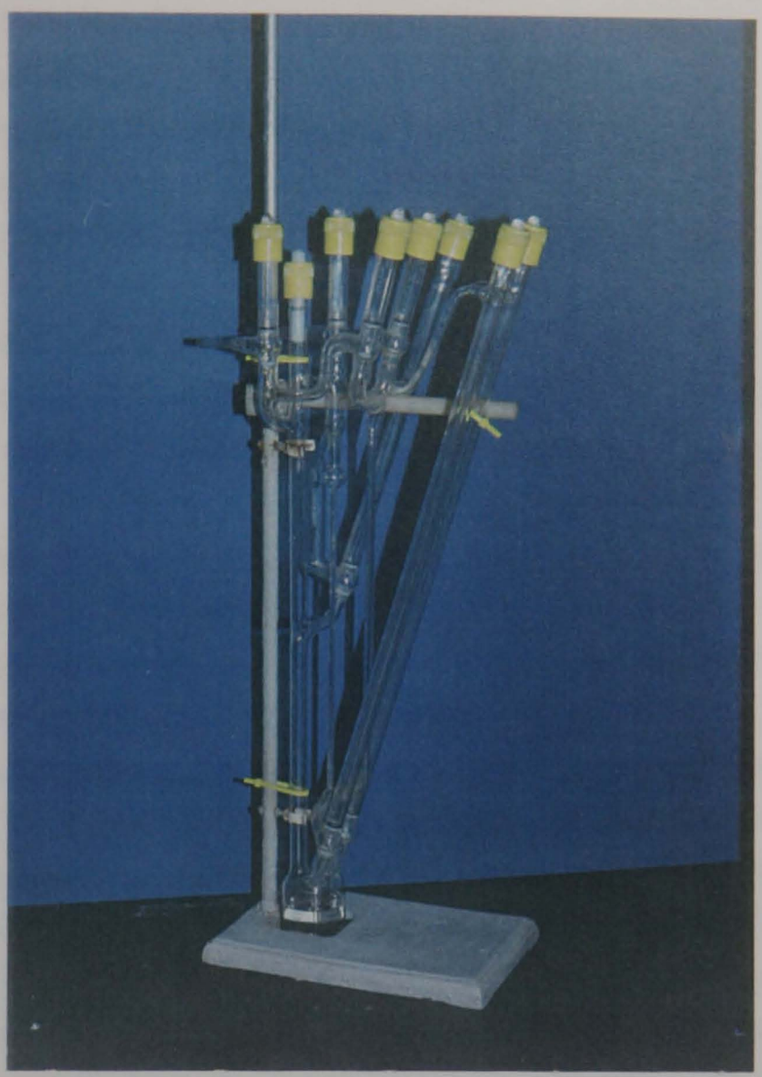

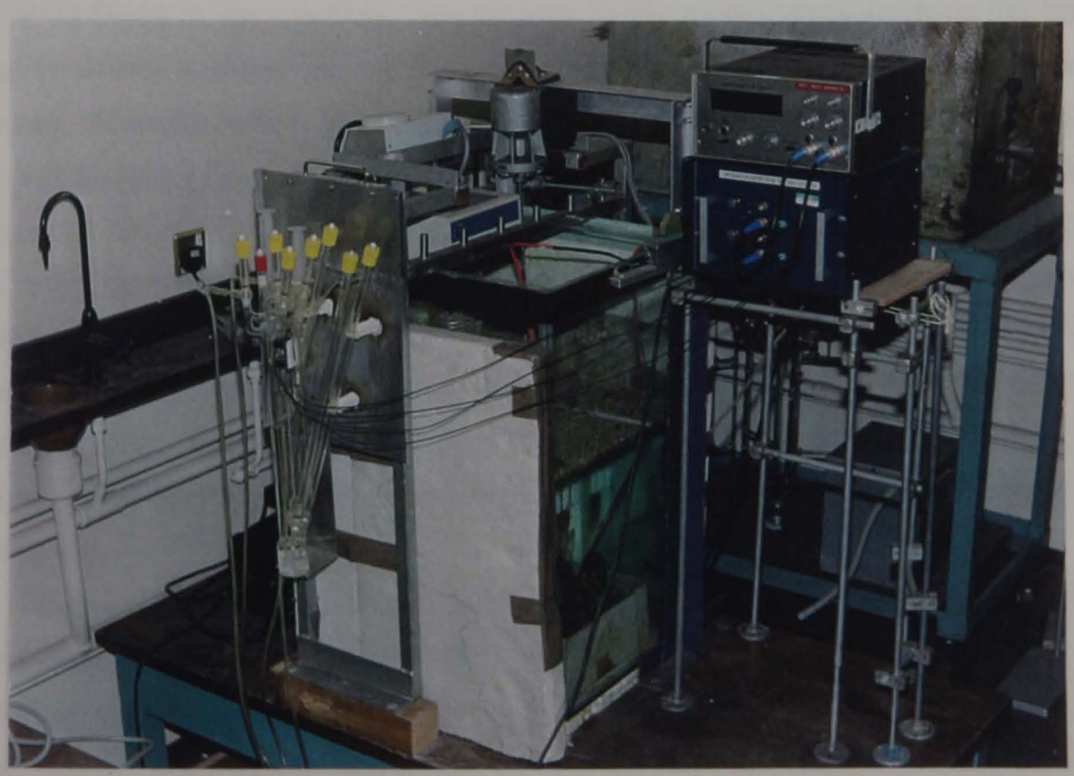

Plate 1: The suspended-level viscometer and the experimental arrangement.

The procedure for the measurement of the flow time of the *lower* phase, starting with all the taps open, is as follows:

1. Tap E is closed.
2. Taps D, B and C are then closed in this order.
3. Pressure is applied through syringe 1, forcing the lower phase up the capillary, until the capillary and bulb are full and the liquid is overflowing into the overflow reservoir.
4. Tap A is closed, syringe 1 is released, and then tap G is also closed.
5. Tap C is opened followed by tap B, and the liquid falls as a suspended column. The meniscus is timed as it falls between two set points above and below the bulb, see below.
6. When the measurement is complete, taps G, A, D and E are opened and the syringes returned to their original positions.

To sample the *upper* phase the procedure is the same except that tap F is closed in place of E in step 1, and opened at the end of the measurement in step 6.

The timing is by means of a digital timer (Venner Electronics TSA6616) reading to 0.01 s, activated by optical fibre sensors set in plastic discs attached above and below the capillary bulb. A plastic spacer ensures that the sensors remain fixed in position at a set distance of separation. Two optical fibre cables are positioned at 180° to each other across the tube for both the upper 'start' signal and the lower 'stop' signal. The intensities are adjusted before each measurement so that a signal is only just detected when liquid is in the capillary and bulb. Since the liquid amplifies the signal, no signal is detected when there is no liquid in the capillary. Any change in the signal starts or stops the timer. The alteration of the intensity allows flow times for both clear and opalescent liquids to be measured. A similar timing device has been described by Habib and Gruner (1988).

For a given phase at each temperature measurements were repeated 4-6 times and an average taken. The precision of successive measurements was often better than ±0.01 s for flow times of 40-60 s, i.e. 0.03-0.05%, although at lower temperatures, for which a cooler was required in the water bath, the range was sometimes ±0.05 s, i.e. about 0.2%. This is more accurate timing than can be achieved with a hand-held stopwatch, where the human element of the error in timing is generally ±0.15 s. The flow times recorded here are short and so the automatic timer ensures a much greater degree of accuracy.

The viscometer and syringes were clipped onto an aluminium back plate which slotted onto a metal frame above the water bath of approximate volume 0.16 m^3. The viscometer and syringes were positioned in the bath so that the liquid sample and the sealed vapour were below the water level. The bath was lagged on three sides with polystyrene and the front face was left open to allow easy viewing of the viscometer. The temperature of the bath was controlled by a thermostat (Techne Tempunit TU 16A) and

was measured by a calibrated platinum resistance thermometer, positioned close to the viscometer capillary, by comparison with a standard 100Ω resistor attached to a resistance bridge (Automatic Systems Laboratories). A stirrer, attached to a separate stand to reduce vibrations, was used to aid water circulation, and at temperatures below 23°C a cooler (Neslab Cryocool CC-80II) was also required. The temperature variation was generally less than ±0.005 K.

The sample in the main viscometer reservoir was stirred prior to each measurement by a Teflon-coated magnetic follower activated by a magnetic stirrer of the same design as that used by Pegg (1982). The stirrer consisted of four coils, sealed in Perspex cement and arranged in a square around the reservoir, which were attached to a plastic base resting on the bottom of the water bath. The signal fed to the coils–four digitally-approximated sine waves of variable frequency each 90° phase shifted from the next–produced a rotating magnetic field around the sample. At a given temperature, the sample was left for a minimum of 80 mins if in a single phase, and for a minimum of 3 hours if in two phases, to equilibrate after stirring. For two-phase mixtures very close to the critical point the mixture was equilibrated for 15 mins between successive measurements on a given phase. Before starting a series of measurements on a given phase the capillary was rinsed clean of the previous phase.

The viscometer was cleaned by soaking overnight in a 5% Decon solution, then rinsing thoroughly with distilled water before drying on a vacuum line. During measurements on the sample mixture the viscometer was sealed under nitrogen to minimise the effects of dissolved oxygen in the perfluorocarbon and of dissolved water in the hydrocarbon. The sample of the required composition was prepared by weighing the components into a filling burette. The sample in the burette was warmed into a single phase and transferred to the viscometer reservoir *via* a long filling tube placed in the viscometer after removing tap H.

The pressure variations during an experimental run were expected to have no greater effect on T_c than the temperature fluctuations of the bath and were therefore neglected.

2.2.2 Materials

The mixture chosen for study was *n*-hexane + perfluoro-*n*-hexane. This mixture contains open chain molecules rather than cyclic molecules as in the alkane + perfluoroalkane mixture methylcyclohexane (MCH) + perfluoromethylcyclohexane (PFMCH) for which the near-critical viscosity has been previously studied along the constant composition, coexistence and isothermal paths, (Davies, 1988; Archer, 1995). Our objectives in the study of the viscosity of hexane + perfluorohexane along the constant composition and coexistence paths in the single-phase and two-phase regions were i) to broaden the base of knowledge of alkane + perfluoroalkane near-critical rheology, ii) to ascertain the need

for a shear-gradient correction and, were one needed, to determine the correlation length amplitude ξ_0–partly in relation to our neutron reflectivity studies and partly to compare with values already published, and lastly iii) to determine the ratio of the critical amplitudes along the constant composition single-phase and coexistence paths to compare with the prediction of Calmettes (1979).

The details of the materials used in this work are given in Table 2.2. Apart from drying the hexane with 4Å molecular sieve the materials were used as received. The density of perfluorohexane is much greater than that of hexane and this aids in the phase separation process and equilibration of the two phases.

Table 2.2: The suppliers, purities, densities ρ, and molar masses M for the liquids used in this work.

material	supplier	purity /mol %	ρ (25°C) /g cm^{-3}	M /g mol^{-1}
hexane	Aldrich	99	0.655[a]	86.18
perfluorohexane	Fluorochem	99 (85% *n*-isomer)	1.672[a]	338.05

[a] Bedford and Dunlap (1958).

The critical point has been determined for this system in a number of studies; details are given in Table 2.3. The differences in T_c and x_c may be due to differing purities of materials, and in the case of T_c to differing thermometer calibrations. Generally, impurities soluble in only one component at T_c tend to raise T_c, and impurities soluble in both phases tend to lower T_c (Snyder and Eckert, 1973). The effects of impurities on x_c or the critical exponent are usually less pronounced (Cohn and Jacobs, 1984). In our measurements, the mixture used was of the critical composition reported by Bedford and Dunlap (1958) for consistency with the densities and coexistence curve used in the calculations of the viscosities. Our critical temperature T_c was determined visually in the viscometer.

Table 2.3: Critical temperatures and mole fractions for hexane + perfluorohexane.

T_c /°C	x_c(perfluorohexane)	reference
22.65	0.370	Bedford and Dunlap (1958)
22.863, 22.472	0.3625	Block *et al.* (1981)
22.66	0.3509	Pozharskaya *et al.* (1984)
22.36-22.41	0.370	this work

The mixture of mole fraction of perfluorohexane of 0.370 was made up by mass. The masses of the components m_1 and m_2 were used to calculate the mass fraction w_1 from equation (2.16), mole fraction x_1 from equation (2.17), or volume fraction ϕ_1 from

equation (2.18), of component 1, using the molar masses M or the densities ρ of the components. In the case of the volume fraction the densities at 25°C were used and the excess volumes were neglected. Conversions between these equations can be made by rearrangement and elimination of m_2/m_1.

$$w_1 = \left(1 + \frac{m_2}{m_1}\right)^{-1} \tag{2.16}$$

$$x_1 = \left(1 + \frac{M_1 m_2}{M_2 m_1}\right)^{-1} \tag{2.17}$$

$$\phi_1 = \left(1 + \frac{\rho_1 m_2}{\rho_2 m_1}\right)^{-1} \tag{2.18}$$

The materials used have relatively low boiling points. The boiling point of hexane is 69°C and of perfluorohexane is 57°C (Aldrich Handbook, 1993).

2.2.3 Calibration

The viscometer was calibrated using distilled water. Flow times t were recorded at eight temperatures over the range 11-61°C. At each temperature the viscosity η and density ρ of water were taken from the data of Weast (1974) and Kell (1975), respectively. The results are given in Table 2.4 and are plotted in Figure 2.3.

Table 2.4: Results of viscometer calibration using distilled water.

temp. /°C	flow time /s	η /cP	ρ /g cm^{-3}	η/ρ /10^{-2} cm^2 s^{-1}
11.16	176.71	1.2647	0.99967	1.2651
18.50	145.97	1.0400	0.99849	1.0416
25.16	124.96	0.8872	0.99700	0.8899
32.49	107.10	0.7570	0.99490	0.7609
39.72	93.29	0.6564	0.99240	0.6615
46.44	82.95	0.5812	0.98971	0.5872
53.29	74.30	0.5181	0.98663	0.5251
60.98	66.34	0.4598	0.98280	0.4678

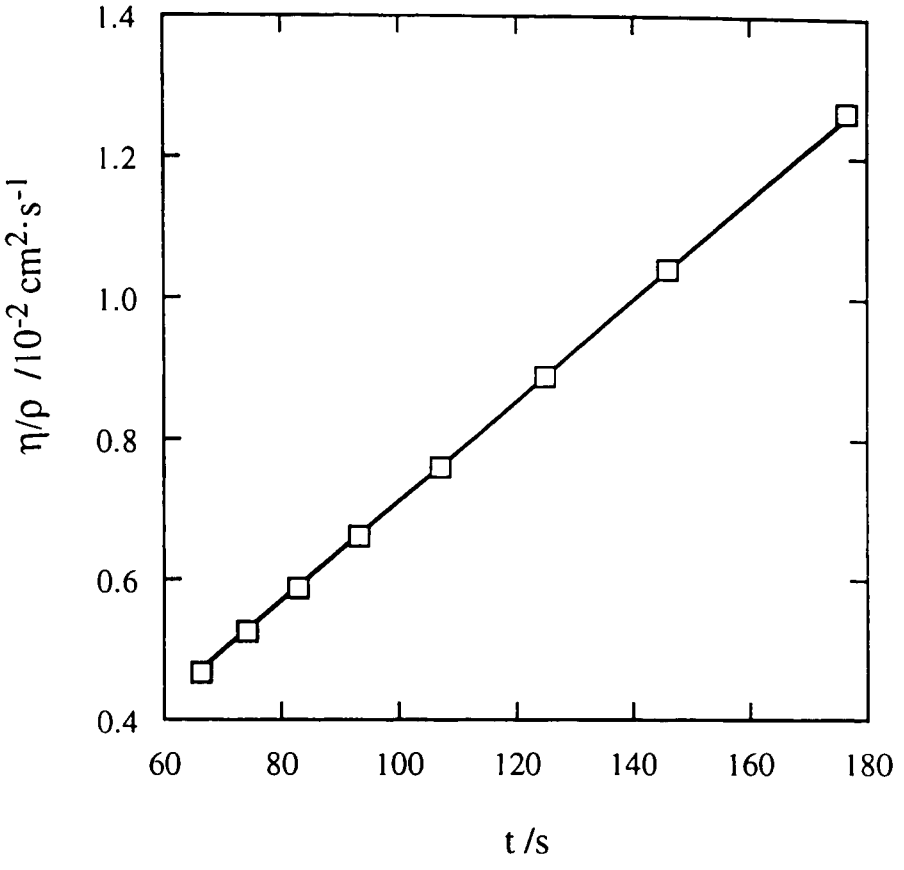

Figure 2.3: Results of viscometer calibration using distilled water, plotting η/ρ as a function of flow time t. The line is drawn from the best fit to equation (2.7) using the value of A quoted in Table 2.5.

The results were fitted, using the program MacCurvefit, to equations of the form of (2.6) and (2.7), reproduced below:

$$(2.6)\quad \frac{\eta}{\rho} = At - \frac{E}{t^2} \qquad \textit{and} \qquad (2.7)\quad \frac{\eta}{\rho} = At$$

where A and E are constants. The results of the fits to each equation are given in Table 2.5. The sum of the squares error SSE and the correlation coefficient R^2, defined in equations (2.19) and (2.20), provide an indication of the goodness of the fit. For a perfect fit SSE = 0 and $R^2 = 1$.

$$SSE = \sum_i (y_i - f(x_i, A, E))^2 \tag{2.19}$$

$$R^2 = 1 - \frac{nSSE}{n\sum_i y_i^2 - (\sum_i y_i)^2} \tag{2.20}$$

In equations (2.19) and (2.20) x_i and y_i are the i^{th} data pair, f is the value of the function, A and E are the coefficients in the function, and n is the number of data points. From the SSE and R^2 values there is not much difference in the fits, but the value of E in equation (2.6) is very poorly defined. The linear form of the equation, (2.7), was therefore adopted. The value of $A = 7.1226 \times 10^{-5}$ cm^2 s^{-2} quoted for this fit in Table 2.5 was used to convert the measured flow times for the hexane + perfluorohexane mixture into the ratio η/ρ.

Table 2.5: Results of fitting the calibration data to equations (2.6) and (2.7).

parameter	fitting to equation (2.6)	fitting to equation (2.7)
$A/10^{-5}$ cm^2 s^{-2}	7.1213	7.1226
error in $A/10^{-5}$ cm^2 s^{-2}	±0.0177	±0.0122
$E/10^{-2}$ cm^2 s	1.2048	-
error in $E/10^{-2}$ cm^2 s	±15.6721	-
SSE	0.00010	0.00011
R^2	0.99980	0.99979

2.3 Results

The flow times of a mixture of hexane + perfluorohexane of critical composition x(perfluorohexane) = 0.370 were measured from 19 K above the upper critical solution temperature T_c in the region of total miscibility to 5 K below T_c in the region of limited miscibility. In the region of liquid-liquid coexistence the flow times were determined for the two phases actually coexisting at each temperature, except at the highest temperature at which only the lower phase could be studied as not enough upper phase was present. The flow times were converted to η/ρ using equation (2.7) with $A = 7.1226 \times 10^{-5}$ cm^2 s^{-2}. The viscosities were then calculated by interpolation of the densities and coexisting compositions reported by Bedford and Dunlap (1958).

The results for η and ρ at different temperatures T are listed for the single-phase mixture in Table 2.6 and for the coexisting phases in Table 2.7. At a given temperature the flow time for the upper phase is greater than that for the lower phase, but the lower perfluorohexane-rich phase has the higher viscosity due to its higher density. The viscosities for the one-liquid phase and the two coexisting liquid phases and their mean are plotted in Figure 2.4.

Table 2.6: The flow times t, shear viscosities η and densities ρ of hexane + perfluorohexane as a function of temperature T in the region of total miscibility.

T /°C	T /K	t /s	ρ /g cm^{-3}	η /cP
41.03	314.18	40.82	1.0685	0.3107
35.03	308.18	43.59	1.0808	0.3356
31.20	304.35	45.66	1.0887	0.3541
28.05	301.20	47.69	1.0951	0.3720
26.02	299.17	49.40	1.0993	0.3868
24.99	298.14	50.51	1.1014	0.3963
24.02	297.17	51.90	1.1034	0.4079
22.97	296.12	54.55	1.1056	0.4296
22.81	295.96	55.25	1.1059	0.4352
22.66	295.81	56.22	1.1062	0.4430
22.49	295.64	58.05	1.1066	0.4575
22.41	295.56	60.20	1.1067	0.4745

Table 2.7: The flow times t, shear viscosities η and densities ρ of hexane + perfluorohexane as a function of temperature T in the region of partial miscibility.

T /°C	T /K	t /s	ρ /g cm^{-3}	η /cP	t /s	ρ /g cm^{-3}	η /cP
			lower phase			upper phase	
22.36	295.51	58.89	1.1436	0.4797			
22.27	295.42	54.63	1.1669	0.4541	55.72	1.0436	0.4142
22.10	295.25	52.81	1.1904	0.4478	54.82	1.0190	0.3979
21.76	294.91	51.35	1.2201	0.4462	54.36	0.9889	0.3829
21.40	294.55	50.69	1.2431	0.4488	54.19	0.9670	0.3732
20.38	293.53	50.15	1.2898	0.4607	54.51	0.9262	0.3596
19.35	292.50	50.21	1.3246	0.4737	55.11	0.8992	0.3530
18.38	291.53	50.53	1.3513	0.4863	55.80	0.8804	0.3499
17.38	290.53	50.94	1.3747	0.4988	56.56	0.8654	0.3486

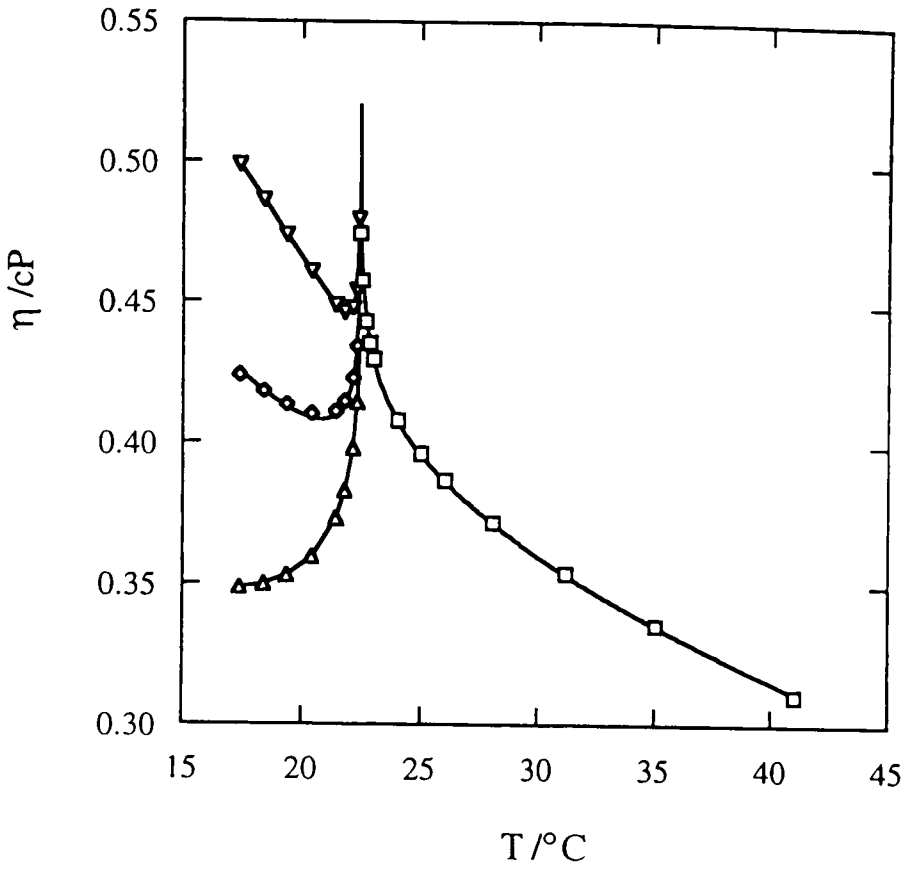

Figure 2.4: The shear viscosity η of a mixture of hexane + perfluorohexane of critical composition in the single phase (□), and the upper and less viscous (△) and the lower and more viscous (▽) phases and their mean (◊) as a function of temperature T close to the optimum upper critical solution temperature $T_{UCS} = 22.38_5$°C. The curves for the mean of the coexisting phases and for the single-phase mixture are drawn after fitting to equation (2.21); the values of A and B are quoted in Table 2.8. For the coexisting phases smooth curves are drawn through the points without theoretical significance.

The viscosities of our mixture are compared with those for other mixtures studied in the group, namely 2-butoxyethanol + water, nitroethane + 3-methylpentane, acetone + hexadecane (Pegg, 1982), and methylcyclohexane + perfluoromethylcyclohexane (Davies, 1988), in Figure 2.5. This figure illustrates the spread of behaviour for mixtures of different kinds exhibiting both upper and lower critical endpoints and whose nonideality springs from different molecular causes. For example, 2-butoxyethanol + water, like nearly all aqueous mixtures exhibiting an LCEP, owes its immiscibility to hydrogen bonding of different strengths and extent between the like and unlike species in the mixture. In contrast, in nitroethane + 3-methylpentane and acetone + hexadecane–as examples of dipole + nonpolar diluent mixtures–the nonideality largely originates from localised dipoles, and in methylcyclohexane + perfluoromethylcyclohexane it originates from a general weakness between the unlike components of the mixture. It is clear that

hexane + perfluorohexane greatly resembles nitroethane + 3-methylpentane in terms of both the magnitude of the viscosity and its near-critical temperature dependence. In contrast, the viscosities of the two alkane + perfluoroalkane mixtures are surprisingly different, with the viscosity of the mixture of cyclic molecules being considerably the higher, even allowing for the difference in T_c.

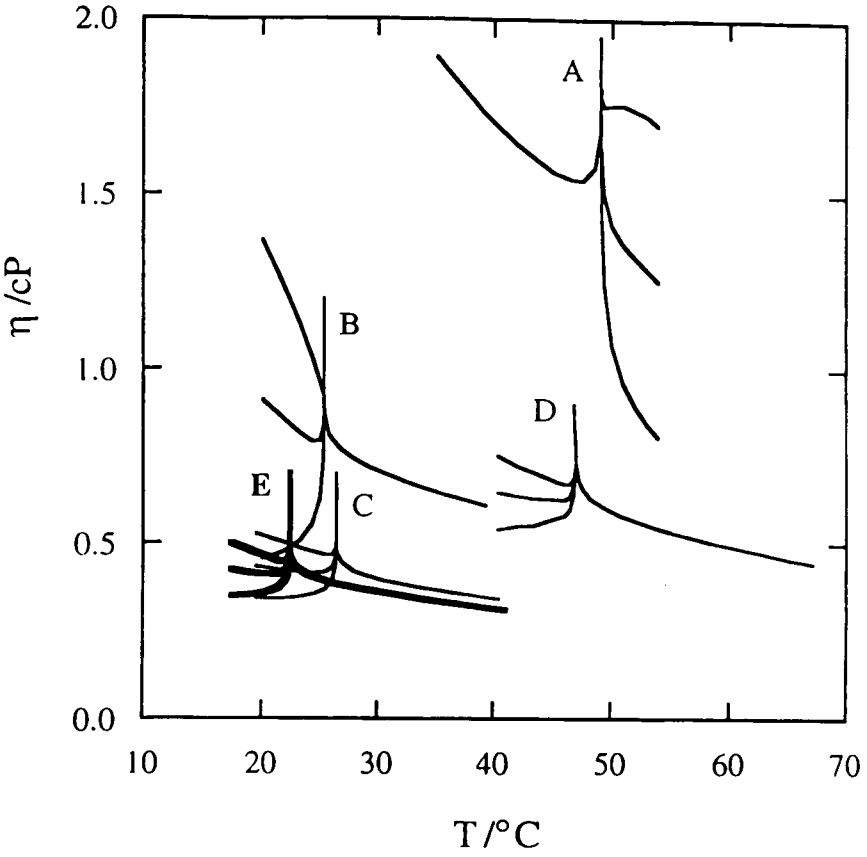

Figure 2.5: The shear viscosities η as a function of temperature T for one mixture near a lower critical endpoint (2-butoxyethanol + water) A and four mixtures near an upper critical endpoint (acetone + hexadecane, nitroethane + 3-methylpentane, methylcyclohexane + perfluoromethylcyclohexane, and hexane + perfluorohexane) B, C, D, and E, respectively. The bold line represents the range of measurements in the present study on hexane + perfluorohexane.

Considering briefly the near-critical viscosities of other mixtures, the viscosity of aniline + cyclohexane is similar in magnitude to that of 2-butoxyethanol + water (D'Arrigo *et al.*, 1977). The viscosity of isobutyric acid + water is notably higher than for these two mixtures, but the viscosity of methanol + cyclohexane is lower and is more comparable with that for MCH + PFMCH (Berg and Moldover, 1988).

2.4 Data analysis and discussion

The shear viscosities have been presented in Tables 2.6 and 2.7 and in Figure 2.4 above. In this section the results are fitted to the expression for the total viscosity–both with and without incorporating the shear-gradient dependence. The analysis with the incorporation of the shear-gradient effects yields the correlation length amplitude ξ_0 for hexane + perfluorohexane. The critical amplitudes for the viscosity–for the single-phase mixture and for the mean of the coexisting phases–are also obtained and the amplitude ratio compared with theoretical predictions.

2.4.1 Shear-gradient dependence

The results for the single phase and for the mean of the coexisting phases can be fitted to an equation of the form discussed previously:

$$\eta = A \exp\left(\frac{B}{T}\right) \varepsilon^{-y} \tag{2.21}$$

where A and B are constants, and the critical exponent y = 0.040 from RG theory. The measurements of the shear viscosity of the single-phase mixture very close to T_c show a reduction or 'rounding off', best portrayed as a flattening on a log η *versus* log ε plot, as in Figure 2.6 below. This is attributed to shear-gradient effects (Oxtoby, 1975), where the shear gradient $\partial v/\partial r$ is the change in velocity of flow with distance measured perpendicular to the direction of flow. Oxtoby suggested that in the critical region the shear gradient is no longer linear and this leads to the reduction of the shear viscosity with increased shear gradient, due to the interaction of the externally imposed shear gradient with the long-wavelength modes that are excited in the critical region. In the absence of shear-gradient effects, the measured viscosities should obey equation (2.21) and thus on a log η *versus* log ε plot, should show a straight line of slope -y for small ε, for which the background term is essentially independent of ε.

In order to fit the measured viscosities to equation (2.21) they must be corrected for the dependence of the viscosity near T_c on the shear gradient. This is accomplished using the procedure of Oxtoby (1975). A dimensionless quantity λ is introduced to aid in the conversion and is defined by:

$$\lambda = \frac{\eta \xi^3 d}{kT} \tag{2.22}$$

where ξ is the correlation length in the fluid, d is the shear gradient, k is the Boltzmann factor and T is the temperature.

In a capillary viscometer the maximum gradient d_{max} is given by (Barr, 1931):

$$d_{max} = \frac{h\rho g r}{2\eta l} \tag{2.23}$$

where h is the maximum height of liquid above the bottom of the capillary, r the radius and l the length of the capillary, g the acceleration due to gravity (9.813 m s^{-2}), and ρ and η the density and viscosity of the fluid, respectively. The dimensions of our viscometer are given in Table 2.1 above.

The shear gradient varies from a maximum at the walls of the capillary to zero at the centre. An effective average value d_{eff} can be calculated assuming the velocity profile in the tube is parabolic (Oxtoby, 1975):

$$d_{eff} = \frac{8}{15} d_{max} \tag{2.24}$$

which with equations (2.22) and (2.23) gives:

$$\lambda_{eff} = \left(\frac{4h\rho g r}{15kTl}\right) \xi^3 \tag{2.25}$$

where $\xi = \xi_0 \varepsilon^{-0.63}$, with ξ_0 the correlation length amplitude. In our calculations of λ_{eff} the average density for the mixtures over the range of measurements was used.

Using λ_{eff}, the viscosities in the absence of shear-gradient effects $\eta(0)$ are obtained from the measured finite-shear-gradient viscosities $\eta(\lambda_{eff})$ *via*:

$$\Delta(\lambda_{eff}) = 1 - \frac{\eta(\lambda_{eff})}{\eta(0)} \tag{2.26}$$

where $\Delta(\lambda_{eff})$ is a universal function of λ_{eff}. This function $\Delta(\lambda_{eff})$ is obtained from the series reported by Lee and Purvis (1977) which describes well the numerical results of Oxtoby for the dependence of $\Delta(\lambda_{eff})$ on λ_{eff}:

$$\Delta(\lambda_{eff}) = 0.0214 + 0.0266\,(\log_{10}\lambda_{eff}) + 0.0078\,(\log_{10}\lambda_{eff})^2 . \tag{2.27}$$

This expression is valid only within the limits $0.1 \le \lambda_{eff} \le 20$. The lower limit reflects a distance from T_c beyond which shear-gradient correction is unnecessary and the upper limit reflects the end of the range of the Oxtoby calculations. The former is approached only for mixtures studied to within a very small distance from T_c and the latter limit is even closer to T_c to an extent unlikely to be met in practice for any mixture. These limits therefore comfortably bracket the range within which shear gradients are observed.

The results of the viscosity measurements were fitted to equation (2.21) using the nonlinear least-squares fitting procedure of Bevington (1969) incorporated into the program viscfit (see appendix) similar to that used by Davies (1988). The critical exponent was set at the RG theory value y = 0.040 and the fitting was carried out both with and without incorporating the effect of the shear gradient. For the case of fitting with the shear-gradient dependence, the correlation length amplitude ξ_0 was obtained. The experimental arrangement using the actual mixture in the viscosity cell did not permit the determination of T_c to better than 0.05 K. Thus in the fitting procedure T_c and ξ_0 were determined by floating the background parameters A and B and seeking the set which gave a minimum χ^2 for a systematic series of fixed T_c and ξ_0. It transpired that the optimum value of T_c was 22.38_5°C. The values of A and B obtained for the one-phase mixture both with and without shear-gradient correction, and for the mean of the viscosities of the coexisting liquid phases are shown in Table 2.8.

Table 2.8: The results of fitting the shear viscosity of hexane + perfluorohexane to equation (2.21), both without and with the correction for the shear-gradient dependence of equation (2.26), assuming the optimum $T_c = 22.38_5$°C and with y = 0.040.

hexane + perfluorohexane	10^3A /cP	B /K	ξ_0 /Å	$10^6\chi^2$
one phase without shear-gradient correction	17.24_8	876.1_4	-	20
one phase with shear-gradient correction	14.26_6	934.2_1	6.4	1
mean of coexisting phases	0.2079_6	$2167._3$	-	3

The experimental results for the one-phase mixture and for the mean of the coexisting phases are displayed as log η *versus* log ε in Figures 2.6 and 2.7, respectively. The functions describing the background viscosity A exp (B/T), the background viscosity + the critical divergence A exp (B/T) ε^{-y}, and the background viscosity + the critical divergence + the shear-gradient dependence A exp (B/T) ε^{-y} [1 - $\Delta(\lambda_{eff})$] are also plotted. The latter function is calculated from equations (2.25)-(2.27) by evaluating λ_{eff} and $\eta(\lambda_{eff})$ over the range of temperatures for which $0.1 \leq \lambda_{eff} \leq 20$. The background viscosity is dependent on the absolute temperature and is essentially independent of ε for $\varepsilon < \sim 10^{-3}$.

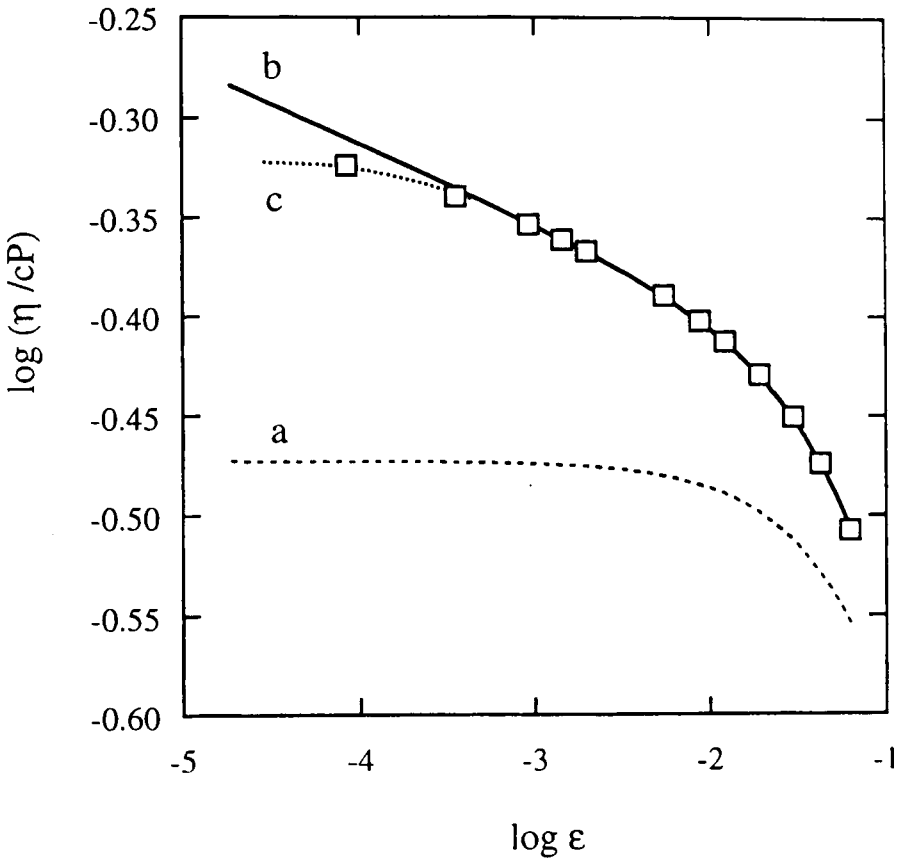

Figure 2.6: The shear viscosity η of the one-phase critical mixture (□) of hexane + perfluorohexane as a function of the temperature response function $\varepsilon = |T_c - T|/T_c$ near the optimum upper critical solution temperature $T_c = 22.38_5$°C displayed as log η *versus* log ε. Curves a = background; b = a + critical divergence; and c = b + shear-gradient dependence.

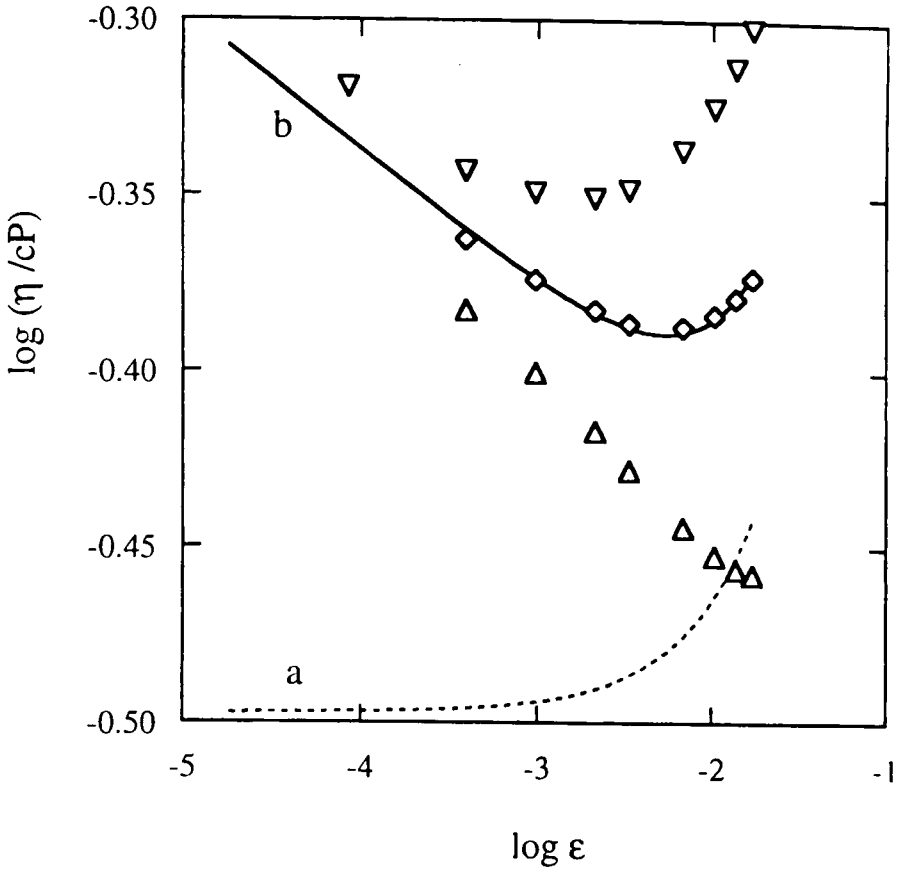

Figure 2.7: The shear viscosity η of the coexisting phases of hexane + perfluorohexane as a function of the temperature response function $\varepsilon = |T_c - T|/T_c$ near the optimum upper critical solution temperature $T_c = 22.38_5$°C displayed as log η *versus* log ε. Curves a = background; and b = a + critical divergence. The mean of the viscosities of the coexisting phases (◊) and the viscosities of the upper (△) and lower (▽) phases are plotted.

The flattening apparent in Figure 2.6 for the experimental points closest to T_c suggests the need for applying the Oxtoby shear-gradient correction. This is confirmed by the value $\lambda_{eff} = 2.6$ for the point closest to T_c, well inside the range $0.1 \leq \lambda_{eff} \leq 20$ within which Oxtoby's calculations identify shear-gradient sensitivity. From the analysis the correlation length amplitude is around 6 Å; the precise evaluation of this quantity depends on a very accurate determination of T_c. The error in our T_c is *ca.* ±0.25 K and within this range around the optimum fitted T_c ξ_0 varies from 4 to 7 Å, although at $T_c = 22.38_5$°C the optimum value is $\xi_0 = 6.4$ Å. A practical assessment of ξ_0 therefore is perhaps $\xi_0 = (5.5 \pm 1.5)$ Å. This compares a little unfavourably with the value (3±1) Å reported by Pozharskaya *et al.* (1984) from light-scattering measurements and even more with the value of Schulz (1996) of (1.9±0.1) Å from turbidity measurements. Shear viscosity measurements may not be the most appropriate method to obtain an accurate value of ξ_0 since the viscosity exhibits only a weak anomaly near the critical point and

various assumptions, see section 2.1.3.3, are made for the equation describing the anomaly and the form of the background term.

2.4.2 Viscosity amplitude ratios

The critical amplitude of the shear viscosity, A exp (B/T) in equation (2.21), is different for different paths to the critical point. The three different paths and their symbols are:

η_+^0 along the critical isochore (constant composition path in the single phase)

$\eta_\sim^0$ along the critical isotherm

η_-^0 along the coexistence curve.

The amplitude ratios η_-^0 / η_+^0 and $\eta_\sim^0 / \eta_-^0$ at the critical point are universal. Calmettes (1979) has reported the theoretical values $\eta_-^0 / \eta_+^0 = 0.950$ and $\eta_\sim^0 / \eta_-^0 = 0.986$. Our value of η_-^0 / η_+^0 for hexane + perfluorohexane, calculated using the values of A and B in Table 2.8 and including the shear-gradient effect for the single phase, is 0.946±0.005, which is within 0.4% of the theoretical value. The results for η_-^0 / η_+^0 should be essentially independent of the fitting of the shear-gradient contribution, since although there is a slight dependence on the choice of T_c and ξ_0 the variation is smaller than our quoted uncertainty. The final value agrees well with the values reported by Maczek *et al.* (1990) for the four mixtures previously reported from our group and with the theoretical value.

2.5 Summary

The near-critical shear viscosity of a mixture of hexane + perfluorohexane of critical composition, x(perfluorohexane) = 0.370, has been measured as a function of temperature both in the single phase up to 19 K above the upper critical solution temperature $T_{UCS} = 22.38_5$°C and for the coexisting phases up to 5 K below T_{UCS}. The viscosity exhibited the expected anomalous divergence at the critical point.

For the single-phase mixture the measured viscosities were corrected for shear-gradient effects in the vicinity of the critical point. The value obtained for the correlation length amplitude $\xi_0 = (5.5\pm1.5)$ Å is somewhat higher than reported in other studies. The value for the ratio of the limiting viscosity amplitudes along the coexistence and constant critical composition paths $\eta_-^0 / \eta_+^0 = 0.946\pm0.005$ is in good agreement with Calmettes' theoretical prediction of 0.950.

Along the constant critical composition and coexistence paths the viscosity has been reasonably well characterised, both experimentally and theoretically. Along the critical isotherm, however, the viscosity has received less attention and thus deserves further investigation. The exact form of the viscosity, and in particular the representation of the background viscosity in the absence of any critical effects, has still to be determined.

CHAPTER 3: MICROSCOPIC VISCOSITY OF NEAR-CRITICAL MIXTURES

3.1 Microviscosity

The anomalous behaviour of the *macroscopic* shear viscosity near a critical endpoint CEP has been described in the previous chapter. The main aim of the present investigation was to determine the *microscopic* viscosity or microviscosity, i.e. the *local* resistance to rotation or translation of a given molecule, in binary mixtures for which the macroscopic viscosity was known. The ultimate objective was to compare the behaviour of the microscopic and the macroscopic viscosities near a CEP. In particular, evidence was sought for any near-critical anomaly at the molecular level that mirrored the well-characterised anomaly in the viscosity at the macroscopic level.

The techniques used to study the microscopic viscosity commonly involve the measurement of the rotational correlation time τ_R of a particular species. The rotational correlation time–effectively the average time taken to rotate through a given angle–is affected by the viscosity of the environment surrounding the molecule. In this study, fluorescent dyes were used to probe the microscopic viscosity. Results are presented here for the measurements of τ_R of various fluorescent dyes in binary liquid mixtures close to their CEPs.

In addition to providing a general measure of the solvent viscosity at a microscopic level, fluorescent molecules of differing lengths may also allow the correlation length ξ_0–which diverges to infinity at the CEP–to be probed. The local environment around a fluorescent molecule may change when ξ_0 becomes comparable to the length of the molecule and this change may possibly be detected. However, there are many properties of the solvent and the probe which influence τ_R and this more refined aspect of study was not pursued in detail here.

An introduction to fluorescence is given in an annexe to this thesis. We turn now to the methods for obtaining a measure of the microscopic viscosity–in particular fluorescence depolarisation since this was used in the present study–and the models used to relate τ_R to the microscopic viscosity.

3.1.1 Methods for obtaining the microscopic viscosity

There are two main methods for obtaining a measure of the viscosity of a solvent on a microscopic level using fluorescence probes. The first, fluorescence depolarisation, involves the measurement of the rotational correlation time τ_R, as discussed above. The second method involves the measurement of the fluorescence lifetime of the probe in a solution with a known concentration of a quencher species; the solvent viscosity affects the rate of translational diffusion of the quencher and fluorescent species and hence the fluorescence lifetime. These methods are discussed in the following sections.

In addition to fluorescence depolarisation, various other methods including nuclear magnetic resonance NMR, electron spin resonance ESR, light scattering, and dielectric and laser relaxation methods can be used to measure τ_R. The values of τ_R can again be

related to the microviscosity, although the language of microviscosity is less common in these other techniques for studying molecular motion. NMR (see for example, Lenk, 1986) is particularly useful since τ_R is measured for the bulk liquid and this route is to be investigated in future extensions to this work. In the technique of ESR the rotational correlation times of free radicals–often nitroxides–are obtained in solution (Marsh, 1989; Marsh and Horváth, 1989). This method should also be of use to probe the microviscosity of our near-critical mixed liquids if suitable spin-labelled molecules can be selected. Recent ESR studies of reorientational motion in glass-forming liquids have been reported by Kowert *et al.* (1996). They observed that the agreement was generally good between their rotational correlation times and those obtained for the same solvent by dielectric relaxation and light scattering techniques. Molecular rotation in liquids studied by methods such as depolarised Rayleigh and Raman scattering has been reviewed by Kivelson and Madden (1980) and Steele (1976).

3.1.1.1 Fluorescence depolarisation

In the present form of time-resolved fluorescence depolarisation experiment the sample is excited by vertically-polarised light and the fluorescence is observed at right angles to the direction of the exciting beam all in the laboratory horizontal plane. Single-photon counting is used to record the fluorescence polarised vertically (parallel) and horizontally (perpendicular) with respect to the electric field vector of the excitation beam as a function of time t after the excitation pulse. The measurement of the fluorescence depolarisation leads to the emission anisotropy r(t) which can be fitted to a sum of exponentials to obtain the rotational correlation times τ_R. The rotational correlation time is a measure of the microscopic viscosity; for a quasi-spherical molecule obeying the Stokes-Einstein-Debye relation τ_R is directly proportional to the viscosity/temperature ratio. This method is discussed in more detail in section 3.1.2.

3.1.1.2 Fluorescence lifetime and quenching

The microscopic viscosity of a system can be determined by fluorescence lifetime measurements. A fluorescent dye (A) dissolved in a liquid mixture and excited with light will fluoresce:

$$A + h\nu \rightarrow A^*$$

$$A^* \rightarrow A + h\nu \qquad \text{fluorescence rate constant} = k_F$$

The excited dye molecule A* can also undergo intramolecular excited state deactivation:

$$A^* \rightarrow A \qquad \text{deactivation rate constant} = k_D$$

or bimolecular excited state deactivation with a quencher molecule Q:

$$A^* + Q \rightarrow A + Q^* \qquad \text{quenching rate constant} = k_q$$

(Demas, 1983).

If a quencher Q is present in greater concentration than A*, the fluorescence lifetime, τ_F, is related to the concentration of quencher by:

$$\tau_F = 1/(k_F + k_D + k_q [Q]). \tag{3.1}$$

The fluorescence lifetime can be measured at different known concentrations of quencher Q at constant temperature to obtain k_q. As molecules of A* and Q have to diffuse together, k_q is a diffusion rate, and is related to the microscopic solvent viscosity η by:

$$k_q = \frac{8RT}{3\eta} \tag{3.2}$$

where R and T have their usual meanings of the gas constant and the thermodynamic temperature.

Oxygen is the most efficient known quencher, but its concentration is not usually well defined. The diffusion of oxygen is also abnormally fast. Compounds containing heavy atoms such as halogens are also used as quenchers, e.g. MeI or CCl_4, and if these are used the samples must be deoxygenated. Other examples of quenchers are given by Ware and Andre (1983).

It seems likely that this translational diffusion route to the microscopic viscosity is most likely to reflect the true viscosity as the probe molecule and the quencher have to diffuse through the solvent rather than just rotate. In the rotational diffusion method, factors such as the solvent structure become more important and these are discussed in the following section. The disadvantages of the translational diffusion method, particularly in the case of our near-critical liquids, are that in addition to a dye a quencher species is also added, so effectively introducing impurities into the system, albeit at low concentrations. The concentration of quencher species must also be known accurately and so the amount of oxygen remaining in each sample after degassing needs to be the same in each case and this can prove difficult. We have therefore used the rotational route to the microviscosity and we now turn to this in more detail.

3.1.2 Details of fluorescence depolarisation

This section gives an account of the technique of fluorescence depolarisation to obtain the rotational correlation time τ_R. We discuss the depolarisation of fluorescence before turning to specific experimental details for time-resolved fluorescence measurements.

3.1.2.1 Polarised light and rotational depolarisation

Plane-polarised light has its electric vector in a particular plane. When plane-polarised light enters a sample it induces oscillations in the electrons of the molecules and the absorption of the light by a particular molecule depends on the orientation of its

transition axis or moment relative to the electric vector of the light, see Figure 3.1. If the molecule is oriented with its transition axis parallel to the electric vector then the probability of absorption is high and absorption takes place readily; if the transition axis is perpendicular to the electric vector then the probability of absorption is zero. To consider the probability of absorption at intermediate orientations the amplitude A of the electric vector can be resolved into two vectors at right angles to each other. In a direction at an angle θ the effective amplitude of vertically polarised exciting light is thus $A\cos\theta$. Since the intensity of the light is proportional to A^2, the intensity at an angle θ is $A^2\cos^2\theta$ and the probability of absorption in this direction is $\cos^2\theta$ (Parker, 1968).

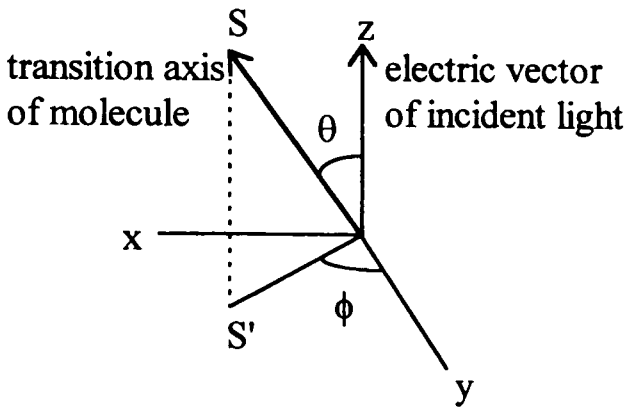

Figure 3.1: The orientation of the transition axis relative to the electric vector of the incident light. S' is the projection of S onto the xy plane.

The transition moment for absorption is not necessarily the same as that for emission but we consider this to be the general case for the purpose of the present discussion. In a solution all the fluorescent probe molecules are generally oriented at random. When polarised light is incident on the solution some of the molecules absorb the light with a $\cos^2\theta$ probability as described above. They are thus excited to a higher electronic state if the incident radiation is of the appropriate frequency corresponding to an energy gap between the ground and excited state electronic levels. The molecules can lose their energy by emission of light and the polarisation of the light emitted depends on the fluorescence lifetime and on how far the molecule rotates in the time period before fluorescence occurs.

The fluorescence polarisation, p, is defined as:

$$p = \frac{I_{\parallel} - I_{\perp}}{I_{\parallel} + I_{\perp}} \tag{3.3}$$

where $I_{\parallel}$ and $I_{\perp}$ are the emission intensities parallel and perpendicular to the plane of the electric vector of the incident light.

The fluorescence anisotropy r(t) is also used as a measure of the fluorescence polarisation:

$$r(t) = \frac{I_{\parallel} - I_{\perp}}{I_{\parallel} + 2I_{\perp}} = \frac{2p}{3-p} \tag{3.4}$$

where $I_{\parallel} + 2I_{\perp}$ is the total emission.

The principal polarisation, p_o, is the polarisation in the absence of any depolarising factors such as rotation. For molecules with parallel transition moments for absorption and emission $p_o = {}^1/_2$ and for molecules with the transition moments for absorption and emission oriented at right-angles $p_o = -{}^1/_3$ (Parker, 1968). These values are obtained by integrating the intensities of the vertical and horizontal components of the light emitted over all possible values for the angles θ and ϕ, see Figure 3.1, defining the orientation of the transition moment with respect to the parallel and perpendicular directions. The corresponding limiting values for r(t) are 0.4 and -0.2, thus a negative anisotropy can sometimes be observed. For the dyes used in our work the limiting values for r(t) were always positive. Values of r(t) apparently greater than 0.4 are often attributed to the detection of scattered light.

The relationship between the observed polarisation p and the principal polarisation p_o for vertically-polarised incident light is:

$$(1/p - 1/3) = (1/p_o - 1/3)\,(3\tau_F/\tau_R + 1) \tag{3.5}$$

where τ_F is the fluorescence lifetime and τ_R is the rotational relaxation time or rotational correlation time.

3.1.2.2 Time-resolved fluorescence

Our experiments were carried out at Daresbury Laboratory on station 12.1, where the incoming light is vertically polarised and a particular wavelength can be selected. The fluorescence is collected at right-angles to the direction of the incident beam so that the collection of stray light due to reflections is minimised.

The fluorescence lifetime is determined by measurement of the fluorescence by single-photon counting techniques. In general, part of the incoming signal is sent *via* a photomultiplier (PM) tube and a constant fraction discriminator (CFD) to start a signal at the time-to-amplitude converter (TAC). The remaining light enters the sample and the fluorescence is detected by a PM tube and a CFD and stops the signal at the TAC. In single-bunch mode, the synchrotron, see section 3.2, emits a pulse of light every 320 ns. Each of these pulses is used to activate the start signal and to induce a single-photon fluorescence event in the sample. The intensity of the fluorescence is kept low by using dilute samples and by adjusting the slit widths; this ensures that the probability of occurrence of a stop pulse is proportional to the probability of a photon being emitted.

The amplitude of the output pulse from the TAC is proportional to the time between the start and stop pulses. The signal is sent to a multi-channel pulse height analyser (MCPHA) which places a count in the appropriate channel. A time calibration allows the channels to be converted to times. The fluorescence is monitored over a period of time to build up a statistical picture of the events. The fluorescence decay is exponential, or if more than one component is present a sum of exponentials is observed.

The instrument response function is usually recorded using Ludox, an aqueous colloidal suspension of silica, at the main emission wavelength of the sample. The Ludox acts as a scattering solution and records the response time of the instrument at the selected wavelength. Scattered light effectively comes straight out after it enters the sample and thus the detection of the difference between the start and stop pulses is a measure of the instrumental factors in the detection process. Ideally, the instrument response should be a sharp peak but broadening is invariably observed due to the failure of the photomultiplier to always respond in exactly the same way. This is attributed to the 'jitter in the transit time of the electrons through the photomultiplier'. To determine the fluorescence lifetime of a dye in a sample, the observed decay has to be deconvoluted from the instrument response.

On station 12.1 the fluorescence is effectively recorded backwards and the plots on the screen show the peak on the right-hand side decaying towards the left-hand side of the screen. The pulse rate from the synchrotron is high–approximately 3×10^6 s^{-1}–so there are too many pulses for the electronics to handle. The fluorescence count rate is adjusted by altering the slit width so that the count rate is no greater than 30,000 s^{-1}. Instead of measuring the time delay from the pulse to the detected fluorescence, the time is counted from the detected fluorescence to the next exciting pulse. In this method the time gap for most of the processes occurring is larger and the detection appears backwards with the peak at long channels as it is furthest in time from the next pulse.

Some level of background is observed in an experiment. This should only be due to thermal electrons leaving the cathode of the PM tube, which is cooled to reduce this; however, higher background levels may be due to the detection of stray light. Before an experiment the box is made as light-tight as possible. The filters may not be perfect and may let in some of the exciting light, particularly if the excitation wavelength is close to the cut-off wavelength of the filter on the exit side. Filters may also be used on the excitation side to help reduce the background level.

During an experiment to determine the fluorescence lifetime of a sample, the polariser is set to the magic angle, $\alpha = 54.7°$ to the vertical, for which $\sin^2\alpha/\cos^2\alpha = \tan^2\alpha = 2$, to effectively collect the total emission $I_{\parallel} + 2I_{\perp}$. (The intensity is proportional to the square of the amplitude, i.e. $I_{\parallel} \propto \cos^2\alpha$ and $I_{\perp} \propto \sin^2\alpha$.) When the decay of the fluorescence anisotropy is measured the polariser is set to move freely and is activated by the computer during the measurement so that it sets to record the fluorescence polarised

parallel and vertical in turn for a given dwell time in each position. The incident vertically polarised light excites the fluorescent species in the sample solution with a probability proportional to $\cos^2\theta$, where θ is the angle between the orientation of the transition axis of the fluorophore and the vertical, as shown above in Figure 3.1. In an experiment to measure rotational correlation times τ_R the fluorescence polarised parallel and perpendicular with respect to the exciting light is recorded and the anisotropy calculated is then fitted to one or more exponentials to obtain τ_R:

$$r(t) = \sum_i r_i(0) \exp(-t / \tau_{R,i}) \tag{3.6}$$

where $r_i(0)$ is the anisotropy at time zero. Models for the relationship between τ_R and the solvent viscosity are described in the next section.

3.1.3 Models for molecular rotation

Several models have been used to describe the molecular rotation of a solute molecule in a liquid, although some have been more successful than others in accurately predicting the values or trends observed experimentally.

The models most often used are based on hydrodynamic models, which treat the solute as a Brownian particle dissolved in a continuum solvent (Ravi and Ben-Amotz, 1994). Approximations can be made to the basic Stokes-Einstein-Debye (SED) equation by introducing extra parameters to describe the 'stick' and 'slip' hydrodynamic boundary conditions. The hydrodynamic models are relatively simple and work surprisingly well given that for a particular solute the rotational correlation time is described only by the solvent temperature and viscosity–which are generally readily available. In some cases, however, deviations from the hydrodynamic boundary conditions are observed and 'superstick' and 'subslip' are invoked to explain this non-hydrodynamic behaviour. The solvent can no longer be described as a continuum and molecular structures have to be considered. Quasi-hydrodynamic models and models based on kinetic theory have been used to treat this behaviour.

Some of the factors involved in hydrodynamic and quasi-hydrodynamic models are discussed below.

3.1.3.1 Stokes-Einstein-Debye equation

The Stokes-Einstein-Debye (SED) equation (Einstein, 1905, 1906; Bartoli and Litovitz, 1972) relates the rotational correlation time τ_R of a spherical solute of volume V to the temperature T and viscosity η of the solvent by:

$$\tau_R = 1/(6D_s) = \eta V/kT \tag{3.7}$$

where D_s is the rotational diffusion constant. A modified form of the equation (Perrin, 1934) takes into account the shape of the molecule by introducing a shape factor f and also includes a boundary condition parameter C dependent on the solute, the solvent and the concentration:

$$\tau_R = (\eta V f C/kT) + \tau_0 \tag{3.8}$$

where τ_0 is the rotational reorientation time at zero viscosity (Roy and Doraiswamy, 1993).

3.1.3.2 Stick limit

In the stick approximation, the solvent is treated as a continuum and a small solvent layer moves with the solute, effectively increasing its size. There is thus strong coupling between the solvent and the solute. The SED equation applies for the stick limit and is usually reasonable for large solute molecules (Ben-Amotz and Drake, 1988). In the stick limit the parameter C in equation (3.8) is set equal to unity.

3.1.3.3 Slip limit

For solute molecules of comparable size to, or smaller than, the solvent molecules, the stick approximation does not hold and the slip limit applies. The molecules rotate faster than predicted by the stick condition and a layer of solvent molecules no longer moves with the solute. Rotation of a non-spherical molecule depends only on displacing some of the surrounding solvent molecules. Spheres or spheroids rotating about a symmetry axis thus experience no frictional drag (Dote *et al.*, 1981). In the slip limit the value of the boundary condition parameter C_{slip} is less than unity (Roy and Doraiswamy, 1993). A transition from slip to stick as a function of increasing solute size has been illustrated by Zwanzig (1978) using a bumpy cylinder model. Values of stick/slip frictional coefficients have been calculated for prolate and oblate spheroids, effectively stretched or flattened spheres, by Hu and Zwanzig (1974) and for ellipsoids by Youngren and Acrivos (1975). The effects of slip and stick on rotational correlation times are shown in Figure 3.2 along with the effects of superstick and subslip, which are discussed in the following section.

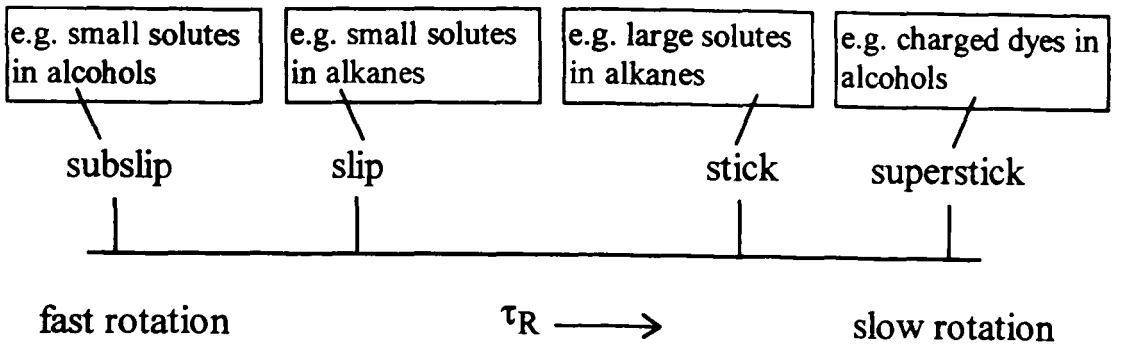

Figure 3.2: The relative effects of subslip, slip, stick and superstick limits on the rotational correlation time τ_R.

3.1.3.4 Superstick and subslip

In the superstick condition the rotational reorientation time of the solute is greater than in the stick approximation, i.e. the solute rotates slower then predicted by the stick condition. This behaviour may occur for charged dye molecules in alcohol solvents (Williams *et al.*, 1994). Two concepts proposed to explain this slower rotation are, i) a solute-solvent interaction increasing the effective volume of the solute molecule, or ii) a long-range dipolar interaction between the solute and the solvent causing an extra frictional effect called dielectric friction (Dutt and Doraiswamy, 1992).

In the subslip case, the rotational reorientation times are smaller than for the slip prediction, i.e. the solute rotates even faster. The parameter C is thus less than C_{slip} (Wirth and Chou, 1991). In this condition the solute is considered to reside in gaps or cavities in the solvent structure, thereby experiencing less resistance to rotation. The solvent is no longer considered to be a homogeneous continuum and this effect can occur in certain solvents if the probe molecules are smaller than the solvent molecules (Dote *et al.*, 1981). It is surprising that under subslip conditions the rotational correlation times also show a linear relationship to the viscosity/temperature ratio as predicted by hydrodynamic theories (Kivelson and Madden, 1980).

3.1.3.5 Gierer-Wirtz model

The Gierer-Wirtz (GW) theory (Gierer and Wirtz, 1953) treats a spherical solute as being surrounded by concentric shells of spherical solvent particles, each shell moving at a constant angular velocity which is greatest for the shell closest to the probe molecule and decreases with the distance of the shell from the probe (Roy and Doraiswamy, 1993). The theory takes into account the relative sizes of the solute and solvent molecules and allows the discontinuous nature of the solvent to be treated. Modified values for the C parameter can be calculated within this quasi-hydrodynamic microfrictional theory. However, a deficiency of the theory is that it does not take into account the free space in the solvent structure.

3.1.3.6 Dote-Kivelson-Schwartz model

The Dote-Kivelson-Schwartz (DKS) model (Dote *et al.*, 1981), also termed the 'free space model' is another quasi-hydrodynamic model that takes account of the relative sizes of the solvent and solute molecules but also includes the effects of the free spaces in the solvent structure. A comparison of the DKS model with the GW and SED models in relation to the predictions of rotational correlation times of probe molecules in alcohols, alkanes and nitriles has been made by Roy and Doraiswamy (1993).

More sophisticated models than the GW and DKS models require statistical quantities which may be difficult to obtain, so the main attraction of the GW and DKS models is their relative simplicity (Ben-Amotz and Drake, 1988).

We turn now to the difference in behaviour observed for various solutes in alcohols and alkanes and the models used to describe the trends.

3.1.3.7 Rotation in alcohols versus alkanes

When the rotational correlation times of relatively small neutral solutes dissolved in alcohols and alkanes of the same viscosity at the same temperature are compared the solutes are found to rotate faster in the alcohols than in the alkanes (Ben-Amotz and Scott, 1987). This behaviour is inconsistent with hydrodynamic theories which predict that for a given solute the rotational correlation times should depend only on the temperature and solvent viscosity.

The rotation of small solutes in alkanes is approximately described by the slip boundary condition. In alcohols, however, the faster rotation leads to subslip. The difference in the rotational correlation times in alcohol and alkane solvents decreases with increasing size of the solute. In the limit for *very* large neutral molecules the rotational correlation times are the same and are consistent with near-stick conditions (Ben-Amotz and Drake, 1988). In both alkane and alcohol solvents plots of the rotational correlation time *versus* viscosity at a given temperature are linear with a small positive intercept at zero viscosity, attributed to the free rotation time of the solute (Ben-Amotz and Scott, 1987).

The fast rotation in alcohols may be due to either structural or dynamic features of the microscopic environment around the solute molecule (Ben-Amotz and Scott, 1987). For example, the hydrogen-bonding structure of the solvent may affect solute rotation in some way. The DKS model has been used to qualitatively predict the effects of the rotation of small solutes in alkanes and alcohols and explains the difference between the rotational correlation times in the two types of solvent in terms of the larger free volume in alcohols than alkanes (De Backer *et al.*, 1996).

Some of the molecules studied and observed to show subslip behaviour in alcohols are relatively large compared to the solvent size, for example 9,10-diphenylanthracene in butanol (Ben-Amotz and Scott, 1987). In these cases, if fluctuations of local number

density occur in the solvent on a greater timescale than the rotational diffusion of the solute then the solute experiences a reduction in the microscopic friction and does not sample the full shear viscosity of the solvent. This type of explanation may be more realistic for fairly large solutes than the size-effect model as it seems less likely that the larger solutes will be able to fit into stable cavities in the solvent structure.

For very large solutes, the changeover towards the stick prediction can be explained by both the dynamic and structural models; the longer rotational time of a larger solute compared with the short timescale fluctuations of the solvent may cause it to experience the full fluctuations and shear viscosity of the solvent, or the solute may be too large to fit into cavities in the solvent structure and so does not experience a reduced friction. It should be noted that other possible effects of alcohols *versus* alkanes may stem from the amphiphilic nature of alcohols. Alcohols thus have the ability to solvate molecules primarily either by the alkyl chain or by the hydroxyl groups.

3.1.4 Some previous work on microviscosity and microstructure using fluorescence techniques

This section briefly describes some of the previous work that has been carried out to determine the microviscosity and microstructure of various solvents and probe environments. The examples are selected to illustrate particular aspects.

Much of the work investigating the microviscosity has been carried out either in pure solvents or in micellar solutions. In micellar solutions the rotational correlation times or fluorescence lifetimes can provide information on the nature of the probe environment in the micelle and the local viscosity around the probe.

The microviscosity of the interior of cetyltrimethylammonium bromide (CTAB) micelles in aqueous solution has been investigated by measuring the fluorescence depolarisation of perylene or 2-methylanthracene (Shinitzky *et al.*, 1971). Fluorescence quenching experiments for pyrene in aqueous CTAB solutions with water-soluble quenchers such as the bromide counterions have also been carried out to study the diffusion rate of the probe in the micellar core (Grätzel and Thomas, 1973).

Pyrene has been used in many studies to probe the microscopic environment. An excimer, or excited dimer, forms in concentrated solutions. The formation of the dimer is controlled by the rate of diffusion of two pyrene species in the solution. The viscosity of the solvent affects the rate of diffusion and by measuring the ratio of intensities of the excimer and monomer peaks in the spectrum a measure of the microscopic viscosity can be obtained. In alkyltrimethylammonium bromide micelles in aqueous solution, pyrene molecules reside in the hydrocarbon interior of the micelles and can thus probe their microviscosity (Pownall and Smith, 1973). The micellar nature of poly(ethylene oxide) polymers endcapped with hydrophobic substituents (Yekta *et al.*, 1993) and poly(ethylene oxide)-poly(propylene oxide) copolymers (Nivaggioli *et al.*, 1995) has

been probed using pyrene and a similar probe, dipyme. Pyrene excimer formation has also been used to study molecular diffusion in thin surfactant films (Papoutsi *et al.*, 1995) and the viscosity of the interface layer of a sapphire-polymer solution (Hamai *et al.*, 1995).

Another effect of pyrene is known as the Ham effect. In polar solvents the intensity of the weak symmetry-forbidden (o-o) band of the pyrene monomer, band I, is enhanced relative to its intensity in nonpolar solvents whereas the intensity of band III shows relatively little change. This effect was first observed by Ham (1953). The intensity ratio of the bands I_1/I_3 provides a measure of the micropolarity of the pyrene environment and has been used *inter alia* to study the hydrophobic regions of micelles.

In addition to providing information on the microviscosity inside micellar structures, fluorescence techniques have been used to investigate the micellar microenvironment in terms of polarity, rigidity, aggregation number and micelle size (Caldararu *et al.*, 1994). Probes can also be selected to study the surface of micelles. The polarity of the surface of aqueous micelles has been investigated using 4-aminophthalimide which binds to the micelle-water surface (Saroja and Samanta, 1995). The formation and stoichiometry of inclusion complexes of a fluorescent probe in cyclodextrin have been examined by time-resolved fluorescence and the microviscosity calculated (Jobe *et al.*, 1988).

Interfaces in surfactant, emulsion and other solutions can also be probed by fluorescence. Fluorescence anisotropy measurements of a modified 1,6-diphenyl-hexa-1,3,5-triene (DPH) probe have been used to study the surface rigidities of emulsion particles at the phospholipid-water interface (Saito *et al.*, 1995). Molecular dynamics computer simulations have been carried out to investigate the possibility of using time-resolved fluorescence to study the microscopic structure of a liquid-liquid interface (Michael and Benjamin, 1995).

3.2 Experimental details

3.2.1 Synchrotron at Daresbury Laboratory

The experiments were carried out on station 12.1 at the CCLRC's Daresbury Laboratory using light from the Synchrotron Radiation Source (SRS) operated in single-bunch mode.

Synchrotron radiation is electromagnetic radiation produced when electrons or positrons move at relativistic energies in a circular path. At Daresbury the synchrotron is an electron synchrotron. The electrons are first linearly accelerated to 12 MeV then injected into a booster synchrotron where they are accelerated to 600 MeV before being injected into the 2 GeV storage ring. Bending magnets are used to define the curved path of the electrons and at each magnet synchrotron radiation is emitted.

The SRS is operated most of the time in multi-bunch mode, but three to five three-day sessions in each six month allocation period are generally reserved for single-bunch operation. In multi-bunch mode 160 bunches of electrons circle the storage ring at 2 ns intervals. In single-bunch operation a single bunch of electrons circles the ring passing a given point at 320 ns intervals. The pulse width is generally 180 ps fwhm (full width at half maximum). The maximum current stored in multi-bunch mode is usually 250-300 mA and in single-bunch is 25-30 mA. In both modes of operation the synchrotron storage ring is generally refilled each morning and the current gradually decreases throughout the day, the lifetime being about 20-30 hours.

The radiation from the SRS covers a wide range of wavelengths from x-rays to far-infrared. On station 12.1 the wavelengths that can be selected lie in the UV and visible regions. The station is mainly used for time-resolved fluorescence work in single-bunch operation. The use of synchrotron radiation for time-resolved fluorescence experiments has been discussed by several authors (Lopez-Delgado *et al.*, 1974; Mills, 1984; Munro *et al.*, 1985; Brocklehurst, 1987).

3.2.2 Data collection and analysis

The fluorescence polarised parallel and perpendicular with respect to the exciting light is recorded by time-resolved single-photon counting, as described in section 3.1.2. The fluorescence is detected using Mullard photomultiplier tubes fitted with Products for Research, Inc. coolers. The tubes available are of two types and the selection of a tube is determined by the wavelength of the fluorescence for a given experiment. The blue tube (XP4278B) is most sensitive at the shorter wavelengths 220-520 nm and the red tube (PM2254) at the longer wavelengths 520-800 nm. The data are analysed on the Daresbury Laboratory Convex C220 computer using the program 'fluor', which deconvolutes the data from the instrument response function.

The anisotropy r(t) is obtained from the fluorescence intensities parallel, $I_{\|}$, and perpendicular, $I_{\perp}$, to the plane of polarisation of the incident beam:

$$r(t) = \frac{I_{\|} - I_{\perp}}{I_{\|} + 2I_{\perp}} = \sum_i r_i(0) \exp(-t / \tau_{R,i}) \qquad (3.9)$$

and thus the rotational correlation times τ_R can be determined. The fluorescence lifetime τ_F can be obtained by direct measurement of the fluorescence with the polariser set at the magic angle (54.7°) or from the parallel and perpendicular fluorescence intensities:

$$I_{\|} + 2I_{\perp} = \sum_i \alpha_i \exp(-t / \tau_{F,i}) \qquad (3.10)$$

where $I_{\|} + 2I_{\perp}$ is the total emission and α is the intensity at time zero.

After each run the instrument response, or prompt, is recorded using Ludox, a colloidal suspension of silica in water supplied by Du Pont. The details of the use of the instrument response have been described in section 3.1.2. The instrument response function is generally 0.7 ns fwhm, due to the beam and the photomultiplier. The timing electronics tend to drift with time; this causes a change in the prompt which therefore has to be recorded at regular intervals, usually after each measurement.

3.2.3 Apparatus

The cells and cell holders used in these experiments are described in the following sections. The experiments were carried out between March 1995 and August 1996. In July 1996 a new copper cell holder was completed to replace the brass holder used in the earlier measurements. The new holder improved the temperature control of our mixtures and was used to repeat some of the previous measurements.

3.2.3.1 Cells

The cells containing the liquid samples are made from either square Pyrex tubing, sealed at one end to form a cuvette, or Pyrex cuvettes (Scientific Glass), joined at the open end to circular Pyrex tubing leading to a Teflon tap, which seals the sample in the cuvette, and a Quickfit joint, for attachment to a vacuum line. The cells made from the Pyrex tubing are particularly suitable for fluorescence lifetime measurements, for which the exclusion of oxygen is important, since the cells can be placed directly in liquid nitrogen during a freeze-pump-thaw degassing cycle. The cuvettes made from the tubing measure 12.3 x 12.3 mm and slot a little too easily into the cell holders, thus achieving only poor thermal contact with the heated cell holders unless packed by brass corner pieces. The standard cuvettes are slightly larger and fit better; these cells are better for anisotropy work, in which degassing of the sample is less vital.

In both types of cell, due to the positioning of the tap, a vapour space is present above the liquid sample. When the brass cell holder was used the upper part of the cell was heated slightly by applying 6 V to two 50 W resistors in parallel–attached with Terry clips just below the tap–since the top of the cell protruded out of the top of the holder. This extra heating was not necessary with the new copper cell holder since the insert holding the cell was set down into the copper block and the thermal contacts between the insert, the cell and the block were also very good.

3.2.3.2 Cell holders

The cell holder on station 12.1 used in most of the measurements is a small brass block, with a slot for the cuvette measuring 12.5 x 12.5 mm and of height 40 mm. The block has slots cut in three of the vertical sides to allow the beam to enter, fluorescence to exit at right-angles and the direct beam be dumped. The fourth side of the block is fitted with

a Peltier element and the temperature of the block is controlled by a Holm Lea Electronics unit. The entire arrangement is contained in a large box, with black spacers to reduce stray reflections, which is covered with a black cloth. On top of the box a top hat arrangement is fitted to give greater clearance of the box from our cells.

There are several disadvantages with this type of cell holder for our work, since we require precise temperature control very close to the critical point. Particularly serious are the open sides of the holder which need to be covered, e.g. with microscope slides, to attempt to reduce heat loss. A further difficulty is the requirement in our experiments to alter the height of the cell holder to study coexisting phases. The new cell holder was designed and built principally to improve the thermal stability of our near-critical mixtures. The features of the new holder include i) Peltier elements on each side of the block to attempt to eliminate temperature gradients across the block, ii) fitted windows to cover the slots for the entrance and exit of the beam and thus reduce heat loss, iii) a carefully machined cell slot to improve the thermal contact of the cell with the block, iv) a stirrer mechanism to allow mixing *in situ*, particularly of coexisting phases, v) platinum resistance thermometers to monitor the temperature as close to the cell as possible, vi) height adjustment to allow measurements of the lower and upper coexisting phases, and vii) several removable central sections so that cells can be equilibrating while an experiment is running.

The new copper cell holder is shown in Figure 3.3 and Plate 2. The main octagonal block measures approximately 10 cm x 10 cm x 11 cm and the sample cell sits in a cylindrical insert which has slots for two cells. The insert is off-set from the centre of the main block and can be rotated while within the block so that either cell is positioned directly in the beam, which enters the block radially. In this way the sample and the prompt can both be equilibrated in the block and the prompt can be measured between each sample run without excessive temperature disruption. The internal surfaces of the insert are blackened to reduce stray reflections. Black paper is also inserted between the two cell positions to eliminate the fluorescence from the sample when running the prompt and to eliminate light scattered from the prompt when running the sample.

A copper taper sits between the main block and the insert. This is loosened to allow the insert to be turned to bring the other cell position into the beam or to allow the height of the insert within the block to be altered to study both upper and lower phases. The taper can be tightened as required to maintain good thermal contact. The block temperature is controlled by four Peltier elements and background heating is supplied by four solder iron heaters connected *via* a Variac.

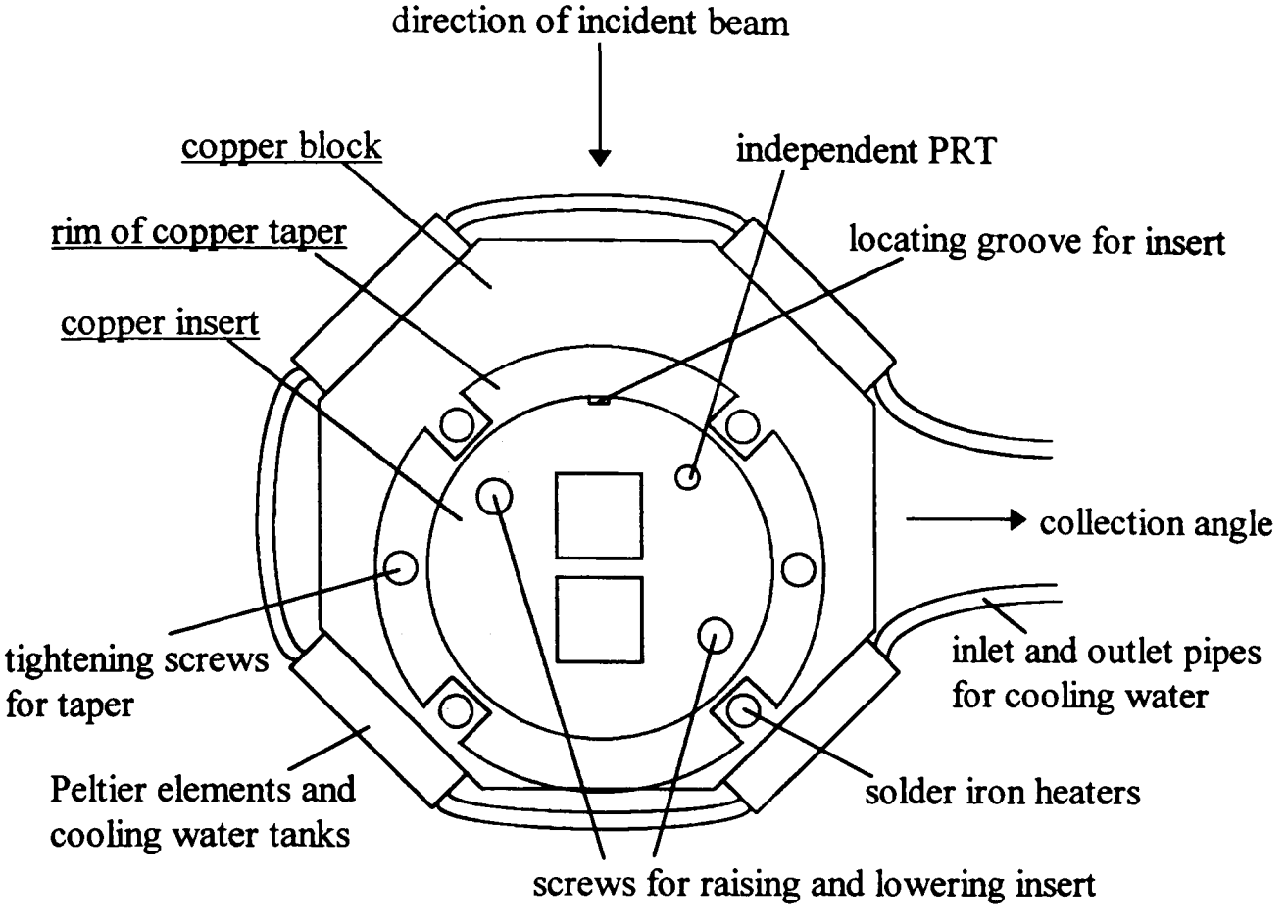

Figure 3.3: Diagrams of the new copper cell holder showing the octagonal block and the insert. The various features are shown on the plan view. In the diagram of the cross-section the taper is omitted for clarity and the shaded regions represent the copper.

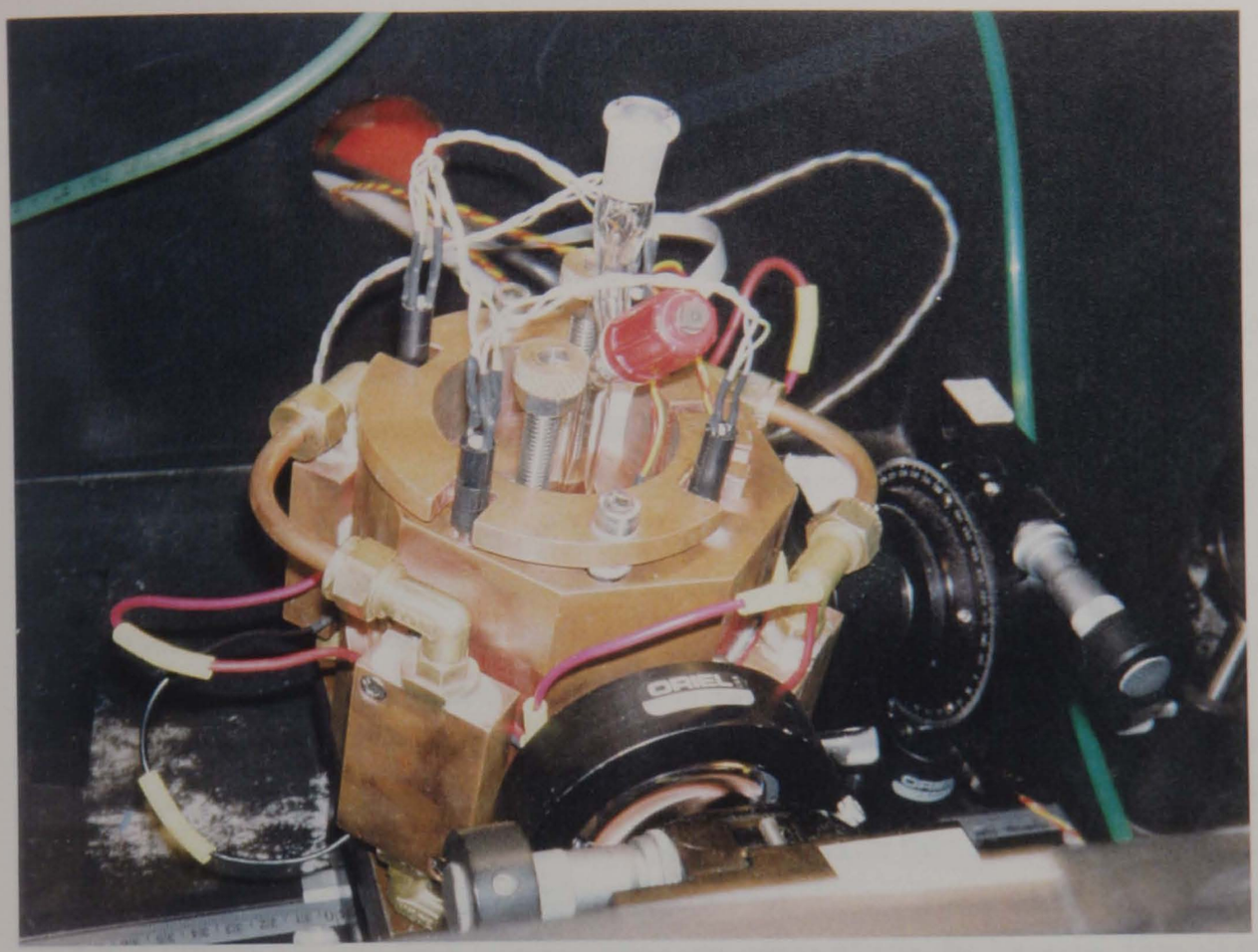

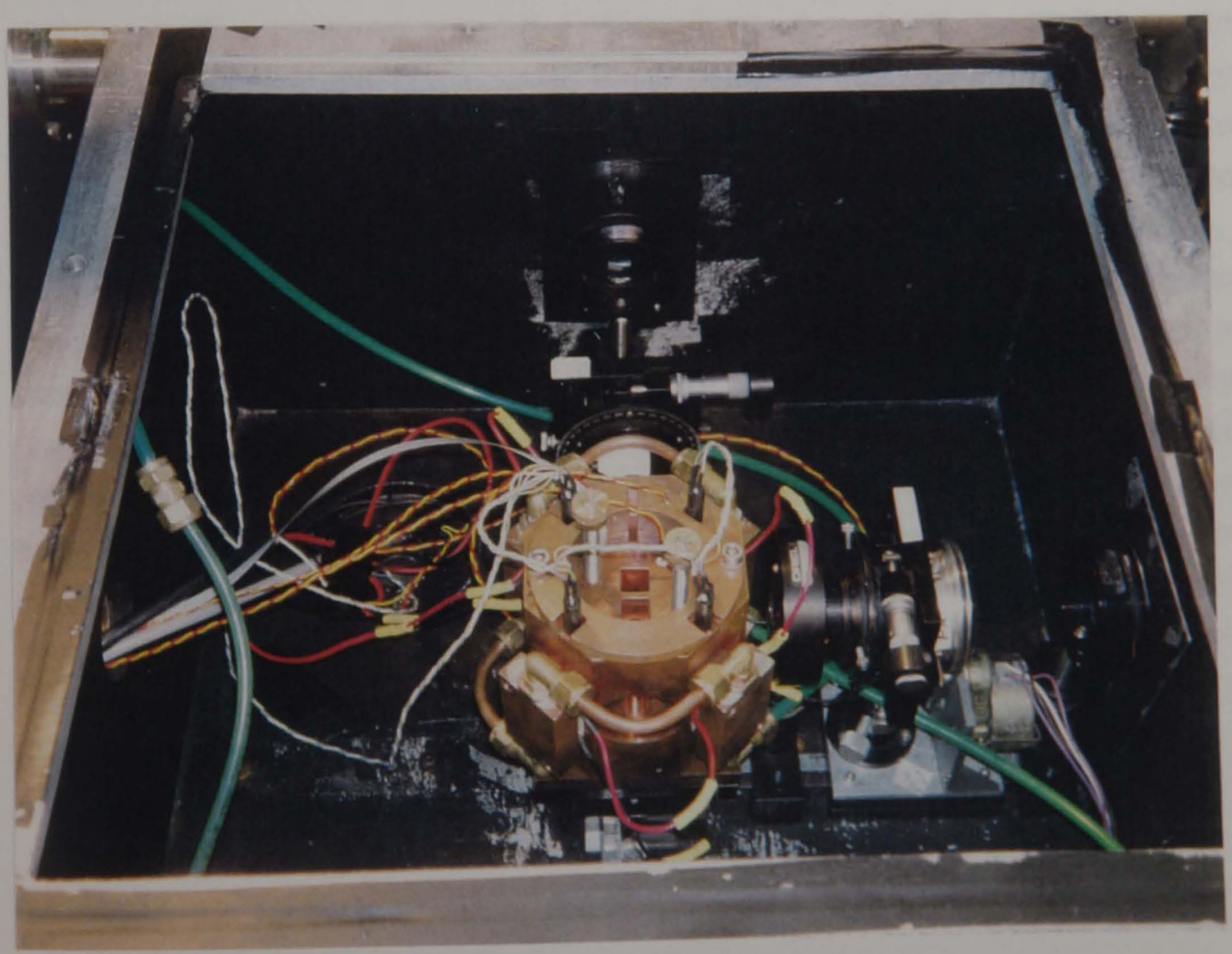

Plate 2: The new copper cell holder.

3.2.4 Choice of systems

The binary liquid mixtures initially considered for study were those for which the form of the macroscopic shear viscosity has already been characterised close to the critical point. These mixtures include *inter alia* nitroethane + 3-methylpentane, hexadecane + acetone and methylcyclohexane (MCH) + perfluoromethylcyclohexane (PFMCH) near their upper critical endpoints (UCEPs) and 2-butoxyethanol + H_2O near its lower critical endpoint (LCEP) (Pegg and McLure, 1984; Maczek *et al.*, 1990). For all these mixtures the viscosity has been determined as a function of temperature both along the path of constant critical composition in the single phase and along each limb of the liquid-liquid coexistence curve. The viscosity of MCH + PFMCH has also been measured as a function of composition along the critical isotherm (Archer, 1995). Of these mixtures 2-butoxyethanol + H_2O has the highest viscosity and is therefore likely to yield the longest rotational correlation time for a given probe; it was thus chosen for study.

The fluorescent dyes chosen were as large and rigid as possible, again to yield the highest rotational correlation times. The fluorescence lifetime of a chosen dye should be between 2 ns and 40 ns. If the fluorescence lifetime is greater than 40 ns the fluorescence does not completely decay away between synchrotron pulses, which occur every 320 ns, and if the lifetime is too short complications can occur due to the response time of the instrument. The rotational correlation time of the dye should be similar to the fluorescence lifetime and ideally about 10 ns. However, our mixtures were not very viscous and it was difficult to find probe molecules with dimensions large enough to achieve the ideal value. In the event, the low rotational correlation times turned out to be measurable, and values exceeding 1 ns were achieved with the largest dye.

In future work the range of mixtures for study can be extended by measuring the macroscopic viscosity of more viscous mixtures, along with the phase diagram if this is not already known. In the present work mixtures of much higher viscosity were considered, such as those formed from silicones with alkanenitriles, alcohols or perfluoroalkanes. The viscous silicones were, however, impure blends and thus unsuitable. Another potential problem with more viscous mixtures is ensuring adequate stirring and equilibration. The addition of glycerol to 2-butoxyethanol + H_2O mixtures should increase the viscosity, but in the ternary mixture formed, the location of the critical point may not be accurately known or easily identified. Mixtures of ethanol with dodecane, tetradecane or hexadecane are slightly more viscous than those used so far, with convenient upper critical solution temperatures T_{UCS} at 12.65°C, 35.25°C and 52.95°C, respectively (Dahlmann and Schneider, 1989; French *et al.*, 1979), and so may be suitable for study. It should be noted that higher mixture viscosities and higher rotational correlation times can also be achieved by working at very low temperatures.

3.2.5 Materials

Details of the liquids used in this work are given in Table 3.1.

Table 3.1: The suppliers, purities, densities and molar masses for the liquids used in this work.

material	supplier	purity /mol %	density at 25°C /g cm^{-3}	molar mass /g mol^{-1}
MCH	Aldrich	99	0.7647[a]	98.18
PFMCH	Fluorochem	95	1.7899[a]	350.06
2-butoxyethanol	Aldrich	99+	0.896[b]	118.18
distilled H_2O	-	-	0.9971[c]	18.02
D_2O	Fluorochem	99.9	1.104[d]	20.03

[a] Heady and Cahn (1973), [b] Pegg (1982), [c] CRC Handbook of Chemistry and Physics (1974), [d] Némethy and Scheraga (1964). MCH = methylcyclohexane, PFMCH = perfluoromethylcyclohexane.

Several fluorescent dyes were used in this work and their structures are shown in Figures 3.4-3.7. Details of the dyes are given in Table 3.2; references for the absorption or fluorescence spectra of each dye, and the filters used throughout this work on the collected fluorescence are also included. The filters are all short-wavelength cut-off filters and should thus transmit only light of longer wavelengths than the stated wavelength, although they are often imperfect. Other types of filter are also available, such as band-pass filters, which transmit light with wavelengths within a given range and cut out any very high or very low wavelengths, and interference filters, which transmit a small range of wavelengths either side of the stated wavelength. Combinations of filters can also be used to further reduce the detection of any scattered incident light in addition to the required fluorescence.

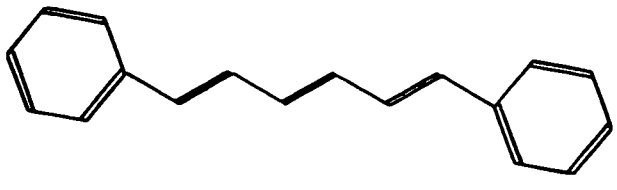

Figure 3.4: Structure of 1,6-diphenylhexa-1,3,5-triene (DPH).

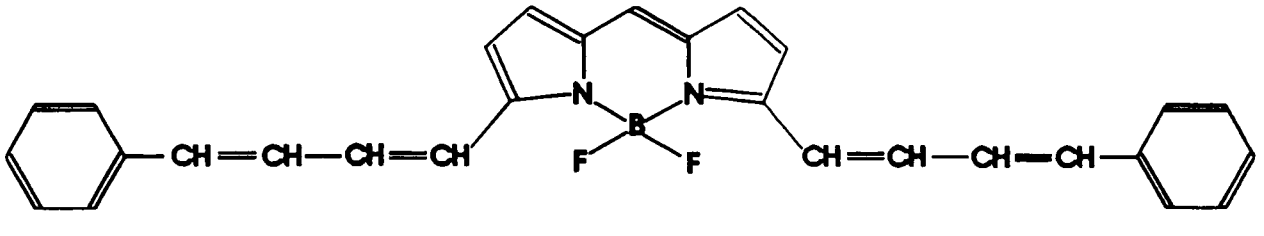

Figure 3.5: Structure of *(E,E)*-3,5-bis-(4-phenyl-1,3-butadienyl)-4,4-difluoro-4-bora-3a,4a-diaza-*s*-indacene (Bodipy 665/676).

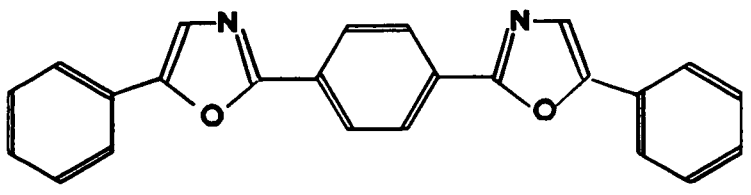

Figure 3.6: Structure of 1,4-di[2-(5-phenyloxazolyl)]benzene (POPOP).

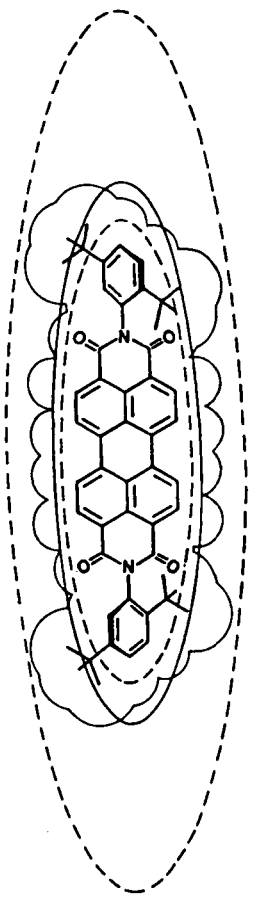

Figure 3.7: Structure of N,N'-bis(2,5-di-*tert*-butylphenyl)-3,4,9,10-perylenedicarboximide (BTBP). (Reproduced from Ben-Amotz and Drake, 1988.)

Table 3.2: The suppliers, purities, molar masses, spectra and other fluorescence data references, and filters used on the fluorescence for the dyes in this work.

dye	supplier	purity /mol %	molar mass /g mol^{-1}	spectra references	filters
DPH	Aldrich	98	232.33	a, b	GG435
Bodipy	Molecular Probes	-	448.32	a, c, d	RG695
POPOP	Lancaster	-	364.41	a, b	GG435
BTBP	Aldrich	-	766.99	a, e, f, g, h	OG570 or OG550

[a] This section, [b] Berlman (1965), [c] Karolin *et al.* (1994), [d] Molecular Probes Catalogue, 1992-94, [e] Rademacher *et al.* (1982), [f] Ben-Amotz and Drake (1988), [g] Ford and Kamat (1987), [h] Bisht *et al.* (1996).

The absorption, excitation or fluorescence spectra of Bodipy, POPOP and BTBP are shown in Figures 3.8-3.10. The spectra for DPH are given in Chapter 4, Figure 4.2. The absorption spectra were run on a Philips PU8700 UV/visible spectrophotometer, against a baseline for the pure solvent, and the fluorescence spectra were run on a Perkin-Elmer LS-5 Luminescence spectrometer.

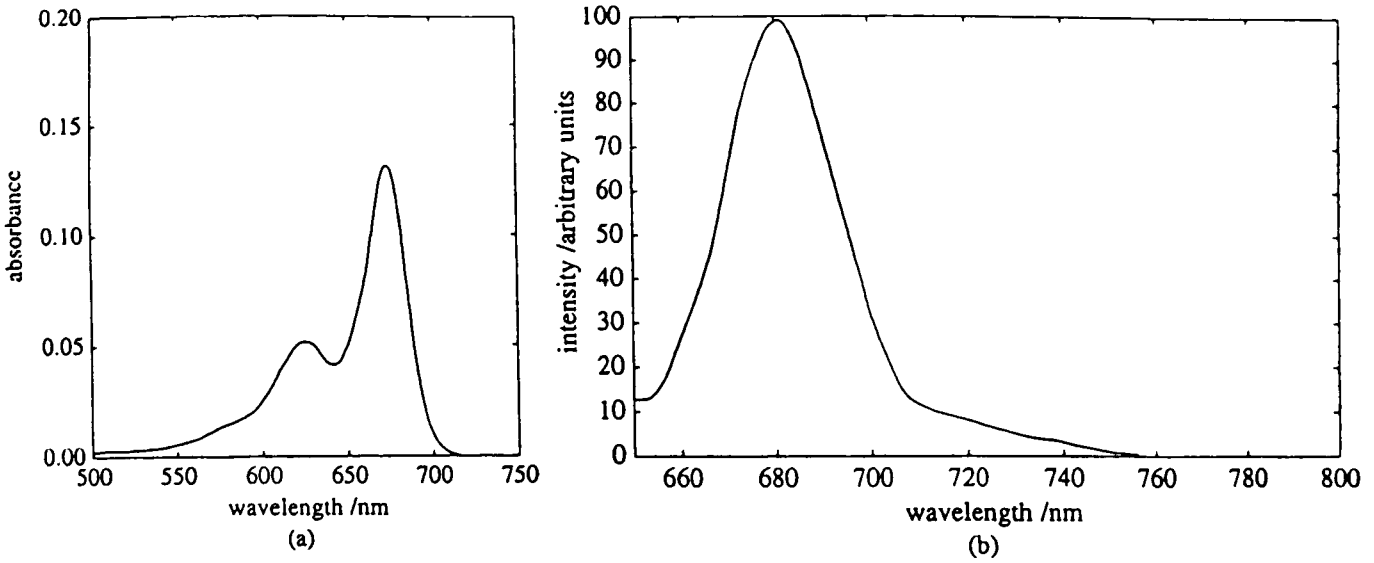

Figure 3.8: (a) The absorption spectrum and (b) the emission spectrum obtained by exciting at 622 nm for Bodipy in 2-butoxyethanol.

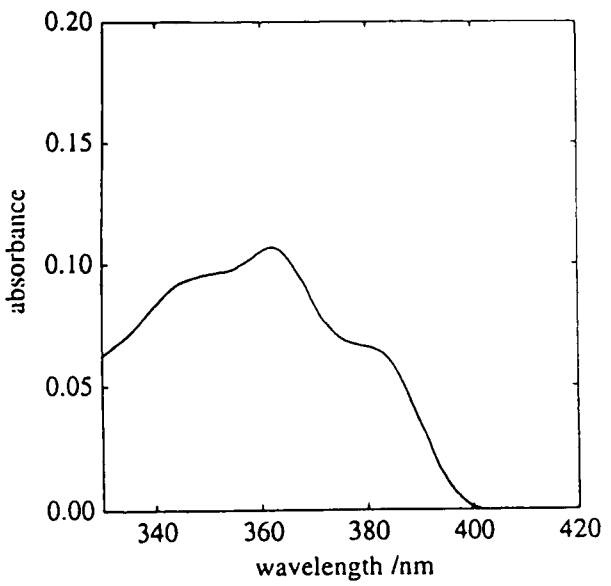

Figure 3.9: The absorption spectrum of POPOP in 2-butoxyethanol.

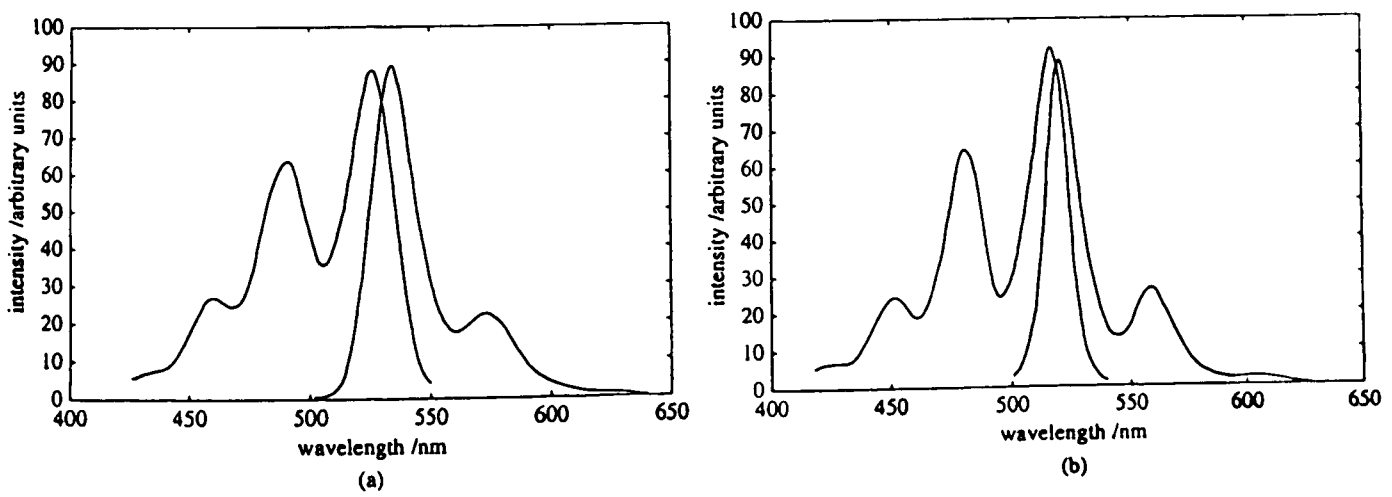

Figure 3.10: (a) The excitation and emission spectra of BTBP in 2-butoxyethanol. The excitation spectrum was obtained at an emission wavelength of 580 nm and the emission spectrum was obtained by exciting at 460 nm. (b) The excitation and emission spectra of BTBP in MCH. The excitation spectrum was obtained at an emission wavelength of 560 nm and the emission spectrum was obtained by exciting at 450 nm.

The details of the mixtures of interest in this work are shown in Table 3.3.

Table 3.3: The critical compositions in terms of mole fraction x, volume fraction ϕ, and mass fraction w and the critical solution temperatures T_{CS} for the mixtures studied in this work. The compositions given are of the fluorocarbon or of 2-butoxyethanol.

mixture	x_c	ϕ_c	w_c	T_{CS} /°C	ref.
MCH + PFMCH	0.361	0.463	0.668	46.13^U	a
2-butoxyethanol + H_2O	0.0602	0.319	0.296	49.052^L	b
2-butoxyethanol + D_2O	0.0602	0.318	0.273	42.5^L	c

[a] Heady and Cahn (1973), [b] Pegg, (1982), c for critical mole fraction as for 2-butoxyethanol + H_2O (Baaken *et al.*, 1990). U = upper critical endpoint; L = lower critical endpoint.

3.2.6 Sample preparation

In some solvents the dye was not very soluble and in such cases a saturated solution was made up and left for a few days to dissolve before filtering. The solutions were diluted until the maximum absorbance was less than 0.1; the concentration was then about 10^{-6} M. Binary mixtures were made up by mass by adding a solution of the dye in the component in which it was more soluble to the other pure component. The liquids were transferred to the cells, which were generally cleaned with acetone before use, by means of a flexible Teflon syringe needle attached to a glass-metal syringe. The samples for which the lifetime measurement was important were degassed by three or four freeze-pump-thaw cycles.

3.2.7 Stirring

Magnetic followers in the cells were activated to achieve mixing of the liquid sample. When the brass cell holder was used this was carried out manually using a magnet. The magnetic followers were lifted out of the liquid during the measurements and held by resting the magnet on the cell holder block. The liquids in the cells used with the new cell holder were stirred by activating smaller magnetic followers by means of an induction coil situated below the cell. However, this did not permit thorough mixing of our samples and so the cells were quickly removed and shaken. A more suitable magnetic follower design or a more powerful stirrer may improve the mixing. In all the experiments the samples were stirred at each temperature and left approximately 15 minutes to equilibrate.

3.2.8 Preliminary experiments

The initial experiments, carried out to find suitable dyes with measurable rotational correlation times τ_R, are listed in Table 3.4. The fluorescence was detected from single-phase mixtures or from the lower phase of two-phase mixtures. The mixture 2-butoxyethanol + H_2O was selected for further study, using the dyes Bodipy and POPOP and also BTBP, and the main results are presented in section 3.3.

Table 3.4: The results of fluorescence lifetime τ_F and rotational correlation time τ_R measurements, and the main conclusions, for the systems studied in the preliminary experiments.

system	conditions			results		conclusions
	x	T /°C	λ_{ex} /nm	τ_F /ns	τ_R /ns	outcome for τ_R
DPH in MCH + PFMCH	x_c	48-50	various	14.0-15.1	~ 0.07	too short - so inaccurate
DPH in C_4E_1 + H_2O	x_c	48-54	various	bi-exp 3.8 (+ 0.4-1.0)	~ 0.13	too short
Bodipy in C_4E_1 + H_2O	x_c	49-54	625	bi-exp 1.0 (+ 4.0)	~ 0.6	measurable
POPOP in C_4E_1	-	45	360	1.2	~ 0.4	measurable

x = composition, x_c = critical composition, λ_{ex} = excitation wavelength, MCH = methyl-cyclohexane, PFMCH = perfluoromethylcyclohexane, C_4E_1 = 2-butoxyethanol. Bi-exp denotes the requirement for a bi-exponential decay; the minor component is given in parentheses.

3.3 Results

The results discussed here are mainly for the dyes Bodipy, POPOP and BTBP, see section 3.2.5, in the same mixture 2-butoxyethanol (C_4E_1) + H_2O, both in the single phase of critical composition below the lower critical solution temperature $T_{LCS} \approx 49°C$ and in the lower H_2O-rich phase of the two-phase mixtures. In the earlier experiments, measurements could not be taken for the upper 2-butoxyethanol-rich phase due to restrictions in the height variation of the brass cell holder, although some measurements were later obtained using both the brass and the new copper cell holders.

For ease of comparison, the decays of the fluorescence polarised parallel and perpendicular to the plane of polarisation of the incident light and the anisotropy decays for each of the four main systems–namely Bodipy, POPOP and BTBP in 2-butoxyethanol + H_2O and BTBP in 2-butoxyethanol + D_2O–are plotted together in Figures 3.11 and 3.12. The fluorescence polarised parallel to the plane of polarisation of the incident light has the higher intensity after the peak, and at longer times, i.e. longer channels, both parallel and perpendicular decays have the same value. The best fits to the anisotropy are also shown. For POPOP the peak at longer times is due to the photomultiplier tube.

The decay of the total fluorescence used to obtain the fluorescence lifetime is plotted for Bodipy in Figure 3.13. Single and bi-exponential fits are shown along with the residuals (the difference between the calculated and experimental values) for each fit. It is clear that a bi-exponential decay is required.

In Figure 3.14 some extra profiles are plotted to illustrate (a) a typical instrument response function, (b) typical residuals for a fit to anisotropy decay data, (c) and (d) the lifetime decays and best fits for POPOP and BTBP in 2-butoxyethanol + H_2O. The lifetime decay for BTBP in 2-butoxyethanol + D_2O is similar to that in 2-butoxyethanol + H_2O.

For all of the plots shown in Figures 3.11-3.14 the number of counts represents the intensity and the channel numbers represent the time; the time calibration is 0.014 ns per channel. The temperatures represented for each system in Figures 3.11-3.14 and the tables quoting the anisotropy parameters for the illustrated fit are given below:

Bodipy in 2-butoxyethanol + H_2O,	T = 45.1°C,	see Table 3.5.
POPOP in 2-butoxyethanol + H_2O,	T = 45.0°C,	see Table 3.9.
BTBP in 2-butoxyethanol + H_2O,	T = 45.0°C,	see Table 3.11.
BTBP in 2-butoxyethanol + D_2O,	T = 37.5°C,	see Table 3.16.

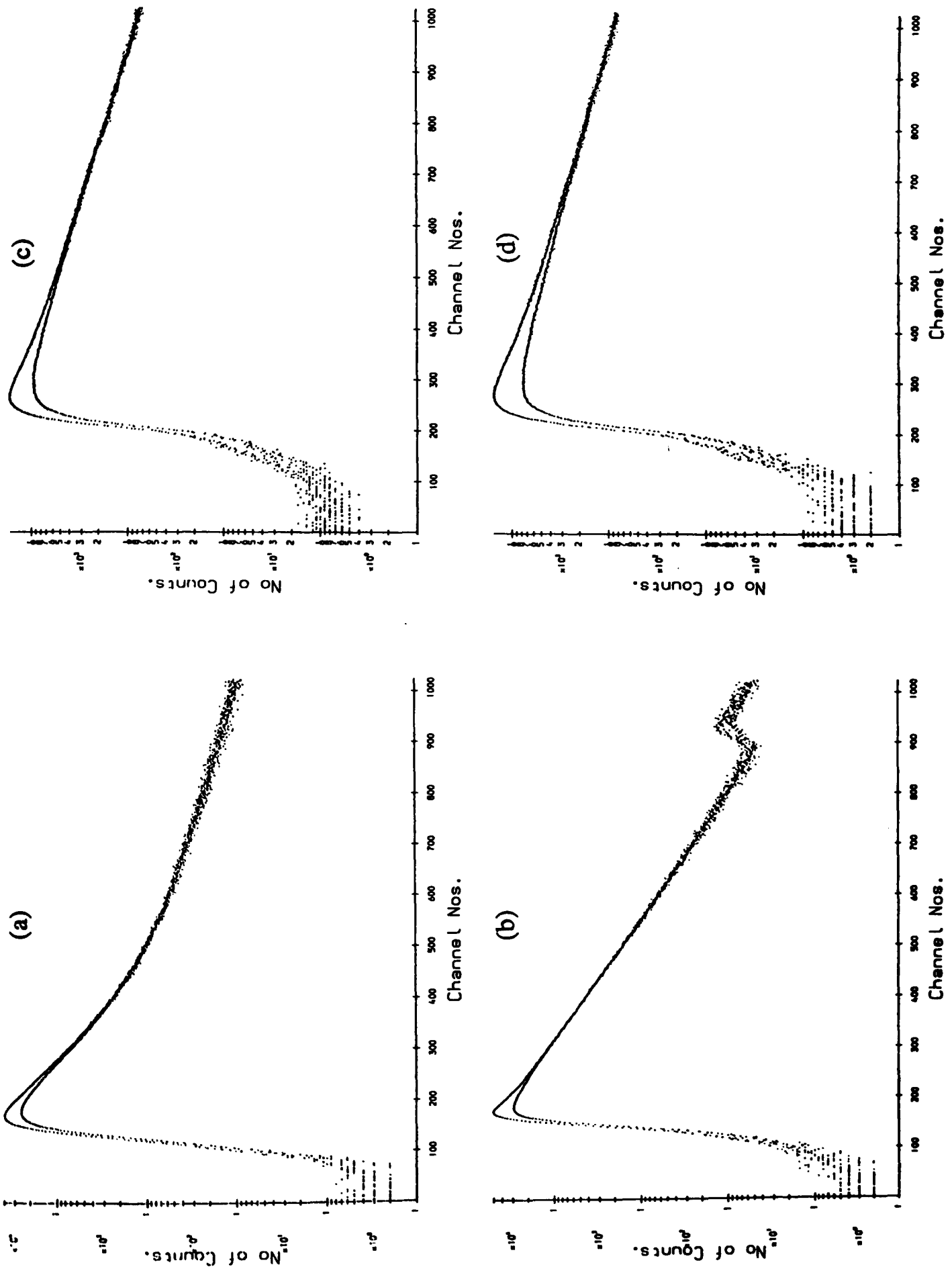

Figure 3.11: Decays of the fluorescence polarised parallel (upper curve) and perpendicular (lower curve) to the plane of polarisation of the incident light for (a) Bodipy, (b) POPOP and (c) BTBP in 2-butoxyethanol + H_2O and (d) BTBP in 2-butoxyethanol + D_2O.

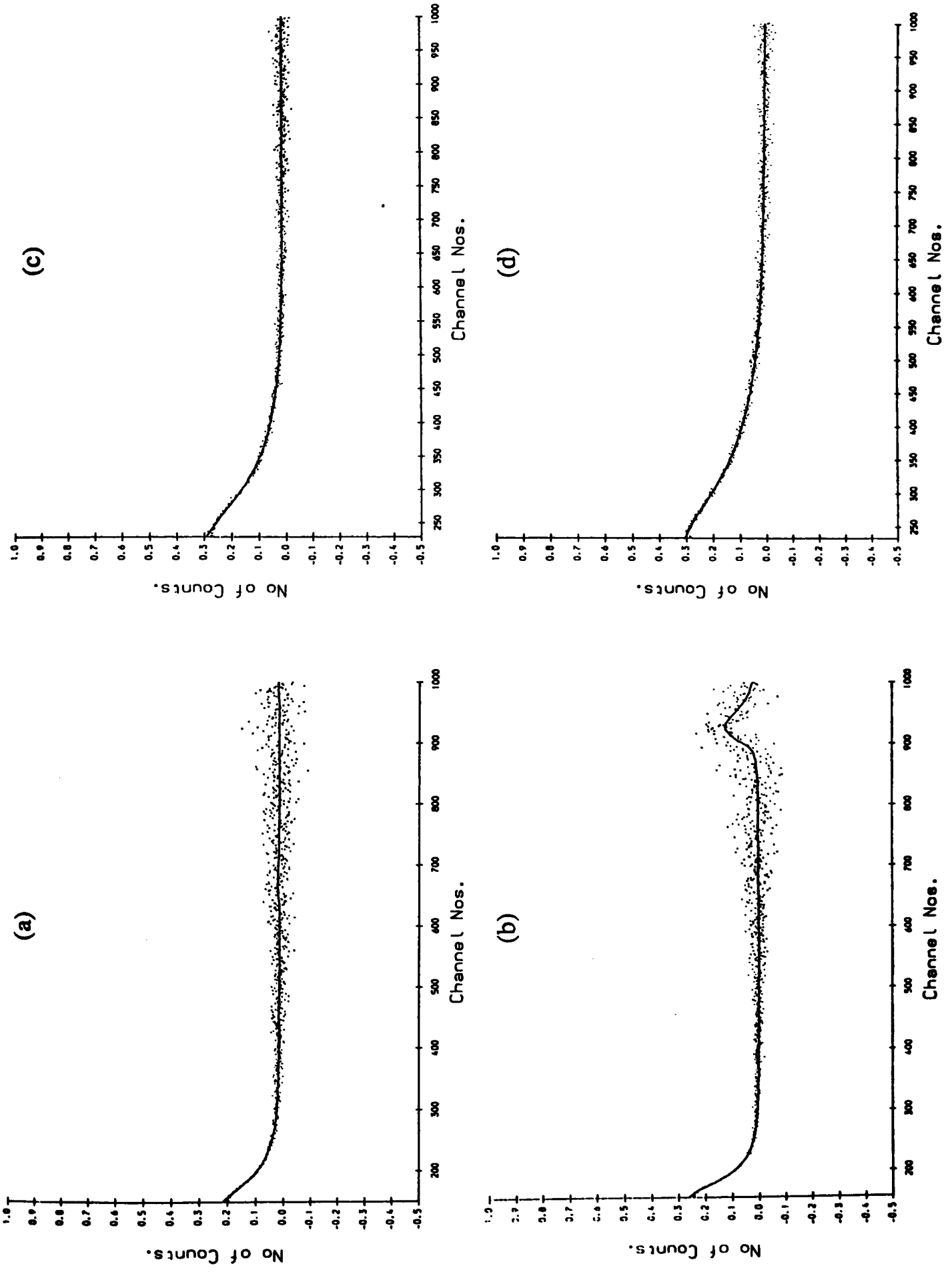

Figure 3.12: Anisotropy decays and fitted lines for (a) Bodipy, (b) POPOP and (c) BTBP in 2-butoxyethanol + H_2O, and (d) BTBP in 2-butoxyethanol + D_2O.

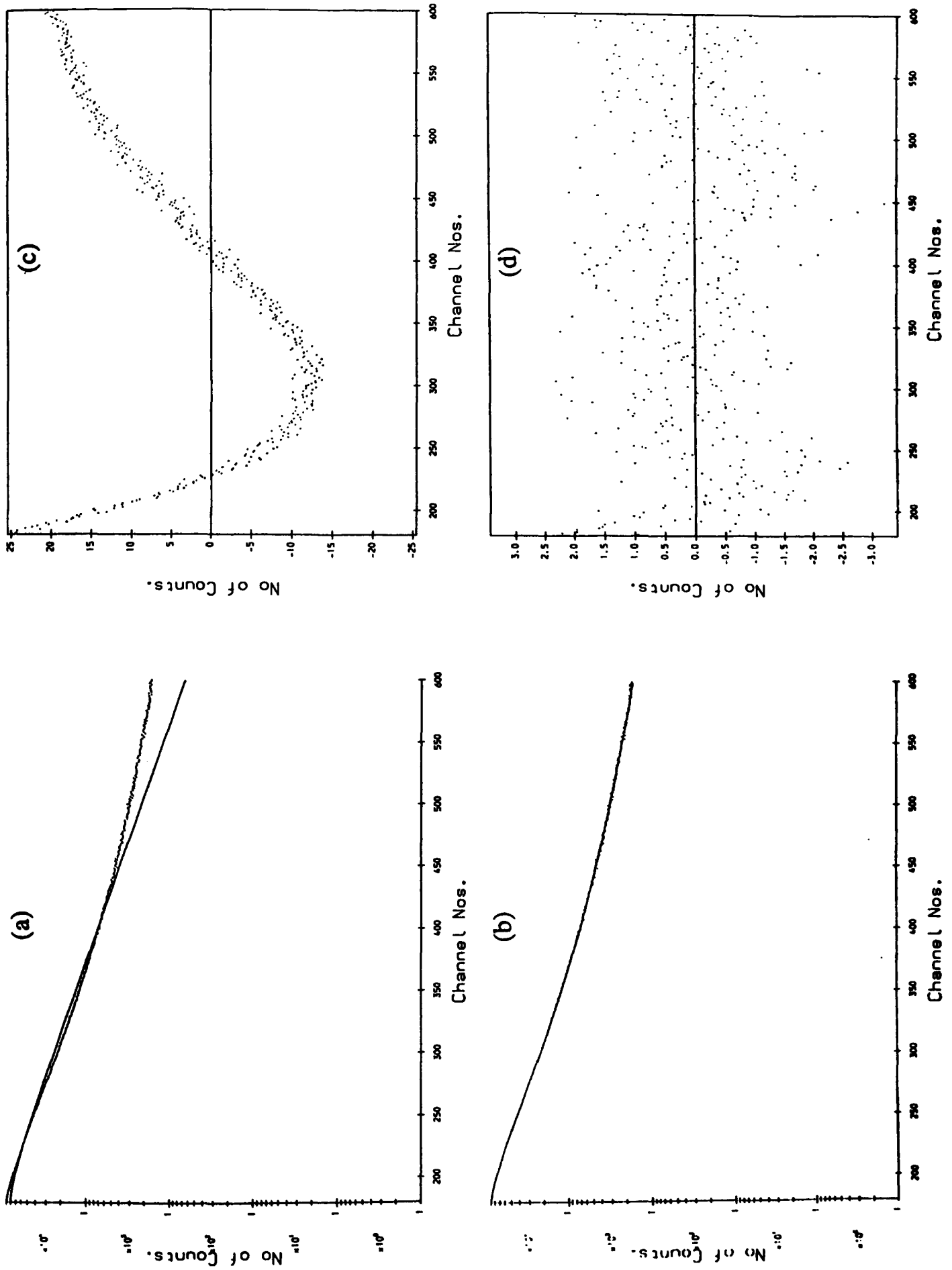

Figure 3.13: (a) Decay of the total fluorescence and a single-exponential fit with τ_F = 1.12 ns, χ^2 = 135.9, (b) decay of the total fluorescence and a bi-exponential fit with α_1 = 0.112, $\tau_{F,1}$ = 0.822 ns, α_2 = 0.011, $\tau_{F,2}$ = 2.723 ns, χ^2 = 1.1, (c) residuals for single-exponential fit, and (d) residuals for bi-exponential fit for Bodipy in 2-butoxyethanol + H_2O.

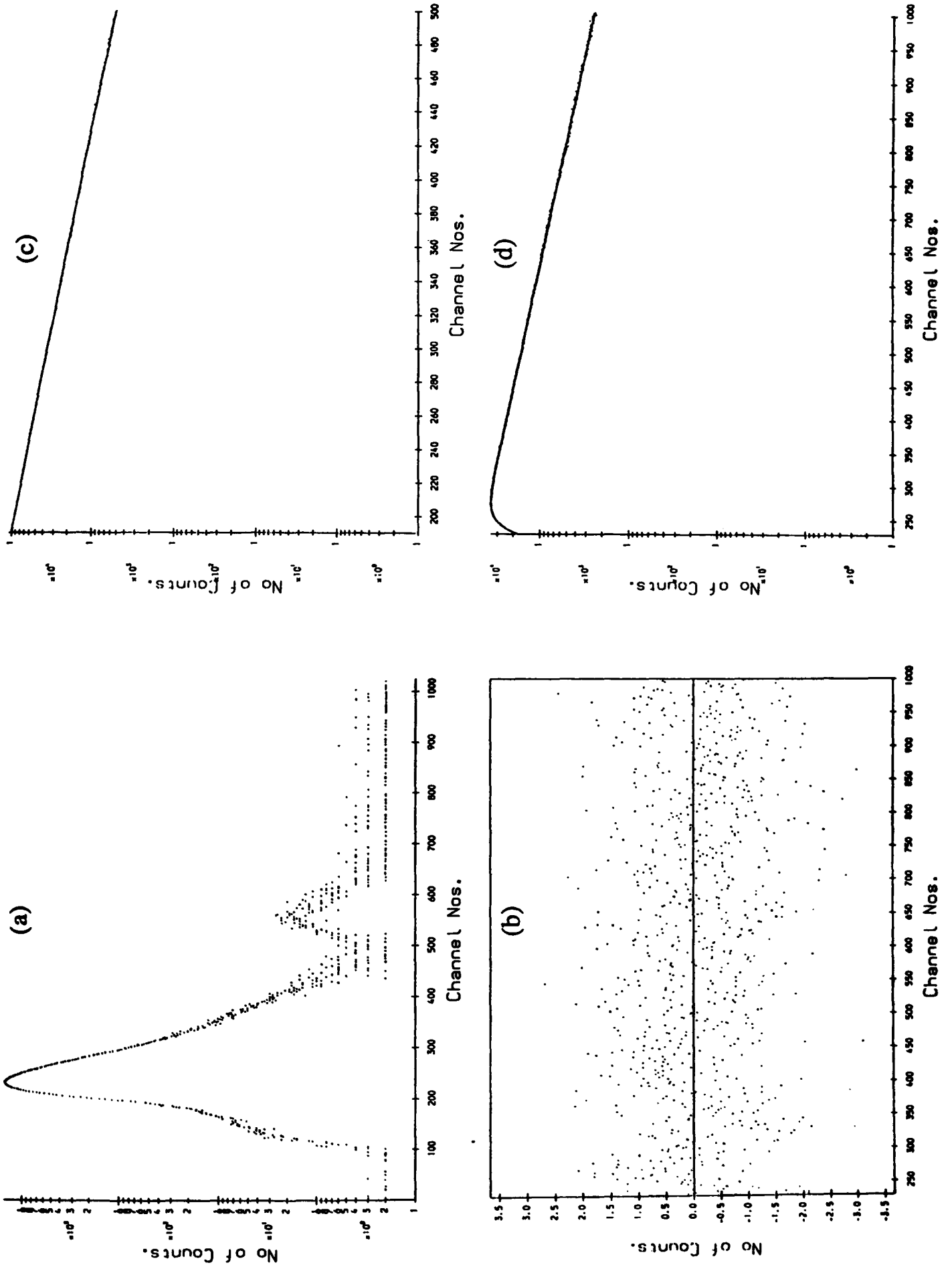

Figure 3.14: (a) A typical instrument response function. (b) Residuals for fit to anisotropy decay data for BTBP in 2-butoxyethanol + H_2O, χ^2 = 1.0. (c) Lifetime data and a single-exponential fit with τ_F = 1.372 ns for POPOP in 2-butoxyethanol + H_2O. (d) Lifetime data and a bi-exponential fit with α_1 = 0.055, $\tau_{F,1}$ = 3.702 ns, α_2 = 0.009, $\tau_{F,2}$ = 0.129 ns for BTBP in 2-butoxyethanol + H_2O.

3.3.1 Bodipy

The first main results obtained were for Bodipy (665/676), a fairly large dye with absorption and fluorescence bands at the higher wavelengths of the visible region. The results from the experiments using Bodipy have been published (Clements *et al.*, 1995).

The fluorescence Stokes' shifts are small for Bodipy, resulting in large spectral overlaps. For example, in methanol the main excitation band is at 665 nm and the main emission is at 676 nm. The absorption and emission spectra for Bodipy in 2-butoxyethanol are shown in section 3.2.5.

The rotational correlation time τ_R of Bodipy in a mixture of 2-butoxyethanol + H_2O of critical composition, $w_{BXE} = 0.294$, was measured over a range of temperatures close to T_{LCS}. Single-phase mixtures below T_{LCS} and the lower H_2O-rich phase of two-phase mixtures above T_{LCS} were studied. The excitation wavelengths used were 622 nm and 670 nm at each temperature. The results at 622 nm are discussed first.

The anisotropy decay data for excitation at 622 nm were fitted well by a single exponential decay; the results are presented in Table 3.5. An anisotropy at infinite time $r(\infty)$ was required to obtain a good fit. This may be due to distortions in the glassware in the fluorescence detection path causing the parallel and perpendicular intensities to be different at long times. The $r(\infty)$ values were all less than 0.02. The values of $r(0)$, the anisotropy at time zero, were 0.26±0.05. This is lower than the value of 0.37 quoted by Karolin *et al.* (1994) for their somewhat different Bodipy derivatives. The χ^2 values indicating the goodness of the fit were equal to 1.0±0.1. The critical temperature T_{LCS} was determined visually as close to 50.1°C (323.25 K). This is about 1.1 K higher than the value of 49.035°C quoted by Pegg (1982) for high purity materials.

The product of the rotational correlation time and the temperature $\tau_R \cdot T$, taken as a measure of the microviscosity, is plotted as a function of temperature in Figure 3.15(a). The increase in the viscosity near T_{LCS} is clearly marked on the approach both from above and below T_{LCS}.

Table 3.5: The results of fitting the anisotropy data for Bodipy in 2-butoxyethanol + H_2O for excitation at 622 nm to a single-exponential decay. The data were fitted from the prompt peak to channel 1000. The anisotropy at time zero r(0) and at infinite time r(∞), and the rotational correlation times τ_R, are given for each temperature. $T_{LCS} \approx$ 50.1°C (323.25 K).

T /°C	T /K	r(0)	τ_R /ns	r(∞)
40.5	313.65	0.253	0.471	0.015
45.1	318.25	0.251	0.415	0.015
47.1	320.25	0.255	0.402	0.013
48.0	321.15	0.257	0.404	0.013
48.9	322.05	0.247	0.398	0.013
49.4	322.55	0.258	0.412	0.012
49.6	322.75	0.219	0.399	0.011
49.7	322.85	0.252	0.395	0.011
49.8	322.95	0.267	0.404	0.011
50.2	323.35	0.261	0.389	0.012
50.3	323.45	0.255	0.390	0.011
50.4	323.55	0.254	0.386	0.010
50.6	323.75	0.248	0.368	0.008
50.8	323.95	0.240	0.373	0.006
51.9	325.05	0.263	0.368	0.010
59.2	332.35	0.305	0.258	0.000

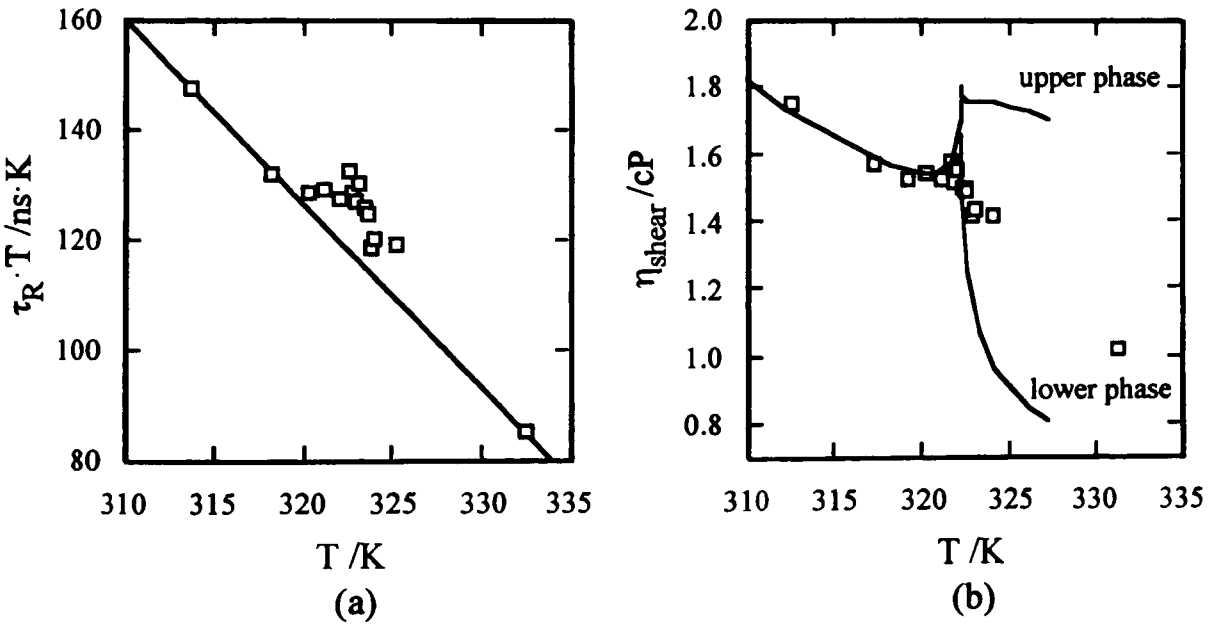

Figure 3.15: (a) The measure of the microviscosity given by the product of the rotational correlation time and temperature $\tau_R \cdot T$ as a function of temperature T for Bodipy in a 2-butoxyethanol + H_2O mixture of critical composition excited at 622 nm. The straight line is drawn only to guide the eye. (b) Scaled $\tau_R \cdot T$ data and shear viscosity η_{shear} (Pegg and McLure, 1984) *versus* temperature T for Bodipy in a 2-butoxyethanol + H_2O mixture of critical composition.

The same results are scaled and plotted in Figure 3.15(b), along with the macroscopic shear viscosity η_{shear} for the 2-butoxyethanol + H_2O mixture (Pegg and McLure, 1984). It is usually difficult in comparing different experimental studies on the critical behaviour of a given mixture to relate all the observations to a common basis of T and composition. This generally arises from differences in component purity and slightly differing local thermometer calibration and these factors can lead to varying determinations of the location of the critical composition and temperature. Our results have thus been scaled by a three-stage process to allow them to be compared with the macroscopic shear viscosity data. In the first stage a multiplicative factor was applied to $\tau_R \cdot T$, with T in Kelvin and τ_R in ns, to make the values comparable to the Pegg and McLure η_{shear}. Next a downwards linear shift of 1.1 K was applied to our temperatures so that our T_{LCS} coincided with T_{LCS} for the η_{shear} data. The final stage was to rescale the $\tau_R \cdot T$ values multiplicatively to bring them into coincidence with the noncritical η_{shear} at a temperature as far from T_{LCS} as possible. The overall factor used to multiply the $\tau_R \cdot T$ values was 1/84. The process is slightly subjective but it allows our data to be compared with those for the macroscopic viscosity. It can be seen in Figure 3.15(b) that our data show a maximum in the effective microscopic viscosity which coincides with that for the macroscopic shear viscosity.

The fluorescence lifetime τ_F was also obtained for excitation at 622 nm. A bi-exponential decay was required to fit the data with a main component of 0.85±0.05 ns and a slightly smaller amount of a longer decay time of 3.1±0.4 ns.

The data obtained by exciting at 670 nm were complicated due to scattered light. This was particularly true for the lower-phase data, which could not be fitted as the apparent anisotropy was too high (greater than 0.4). Close to a critical endpoint opalescence occurs and light is scattered. The effects of scattered light should have been eliminated in our experiments due to the use of filters to cut out the wavelength of the incident light. However, for the incident light of 670 nm scattered light got through the RG695 filter. The cut-off wavelength of 695 nm is not sharp and the transmission tails off below this wavelength. The data at 670 nm were instead fitted by taking the crude anisotropy point by point and analysing to include the effects of scattered light. The results are given in Table 3.6. The procedure is useful to allow some analysis of the data, but the values of χ^2 were poor and thus the data at 622 nm lend themselves better to further fitting and comparison with the macroscopic viscosity. Both the rotational correlation time τ_R and the scattered light intensity as a function of temperature for excitation at 670 nm are plotted in Figure 3.16. It can be seen that the rotational correlation time, as for excitation at 622 nm, increases at T_{LCS}. It is also apparent that the light is scattered strongly close to the critical point, and provides an extra indication of the proximity to T_{LCS}.

Table 3.6: The results of fitting the anisotropy data for Bodipy in 2-butoxyethanol + H_2O for excitation at 670 nm from channels 160-200. The rotational correlation times τ_R and the scattered light values SL (in arbitrary units) are given for each temperature.

T /°C	τ_R /ns	SL /arbitrary units
47.1	0.918	0.047
48.0	0.956	0.052
48.9	0.987	0.046
49.4	0.955	0.043
49.6	0.956	0.053
49.7	1.017	0.062
49.8	1.068	0.067
50.2	1.194	0.092
50.3	1.068	0.081
50.4	1.615	0.122
50.6	1.155	0.134
50.8	1.179	0.103
51.9	0.726	0.101

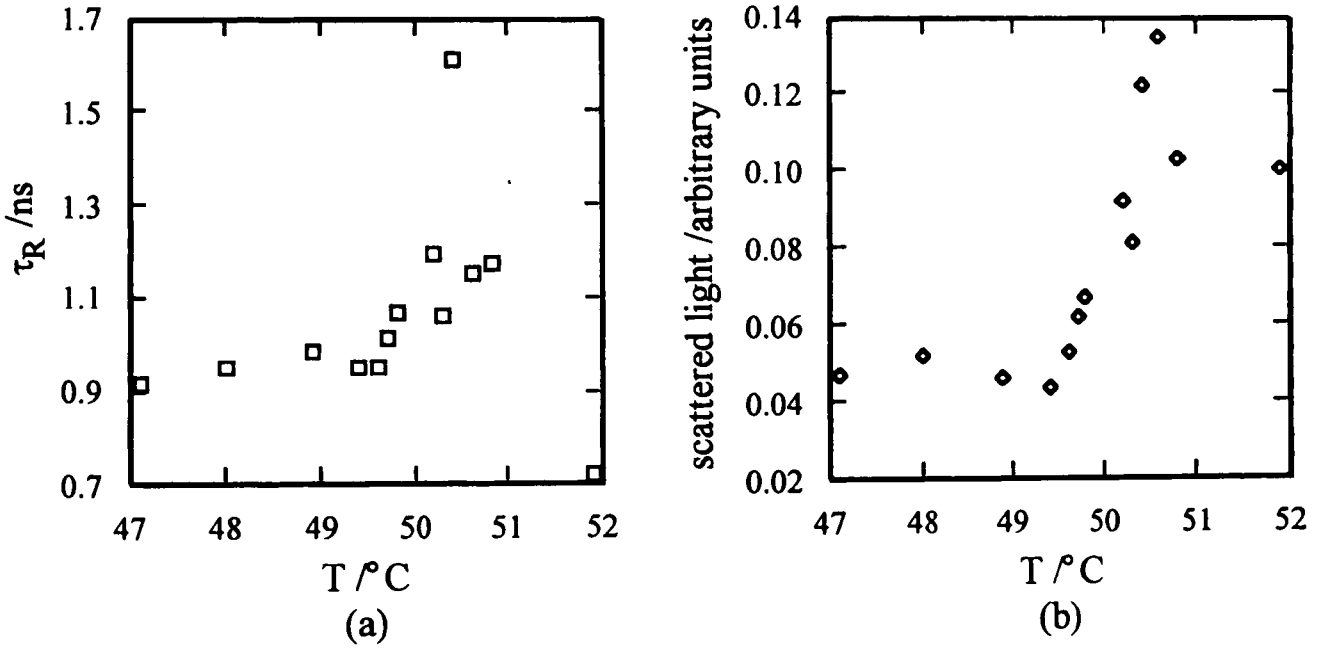

Figure 3.16: (a) The rotational correlation time τ_R *versus* temperature T and (b) the scattered light intensity *versus* T for Bodipy in a 2-butoxyethanol + H_2O mixture of critical composition excited at 670 nm.

After the results presented above were obtained, it was observed that the solutions of Bodipy in 2-butoxyethanol and in 2-butoxyethanol + H_2O were changing significantly with time. The solutions were initially blue, then after a few days changed to pink and then finally became colourless. The changes occurring showed up clearly in the absorption spectra and these are discussed below. The maximum absorbance varies for different samples as the spectra were run at slightly different concentrations.

For Bodipy in 2-butoxyethanol solutions, there was no significant change in the absorption spectrum over a timescale of 7 hours after dissolution. The absorption spectrum of a fresh sample is shown in section 3.2.5 above.

After about 24 hours the intensity of the peak at 670 nm began to decrease and the intensity of the peak at 622 nm began to increase. A significant change was observed after 31 hours, particularly in the 670 nm peak intensity, and was very pronounced after 4 days. A slight shoulder at 590 nm also began to appear. The solution was still blue in appearance. The spectra for 1 hour and 4 day old samples are compared in Figure 3.17(a). The absorption spectrum to shorter wavelengths for a sample after 4 days is plotted in Figure 3.17(b). An odd peak at 377 nm was observed. The long-wavelength spectrum after 18 days is shown in Figure 3.17(c). The spectra for samples after 1 hour and 34 days are compared in Figure 3.17(d). After 34 days the sample appeared pink and all the main bands had shifted so that the sample was absorbing at shorter wavelengths.

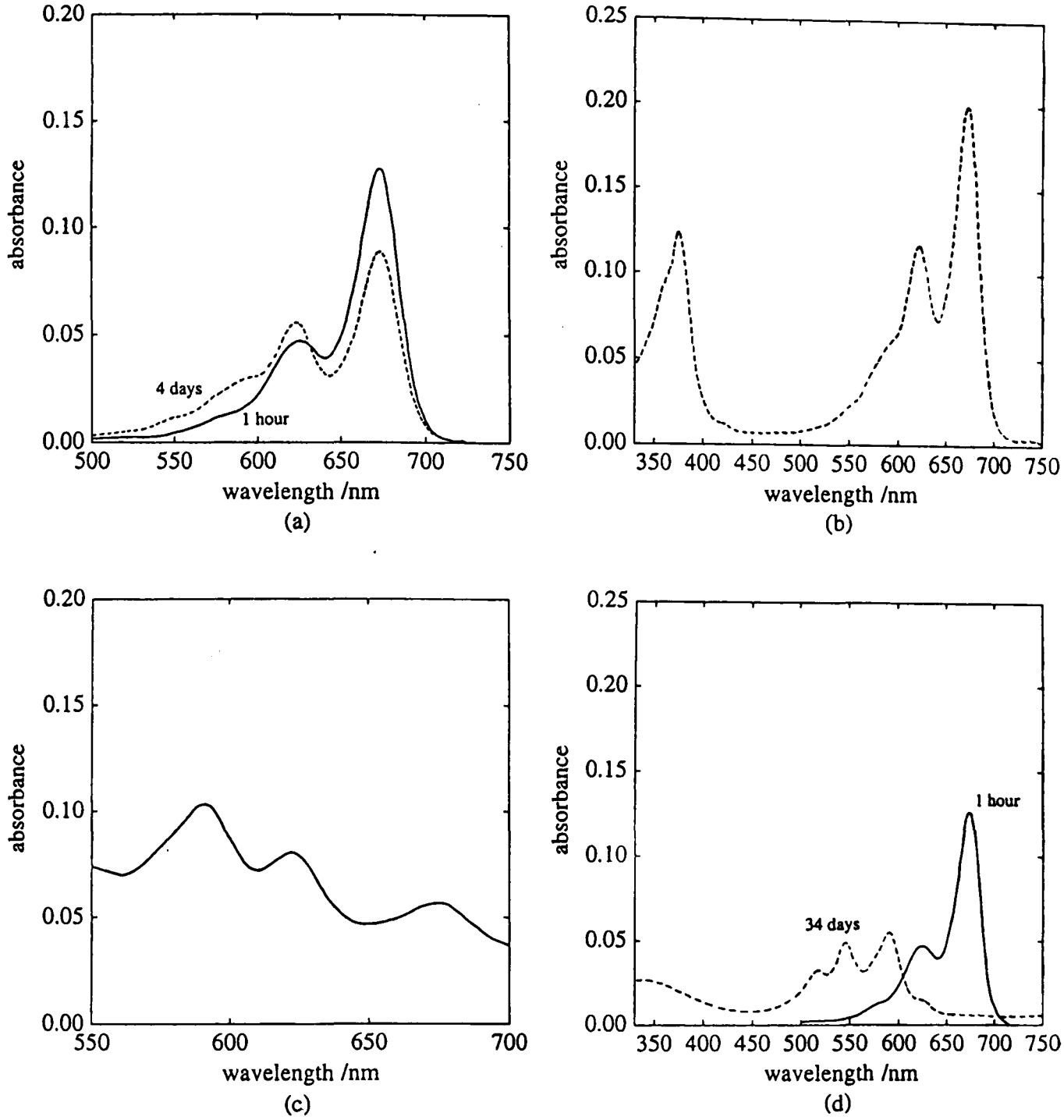

Figure 3.17: Absorption spectra for Bodipy in 2-butoxyethanol (a) after 1 hour and after 4 days, (b) after 4 days showing the shorter wavelengths, (c) after 18 days, (d) after 1 hour and after 34 days.

The changes in the spectra with time may have been due to decomposition, or, as suggested by Molecular Probes, to aggregation of the nonpolar dye in our polar solvents. Further experiments were carried out to attempt to clarify this effect.

Solutions of Bodipy 2 hours old, 4 days old and 6 days old in 2-butoxyethanol were studied at 45°C and at excitation wavelengths λ_{ex} = 546, 591, 622 and 670 nm. The results are presented in Tables 3.7 and 3.8. Differences were observed in τ_F and the excitation scans for each sample but no significant differences were observed in τ_R.

Table 3.7: The fluorescence lifetimes τ_F and the amplitudes α, effectively the emission intensities at time zero, for bi- and tri-exponential fits to the decays, for samples of Bodipy in 2-butoxyethanol of 1 hour, 4 days and 6 days old at 45°C, for excitation at 546, 591, 622 or 670 nm.

λ_{ex} /nm	age of sample					
	1 hour		4 days		6 days	
	α	τ_F /ns	α	τ_F /ns	α	τ_F /ns
546	-	-	0.017	0.946	-	-
			0.021	3.465		
591	-	-	0.016	1.044	0.020	0.929
			0.013	3.459	0.024	3.414
622	-	-	0.044	0.274	-	-
			0.129	1.015		
			0.056	3.400		
670	0.135	0.103	0.078	0.291	0.009	0.431
	0.118	1.010	0.296	1.011	0.064	1.014
			0.0004	3.575	0.0001	4.545

Table 3.8: The anisotropy at time zero r(0) and at infinite time r(∞), and the rotational correlation times τ_R for single-exponential fits to the decays, for samples of Bodipy in 2-butoxyethanol of 1 hour, 4 days and 6 days old at 45°C, for excitation at 546, 591, 622 or 670 nm.

λ_{ex} /nm	age of sample								
	1 hour			4 days			6 days		
	r(0)	τ_R /ns	r(∞)	r(0)	τ_R /ns	r(∞)	r(0)	τ_R /ns	r(∞)
546	-	-	-	0.238	0.376	0.015	-	-	-
591	-	-	-	0.276	0.437	0.014	0.282	0.411	0.013
622	-	-	-	0.242	0.403	0.013	-	-	-
670	0.186	0.396	0.018	0.235	0.406	0.017	0.288	0.383	0.017

Considering first the fluorescence lifetimes in Table 3.7. The following points can be noted: i) the τ_F = 0.1-0.5 ns component present for excitation at 622 and 670 nm is probably due to scattered light, ii) the $\tau_F \approx 1.0$ ns present in all samples is the Bodipy, iii) for samples 4 or 6 days old a longer τ_F component is observed, iv) for the 4-day-old and 6-day-old samples the amount of this longer component relative to the amount of Bodipy, as seen from the α values, increases with decreasing excitation wavelength; excitation at 670 nm thus excites mainly the Bodipy. The time-resolved scans showed that the component/impurity present in the older samples is the long-lifetime component, confirming that $\tau_F \approx 1.0$ ns is due to Bodipy.

Turning now to the rotational correlation times in Table 3.8, it can be seen that the times vary slightly with excitation wavelength, but there does not appear to be any real trend. The values for τ_R are all fairly similar. As the Bodipy component has the shorter fluorescence lifetime, we should have been observing Bodipy in the previous rotational correlation time measurements at short timescales.

Due to the changes occurring in Bodipy it was deemed unsuitable for further microviscosity experiments; other dyes were therefore sought. An effect in the absorption spectrum with time, similar to that observed for Bodipy, was observed for the ionic dye 3,3'-diethylthiadicarbocyanine iodide in 2-butoxyethanol or H_2O. The solutions visibly changed from blue to red to colourless, so this dye was also unsuitable.

A more stable dye, POPOP, was selected to use in 2-butoxyethanol + water to attempt to investigate the anomaly more closely.

3.3.2 POPOP

POPOP is a fairly large and rigid molecule which is planar in the excited state. Its absorption spectrum is shown in section 3.2.5. The spectrum is fairly broad with the main peak at 362 nm. The main emission bands in cyclohexane are at 387, 410 and 435 nm (Berlman, 1965).

The rotational correlation time τ_R of POPOP in a mixture of 2-butoxyethanol + H_2O of critical composition, w_{BXE} = 0.295, was measured over a range of temperatures close to the lower critical solution temperature T_{LCS}. Single-phase mixtures below T_{LCS} and the lower H_2O-rich phase of two-phase mixtures above T_{LCS} were studied. The excitation wavelength used was 360 nm. The data were obtained during two separate runs; the rotational correlation times measured during run 2 were slightly shorter than those for run 1 at the same temperature.

The anisotropy decay data were fitted to single-exponential decays and the results are given in Table 3.9. The values for χ^2 indicating the goodness of the fit were generally 1.1±0.1. T_{LCS} was determined visually as 50.1°C (323.25 K).

Table 3.9: The results of fitting the anisotropy data for POPOP in 2-butoxyethanol + H_2O to single-exponential decays. The data were fitted from the prompt peak to channel 1000 with the anisotropy at infinite time r(∞) fixed at zero. The anisotropy at time zero r(0) and the rotational correlation times τ_R are given for runs 1 and 2. $T_{LCS} \approx 50.1$°C.

run 1				run 2			
T /°C	T /K	r(0)	τ_R /ns	T /°C	T /K	r(0)	τ_R /ns
39.7	312.85	0.319	0.551	49.6	322.75	0.252	0.307
45.0	318.15	0.335	0.423	49.9	323.05	0.321	0.272
49.0	322.15	0.315	0.356	50.0	323.15	0.286	0.264
49.2	322.35	0.278	0.339	50.1	323.25	0.315	0.301
49.4	322.55	0.304	0.339	50.3	323.45	0.335	0.292
49.6	322.75	0.314	0.324	50.4	323.55	0.341	0.287
49.9	323.05	0.316	0.315	50.7	323.85	0.345	0.297
				51.3	324.45	0.316	0.298
				53.1	326.25	0.306	0.275
				55.4	328.55	0.389	0.248

The product $\tau_R \cdot T$, taken as a measure of the microviscosity, is plotted as a function of temperature for both runs in Figure 3.18. A decrease in the product $\tau_R \cdot T$ near T_{LCS} is observed on approach both from above and below T_{LCS}. This is the opposite effect to that observed for Bodipy in the same mixture.

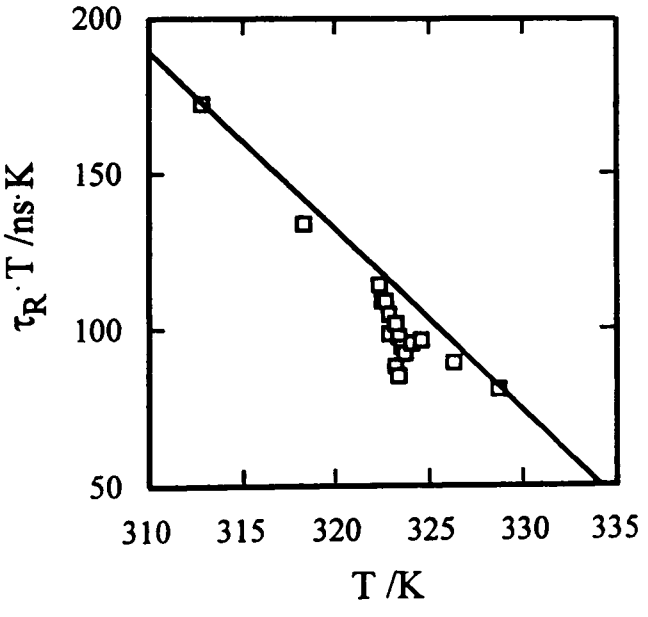

Figure 3.18: The measure of the microviscosity given by the product of the rotational correlation time and temperature $\tau_R \cdot T$ as a function of temperature T for POPOP in a 2-butoxyethanol + H_2O mixture of critical composition. The straight line is drawn to guide the eye.

The fluorescence lifetimes τ_F of POPOP measured were 1.21 ns in 2-butoxyethanol and 1.36±0.04 ns in 2-butoxyethanol + H_2O mixtures. These values agree with the quoted value of 1.26 ns for the lifetime of POPOP in benzene (Berlman, 1965).

The rotational correlation time τ_R of POPOP has been determined as 0.11 ns in ethanol and 0.047 ns in hexane, both at 45°C (Lakowicz and Maliwal, 1985). Our τ_R in 2-butoxyethanol + H_2O are generally longer than these values–as expected from the higher viscosity of our mixture at the same temperature.

The values quoted for the volume of POPOP and its axial ratio if it is assumed to be a spheroid are 331 $Å^3$ and 4.39, respectively (Ben-Amotz and Drake, 1988). Our calculated volume is slightly larger, 361 $Å^3$, see Table 3.13 below.

We turn now to another dye, BTBP, which is larger than POPOP and thus has a higher τ_R for a given mixture viscosity and temperature.

3.3.3 BTBP

The excitation and emission spectra for BTBP in 2-butoxyethanol and in MCH are shown in section 3.2.5. The main absorption bands for BTBP in 2-butoxyethanol occur at 460, 491 and 527 nm and the main emission peaks at 535 and 570 nm. In MCH the peaks in the absorption spectrum for BTBP are shifted by about 10 nm to lower wavelengths and the emission spectrum is shifted by about 15 nm to lower wavelengths relative to 2-butoxyethanol solutions. In 2-butoxyethanol + H_2O mixtures of critical composition the absorption spectrum is the same as in 2-butoxyethanol.

BTBP was studied in 2-butoxyethanol + H_2O or D_2O mixtures using both cell holders and the results are presented in the following sections. The rotational correlation times τ_R in 2-butoxyethanol + H_2O were larger for BTBP than for either Bodipy or POPOP in the same mixture. In 2-butoxyethanol + D_2O, the τ_R values were even longer and thus more easily measured. The effect of substitution of H_2O by D_2O in 2-butoxyethanol + H_2O mixtures has been discussed briefly in Chapter 1, section 1.5.5.

BTBP was also studied in methylcyclohexane + perfluoromethylcyclohexane. However, the results are not presented in detail since the rotational correlation times τ_R times were very short–much shorter than expected from a comparison of the shear viscosities of MCH + PFMCH and 2-butoxyethanol + H_2O. The variation in τ_R was between 0.25 ns and 0.27 ns over a range of 10 K close to T_{UCS}. The values were thus too small to be measured accurately and any variations with temperature were smaller than differences obtained by exciting at the different wavelengths of 482 nm and 517 nm.

3.3.3.1 BTBP in 2-butoxyethanol + H_2O

The rotational correlation time τ_R of BTBP in a mixture of 2-butoxyethanol + H_2O of critical composition, $w_{BXE} = 0.296$, was measured over a range of temperatures close to T_{LCS}. In the earlier experiments using the old cell holder, single-phase mixtures below T_{LCS} and the lower H_2O-rich phase of two-phase mixtures above T_{LCS} were studied using an excitation wavelength of 527 nm. In the experiments repeated using the new cell holder, single-phase mixtures below T_{LCS} and both coexisting phases above T_{LCS} were studied using an excitation wavelength of 491 nm. The shorter excitation wavelength was used to reduce the scattered light passing through the filter.

The anisotropy decay data were fitted to single-exponential decays and the results are given for the old cell holder in Table 3.10 and for the new cell holder in Tables 3.11 and 3.12. The values for χ^2 were generally equal to 1.0±0.2. T_{LCS} was determined visually as 49.9°C (323.05 K) in both sets of experiments.

Table 3.10: The results of fitting the anisotropy data for BTBP in 2-butoxyethanol + H_2O in the single phase and the lower phase using the *old* cell holder to single-exponential decays. The data were fitted from the prompt peak to channel 900 with the anisotropy at infinite time r(∞) fixed at 0.008. The anisotropy at time zero r(0) and the rotational correlation times τ_R are given for each temperature. $T_{LCS} \approx 49.9$°C.

T /°C	T /K	r(0)	τ_R /ns
40.3	313.45	0.338	1.401
45.0	318.15	0.338	1.231
46.6	319.75	0.337	1.165
48.0	321.15	0.332	1.117
48.9	322.05	0.321	1.077
49.5	322.65	0.310	0.993
49.6	322.75	0.306	0.930
49.7	322.85	0.311	0.934
49.8	322.95	0.324	1.046
49.9	323.05	0.323	1.027
50.0	323.15	0.323	1.040
50.2	323.35	0.335	0.998
50.3	323.45	0.324	1.020
50.4	323.55	0.325	1.011
50.6	323.75	0.322	0.973
50.9	324.05	0.305	0.928
52.0	325.15	0.330	0.958

Table 3.11: The results of fitting the anisotropy data for BTBP in 2-butoxyethanol + H_2O in the *single phase* using the *new* cell holder to single-exponential decays. The data were fitted from the prompt peak to channel 1000 with the anisotropy at infinite time r(∞) fixed at the values obtained by fitting first from channels 600-1000. The anisotropy at time zero r(0), the rotational correlation times τ_R, and r(∞) are given for each temperature. T_{LCS} = 49.9°C (323.05 K).

T /°C	T /K	r(0)	τ_R /ns	r(∞)
40.0	313.15	0.324	1.313	0.013
42.5	315.65	0.322	1.222	0.013
45.0	318.15	0.319	1.168	0.010
47.5	320.65	0.320	1.086	0.010
49.0	322.15	0.317	1.053	0.009
49.2	322.35	0.307	1.007	0.007
49.4	322.55	0.305	0.996	0.010
49.6	322.75	0.303	0.967	0.008
49.8	322.95	0.300	0.942	0.008

Table 3.12: The results of fitting the anisotropy data for BTBP in 2-butoxyethanol + H_2O in both *coexisting phases* using the *new* cell holder to single-exponential decays. The data were fitted from the prompt peak to channel 1000 with the anisotropy at infinite time r(∞) fixed at the values obtained by fitting first from channels 600-1000. The anisotropy at time zero r(0), the rotational correlation times τ_R, and r(∞) are given for each temperature. T_{LCS} = 49.9°C (323.05 K).

T /°C	T /K	upper phase			lower phase		
		r(0)	τ_R /ns	r(∞)	r(0)	τ_R /ns	r(∞)
50.1	323.25	0.310	0.911	0.008			
50.3	323.45	0.305	0.977	0.008	0.323	0.961	0.009
50.5	323.65	0.319	0.990	0.008	0.325	0.932	0.011
50.7	323.85	0.330	0.997	0.009	0.313	0.934	0.011
50.9	324.05	0.326	0.981	0.009	0.317	0.931	0.011
53.4	326.55	0.327	0.937	0.005	0.289	0.797	0.013
55.9	329.05	0.326	0.875	0.006	0.324	0.657	0.005

The product of the rotational correlation time and the temperature $\tau_R \cdot T$ is plotted as a function of temperature in Figure 3.19 both for the data obtained using the old cell holder and for those obtained with the new cell holder. A decrease in the product $\tau_R \cdot T$ near T_{LCS} is observed on approach both from above and below T_{LCS}. This negative anomaly is similar to that observed with POPOP, but is the opposite effect to that observed with Bodipy and that shown by the macroscopic viscosity.

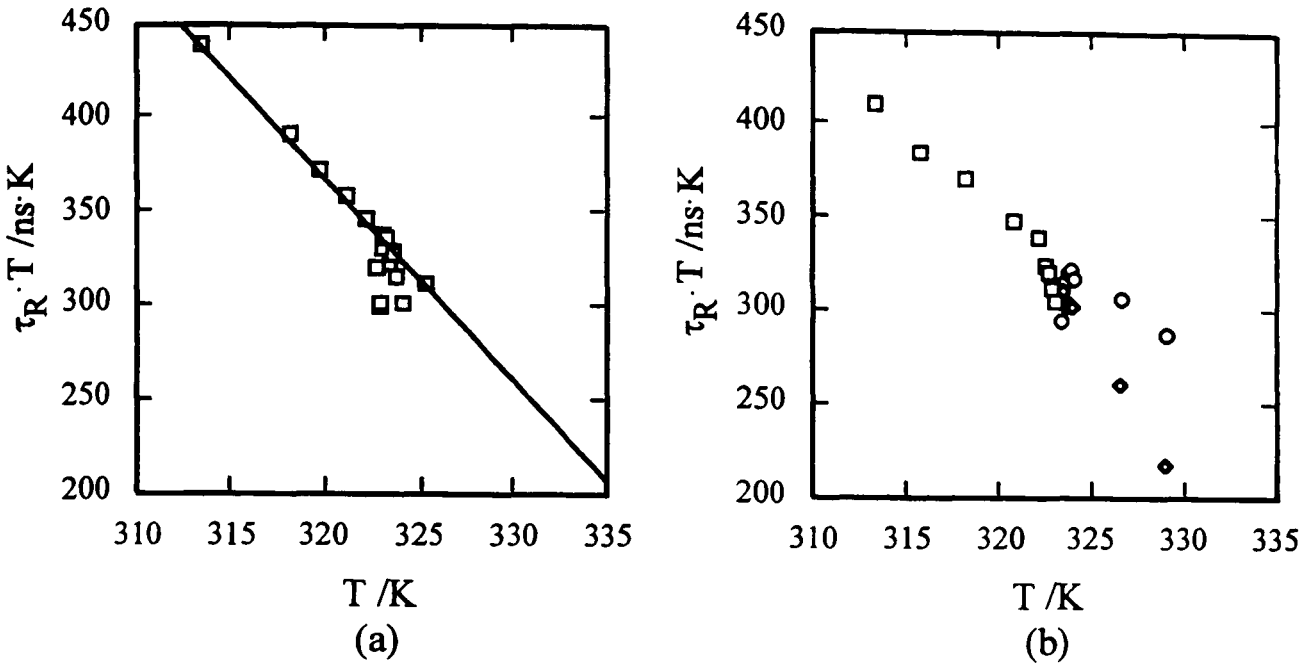

Figure 3.19: The measure of the microviscosity given by the product $\tau_R \cdot T$ as a function of temperature T for BTBP in a 2-butoxyethanol + H_2O mixture of critical composition. (a) In the single phase and the lower water-rich phase using the old cell holder. The straight line is drawn to guide the eye. (b) In the single phase (□) and in the upper (O) and lower (◊) phases using the new cell holder.

It is clear both from the tabulated results in Tables 3.10-3.12 and from Figure 3.19 that the data obtained using the new cell holder show less scatter than those obtained using the old cell holder, although the overall result of a negative anomaly is apparent in both data sets.

At a given temperature, the lower water-rich phase has the shorter rotational correlation time as expected since this phase is less viscous than the 2-butoxyethanol-rich phase. The $\tau_R \cdot T$ data obtained using the new cell holder were converted to viscosities to allow direct comparison with the macroscopic shear viscosities. This conversion is discussed below and was accomplished using an equation of the form of equation (3.7) and approximating the molecule as an ellipsoid.

An ellipsoid has three different orthogonal axial dimensions and all three cross-sections through these axes are ellipses. This is in contrast with a spheroid in which two of the axes have the same dimensions. If the two equivalent dimensions are smaller than the third, then the body is a prolate spheroid, a 'stretched sphere'; if the two dimensions are greater than the third, it is an oblate spheroid, a 'squashed' sphere. In a spheroid, two of the cross-sections through the axes are thus circles and the third is an ellipse.

The dimensions of BTBP were obtained using Macromodel, a graphical molecular mechanics program (Mohamadi *et al.*, 1990), which calculates the dimensions and moments of inertia for the minimum energy conformation of the molecule. The dimensions are obtained using the sum of the covalent radii (Huheey, 1983) in the molecule, and the van der Waals radii (Bondi, 1964) for the edge atoms in each direction. (The covalent radius is half the distance of separation of two bonded atoms. The van der Waals radius is half the intramolecular separation of two equivalent atoms at the point of minimum energy; the values are obtained from crystal x-ray diffraction data.) The program ellipso (see appendix) was used to calculate the appropriate factor for an ellipsoid–used in place of the volume of the spheroid in equation (3.7) to account for the rotation about one of the two shorter axes–from the BTBP dimensions using the Perrin integrals (Perrin, 1934) and the Youngren and Acrivos parameters (Youngren and Acrivos, 1975) and assuming the stick condition. (The program ellipso takes the input hemi-axis dimensions as for a rectangular block and converts them to the dimensions of an ellipsoid with the same volume. However, this conversion was not performed here.)

Our $\tau_R \cdot T$ values were converted to viscosities as discussed above. The resulting values were then further scaled by a multiplicative factor of 0.85 to account for the 15% deviation from stick conditions noted by Ben-Amotz and Drake (1988). The results are plotted in Figure 3.20 along with the macroscopic viscosities, which have been scaled by +0.9 K in temperature to ensure coincidence of the critical temperatures. Our single-phase microscopic viscosities obtained by the conversions discussed above are essentially the same as the macroscopic viscosities at temperatures removed from T_{LCS}. At temperatures removed from T_{LCS} in the two-phase region, however, the values for the microscopic and macroscopic viscosities of coexisting phases are different, although they are of the same order of magnitude. Both above and below T_{LCS} the anomaly in the microscopic viscosity is in the opposite sense to that in the macroscopic viscosity but, particularly in the single phase, it appears to be of a similar magnitude.

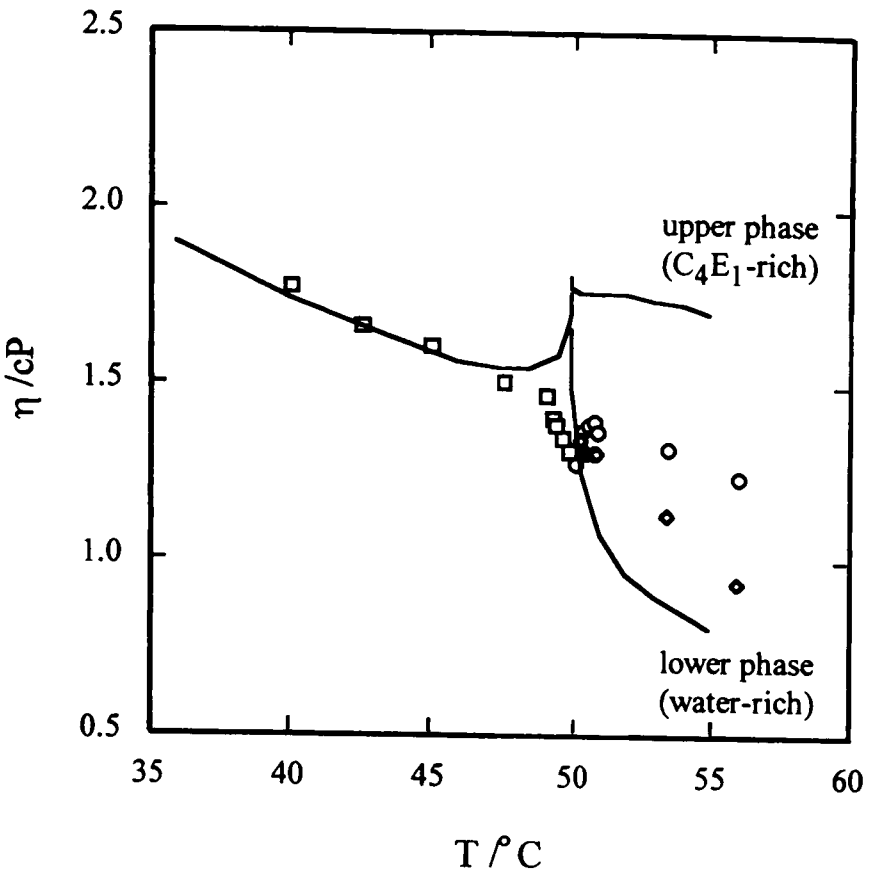

Figure 3.20: The macroscopic shear viscosity η and the microscopic viscosity calculated from $\tau_R \cdot T$ *versus* temperature T for BTBP in a 2-butoxyethanol + H_2O mixture of critical composition in the single phase (□) and in the upper (O) and lower (◊) phases.

The volume of an ellipsoid can be calculated from $(4\pi abc)/3$, where a, b and c are the hemi-axis lengths. The volume of BTBP, assuming it can be modelled as an ellipsoid, and the dimensions obtained from Macromodel are given in Table 3.13. The dimensions of Bodipy and POPOP are also included for comparison.

Table 3.13: The orthogonal axes dimensions x,y,z and volumes V, assuming ellipsoids, of the dyes used in this work.

dye	x /Å	y /Å	z /Å	V /Å^3
BTBP	25.19	11.90	9.22	1447
POPOP	21.61	9.26	3.45	361
Bodipy	21.03	14.71	5.17	837

The fluorescence properties of BTBP including its fluorescence lifetime and rotational correlation time have been studied by Ben-Amotz and Drake (1988) in a range of alkane and alcohol solvents of different viscosities and at various temperatures. They observed that the rotational diffusion times of BTBP in alkanes and alcohols plotted *versus* the viscosity/temperature ratio fell on the same line. The orientation of the transition dipole of BTBP is not known but evidence suggests that it lies along or nearly along the major axis. The values of r(0) are close to 0.4 which indicates that the dipoles for absorption and fluorescence have the same orientation relative to the molecular axes. The fluorescence quantum yield of BTBP has been determined as 0.99 (Rademacher *et al.*, 1982). The fluorescence lifetime of BTBP measured by Ben-Amotz and Drake in *n*-alcohol and *n*-alkane solvents over a range of temperatures 10-90°C was found to be 3.7±0.1 ns. Our measured lifetimes in 2-butoxyethanol + H_2O or D_2O were within this range. The central five-ring structure of the BTBP molecule is perylene. The absorption spectrum of BTBP is shifted by about 100 nm to longer wavelengths than perylene.

Ben-Amotz and Drake (1988) modelled BTBP as a prolate spheroid. They fixed the major axis dimension to the sum of the geometric bond lengths and van der Waals radii, quoted as 26 Å. The two equal minor axis dimensions were determined by requiring the volume of the spheroid to be equal to the van der Waals volume calculated using van der Waals increments, quoted as 733 $Å^3$. This volume is much smaller than our calculated ellipsoid volume; the discrepancy may be due to different approximations of molecular shape and different methods of calculation of the molecular dimensions.

In the experiments using the new cell holder, for which the results are reported in Tables 3.11 and 3.12, data were collected at temperatures closer to T_{LCS}. However, the data could not be fitted by a simple single-exponential decay, instead requiring a bi-exponential with some small amount of a component attributed to scattered light. The detection of scattered light was probably enhanced by the opalescence of the sample.

During a separate allocation of beamtime, tests were carried to investigate other aspects of the experiment such as the effects of the equilibration time and the excitation wavelength; the outcomes are discussed here. The fluorescence anisotropy of single-phase samples of BTBP in 2-butoxyethanol + H_2O was measured at 40.0°C and at 49.8°C to investigate the variation in τ_R with the equilibration time for clear and opalescent samples. For the sample at 40°C, results were obtained after equilibration times of 1, 20, 38 and 55 mins. The variation in τ_R over this timescale was small: τ_R = (1.312±0.012) ns and r(0) = 0.332±0.001. For the near-critical sample at 49.8°C, results were obtained after equilibration times of 10, 28 and 46 mins. The variation in τ_R was again small: τ_R = (0.918±0.003) ns and r(0) = 0.318±0.002. This range of values was smaller than previously observed during different experimental runs. In our experiments the samples were generally equilibrated for a minimum of 15 mins and it seems that longer equilibration times would not have altered the outcome.

The same sample at 40°C was also studied at different wavelengths of the incident light: 491, 504 and 527 nm. At 491 nm and 527 nm the excitation spectrum shows a peak and at 504 nm a trough. The variations in τ_R were again small: τ_R = (1.303±0.003) ns and r(0) = 0.334±0.002 thus validating our choice of wavelength in the main experiments. Tests using different filters showed that the OG550 and OG570 filters were both suitable for our purpose.

3.3.3.2 BTBP in 2-butoxyethanol + D_2O

The rotational correlation time τ_R of BTBP in a mixture of 2-butoxyethanol + D_2O of critical composition, w_{BXE} = 0.274, was measured over a range of temperatures close to T_{LCS}. Single-phase mixtures below T_{LCS}, and both the lower D_2O-rich phase and the upper phase of two-phase mixtures above T_{LCS}, were studied using both cell holders. The measurements obtained with the new cell holder were repeated a second time to characterise the variation of τ_R with temperature more fully in the two-phase region ensuring that the sample was fully mixed. The excitation wavelength used was 491 nm.

The anisotropy decay data were fitted to single-exponential decays, but from 15 or 20 channels after the prompt peak to exclude the effects of scattered light which were particularly apparent close to T_{LCS}. This method was adopted instead of fitting bi-exponential decays from the prompt peak since in fitting a bi-exponential decay the two components are effectively coupled and the solution need not be unique. The values for χ^2 were generally equal to 1.1±0.1. T_{LCS} was determined visually as approximately 46.6°C (319.75 K) using the old cell holder, and as 43.0°C (316.15 K) and later as 43.2°C (316.35 K) using the new cell holder. The main discrepancy is due to poor contact between the electrical connections to the old cell holder so that the temperature setting, which was the recorded temperature, was higher than the actual temperature of the mixture.

For the results using the new cell holder, a G factor was used in fitting; thus eliminating the requirement for an r(∞) term. This was determined at the time of the experiments with the polariser on the entrance side set to horizontal and by measuring the intensities of the fluorescence with the exit polariser set in turn to perpendicular and parallel. An average of the counts for each polariser position was determined and the G factor was calculated from: G factor = (perpendicular counts)/(parallel counts). Deviations from G factor = 1 occur due to factors such as distortions in the lenses, the angle of the beam and the position of the photomultiplier tube.

The results using the old cell holder are given in Tables 3.14 and 3.15 and the results using the new cell holder are given for run 1 in Tables 3.16 and 3.17 and for run 2 in Tables 3.18 and 3.19.

Table 3.14: The results of fitting the anisotropy data for BTBP in 2-butoxyethanol + D_2O in the *single phase* using the *old* cell holder to single-exponential decays. The data were fitted from 15 channels after the prompt peak to channel 1000 with the anisotropy at infinite time r(∞) allowed to vary. The r(∞) values are all < 0.015. The anisotropy at time zero r(0), the rotational correlation times τ_R, and r(∞) are given for each temperature. $T_{LCS} \approx 46.6°C$ (319.75 K).

T /°C	T /K	r(0)	τ_R /ns	r(∞)
33.8	306.95	0.324	1.826	0.014
38.1	311.25	0.327	1.754	0.008
43.5	316.65	0.332	1.744	0.009
44.7	317.85	0.330	1.673	0.008
46.3	319.45	0.338	1.640	0.006

Table 3.15: The results of fitting the anisotropy data for BTBP in 2-butoxyethanol + D_2O in both *coexisting phases* using the *old* cell holder to single-exponential decays. The data were fitted from 15 channels after the prompt peak to channel 1000 with the anisotropy at infinite time r(∞) allowed to vary. The r(∞) values are all < 0.009. The anisotropy at time zero r(0), the rotational correlation times τ_R, and r(∞) are given for each temperature. $T_{LCS} \approx 46.6°C$ (319.75 K).

T /°C	T /K	upper phase			lower phase		
		r(0)	τ_R /ns	r(∞)	r(0)	τ_R /ns	r(∞)
46.8	319.95	0.308	1.287	0.005	-	-	-
47.5	320.65	0.334	1.276	0.004	-	-	-
47.7	320.85	0.327	1.294	0.004	0.328	1.241	0.006
47.9	321.05	0.335	1.256	0.004	0.311	1.154	0.008
48.6	321.75	0.289	1.220	0.004	0.318	1.121	0.005
50.0	323.15	0.332	1.159	0.003	-	-	-
51.1	324.25	0.323	1.136	0.004	0.341	1.210	0.002
52.7	325.85	-	-	-	0.263	1.003	0.006
52.8	325.95	0.301	1.074	0.003	-	-	-
55.3	328.45	-	-	-	0.314	1.041	0.007
55.4	328.55	0.289	1.008	0.005	-	-	-

Table 3.16: The results of fitting the anisotropy data for BTBP in 2-butoxyethanol + D_2O in the *single phase* using the *new* cell holder (*run 1*) to single-exponential decays. The data were fitted from 20 channels after the prompt peak to channel 1000 with the G factor = 0.965 and the anisotropy at infinite time $r(\infty) = 0$. The anisotropy at time zero r(0) and the rotational correlation times τ_R are given for each temperature. $T_{LCS} \approx$ 43.0°C (316.15 K).

T /°C	T /K	r(0)	τ_R /ns
30.0	303.15	0.342	2.128
32.5	305.65	0.340	1.943
35.0	308.15	0.337	1.780
37.5	310.65	0.335	1.624
42.5	315.65	0.325	1.364
42.7	315.85	0.333	1.355
42.8	315.95	0.318	1.351
42.9	316.05	0.311	1.301
43.0	316.15	0.303	1.208

Table 3.17: The results of fitting the anisotropy data for BTBP in 2-butoxyethanol + D_2O in both *coexisting phases* using the *new* cell holder (*run 1*) to single-exponential decays. The data were fitted from 20 channels after the prompt peak to channel 1000 with the G factor = 0.965 and the anisotropy at infinite time $r(\infty) = 0$. The anisotropy at time zero r(0) and the rotational correlation times τ_R are given for each temperature. $T_{LCS} \approx$ 43.0°C (316.15 K).

T /°C	T /K	upper phase		lower phase	
		r(0)	τ_R /ns	r(0)	τ_R /ns
43.1	316.25	0.318	1.335	0.323	1.333
43.2	316.35	0.323	1.348	0.321	1.295
43.3	316.45	0.315	1.316	0.320	1.318
43.4	316.55	0.333	1.348	0.306	1.285
43.5	316.65	0.333	1.337	0.334	1.324
43.7	316.85	0.327	1.384	0.322	1.344
44.0	317.15	0.335	1.337	0.303	1.285
45.0	318.15	0.337	1.280	0.328	1.256
47.5	320.65	0.317	1.221	0.329	1.141
50.0	323.15			0.363	0.611

Table 3.18: The results of fitting the anisotropy data for BTBP in 2-butoxyethanol + D_2O in the *single phase* using the *new* cell holder (*run 2*) to single-exponential decays. The data were fitted from 20 channels after the prompt peak to channel 1000 with the G factor = 0.967 and the anisotropy at infinite time $r(\infty) = 0$. The anisotropy at time zero r(0) and the rotational correlation times τ_R are given for each temperature. $T_{LCS} \approx$ 43.2°C (316.35 K).

T /°C	T /K	r(0)	τ_R /ns
40.0	313.15	0.337	1.513
42.5	315.65	0.321	1.393
43.0	316.15	0.304	1.342
43.2	316.35	0.308	1.257

Table 3.19: The results of fitting the anisotropy data for BTBP in 2-butoxyethanol + D_2O in both *coexisting phases* using the *new* cell holder (*run 2*) to single-exponential decays. The data were fitted from 20 channels after the prompt peak to channel 1000 with the G factor = 0.967 and the anisotropy at infinite time $r(\infty) = 0$. The anisotropy at time zero r(0) and the rotational correlation times τ_R are given for each temperature. $T_{LCS} \approx 43.2$°C (316.35 K).

T /°C	T /K	upper phase		lower phase	
		r(0)	τ_R /ns	r(0)	τ_R /ns
43.3	316.45	0.322	1.315	0.348	1.253
43.4	316.55	0.250	1.153	0.319	1.252
43.8	316.95	0.328	1.300	0.315	1.299
44.3	317.45	0.332	1.297	0.324	1.244
46.0	319.15	0.320	1.247	0.328	1.190
48.0	321.15	0.330	1.144	0.328	1.051
50.0	323.15	0.339	1.058	0.361	0.918
51.5	324.65	0.338	1.035		
53.0	326.15	0.334	0.964		

The product of the rotational correlation time and the temperature $\tau_R \cdot T$ is plotted as a function of temperature in Figure 3.21 for the results obtained using the old cell holder. No particular anomaly is observed in $\tau_R \cdot T$ in the single phase, but a slight increase is detected for both the upper and lower phases as T_{LCS} is approached. An interesting point to note is that the microviscosity seems to have similar values in the upper and lower phases, unlike the expected macroscopic viscosity. This may indicate that the probe is in a similar environment in each phase; however, the results obtained for the coexisting phases using the new cell holder are not so similar.

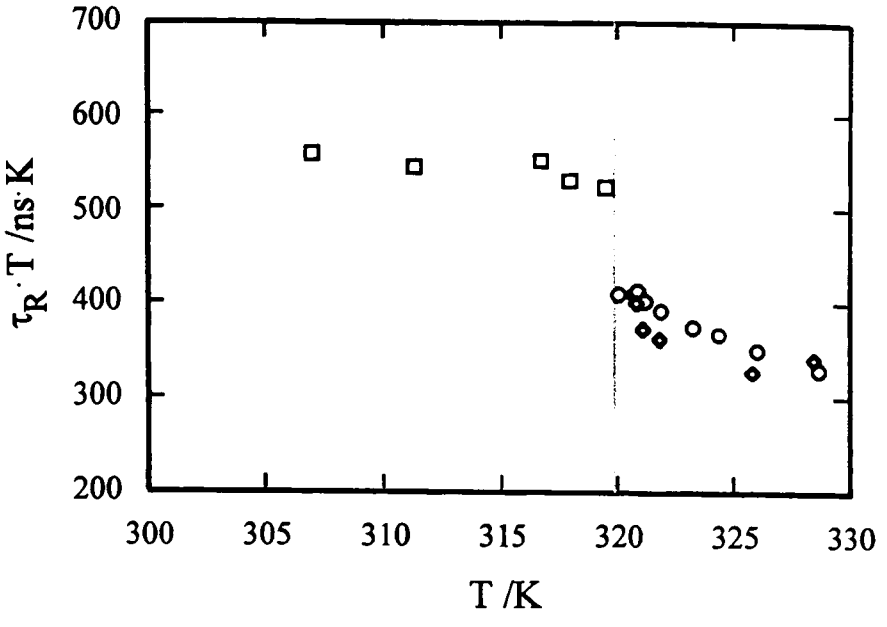

Figure 3.21: The measure of the microviscosity given by the product $\tau_R \cdot T$ as a function of temperature T for BTBP in a 2-butoxyethanol + D_2O mixture of critical composition in the single phase (□) and in the upper (O) and lower (◊) phases using the old cell holder. The vertical line marks T_{LCS}.

The product $\tau_R \cdot T$ is plotted for the results obtained using the new cell holder in Figure 3.22. The values plotted are for runs 1 and 2 for the single-phase mixture and for run 2 for the coexisting phases. For run 1 the temperatures are scaled by +0.2 K so that the critical temperatures for each run coincide. For the coexisting phases the y-axis range is decreased so that the points can be seen more clearly. The results obtained for both runs 1 and 2 agree within a reasonable experimental error. In contrast to the results obtained using the old cell holder, those obtained with the new cell holder show a negative anomaly as T_{LCS} is approached from the single-phase region. However, no anomaly is observed as T_{LCS} is approached along either limb of the coexistence curve.

The discrepancy in the trends observed for $\tau_R \cdot T$ *versus* T for the experiments using the different cell holders may be due to poor equilibration in the old cell holder. The results obtained using the new cell holder are more likely to reflect the 'true' trend.

Close to T_{LCS} a negative anomaly is observed in r(0) for the results obtained using the new cell holder. This is particularly pronounced for the single phase; more scatter is observed in r(0) for the coexisting phases. This effect is shown in Figure 3.23. A similar effect is observed for BTBP in 2-butoxyethanol + H_2O and these results are also plotted. The decrease in r(0) close to T_{LCS} may be due to the increase in the opalescence of the sample, leading to an increase in the amount of multiply scattered exciting light and fluorescence which may alter the polarisation.

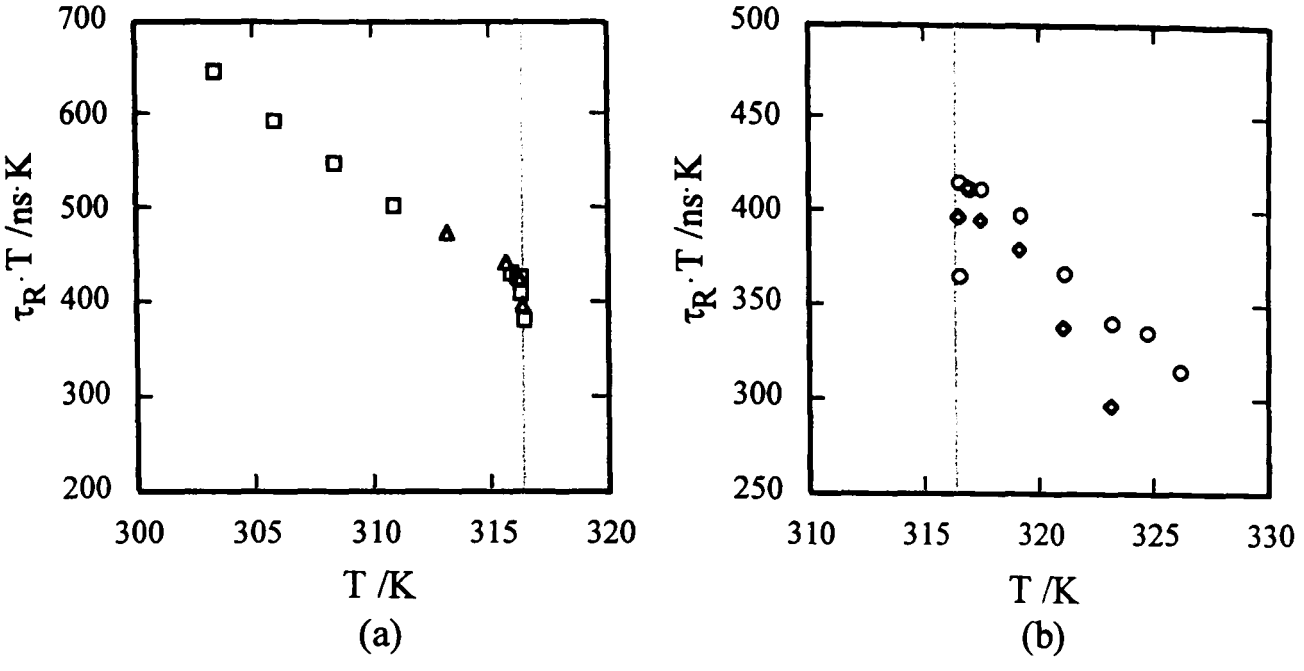

Figure 3.22: The measure of the microviscosity given by the product $\tau_R \cdot T$ as a function of temperature T for BTBP in a 2-butoxyethanol + D_2O mixture of critical composition (a) in the single phase, run 1 (□) and run 2 (Δ), and (b) in the upper (O) and lower (◊) phases using the new cell holder. The vertical lines mark T_{LCS}.

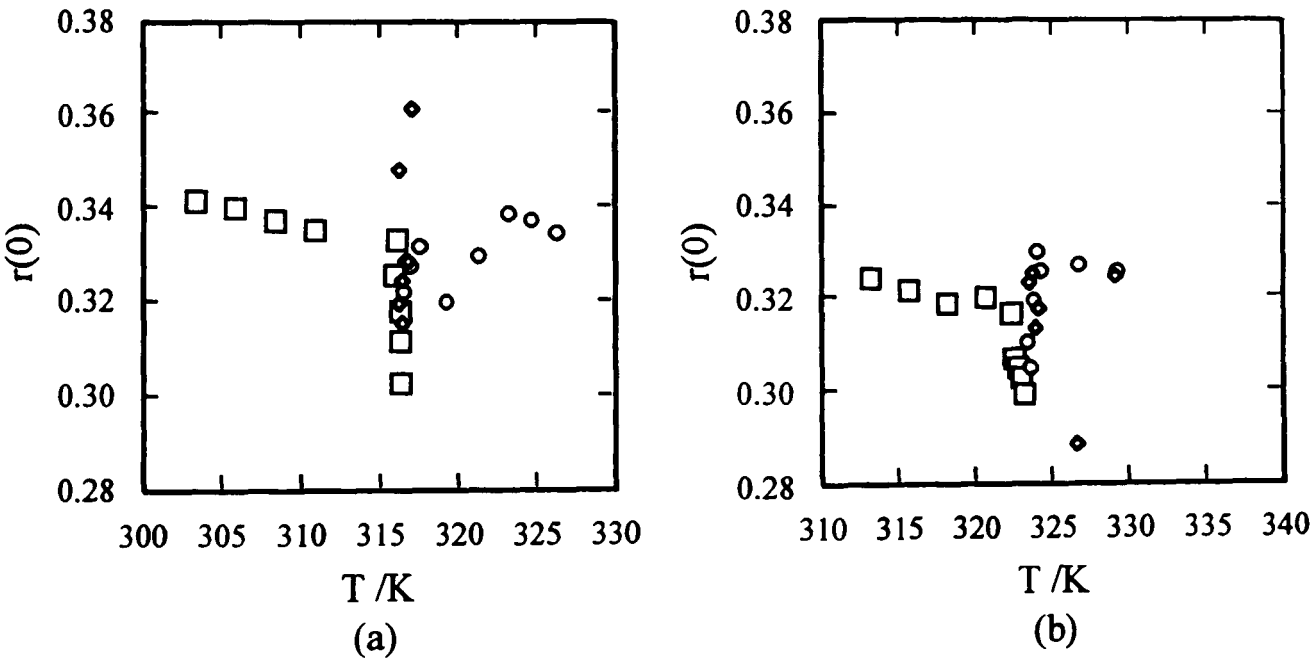

Figure 3.23: The anisotropy at time zero r(0) as a function of temperature T for critical composition mixtures of BTBP in (a) 2-butoxyethanol + D_2O and (b) 2-butoxyethanol + H_2O in the single phase (□) and in the upper (O) and lower (◊) phases using the new cell holder.

3.4 Discussion

The microviscosity of four different systems as a function of temperature close to the critical point has been studied by measuring the rotational correlation time τ_R of a fluorescence probe. The systems are: Bodipy, POPOP and BTBP in 2-butoxyethanol + H_2O and BTBP in 2-butoxyethanol + D_2O. The main outcomes are that Bodipy exhibits an unsurprising *positive* anomaly similar to that observed in the macroscopic viscosity, but a *negative* anomaly is observed for each of the other three systems. In each case the anomaly is more pronounced for the approach to T_{LCS} from the single phase than from the two-phase region.

The essential issue to be resolved is that of reconciling the variety of microviscosity temperature dependence observed here near a liquid-liquid critical point with the well known divergence of the correlation length ξ according to the expression $\xi = \xi_0 \varepsilon^{-\nu}$, where the critical index $\nu = 0.63$–see Chapter 1, section 1.1.4–that occurs in all near-critical systems, whatever their nature–magnetic, gas-liquid, or, as here, liquid-liquid. This divergence in ξ is believed to be the cause of all critical phenomena and is clearly independent of any molecular processes simultaneously in train in any particular system at a critical point. In particular, the issue is the unexpected observation that in some of our systems the correlation length divergence, and its usual manifestation of a divergence in shear viscosity is apparently overwhelmed by another effect, such that this divergence is not observed in our results. By contrast, the identification of the causes of the anomaly observed in some mixtures and not in others, although possibly offering a clue to the main issue, is for the moment secondary.

The reason for the 'normal' anomaly in the shear viscosity at a critical point is usually attributed to the increase in effective rigidity in liquid structure caused by the divergence in ξ. This must be happening in all our mixtures, indeed we have measured it macroscopically in the most studied of our mixtures: 2-butoxyethanol + H_2O. The cause of the observed drop in ξ must therefore be a purely local event that heavily conditions the environment of the probe molecule.

We have discussed in section 3.1.3 the features of local environment which have been invoked to account for an *increase* in local fluidity, manifest as a decrease in the rotational correlation time τ_R, in a liquid–slip and subslip, usually attributed to liquid structure modification in the environment of the probe–and for a *decrease* in local fluidity, manifest as an increase in the rotational correlation time τ_R, in a liquid–stick and superstick, usually attributed to solvation of the probe. In mixtures, and particularly mixtures in the vicinity of a liquid-liquid critical point, there must be added a third factor which can be seen as related to the molecular conditions for stick and superstick, namely the large change in local environment likely to occur in a mixture close to phase separation, i.e. the large fluctuations in local concentration which accompany the fluctuations in density which occur in all near-critical fluid systems.

The effect of fluctuations in composition on the probe environment depends on the differential susceptibility of the probe to solvation by the components of the mixture. For example, in mixtures whose components are broadly speaking similar and whose mutual partial miscibility rests on a specific *weakness* in the unlike interaction, for example hydrocarbon + perfluorocarbon mixtures, specific solvation with associated structural changes might be expected to be less pronounced than in those in which the partial miscibility reflects large differences in the nature of the components. Such mixtures, for example, encompass alkane + alkanol mixtures and aqueous mixtures such as 2-butoxyethanol + water. In mixtures of these kinds the molecular environment in the coexisting phases in the two-liquid region of coexistence are likely to be very different and so give rise to very different effects of near-criticality even in the one-liquid phase region as composition fluctuations increase sharply towards the critical point.

Perhaps the most likely effect of these fluctuations in relation to a probe molecule is to change the opportunity for slip and for stick phenomena. For example, with the alcohol solutions discussed above, the lower τ_R compared to that in 'corresponding' alkanes is attributed to the formation of 'cages' or clathrate-like holes within which the probe can rotate more easily than in a liquid of similar viscosity but lacking the structural characteristics required to generate cages of suitable size or any cages at all. Changes in local composition near a critical point could be imagined as reducing the ease of formation of such cages and thus increasing τ_R and suggesting an increase in viscosity. Conversely, if the changes in the local structure increase the ease of cage formation, τ_R will decrease suggesting a drop in viscosity. We turn now to the application of these ideas to the systems under consideration.

The observation of a decrease in τ_R close to T_{LCS} in some of our systems was quite unexpected. Among the main issues that demand consideration are:

(i) The reasons for the observation of a *positive* anomaly in the microscopic viscosity measured using Bodipy as a probe but of a *negative* anomaly using other probes in the same liquid mixture.

(ii) The effects that could contribute to the observation of a negative anomaly in the microscopic viscosity, particularly since the macroscopic viscosity shows a positive anomaly.

In an attempt to answer part (i), the structures of the dyes can be compared. The molecules are all neutral, although there is nominally some partial charge separation in Bodipy across the B-N bond. One notable difference, which may possibly account for the difference in behaviour in our hydrogen-bonded mixtures, is that POPOP and BTBP have the potential to form hydrogen bonds with the solvent molecules, but this capability is apparently absent in Bodipy, although the B-F bond may be polar enough for some kind of specific interaction to occur.

Turning now to point (ii), as mentioned earlier, for example in section 3.1.3, shorter rotational correlation times for small solutes have been observed in alcohols than in alkanes. This has been termed subslip and is explained either by structural or by dynamical effects at molecular level within the solvent. Such explanations may possibly be applied near a critical point by considering the changes occurring in the solvent. The structures present in 2-butoxyethanol + water mixtures have been discussed in Chapter 1, section 1.5.5. The two expected entities are clathrate-hydrate like structures with 50 H_2O molecules per 2-butoxyethanol molecule and micelle-like structures with 4 H_2O molecules per 2-butoxyethanol molecule.

Bodipy may be most likely to reside in 2-butoxyethanol-rich regions so that the molecule is in contact mostly with the alkyl chains. Bodipy may thus effectively probe the 'true' microscopic viscosity as the interactions with the solvent are likely to be less pronounced.

Close to T_{LCS}, POPOP and BTBP rotate faster than expected. The molecules are relatively large, probably too large to sit inside 2-butoxyethanol micelles. They are thus more likely to be linked to the clathrate-hydrate structures. The dye molecules are present in small amounts and so the extensive structure is unlikely to be largely disrupted. POPOP and BTBP have the potential to interact *via* hydrogen bonds with the solvent, although they are largely aromatic and may prefer an alkyl-rich environment. The fast rotational correlation times suggest subslip behaviour which may occur as the solvent reorganises close to the critical point. However, hydrogen-bonding linkages will increase the effective size of the molecule and thus also τ_R and the molecules may be too large to sit inside cavities in the solvent structure. Furthermore, BTBP has been observed to show near-stick behaviour in alcohols and alkanes.

A more likely explanation may involve the fluctuations occurring in the solvent near a critical point. If the timescale of the solvent fluctuations increases along with the correlation length, then the probe may no longer experience the full viscosity of the solvent and this may also lead to subslip behaviour.

Another totally separate factor which may affect the results is that of critical opalescence. In theory this should not be a prominent factor since light scattering is elastic and we have endeavoured to eliminate the collection of light of the incident wavelength along with the longer wavelength fluorescence by the use of filters. However, in practice this is not easily achieved as indicated by the change in r(0) as the critical point is approached. This possible complicating factor might be investigated further using isooptic mixtures, for example nitroethane + 3-methylpentane, in which the refractive indices of the phases are matched and thus critical opalescence is reduced.

It is noted here that recent results using BTBP in a mixture of ethanol + hexadecane of critical composition indicate the presence of a positive anomaly in τ_R near T_{UCS}. This further suggests that the negative effects discussed here for the same dye in different mixtures may be due to the changes occurring in the solvent near the critical point, rather than to particular effects of the dye. The results also serve to validate this dye as a suitable probe for microviscosity in selected mixtures.

We now turn to thoughts of avenues for testing the ideas outlined above. The obvious course is to expand the range of observed phenomenology. The most pressing matter is to explore the composition dependence of τ_R. If there are competing processes affecting τ_R, it is unlikely that the dependence on mixture composition will be the same for all factors affecting τ_R. Equally, but less efficiently accomplished, it is clearly desirable to expand the body of knowledge of the microviscosity of mixtures studied by fluorescence depolarisation to attempt to deconvolve the dominant factors in different situations. For example, data are needed on many more near-critical mixtures of different kinds–to check whether the details of the depolarisation process differ with changes in the molecular causes of partial miscibility–and on different probes–to check the aspects of local structural environment.

Measurements of the depolarised Rayleigh linewidths in the critical region of binary liquid mixtures have been carried out by Petrula *et al.* (1978) and Phillies *et al.* (1978) to obtain reorientational relaxation rates. They observe at best a weak anomaly in the relaxation times at the critical point. However, some differences are apparent between their work and our own. In our work we are looking at the rotation of a probe molecule in the liquid rather than the collective motion of the liquid itself and we are thus considering wavelengths of the order of the length of a probe molecule, i.e. shorter than the wavelengths of light. Due to the differences in our method of study and range of probe wavelength compared with those of previous workers, it is not totally surprising that the outcomes from each study are not the same, but this aspect deserves consideration in future investigations.

3.5 Summary

Both anomalous increases and anomalous decreases have been observed in the product $\tau_R \cdot T$, which is used as a measure of the microviscosity, for different dyes in the same mixture 2-butoxyethanol + H_2O. The reason for the differences in behaviour is not clear and deserves further investigation.

The mixtures investigated here may be usefully studied across the composition range using BTBP as a probe, both along the isothermal path to the critical point and at temperatures removed from the critical region to study the non-critical behaviour. The mixture 2-butoxyethanol + H_2O could also be investigated using a suitable ionic dye to investigate the hydrogen-bonding nature of the solvent and changes in the solvent structure near the critical endpoint. Other large nonionic dyes may also be useful. A porphyrin dye was briefly investigated in this work, but only scatter was detected, although other similar dyes may prove better probes. The fluorescence properties of some porphyrins in micelles have been studied by Maiti *et al.* (1995).

Other mixtures exhibiting closed loops and those exhibiting upper critical endpoints may be interesting to allow some comparison between mixtures of different chemical composition, particularly more viscous mixtures in which no hydrogen bonding occurs.

Finally, other methods of obtaining the rotational correlation time, such as NMR and ESR, should prove useful complementary studies to provide greater insight into the microscopic viscosity and structure of binary mixtures near critical points.

CHAPTER 4: CRITICAL-POINT WETTING AT THE SOLID-LIQUID INTERFACE

4.1 Evanescent-wave-generated fluorescence spectroscopy

In the previous chapter the use of fluorescence in the study of the microscopic rheological properties of mixtures has been discussed. We turn now to a different fluorescence technique, that of evanescent-wave-generated fluorescence spectroscopy (EWGFS), also known as total-internal-reflection fluorescence (TIRF), which we have used to study the wetting behaviour at the solid-liquid interface in mixtures near a critical endpoint.

As a critical endpoint is approached from the two-phase region, one of the phases preferentially wets the noncritical phase such as the solid container or the vapour, and a transition from partial to complete wetting occurs at some temperature T_w not quite at the critical temperature T_c. The details of critical-point wetting at the solid-liquid interface have been discussed in Chapter 1, sections 1.3.2 and 1.3.3. In this chapter the technique of EWGFS and its application in this area is considered.

The issues in critical-point wetting include the nature of the wetting phase, the value of the transition temperature T_w, the order of the transition, and the thickness of the interposing wetting layer. The main aim of this work was to identify T_w for the binary mixture studied by two different methods of detection of the fluorescence. In addition, we planned to investigate the order of the transition and to determine the nature and thickness of the wetting film and their variations with temperature.

In the following sections, EWGFS, the different methods for the detection of the fluorescence and the particular properties of the fluorescent dye used in this work are discussed. Later sections describe the details of the experimental arrangements and the results.

4.1.1 Technique of evanescent-wave-generated fluorescence spectroscopy

4.1.1.1 Evanescent waves

The spectroscopic technique of EWGFS utilises the evanescent wave which is generated when total internal reflection occurs. The accompaniment of total reflection by an evanescent wave was first noted by Sir Isaac Newton (Newton, 1704). When light is incident at the boundary between two transparent media of different optical densities, it is totally reflected if the incident beam is in the optically dense medium, i.e. the medium of higher refractive index, and the angle of incidence measured relative to the normal is greater then the critical angle α_c.

The relationship between α_c and the refractive indices of the two adjoining media is:

$$\sin\alpha_c = n_0/n_1 \tag{4.1}$$

where n_0 and n_1 are the refractive indices of the optically rare and optically dense media, respectively. An evanescent wave accompanies total reflection and propagates along the boundary between the two media with a decaying amplitude into the medium of lower refractive index. The intensity I of the electric field of the evanescent wave decays exponentially with perpendicular distance z from the totally reflecting boundary:

$$I(z) = I_0 \exp(-2z/z_{0,1}) \tag{4.2}$$

where I_0 is an amplitude and $z_{0,1}$ is the penetration depth of the evanescent wave. The penetration depth is the distance required for the electric field amplitude to decay to 1/e of its original value and is given by:

$$z_{0,1} = (\lambda_{ex}/2\pi)\,[(n_1\sin\alpha_{ex})^2 - (n_0)^2]^{-1/2} \tag{4.3}$$

where λ_{ex} is the wavelength of the incident light and α_{ex} is the angle of incidence. The penetration depth may be several tens of nm and the evanescent wave can thus probe the medium of lower refractive index, generally a liquid, close to the interface, e.g. a solid-liquid boundary.

4.1.1.2 General experimental arrangement

In our and other studies of critical-point wetting the liquid film at a solid-liquid interface has been studied by using the evanescent wave to excite fluorescent molecules in the liquid. If the liquid is not naturally strongly fluorescent, a fluorescent dye may be added. In these kinds of experiment the arrangement generally consists of a light beam directed radially through a hemicylindrical prism onto its planar surface which is in contact with the liquid, as shown in Figure 4.1.

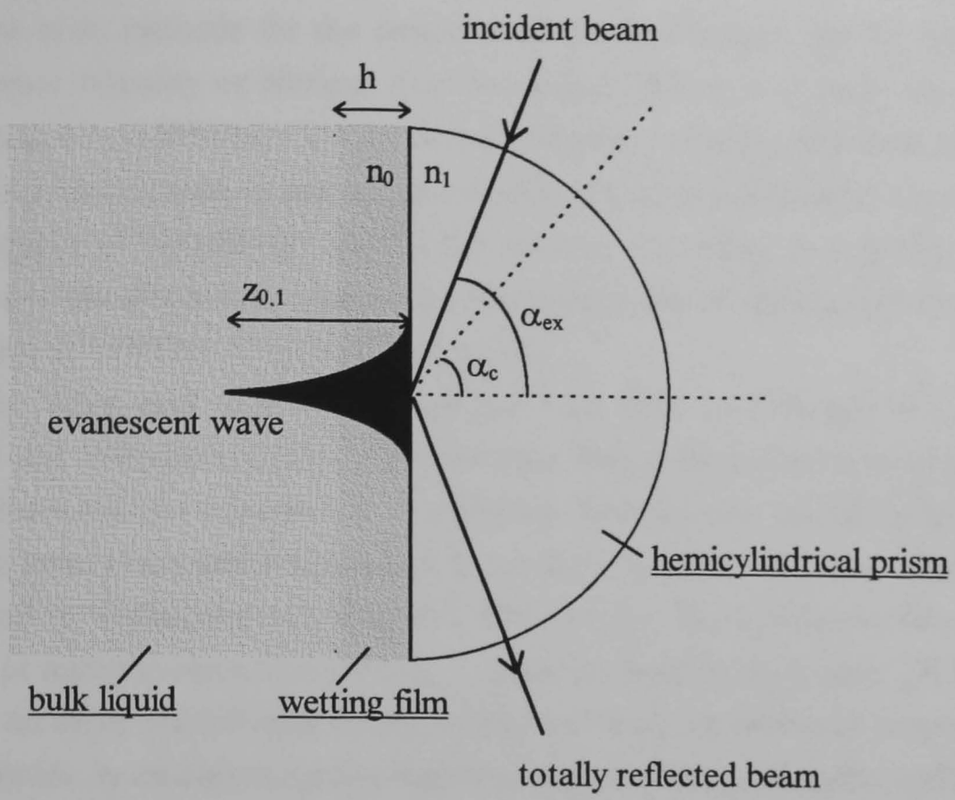

Figure 4.1: Schematic diagram showing general arrangement for an evanescent-wave-generated fluorescence spectroscopy experiment.

If the light is incident at angles greater than the critical angle the evanescent wave generated penetrates the liquid film close to the interface. To investigate the bulk liquid the angle of incidence is reduced to less than the critical angle and the refracted beam can then excite any fluorescent species in the bulk phase.

The prism can be made of a variety of materials such as different glasses, although the refractive index of the prism needs to be greater than that of the liquid. The prism should also be resistant to chemical attack by the solution and must not fluoresce at the chosen wavelength. In our work a *synthetic quartz* prism was used.

4.1.2 Methods of fluorescence detection

In an EWGFS experiment the evanescent wave excites fluorescent molecules close to the solid-liquid boundary and the emitted fluorescence is detected. Since critical-point wetting films are expected to be of the order of 10's of nm thick, which corresponds to typical penetration depths of evanescent waves $z_{0,1}$, EWGFS is a useful technique for the investigation of wetting layers in near-critical binary mixtures. The evanescent wave may, however, also penetrate through the wetting film into the bulk phase, depending on the thickness of the film and $z_{0,1}$. The natural fluorescence of one of the components or of a dissolved dye is exploited to provide a means of discrimination between the phases. The fluorescence detected from one phase needs to be different from that detected from the other so that, when a change in the wetting behaviour at the solid-liquid interface

occurs on changing the temperature, the formation of the wetting film is observed and its identity established.

The main methods for the detection of the fluorescence are by measurement of fluorescence intensity or lifetime. The two liquid phases in a binary mixture may be discriminated by a difference in fluorescence intensity collected from each phase due to i) the natural fluorescence of one of the components, ii) the differential solubility of a dye in each phase of the mixture, and iii) the selective excitation, or selective collection of emission, of the dye in each phase. The phases may also be distinguished by a difference in fluorescence lifetime of a dye in each phase.

The differential solubility method has been used by Fattinger *et al.* (1987) and McLure and Williamson (1996). Both studies used a laser dye DCM in 2,6-lutidine + water which exhibits a lower critical endpoint. The dye was essentially insoluble in the lower aqueous phase which was found to wet the solid wall. Selective excitation has also been used by Williamson and McLure (1996) for the dye 1,6-diphenylhexa-1,3,5-triene (DPH) in methylcyclohexane (MCH) + perfluoromethylcylcohexane (PFMCH) which exhibits an upper critical endpoint. In our present work the particular properties of DPH, of a variation in excitation spectra and fluorescence lifetime in perfluoroalkanes relative to alkanes, have been exploited in the methods involving the measurement of the fluorescence intensity and lifetime. The properties of DPH are discussed in detail in the next section. A preliminary account of fluorescence is given in an annexe to this thesis.

4.1.3 Fluorescence of 1,6-diphenylhexa-1,3,5-triene

The fluorescence of all-*trans*-1,6-diphenylhexa-1,3,5-triene (DPH) is of interest in this work, since this dye has been used in both our steady-state and our time-resolved EWGFS work to be discussed in this chapter.

The electronic states involved in the absorption and emission transitions in DPH and other linear diphenylpolyenes have been the subject of discussion for several years and the exact ordering and energy levels of the excited states, particularly in diphenylbutadiene in which they are very close, has still not been fully resolved (Allen and Whitten, 1989). DPH is of interest as it shows anomalous behaviour in its fluorescence lifetime and its emission spectrum, discussed below. It also has the unusual characteristic of showing significantly different lifetimes and pronounced shifts in bands in the excitation spectra in different solvents, such as alkanes and perfluoroalkanes.

DPH has been used in the EWGFS experiments to identify the wetting film at the quartz-liquid interface in heptane + perfluorohexane, both by the intensity method of selective excitation and by the measurement of the fluorescence lifetime. The excitation and emission spectra for DPH in heptane and perfluorohexane in Figure 4.2 clearly show the difference in the excitation spectra. In our intensity experiments, the incident light at 371 nm effectively excites only DPH in the heptane-rich phase. This effect is heightened

by the greater solubility of DPH in the heptane-rich phase compared with the perfluorohexane-rich phase. The lifetime dependence of the fluorescence of DPH on the composition of a heptane + perfluorohexane mixture has been studied and the outcome is presented later in this chapter.

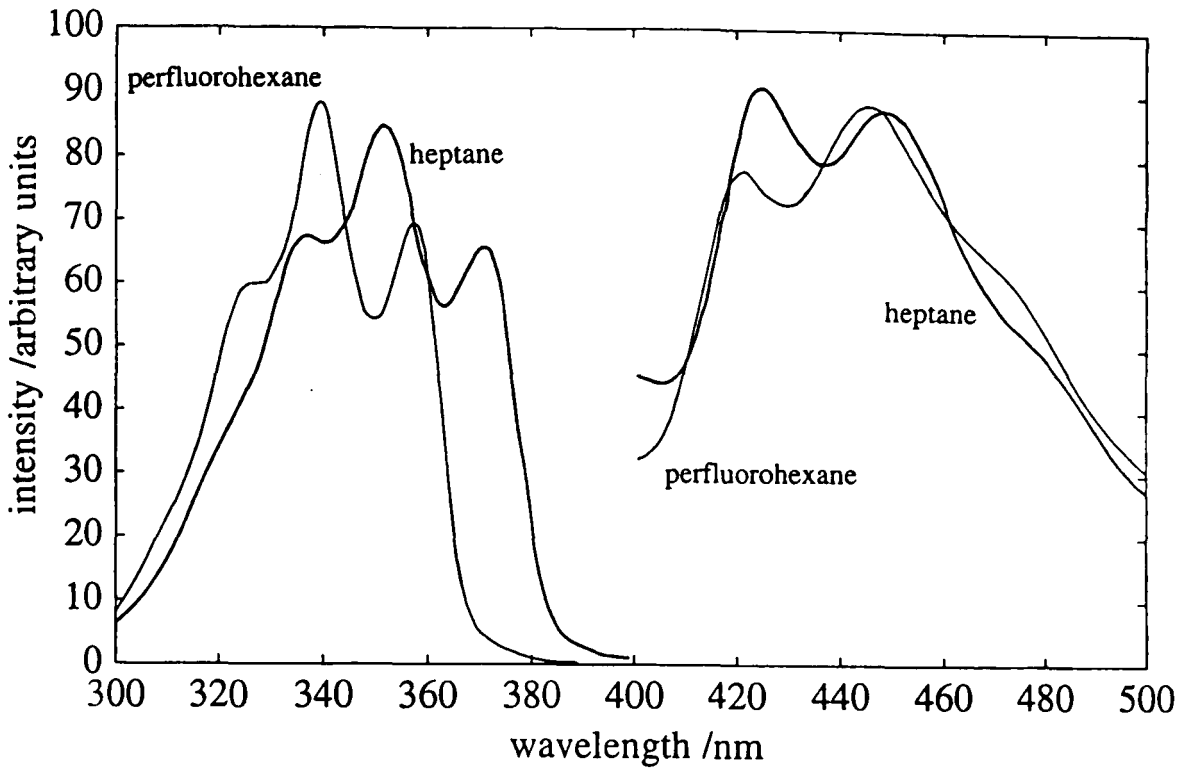

Figure 4.2: Excitation and emission spectra for 1,6-diphenyl-hexa-1,3,5-triene (DPH) in heptane and perfluorohexane.

4.1.3.1 Fluorescence properties of DPH

The observed fluorescence decay time or lifetime of DPH is generally longer than the value calculated from the absorption. The emission spectra in various solvents do not show a mirror-image relationship with the absorption spectra and are broader and less structured. The longest wavelength absorption band and the shortest wavelength emission band in the spectra are separated and show little overlap (Cehelnik *et al.*, 1974).

The absorption spectrum shows a bathochromic shift, i.e. a shift to longer wavelengths, as the polarisability α_e of the solvent is increased, whereas the emission spectra do not change appreciably in different solvents (Cehelnik *et al.*, 1975; Hudson and Kohler, 1973). The effective electronic polarisability α_e of the solvent can be calculated from:

$$\alpha_e = \frac{n^2 - 1}{n^2 + 2} \tag{4.4}$$

where n is the refractive index of the solvent. The shift in the absorption spectrum means that the separation of the absorption and emission spectra of DPH is smaller in heptane

than in perfluorohexane, see Figure 4.2, since the greater polarisability of heptane following from its higher refractive index, 1.387 compared with 1.252 for perfluorohexane for the sodium D-line at 20°C (Aldrich Handbook, 1992-93), causes a shift of the absorption spectrum to longer wavelengths.

Absorption and emission spectra, and fluorescence lifetimes, have been determined for several DPH derivatives in different solvents (Alford and Palmer, 1982, 1983, and 1986). The derivatives include the molecules formed by addition of a fluorine or a chlorine atom, or a methyl, isopropyl or a methoxy group on each phenyl ring. For a given derivative the fluorescence lifetimes decrease with increasing polarisability of the solvent, although the fluorescence quantum yields are similar in non-polar solvents. This property is unusual and makes DPH and its derivatives somewhat special. In particular, the fluorescence lifetime is very different in perfluoroalkane and alkane solvents; the lifetime of DPH in perfluorohexane is 32.5 ns and in heptane is 15.6 ns (Cehelnik *et al.*, 1974).

4.1.3.2 Reasons for the particular behaviour of DPH

The reasons for the particular behaviour of DPH can be discussed with reference to an energy level diagram, see Figure 4.3.

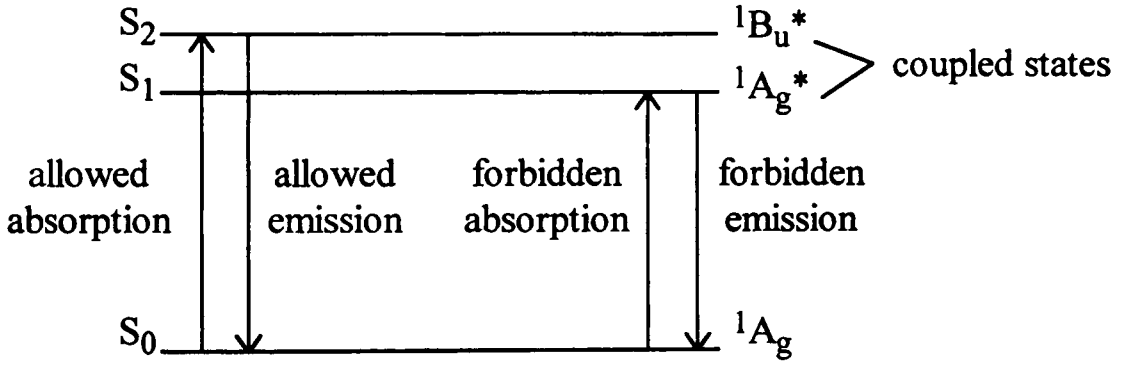

Figure 4.3: Schematic energy level diagram for DPH in heptane or perfluorohexane solutions.

The behaviour of DPH has been attributed to the existence of a low-lying ^1A_g* excited state (S_1) coupled to a higher-energy ^1B_u* excited state (S_2) (Birks and Birch, 1975; Birks, 1978; Birks *et al.*, 1978; Alford and Palmer, 1982). The energy gap between these first two excited states is small for DPH in hydrocarbon solutions. The ground state is a singlet state ^1A_g and the allowed absorption process is to the ^1B_u* state. The emission takes place from both the ^1A_g* and the ^1B_u* states and thermal repopulation of S_2 from S_1 has been proposed to occur at a rate comparable to radiative and non-radiative decay from S_1 (Alford and Palmer, 1983). This process connects the two states and emission occurs from both states even though the ^1A_g*-^1A_g transition is symmetry forbidden. Most of the intensity in the emission spectrum is due to the ^1A_g*-^1A_g transition (Itoh and Kohler, 1987) but in certain solvents a weak high energy band

due to the $^1B_u^*$-^1A_g transition can be observed in the region where it is not masked by the main $^1A_g^*$-^1A_g transition and this overlap of spectra due to different transitions also contributes to the loss of structure (Alford and Palmer, 1983).

The ordering of the energy levels accounts for the differences between the absorption and emission spectra as the transitions occur between different electronic states. The absorption and emission spectra are separated as emission takes place from a lower energy electronic state than that which is involved in the absorption process. The lifetimes of DPH are longer than the calculated values for the allowed transition as S_1-S_0 emission is slow due to the small transition moment of the symmetry-forbidden transition (Allen and Whitten, 1989).

The absorption spectrum of DPH changes in different solvents as the relative positions of the first two excited states are altered in solvents of varying polarity and polarisability. This is due to the covalent nature of the A_g state compared with the more 'ionic' nature of the B_u state. This means that the B_u state is stabilised, i.e. lowered in energy, by polar and highly polarisable solvents but the A_g state is unchanged. In polar and more polarisable solvents the energy gap between the S_0 and S_2 states is smaller and thus the bands in the absorption spectra are at longer wavelengths (Allen and Whitten, 1989). The change in energy levels can occur to such an extent that a cross-over in the ordering of the $^1A_g^*$ and $^1B_u^*$ energy levels occurs for DPH in the highly polarisable solvent CS_2 at 77 K and fluorescence is observed from the $^1B_u^*$ state which is the lowest energy excited state (S_1) in this system (Kohler and Itoh, 1988).

A change in the ordering of the energy levels is also observed in other diphenylpolyenes. For *trans*-stilbene (1,2-diphenylethylene) and 1,4-diphenylbutadiene in hydrocarbon solvents an allowed emission transition takes place from the $^1B_u^*$ state which is the lowest excited singlet state. The rates of fluorescence fit in with this being an allowed transition. In DPH and 1,8-diphenyloctatetraene (DPO) emission takes place mainly from the $^1A_g^*$ excited state. The fluorescence rate for DPH is slower than for *trans*-stilbene due to a formally disallowed transition from the lowest excited singlet state $^1A_g^*$, which is weakly allowed due to coupling with the $^1B_u^*$ state. The rate of emission in DPO is slower than in DPH as the S_1-S_2 energy gap is larger so emission from the $^1A_g^*$ (S_1) state is more forbidden (Allen and Whitten, 1989). In DPH the shortening of the lifetime in solvents of increasing polarisability is accounted for by the stabilisation of the $^1B_u^*$ state, thus bringing it closer in energy to the $^1A_g^*$ state so the emission transition is more allowed and the rate of emission is faster.

In this section the main fluorescence properties of DPH have been summarised. It is clear that DPH has been widely researched and possesses a number of useful properties. Some of these properties, particularly the difference in fluorescence excitation spectra and in fluorescence lifetimes in alkane and perfluoroalkane solvents, have been exploited in our investigations.

We turn now to the fluorescence intensity and fluorescence lifetime methods used with DPH in this work. In particular we look at the factors involved in each method, the expected results, and the critical-point wetting issues that can be investigated.

4.1.4 Fluorescence intensity method

In previous work measuring the intensity of the fluorescence emitted (Williamson, 1990; McLure and Williamson, 1996; Williamson and McLure, 1996) excitation was by means of a laser. In the present investigation synchrotron radiation, see section 3.2, was used. Synchrotron radiation has the advantage that a wide range of excitation wavelengths can be selected, although the incident beam is generally of lower intensity than that produced by a laser.

4.1.4.1 Factors involved in intensity method

In any investigation of critical-point wetting by EWGFS the wetting transition temperature T_w should be far enough away from the critical temperature T_c that the phases are still significantly different in composition close to T_w. There are many additional factors involved in the measurement of the fluorescence intensity method of EWGFS and these are listed below. The discussion is mainly concerned with selective excitation since this technique has been used in our study.

1. *Change in refractive index with temperature.*

The refractive index n is the ratio of the speed of light in a vacuum to the speed of light in the medium and thus depends on the medium, the frequency of the light and the temperature.

i) Change in refractive index with temperature for a single phase.
Williamson (1990) found that the refractive indices of solutions of DCM in 2,6-lutidine and DCM in 2,6-lutidine + water in the one-phase region below the lower critical endpoint decreased slightly with increasing temperature. The effect was small, $dn/dT \sim -2.2 \times 10^{-4}\ K^{-1}$, and is not expected to affect the results.

ii) Change in refractive index with temperature for coexisting phases.
In a binary liquid mixture the refractive index also varies with temperature due to the changing compositions of the two coexisting phases. The effect of changing the refractive index is to alter both the critical angle α_c and the depth of penetration of the evanescent wave. The penetration depth of the evanescent wave $z_{0,1}$, given by equation (4.3), decreases with increasing angle of excitation α_{ex} providing $\alpha_{ex} > \alpha_c$. The penetration depth thus depends on the nearness of the excitation angle to the critical angle. If α_{ex} is too large the penetration depth of the evanescent wave is small and thus fewer fluorescent molecules are excited leading to a fluorescence intensity too low to be detected.

2. *Change in the fluorescence intensity with temperature.*
   A decrease in the intrinsic fluorescence intensity with increasing temperature occurs in general due to the greater frequency of molecular collisions at higher temperatures thus providing radiationless pathways for deactivation of the probe dye molecules.
3. *Dependence of the fluorescence intensity on the emission angle α_{em} at which the fluorescence is collected.*
   The intensity of the fluorescence rises to a maximum at α_{em} equal in value to the critical angle α_c' for evanescent wave excitation of the surface (Fattinger, 1987; Fattinger *et al.*, 1987; Williamson, 1990) and for excitation of the bulk (Williamson, 1990). For a single phase, the overall intensity is generally lower for evanescent wave excitation than for excitation of the bulk phase as only molecules close to the surface are excited by an evanescent wave. For excitation by an evanescent wave, the fluorescence intensity decreases for collection at angles $\alpha_{em} > \alpha_c'$ and may then apparently increase again at higher angles due to the detection of the totally reflected beam, which occurs when α_{em} is equal to the angle of incidence α_{ex} but on the other side of the normal, if this is not blocked or filtered out. For α_{ex} too close to α_c, the high fluorescence intensity at α_{em} close to α_c' may be masked by the detection of the totally reflected beam.
4. *Effect of temperature on the partitioning of the dye between two coexisting phases.*
   The partitioning of the probe dye between the two phases may change with temperature as the compositions of the phases vary. Any change in the concentration of the dye close to the interface affects the fluorescence intensity.
5. *Effect of temperature on the thickness of the wetting film.*
   If the wetting film thickness h varies with temperature the intensity may also vary. The effect on the intensity depends on whether the dye is in the wetting phase, i.e. the phase that wets the solid-liquid interface, or in the other wetted phase. If the probe is in the wetting phase the fluorescence intensity is expected to increase with increasing thickness of the film as more probe molecules are present in the vicinity of the interface if the concentration remains constant. If the probe is in the wetted phase the opposite effect is expected; as the wetting film thickness increases the evanescent wave penetrates less deeply into the wetted phase containing the dye, so fewer molecules are excited and the observed fluorescence intensity decreases. For a fluorescent probe soluble in the wetted phase, and neglecting the differences in refractive indices of the two liquid phases, Fattinger *et al.* (1987) give the fluorescence intensity I(h) as a function of the wetting film thickness h as:

$$I(h) = I(0) \exp(-2h/z_{0,1}) \tag{4.5}$$

where $z_{0,1}$ is the penetration depth of the evanescent wave defined in equation (4.3).

6. *Effect of temperature on the composition of coexisting phases and hence on the absorption and emission spectra of the fluorescent species.*

   As the temperature varies, the compositions of the coexisting phases change and this may produce a shift in the absorption or emission spectra. This is of importance if differential excitation is being used since, as the phases become more similar, the excitation peaks in the spectra for each phase may move closer together and the selected excitation wavelength may not be positioned at a constant peak in intensity. It is not really known whether the wavelengths of intensity maxima show a linear change with composition, or whether they are more similar to the positions in one of the components due to preferential solvation of the probe molecules by one of the components of the mixture.

The factors discussed above apply to the technique and the system. Further experimental factors which require attention include:

1. *Change in intensity of the synchrotron beam.*

   Another factor affecting the fluorescence intensity for the work carried out using the synchrotron radiation source at Daresbury Laboratory is the change in the fluorescence intensity due to the decrease in intensity of the synchrotron beam with time after refilling. The fluorescence of a standard may need to be recorded to allow the results to be scaled. Any drift in the beam position with time will also affect the intensity of the fluorescence.

2. *Effects due to stray light.*

   Although filters may be used on both the incident light and emitted fluorescence, they are usually not perfectly efficient and some effects of stray light may still cause problems. The width of the reflected beam due to the curved surface of the prism may also affect results due to the detection of the reflected beam in addition to the fluorescence. The various effects of scatter may thus obscure any fluorescence.

3. *Aggregation of dye at the liquid-liquid interface or deposition on solid walls of container.*

   Any aggregation or adsorption of dye molecules at an interface with time or temperature affects the concentration remaining in the liquid and thus the intensity of the fluorescence.

The effects of some of these factors can be measured experimentally, although the influence of others is not easily determinable. In many cases, changes may occur over the full temperature range of an experiment but may be negligible over a narrow temperature range close to T_w so the wetting transition may still be identified. In section 4.2.9 we consider the factors in relation to our materials and experiments.

The use of a mixture in which one of the components is naturally strongly fluorescent should simplify several aspects of the experiment and dispense with the problem of the dye partitioning and adsorption/aggregation effects. One possible mixture is hexane + nitrobenzene in which the natural fluorescence of nitrobenzene can be utilised.

4.1.4.2 Predicted intensity-temperature profiles

There are several types of system that can be investigated. The binary mixture may exhibit an upper critical endpoint UCEP or a lower critical endpoint LCEP and in each case the main fluorescence intensity may be detected from the wetting phase or the wetted phase. Here we consider the intensity of the fluorescence for a binary mixture, with the incoming light incident at the boundary of the solid with the liquid phase, either upper or lower, at which a change in the wetting properties occurs. The schematic profiles predicted for the various scenarios are shown in Figures 4.4-4.7 and have also been submitted for publication (McLure and Clements, 1996). It is assumed that the transition is second order with the wetting film thickness displaying a simple form with a maximum at the wetting transition temperature T_w as observed by Fattinger *et al.* (1987). In each case the contributions are as follows:

a) The intensity-temperature profiles assuming first of all that the coexisting liquid phase compositions are independent of temperature and that no wetting occurs.
b) Incorporating the decrease of the intensity of the fluorescence with temperature due to the increasing inefficiency of fluorescence as a deexcitation mechanism.
c) Relaxing the fixed coexisting phase compositions to follow the shape of the coexistence curve.
d) The wetting film thickness h-temperature profile assumed.
e) The predicted intensity-temperature profile including a wetting film.

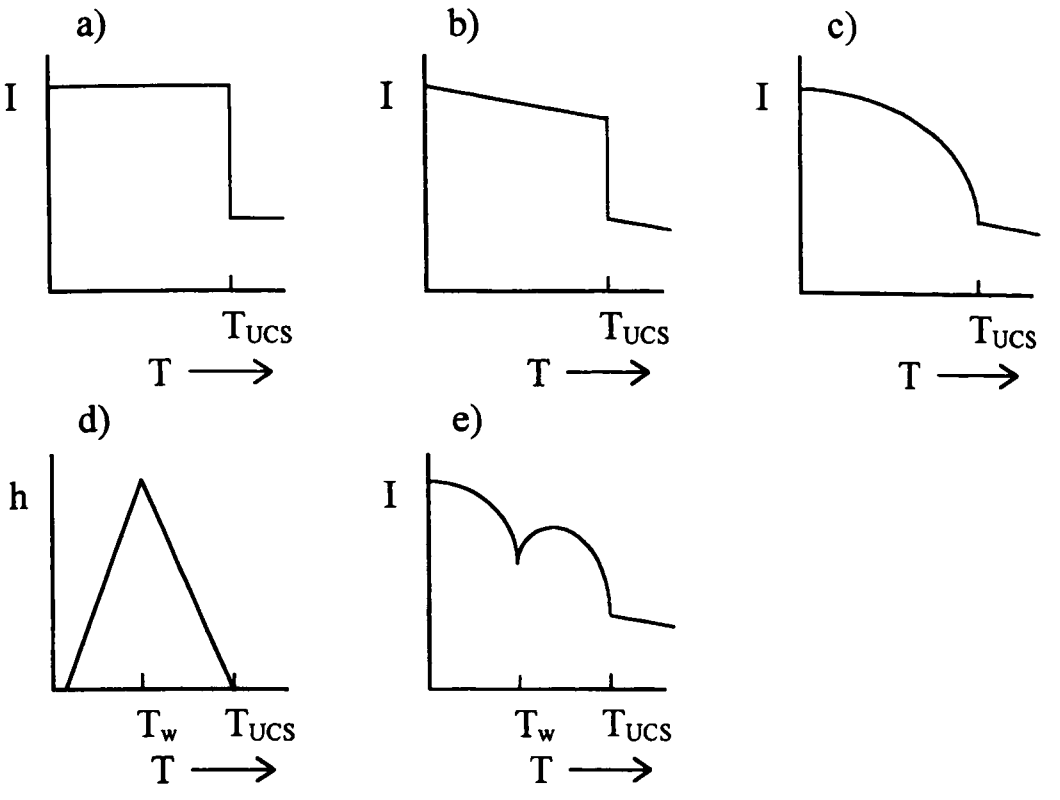

Figure 4.4: Factors contributing to the predicted overall intensity-temperature I-T profile e) for a binary mixture exhibiting an upper critical endpoint UCEP and with the dye in the wetted phase.

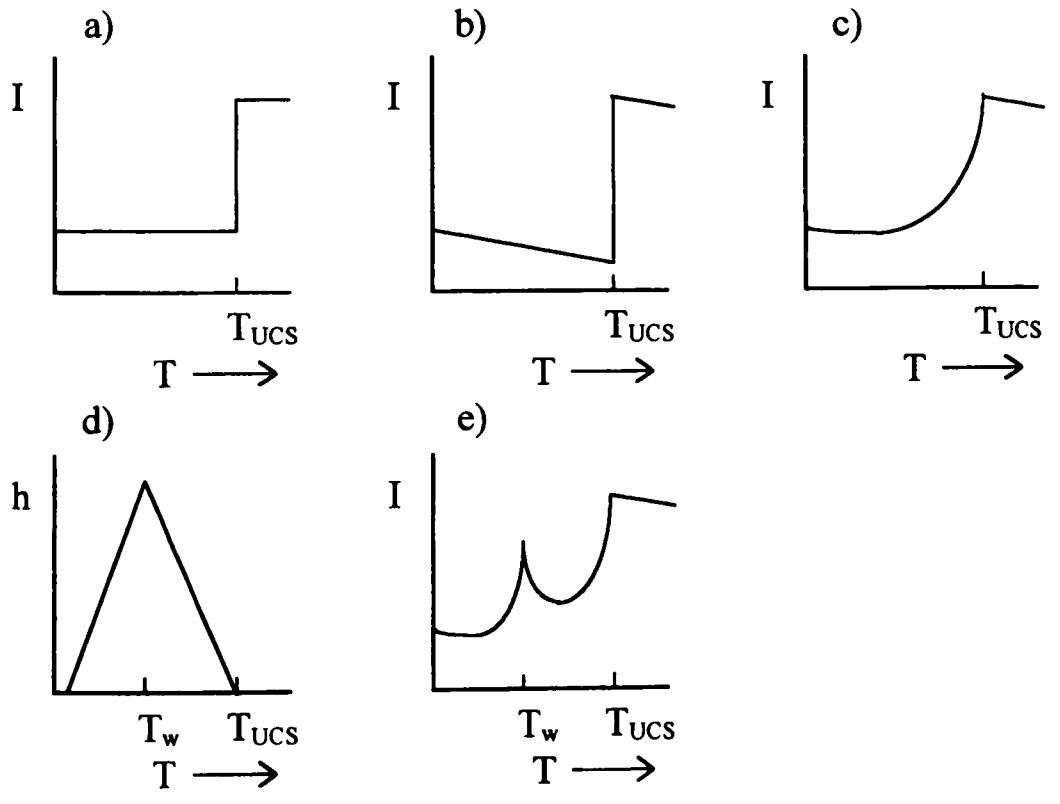

Figure 4.5: Factors contributing to the predicted overall intensity-temperature I-T profile e) for a binary mixture exhibiting an upper critical endpoint UCEP and with the dye in the wetting phase.

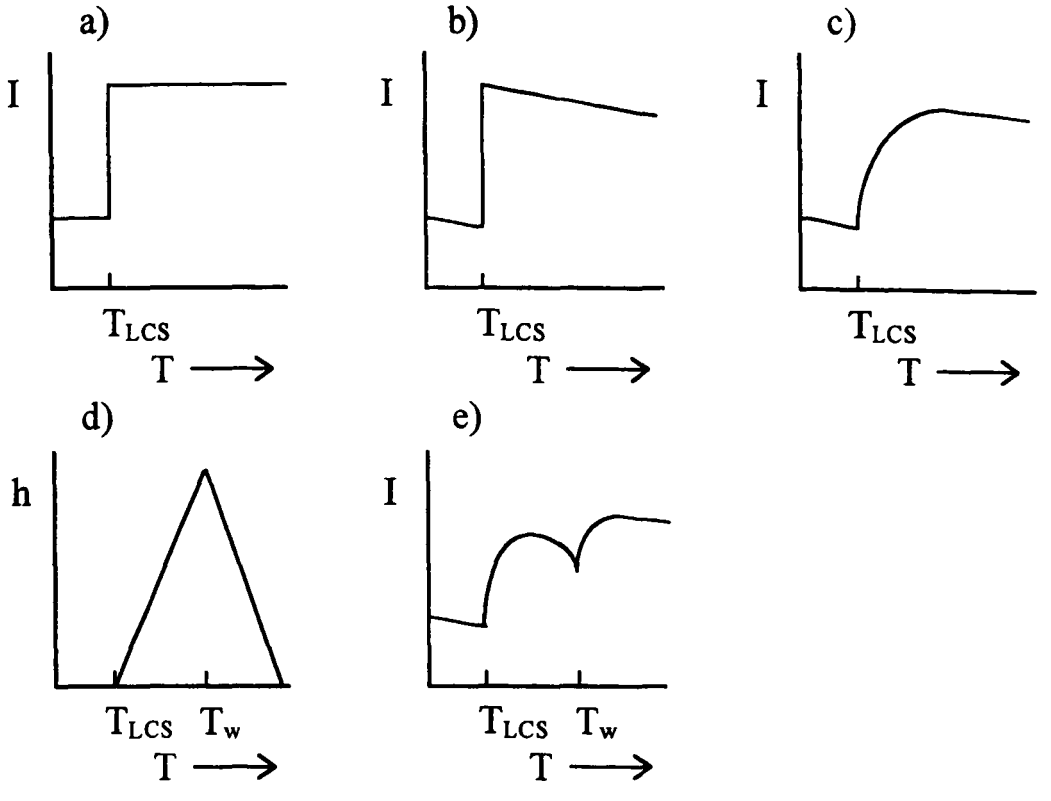

Figure 4.6: Factors contributing to the predicted overall intensity-temperature I-T profile e) for a binary mixture exhibiting a lower critical endpoint LCEP and with the dye in the wetted phase.

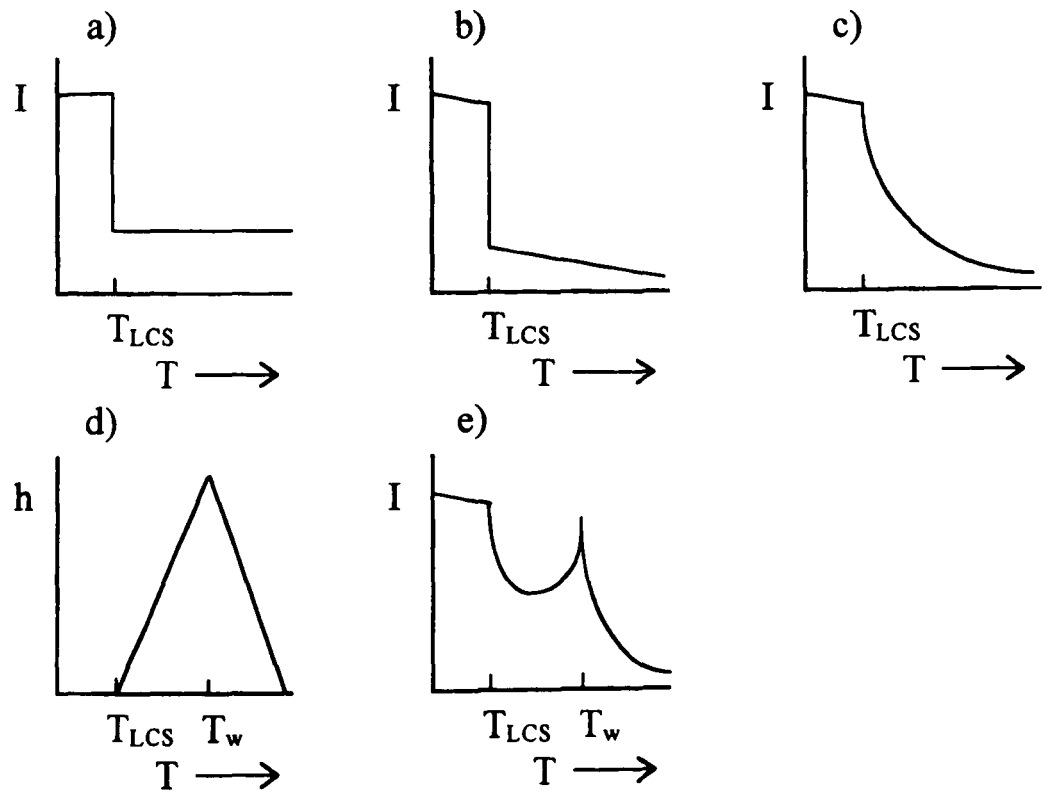

Figure 4.7: Factors contributing to the predicted overall intensity-temperature I-T profile e) for a binary mixture exhibiting a lower critical endpoint LCEP and with the dye in the wetting phase.

Figure 4.6 corresponds to the situation studied by Fattinger *et al.* (1987). Our predicted result agrees with their experimental result close to T_w, although differs close to T_{LCS} as, due to the absence of any stirring in their experiment, their phases did not remix on cooling below T_{LCS}, and so the signature of the critical point was not observed. Figure 4.5 corresponds to a possible outcome of our experiment with DPH in heptane + perfluorohexane.

4.1.4.3 Issues that can be investigated by intensity method

The main issues of interest in critical-point wetting, such as the nature of the wetting film, the wetting transition temperature T_w, the order of the transition and the thickness of the wetting film, should be accessible by collection of the fluorescence intensity. The wetting transition temperature is marked by a minimum or a maximum in the intensity. If measurements are made at small temperature intervals the order of the transition can in theory be determined. The elucidation of the thickness of the wetting film has been achieved by Fattinger *et al.* (1987) by measurement of the angular distribution of the emitted fluorescence intensity. The experimental results for s-polarised intensity of the evanescent-wave-excited fluorescence were compared with the angular distributions of s-polarised intensity calculated using the theory developed by Lukosz (1979, 1981). At a given temperature the peak in the intensity occurred at an emission angle equal to the critical angle, and it was shown that the interposition of a non-fluorescent wetting layer of thickness $h \geq z_{0,1}/10$ would lead to an observable change in the intensity for emission angles $\alpha_c' \leq \alpha_{em} \leq 90°$. The water-rich wetting film thickness observed by Fattinger *et al.* (1987) in 2,6-lutidine + water was approximately 15 nm with a penetration depth of the evanescent wave of about 80 nm, see equation (4.5).

4.1.5 Fluorescence lifetime method

In this method the fluorescence lifetime of a probe molecule is measured. The detection is generally by single-photon counting techniques which have been discussed in section 3.1. The time-resolved work presented here used a laser as the source of fluorescence excitation.

4.1.5.1 Factors involved in lifetime method

One major factor in the use of EWGFS in any study of critical-point wetting is that $|T_w - T_c|$ must be large enough that the sensitivity is not decreased at the wetting transition temperature T_w as the phases become more alike approaching the critical temperature T_c.

Another factor, probably essential in most cases using the lifetime method, is ensuring the exclusion of oxygen from the sample. Dissolved oxygen has the effect of reducing the lifetime due to encounters with the fluorescent molecules providing

radiationless pathways for deactivation. The effect is more pronounced for long lifetimes and any difference in lifetime between the two phases is significantly reduced. The fluorescence intensity is also reduced but probably to a similar extent for both phases.

Some possible additional affects are discussed in section 4.2.10. The influencing factors in the intensity method discussed above are generally not significant for the lifetime method and thus this method should provide a clearer picture of the wetting behaviour. In our work we have used 1,6-diphenylhexa-1,3,5-triene (DPH) in heptane + perfluorohexane for which the difference in lifetime between the pure solvents is about 16 ns.

4.1.5.2 Predicted lifetime-temperature profiles

For our case of a mixture exhibiting an upper critical endpoint UCEP and with the higher lifetime in the wetted or non-wetting perfluorocarbon-rich phase, we consider the variation in lifetime with temperature for the film at the interface of the solid with the liquid phase at which a change in the wetting occurs, in this case the lower perfluorocarbon-rich phase. As the composition changes along the coexistence curve the lifetimes vary accordingly. The predicted profile is shown in Figure 4.8 assuming a first-order transition.

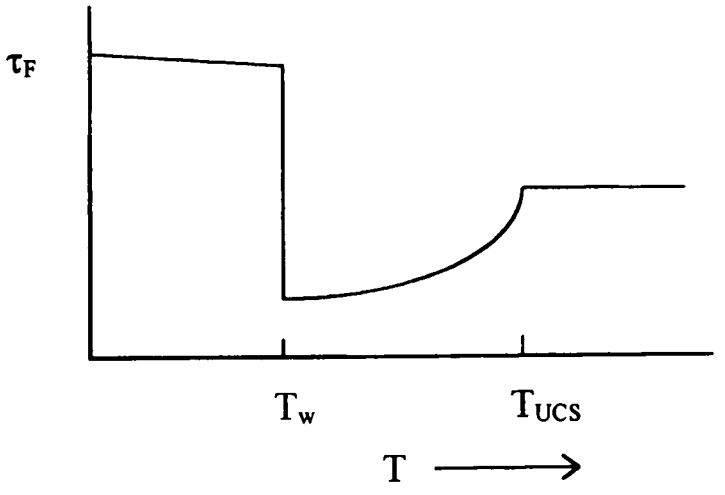

Figure 4.8: Predicted fluorescence lifetime τ_F-temperature profile for DPH in heptane + perfluorohexane at the surface of the lower phase.

4.1.5.3 Issues that can be investigated by lifetime method

If the difference in the lifetimes of the two phases at T_w is large enough, then T_w and the order of the transition can be determined by recording the lifetime at small intervals of temperature. This technique also shows promise for estimation of the thickness of the wetting film by collection of the fluorescence as a function of excitation angle. The variation of the excitation angle alters the penetration depth of the evanescent wave and may thus possibly allow various depths through the wetting film to be probed. This is discussed in more detail later.

4.1.6 Some previous work using evanescent-wave techniques

The details and principles of EWGFS have been described above. We now briefly consider the scope of evanescent-wave techniques in different applications.

The excitation of fluorescence by an evanescent wave has previously been used to study various solid-liquid interfaces in biological systems (Axelrod *et al.*, 1984) and in polymer solutions (Rondelez *et al.*, 1987). EWGFS has also been used in spectroscopic studies, for example to investigate pyrene excimer formation in an interface layer of a sapphire-polymer solution (Hamai *et al.*, 1995) and the effect of adsorption on the fluorescence properties of the triphenylmethane dye malachite green at an aqueous-quartz interface (Bell *et al.*, 1994). Evanescent-wave-induced fluorescence has been measured for dyes dissolved in solution close to a glass interface (Fattinger *et al.*, 1986a) and it was observed that the fluorescence lifetimes for molecules close to the surface were slightly smaller than for molecules in bulk solution, but that the decay times for adsorbed molecules were shorter by a factor of three than those for molecules in solution.

Beysens and Leibler (1982) used EWGFS to study critical adsorption in the binary mixture nitrobenzene + hexane at a silica interface, utilising the natural fluorescence of nitrobenzene. Fattinger *et al.* (1986b) observed a surface-pressure-induced wetting transition at a solid wall in a two-phase solid-liquid system of dimethylsulphoxide close to its melting point. Wetting transitions were then investigated in binary liquid mixtures in contact with a solid surface using differential solubility of a dye in each phase (Fattinger *et al.*, 1987). This work on wetting in binary mixtures has since been extended, recording the fluorescence intensity and using the methods of differential solubility and selective excitation (Williamson, 1990; McLure and Williamson, 1996; Williamson and McLure, 1996).

In this chapter the methods and results are presented for further work on the selective excitation intensity method and for measurements of the fluorescence lifetime to identify a wetting transition. This latter work has been submitted for publication (Bowers *et al.*, 1996c).

4.2 Experimental details

4.2.1 Experimental arrangement

The arrangement for an EWGFS experiment generally consists of a source of light directed radially at the axis of a hemicylindrical prism at an angle greater than the critical angle. The evanescent wave induced excites fluorescent species in the sample in contact with the planar surface of the prism close to the interface. The cell, containing the sample and the prism, is attached to a rotatable goniometer table. The fluorescence is emitted in all directions but is usually collected after transmission through the prism by the use of a photomultiplier PM tube attached to a rotatable arm of the goniometer. Rotation of the cell varies the angle of incidence, so evanescent wave excitation of the surface and direct beam refraction into the bulk liquid are possible, and rotation of the detector arm varies the angle of collection of the fluorescence. This type of arrangement was used in our experiments and is shown in Figure 4.9.

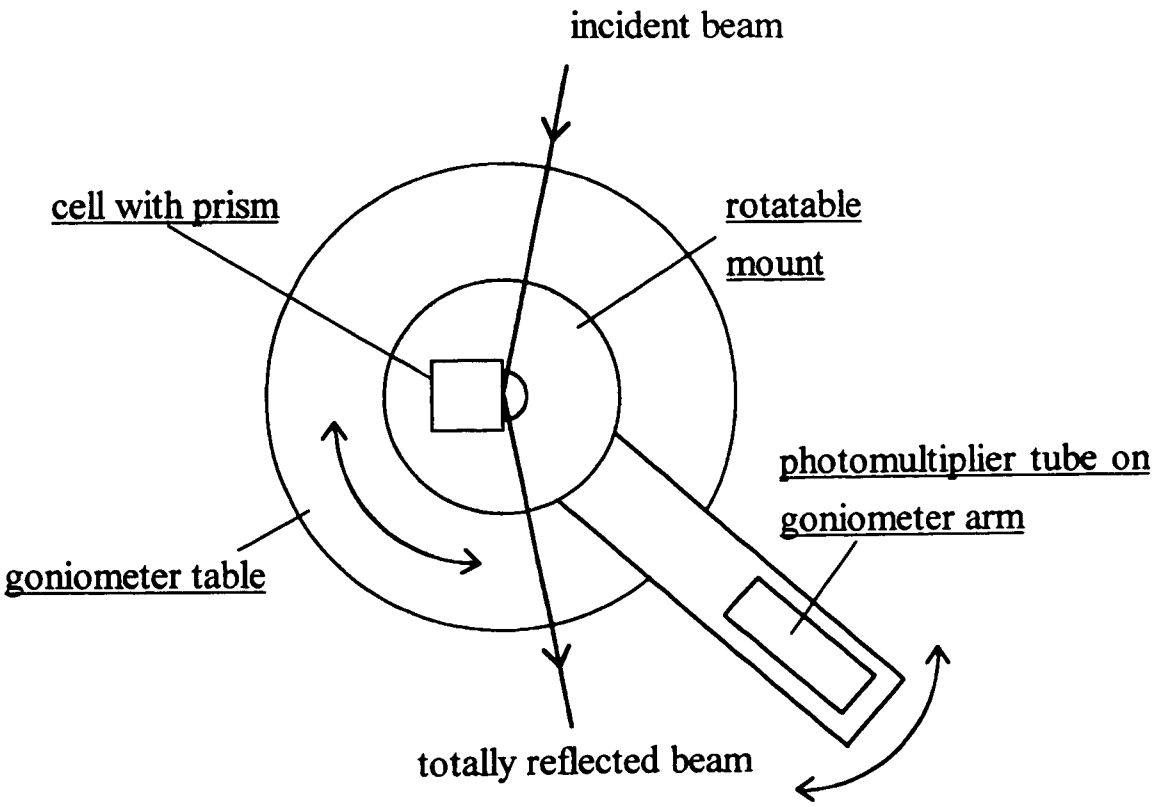

Figure 4.9: Plan view of general arrangement in our EWGFS experiments.

4.2.2 Features of the cell

The cell in our experiments consists of a heated copper block in which a stainless-steel insert containing the liquid sample is in contact with a hemicylindrical synthetic Spectrosil quartz prism (Robson Scientific, radius 12.5 mm) clasped onto the block. A seal is obtained between the prism and the sample insert by means of a Viton O-ring (James Walker Ltd., internal diameter i.d. 17.6 mm, cross-section 2.4 mm^2) set in a recess on the front face of the insert. The cell is drawn schematically in Figure 4.10 and is shown in Plate 3.

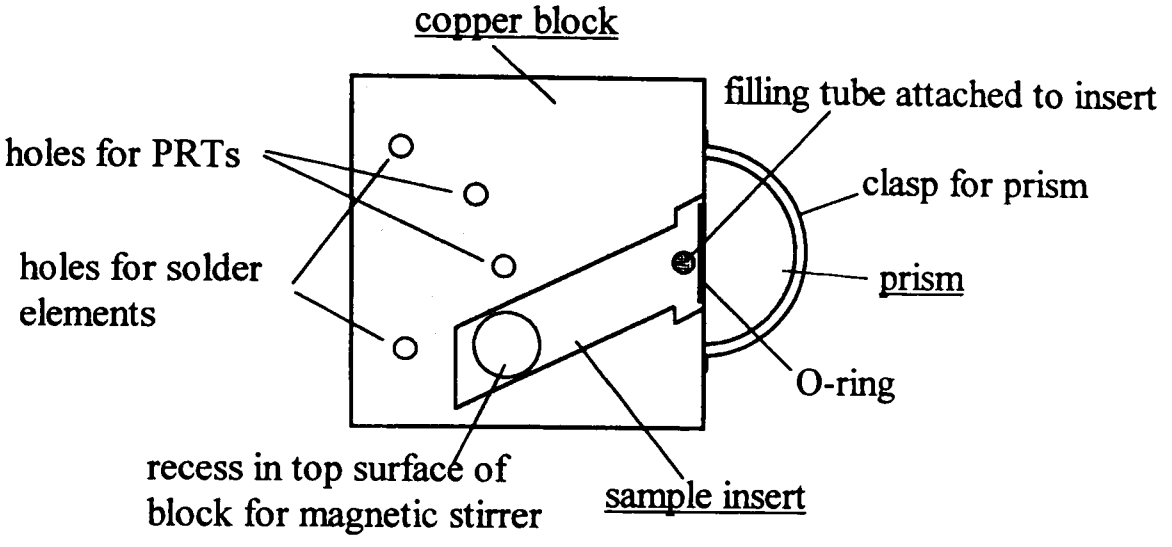

Figure 4.10: Schematic diagram of EWGFS cell.

The sample insert is a tube with a removal base sealed by a screw thread and a second Viton O-ring wrapped in Teflon tape. The front face of the insert is open and close to the front face a filling tube (i.d. 1/8") with a Whitey ball valve and a Swagelok fitting (1/8") is attached so that the sample can be transferred to the cell with the prism clasped in place over the open face. The insert is not normal to the planar face of the prism, but is angled to allow the incident beam to be 'buried' thereby reducing stray reflections.

The stirrer used originally was a glass-coated magnetic follower on a rotatable glass setting placed inside the sample insert and activated by a motor-operated rotating magnet set close to the insert in the copper block. This means of stirring was not very effective and prior to most measurements the cell was shaken vigorously to mix the contents. Later a Teflon-coated magnetic follower was activated by a magnet and more powerful motor.

The block is heated and thermostatically controlled by means of two 15 W solder iron heaters and a platinum resistance thermometer PRT (Sensing Devices Ltd.) set in recesses in the copper block and connected to a CAL 9000, or a CAL 9900, controller. An independent readout of the temperature is also provided by a PRT connected to a

Newport digital meter and situated in the copper block as close to the sample insert as possible. The cell is insulated by a Sindanyo-like base.

The cell is based on the one used by Williamson (1990), and incorporates modifications by Bowers (1995).

4.2.3 Specific arrangement and data collection for intensity work

The measurements of the fluorescence intensity were carried out at the Synchrotron Radiation Source at Daresbury Laboratory on station 12.1. The synchrotron has been described in section 3.2 and was used throughout this work in multi-bunch operation. The range of wavelengths available extended from the UV through the visible region.

The complete EWGFS arrangement of cell, goniometer table and PM tube was contained in a large 'black box', as shown in Plate 4. The incident light at 371 nm was reflected by a mirror through a slit in the box and was focused by a lens on to the axis of the prism. On station 12.1 the incident light is essentially unpolarised. Angular readouts were made from the goniometer at the base of the cell and from the PM tube arm to determine the angles of excitation and emission. The emission angles in particular were only a rough indication of α_{ex} as the width of the PM tube aperture was approximately 5 cm so a range of angles was sampled in any one position.

The cell height was altered to look at the upper or lower phase of the mixture by means of aluminium spacers placed under the base of the cell. When recording the intensity from the lower phase, the upper phase, in which the dye was more soluble, and the liquid-liquid interfacial region were masked using black tape to eliminate fluorescence recorded from the unwanted phase due to stray reflections.

The intensity of the fluorescence was recorded manually as counts per second from a dial, however this was not very accurate and in future work should be automated. Due to the decrease in intensity of the synchrotron with time after refilling, the intensity of a standard solution, DPH in heptane of absorbance ~0.1, was recorded regularly to allow the sample intensities to be scaled. The intensity recorded for the standard decreased linearly with decreasing ring current throughout the day.

4.2.4 Specific arrangement and data collection for lifetime work

The lifetime work was carried out at the Central Laser Facility (CLF) at the Rutherford Appleton Laboratory (RAL). The laser used was a Nd:YAG pumped cavity dumped tuneable dye laser with an output in the range 550-620 nm afforded by the dye Rhodamine 6G in ethylene glycol. The system operated at saturated gain and the resulting output pulse width was approximately 6 ps. The maximum wavelength of 620 nm was selected and was frequency doubled by means of a β-barium oxide (BBO) crystal to 310 nm, which was the wavelength used to excite the dye in our sample.

The experimental arrangement was contained in a black box in a dark room. The incoming beam was directed by mirrors and lenses and focused onto the cell, and was horizontally or p-polarised. The fluorescence was detected by a microchannel plate photomultiplier tube MCP and was imaged using a simple two-lens telescope arrangement onto a 330 nm short-wavelength cut-off filter at the entrance slit of a monochromator set at 440 nm in front of the MCP. This ensured that significant intensity was collected to measure a lifetime from the lower perfluorocarbon-rich phase. The totally reflected beam was dumped. The excitation angles, read from the goniometer base, and the emission angles, read from the location of the detector arm, were generally selected such that a reasonably high intensity of fluorescence was collected.

The cell height was adjusted using aluminium spacers to allow excitation of the dye in the upper and lower phases. As in the intensity work, the upper phase and interfacial regions were masked while measurements were made on the lower phase. The arrangement of the cell on the goniometer table is shown in Plate 4.

The fluorescence lifetimes were measured using time-correlated single-photon counting, see section 3.1. The instrument response, to take account of factors such as the pulse width of the laser and the response time of the electronics, was recorded by scattering laser light at 310 nm from the optical components in the system. To determine the fluorescence lifetimes the observed decay was deconvoluted from the instrument response using the lifetime-fitting software LIFETIME available at the CLF. The instrument response for the time-resolved microviscosity work in Chapter 3 using synchrotron radiation could be recorded at the fluorescence emission wavelength, but this was not possible here due to the limited wavelengths of the laser. The absolute timescale was determined by means of a time calibration using the known time difference between the main pulse and after pulse of the laser, approximately 12 ps, and the measured channel difference. The data collected were fitted to an exponential decay function of the form:

$$\text{Number of counts} = \sum_i A_i \exp(-t / \tau_{F,i}) \tag{4.6}$$

where the A_i are amplitudes and the $\tau_{F,i}$ are fluorescence lifetimes.

The laser and optical arrangements were conventional and are shown in Figures 4.11 and 4.12.

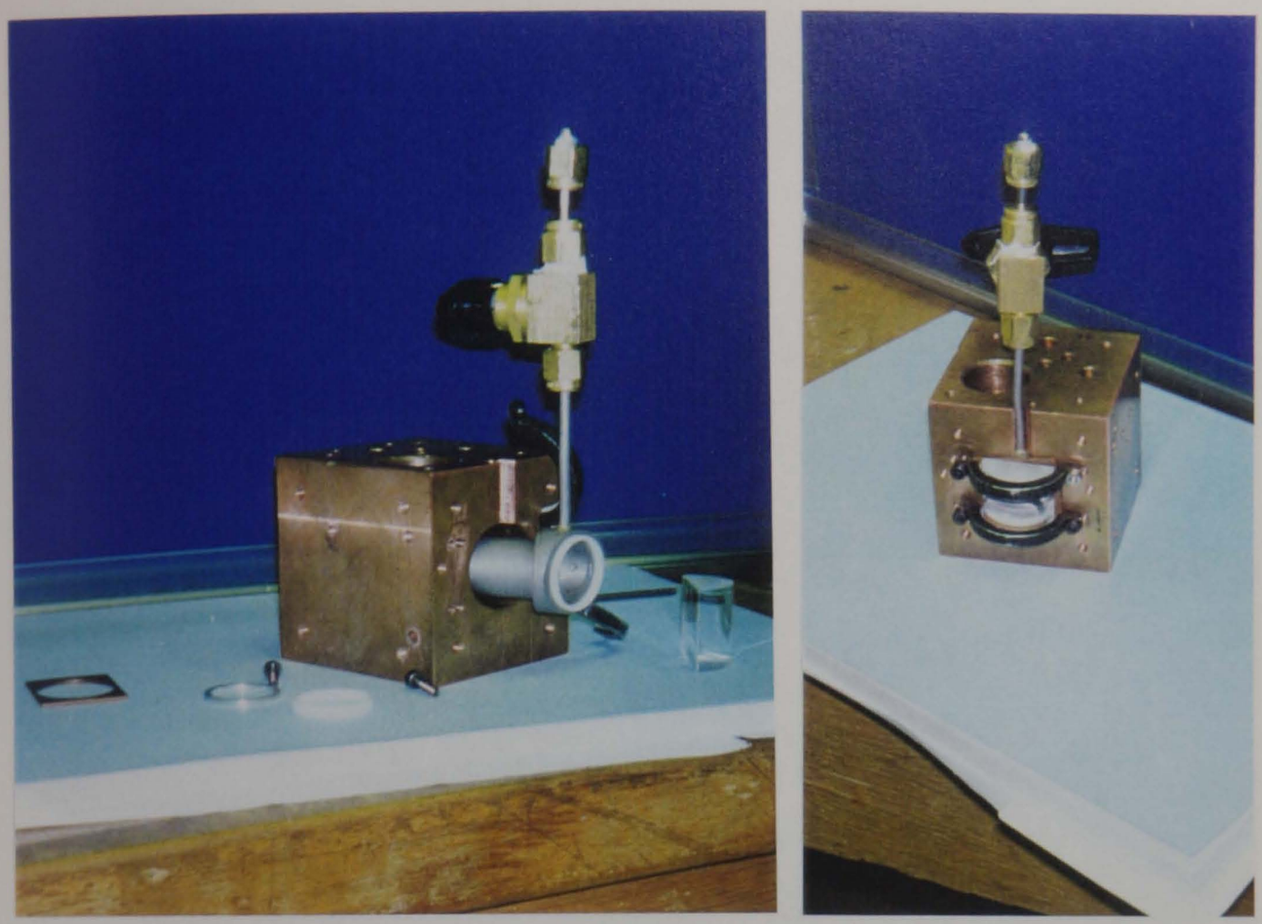

Plate 3: The EWGFS cell and the arrangement for degassing.

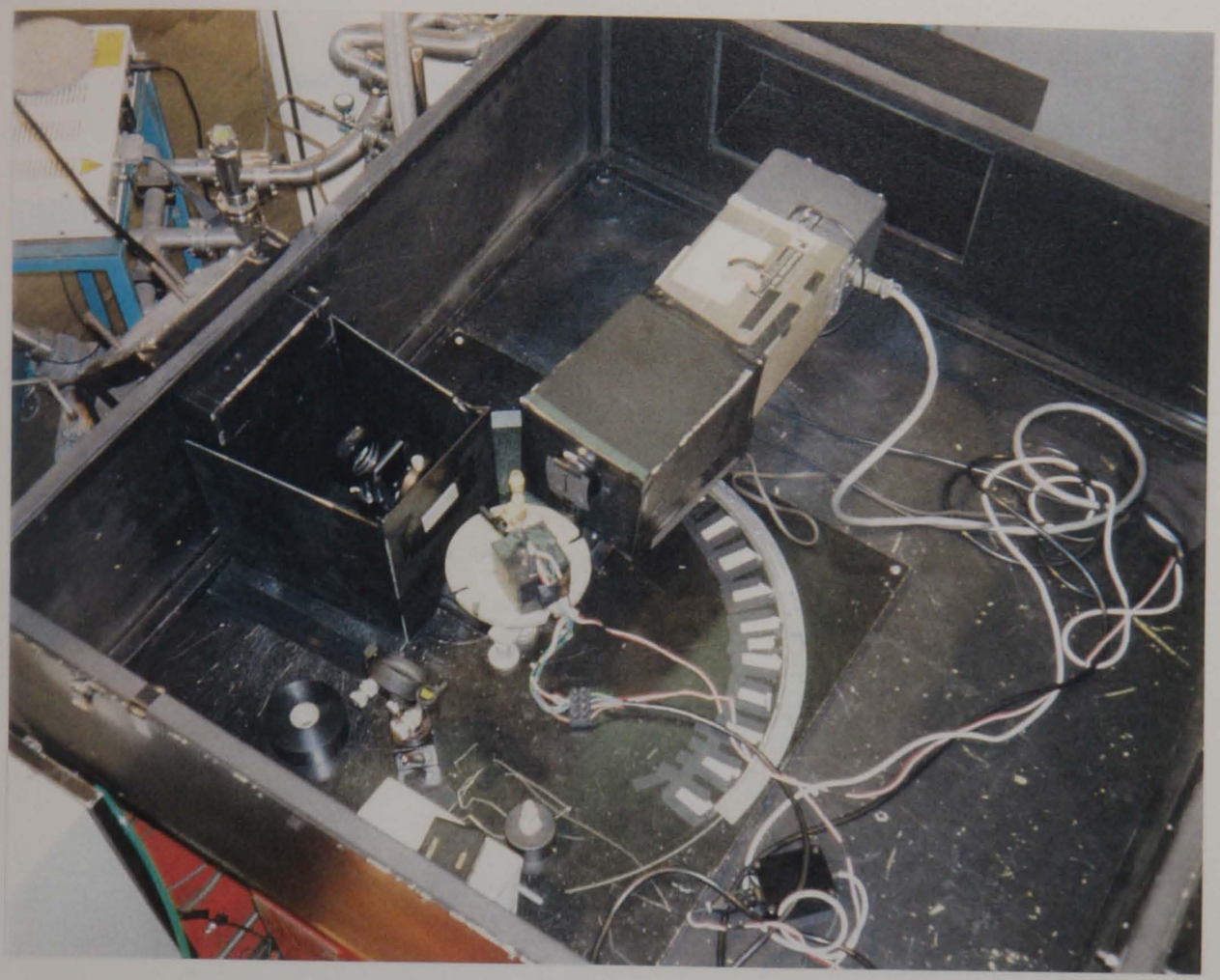

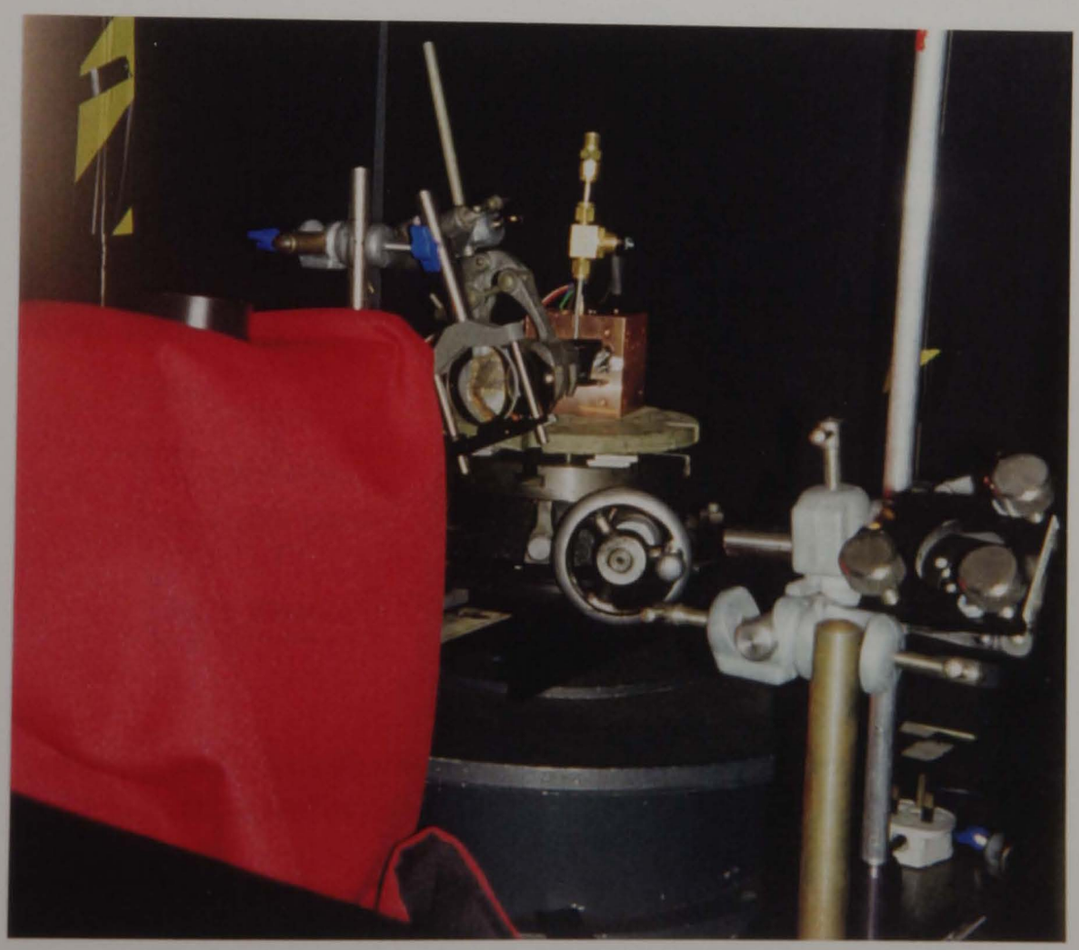

Plate 4: The arrangement of the EWGFS cell on the goniometer table for (a) the intensity work and (b) the lifetime work.

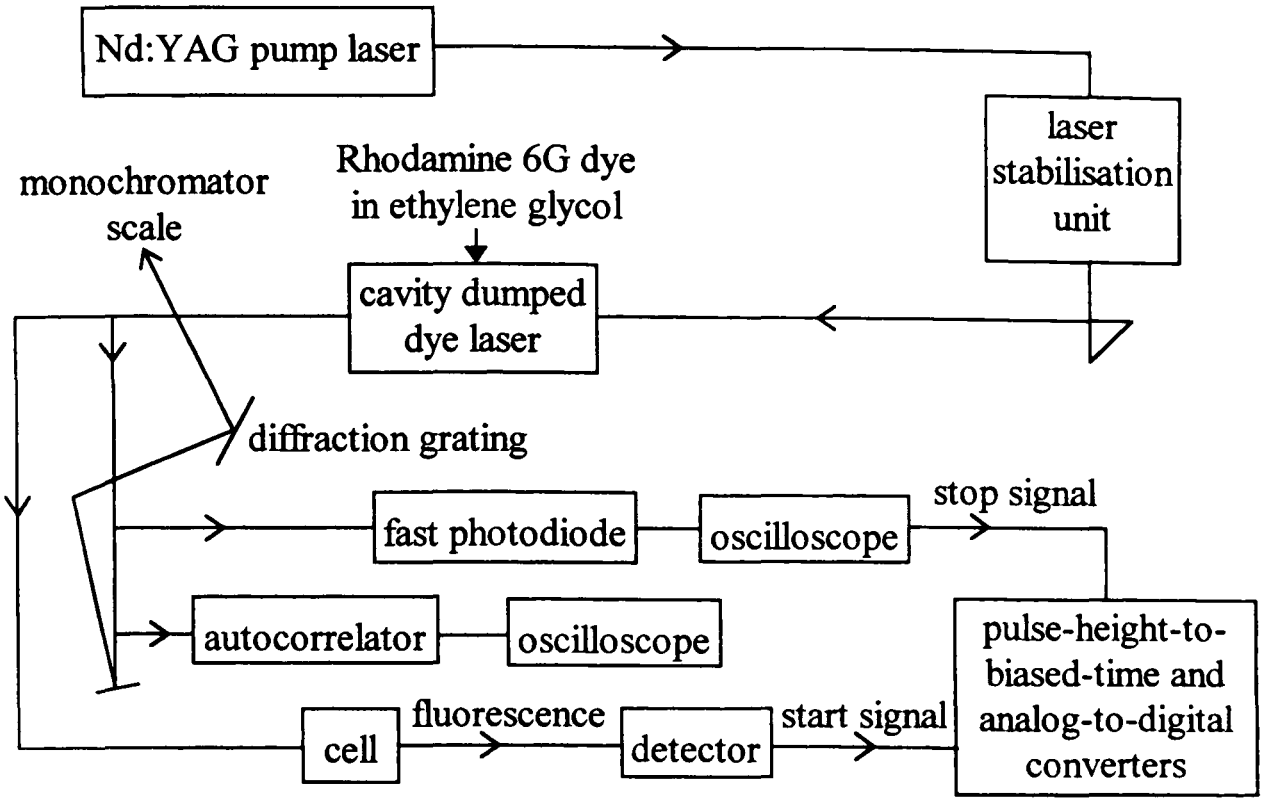

Figure 4.11: Laser assembly used for the lifetime experiments at the Central Laser Facility at the Rutherford Appleton Laboratory.

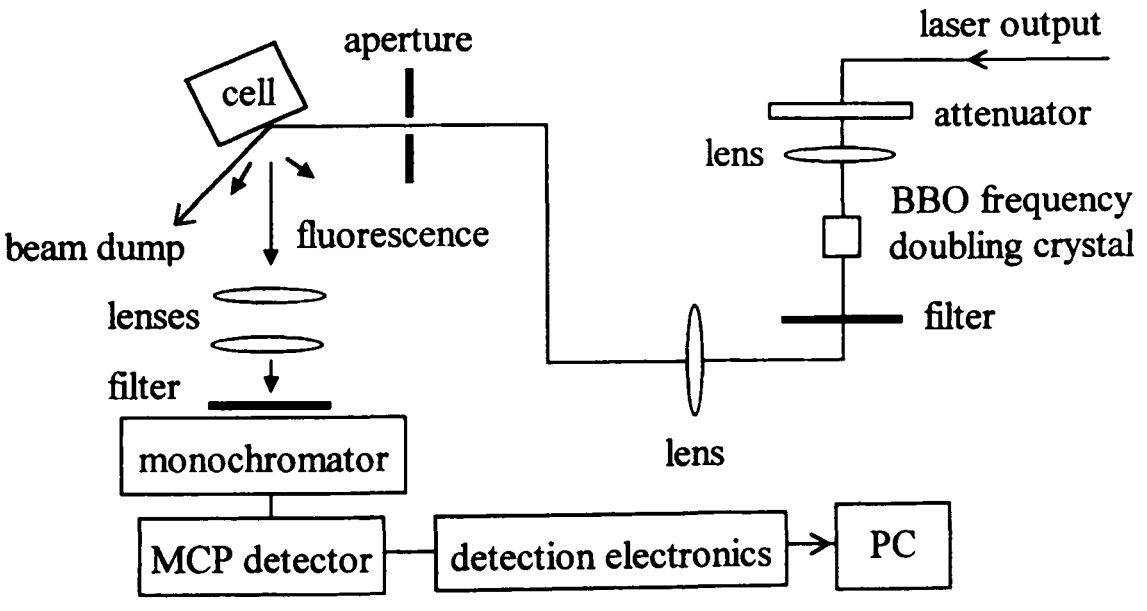

Figure 4.12: Optical arrangement used for the lifetime experiments at the Central Laser Facility at the Rutherford Appleton Laboratory.

4.2.5 Choice of system

As discussed in section 4.1.3, the dye 1,6-diphenylhexa-1,3,5-triene (DPH) possesses several particular properties which can be of use in discriminating between different solvents. Alkanes + perfluoroalkanes constitute a solvent pair in which DPH is very effective. Much of the work in the group has focused on the critical behaviour of alkane + perfluoroalkane mixtures and so a mixture of this type, *n*-heptane + perfluoro-*n*-hexane with a convenient upper critical solution temperature $T_{UCS} \approx 43°C$, was chosen for study. Initially DPH in methylcyclohexane (MCH) + perfluoro-methylcyclohexane (PFMCH), studied by Williamson (1990) at a Schott SF6 glass interface using the selective excitation intensity method, was to be used in the lifetime work, but the high lifetime expected for DPH in PFMCH was not, inexplicably, observed.

4.2.6 Materials

The sources and data used for *n*-heptane and perfluoro-*n*-hexane in this work are given in Table 4.1. The fluorescent dye 1,6-diphenylhexa-1,3,5-triene (DPH) of purity 98 mol % was obtained from Aldrich. The *n*-heptane was dried over 4 Å Molecular Sieves and the other materials were used as received.

Table 4.1: The suppliers, purities, densities ρ, molar masses M, and refractive indices n for the liquids used in this work.

material	supplier	purity /mol %	ρ (25°C) /g cm^{-3}	M /g mol^{-1}	n (20°C, 589.3 nm)[a]
heptane	Fisons	99+	0.680[b]	100.21	1.387
perfluorohexane	Fluorochem	99 (85% *n*-isomer)	1.672[c]	338.05	1.252

[a] Aldrich Handbook 1992-93, for sodium D-line, [b] Hildebrand *et al.* (1950), [c] Bedford and Dunlap (1958).

The coexistence curve in terms of volume fraction ϕ for (1-ϕ) heptane + ϕ perfluorohexane has been measured by Whitfield (1996) and is reproduced in Figure 4.13. The upper critical solution temperature T_{UCS} = 43°C and the critical composition ϕ_c = 0.44.

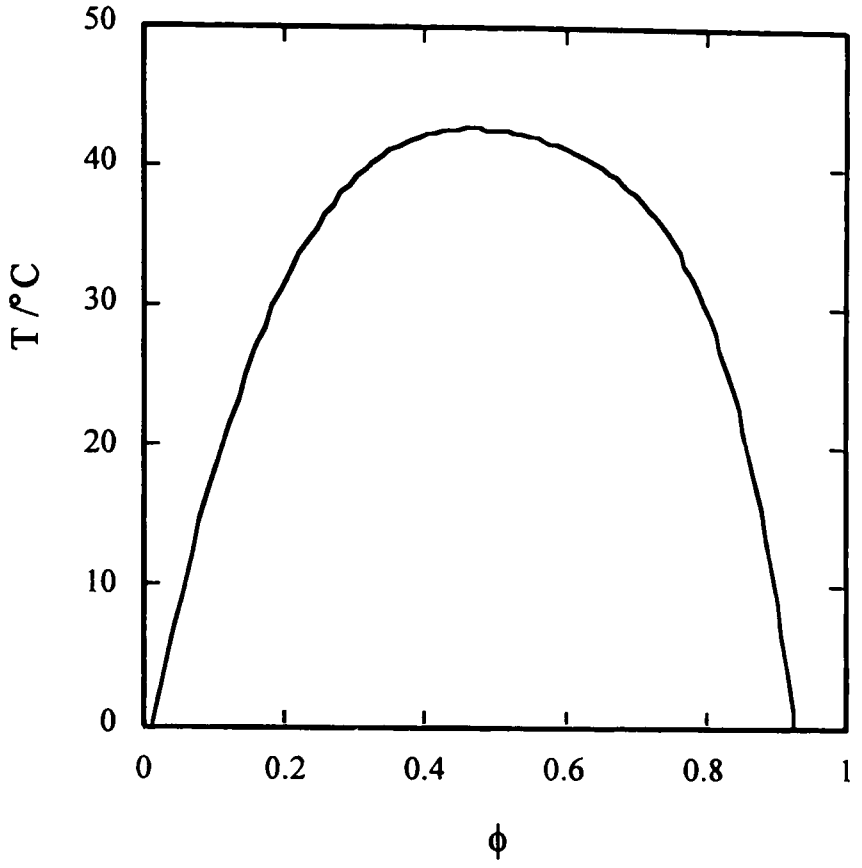

Figure 4.13: Coexistence curve for (1-ϕ) heptane + ϕ perfluorohexane. (Taken from Whitfield, 1996). T_{UCS} = 43°C, ϕ_c = 0.44.

The refractive index change with temperature due to changing compositions in a binary mixture can be either measured experimentally or calculated from the Lorentz-Lorenz equation:

$$\left(\frac{n_{mix}^2-1}{n_{mix}^2+2}\right)=\left(\frac{n_1^2-1}{n_1^2+2}\right)\phi_1+\left(\frac{n_2^2-1}{n_2^2+2}\right)\phi_2 \qquad (4.7)$$

where n_i is the refractive index of component i, n_{mix} is the refractive index of the mixture and ϕ_i is the ideal volume fraction of component i evaluated at 25°C. The volume fraction of component i in each phase at a given temperature can be obtained from the coexistence curve, Figure 4.13, and with the refractive indices of the pure components, Table 4.1, used to calculate the refractive indices of the coexisting phases n_{mix} as a function of temperature, as shown in Figure 4.14.

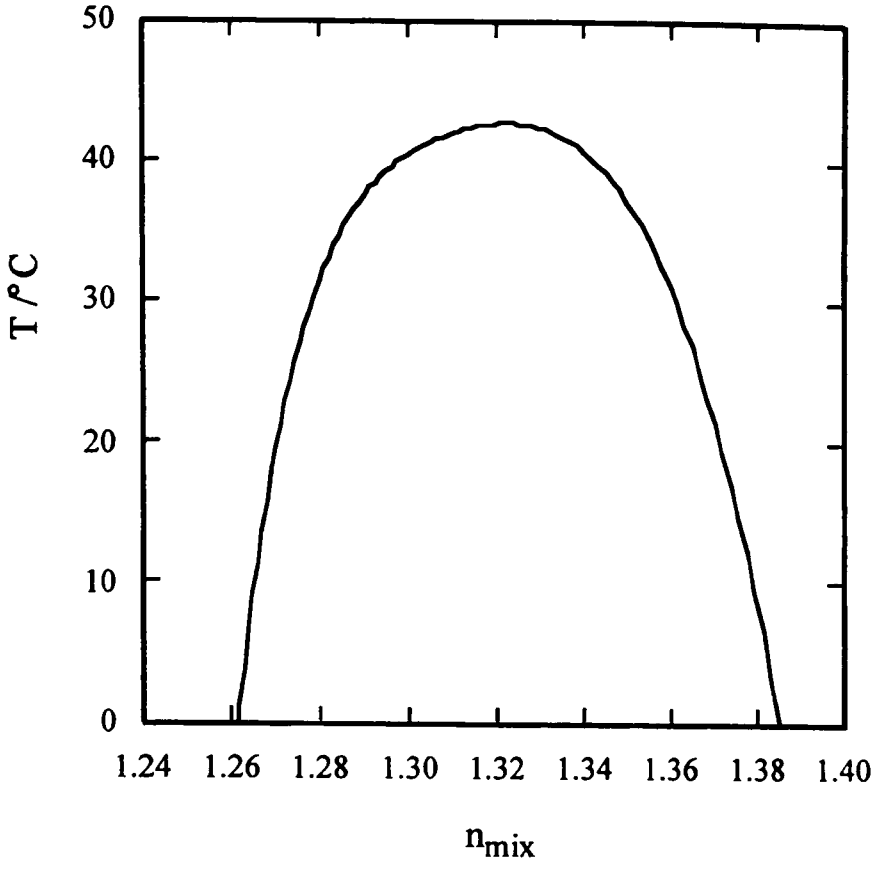

Figure 4.14: Temperature-refractive index plot for coexisting phases in a mixture of heptane + perfluorohexane.

4.2.7 Sample preparation

For the intensity experiments the mixture was made up by injecting a DPH in heptane solution, of absorbance < 0.1, and perfluorohexane by syringe into the cell through the filling tube with the prism clasped in place on the front of the cell. The measurements were carried out for two-phase mixtures below T_{UCS} and so the exact composition of the mixture did not need to be known.

In the lifetime work the samples were required to be oxygen-free. Mixtures of composition close to critical were made up in Whitey bottles from heptane solutions–saturated with DPH–and perfluorohexane. In this work the DPH in heptane solutions were saturated, and then filtered. Saturated solutions were needed to obtain a measurable fluorescence signal since the excitation wavelength of 310 nm was on the low-wavelength low-intensity edge of the excitation spectrum for DPH in heptane or perfluorohexane. The samples were degassed by about four freeze-pump-thaw cycles in the Whitey bottles and transferred on the stainless steel vacuum line by gravity into the cell, which was attached via the Swagelok fitting on the filling tube, as illustrated in Plate 3. The cell and Whitey bottle were generally cleaned using methanol.

4.2.8 Filters

Different types of filters have been discussed briefly in section 3.2. For the EWGFS intensity work it was found that the choice of filters was very important and an interference filter 370 nm was used on the excitation beam of 371 nm selected using a monochromator and a short-wavelength cut-off filter GG435 on the collected fluorescence. This combination of filters was still not ideal as an increase in intensity was generally observed at emission angles equal to the excitation angle and in future experiments the totally reflected beam should also be dumped. The intensity of the fluorescence signal was decreased significantly by the use of the filters.

Throughout the lifetime measurements, using an excitation wavelength of 310 nm, a filter was used on the incident beam to cut out 620 nm light and, as mentioned above, a 330 nm short-wavelength cut-off filter was used on the fluorescence in addition to a monochromator set at 440 nm.

4.2.9 Further considerations for intensity experiments

As discussed in section 4.1.4.1 there are many factors involved in the measurement of the fluorescence intensity to study critical-point wetting. In this section the expected effects of some of the factors on our selective excitation measurements on DPH in heptane + perfluorohexane are considered in more detail.

The variation of the refractive index n of each coexisting phase with temperature has been plotted in Figure 4.11. This variation affects the critical angle $\alpha_c = \sin^{-1}(n_{mix}/n_{quartz})$. At 20°C, $n_{quartz} = 1.474$ at 371 nm, the wavelength used in the intensity work, and $n_{quartz} = 1.485$ at 310 nm, the wavelength used in the lifetime work. These values were calculated from:

$$n^2 = 1 + \frac{0.696\lambda^2}{\lambda^2 - 0.0047} + \frac{0.408\lambda^2}{\lambda^2 - 0.0135} + \frac{0.897\lambda^2}{\lambda^2 - 97.934} \qquad (4.8)$$

where λ is the wavelength in μm (Robson Scientific). The refractive index of quartz also changes with temperature, but the effect on the critical angle for each phase at a given temperature is expected to be similar and so this effect is neglected here. At 30°C and taking n_{quartz} at 371 nm, at the boundary of the quartz prism with the upper heptane-rich phase $\alpha_c = 67.4°$ and with the lower perfluorohexane-rich phase $\alpha_c = 60.2°$. Similarly at 40°C, $\alpha_c = 65.6°$ at the heptane-rich phase and $\alpha_c = 61.8°$ at the perfluorohexane-rich phase, the angles becoming closer in value closer to $T_{UCS} = 43°C$ as the phases become more similar.

Another effect of the refractive index change is to alter the penetration depth of the evanescent wave $z_{0,1}$, given earlier by equation (4.3) and reproduced below:

$$z_{0,1} = (\lambda_{ex}/2\pi)\,[(n_{quartz}\,\sin\alpha_{ex})^2 - (n_{mix})^2]^{-1/2} \qquad (4.9)$$

where in our intensity experiments λ_{ex} = 371 nm. As α_{ex} approaches α_c, $z_{0,1}$ tends to infinity, and thus the highest penetration depths are obtained for α_{ex} close to α_c. The variation in $z_{0,1}$ with α_{ex} for each phase at 30°C is shown in Figure 4.15. For a given α_{ex} less than both critical angles, $z_{0,1}$ is greater in the heptane-rich phase. At higher temperatures the penetration depths in each phase become more similar.

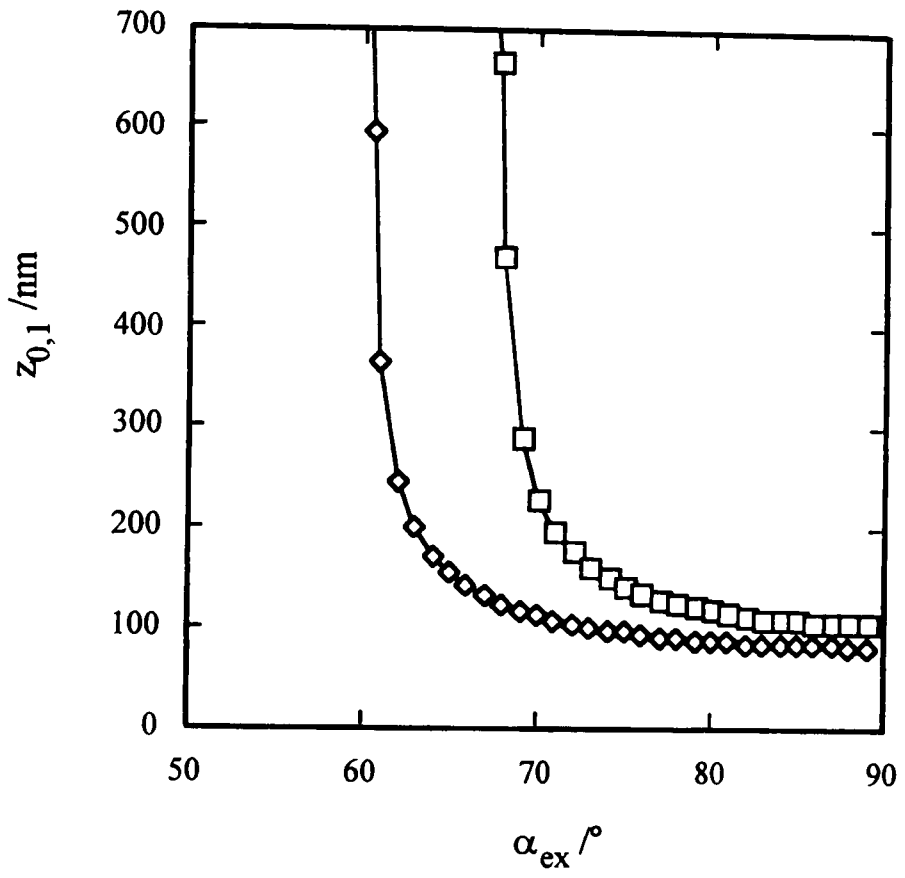

Figure 4.15: Variation in the penetration depth of the evanescent wave $z_{0,1}$ with excitation angle α_{ex} for the heptane-rich (□) and perfluorohexane-rich (◊) phases coexisting at 30°C.

The decrease in the intrinsic fluorescence intensity with temperature is another factor that needs to be considered in interpreting any results, although this is expected to be a fairly consistent effect. The form of the fluorescence intensity-temperature profile for DPH in the pure solvents methylcyclohexane (MCH) and perfluoro-methylcyclohexane (PFMCH) has been studied by Williamson (1990). With increasing temperature, an initial increase then a decrease in intensity was observed in MCH, and a monotonic decrease in intensity was found in PFMCH.

The fluorescence intensity also depends on the emission angle at which the fluorescence is collected. In our experiments the fluorescence intensity was recorded for a range of emission angles, although in some cases this was limited, particularly for the

bulk phase, by the possible positions of the PM tube with respect to the prism and cell. The excitation angles need to be carefully selected to ensure that a reasonable penetration depth of the evanescent wave is achieved, but so that the collection of fluorescence at emission angles close to the critical angle is not obscured by the totally reflected beam. For careful angular work slits should be used on the collected fluorescence to ensure that only a narrow angular range is collected at any one time. In our work a large range of angles was collected for any position of the PM tube, so the angles were only approximate. Since the PM tube could only be accurately located every 10°, measurements were only possible at 5° intervals by setting at intermediate positions, and in further work angular intervals of 1° should be incorporated in the set-up. It should be noted that measurements taken at high emission angles may not be accurate due to edge effects as some of the fluorescence is obscured by the cell.

The partitioning of the dye between the phases may alter with temperature, but probably not by much for a small range of temperatures close to the wetting transition temperature T_w, and this is expected to be a minor factor compared with others discussed here. The effect of temperature on the thickness of the wetting film and hence on the fluorescence intensity is of interest and future results may allow this to be determined. Any change in the excitation and emission spectra of DPH with composition and temperature may be of importance in this work. In future work this aspect should be looked at more closely, in particular to determine the form of the shift in the excitation peaks with composition of a binary mixture. Some work in this area was undertaken by Williamson (1990) who showed that for DPH in MCH + PFMCH excited at 375 nm, the intensity of the fluorescence increased with the mole fraction of MCH, although not linearly, for all emission wavelengths considered.

The decrease in incident beam intensity with time throughout the day, due to the decreasing current of the synchrotron with time after refilling, was accounted for by recording the fluorescence from a standard as described in section 4.2.3. The synchrotron ring current dropped over about 13 hours from 230 mA to 150 mA resulting in a drop in intensity of the reference from 33,000 counts s^{-1} to 8,000 counts s^{-1}. Possibly one of the major factors affecting the experiment was the detection of stray scattered light instead of fluorescence. Further effects were due to shifts in the position of the beam–at times the incident beam was observed to catch on the entrance slit to the black box–and changes in the focusing of the beam. All the results quoted were obtained on the same day as changes in the beam on refilling were noticed. The cell also had to be fixed onto the base by two locating screws, to ensure that the reference angle, i.e. the angle corresponding to $\alpha_{ex} = 0$, remained unchanged during a run. The reference angle read from the goniometer was used to calculate the excitation and emission angles and was obtained by rotating the cell to determine the position for

which the incident and reflected beams coincided, i.e. when the incident beam bisected the hemicylindrical section of the prism.

In some experiments, solid deposits were noticed at the liquid-liquid interface which were probably dust particles. The precipitation of dye at the interface was unlikely since the mixture was made up from a fairly dilute solution of DPH in heptane by adding perfluorohexane.

4.2.10 Preliminary lifetime experiments

The preliminary experiments carried out prior to the lifetime work presented here were as follows:

1. DPH was deposited on the prism and the fluorescence lifetime τ_F was measured from the bulk and surface of a solution of DPH in methylcyclohexane (MCH) (Bowers, 1995; Whitfield, 1996). The lifetimes were the same indicating that problems should not be encountered due to adsorption/deposition of the dye on the prism affecting the lifetime.
2. The fluorescence lifetime for DPH in cyclohexane + perfluorohexane was measured at room temperature, well below $T_{UCS} = 75°C$ so no wetting was expected. The intensity from the lower phase was very low showing that no notable adsorption of the hydrocarbon-rich phase onto the prism had occurred.
3. A standardisation test was carried out by measuring the lifetimes of an anthracene in ethanol solution, both with and without degassing. The values obtained agreed well with the literature values (Demas, 1983).
4. Lifetimes were measured for DPH in pure heptane $\tau_F = 15.5$ ns and in pure perfluorohexane $\tau_F = 29.8$ ns and agreed well with the literature values of 15.6 ns and 32.5 ns in heptane and perfluorohexane, respectively (Cehelnik *et al.*, 1974). The fluorescence lifetime of DPH in heptane was also measured at the surface and in the bulk solution and the values obtained were essentially the same.

Tests were also carried out to ensure that the mixtures were adequately degassed and that the seal on the cell held over long periods of time.

4.3 Results and discussion

4.3.1 Fluorescence intensity method

Throughout this work an excitation wavelength of 371 nm was used to excite the dye in the heptane-rich phase only. A preliminary experiment was carried out for DPH in heptane and the critical angle $\alpha_c = 69°$ determined agreed fairly well with the calculated value $\alpha_c = 70.2°$. This sample was also used to decide which excitation angles to use throughout the experiment.

The main experiment for DPH in heptane + perfluorohexane produced various results which are outlined below. The measured intensities were much lower than the allowed maximum of 70,000 counts s^{-1} due to the filters cutting down the intensity and the drop in intensity throughout the day. The measured values were divided by the intensity of the reference for the same ring current and then multiplied by a constant factor to yield numbers that were easily comparable. The excitation angles α_{ex} selected were 30° for excitation of the bulk phases and 75° and 80° for evanescent wave excitation of the surface phases. At a given temperature and α_{ex}, measurements were made for both the upper and lower phases. After the sample had reached the required temperature, the contents were mixed and then left to equilibrate for at least 30 minutes. The temperatures were recorded from both the CAL controller setting and an independent thermometer. The values quoted are those from the CAL; the independent reading was generally 1.7 Kelvin lower. The upper critical solution temperature $T_{UCS} \approx 47.0°C$ (on the CAL) was determined by observing the transition from two phases to a single phase. The temperatures recorded are thus probably about 4 K too high, from a comparison with the accepted value of T_{UCS}. This variation can be attributed to different thermometer calibrations and impurities.

The intensity-emission angle α_{em} profiles at 35.0°C for the lower and upper phases at different excitation angles are shown in Figures 4.16 and 4.17. This temperature is expected to be below the wetting transition temperature T_w. Similar profiles were observed at other temperatures in the range 29.3-42°C. The intensities are low and at smaller α_{em} are only slightly larger in the upper heptane-rich phase than in the lower phase, although the numbers are too small to compare accurately.

For surface excitation of both the upper and lower phases, the increase in intensity at higher α_{em} is likely to be due to the detection of the totally reflected beam, since the increase is large and is observed close to $\alpha_{em} = \alpha_{ex}'$. The further decrease observed at the highest emission angles may be artefactual possibly due to edge effects. For the surface phases, the small local maximum in intensity observed at 50° for the lower phase and 55° for the upper phase, particularly for $\alpha_{ex} = 80°$, may be caused by nearness to the critical angle as indicated by Fattinger (1987), although the calculated critical angles, 60° and 67°, are somewhat larger and thus indicate that this may be unlikely. In order to confirm this more fully all the angles must be better defined and the intensity collected at smaller angular intervals. The differences in intensity recorded by collection at slightly different angles are apparent.

From the lower bulk phase the fluorescence intensity is very small as expected due to the low DPH concentration and the low absorbance at the selected excitation wavelength. In contrast, from the upper bulk phase the intensity is higher. The increase at lower α_{em} is again probably due to the detection of the imperfectly filtered out totally reflected beam. Whatever its cause, however, one consequence would be the masking of the signature of the critical angle.

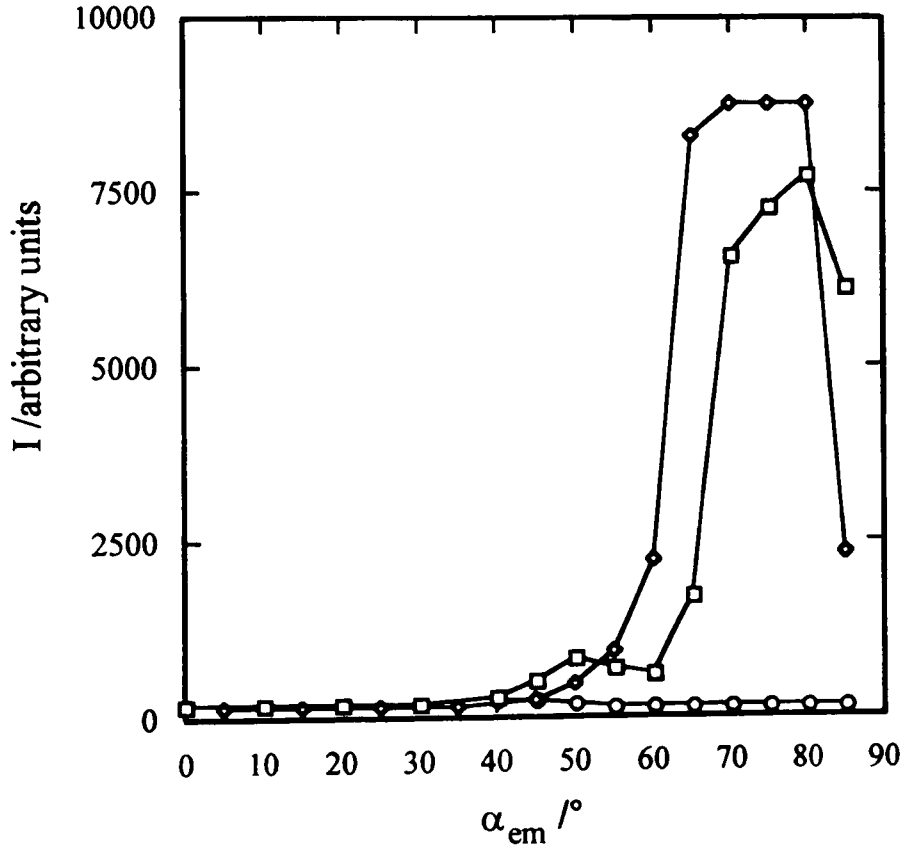

Figure 4.16: Scaled fluorescence intensity I-emission angle α_{em} profiles at 35.0°C and excitation angles α_{ex} of 30° (O), 75° (◊) and 80° (□) for the lower perfluorohexane-rich phase.

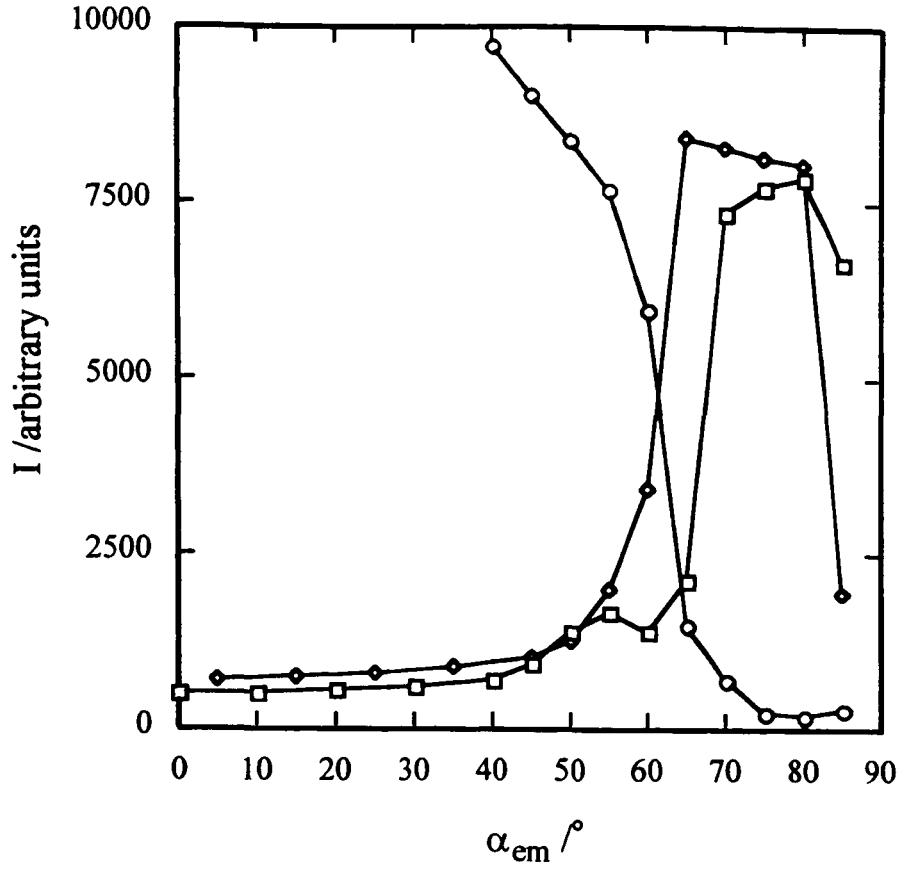

Figure 4.17: Scaled fluorescence intensity I-emission angle α_{em} profiles at 35.0°C and excitation angles α_{ex} of 30° (O), 75° (◊) and 80° (□) for the upper heptane-rich phase.

The differences in the scaled intensities of the upper and lower surface phases as a function of temperature for $\alpha_{ex} = 75°$ and 80° and for $\alpha_{em} = 50°$ are shown in Figure 4.18. Over the temperature range, the intensity recorded from the upper phase is higher than that from the lower phase, as expected, even for temperatures at which the presence of a wetting film of the upper phase between the lower bulk phase and the solid wall is expected, since the evanescent wave may penetrate through the wetting film into the bulk phase. At 37°C the two surface phases become most similar and this may possibly be interpreted as the wetting temperature T_w. However, although similar profiles were observed for $\alpha_{em} = 45°$ and 55°, different profiles were observed at higher $\alpha_{em} = 60°$, 65°, 70° and 75°, as shown for $\alpha_{em} = 60°$ in Figure 4.19, corresponding to angles in the intensity-emission angle profiles at which the detection of the totally reflected beam was suspected.

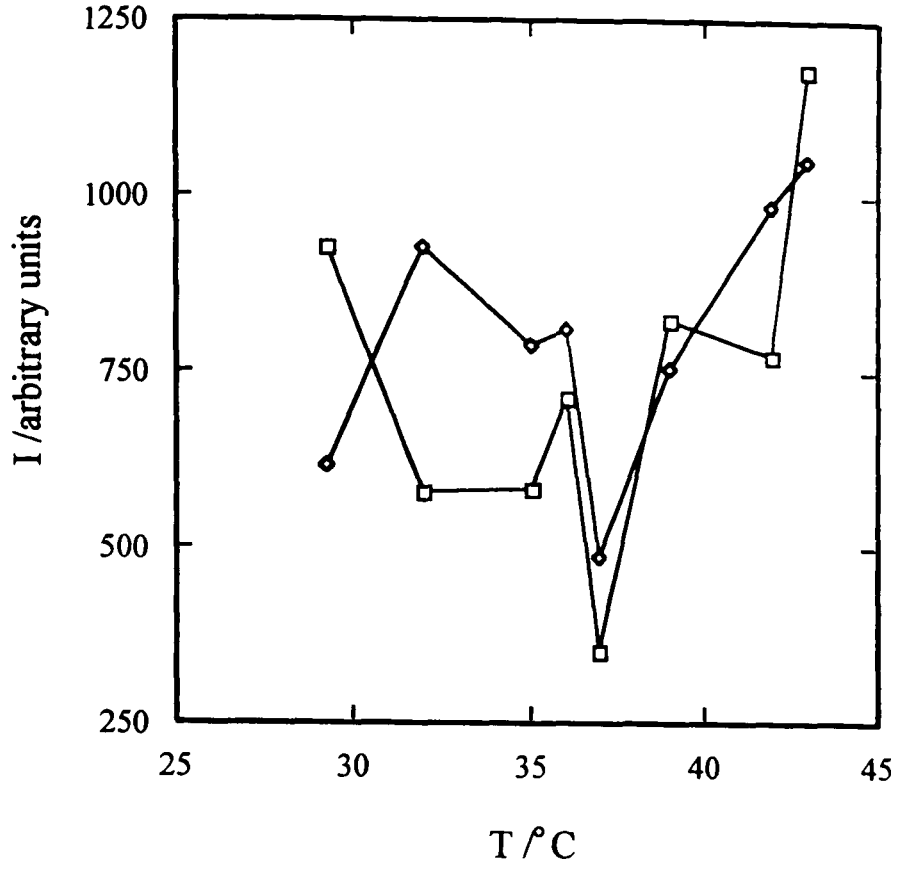

Figure 4.18: Scaled intensities I for (upper phase - lower phase) as a function of temperature for excitation angles α_{ex} = 75° (◊) and 80° (□) and for an emission angle α_{em} = 50°.

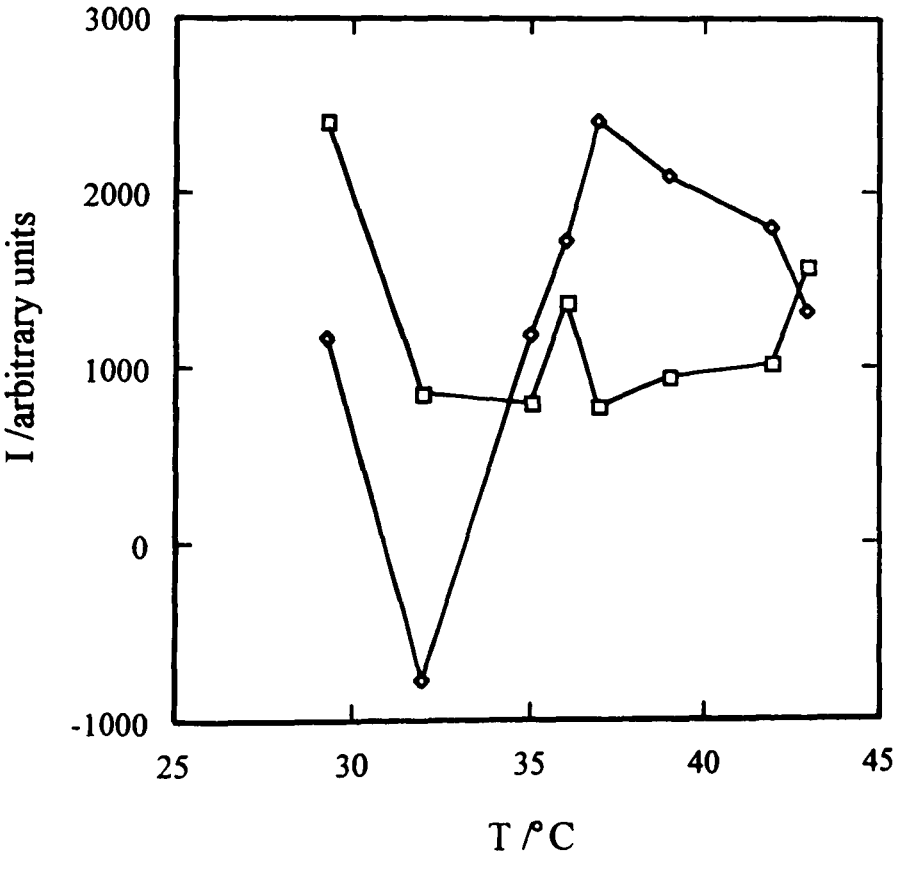

Figure 4.19: Scaled intensities I for (upper phase - lower phase) as a function of temperature for excitation angles α_{ex} = 75° (◊) and 80° (□) and for an emission angle α_{em} = 60°.

For $\alpha_{em} = 50°$, the intensity-temperature profile for the lower surface phase was as predicted, see section 4.1.4.2, however, a similar profile was also observed for the upper phase. The results presented here highlight some of the problems with the experiment and do not clearly show a wetting transition since many of the obscuring factors discussed previously could not be eliminated.

In future experiments the intensity of the fluorescence collected must be increased and must be measured more accurately since the differences in intensity due to a wetting transition may be small (Fattinger *et al.*, 1987; Williamson, 1990), possibly of the order of 10-20%. The totally reflected beam must be eliminated along with stray light effects which obscure the fluorescence.

In recent work on this technique, using either the synchrotron for selective excitation, or a HeNe laser at 632 nm with a Bodipy dye for differential solubility, problems have been encountered in the true detection of fluorescence due to scatter from optical elements in the system (Bowers, 1996a; Whitfield, 1996).

We turn now to the results obtained by the method of fluorescence lifetime difference in each phase, which has fewer associated problem-causing factors.

4.3.2 Fluorescence lifetime method

In all the measurements on DPH in heptane + perfluorohexane the incident wavelength was set at 310 nm and the fluorescence was collected at 440 nm. The excitation angles α_{ex} were chosen to ensure that total internal reflection occurred and that a reasonably high fluorescence intensity was detected. The fluorescence was generally recorded from the surface and bulk regions of both the upper and lower phases at a given temperature, after equilibrating for about 30 minutes once mixed. The lifetimes were obtained by fitting the decays to single-exponentials, or bi-exponentials if the fluorescence intensity was low to account for the short decay time of about 1 ns of the cell and the prism. The fluorescence decay of the cell and the prism, with no sample, is shown in Figure 4.20.

Two different temperature runs were carried out on the same degassed mixture. In run 2 the wetting transition temperature T_w was located more accurately by stepping in smaller intervals of temperature. The results obtained from runs 1 and 2, along with the excitation angles α_{ex} for the generation of an evanescent wave at the surface phases and the calculated critical angles for the bulk phases, are given in Tables 4.2 and 4.3. Figure 4.21 shows representative fluorescence decays for the bulk and surface of the upper heptane-rich phase below and above T_w. Figures 4.22 and 4.23 show fluorescence decays for the bulk and surface of the lower perfluorohexane-rich phase below and above T_w, respectively. The difference in the bulk and surface decays above T_w is clearly shown.

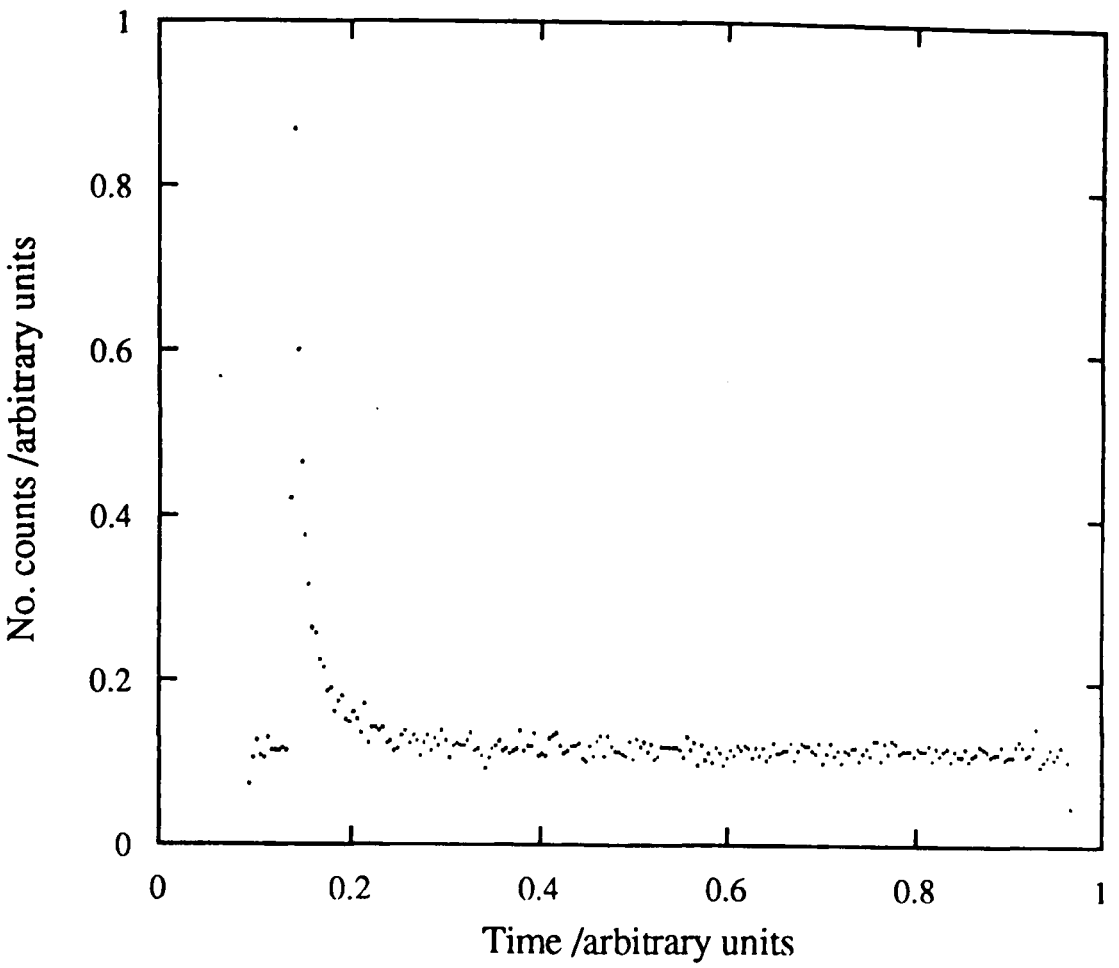

Figure 4.20: Fluorescence decay of the cell and prism, with no sample, excited at 310 nm.

Table 4.2: Run 1. The fluorescence lifetimes τ_F of DPH measured from the bulk and surface regions of the upper and lower phases of a heptane + perfluorohexane mixture. The excitation angles α_{ex} at the surface phases and the calculated critical angles α_c for the bulk phases are also included.

T/°C	lower phase				upper phase			
	$\tau_{F,bulk}$ /ns	$\tau_{F,surf}$ /ns	α_{ex} /°	α_c /°	$\tau_{F,bulk}$ /ns	$\tau_{F,surf}$ /ns	α_{ex} /°	α_c /°
19.3	28.2	29.1	60.9	58.8	17.1	-	-	67.6
26.7	26.3	26.9	61.3	59.2	17.8	-	-	66.9
31.7	24.9	25.2	63.7	59.6	17.9	-	-	66.2
36.6	24.2	18.0	65.7	60.1	17.9	-	-	65.6
38.6	23.7	18.3	65.0	60.6	18.1	18.3	70.2	65.1

Table 4.3: Run 2. The fluorescence lifetimes τ_F of DPH measured from the bulk and surface regions of the upper and lower phases of a heptane + perfluorohexane mixture. The excitation angles α_{ex} at the surface phases and the calculated critical angles α_c for the bulk phases are also included.

T/°C	lower phase				upper phase			
	$\tau_{F,bulk}$ /ns	$\tau_{F,surf}$ /ns	α_{ex} /°	α_c /°	$\tau_{F,bulk}$ /ns	$\tau_{F,surf}$ /ns	α_{ex} /°	α_c /°
19.3	25.3	24.4	60.7	58.8	16.8	16.8	74.9	67.6
26.7	23.1	21.7	61.7	59.2	17.6	17.2	74.5	66.9
31.4	24.1	22.2	62.2	59.5	16.6	16.4	73.7	66.2
31.6	22.2	16.4	64.7	59.6	-	-	-	66.2
31.9	23.5	17.4	64.7	59.6	16.6	16.6	71.0	66.2
32.4	23.5	16.8	64.2	59.7	16.3	16.5	70.7	66.0

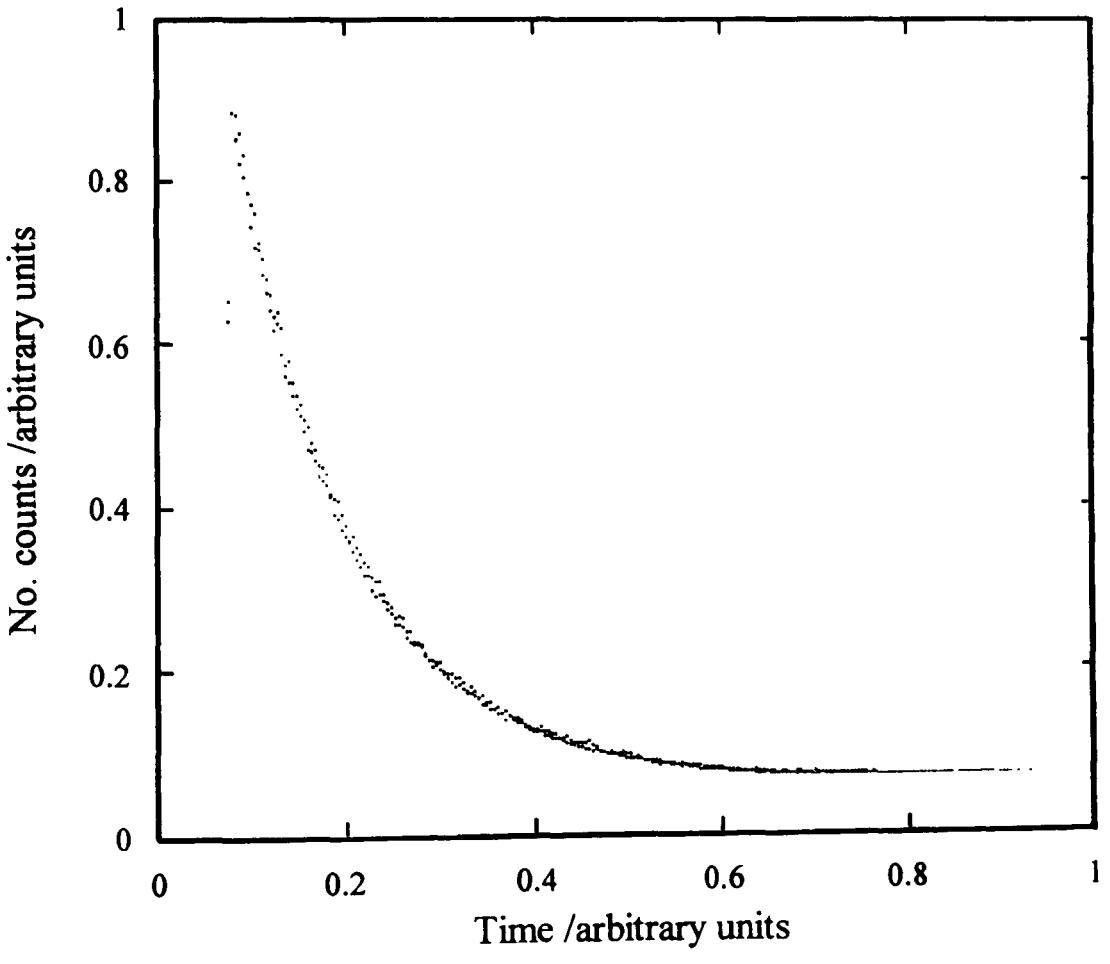

Figure 4.21: Fluorescence decays of DPH from the bulk and surface regions of the upper heptane-rich phase below and above T_w, for excitation at 310 nm and collection at 440 nm.

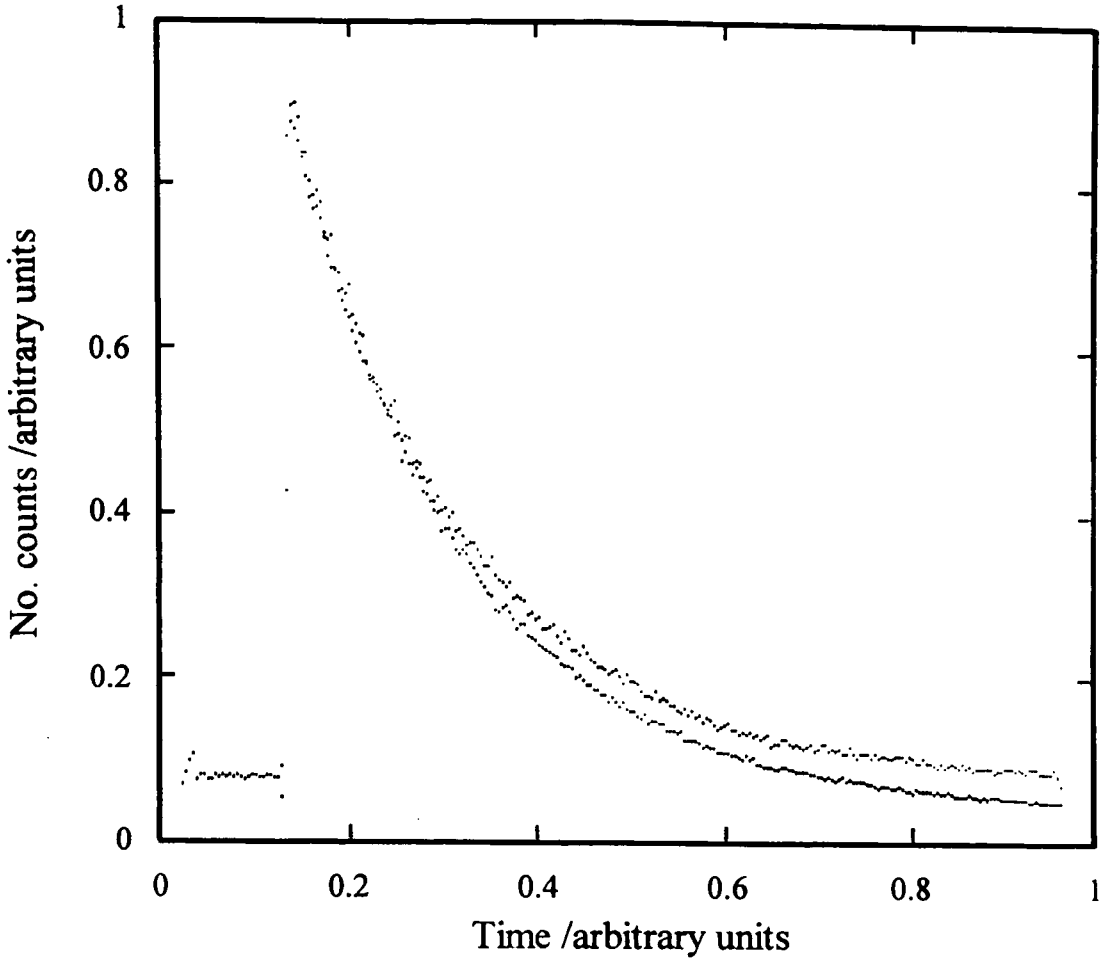

Figure 4.22: Fluorescence decays of DPH from the bulk and surface regions of the lower perfluorohexane-rich phase below T_w, for excitation at 310 nm and collection at 440 nm.

The fluorescence lifetimes τ_F from Tables 4.2 and 4.3 are plotted as a function of temperature for runs 1 and 2 in Figures 4.24 and 4.25, respectively. There is some slight discrepancy in τ_F at a given temperature between runs 1 and 2, due to a slow leak in the apparatus during run 2 resulting in a small reduction in the lifetime of the perfluorohexane-rich phase. The differences between the two phases, however, is still clear. At lower temperatures the lifetimes for the lower surface phase correspond to those for the bulk lower phase, but a transition in the lifetimes of the lower surface phase is observed at higher temperatures and they become more similar to those measured from the upper bulk phase. This indicates the interposition of a heptane-rich wetting film between the lower perfluorohexane-rich phase and the quartz. The wetting transition temperature T_w is identified from Figure 4.25 as $T_w = 31.5°C$ and thus lies about 11 K below T_{UCS}. The value of T_w was also indicated by the measurement at 31.4°C, since on heating to this temperature the controller slightly overshot the preset temperature and a wetting film was observed. This film was displaced on mixing and equilibrating at the required temperature. The change in lifetime is observed to occur within a 0.2 K temperature interval, indicating that the transition may be of first order, but further work needs to be carried out to confirm this.

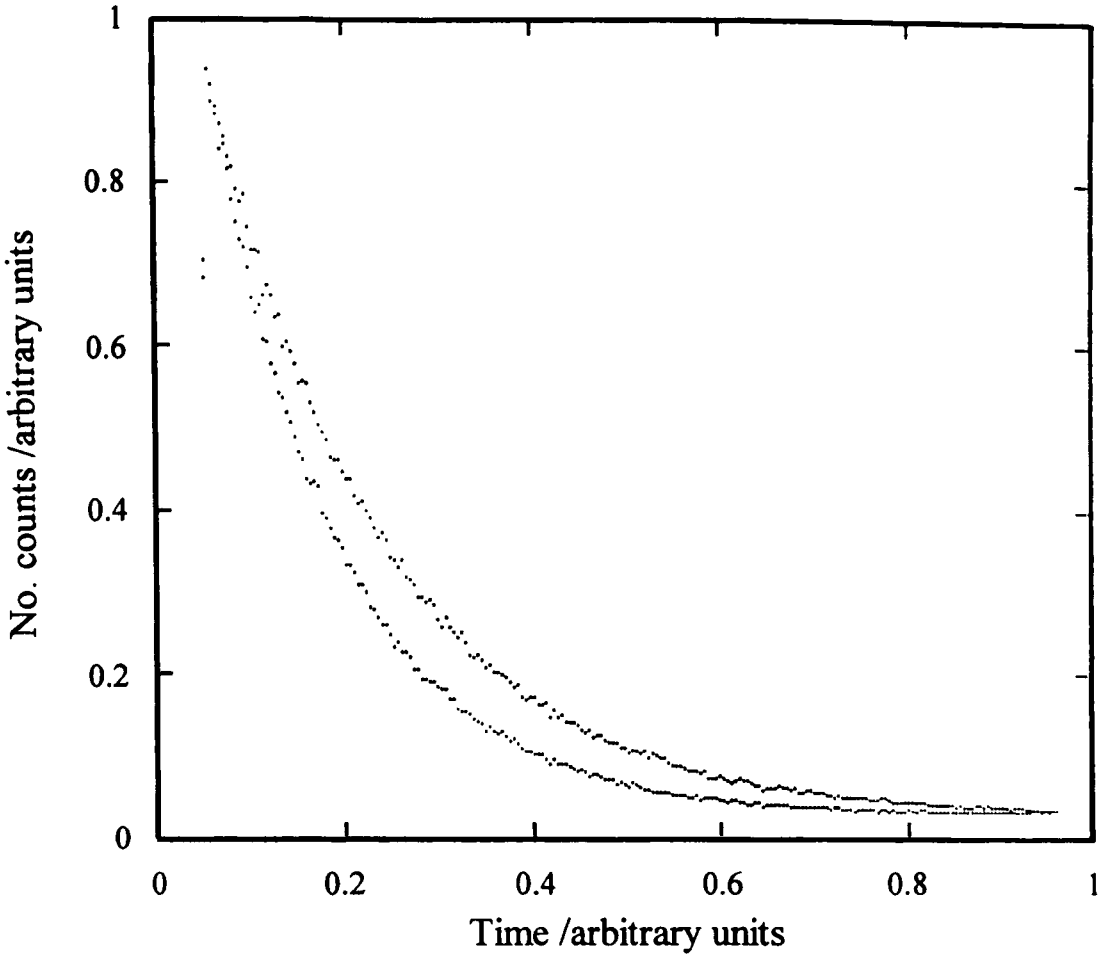

Figure 4.23: Fluorescence decays of DPH from the bulk and surface regions of the lower perfluorohexane-rich phase above T_w, for excitation at 310 nm and collection at 440 nm.

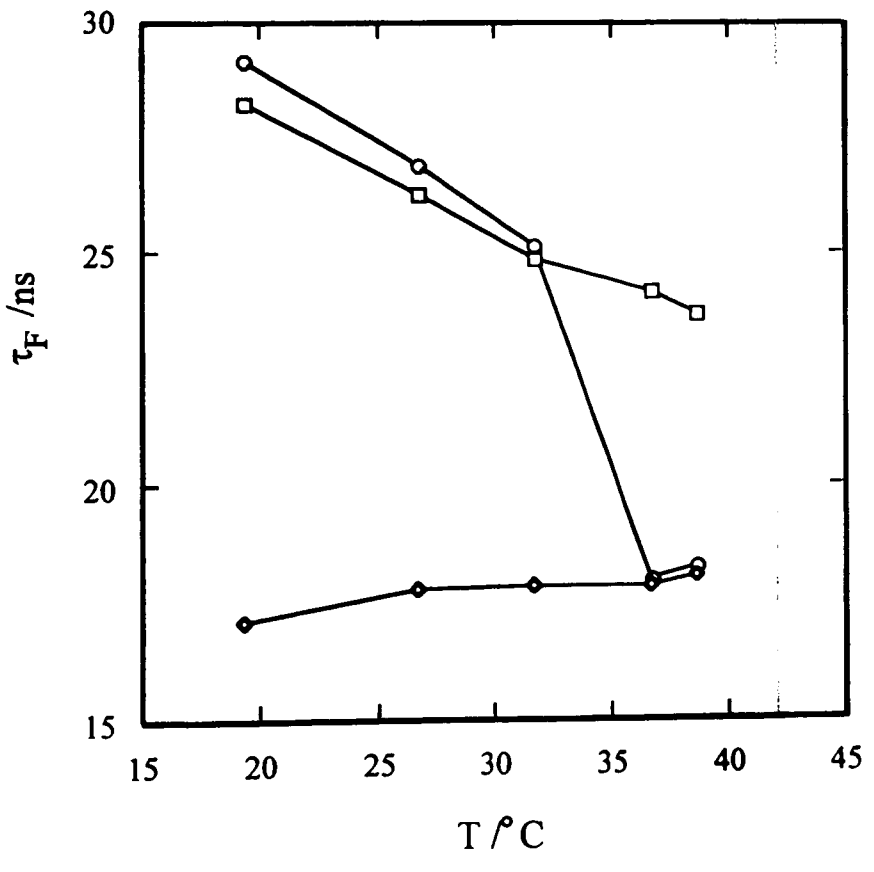

Figure 4.24: Run 1. Fluorescence lifetimes τ_F for DPH, excited in the bulk upper (◊) and lower (□) phases and at the surface in the lower (O) phase, as a function of temperature. The vertical line marks T_{UCS}.

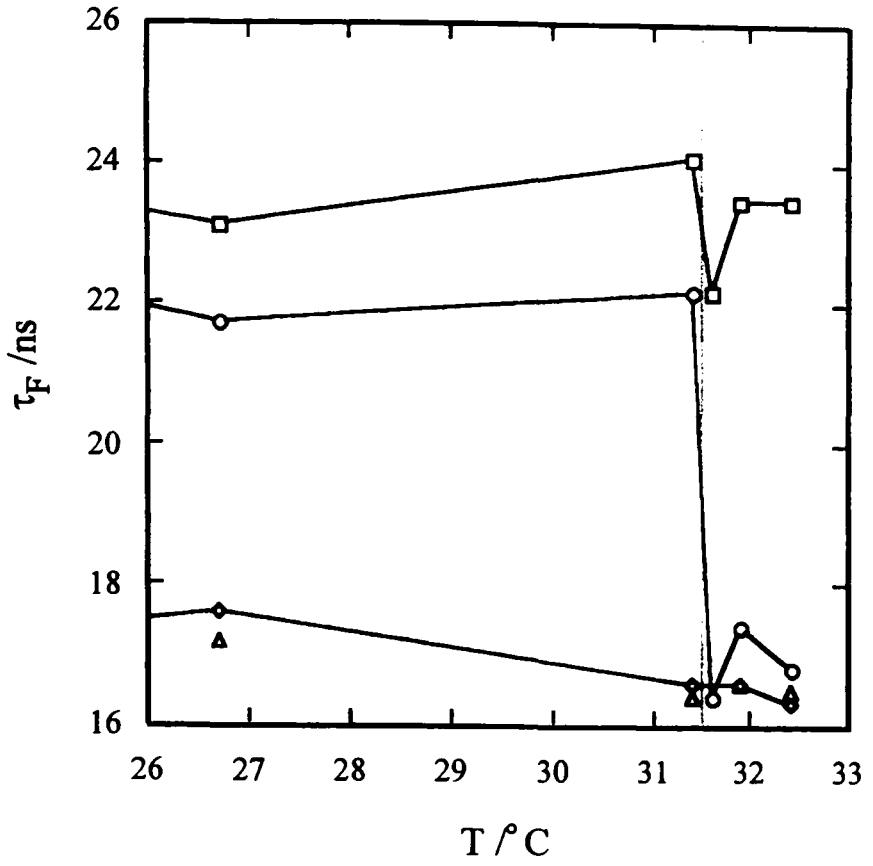

Figure 4.25: Run 2. Fluorescence lifetimes τ_F for DPH, excited in the bulk upper (◊) and lower (□) phases and at the surface in the upper (Δ) and lower (○) phases, as a function of temperature. The vertical line marks T_w.

The dependence of τ_F of DPH on the composition x of a mixture of heptane + perfluorohexane, where x is the mole fraction of one of the components, was obtained by relating the values of τ_F in each coexisting bulk phase at a given temperature to the compositions of the phases calculated from the coexistence curve. These values as a function of x around the coexistence curve, as well as those obtained for the pure components, agreed well with those obtained using the Synchrotron Radiation Source (SRS) at Daresbury Laboratory (DL) while carrying out the microviscosity experiments in Chapter 3. These latter measurements were obtained at 45°C for degassed single-phase mixtures in sealed Pyrex cuvettes using incident light at 340 nm and collecting a range of emission wavelengths. Both sets of results are tabulated in Table 4.4 and plotted in Figure 4.26, which shows that the dependence of τ_F on x(perfluorohexane) is not linear. Originally a very high lifetime of 57.1 ns was obtained at Daresbury for DPH in pure perfluorohexane, but this was not reproducible and values of about 31 ns were later measured.

Table 4.4: Fluorescence lifetimes τ_F for DPH in heptane + perfluorohexane obtained at 45°C, using the Synchrotron Radiation Source (SRS) at Daresbury Laboratory (DL) for excitation at 340 nm and collection over a range of emission wavelengths, and at different temperatures around the coexistence curve, using the Central Laser Facility (CLF) at Rutherford Appleton Laboratory (RAL) for excitation at 310 nm and collection at 440 nm.

DL		RAL	
x (perfluorohexane)	τ_F /ns	x (perfluorohexane)	τ_F /ns
0	16.0	0	15.5
0.270	19.4	0.08	17.1
0.410	22.5	0.12	17.8
0.650	24.3	0.15	17.9
0.840	27.8	0.20	17.9
0.920	29.1	0.23	18.1
0.977	30.9	0.61	23.7
0.996	30.4	0.66	24.2
1	31.1	0.72	24.9
		0.77	26.3
		0.82	28.2
		1	29.8

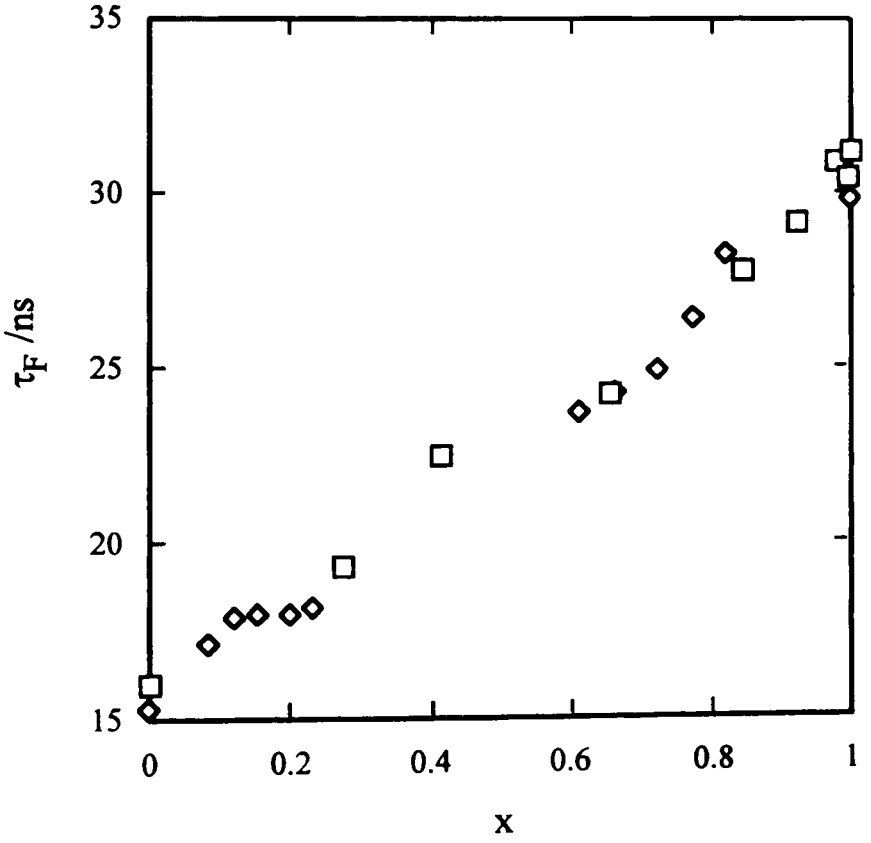

Figure 4.26: Fluorescence lifetimes τ_F as a function of mole fraction x of perfluorohexane for DPH in heptane + perfluorohexane. Results at 45°C (□), obtained using the SRS at DL for excitation at 340 nm and collection over a range of emission wavelengths, and at different temperatures around the coexistence curve (◊), obtained using the CLF at RAL for excitation at 310 nm and collection at 440 nm.

In Table 4.5, fluorescence lifetime measurements taken as a function of excitation angle α_{ex} for the lower surface and bulk phases at 38.6°C, which is above T_w, are tabulated. The lifetimes are quoted here, and in the following tables, to more significant figures than may be strictly accurate to highlight the small changes in the later values. The results, plotted in Figure 4.27, show some well-defined structural features. These features are attributed to structure within the wetting layer rather than to the adsorption of dye at the quartz surface, since corresponding experiments in the phases in which no critical-point wetting layer is present show no such features, as discussed below.

A plausible explanation for the observed structure is as follows. At lower α_{ex} the laser beam is partially reflected but the majority of the intensity is transmitted to the bulk of the mixture where fluorescence is induced. As the critical angle α_c for total reflection is approached, the measurement is sensitive to both surface and bulk contributions so a drop in the lifetime is observed as the surface layer is increasingly sampled in the measurement. There is then a further rapid drop in the lifetime at α_c, about 60.1°, the measured lifetime being consistent with the presence of a heptane-rich wetting film. This is now the region of total reflection. As α_{ex} increases above α_c the penetration depth $z_{0,1}$ of the evanescent wave decreases. The three apparent steps in the profile i)-iii) can be interpreted as:

i) $z_{0,1}$ large, thus probing both the wetting film and the bulk,

ii) $z_{0,1}$ smaller, thus probing only the wetting film,

iii) preferentially adsorbed heptane at the quartz surface.

Measurements could not be obtained at higher α_{ex} as the fluorescence intensity was too low. These effects suggest that measurements of this kind may have the potential to allow the thickness of the wetting film and the order of the transition to be determined, since the extent of the second step with α_{ex} may possibly be related to the thickness of the layer.

Table 4.5: Fluorescence lifetime τ_F as a function of excitation angle α_{ex} for the lower surface and bulk phases at 38.6°C, which is above T_w, where the critical angle $\alpha_c = 60.1°$.

α_{ex} /°	τ_F /ns
56.7	23.48
57.7	23.39
58.7	23.17
59.7	22.94
60.7	22.12
61.7	18.90
62.7	18.81
63.7	18.67
64.7	17.96
65.7	18.01
66.7	17.90
67.7	17.94
68.7	17.46

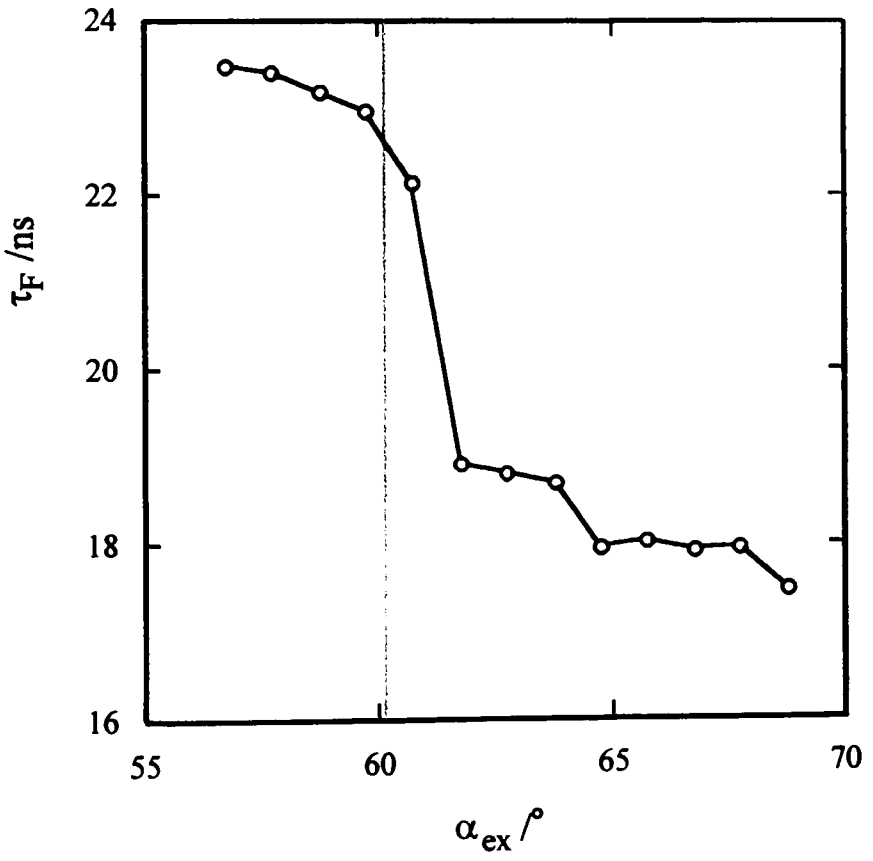

Figure 4.27: Fluorescence lifetime τ_F as a function of excitation angle α_{ex} for the lower surface and bulk phases at 38.6°C, which is above T_w, where the critical angle $\alpha_c = 60.1°$ is marked by the vertical line.

For comparison, the dependence of τ_F on α_{ex} was also measured for the upper and lower phases at 19°C, which is below T_w, and the results are given in Table 4.6. The lifetimes are higher for the lower perfluorohexane-rich phase than for the upper heptane-rich phase, as expected, and in both phases no significant change in τ_F with α_{ex} was observed in this partial wetting regime.

Table 4.6: Fluorescence lifetime τ_F as a function of excitation angle α_{ex} for the lower and upper phases at 19°C, which is below T_w, with the critical angles $\alpha_c = 58.8°$ for the lower phase and $\alpha_c = 67.6°$ for the upper phase.

lower phase		upper phase	
α_{ex} /°	τ_F /ns	α_{ex} /°	τ_F /ns
55.7	26.43	68.7	16.71
56.7	26.02	69.7	16.70
57.7	25.85	70.7	16.83
58.7	25.58	71.7	16.64
59.7	26.01	72.7	16.67
60.7	26.20		

At 19°C, values of τ_F were also measured for the upper and lower phases using incident light polarised horizontally, as used in all the other measurements, and vertically. Lifetimes of 16.76 ns and 16.80 ns in the upper phase, and 26.43 ns and 26.30 ns in the lower phase, were obtained for horizontally and vertically polarised light, respectively. No significant dependence of the lifetime on polarisation of the incident light was thus observed.

The lifetime method has been used successfully to determine T_w and shows promise for the study of the thickness of the wetting film and the order of the transition. A comparison of the fluorescence lifetimes showed that the wetting layer observed was of approximately the same composition as the bulk heptane-rich phase.

4.4 Summary

A wetting transition has been observed at the quartz-liquid interface in the binary mixture heptane + perfluorohexane below $T_{UCS} = 43°C$. The wetting transition temperature T_w, at which the transition from partial to complete wetting of the quartz by the upper heptane-rich phase occurred, was identified as $T_w = 31.5°C$. The transition was located by the measurement of the fluorescence lifetime of 1,6-diphenyl-hexa-1,3,5-triene (DPH) in each coexisting liquid phase. The measurements of the fluorescence intensity, after selective excitation of DPH in the heptane-rich phase, did not yield such strong conclusions.

There are many more issues in critical-point wetting in this and other systems that lend themselves to further study. In addition, modified surfaces can be used to attempt to reverse the wetting behaviour and to vary the order of the transition.

CHAPTER 5: ADSORPTION AND WETTING AT THE LIQUID-VAPOUR INTERFACE

5.1 Neutron reflection

In the previous chapter critical-point wetting at the solid-liquid noncritical interface was discussed. In this chapter we turn to critical-point wetting and critical adsorption in binary mixtures at the *liquid-vapour* interface, and the activity of perfluoroalkylalkanes at the alkane-vapour or perdeuteroalkane-vapour interface. The liquid-vapour interface can be studied using the technique of specular neutron reflection which is a powerful tool for the elucidation of surface structure on the Ångstrom scale. The reflectivity data collected during an experiment provide information on the neutron refractive index profile normal to the interface to a depth of a few thousand Ångstroms, and thicknesses of surface layers can be determined to within a few Ångstroms.

The details of adsorption and wetting in near-critical mixtures and surfactant solutions have been discussed in Chapter 1, sections 1.3 and 1.4. The components of the mixtures used in this work include alkanes, perfluoroalkanes, perfluoroalkylalkanes, hexamethyldisiloxane, deuterium oxide and 2-butoxyethanol; these mixtures have been described in Chapter 1, section 1.5. We begin here with an introduction to neutrons and neutron reflectivity.

5.1.1 Neutrons

Neutrons are sub-atomic uncharged particles with a mass of 1.675×10^{-27} kg and a spin of $^1/_2$. Neutrons are generally produced for neutron scattering experiments in one of two ways, i) in a nuclear reactor, where the neutrons are formed by fission of uranium-235 nuclei, or ii) in a pulsed accelerator source, where charged particles are accelerated and directed towards a target of uranium or tantalum, or other similar material, and the neutrons are produced by reaction of these charged particles with the nuclei of the target. Method ii) is used to produce the neutrons at the ISIS facility at the Rutherford Appleton Laboratory, Didcot, Oxon where the work reported here was carried out. The charged particles used at ISIS are protons and the method is known as *spallation*. The protons are accelerated to high energies, of the order of 800 MeV, by a combination of an H^- linear accelerator and a proton synchrotron. In both methods of neutron production, the neutrons are slowed by collisions with a moderator such as liquid methane at 100 K, ambient water, or hydrogen at 25 K. The resulting thermal or cold neutrons generally have wavelengths comparable with the wavelengths of x-rays used in x-ray diffraction experiments, typically of the order of 1 Å. The technology used for neutron production has been described in more detail by Windsor (1981) and Byrne (1994).

Thermal neutrons can be treated as waves with the relationship between the wavelength λ and momentum p expressed by the de Broglie relation:

$$\lambda = \frac{h}{p} = \frac{h}{mv} \tag{5.1}$$

where h is Planck's constant, m is the neutron mass and v is its velocity. The velocity of a neutron is thus inversely proportional to its effective wavelength. The neutron wavelengths selected as ISIS are short and can be used to probe molecular lengths. The wave nature of neutrons means that they can undergo reflection, refraction, diffraction and interference and thus exhibit the characteristics associated with electromagnetic radiation. The reflection of neutrons can thus be treated using a classical optics approach.

In neutron scattering experiments the neutrons interact with the nuclei of the constituent atoms of the molecules. The scattering thus depends on the nuclei, and the scattering of neutrons is different from different isotopes of the same element. This is in contrast to x-ray scattering experiments in which the x-rays interact with the electrons of the constituent atoms and the scattering then depends on the electron density. Neutrons also possess a spin magnetic moment and can interact with electrons of unpaired spin– this is known as magnetic scattering.

The scattering of a neutron by a nucleus can be treated by the solution of a one-body Schrödinger equation:

$$\nabla^2\Psi(r) + \frac{2m}{\hbar^2}[E - V(r)]\Psi(r) = 0 \tag{5.2}$$

where ∇^2 is the differential operator $(\partial^2/\partial x^2 + \partial^2/\partial y^2 + \partial^2/\partial z^2)$, $\psi(r)$ is the neutron wavefunction, m is the neutron mass, $\hbar = h/(2\pi)$, V(r) is the potential representing the interaction of the neutron with the system and E is the incident neutron energy. All neutron optics are based on this equation and rigorous treatments of the derivations of the expressions in this chapter are given by Sears (1989).

5.1.1.1 Momentum transfer vector

In a neutron reflection experiment the incoming neutron beam has a wavevector $\mathbf{k_{in}}$ and the outgoing reflected beam has a wavevector $\mathbf{k_{out}}$. The momentum transfer vector normal to the interface **Q**, see Figure 5.1, is defined as:

$$\mathbf{Q} = \mathbf{k_{out}} - \mathbf{k_{in}} \ . \tag{5.3}$$

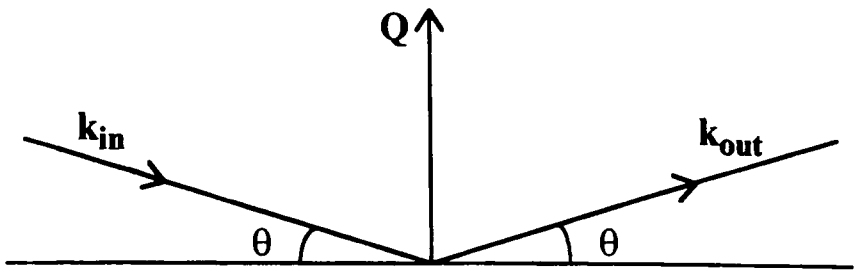

Figure 5.1: The momentum transfer vector **Q** for specular neutron reflection, defined in terms of the incident and reflected wavevectors $\mathbf{k_{in}}$ and $\mathbf{k_{out}}$.

For specular elastic scattering the glancing angle of incidence θ is equal to the glancing angle of reflection and the magnitudes of the incident and reflected wavevectors are the same, $k = |\mathbf{k_{out}}| = |\mathbf{k_{in}}|$. By equating the incoming and outgoing wavevectors, using the law of cosines and the identity $\cos(2\theta) = 1 - 2\sin^2\theta$, the equation relating the momentum transfer Q, where $Q = |\mathbf{Q}|$, to the wavelength λ of the neutrons and the glancing angle of incidence θ measured relative to the interface is:

$$Q = 2k\sin\theta = \frac{4\pi\sin\theta}{\lambda} \tag{5.4}$$

where the magnitude of the wavevector $k = 2\pi/\lambda$, by definition. In a neutron reflection experiment the reflectivity, see section 5.1.2, is measured as a function of Q, and either the angle or the wavelength is usually fixed and the other varied. In our experiments it is the angle that is fixed and the wavelength that is varied. For a fixed angle of 1.5° generally used on the spectrometers CRISP and SURF at ISIS and a wavelength range of 0.5-6.5 Å, the corresponding Q range is 0.05-0.66 $Å^{-1}$.

5.1.1.2 Neutron scattering length

In a neutron beam a single nucleus acts like a point scattering centre. The forces between a neutron and an atomic nucleus have a range of the order of 10^{-15} m. This distance is small compared with the wavelength of a thermal neutron and the scattering cross-section $\sigma_s = 4\pi|b|^2$, see below, and the scattering length b, characterising the scattering from a single nucleus, are independent of the angle of scattering. The effective coherent neutron scattering length has the dimensions of length and is effectively a measure of the scattering strength and the neutron-nucleus interaction. As neutrons are scattered by the nuclei, the neutron scattering length is different for different isotopes of the same element, and no linear increase in scattering length with atomic number occurs as for x-ray scattering lengths. The factors determining neutron scattering lengths are the

nuclear radius and the allowed energies of the nucleus. For hydrogen b is small and negative, but for deuterium it is large and positive. A positive b value indicates a phase change of π on scattering whereas a negative b indicates a phase change of 2π; very few isotopes have negative scattering lengths. Values of b for different isotopic species of the elements are tabulated (Koester and Yelon, 1982; Byrne, 1994) and Table 5.1 shows some of the values for the elements forming the constituents of the molecules used in this work.

Table 5.1: Coherent neutron scattering lengths b and abundances for some of the isotopes of importance in this work. The values are taken from Koester and Yelon (1982) and Byrne (1994). The average scattering length for a nucleus in natural abundance can be calculated by summing the values of b for each constituent isotope weighted by the fractional abundance.

nucleus	% abundance	10^{14} b /m
^{1}H	99.985	-0.3741
^{2}H	0.015	0.6674
^{12}C	98.9	0.6653
^{13}C	1.1	0.62
C (nat. ab.)	-	0.6648
^{14}N	99.6	0.937
^{16}O	99.76	0.5805
^{19}F	100	0.565
^{28}Si	92.2	0.4106
^{29}Si	4.7	0.47
^{30}Si	3.1	0.458
Si (nat. ab.)	-	0.4149

For a molecule, the neutron scattering length is calculated from the sum of the products of the number n_i of atoms of type i with scattering length b_i in the molecule normalised by the total number of atoms in the molecule n_{tot}:

$$b = \sum_i n_i b_i / n_{tot} \,. \tag{5.5}$$

The neutron scattering length usually forms part of any equations as the quantity Nb, the neutron scattering length density, which has dimensions of area^{-1}. The number density N is the number of nuclei per unit volume, and is calculated from:

$$N = \rho N_A n_{tot} / M_r \tag{5.6}$$

where ρ is the density in g·Å^{-3}, N_A is the Avogadro constant (6.022×10^{23} mol^{-1}) and M_r is the molar mass in g·mol^{-1}, giving N in Å^{-3}. Table 5.2 shows the scattering length densities for the molecules of interest in this work.

Table 5.2: Calculated scattering length densities Nb for the molecules of interest in this work.

molecule	10^5Nb /Å^{-2}
cyclohexane	-0.0286
hexane	-0.0576
methylcyclohexane	-0.0274
octane	-0.0524
perdeuterocyclohexane	0.668
perfluorohexane	0.354
perfluoromethylcyclohexane	0.387
perfluorooctane	0.376
hexamethyldisiloxane	-0.0376
2-butoxyethanol	-0.004
H_2O	-0.0560
D_2O	0.635

For a mixture, the scattering length density is calculated from the scattering length densities of each constituent molecule summed in proportion to the relative volumes of each species present. For a mixture of two components 1 and 2:

$$(Nb)_{mixture} = \phi_1(Nb)_1 + \phi_2(Nb)_2 \qquad (5.7)$$

where ϕ_i is the volume fraction of component i and is generally evaluated using the densities at 25°C and neglecting the excess volumes.

5.1.1.3 Coherent and incoherent scattering

Scattering measurements are generally made from assemblies of atoms. The waves scattered from atoms in different spatial positions interfere and may have different phase relationships. Coherent scattering occurs when there are defined phase relationships between waves scattered by neighbouring atoms, giving rise to an interference pattern. Incoherent scattering arises from random scattering events, which occur because not all the nuclei of an element are identical due to different isotopes or different nuclear spin states, and is isotropic. The incoherent scattering causes a background level in the reflectivity. Hydrogen has a larger incoherent scattering length than deuterium and this leads to a higher background reflectivity from H_2O than from D_2O. Values for incoherent scattering lengths can be found in various sources (for example, Byrne, 1994). The main neutron optical phenomena are due to coherent scattering which is elastic. In addition to coherent and incoherent scattering, absorption of a neutron by a nucleus may occur. This radiative capture means that no neutron leaves the sample.

5.1.1.4 Scattering cross-section

The total scattering cross section σ_s for thermal neutrons is defined as the average number of neutrons scattered by a given nucleus in unit time per unit incident flux, i.e. the number per unit area and time. The scattering cross section is related to the effective scattering length b by:

$$\sigma_s = 4\pi |b|^2. \tag{5.8}$$

The total scattering cross section is equal to the sum of the bound coherent and incoherent scattering cross sections:

$$\sigma_s = \sigma_c + \sigma_i \tag{5.9}$$

where $\sigma_c = 4\pi |b_c|^2$ and $\sigma_i = 4\pi |b_i|^2$, where b_c and b_i are the bound coherent and incoherent scattering lengths, respectively. Coherent and incoherent cross sections are also given by Byrne (1994).

5.1.1.5 Neutron refractive index

The index of refraction for neutrons at the boundary of a medium is defined as:

$$n = k_1 / k_0 \tag{5.10}$$

where k_1 and k_0 are the magnitudes of the wavevectors inside and outside the medium, respectively. The full expression for the neutron refractive index includes a complex term that can be ignored if the medium is not strongly absorbing, as in all the cases described here, thus the neutron refractive index for thermal and cold neutrons is:

$$n \approx 1 - \frac{\lambda^2 Nb}{2\pi} \tag{5.11}$$

where Nb is the scattering length density defined above and λ is the neutron wavelength.

5.1.1.6 Critical reflection of neutrons

As neutrons can be treated in a similar way to electromagnetic radiation, a parallel to Snell's Law of refraction can be formulated. For electromagnetic radiation, Snell's Law is usually written:

$$n_0 \sin\alpha_0 = n_1 \sin\alpha_1 \tag{5.12}$$

where α_i is the angle made in the medium of refractive index n_i. The angles are defined relative to the normal at the point of refraction at the interface. For neutrons the angles

are conventionally defined relative to the interface or boundary, so the equation becomes:

$$n_0 \cos\theta_0 = n_1 \cos\theta_1 \qquad (5.13)$$

where $\theta° = (90 - \alpha°)$ is the *glancing* angle. The reflection and refraction of neutrons at a planar interface is illustrated in Figure 5.2.

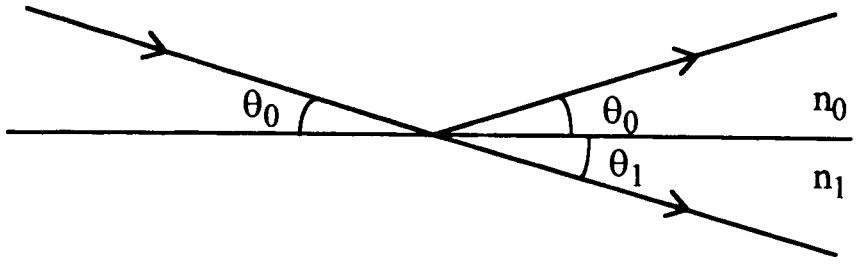

Figure 5.2: Reflection of neutrons from a planar interface.

At the critical angle of incidence the angle of refraction is zero and the refracted beam propagates along the interface. Thus for incidence from medium 0 to medium 1 (with $n_0 > n_1$), $\cos\theta_1 = 1$. From equation (5.13), the critical angle θ_c is thus:

$$\cos\theta_c = n_1 / n_0. \qquad (5.14)$$

In contrast to refractive indices for light, neutron refractive indices are generally less than unity for condensed matter as most values of b are positive. In reality, neutron refractive indices are often very close to unity since Nb values are generally of the order 10^{-6} Å^{-2}, see equation (5.11). In the experiments described here, the neutron beam is incident on the sample from air, for which Nb is effectively zero and thus $n_0 = 1$, and so $\cos\theta_c = n_1 \approx 1$, so θ_c is very small. For example, for D_2O, Nb = 0.635×10^{-5} Å^{-2} so for a neutron wavelength of 1 Å, from equations (5.11) and (5.14), $\theta_c = 0.081°$ for the D_2O-air interface. If the beam is incident from the medium of greater neutron refractive index at an angle less than the critical glancing angle, total reflection occurs. For small angles the approximation for $\cos\theta \approx 1 - (\theta^2/2)$ can be used and thus for incidence from air:

$$\theta_c \approx \lambda\left(\frac{Nb}{\pi}\right)^{1/2} \qquad (5.15)$$

where θ_c is in radians. For a medium with a scattering length density Nb the critical angle depends only on the wavelength λ of the neutrons incident on the medium.

5.1.2 Neutron reflectivity

The reflectivity R is the quantity measured in a typical neutron reflectivity experiment. R is defined most simply as the intensity of the exit beam I_{out} relative to the intensity of the incoming beam I_{in}:

$$R = I_{out} / I_{in} \tag{5.16}$$

which gives the fraction of the incident neutrons that are reflected at the interface. In an experiment the reflectivity measured is usually plotted versus the momentum transfer vector Q, as shown schematically in Figure 5.3. Beyond the critical reflection edge the reflectivity falls off rapidly. In our experiments R is typically 10^{-3} to 10^{-5} so we only consider a narrow range of the profile beyond the critical edge.

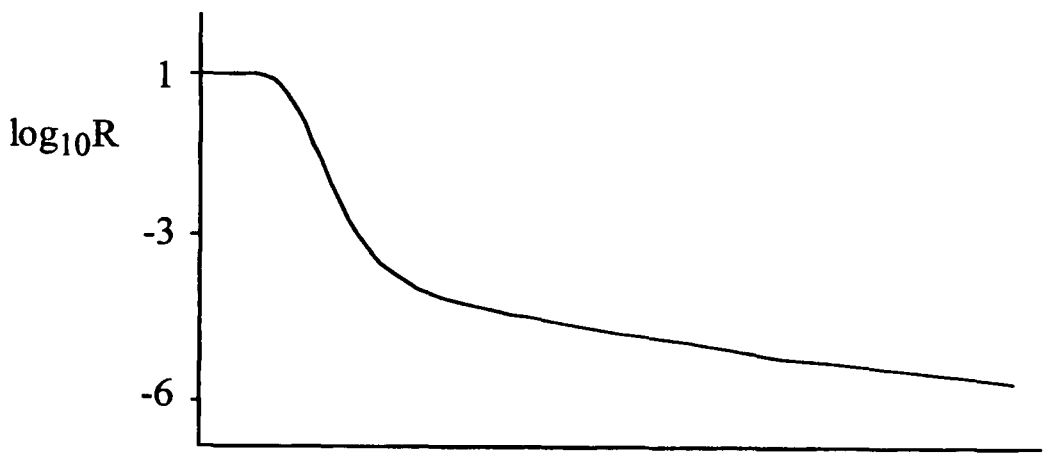

Figure 5.3: Schematic neutron reflectivity profile for a single plane surface.

In our experiments the angle of incidence is usually fixed at 1.5° which is close enough to the critical angle to see both reasonable reflectivity and some background level. The angle can be taken to smaller values by the use of a supermirror, but very shallow glancing angles are difficult to work with, especially if the liquids are organic and do not sit very proud of the sample trough.

In the following sections, the reflection of neutrons from different surface structures is described.

5.1.2.1 Reflection from a plane surface

The reflection coefficient r is defined as the ratio of the amplitude of the reflected wave A_r to the amplitude of the incident wave A_i:

$$r = A_r / A_i. \tag{5.17}$$

As the intensity of a wave is equal to the amplitude squared, r^2 is the reflectivity R. At angles less than the critical glancing angle all the neutrons are reflected and the reflectivity is equal to 1. At angles greater than the critical angle, the reflectivity falls off according to Fresnel's Law with:

$$R = r^2 = \left| \frac{n_0 \sin\theta_0 - n_1 \sin\theta_1}{n_0 \sin\theta_0 + n_1 \sin\theta_1} \right|^2 \qquad (5.18)$$

for the angle of incidence in medium 0 and the angle of refraction in medium 1.

For a rough interface the reflectivity falls off more quickly with increasing Q than for a smooth surface, for which Fresnel's Law is obeyed. The Fresnel equation assumes a sharp boundary between the two media, but in reality there may be a more gradual change in refractive index. This can be accounted for by the inclusion of a surface roughness factor that is the width of the half Gaussian-shaped profile needed to provide a better approximation of the interfacial profile. The roughness is on a microscopic scale. If the interface is too rough reflectivity information is lost. The effect of surface roughness on the reflectivity profile is illustrated in Figure 5.4 for a bare perfluoro-methylcyclohexane subphase.

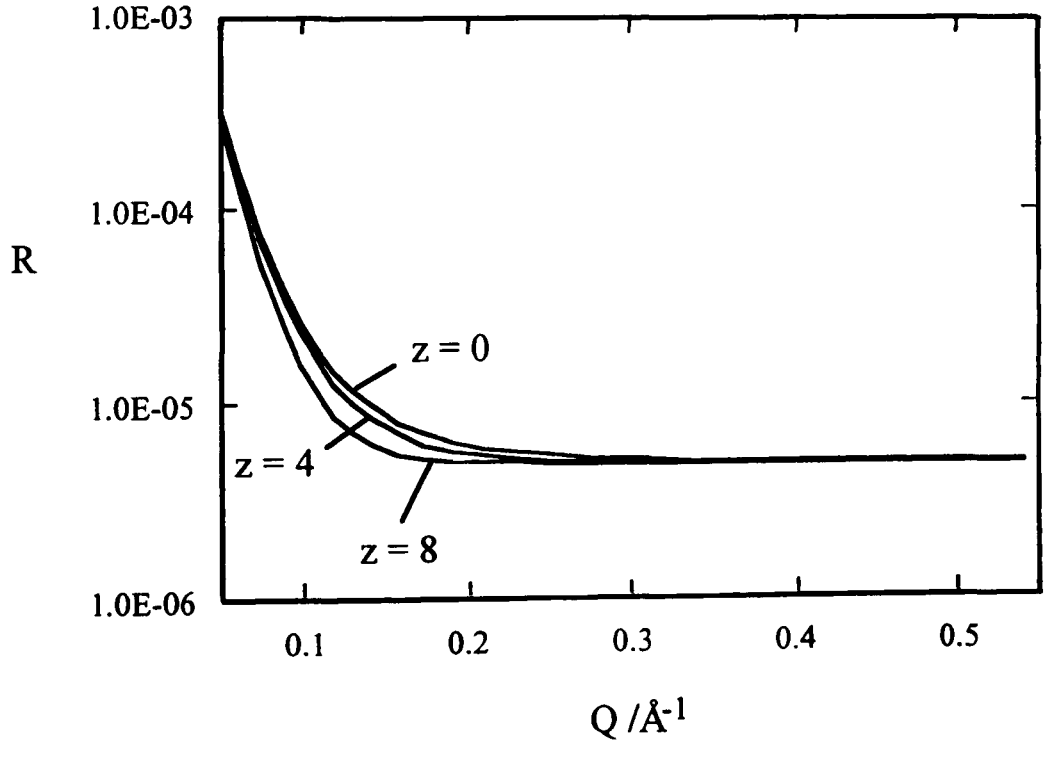

Figure 5.4: The effect of surface roughness on the simulated reflectivity profile for a bare subphase of perfluoromethylcyclohexane. The roughnesses are 0, 4 and 8 Å and increasing the roughness lowers the reflectivity in the mid-Q range.

5.1.2.2 Reflection from a monolayer at the interface

As neutrons enter the sample from air at an angle greater than the critical glancing angle they are refracted at the interface as well as reflected. The refracted beam passes into the sample and is further refracted and reflected at a second boundary between media of different neutron refractive indices. The reflected beams from each boundary have a path difference, which depends on the thickness of the layer d, the refractive indices of the media, and the angle of incidence in the air, and may thus constructively or destructively interfere. The interference pattern can be calculated using the Fresnel equations which apply to each boundary. This kind of calculation can be carried out fairly easily for one or two layers, but it becomes much more complex when many layers are considered.

The reflection of neutrons from a monolayer is illustrated in Figure 5.5. The angles of incidence and refraction and their differences are exaggerated to emphasise the path difference.

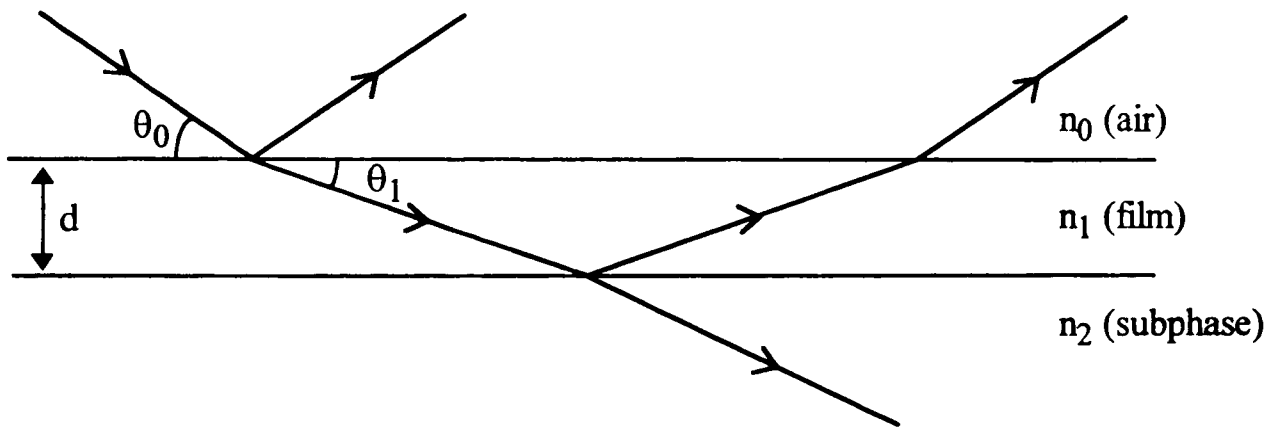

Figure 5.5: Reflection of neutrons from a monolayer at the interface.

5.1.2.3 Reflection from multilayers

For reflection from multilayers the equations are usually solved by matrix methods. The most common method used at ISIS is the optical matrix method of Abèles (Heavens, 1955; Penfold, 1988). Matrices formed from the Fresnel coefficients including the effects of path differences are used to describe each layer. The roughnesses at each layer boundary can also be taken into account.

Features or fringes in the R-Q profiles can be observed for multilayer systems or, for example, for thick polymer films. Well-defined fringes in multilayer systems allow the determination of the thickness and scattering length density of each layer.

5.1.2.4 Modelling neutron reflectivity data

There are two basic approaches to modelling neutron reflectivity data. The first is the dynamic optical approach used in this work. In this method the structure is broken down into a series of layers each with a characteristic scattering length density and thickness and the reflectivity is calculated for each layer by a matrix calculation, as mentioned above and discussed in detail by Lekner (1991). The matrix calculation is tedious but is exact for a given model. The experimental reflectivity data are compared with the results of the matrix calculations; the model is then modified and the calculations repeated until good agreement is reached between the calculated and observed reflectivity profiles.

The second type of approach is based on approximations. A number of approximate methods exist for calculating reflectivity profiles (Lekner, 1987), of which the kinematic method has so far proved the most useful. In the kinematic approximation the reflectivity R is related to the Fourier transform of the scattering length density profile through the interface:

$$R(Q) = \frac{16\pi^2}{Q^4}\left|\int_{-\infty}^{+\infty} \exp(iQz)\left(\frac{d\,Nb(z)}{dz}\right)dz\right|^2 \qquad (5.19)$$

where z is the distance from the interface at which z = 0. This method has been used by Thomas and coworkers to obtain information about the structure of the surface of surfactant solutions (Lu *et al.*, 1992, 1993).

The various methods for the analysis of neutron reflectivity data have been discussed by several authors (for example, Lekner, 1987; Penfold and Thomas, 1990) and a fairly recent issue of *Physica B* (1991, 173) has been devoted to this subject.

5.1.3 Applications of neutron reflection

In this section some of the applications of neutron reflection are described. The discussion is mainly confined to the application of specular neutron reflection to the study of surfaces and interfaces, and in particular to the liquid-vapour interface since this is the interface studied in the present work.

In order for a layer structure at an interface to be studied by neutron reflectivity measurements, the neutron refractive index, and hence the scattering length density, must be significantly different for each layer. If the scattering length densities of two consecutive layers are the same, no reflectivity is detected due to the presence of the interface. The scattering length density of a mixture is determined from the volume fractions and the scattering length densities of the individual components, see equation (5.7) above. In many cases the scattering length densities of the components of a mixture may not be significantly different, but in these cases isotopic substitution may be used.

Isotopic substitution is one main advantage of the use of neutrons rather than x-rays in structural studies. The differences in the scattering lengths of various isotopes of an element may be large. For example, the scattering lengths of hydrogen and deuterium are of opposite sign and the substitution of hydrogen by deuterium provides a particularly useful contrast. In this case, due to the differences in sign, many hydrogenated and deuterated species can be mixed in the required proportions to form a mixture with a scattering length density of zero; for example Nb = 0 for a $D_2O + H_2O$ mixture of mole ratio D_2O/H_2O of 0.088. Since the resulting scattering length density is zero, the neutron refractive index is unity, as for air, and the $D_2O + H_2O$ mixture is said to be null or *contrast matched* and the only reflectivity observed is the background level.

The scattering length density can also be adjusted to a range of values between those for the pure hydrogenated and deuterated compounds by altering the relative proportions. This technique is useful–if the thermodynamics is unaltered by deuteration–to check the model profile used to fit the reflectivity data for a surface structure on a subphase. The model is assumed to be unchanged by alteration of the scattering length density of the mixture and the experiment is repeated using a subphase of a different scattering length density to reveal any layers which were previously hidden. Contrast variation has been used extensively in the study of the surface structure of aqueous surfactant mixtures (Crowley *et al.*, 1991).

The technique of contrast matching can also be applied to alkane solvents as used in our work, for example a contrast-matched mixture of perdeuterocyclohexane + cyclohexane has a mole ratio of d_{12}-cyclohexane/h_{12}-cyclohexane of 0.041, but may not be as useful in our near-critical studies due to the possible change in surface structure on deuteration. For binary mixtures of cyclohexane or perdeuterocyclohexane with perfluorohexane, the upper critical solution temperature T_{UCS} is lowered by approximately 8.5 K by deuteration, as discussed in more detail in Chapter 6. Since T_{UCS} is altered greatly by deuteration of the alkane component it may not be reasonable to assume that any surface structure is unchanged. A further effect of deuteration is to alter the bulk liquid density and this may in turn possibly affect the wetting behaviour. This effect was exploited by Schmidt (1986).

Specular neutron reflection has been applied at many different types of interface. A discussion of some of the results and the background theory is given in a review article by Penfold and Thomas (1990). In particular, neutrons have been used at the liquid-air interface to look at monolayers and multilayers of polymers and surfactants. Isotopic substitution in different parts of a long-chain surfactant molecule has been used to selectively highlight the structure, for example to determine the orientation of surfactant monolayers (Lu *et al.*, 1993c) and the separation and overlap of the surfactant molecules in an adsorbed layer (Lu *et al.*, 1993b). The penetration of water into the surfactant layer (Lu *et al.*, 1992) and the effects of the counterions in ionic surfactants on the structure

(Lu *et al.*, 1993a) can also be investigated. The existence of structured surfactant-rich, surfactant-depleted and micellar layers at the air-water interface of an ionic surfactant mixture have been identified using neutron reflection (Lu *et al.*, 1993d). At the air-water interface, neutron reflection has also been used to identify the degree of hydration of nonionic surfactant and phospholipid monolayers (Barlow *et al.*, 1995; Naumann *et al.*, 1995).

At the solid-air interface magnetic materials have been studied using neutrons (Penfold and Thomas, 1990). Neutron reflection has also proved a useful technique for the study of Langmuir-Blodgett films, and polymer films (Arrighi *et al.*, 1993/94). In addition, the solid-solid and solid-liquid interfaces have been studied as the neutrons can enter through one of the solids. The liquid-liquid interface, however, is more difficult to study using neutrons since intensity is lost as the beam passes through a liquid sample, but can be investigated using x-rays (Roser *et al.*, 1994). Some of the applications of specular neutron reflection using the CRISP spectrometer at ISIS at the Rutherford Appleton Laboratory have been discussed by Penfold (1991).

The above discussion has been concerned with surfaces, and in particular with the studies of the surface activity of surfactant molecules in aqueous solutions. In the presence of an oil, and in some cases a cosurfactant, an aqueous surfactant solution can form a microemulsion, see Chapter 1, section 1.4.1. Microemulsions form the subject of extensive investigations using small-angle neutron scattering (SANS) (for example, Teubner and Strey, 1987; Gradzielski *et al.*, 1995). In SANS experiments the microemulsion dimensions can be probed and the contrast changed by deuteration of one or more of the components.

5.2 Experimental details

5.2.1 ISIS

ISIS is the pulsed spallation source at the Central Laboratory of the Research Council's Rutherford Appleton Laboratory near Oxford. The first neutrons at ISIS were produced in late 1984 and the facility was officially opened in October 1985.

Several stages are involved in the production of the neutrons. Basically, an ion source produces H^- ions which are accelerated in a pre-injector column and a linear accelerator. The electrons are then stripped from the H^- ions at injection into the proton synchrotron, where the protons are further accelerated before extraction to the target station. At ISIS the target is usually tantalum. Uranium has also been used and produces a higher neutron flux, but problems have been experienced due to radiation damage of the crystal structure. The high energy protons produce neutrons by chipping nuclear fragments from the nuclei of the target. Moderators of ambient water, liquid methane or liquid hydrogen slow down the neutrons before they are channelled to the individual

instruments positioned around the target. The instruments used in this work, CRISP and SURF, are described in the next section.

The source at ISIS is a pulsed source and each pulse contains neutrons with a wide range of velocities, and hence wavelengths. The resulting beam is thus termed a 'white beam'. The ISIS beam hall and the arrangement of the instruments around the target are shown in Plate 5.

5.2.2 CRISP and SURF

CRISP and SURF are the reflectometers used in this work. A full description of CRISP is given by Penfold *et al.* (1987). SURF is a new instrument built for looking at liquid surfaces. The beam can be focused so that smaller sample areas can be used to reduce evaporation of the liquids without too great a loss in flux.

On both CRISP and SURF the incident angle is usually fixed at 1.5°, although smaller angles can be achieved by insertion of a supermirror in the path of the beam. A schematic diagram of the arrangement on CRISP is shown in Figure 5.6; a similar arrangement is used on SURF. The chopper selects the neutrons of wavelengths of 0.5-6.5 Å, corresponding to a Q range of 0.05-0.66 $Å^{-1}$, after they have been moderated to thermal velocities by a hydrogen moderator at 20 K. Cadmium slits, S_1 and S_2, define the height and width of the incident neutron beam, which is typically 40 mm wide and 2 mm high. The frame overlap mirrors, which are silicon wafers coated with nickel, reflect out any slow neutrons to prevent slow neutrons from the previous pulse arriving at the sample along with the current pulse. Frame-overlap contamination is also partially reduced by the chopper. The slits S_3 and S_4 collimate the reflected beam which is detected by a ^3He gas detector.

For an angle of incidence of 1.5° the footprint size of the beam at the sample is generally 40 mm x 76 mm. The height of the sample is observed using a HeNe laser beam with the same alignment as the neutron beam. The laser is used at the start of a set of experiments to position the sample trough and cell centrally in the beam at the correct height. Between each experiment the liquid level in the trough is checked by ensuring that the laser beam still passes through the slits S_3 and S_4, that the footprint is still central on the liquid surface, and that there is no flaring of the laser beam on the edge of the trough. The flaring on the edge of the trough is a clear indication of a drop in liquid level of our samples. The height of the trough needs to be carefully checked as our organic liquids have low surface tensions and, unlike the D_2O used in the calibrations, do not sit proud of the trough lip.

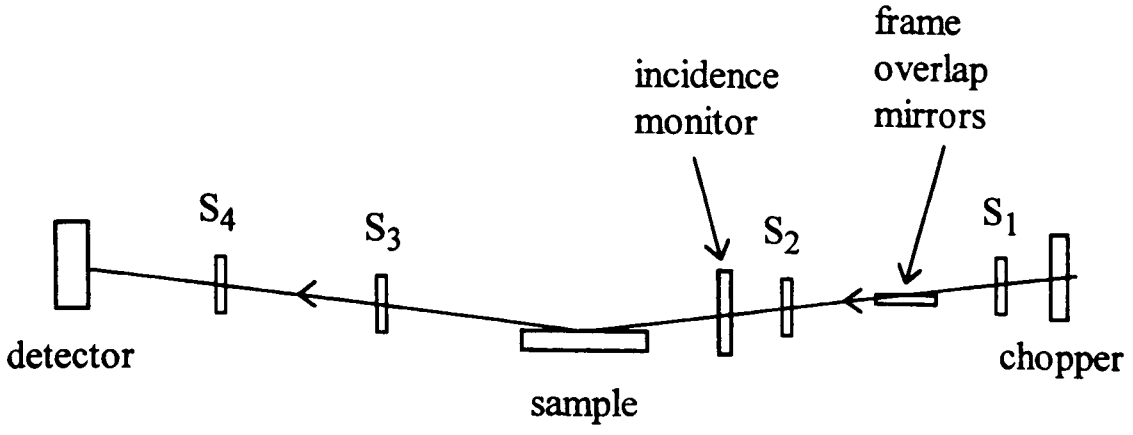

Figure 5.6: Schematic diagram of the CRISP reflectometer.

5.2.3 Data collection and analysis

5.2.3.1 Data collection

The run lengths were generally between one and two hours and 200 μA of incidence flux were typically collected. In some cases the run lengths were extended to gain better statistics, and occasionally shorter runs were used to ensure that equilibrium had been reached and that a stable liquid level had been established in the trough. When several shorter runs, of for example 50 μA, were collected they were added together if the reflectivities were the same with respect to the statistics.

On CRISP and SURF the reflectivity data are analysed by a time-of-flight (TOF) technique. This technique can be used for pulsed sources such as ISIS. The neutrons from each pulse are collected in histogram format according to their time of arrival at the detector. The times are then used to calculate the neutron velocity and hence the wavelength. A monitor in the incident beam measures the wavelength spectrum of the incident neutrons. The reflectivity is determined from the ratio at each wavelength of the number of neutrons reflected to the number of incident neutrons. The calculation of the neutron wavelengths is performed by the QUICK routine within the GENIE program. In the TOF method the reflectivity is measured simultaneously for a wide range of Q. This is in contrast to the method usually used at reactor sources where the wavelength is fixed and a range of angles is scanned.

5.2.3.2 Modelling the reflectivity

The reflectivities are modelled on the ISISE computer using MULF, a non-linear least-squares fitting routine which uses the optical matrix method. The model is a slab layer model with allowance for roughness factors. The model input includes the number of layers, the scattering length densities of the layers, the thicknesses of the layers, the

scattering length density of the substrate and the roughness factors at each interface. Some of these parameters are fixed and some are allowed to vary, until a good fit–indicated by a minimum in the value of χ^2 and the similarity of the calculated and measured reflectivity profiles–is achieved. The other values input into the fitting program are the angle of incidence, the angular resolution and the background reflectivity.

The main problems with the fitting method are (i) that a model has to be preselected and (ii) that a solution which yields a good fit may not be unique. The fitting procedure in some cases was improved by using the programs nrfit and nrmodfit, see appendix. The program nrmodfit fits the reflectivity to a damped oscillating profile for the scattering length density variation through the interface. This type of profile–with layers of alternating scattering length density corresponding to layers rich in each of the two components and both types of layer becoming more similar to the bulk scattering length density at further distances from the liquid-vapour interface–was useful in describing the reflectivity for some systems. The program nrfit uses a similar layer method to that used in MULF, but permits the increment of the explored variations in each parameter to be specified. When fitting damped oscillatory profiles with many layers, such as for D_2O + 2-butoxyethanol, nrmodfit was used, followed by nrfit to allow the parameters to relax slightly from those specified by the damped model and an optimum fit to be achieved.

A model-independent method of Reverse Monte Carlo type was developed by Bowers and Burgess (Bowers, 1996b) and used to generate models to fit the reflectivity data and to check independently any models previously used to describe the reflectivity spectra. The optical matrix method was still used but this fitting did not involve the presumption of any adsorption. The interfacial region was divided into 2 Å layers of initial scattering length density equal to that of the bulk mixture. Random numbers were used to select a layer and to decide whether to increase or decrease its scattering length density and a smoothness factor was used to impose a realistic roughness. In this way an Nb profile describing the reflectivity was built up.

In some cases the reflectivity data could not be fitted using simple layer models and the possibility of the formation of 'islands', i.e. regions of different scattering length densities on the surface, was considered. Richardson and Roser (1991) have discussed the theory of reflection from a patchy surface and the model has been used, for example, by Eaglesham and Herrington (1995). Fitting of some of our data by an islands model was attempted by Bowers (1996b) but with at best indifferent success. The specific cases are described in the results section.

The program 'profile', see appendix, was used to calculate the scattering length density profiles normal to the interface as a function of distance z through the interface for a given model. The effects of the roughness factors are incorporated in the resulting profile. In this model $z = 0$ at the subphase-film boundary.

5.2.4 Sample environment

5.2.4.1 Trough and cell

Our liquid samples were contained in a PTFE trough of dimensions of the liquid environment of 123 mm x 51 mm with a depth of 4 mm surrounded by a moat, as shown in Figure 5.7 and Plate 6. The trough was constructed from two sections of PTFE measuring 174 mm x 123 mm, one virgin PTFE and the other glass-filled PTFE, glued together sandwiching an aluminium base plate. An aluminium frame or surround was screwed on afterwards and a seal was provided between the aluminium and the glass-filled PTFE by a gasket. The first gasket material was silicone rubber, but this absorbed hydrocarbons and expanded producing a leak. A second gasket of cardboard also offered a poor seal and so was later replaced by Viton. A small platinum resistance thermometer PRT (Sensing Devices Ltd.) can be sited below the trough close to the liquid to give an independent temperature readout.

The trough was made of the required dimensions to screw into a sealed casing cell of aluminium which was kindly loaned to us by Dr R. Richardson and Dr. A. Zarbakhsh from the University of Bristol. The aluminium surround attached to the trough is seated on a large Viton O-ring set in a recess on the cell to provide a seal below the trough. A seal is provided above the trough by the lid of the cell which screws onto another large Viton O-ring set in a recess in the rim of the cell. The attachments to the trough for heating and stirring are all underneath and the tubing for the services leave the casing through a slot in the underside of the casing cell. The slot was originally very small and it was difficult to get all the tubing and wiring out through the bottom, but the slot was later widened to open up the full base of the cell.

All four sides of the cell and the lid are fitted with double-glazed mica windows, essentially transparent to neutrons, to allow the beam to enter and exit and to allow the liquid in the trough and the laser beam footprint to be viewed.

PTFE is the material generally used for troughs since most work is carried out on aqueous systems and with PTFE the liquid-vapour interface sits proud of the trough. A further reason for the use of PTFE is that it is easily cleaned. In our nonaqueous mixtures, however, proud interfaces are not observed, and in near-critical studies good temperature control is essential and this is not easily achieved using PTFE at higher temperatures than room temperature. A further problem noted during our studies on perfluoroalkylalkanes PFAAs in alkanes, was the competing adsorption of the PFAAs at the PTFE-liquid and the liquid-vapour interfaces. Another trough material was therefore sought.

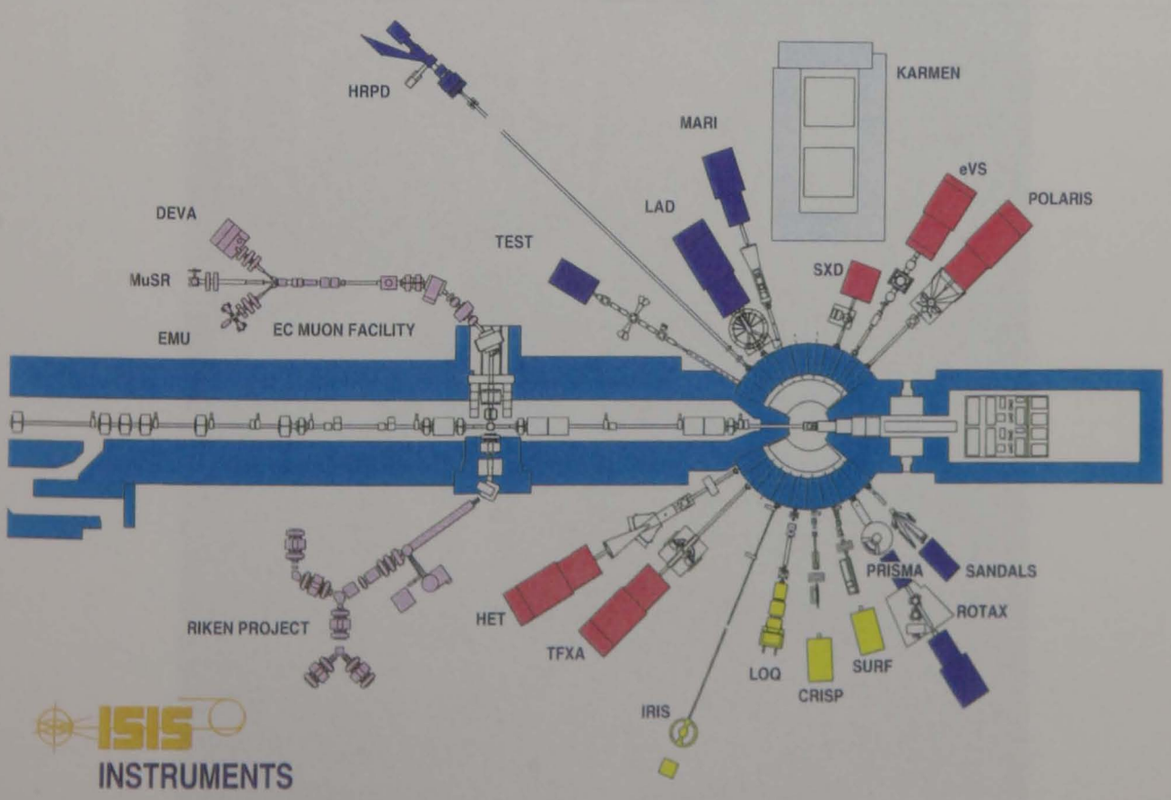

Plate 5: The ISIS beam hall and the arrangement of the instruments around the target.

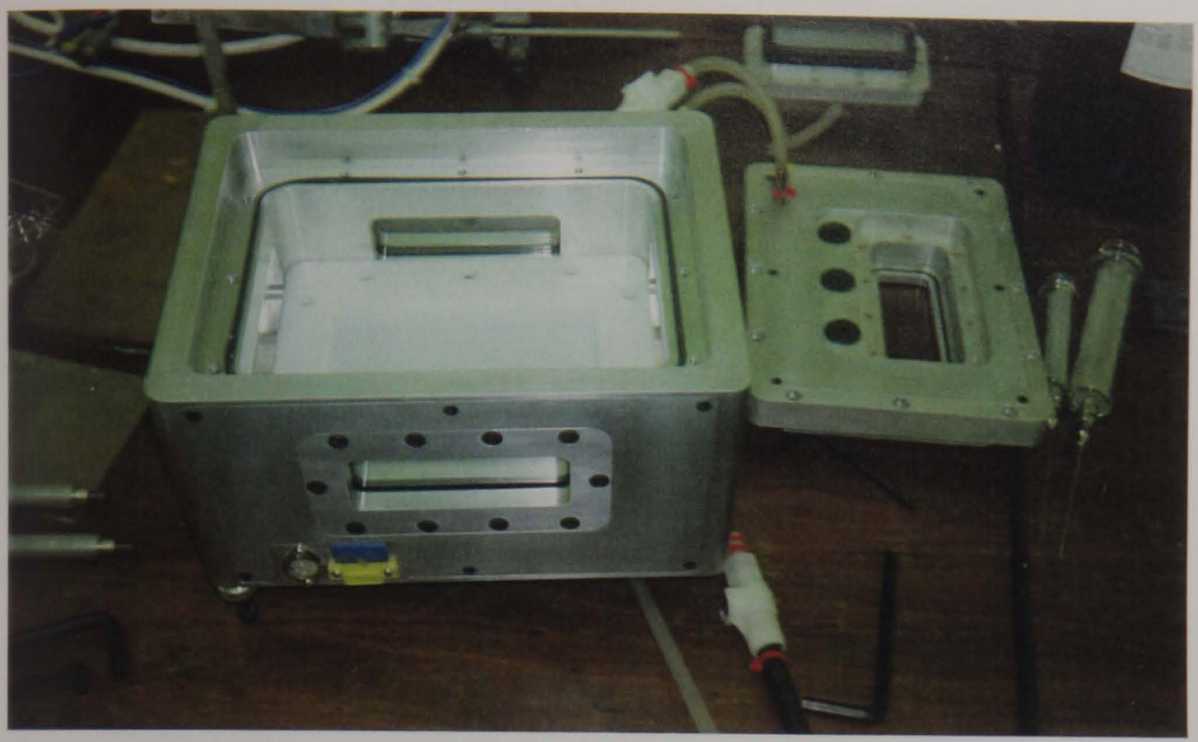

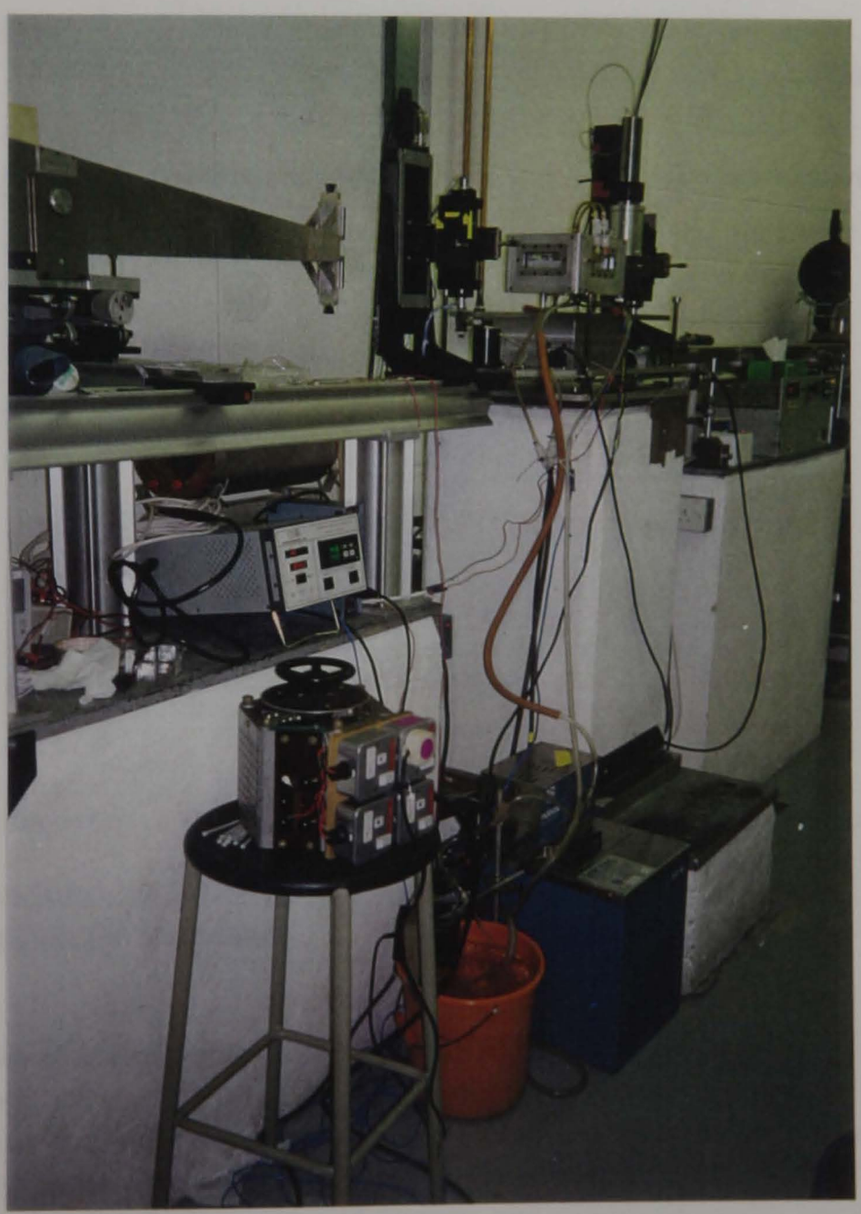

Plate 6: The PTFE trough in the outer cell and the experimental arrangement on CRISP.

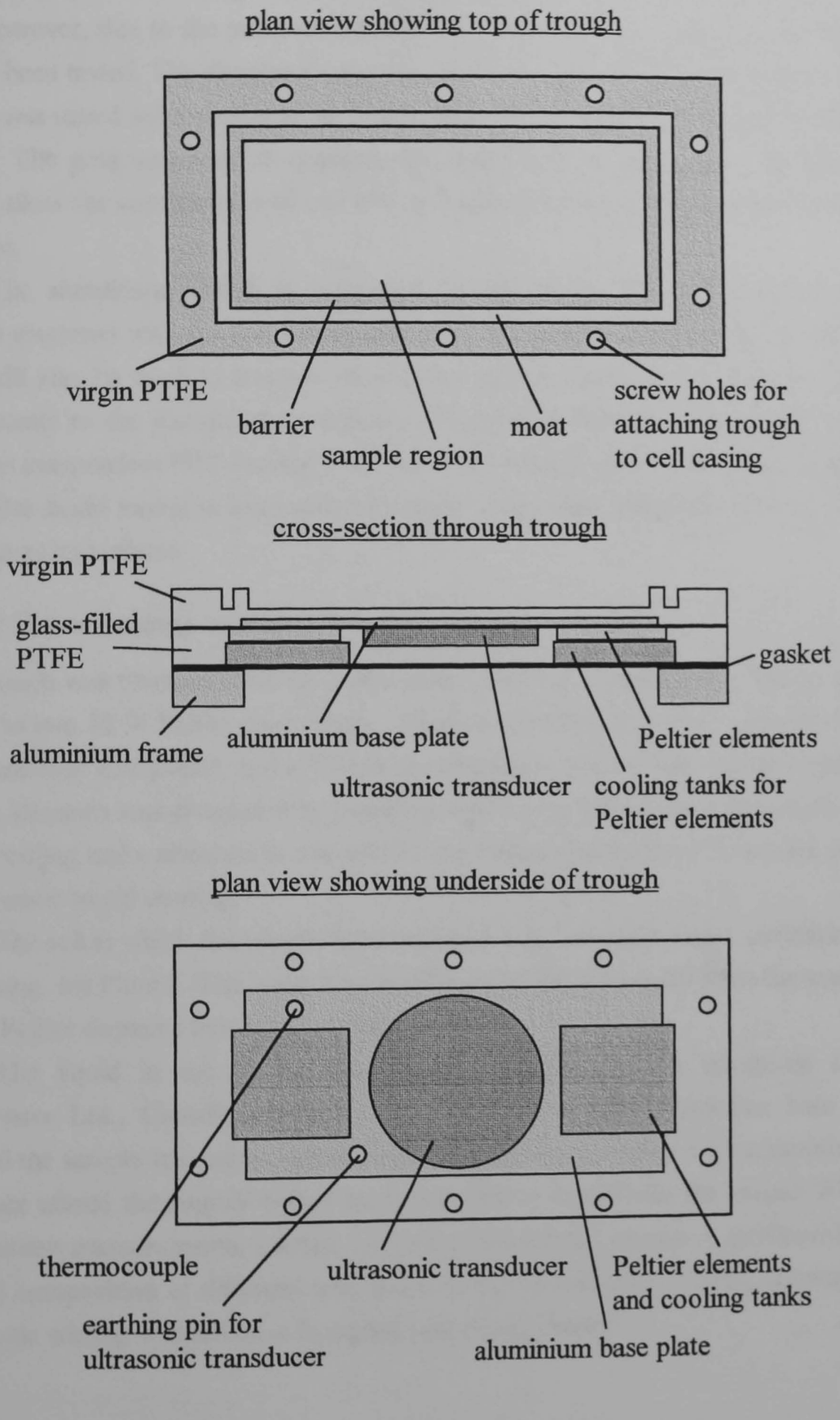

Figure 5.7: Diagrams of our PTFE trough. The various connections are not shown but include: Peltier and thermocouple connections to Marlow controller, ultrasonic transducer connections to power supply, thermometer connections to Newport box, tubing for Peltier cooling water circulated via pump and bucket, and tubing for water circulated round cell body.

Recently a new trough has been fabricated from 95% aluminium sputtered with gold; however, due to the postponement of two allocations of beamtime, the trough has not yet been tested. The aluminium was required to be reasonably pure and the lip of the trough was raised with respect to the surround to reduce additional scattering due to the trough. The gold was used to improve the cleanliness of the trough. The new trough should allow the continuation of our PFAA studies and better temperature control in all mixtures.

The aluminium trough is composed of the layers: aluminium with the trough surface sputtered with gold, a Viton gasket, and an aluminium surround; a polyurethane filler will also be used to insulate around the thermocouple sensor and the PRT. The attachments to the aluminium trough are the same as those for the PTFE trough, but with the independent PRT located in the lip of the trough close to the liquid sample.

Our liquid mixtures were generally made up by mass and transferred to the trough while in a single phase.

5.2.4.2 Thermostatting and stirring

The trough was thermostatted by a controller (Marlow Industries Inc. Model SE 5010) linked to two 18 W Peltier heat pumps, which were attached to the aluminium base plate with heat-sink compound, and a T-type thermocouple sensor. The cooling water for the Peltier elements was circulated by pumping water externally from a bucket through the small cooling tanks attached to one side of the Peltier elements. At times, ice was added to the water to aid cooling.

The cell in which the trough was contained was heated by water circulating around the casing, see Plate 6. The water was heated or cooled separately from the water supply to the Peltier elements below the trough.

The liquid in the trough was stirred by means of an ultrasonic transducer (Ultrawave Ltd., Cardiff) attached to the underside of the aluminium base plate. In general the sample was taken slowly to the required temperature with occasional stirring and then stirred thoroughly before being allowed to equilibrate for around 20 minutes. Preliminary measurements, carried out on a mixture of hexane + perfluorohexane of critical composition at different temperatures before and after stirring, showed that the ultrasonic stirring was effective in mixing coexisting phases.

5.2.4.3 Improvements to experimental arrangement

One of the main difficulties experienced during the earlier experiments was reducing the vibrations of the trough due to the water circulation pipes to the Peltiers and through the cell casing having to rest on the optical table on which the trough was positioned. The vibrations were reduced as much as possible by supporting the tubing and taping it to the table.

Temperature control was another cause for concern. In the earlier experiments the position of the pipes for cooling water for the Peltiers was such that the plastic tubing was constricted in being forced through the hole in the base of the casing, which was only just large enough for all the service tubes and wires, causing the temperature to rise as no cooling water was being supplied to the Peltiers. The water circulation was improved by repositioning the water pipes.

The temperature was read from the Marlow controller for the Peltier elements, but a small PRT could be sited below the trough close to the liquid. However, this probe was still in the PTFE and seemed to be affected by the Peltiers; thus an accurate measure of the temperature of the liquid in the trough during an experimental run could not easily be obtained. In the new aluminium trough the PRT was located in the lip of the trough so that it was closer to the liquid sample.

At high temperatures, liquid was found to condense on the windows and lid of the casing during the first set of experiments. This effect was eliminated by setting the temperature of the cell casing at about 5°C higher than that of the trough.

Possibly the greatest experimental problem was in ensuring that the trough was totally sealed in the casing. The fall in liquid level if a seal was not complete was significant with our volatile organic liquids and could be detected by a drop in the background level of the plotted reflectivity data with time. A sealed sample environment was achieved by using good O-rings and screwing the trough and the casing lid firmly in place.

5.2.4.4 Trough cleaning and drying

Deionised water was used to clean the trough before the D_2O calibration. The trough was initially dried by removing as much of the liquid as possible with a dropping pipette and then wiping out with tissues. However, rubbing with tissues was found to cause static problems leading to non-self-levelling liquids. In the organic mixtures used any charge built up could not be easily dissipated, although it disappeared with time. The trough was thus better dried by dabbing with a tissue and then using a hairdryer. The use of a metal trough should reduce this problem.

5.2.4.5 Calibration

Once the trough had been placed in position and aligned at the start of a set of experiments, a calibration was run with D_2O in the trough. The reflectivity from pure D_2O was modelled using MULF, usually with the background level varied, the substrate scattering length density fixed at the value for D_2O of 0.635 x 10^{-5} $Å^{-2}$, and the roughness factor varied systematically for each fit between 2.5 Å and 4 Å, in steps of 0.5 Å, until the best fit was obtained. The scale factor obtained for the best fit was noted. The reflectivities measured from different samples throughout a set of experiments were then put on an absolute scale by dividing by the scale factor.

5.2.5 Choice of mixtures

Several of the mixtures studied were alkane + perfluoroalkane mixtures. In alkane + perfluoroalkane mixtures deuteration to highlight one of the species is not necessary as the scattering length of fluorine is large and positive in contrast to the negative scattering length of hydrogen. The scattering length densities for most perfluoroalkanes are thus large and positive, whereas those for alkanes are, in general, small and negative, see Table 5.2 above. This provides a natural contrast and, in principle, a wetting layer of a perfluoroalkane on an alkane subphase can be readily detected by neutron reflectivity measurements.

The binary mixtures selected for the study of wetting and adsorption near a critical endpoint and reasons for their selection are given below:

1. Hexane + perfluorohexane: an archetypal alkane + perfluoroalkane mixture.
2. Methylcyclohexane (MCH) + perfluoromethylcyclohexane (PFMCH): previously studied by ellipsometry (Kwon *et al.*, 1982; Schmidt, 1990).
3. Hexamethyldisiloxane + perfluorohexane: similar to hexane + perfluorohexane, see Chapter 1, section 1.5.
4. Deuterium oxide + 2-butoxyethanol: a primitive nonionic surfactant solution. H_2O + 2-butoxyethanol previously studied by ellipsometry (Bennes *et al.*, 1985; Hirtz *et al.*, 1993).

Mixtures 1-3 exhibit upper critical endpoints (UCEPs) with an upper critical solution temperature T_{UCS} and mixture 4 exhibits a lower critical endpoint (LCEP) with a lower critical solution temperature T_{LCS}. These mixtures have been used in other studies within the group and their phase behaviour and properties have been well characterised. The critical compositions and temperatures are given in Table 5.3 along with the references for the phase diagrams. The surface activity of the perfluoroalkylalkane F_8H_8 has also been studied on cyclohexane and perdeuterated cyclohexane. All these mixtures have been discussed in Chapter 1, section 1.5.

Table 5.3: The critical compositions in terms of mole fraction x, volume fraction ϕ, and mass fraction w and the critical solution temperatures T_{CS} for the mixtures studied in this work. The compositions given are of the fluorocarbon or of 2-butoxyethanol.

mixture	x_c	ϕ_c	w_c	T_{CS} /°C	ref.
hexane + perfluorohexane	0.367	0.471	0.695	22.61^U	a
MCH + PFMCH	0.361	0.463	0.668	46.13^U	b
hexamethyldisiloxane + perfluorohexane	0.510	0.497	0.684	23.50^U	a
deuterium oxide + 2-butoxyethanol	0.0602	0.318	0.273	42.5^L	c

[a] This work, Chapter 6, see also Bedford and Dunlap (1958) for similar values for hexane + perfluorohexane, [b] Heady and Cahn (1973), [c] for critical mole fraction as for H_2O + 2-butoxyethanol (Baaken *et al.*, 1990), measured by Pegg (1982). U = upper critical endpoint; L = lower critical endpoint.

Conversions from the mole fraction of component 1, x_1, to volume fraction ϕ_1 and mass fraction w_1 can be achieved using the following equations:

$$\phi_1 = \left[1 + \left(\frac{1-x_1}{x_1}\right)\frac{M_2\rho_1}{M_1\rho_2}\right]^{-1} \tag{5.20}$$

$$w_1 = \left[1 + \left(\frac{1-x_1}{x_1}\right)\frac{M_2}{M_1}\right]^{-1} \tag{5.21}$$

where M_i and ρ_i are the molar mass and density of component i, respectively, and are given in Table 5.4 below.

5.2.6 Materials

Details of the materials used in this work are given in Table 5.4.

Table 5.4: The suppliers, purities, densities ρ and molar masses M for the materials used in this work.

material	supplier	purity /mol %	density at 25°C /g cm^{-3}	molar mass /g mol^{-1}
cyclohexane	Sigma-Aldrich	99.9+ (HPLC grade)	0.7735[a]	84.16
hexane	Aldrich	99+	0.655[b]	86.18
methylcyclohexane	Aldrich	99	0.7647[c]	98.18
perdeuterocyclohexane	Eurisotop (via Fluorochem)	99.7	0.8872[a]	96.2
perfluorohexane	Fluorochem	99 (85 *n*-isomer)	1.672[b]	338.05
perfluoromethyl-cyclohexane	Fluorochem	95	1.7899[c]	350.06
hexamethyldisiloxane	Aldrich	99.5+ (NMR grade)	0.762[d]	162.38
2-butoxyethanol	Aldrich	99+	0.896[e]	118.18
D_2O	Fluorochem	99.9	1.1044[f]	20.03

[a] Houessou *et al.* (1985), [b] Bedford and Dunlap (1958), [c] Heady and Cahn (1973), [d] McLure *et al.* (1977), [e] Pegg (1982), [f] Némethy and Scheraga (1964).

The scattering length density of a mixture of given composition can be calculated from the volume fraction using equation (5.7) or directly from the mole fraction x using:

$$(\mathrm{Nb})_{\mathrm{mixture}} = \frac{x_1[(\mathrm{Nb})_1 M_1 \rho_2 - (\mathrm{Nb})_2 M_2 \rho_1] + (\mathrm{Nb})_2 M_2 \rho_1}{x_1[M_1 \rho_2 - M_2 \rho_1] + M_2 \rho_1} \qquad (5.22)$$

where $(\mathrm{Nb})_i$ is the scattering length density of component i, and M_i and ρ_i are the molar mass and density of component i, respectively.

5.3 Results and discussion

In this section the results are presented of our surface studies on the mixtures hexane + perfluorohexane, methylcyclohexane + perfluoromethylcyclohexane, hexamethyldisiloxane + perfluorohexane, deuterium oxide + 2-butoxyethanol, and perfluorooctyloctane + cyclohexane and perdeuterocyclohexane.

5.3.1 Hexane + perfluorohexane

A mixture of hexane + perfluorohexane of critical composition, approximate mole fraction of perfluorohexane $x_c = 0.37$ or volume fraction $\phi_c = 0.47$, was studied as a function of temperature from 7 K above the upper critical solution temperature T_{UCS} = 22.65°C to 11 K below T_{UCS}. The compositions and scattering length densities of coexisting phases at temperatures below T_{UCS} are shown in Figure 5.8. Further details of the phase diagram are given in Chapter 6.

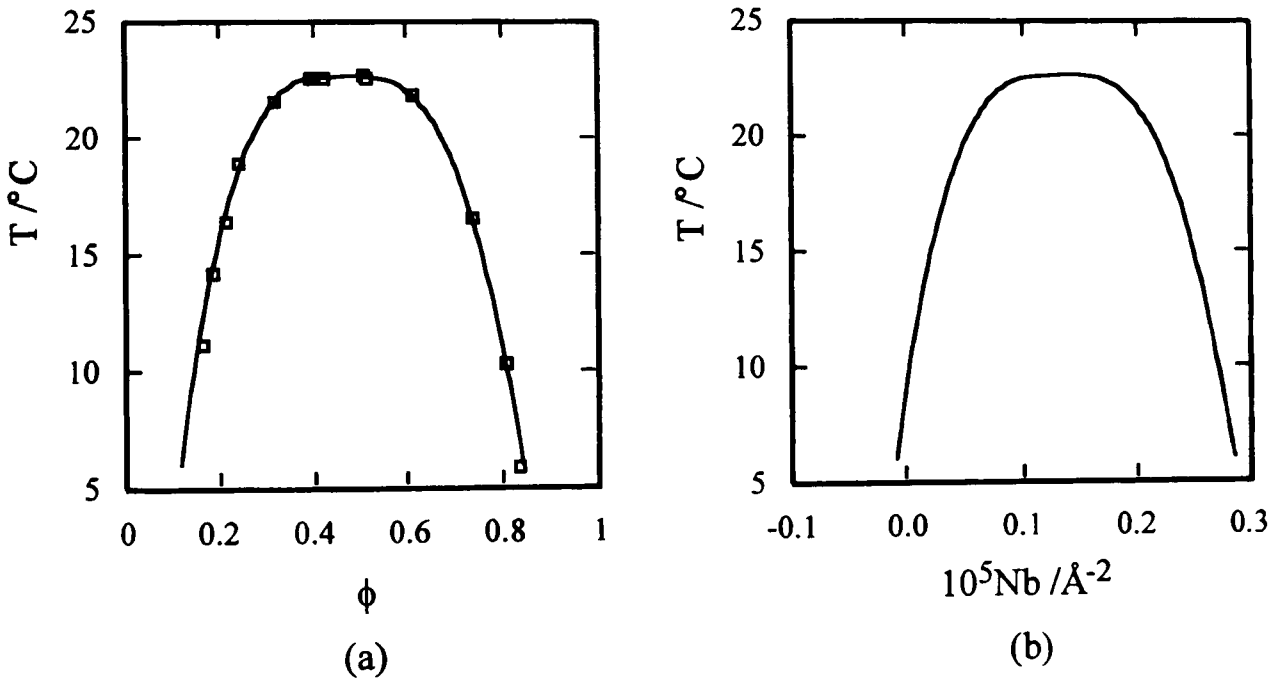

Figure 5.8: (a) Volume fraction ϕ and (b) scattering length density Nb for coexisting phases of (1-ϕ) hexane + ϕ perfluorohexane. For a critical mixture $\phi_c = 0.471$, T_{UCS} = 22.61°C, Nb = 0.136 x 10^{-5} Å^{-2}.

The reflectivity measurements were carried out on both CRISP and SURF in January-March and August-September 1995. The results were fitted to a layer model using the optical matrix method. The scattering length densities Nb and thicknesses of the layers are coupled to some extent. The parameters quoted are thus not unique but are optimised solutions; however the qualitative model still holds despite deviations from these optimised parameters.

The results obtained above and below T_{UCS} are reported in Tables 5.5 and 5.6, respectively. The general model is a perfluorohexane-rich subphase with or without the incorporation of a monolayer of pure perfluorohexane. The simple slab model employed is the only simple model which both fitted the reflectivity adequately and was in agreement with the expected thermodynamics. Neither the expected bulk subphase of the critical composition mixture above T_{UCS} (Nb = 0.136 x 10^{-5} Å^{-2}) nor the upper hexane-rich phase of the phase separated mixture below T_{UCS} were detected directly and so the overall thickness of the perfluorohexane-rich surface layer could not be determined. If the reflectivity data were modelled by the ultimate subphase capped by a thick perfluorohexane-rich layer, the fitting was insensitive to the thickness of the layer since it was too thick. The thickness of the perfluorohexane monolayer is fitted to an accuracy of ±1 Å and the scattering length densities to ±0.01 x 10^{-5} Å^{-2}, but in some cases are quoted to greater accuracy to allow comparison of similar values. The reflectivity spectra measured correspond to three distinct temperature regimes: above T_{UCS}, immediately below T_{UCS}, and further below T_{UCS}. Representative reflectivity spectra for these three regimes are shown in Figure 5.9. R is generally plotted on a logarithmic scale and Q is usually plotted on a linear scale; however, here and in some later figures both R and Q are plotted on logarithmic scales to highlight the differences in the spectra at low Q values.

Table 5.5: Details of fitting to the reflectivity data *above* T_{UCS} for a hexane + perfluorohexane mixture of critical composition. The model used is a layer of perfluorohexane (Nb = 0.354 x 10^{-5} Å^{-2}) capping a subphase enriched in perfluoro-hexane with respect to the bulk critical mixture (Nb = 0.136 x 10^{-5} Å^{-2}). The volume fraction ϕ and mole fraction x of perfluorohexane in the subphase are calculated from the subphase Nb. For the bulk critical mixture ϕ_c = 0.47, x_c = 0.37. All roughnesses are 4 Å.

T /°C	10^5Nb subphase /Å^{-2}	ϕ subphase	x subphase	thickness of perfluorohexane layer /Å
30	0.160	0.51	0.41	9.5
26	0.180	0.56	0.45	13.0
25	0.185	0.59	0.48	13.6
24	0.200	0.62	0.51	13.3
23	0.216	0.66	0.55	14.7

Table 5.6: Details of fitting to the reflectivity data *below* T_{UCS} for hexane + perfluorohexane. The surface structure is modelled by a macroscopic perfluorohexane-rich subphase capped, where indicated, by a monolayer of perfluorohexane (Nb = 0.354 x 10^{-5} Å^{-2}). The scattering length density calculated from the phase diagram is included for comparison. The roughnesses are 4 Å for the data requiring a monolayer and are otherwise about 6 Å. The values in *italics* are measurements repeated on a separate occasion.

T /°C	10^5Nb subphase (ex reflectivity) /Å^{-2}	10^5Nb subphase (ex phase diagram) /Å^{-2}	thickness of perfluorohexane layer /Å
22	0.185	0.186	13.2
21	0.230	0.210	11.4
21	*0.225*	*0.210*	*10.0*
20	0.219	0.220	10.0
18	0.250	0.237	10.0
16	0.220	0.248	10.0
16	*0.230*	*0.248*	*no layer*
14	0.260	0.258	no layer
13	0.256	0.261	no layer
11.5	0.266	0.265	no layer

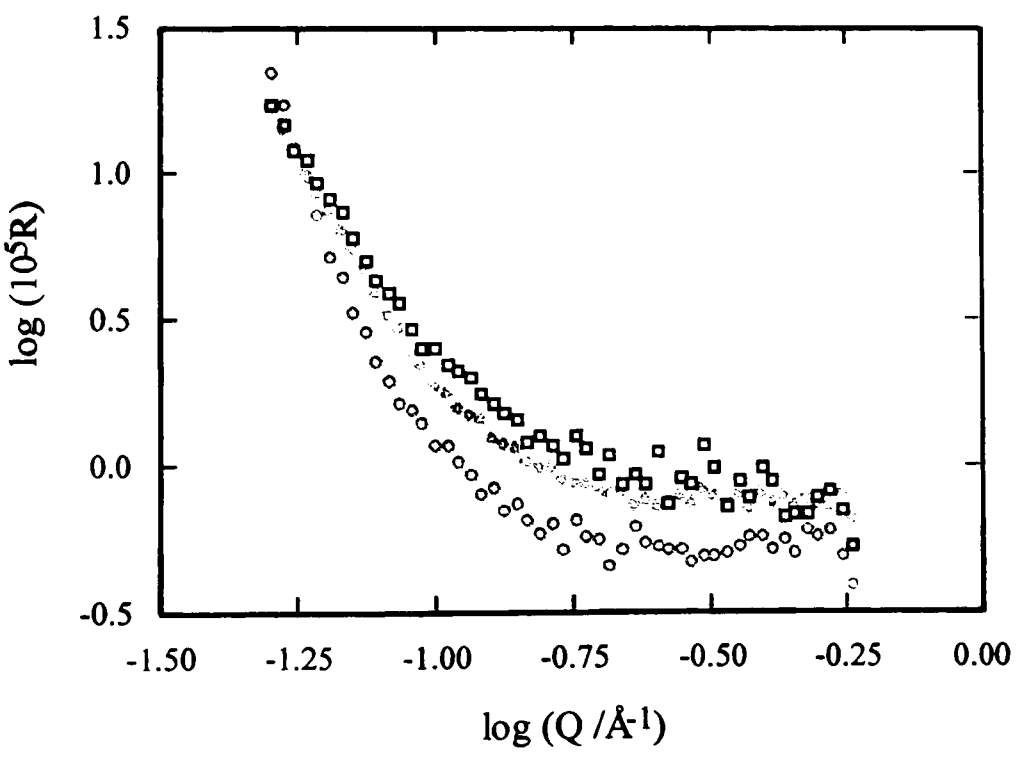

Figure 5.9: Reflectivity R against momentum transfer Q spectra for a mixture of hexane + perfluorohexane of critical composition at temperatures of 23°C (□), 18°C (◊), and 13°C (O). Logarithmic scales have been used to highlight the difference between the spectra at low Q values. The drop in background level correlates with the increase in scattering length density of the subphase.

Above T_{UCS} the reflectivity is best modelled by a perfluorohexane-rich subphase capped by a layer whose scattering length density and thickness correspond to a perfluorohexane monolayer. It is clear from inspection of the scattering length densities Nb in Table 5.5 that the subphase becomes increasingly enriched in perfluorohexane as T_{UCS} is approached. This is consistent with the qualitative predictions of the Total Surface Segregation (TSS), see Chapter 1, section 1.3.1, which interprets the subphase as being an adsorbed layer with a macroscopic thickness. The monolayer increases in thickness close to T_{UCS}; this may be attributed to approximating critical adsorption with an over-simplified model. This model describes the data, although a more realistic interfacial structure is probably a gradually decaying profile from pure perfluorohexane at the vapour interface to the bulk critical composition further into the liquid (Fisher and de Gennes, 1978; Liu and Fisher, 1989). In future work, with more precise data obtained under conditions of stricter temperature control, it may be possible to fit the data more rigorously using slowly decaying profiles.

Immediately below T_{UCS} the reflectivity is most successfully modelled by a macroscopically thick layer–with a scattering length density at a given temperature corresponding to that calculated from the phase diagram for the lower bulk perfluorohexane-rich phase–capped by a layer whose scattering length density and thickness are consistent with a perfluorohexane monolayer, as shown in Table 5.6.

The presence of a macroscopic perfluorohexane-rich phase is in agreement with the expectations of critical-point wetting. For this mixture a wetting layer of 400 Å would result in fringes, or features, in the neutron reflectivity spectrum, but for thicker layers the features should disappear. As shown in Figure 5.9, our reflectivity profiles are relatively featureless and so the wetting layer, although indeterminate from our present measurements, may possibly have a thickness in agreement with the predictions of Widom (1978) of the order of 10^4 Å. It certainly appears from our results that the wetting layer has the same composition as the bulk phase from which it originated. The layer of pure perfluorohexane increases in thickness as T_{UCS} is approached and this is again believed to be due to approximating critical adsorption with a simplified model.

Further below T_{UCS}, at $(T_{UCS} - T) \approx 7$ K, the perfluorohexane monolayer is absent from the model. At temperatures for which the monolayer is observed, the composition of the immediately underlying perfluorohexane-rich phase correlates with compositions of perfluorohexane ($x = 0.2$-0.7) at which the monolayer was observed in previous studies in the group investigating the surface structure as a function of composition in the one-liquid phase region at T = 24.5°C (Bowers *et al.*, 1996a).

The scattering length density profile normal to the interface as a function of distance z through the interface, where in this case z = 0 at the subphase-surface layer boundary, is plotted in Figure 5.10 for temperatures representative of the three regimes: above T_{UCS}, immediately below T_{UCS}, and further below T_{UCS}.

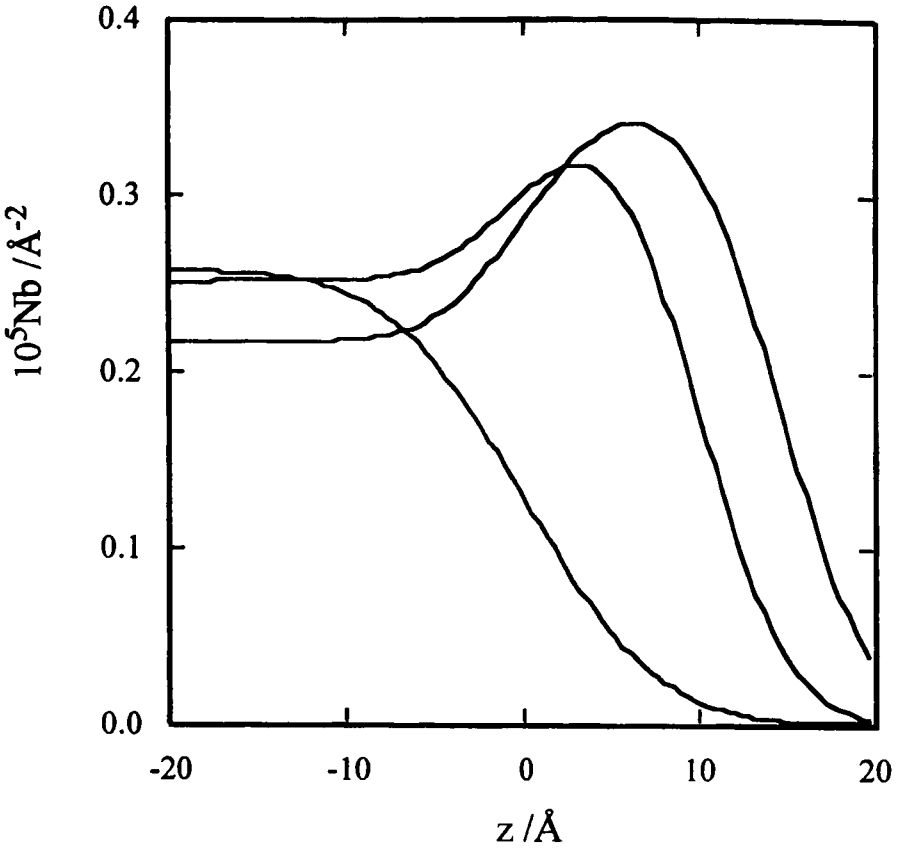

Figure 5.10: Scattering length density Nb profiles normal to the interface as a function of the distance z through the interface for hexane + perfluorohexane at 13°C, 18°C and 23°C reading from top to bottom on the left-hand axis. The effect of the surface roughness is apparent in smoothing the step-like profile.

The scattering length density of the subphase as a function of temperature both above and below T_{UCS} is plotted in Figure 5.11. The monolayer is neglected. In the single-liquid-phase region the enrichment of the interface with perfluorohexane as T_{UCS} is approached is clearly demonstrated. Below T_{UCS} the scattering length densities obtained from the reflectivities are shown together with the scattering length densities of the perfluorohexane-rich phase calculated from the phase diagram.

For two of the temperatures below T_{UCS} the results were repeated in a separate session and are *italicised* in Table 5.6. Some discrepancy remains between the Nb values obtained from the reflectivity and those calculated from the phase diagram and is attributed to non-equilibrium conditions. The inconsistency in the presence of a monolayer at 16°C is probably due to the cut-off temperature for the monolayer lying close to 16°C and any non-equilibrium conditions upsetting this balance. It was important to ensure that the sample reached thermal equilibrium before the final stirring of the mixture and that it was allowed to settle for sufficiently long periods of time. Unfortunately, owing to time constraints on the instrument these times were often shorter than desired, which accounts for some of the poorer results.

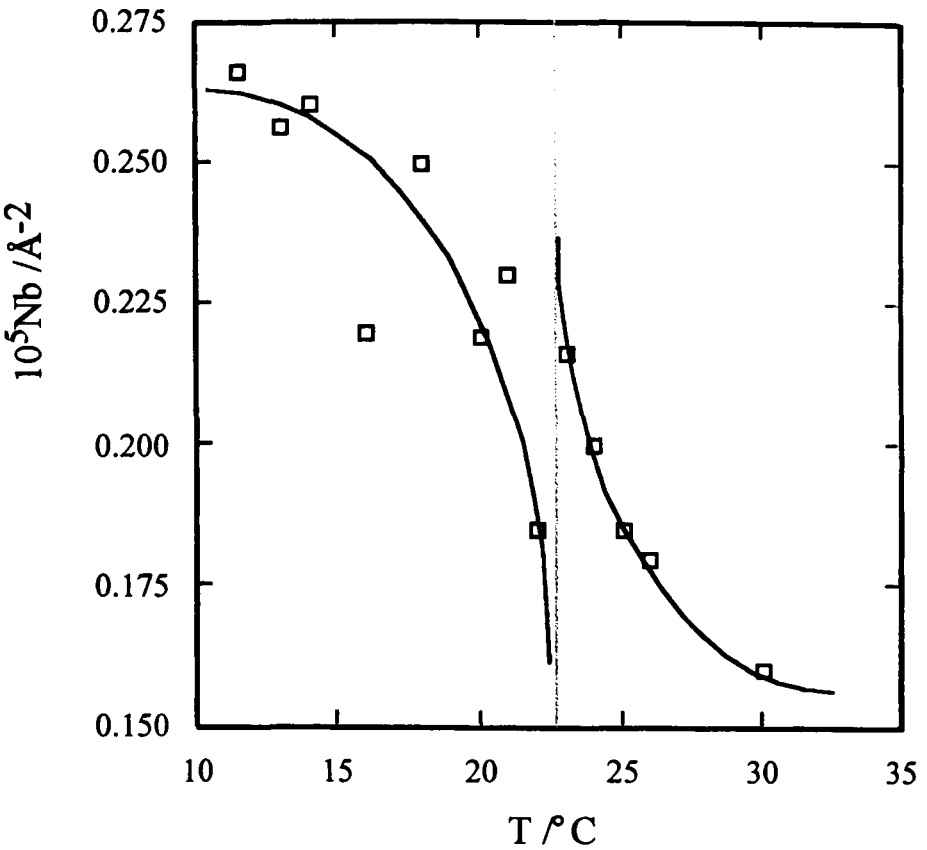

Figure 5.11: The scattering length density Nb of the subphase as a function of temperature T for a mixture of hexane + perfluorohexane of critical composition. The vertical line indicates T_{UCS}. The points represent the Nb obtained from the reflectivity measurements. Above T_{UCS} the line is included to guide the eye. Below T_{UCS} the line is the Nb of the bulk perfluorohexane-rich phase calculated from the phase diagram.

A model-independent method of fitting the reflectivity data obtained at 26°, see section 5.2.3.2, encouragingly indicates the enrichment of perfluorohexane at the interface. It also shows the presence of a monolayer which is of comparable thickness, scattering length density and roughness to that used in the fitting using MULF, for which the results are presented above.

5.3.2 Methylcyclohexane + perfluoromethylcyclohexane

The surface structure of a mixture of methylcyclohexane (MCH) + perfluoromethylcyclohexane (PFMCH) of critical composition, mole fraction of PFMCH $x_c = 0.36$ or volume fraction $\phi_c = 0.46$, was studied as a function of temperature from 4 K above $T_{UCS} = 46.13°C$ to 23 K below T_{UCS}. Measurements in the single-phase region further above T_{UCS} were not possible due to evaporation of the liquid at these high temperatures. The compositions and scattering length densities of coexisting phases of MCH + PFMCH below T_{UCS} are shown in Figure 5.12.

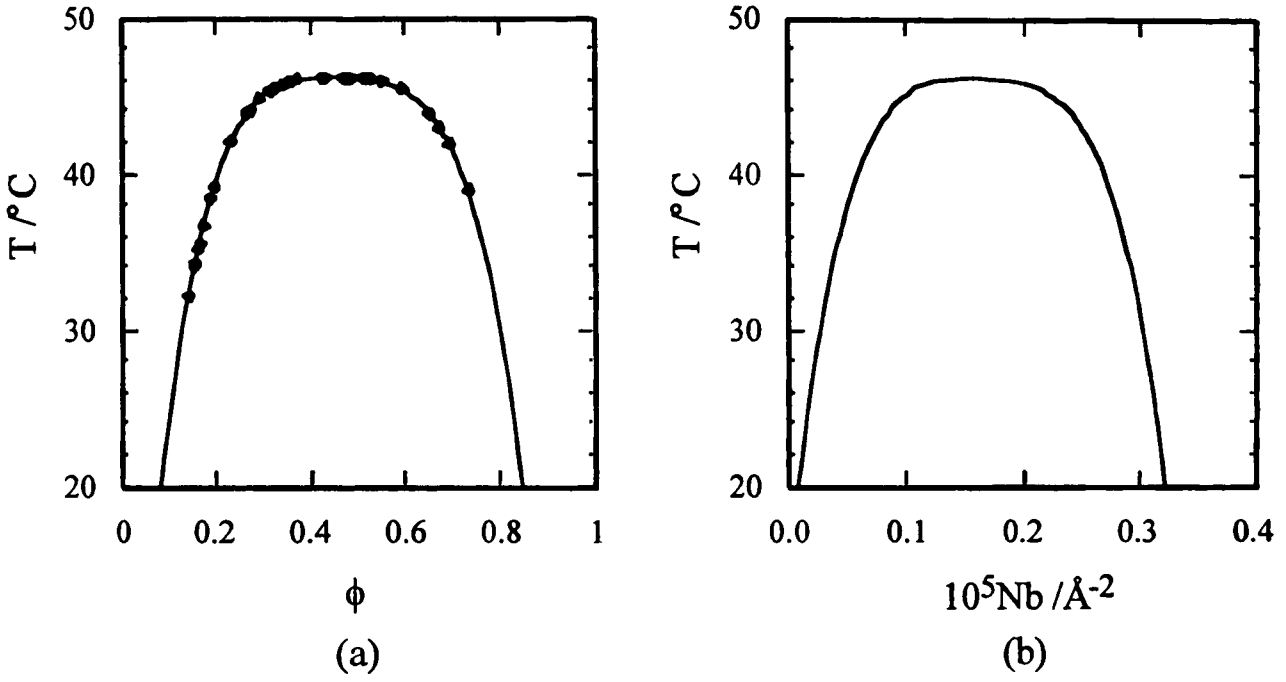

Figure 5.12: (a) Volume fraction ϕ and (b) scattering length density Nb for coexisting phases of (1-ϕ) methylcyclohexane + ϕ perfluoromethylcyclohexane calculated from the coexistence curve of Heady and Cahn (1973). For a critical mixture $\phi_c = 0.463$, $T_{UCS} = 46.13°C$, $Nb = 0.164 \times 10^{-5}$ Å^{-2}.

The reflectivity measurements were carried out on SURF in August-September 1995. The equilibration times were generally at least 15 minutes, but at 44°C the sample was equilibrated for 17 hours. The results were fitted using MULF to a slab model similar to that used to describe the hexane + perfluorohexane data discussed above. The outcome of this fitting is shown in Table 5.7. The basic model is a PFMCH-rich subphase capped where necessary by a layer of pure PFMCH. As in hexane + perfluorohexane neither the bulk critical composition mixture above T_{UCS} nor the upper hydrocarbon-rich phase below T_{UCS} are detected within a reasonable sensitivity.

Table 5.7: Details of fitting to the reflectivity data for a mixture of MCH + PFMCH of critical composition both above and below $T_{UCS} \approx 46.1°C$ using a simple *one-layer* model. The surface structure is modelled by a macroscopic PFMCH-rich subphase capped, where indicated, by a monolayer of PFMCH ($Nb = 0.387 \times 10^{-5}$ Å^{-2}) of thickness d Å. The scattering length densities for the bulk critical mixture above T_{UCS} and for the PFMCH-rich phase below T_{UCS}, calculated from the phase diagram, are included for comparison. The interfilm roughnesses are 0 Å. The background is set at 0.5×10^{-5}, except at 38°C where it is 0.45×10^{-5} due to a slight drop in liquid level. χ^2 indicates the goodness of fit.

T /°C	10^5Nb subphase (ex reflectivity) /Å^{-2}	10^5Nb subphase (ex phase diagram) /Å^{-2}	d /Å	air-film roughness /Å	χ^2
50	0.231	0.164	8.6	4	0.9
48	0.222	0.164	10.6	4	1.6
46	0.220	0.192	8.0	0	2.1
44	0.210	0.240	9.0	0	1.9
42	0.227	0.257	7.8	4	1.0
38	0.264	0.280	7.0	8	1.2
28	0.308	0.310	no layer	6	1.6
23	0.333	0.315	no layer	8	1.6

Above T_{UCS} the reflectivity can be described by a model with a layer of PFMCH capping a subphase enriched in PFMCH with respect to the bulk critical composition. These measurements indicate that the thickness of the PFMCH layer increases as T_{UCS} is approached. The scattering length density of the subphase does not also show an increase to indicate enhanced PFMCH adsorption close to T_{UCS}. However, this mixture was only studied at two temperatures above T_{UCS} so general conclusions of the basic trend cannot be drawn.

Below T_{UCS} the model is a macroscopic PFMCH-rich phase–with a scattering length density roughly corresponding to that expected for the lower PFMCH-rich bulk phase–which immediately below T_{UCS} is capped by a monolayer of pure PFMCH. Further below T_{UCS} this monolayer disappears.

It is unclear whether the mixture at 46°C is phase separated since direct observation of phase separation of the sample in the trough is not possible. Calibration tests suggest that at high temperatures the liquid in the trough may be at a lower temperature than that recorded. The mixture is thus expected to be in two phases at 46°C, although it may be near-critical and any temperature fluctuations may cause large variations in composition.

At 38°C the model is only approximate as the data are poor due to a slight drop in liquid level indicated by the requirement for a lower background. Unfortunately, there was insufficient time to repeat the run at this temperature.

Data were also recorded at 33°C; however the reflectivity could not be fitted to the same model. The best fit obtained was with a three-layer model of: 11 Å of Nb = 0.387×10^{-5} Å^{-2} (pure PFMCH), 22 Å of Nb = 0.369×10^{-5} Å^{-2} and 33 Å of Nb = 0.361×10^{-5} Å^{-2} on a subphase with Nb fixed at the value calculated from the phase diagram, namely 0.295×10^{-5} Å^{-2}. All the roughnesses were 8 Å. This model is a crude approximation to a decaying profile, although it does not decay smoothly to the bulk value. This temperature may be in the cross-over regime between two different surface structures and may be very sensitive to any temperature fluctuations. Unfortunately, there was again insufficient time to repeat this measurement to check whether the very different reflectivity was reproducible.

This model seems to adequately describe all the data, except those obtained at 33°C. Nevertheless, we have some reservations about the model since the fitting was very sensitive to the air-film roughness factors quoted in Table 5.7. In particular, air-film roughnesses of zero for the data at 46°C and 44°C were required; although this may possibly be attributed to a difficulty in fitting near-critical data. Generally, when fitting reflectivity data the roughnesses are fixed at reasonable values, e.g. 2 or 4 Å, and any changes in these values do not significantly affect the goodness of fit. In this case, however, the fit was very dependent on the roughness, hence the variation in the values quoted for different data sets. The effect of roughness on the reflectivity from a bare subphase of PFMCH is shown in Figure 5.4 above.

The sensitivity of the data to the air-film roughness may indicate that the model is not the best one to describe the data. The model-independent method, see section 5.2.3.2, suggested the need for the incorporation of some surface layering. The reflectivity was therefore refitted keeping all the roughnesses fixed at 4 Å. The results are tabulated in Table 5.8. The model consists of three layers of alternating Nb with pure PFMCH at the surface, then an MCH-rich layer, then a PFMCH-rich layer, on a PFMCH-rich subphase. The PFMCH-rich subphase was generally of the same Nb as obtained from the single-layer model at a given temperature and of slightly lower Nb than that calculated from the phase diagram.

Table 5.8: Details of fitting to the reflectivity data for a mixture of MCH + PFMCH of critical composition both above and below $T_{UCS} \approx 46.1°C$ using a *three-layer* model. The surface structure is modelled by a macroscopic PFMCH-rich subphase capped by three layers of thicknesses d Å of alternating high and low scattering length densities with the top layer equivalent to pure PFMCH (Nb = 0.387×10^{-5} Å^{-2}). One-layer models are also included for 50°C and 48°C. All roughnesses are 0 Å. The background is set at 0.5×10^{-5}, except at 38°C where it is 0.45×10^{-5} due to a slight drop in liquid level. χ^2 indicates the goodness of fit.

T /°C	10^5Nb subphase /Å^{-2}	layer 1		layer 2		layer 3		χ^2
		d /Å	10^5Nb /Å^{-2}	d /Å	10^5Nb /Å^{-2}	d /Å	10^5Nb /Å^{-2}	
50	0.219	11.9	0.387	9.0	0.133	7.9	0.262	1.0
	0.221	*13.8*	*0.307*	-	-	-	-	*1.0*
48	0.200	13.3	0.387	10.7	0.133	8.4	0.251	1.4
	0.209	*13.5*	*0.340*	-	-	-	-	*1.7*
46	0.220	13.4	0.387	10.4	0.130	10.1	0.251	1.2
44	0.210	13.7	0.387	10.6	0.131	8.9	0.239	1.8
42	0.238	11.6	0.387	8.3	0.131	6.2	0.269	1.1
38	0.268	7.2	0.387	7.4	0.099	5.3	0.300	1.1

At 50°C and 48°C the reflectivity spectra can be described by the three-layer model, but fits to one-layer models are also quoted for comparison. At 50°C no significant improvement on the one-layer model is made by incorporating three layers. This one-layer model in Table 5.8 can be compared with the one in Table 5.7 for a pure PFMCH layer rather than a PFMCH-rich layer and provides an indication of the coupling between the thickness and the Nb of a layer. It is unclear whether the data at 50°C are best modelled using a one-layer or a three-layer model since the error bars on the data are not small enough to allow a rigorous analysis. At 48°C, although a reasonable fit is obtained using one layer, a subtle improvement is made with the three-layer model. It should perhaps be pointed out here that the χ^2 values indicating the goodness of fit (a very good fit has $\chi^2 = 1$) can be compared for different fits to the same data set, but are not so useful in assessing the accuracy of a given model for different data sets. This is because the error bars for some data sets are larger than for others and a smaller χ^2 can thus be obtained more easily.

The data at 33°C were again inadequately described by the three-layer model. At 28°C and 23°C, no improvements on the previous bare subphase model were made using the three-layer model. The high air-film roughnesses needed at these temperatures may be reasonable for a bare subphase and may be due to thermal fluctuations.

From the results of the fitting and from a comparison of the reflectivity profiles it appears that the measurements below T_{UCS} fall into three main temperature regimes: 46-38°C, 33°C and 28-23°C. The reflectivity profiles above T_{UCS} at 50°C and 48°C are similar to those just below T_{UCS}. Representative reflectivity spectra from each regime are plotted in Figure 5.13; the temperatures chosen are those for which the best data were collected. The fits quoted in Table 5.8 are also plotted for each data set.

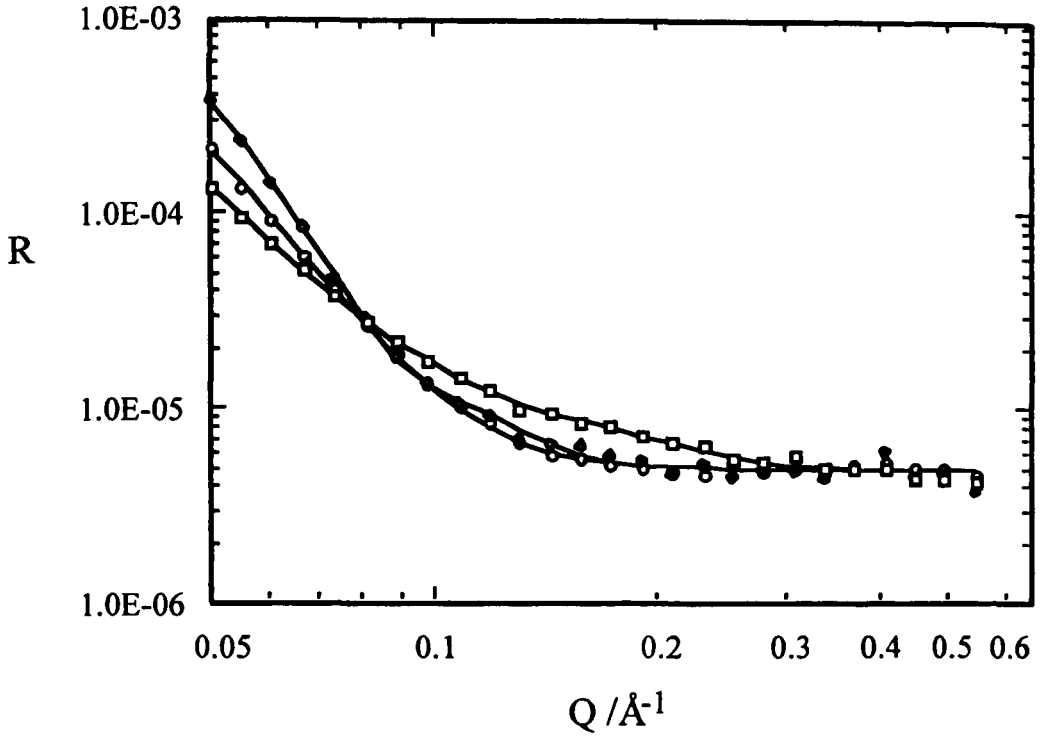

Figure 5.13: Reflectivity R against momentum transfer Q spectra for a mixture of MCH + PFMCH of critical composition at 33°C (◊), 23°C (O), and 46°C(□) reading from top to bottom on the R axis. Logarithmic scales have been used to highlight the difference between the spectra at low Q values.

The scattering length density Nb-distance z through the interface profiles are plotted in Figure 5.14 for the one-layer and three-layer models used to represent the data at 46°C, see Tables 5.7 and 5.8. The profiles for the other temperatures using the three-layer model are similar and for the one-layer model are smoothed if a roughness factor is used in the fitting. The Nb of the subphase is plotted as a function of temperature in Figure 5.15 with the Nb for the PFMCH-rich phase calculated from the phase diagram. It should be noted that the phase diagram is not known very accurately at low temperatures, particularly for the PFMCH-rich phase at temperatures below 38°C, see Figure 5.12, so the Nb values are obtained by extrapolation and are thus only approximate.

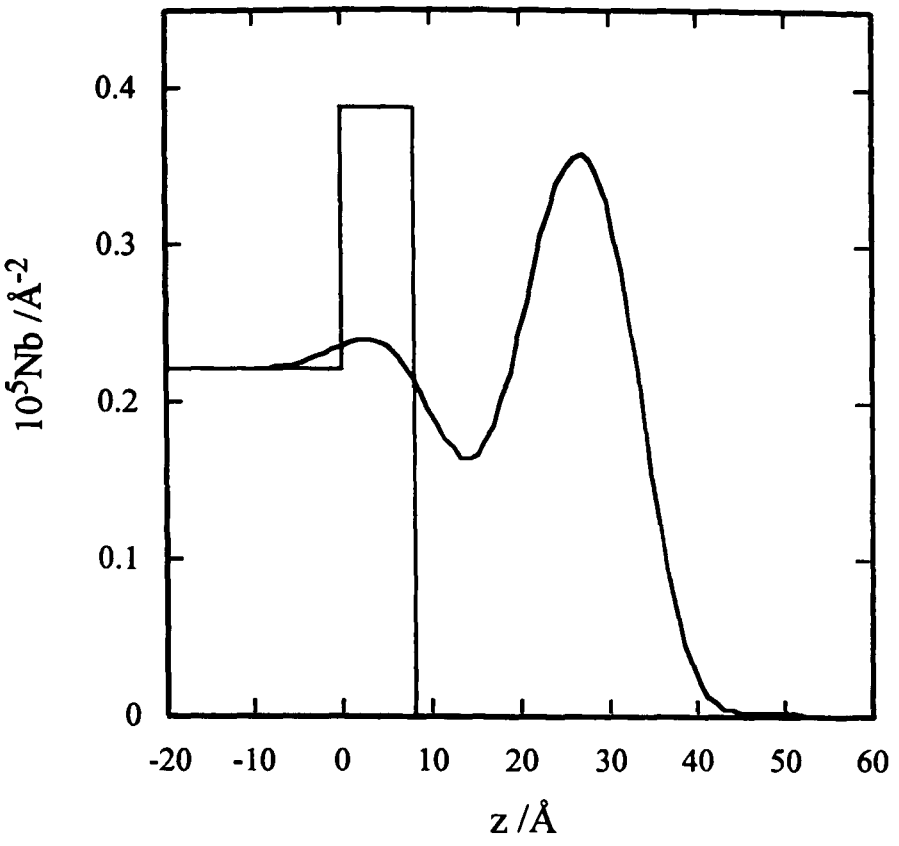

Figure 5.14: Scattering length density Nb profiles normal to the interface as a function of the distance z through the interface for the one-layer and three-layer models used to describe the MCH + PFMCH data at 46°C.

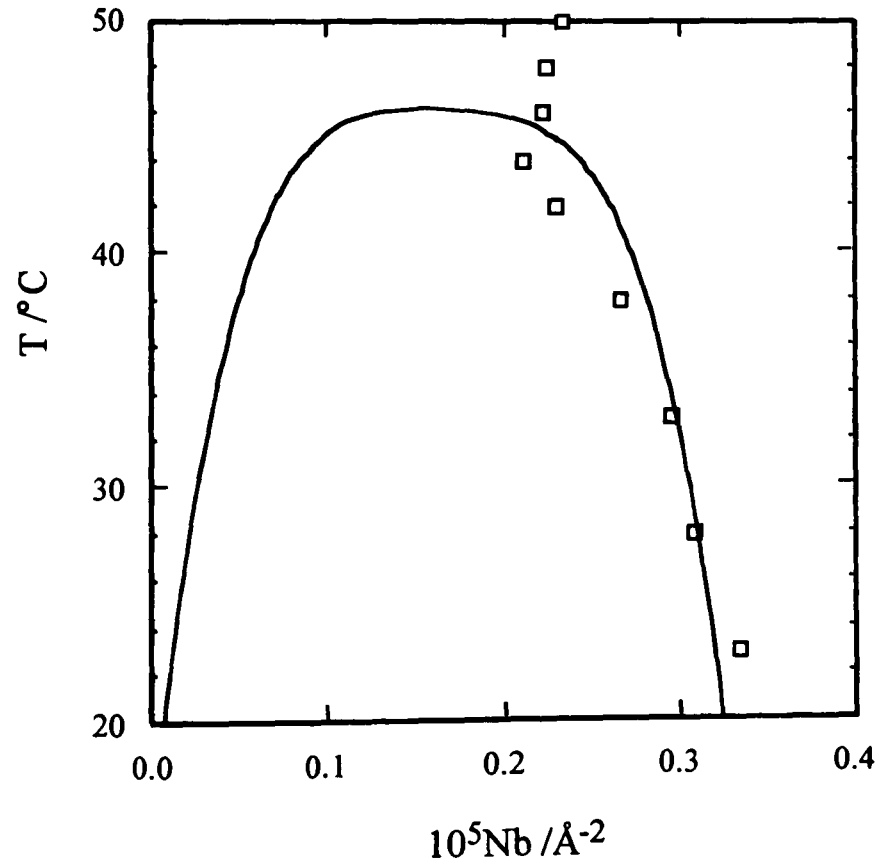

Figure 5.15: The scattering length density Nb of the subphase as a function of temperature T for a mixture of MCH + PFMCH of critical composition. The points represent the Nb obtained from the reflectivity measurements. The line is the Nb for coexisting phases below T_{UCS} calculated from the phase diagram.

At all temperatures studied the surface is rich in PFMCH. This is in agreement with the expectations of critical-point wetting and adsorption. The surface structure of this mixture of cyclic molecules can be modelled in a similar way to the straight-chain mixture hexane + perfluorohexane, although at some temperatures a model incorporating more surface layering provides a better description of the reflectivity.

The liquid-vapour interface of MCH + PFMCH mixtures has been studied by ellipsometry both below T_{UCS} (Kwon *et al.*, 1982) and above T_{UCS} (Schmidt, 1990). Kwon *et al.* used a model of a PFMCH-rich wetting layer with the same composition as the bulk PFMCH-rich phase on a subphase of the same composition as the bulk MCH-rich upper phase. They determined the thickness of the PFMCH-rich wetting layer as about 400 Å. From our neutron reflectivity measurements we were unable to determine the precise thickness of the wetting layer. This may be due to the weak scattering nature of the bulk upper MCH-rich phase compared with the PFMCH-rich wetting layer. However, since no fringes were observed in the reflectivity profile our estimated wetting layer thickness is much greater than 400 Å, possibly of the order of microns as predicted by Widom (1978).

Further work is required on MCH + PFMCH to check the detailed surface structure and the existence of three temperature regimes below T_{UCS}. The analysis could also be extended a greater distance into the single phase region above T_{UCS} if higher temperatures of the liquid in the trough can be achieved and maintained. The study of the surface structure across the composition range at a temperature in the one-phase region close to T_{UCS} and at higher temperatures would also be of interest and may inform on the composition in the two-phase region at which a surface layer of pure PFMCH is no longer required.

5.3.3 Hexamethyldisiloxane + perfluorohexane

The surface structure of hexamethyldisiloxane + perfluorohexane was studied as a function of composition for single-phase mixtures at T = 24.4±0.2°C. A mixture of critical composition, mole fraction of perfluorohexane x = 0.52, was also studied as a function of temperature from 1.7 K above T_{UCS} = 23.5°C to 4.2 K below T_{UCS}. The sample temperatures were obtained by measuring, using a calibrated platinum resistance thermometer, the temperature of a sample of water in the trough at the same temperature settings on the controller as those used in the experiment. These measurements were carried out on CRISP in January and July 1996.

The compositions and scattering length densities of coexisting phases below T_{UCS} are shown in Figure 5.16. Further details of the coexistence curve are given in Chapter 6. The scattering length density as a function of composition in terms of both volume fraction and mole fraction is plotted in Figure 5.17.

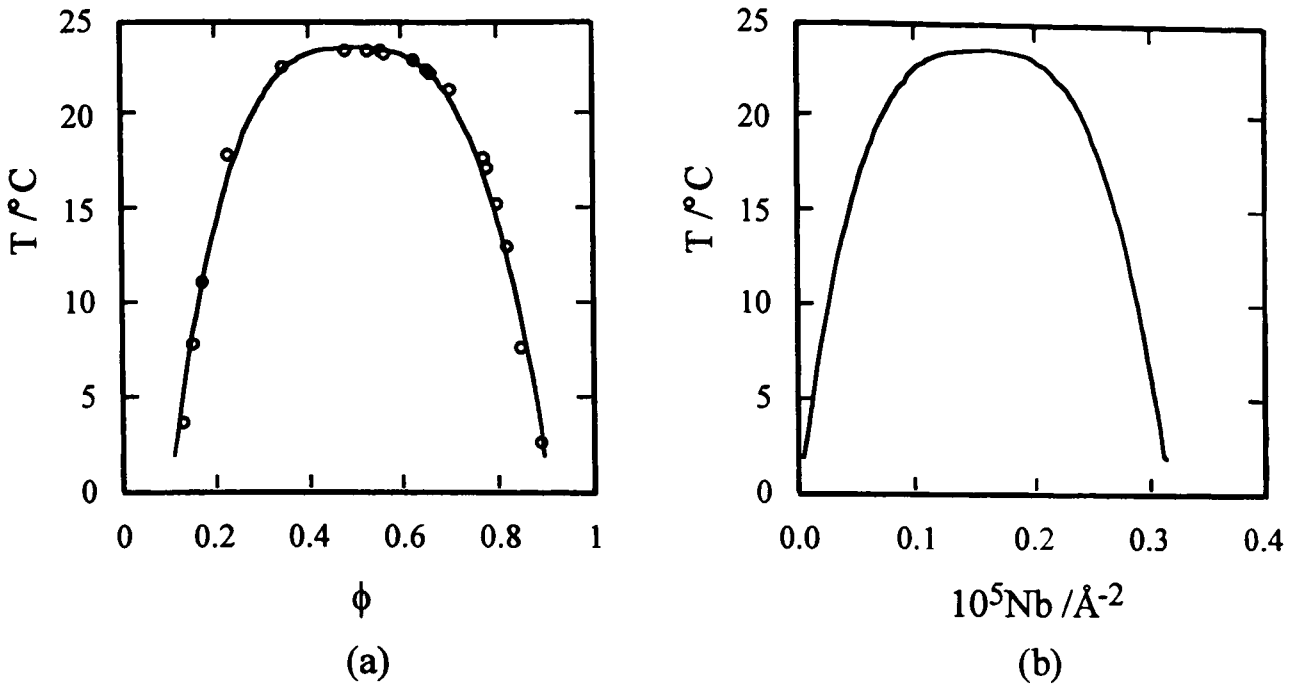

Figure 5.16: (a) Volume fraction ϕ and (b) scattering length density Nb for coexisting phases of (1-ϕ) hexamethyldisiloxane + ϕ perfluorohexane. For a critical mixture ϕ_c = 0.497, T_{UCS} = 23.50°C, Nb = 0.157 x 10^{-5} Å^{-2}.

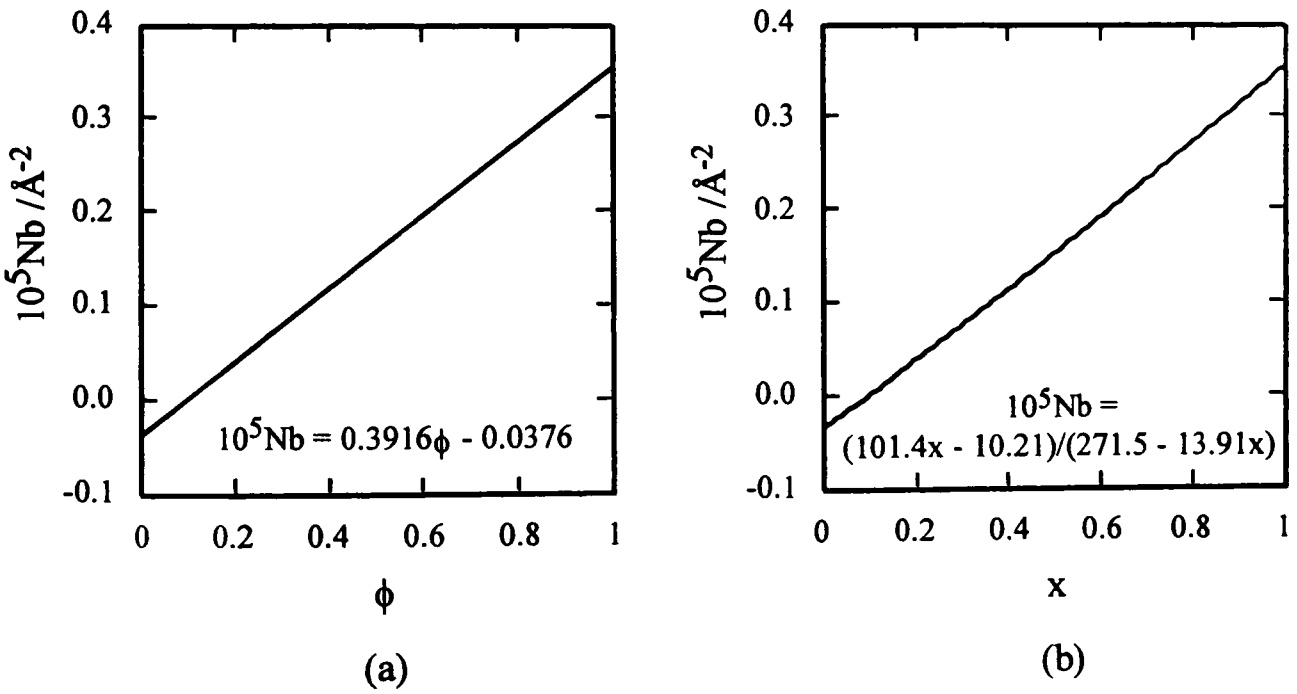

Figure 5.17: Scattering length density Nb of (1-φ) hexamethyldisiloxane + φ perfluorohexane as a function of composition φ for (a) φ = volume fraction ϕ and (b) φ = mole fraction x.

The results of fitting the reflectivities as a function of composition at 24.4°C to three-layer and four-layer models are shown in Table 5.9. The substrate Nb is fixed at the value calculated for the bulk mixture. For the top layer the Nb is fixed as for pure perfluorohexane, Nb = 0.35 x 10^{-5} Å^{-2}. For layers 2 and 4, Nb is closer to that for hexamethyldisiloxane, Nb = -0.0376 x 10^{-5} Å^{-2}, but layer 3 is again rich in perfluorohexane. Two four-layer models are included for x = 0.51 to indicate the extent of the

coupling between the thicknesses and scattering length densities. A simple monolayer model like that used for hexane + perfluorohexane could not describe the data. The most striking change with increasing perfluorohexane content is the apparent decrease in thickness of the hexamethyldisiloxane-rich layer 2 which must eventually vanish when x = 1. Five different compositions were studied and the outcome of the fitting is summarised below.

x = 0.10 The measured reflectivity was just background signifying no excess adsorption of perfluorohexane.

x = 0.51 A four-layer model best describes the data, although a three-layer model can be used.

x = 0.77 A four-layer model is required, although a three-layer model approximately describes the reflectivity.

x = 0.91 At this aneotropic composition the data can be roughly fitted by a four-layer model. This model fits the reflectivity well at low Q, but not so well at high Q partly due to the sloping background. One and two-layer models do not improve the fit. Fitting roughly to an 'islands' model also leads to a poor representation.

x = 0.96 The reflectivity can be modelled by a bare subphase if the sloping background is neglected.

Table 5.9: Details of fitting to the reflectivity data for (1-x) hexamethyldisiloxane + x perfluorohexane at 24.4°C using three-layer and four-layer models. The surface structure is modelled by the bulk subphase capped by layers of thicknesses d Å of alternating high and low scattering length densities with the top layer equivalent to pure perfluorohexane (Nb = 0.35×10^{-5} Å^{-2}). The air-film roughnesses are 4 Å and the interfilm roughnesses are 2 Å. The background (bgd) level is quoted. χ^2 indicates the goodness of fit.

x	10^5Nb	layer 1		layer 2		layer 3		layer 4		10^5bgd	χ^2
	subphase /Å^{-2}	d /Å	10^5Nb /Å^{-2}	d /Å	10^5Nb /Å^{-2}	d /Å	10^5Nb /Å^{-2}	d /Å	10^5Nb /Å^{-2}		
0.51	0.16	19.5	0.35	11.7	0.01	8.4	0.30	6.6	0.10	0.71	1.0
	0.16	20.0	0.35	10.0	-0.03	10.0	0.28	10.0	0.12	0.71	1.1
	0.16	19.3	0.35	9.9	0.02	9.8	0.22	-	-	0.71	1.2
0.77	0.26	25.1	0.35	8.7	0.01	14.2	0.34	6.1	0.19	0.91	1.1
	0.26	25.0	0.35	7.9	0.02	11.1	0.32	-	-	0.91	1.4
0.91	0.32	25.5	0.35	4.5	0.01	19.2	0.35	7.6	0.25	0.58	3.3
	0.32	24.9	0.35	3.6	0.01	10.0	0.35	-	-	0.61	5.1
0.96	0.34	-	-	-	-	-	-	-	-	0.50	6.7

The reflectivity profiles for different compositions are plotted in Figure 5.18. The points represent the experimental data and the lines are the fitted curves for the best fits quoted in Table 5.9. All the profiles except at x = 0.96 seem to show a 'bulge' in the mid-Q range. This seems to be real, rather than an effect due to scattering from the trough, as when the reflectivity of a sample of pure perfluorohexane at the same liquid level was measured directly afterwards it fitted well to the expected bare subphase and the shoulder was not present. Another feature of the reflectivity, particularly for the perfluorohexane-rich samples, is the sloping background. The reason for this is not known, but it caused some difficulties in determining the 'goodness' of a given fit. Generally the fit is deemed satisfactory if the fitted curve passes through the points in the low-mid Q range.

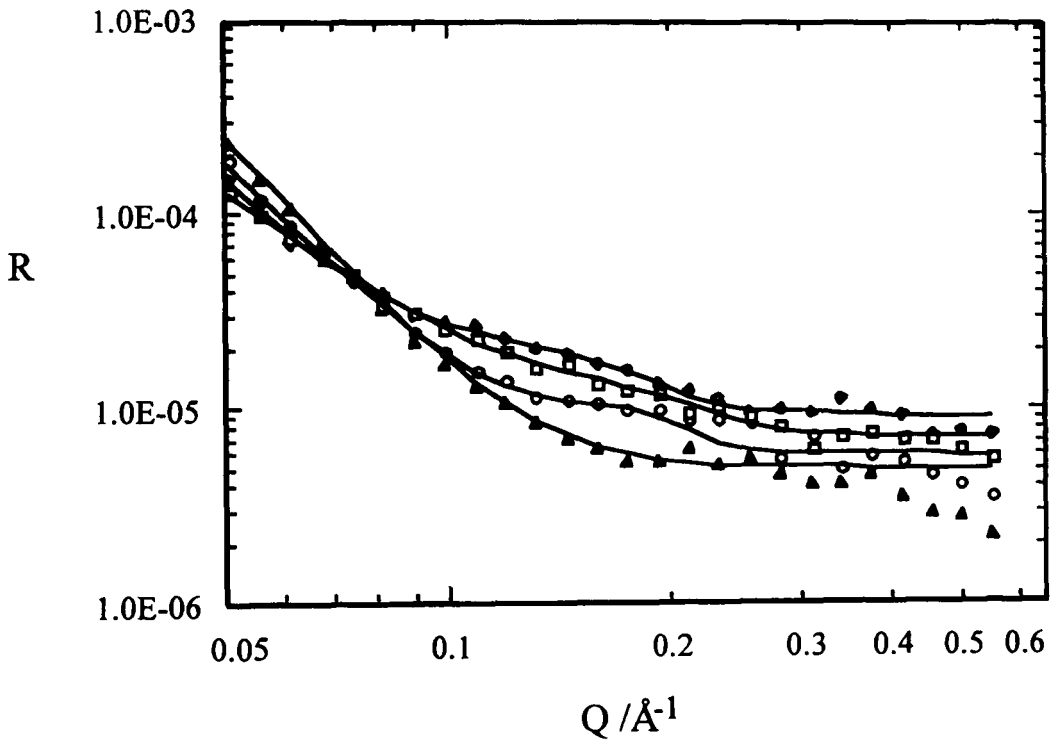

Figure 5.18: Reflectivity R against momentum transfer Q spectra for (1-x) hexamethyldisiloxane + x perfluorohexane at 25°C for x = 0.51 (□), 0.77 (◊), 0.91 (O) and 0.96 (Δ) reading from bottom to top on the R axis. Logarithmic scales have been used to highlight the difference between the spectra at low Q values.

The details of fitting the reflectivity measurements for the mixture of critical composition x = 0.52 as a function of temperature to similar four-layer models are given in Table 5.10. The use of one, two or three-layer models did not yield good agreement with the reflectivity data. At 25.2°C the profile is similar to that used to describe the reflectivity of a critical composition mixture at 24.4°C, see Table 5.9. At 19.3°C the data are not good enough to be fitted rigorously.

Table 5.10: Details of fitting to the reflectivity data for a mixture of hexamethyldisiloxane + perfluorohexane of critical composition, x = 0.52, both above and below T_{UCS} = 23.5°C using four-layer models. Above T_{UCS} the surface structure is modelled by the bulk subphase (Nb = 0.16 x 10^{-5} Å^{-2}) capped by layers of thicknesses d Å of alternating high and low scattering length densities with the top layer equivalent to pure perfluorohexane (Nb = 0.35 x 10^{-5} Å^{-2}). A similar model is used below T_{UCS} but with the subphase Nb fixed at the value for the bulk perfluorohexane-rich phase calculated from the phase diagram. The air-film roughnesses are 4 Å and the interfilm roughnesses are 2 Å. The background level is 0.7 x 10^{-5}. χ^2 indicates the goodness of fit.

T /°C	10^5Nb	layer 1		layer 2		layer 3		layer 4		χ^2
	subphase /Å^{-2}	d /Å	10^5Nb /Å^{-2}	d /Å	10^5Nb /Å^{-2}	d /Å	10^5Nb /Å^{-2}	d /Å	10^5Nb /Å^{-2}	
25.2	0.16	19.7	0.35	10.8	0.01	9.1	0.25	8.5	0.13	1.8
24.4	0.16	20.0	0.35	10.4	0.01	9.2	0.25	9.4	0.13	1.6
23.5	0.16	19.9	0.35	10.1	0.01	10.0	0.23	11.1	0.14	1.7
22.7	0.21	20.3	0.35	9.9	0.04	9.3	0.31	12.3	0.18	0.8
20.8	0.24	18.4	0.35	9.9	0.07	9.0	0.33	10.1	0.20	1.3
19.3	0.25	15.9	0.35	8.9	0.07	7.8	0.33	14.1	0.22	1.7

Above T_{UCS} the reflectivity is best modelled by a damped oscillatory composition profile, oscillating about the bulk critical composition. Reasonable fits are achieved using a four-layer model. No definite effects of critical adsorption are observed approaching T_{UCS}. The surface oscillations dominate the reflectivity and no change in the subphase scattering length density could be detected.

Below T_{UCS} the reflectivity is again modelled by an oscillating profile, this time about the composition of the bulk perfluorohexane-rich phase. This is consistent with the presence of a perfluorohexane-rich wetting layer at the interface, although the scattering length density of the subphase was imposed. For the fits quoted, the scattering length density of the subphase is fixed at the value calculated from the phase diagram for each temperature, but variations in this value within the perfluorohexane-rich range still yield reasonable agreement. However, if the subphase is modelled as hexamethyldisiloxane-rich, a realistic composition profile cannot be fitted. Both above and below T_{UCS} the model is unaffected by changes in the roughness factors.

The reflectivity profiles for the critical composition mixture at 25.2, 22.7, 20.8 and 19.3°C are plotted in Figure 5.19 along with the fitted curves from the values quoted in Table 5.10. The calculated reflectivity for a bare subphase of the critical composition mixture with a roughness of 4 Å is also shown. The profiles at 24.4 and 23.5°C are identical to the one at 25.2°C. As the temperature is decreased below T_{UCS} = 23.5°C the reflectivity exhibits a systematic lowering in the mid-Q range.

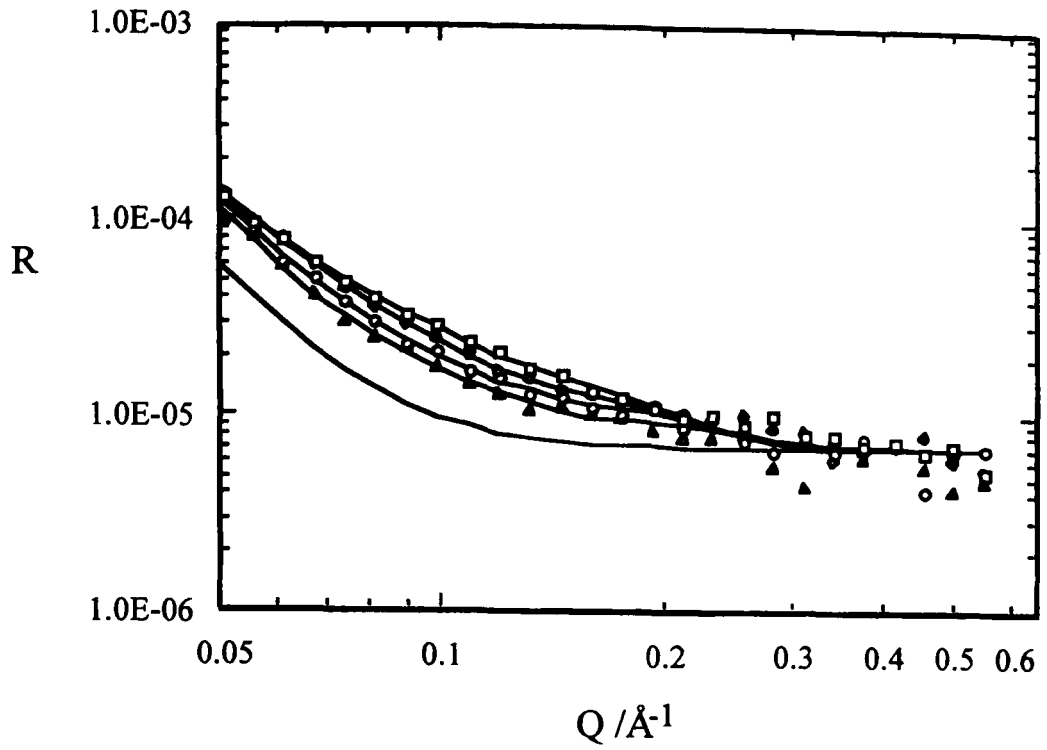

Figure 5.19: Reflectivity R against momentum transfer Q spectra for a mixture of hexamethyldisiloxane + perfluorohexane of critical composition at 25.2°C (□), 22.7°C (◊), 20.8°C (O), and 19.3°C (Δ) reading from top to bottom at Q = 0.1 $Å^{-1}$. The calculated R-Q plot for a bare subphase of critical composition is also shown. Logarithmic scales have been used to highlight the difference between the spectra at low Q values.

At 19.3°C the composition of the bulk perfluorohexane-rich phase and hence of the wetting layer is close to x = 0.77. This is the same composition as one of the bulk single-phase mixtures studied at 24.4°C. Similar models are used to fit both data sets. However, the reflectivity of the single-phase mixture is higher than that of the two-phase mixture, see Figures 5.18 and 5.19, and this is accounted for in the fitting parameters by a thicker top perfluorohexane layer for the single-phase mixture. The main distinction between the two mixtures is that for the two-phase mixture a further change in scattering length density must occur further from the interface due to the upper hexamethyldisiloxane-rich phase. If this difference in the reflectivity is real, it indicates that the long-range forces may play some role in the resulting surface structure.

As a function of composition in the single-phase region and as a function of temperature for a mixture of critical composition both above and below T_{UCS} an oscillatory composition profile at the interface can be used to represent the reflectivity data. Typical scattering length density Nb-distance z through the interface profiles for three-layer and four-layer models are shown in Figure 5.20. It appears that the surface structure of this mixture is more complex than in hexane + perfluorohexane and that the interfacial region extends over about 40 Å.

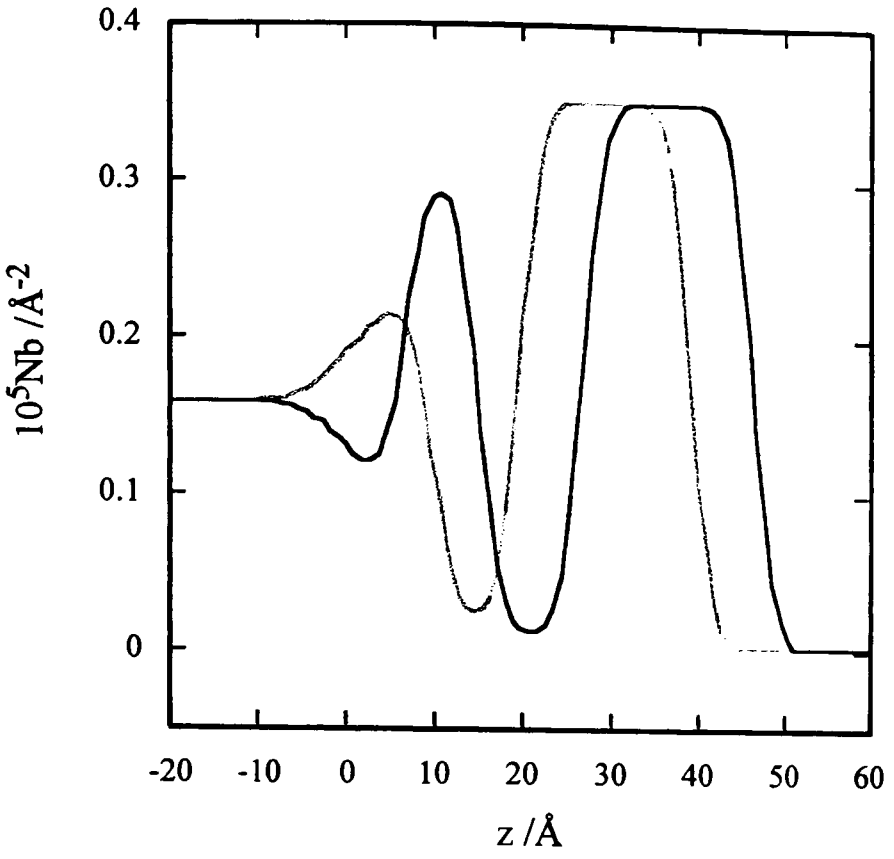

Figure 5.20: Scattering length density Nb profiles normal to the interface as a function of the distance z through the interface for a mixture of hexamethyldisiloxane + perfluorohexane of critical composition at 24.4°C for the three-layer and four-layer models quoted in Table 5.9.

For the aneotropic composition, see Chapter 1, a similar profile to that used for the other compositions approximately describes the data. For this mixture the surface composition is expected to be the same as the bulk composition, i.e. no net adsorption. Although surface layering is observed, the composition oscillates about the bulk composition and this may be in agreement with the expectations from theory.

The suitability of a layer profile of alternating high and low scattering length density to describe the reflectivity data is supported by a model-independent method of fitting (Bowers, 1996b) which shows oscillations in the scattering length density profile normal to the interface with the presence of a minimum of three layers on the bulk subphase. The plausibility of such a model to represent the surface structure at the liquid-vapour interface of a binary mixture is examined in the following section, with particular reference to the longer-ranged profile at the liquid-vapour interface of deuterium oxide + 2-butoxyethanol mixtures.

5.3.4 Deuterium oxide + 2-butoxyethanol

The reflectivity was measured from the surface of a mixture of D_2O + 2-butoxyethanol (C_4E_1), with weight fraction of 2-butoxyethanol w = 0.25 (the critical composition w = 0.273), at temperatures of 30, 35, 37.5, 38.5, 39.5, 40.5 and 41.5°C (on the Marlow controller) in the one-liquid phase region close to T_{LCS} = 42.5°C. The measurements were carried out on CRISP in January 1996.

The reflectivity data cannot be fitted by a bare subphase or by simple one-layer and two-layer models. Extensions to three-layer and four-layer models yield partial success suggesting layering at the interface. To fully describe the measured reflectivities a ten-layer model is required. The features of the model are:

1. Ten layers of alternating high and low scattering length densities oscillating about the bulk critical composition (Nb = 0.451 x 10^{-5} Å^{-2}).
2. The first (top) layer is of Nb fixed as for pure D_2O (Nb = 0.635 x 10^{-5} Å^{-2}) and the other odd-numbered layers are D_2O-rich, but approach closer to the bulk composition with increasing distance from the liquid-air interface.
3. The even-numbered layers are 2-butoxyethanol-rich, with layer 2 close to pure 2-butoxyethanol (Nb = -0.004 x 10^{-5} Å^{-2}), and also approach the bulk composition.
4. As the bulk mixture is approached, the D_2O-rich layers decrease in thickness and the 2-butoxyethanol-rich layers increase in thickness.
5. The top D_2O layer is about 30 Å thick.
6. The overall extent of the surface region is about 150-200 Å.

The reflectivity measurements were fitted to this model using nrmodfit and nrfit (see section 5.2.3 and the appendix). The interfilm roughness factors were fixed at 2 Å, to allow for roughness of the order of the D_2O molecular size, and the air-film roughnesses were floated and were 1-3 Å. All the data were described well by this model. An example of the parameters used is given for one data set in Table 5.11.

Table 5.11: Details of fitting to the reflectivity data for a mixture of deuterium oxide + 2-butoxyethanol of weight fraction composition w = 0.25 at 30°C using a ten-layer model. The bulk scattering length density is fixed at the value calculated for this overall composition, Nb = 0.451 x 10^{-5} Å $^{-2}$. The air-film roughness is 2.2 Å and the interfilm roughnesses are 2 Å. The background level is 0.61 x 10^{-5}. χ^2 = 1.1.

D_2O-rich layers			2-butoxyethanol-rich layers		
layer no.	thickness /Å	10^5Nb /Å^{-2}	layer no.	thickness /Å	10^5Nb /Å^{-2}
1	27.5	0.635	2	8.3	0.006
3	16.0	0.544	4	11.5	0.233
5	10.7	0.497	6	16.2	0.344
7	6.1	0.467	8	20.7	0.399
9	4.1	0.460	10	24.5	0.428

The reflectivity profile for the data at 30°C and the fitted curve, for which the parameters are given in Table 5.11, are plotted in Figure 5.21, along with the Fresnel reflectivity for a bare subphase. The reflectivity profiles for the other temperatures in the range 30-41.5°C are very similar. The scattering length density profile through the interface is shown in Figure 5.22.

Since all the reflectivity profiles are similar in the one-phase region approaching T_{LCS} and can be fitted by the same model, no critical adsorption is apparent from our measurements. This may possibly be because our composition is not close enough to the true critical composition. The results are, however, interesting and may inform upon the non-critical behaviour of this mixture. It is expected that the outermost layer is of 2-butoxyethanol, but this cannot be detected by the neutrons due to the very small scattering length density. The modelled profile is of surprisingly long range for this off-critical mixture, although polymer solutions and near-critical binary mixtures possess very thick interfaces.

A model-independent method of fitting the reflectivity data, see section 5.2.3.2, yields an oscillating interfacial scattering length density profile with a damped amplitude. The outermost layer detected appears to be of nearly pure D_2O with a thickness of 20-40 Å, which is consistent with the model used in the fitting described above. After this first D_2O layer the period of the oscillations, i.e. the thickness of the layers, is reasonably constant. This is in contrast to the varying period discussed above.

The model that we have used to describe the data assumes that the in-plane surface is homogeneous. However, it is possible that the surface is patchy, i.e. constituted of 'islands', due to some kind of surface phase separation. To assess this possibility the data were fitted to a simple islands model with single-layer D_2O-rich and 2-butoxyethanol-rich islands, but no realistic good fits could be achieved.

The reflectivity profiles, see Figure 5.21, look relatively featureless; however, a complex damped oscillatory model is required to describe the data. We now attempt to account for this type of profile in D_2O + 2-butoxyethanol and in our other mixtures from previous experimental and theoretical work by various groups on different systems. Further details are given in the paper in preparation on this topic (Bowers *et al.*, 1996b).

X-ray reflectivity studies of the liquid-vapour interface of mercury by Magnussen *et al.* (1995) have shown the existence of a damped oscillatory density profile in agreement with the theoretical predictions for simple metals by Sluis, D'Evelyn and Rice (1983) and D'Evelyn and Rice (1983). In liquid mixtures, a weak damped oscillatory decay of the liquid-vapour density profile into the bulk liquid is predicted theoretically by Evans *et al.* (1993, 1994). Molecular dynamics simulations by Toxvaerd and Stecki (1995) of an immiscible binary mixture of simple particles reveal similar oscillatory structures in the density profiles at the liquid-liquid interface. These density oscillations

may possibly be due to packing effects or to fluctuations in composition, or to contributions from both.

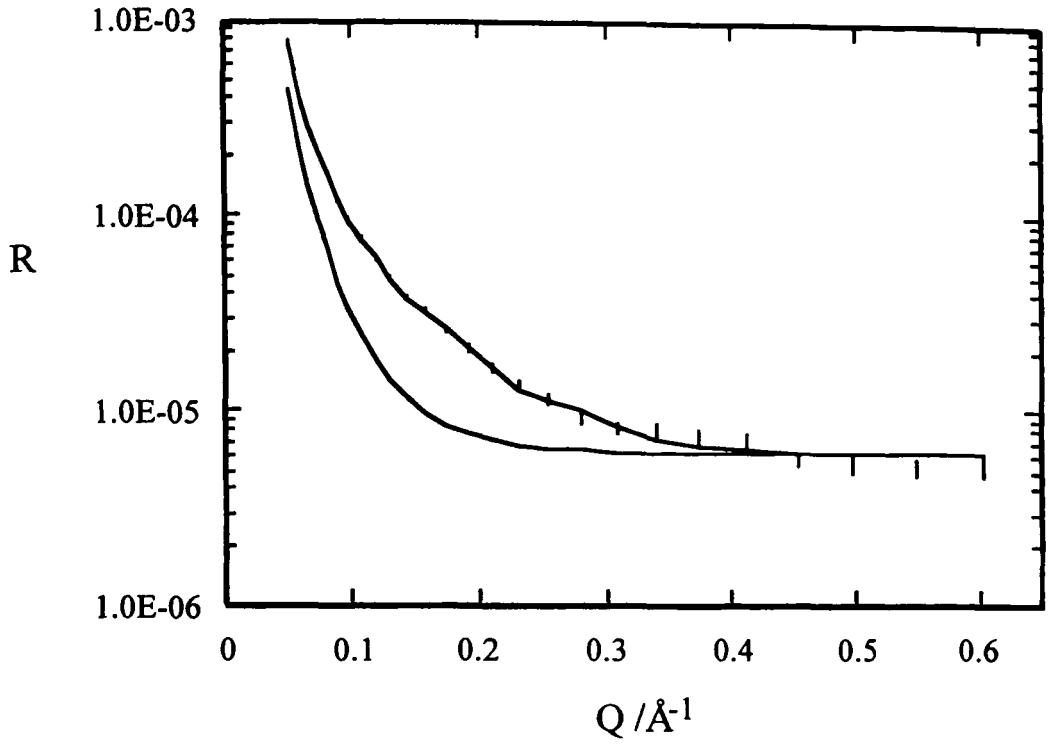

Figure 5.21: Reflectivity R against momentum transfer Q spectra for (1-w) D_2O + w 2-butoxyethanol at 30°C for weight fraction w = 0.25. The reflectivity for a bare subphase is also shown.

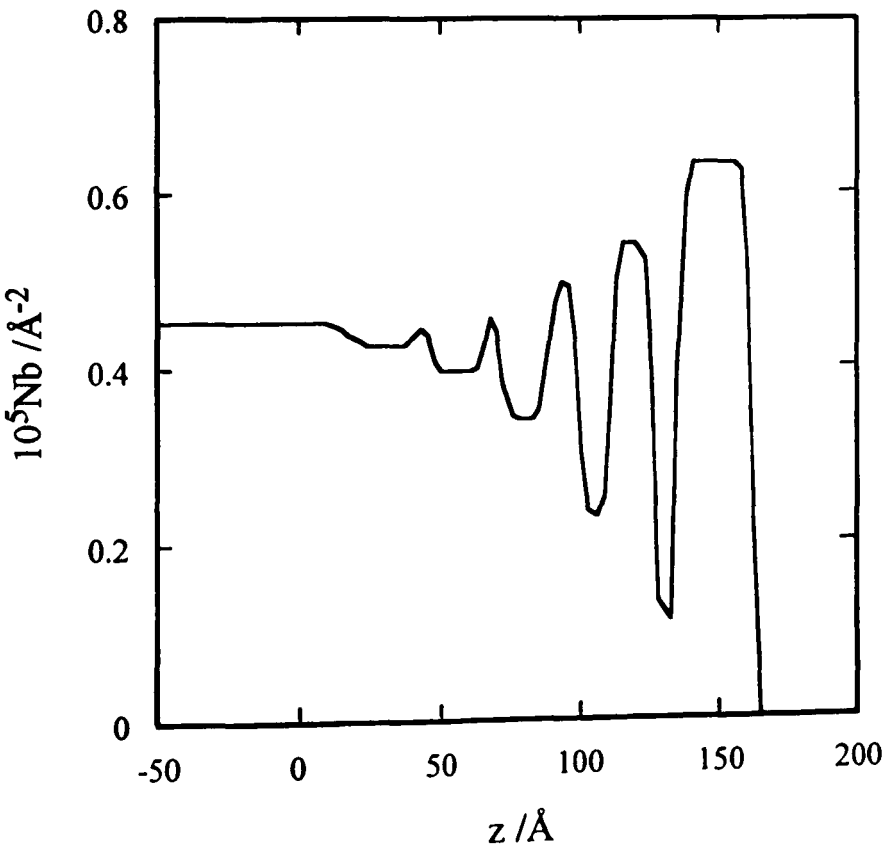

Figure 5.22: Scattering length density Nb profile normal to the interface as a function of the distance z through the interface for (1-w) D_2O + w 2-butoxyethanol at 30°C for weight fraction w = 0.25.

There do not appear to have been any reports of oscillating composition profiles in mixtures like those in our work, but some similar features such as surface layering have been observed experimentally in related mixtures. For example, a damped oscillatory composition profile has been observed in a $C_{10}E_4$ + D_2O + octane microemulsion mixture at a hydrophobically-coated silicon interface by Lee *et al.* (1995). In an aqueous surfactant solution, $C_{12}E_4$ + D_2O, which is related to that used in our study, Steitz *et al.* (1996) have obtained reflectivity measurements at a hydrophobically-coated silicon interface which suggest the existence of a damped oscillatory decaying density profile with an overall range of around 300 Å. A similar oscillatory composition profile has been observed at the liquid-air interface in polymer solutions undergoing spinodal decomposition after rapid quenching to an unstable state by Jones *et al.* (1991).

In methanol + cyclohexane mixtures surface layering of methanol molecules has been reported in the two-liquid phase region in the wetting regime and has been attributed to hydrogen bonding between the methanol molecules (Bonn *et al.*, 1992, 1993).

Since oscillatory density and composition profiles and surface layering have been observed in systems not too unlike our own D_2O + 2-butoxyethanol mixture it seems that our interpretation of the reflectivity profiles in terms of an oscillating composition profile is reasonable. The profile fitted may be an average due to various effects, such as hydrogen bonding and packing. Thus the period of oscillation does not correspond to molecular lengths of the components, although the characteristic sizes are not far from the estimated dimensions of D_2O of 2-3 Å and of 2-butoxyethanol of 9 Å (single extended molecule) or 13 Å (bilayer due to interacting O and OH groups). In long-chain surfactant mixtures water-rich layers have been observed below the surfactant monolayer, see Chapter 1, section 1.4.2, and in nonionic systems near the lower critical endpoint the adsorption behaviour is unusual in that the component of higher surface tension, i.e. the water, is more heavily adsorbed. In our short-chain surfactant mixture the interfacial structure seems to extend over a long range and the oscillating profile may possibly indicate that there is no preferential adsorption of either component.

Reflectivity data were also obtained for the w = 0.25 mixture closer to T_{LCS} and at higher temperatures in the two-phase region, although the exact distance in temperature from T_{LCS} was not known since the phase separation could not be observed directly. With increasing temperature the reflectivity at low Q drops systematically, possibly consistent with critical adsorption and in the two-phase region with the enrichment of the upper phase in 2-butoxyethanol. However, the temperature control at these high temperatures was not good enough to warrant rigorous analysis of the data. Slight changes in temperature close to T_{LCS} can also bring about large changes in the composition. In future work the near-critical region should be revisited and the new aluminium trough should ensure better thermostatting. The surface tension of this

mixture is also large enough that smaller angles of incidence may be possible without clipping the edge of the trough, and may therefore allow the collection of data at lower Q. Preliminary measurements at other compositions of w = 0.27 and w = 0.30 also suggested the presence of surface composition oscillations, but again the temperature control was less than adequate.

5.3.5 Perfluoroalkylalkanes on cyclohexane and perdeuterocyclohexane

The surface activity of the perfluoroalkylalkane (PFAA), perfluorooctyloctane F_8H_8, has been studied in cyclohexane and perdeuterocyclohexane solvents at temperatures in the range 20-30°C. This work was carried out on CRISP in September 1995 and January 1996.

Previously an interpenetrating trilayer of F_8H_8 was observed on cyclohexane and on deuterated cyclohexane (Bowers, 1995; Whitfield, 1996). The aim of the present experiment was to study solutions of increasing concentration in an attempt to observe monolayer and then interpenetrating multilayer formation. A further objective was to investigate the effect, if any, of deuteration of the subphase on the surface structure. However, the results obtained are conflicting and confusing. The main reason for this is believed to be the competing adsorption of the F_8H_8 between the PTFE trough-liquid and the liquid-air interfaces, as discussed below.

During the first experiment in September 1995, increasing amounts of F_8H_8 were added to the cyclohexane while the temperature was low, about 10°C, since this was expected to promote surface adsorption. After the addition of a total of 800 µl in 200 µl aliquots–yielding an estimated total concentration of 0.08 mol dm^{-3}–no reflectivity was observed above the background level. When the temperature was increased to 25°C and the mixture stirred more thoroughly using the ultrasonic stirrer some non-background reflectivity–attributed to a surface excess of F_8H_8–was observed. With increasing temperature the reflectivity increased and then decreased and was not reproducible on returning to an earlier temperature. At a given temperature, the reflectivity was also not stable but decreased with increasing time signifying non-equilibrium conditions, possibly due to drainage of the F_8H_8 from the interface. When 800 µl of F_8H_8 was added to deuterated cyclohexane at 22.5°C, no surface activity was observed. This is not believed to be due to an isotope effect, but rather to the competing adsorption and non-equilibrium conditions.

A similar experiment was carried out during the second allocation of beamtime in January 1996, but this time the 200 µl aliquots were added while the temperature was at 25°C. When 800 µl had been added no reflectivity was observed, in contrast to the previous experiment with the same concentration and at the same temperature. On decreasing the temperature to 20°C some low reflectivity was detected. At 30°C the reflectivity remained low, but on decreasing the temperature to 25°C, and then further to

20°C, any F_8H_8 at the surface disappeared. On removing the lid of the cell and scraping the bottom of the trough with a pipette, some low reflectivity above background was again measured at 20°C.

The data from both experiments were crudely fitted using a single-layer model. The thicknesses and scattering length densities were allowed to vary freely since fixing one of them to allow a direct comparison between measurements led to poor fits. The scattering length density of the substrate was fixed at the value for pure cyclohexane, Nb = -0.028×10^{-5} Å^{-2}, although an increase to allow for any dissolved F_8H_8 did not greatly alter the fitted values or the quality of the fit. The F_8H_8 is estimated to have Nb = 0.2×10^{-5} Å^{-2}. For the first experiment the results can also be modelled by an interpenetrating trilayer model, but the quality of the data do not promote such rigorous fitting. The results are shown in Tables 5.12 and 5.13.

Table 5.12: Details of fitting using a one-layer model to the reflectivity data for F_8H_8 on cyclohexane obtained in *September 1995*. The bulk scattering length density is fixed at the value for cyclohexane, Nb = -0.028×10^{-5} Å^{-2}. The roughness are zero and the background level is 0.6×10^{-5}.

order of experiments	T /°C	thickness of layer /Å	10^5Nb layer /Å^{-2}	χ^2
5	20	40.1	0.051	2.9
2	22.5	31.8	0.113	4.4
1	25	35.1	0.124	2.4
3	27.5	31.3	0.150	2.1
4	30	32.1	0.110	3.0

Table 5.13: Details of fitting using a one-layer model to the reflectivity data for F_8H_8 on cyclohexane obtained in *January 1996*. The bulk scattering length density is fixed at the value for cyclohexane, Nb = -0.028×10^{-5} Å^{-2}. The roughness are zero and the background level is 0.6×10^{-5}.

order of experiments	T /°C	thickness of layer /Å	10^5Nb layer /Å^{-2}	χ^2
1	20	39.4	0.053	1.3
6	20	28.3	0.030	1.1
2	25	33.7	0.080	1.2
3	25	29.1	0.065	1.3
4	30	28.2	0.086	0.9
5	30	31.6	0.053	1.9

In summary, some surface activity of F_8H_8 on cyclohexane has been observed. However, any detailed analyses of structure and the effects of concentration and temperature were complicated by competitive adsorption at the PTFE-liquid and liquid-air interfaces. A new gold-sputtered aluminium trough has been built for future experiments and it is hoped that a stable liquid-vapour interface will be formed since the metal should not promote adsorption of the PFAA and should aid in attaining thermal equilibrium. If this can be achieved there is much scope for further studies on this system and those of other PFAAs in both hydrogenated and perdeuterated solvents. The surface structures of PFAAs of differing alkyl and perfluoroalkyl chain lengths can also be compared in pure and mixed alkane and perfluoroalkane solvents to investigate the nature of the surfactancy in these systems.

5.4 Summary

The liquid-vapour interface of various binary mixtures has been studied in the vicinity of their critical endpoints by specular neutron reflection. In hexane + perfluorohexane the surface structure is modelled by a macroscopic perfluorohexane-rich subphase capped close to the critical point–in both the one-phase and two-phase regions–by a monolayer of perfluorohexane. In a related alkane + perfluoroalkane mixture, MCH + PFMCH, although the reflectivity can be modelled in a similar way to hexane + perfluorohexane, it is possibly best modelled by a PFMCH-rich subphase, capped close to the critical point by three layers of alternating high and low scattering length densities. In hexamethyldisiloxane + perfluorohexane a damped oscillatory interfacial composition profile of three or four layers with a range of around 40 Å is again observed on the bulk subphase in one-phase mixtures or on a perfluorohexane-rich wetting layer in two-phase mixtures. In deuterium oxide + 2-butoxyethanol, the oscillating composition profile decays to the bulk composition over a much longer range, about 150-200 Å, and ten layers are required to describe the reflectivity.

These complex structures were unexpected in our relatively simple mixtures and deserve future investigation. The surface structures due to the presence of wetting layers and critically adsorbed components remain to be elucidated from the non-critical effects.

The surface activity of the PFAA F_8H_8 has also been investigated in cyclohexane. Both this system and the near-critical binary mixtures should benefit from further study using the new gold-sputtered aluminium trough.

CHAPTER 6: TERNARY MIXTURES

6.1 Introduction

The earlier sections of this thesis have been devoted to the rheological and interfacial properties of binary liquid mixtures near critical endpoints. However, most substances encountered contain many components. In this chapter the phase behaviour of simple ternary mixtures, in which two of the components are related in one way or another, is addressed. This is the first part of what should be a more extensive modern study of ternary mixtures, both to determine the phase behaviour and to investigate the near-critical properties. It is hoped that this may bring the study of more complex multicomponent mixtures, such as microemulsions, into the same framework that is used for normal binary mixtures.

The work presented in this chapter on a series of three ternary mixtures exhibiting tunnel phase behaviour has been published or submitted for publication in *J. Chem. Soc. Faraday Trans.* These narratives describe the entire range of investigation and are included here in their completed forms. The three mixtures are (i) cyclohexane + perdeuterocyclohexane + perfluorohexane, (ii) hexane + decane + propanenitrile, and (iii) hexane + hexamethyldisiloxane + perfluorohexane. The general common feature of these mixtures is that they all comprise two components A' and A" which are fully miscible within the considered temperature range but display partial miscibility with the third component B exhibiting binary upper critical endpoints. Each mixture has been studied experimentally by measuring phase separation temperatures both for the binary mixtures and for ternary mixtures whose compositions lie along quasibinary slices passing through the B vertex. The phase behaviour of mixture (iii) has also been studied theoretically using SAFT-HS theory.

Although sharing common characteristics, the molecular reasons for determining the observed phase behaviour are very different in each case. Mixture (i) is of interest for our neutron reflectivity studies in relation to the deuteration of mixture components. The alkanes in mixture (ii) were chosen so that the binary upper critical solution temperatures T_{UCS} were separated in temperature, but still within an easily accessible temperature range, thus hopefully to yield a 'regular' ternary mixture. The components of mixture (iii) were selected because the two binary T_{UCS} are within 1 K; the aim of this study was to determine the detailed shape of the two-phase region experimentally and so to describe it accurately theoretically.

Thermodynamics of ternary mixtures exhibiting tunnel phase behaviour

Part 1.–Cyclohexane–perdeuterocyclohexane–perfluorohexane

Hannah K. Batchelor, Patricia J. Clements and Ian A. McLure*
Department of Chemistry, The University, Sheffield, S3 7HF, UK

The liquid-liquid phase separation temperatures T_{sep} for the binary mixtures cyclohexane or perdeuterocyclohexane–perfluorohexane and for the ternary mixture (equivolume cyclohexane-perdeuterocyclohexane)–perfluorohexane have been determined by visual observation. Perdeuteration of cyclohexane lowers the upper critical solution temperature T_{UCS} from 346.16 K to 337.69 K but the shape of the phase diagram in terms of the Wegner extended scaling series is unaltered. In contrast, although the maximum separation temperature of the ternary mixture $T_{sep,\,max}$ is little different from T_{UCS} of cyclohexane-perfluorohexane, the shape of the T_{sep} *versus* perfluorohexane mole fraction curve is substantially different. The results cast some doubt on the assumption that the thermodynamics of a solution, and hence the surface structure, in a contrast-matched solvent in reflectivity measurement is the same as would be obtained in the pure solvent.

1. Introduction

Partly because the theory of binary liquid mixtures has reached a plateau of maturity and partly because the majority of straightforward binary liquid mixtures have been studied experimentally, there has been a renaissance of interest in the precise study of the thermodynamics of ternary mixtures.[1] Most of this effort has been focused on the traditional area of liquid-liquid phase equilibria although, increasingly, attention is being paid to the measurement and analysis of excess properties.[2] The great disparity in nature of the components of many of the mixtures which have been studied–and the consequent complexity of their liquid-liquid phase diagrams–suggests that there is little hope of a satisfactory general theoretical resolution of their behaviour in the foreseeable future. Nevertheless, the intrinsic interest of these systems and their obvious practical applications, notably in the rich phase behaviour of oil-water-surfactant mixtures,[3] make all the more important the understanding of relatively simple three-component mixtures as a contribution towards the understanding of the more complex mixtures.

One approach to the effective study of simple three-component mixtures is the study of ternary mixtures in which two of the components are chemically related in one way or another, e.g. mixtures of an *n*-alkanenitrile with two *n*-alkanes. This simplification offers advantages similar to those obtained for binary mixtures through the study of unihomologous mixtures, i.e. mixtures of chain molecules drawn from the same homologous series, e.g. mixtures of two *n*-alkanes. This approach has been used in the past to generate a quasi-binary mixture in which one 'component'–although actually a mixture of two substances–is used in place of a hypothetical substance possessing one or more desirable properties[4]. One further advantage of this ability to 'tune' component properties is the opportunity in the study of critical phenomena to study the transition from true binary mixtures to true ternary mixtures and, in particular, the effect of renormalization of critical exponents.[5]

The simplest kind of three-component phase diagram exhibiting liquid-liquid phase separation is of the type A'-A"-B, where A' and A" are sufficiently chemically related in the sense indicated above to be totally

miscible within the temperature range considered but each exhibits partial miscibility with B forming binary upper critical endpoints (UCEP) at upper critical solution temperatures T_{UCS}' and T_{UCS}'', respectively.

At any temperature between T_{UCS}' and T_{UCS}'' such mixtures show an isothermal phase diagram characterised by a plait point, the ternary analogue of a binary critical point. The full temperature-composition phase diagrams are conveniently represented by a right triangular prism with temperature represented by the long axis and in which the binary partial miscibility gaps are represented on two faces of the prism. In many cases there is a locus of plait points at temperatures between T_{UCS}' and T_{UCS}'' and at lower temperatures there is a region of partial miscibility extending between the A'-B and the A"-B binary miscibility gaps. This region we term a tunnel of immiscibility and ternary mixtures which display it we term tunnel mixtures.

The nature of the chemical similarity necessary for the designation of tunnel behaviour can take several forms. The three forms discussed in this paper and its immediate successors are:

1. Isotopomerism–in which chemically identical substances differ only by the complete substitution of all of one kind of constituent atom by an isotopically different atom, usually D for H. Mixtures of such species alone have been termed nuclidic mixtures.[6]
2. Homologously related substances–e.g. members of the same series differing only in chain length or ring size.
3. Perhaps, least obviously, substances which are congruent in terms of the near-equality of their corresponding-states reduction factors which results in their sharing reduced temperature and pressure at any actual temperature and pressure and behaving in essentially similar fashion in many theories of mixtures, e.g. *n*-hexane-hexamethyldisiloxane.

Here we concentrate on A'-A"-B mixtures of the first kind in which A' is cyclohexane, A" is perdeuterocyclohexane and B is perfluorohexane. Apart from the intrinsic interest of such mixtures, there is a special reason that drew us first to their study, and that is the use of the nuclidic mixture cyclohexane-perdeuterocyclohexane as a mixed solvent in neutron reflectivity. In neutron reflectivity measurements a common technique, particularly in the study of aqueous solutions of surfactants,[7] is the employment of a mixed solvent of isotopomers of such a composition that the effective average scattering length density is zero.

Since the proton and deuteron scattering lengths are of opposite sign, a H_2O-D_2O mixture containing 8.1 mol % of the latter forms a contrast-matched solvent. In a neutron reflection experiment on a surfactant dissolved in this mixed solvent the neutron beam is therefore essentially indifferent to the solvent and the observed reflectivity records the surface structure only. It is implicit in this technique that the surface structure is unaffected by the isotopic composition of the solvent and that the structure of the surfactant layer on pure water can be inferred confidently from the structure determined for a layer on contrast-matched water. In effect this also amounts to the assumption that the thermodynamics of the system is unaffected by the isotopic composition of the 'mixed' solvent. Outside the field of aqueous solution chemistry, e.g. in polymer solutions and melts[8,9] and in mixtures of very small molecules,[10] this assumption is known to be unsafe and a rich literature exists describing the thermodynamics of 'isotope effects' in nuclidic mixtures.

The secondary motivation for undertaking this study was therefore to explore the thermodynamic consequences of employing a contrast-matched cyclohexane-perdeuterocyclohexane mixture in neutron reflectivity studies of wetting in near-critical alkane-perfluoroalkane mixtures and of perfluoroalkylalkanes in alkanes or perfluoroalkanes. The mole fraction of c-C_6D_{12} in the contrast-matched c-C_6H_{12}-c-C_6D_{12} is 3.9%, rather smaller than the analogous figure for H_2O-D_2O, 8.1%. In the event a contrast-matched solvent was not needed since the contrast available with pure cyclohexane as the solvent was satisfactory for modelling purposes. As will emerge, the thermodynamics of the ternary contrast-matched mixture with perfluorohexane, at least insofar as this is typified by $T_{sep,max}$, is relatively little different from that of pure cyclohexane-perfluorohexane. By contrast, however, the thermodynamics as expressed by T_{UCS}' of the cyclohexane–perfluorohexane mixture is significantly affected by greater proportions of deuterated isotopomer than in the contrast-matched mixture. This finding signalled the need for exercising care to allow for variations in component isotopic content in near-critical point studies.

This paper describes the outcome of an investigation into the liquid-liquid phase behaviour of the two binary mixtures cyclohexane–perfluorohexane and perdeuterocyclohexane–perfluorohexane and of the tunnel ternary mixture comprising a mixed solvent containing equal volumes, and coincidentally near-equal moles, of cyclohexane and perdeuterocyclohexane with perfluorohexane as the third component. This work formed part of a study of ternary mixtures ongoing in this laboratory.

2. Experimental

Materials

The cyclohexane was HPLC grade supplied by Aldrich with a stated purity of 99.7 mol%; the perdeuterocyclohexane was supplied by Eurisotop with a stated purity of 99.7 mol%; the perfluorohexane was supplied by Fluorochem with a stated purity of 99 mol%. All materials were used as supplied.

Procedure

Mixtures were made up by mass in sealed vessels containing approximately 2 cm^3 samples immersed in a small Silicone oil-filled thermostat bath. Ternary mixtures were made up from an equivolume stock mixture of c-C_6H_{12}–cC_6D_{12}. The temperatures of liquid-liquid phase separation were determined using a calibrated platinum resistance thermometer as the temperature was cycled slowly up and down around the point of phase separation. The temperature of phase *separation* T_{sep} rather than that of single-phase *reappearance* was recorded since it was the more reproducible. The mole fraction was determined to ± 0.0001 and T_{sep} to ± 0.01 K; the accuracy is probably no better than 0.05 K. The T_{sep} of ternary mixtures were more difficult to observe and for them the uncertainty is probably closer to ± 0.1 K.

3. Results

The liquid-liquid separation temperatures T_{sep} for mixtures of known mole fraction x and volume fraction ϕ are recorded in Table 1; throughout the paper the composition variable refers to perfluorohexane. The densities used to calculate ϕ from x are given in Table 2.

The results are shown in Figure 1 in which the projection of the ternary mixture is matched to the binary phase diagrams. The (T_{sep} + ϕ) results were fitted to expressions of the form:

$$\phi_{\pm} = \phi_C + [C\varepsilon + C_1\varepsilon^{\psi} + C_2\varepsilon^{\psi} + \Delta_1 + \ldots] \pm {}^1/_2[B\varepsilon^{\beta} + B_1\varepsilon^{\beta+\Delta_1} + B_2\varepsilon^{\beta+2\Delta_1} + \ldots] \quad (1)$$

where the $\phi_{\pm}$ are compositions on either side of the critical composition ϕ_c, the C_i are the diameter amplitudes, ψ is the critical index for the diameter $(\phi_+ + \phi_-)/2$, the B_i are the amplitudes for the order parameter $(\phi_+ - \phi_-)$, β is the order-parameter critical index and Δ_1 is the Wegner gap exponent for the order parameter. The Renormalization Group values for the critical indices were adopted: $\beta = 0.325$, $\psi = 1 - \alpha = 0.89$ and $\Delta_1 = 0.5$.[11]The fitting was carried out using a pre-optimised value for T_c. The results of the fitting routine are listed in Table 3.

The full form of fitting expression offered in equation (1) is usually only required for extensive sets of (T_{sep} - ϕ) results. Our data were not collected for the purpose of a stringent test of the form of this equation, particularly in relation to the need *inter alia* for a critical anomaly term in the diameter and the identification of the correct index or to the number of Wegner correction terms needed in the off-critical region, and so are limited in amount and precision. It is therefore not too surprising that only the first B and C terms were required for a satisfactory representation of our results. This judgment was reached on the basis of a consideration of the behaviour of the reduced χ^2 as the number of coefficients was increased. The maximum value of ε is around 0.1 and it is mildly unexpected that over such a large range of temperature away from T_{UCS} so few fitting constants and no Wegner terms are required to represent our liquid-liquid coexistence curve results.

4. Discussion

Binary mixtures

Fig. 1 shows the liquid-liquid coexistence curves for the two binary mixtures in terms of T_{sep} *versus* mole fraction x of perfluorohexane and Fig. 2 the same information in the volume fraction ϕ representation. The most striking features are the substantial difference in the upper critical solution temperatures T_{UCS}(c-C_6H_{12}–C_6F_{14}) = 346.16 K and T_{UCS}(c-C_6D_{12}-C_6F_{14}) = 337.69 K, a drop of 8.5 K, and the close similarity of the critical mole fractions: x_c = 0.3234 and 0.3195, respectively, (ratio = 1.012), and ϕ_c = 0.4505 and 0.4620, respectively, (ratio = 0.9751). Within the experimental error of the results and the uncertainties in the fitting procedure occasioned by different numbers and distribution patterns over composition of the data points these values for x_c and ϕ_c can be regarded as equal.

Figs. 1 and 2 also show the diameters–$(x_+ + x_-)/2$ and $(\phi_+ + \phi_-)/2$, where the subscript + refers to points richer and the subscript - to mixtures poorer in perfluorohexane than the critical mixture–calculated from the fitting expression (1). The similarity of the slopes of the diameters, especially for the volume fraction representation of the coexistence curve is clear. We shall return below to the molecular basis for these similarities and differences.

The shape of the curves is very similar and is perhaps best represented in Fig. 3 and 4 in which, following Munson,[12] we portray the results of the liquid-liquid coexistence curve in terms of a reduced temperature T_{sep}/T_{UCS} *versus* x and ϕ, respectively. It is clear that the coexistence curves are very well mapped indeed, as is confirmed by the similar values of the amplitudes B and C in Table 3. It is particularly striking that the coexistence curves, the diameters, and the critical compositions are essentially identical within experimental error. This degree of congruence lends agreeable confidence to the quality of the observations.

Figs. 1-4 illustrate the well known improvement in symmetry of the liquid-liquid coexistence curves for alkane-perfluoroalkane mixtures when displayed in terms of volume fractions rather than mole fractions. It is helpful to recall that symmetry in this case has the alternative meaning of either a critical composition close to 0.5 in whatever composition variables seem appropriate or a diameter that is parallel to the temperature axis. It is apparent from Figs. 3 and 4 that the volume fraction representation is the more symmetrical in both senses.

Ternary mixtures

Fig. 5 shows upper critical solution temperatures T_{UCS} for cyclohexane-perfluorohexane and perdeuterocyclohexane-perfluorohexane and the maximum phase separation temperature $T_{sep,max}$ for the ternary mixture as a function of the cyclohexane mole fraction x(c-C_6H_{12}) in the cyclohexane-perdeuterocyclohexane solvent. It is clear that the locus of the line through these points is not linear. Since it is not obvious without more investigation than we have undertaken that $T_{sep,max}$ is a critical point, this finding calls for no immediate explanation.

The results for the ternary mixture are shown as $T_{sep}/T_{sep,max}$ along with those for the binary mixtures as T_{sep}/T_{UCS} in Figs. 6 and 7 as functions of x and ϕ, respectively. It is important to be aware that the ternary T_{sep}/T_{UCS} diagram differs significantly from the superficially different binary coexistence curves. The difference arises from the fact that there is no sense in which the two limbs of the curve for the quasi-binary ternary mixture actually bear any canonical relationship to one another, i.e. no two points at any given temperature necessarily represent mutually coexisting phases. An alternative way of saying this is to say that the tie line linking coexisting-phase compositions at a given temperature need not lie on the plane of constant x(c-C_6H_{12})/x(c-C_6D_{12}) in the (T - x' - x") representation. It is therefore unsurprising that the shape of the quasi-binary T_{sep} *versus* composition curves, though necessarily casually similar, is quite different to that of either of the binary mixture coexistence curves and this is explored below.

Molecular thermodynamics of isotopomeric mixtures

Deviations from ideality in liquid mixtures varies from the relatively small to the relatively large. The former arise from minor differences between the unlike molecules and mixtures of such molecules almost never exhibit liquid-liquid phase separation. In the field of isotopomer mixtures they are well represented by nuclidic mixtures in which the deviations arise entirely from differences in isotopic content in otherwise identical molecules. The latter arise from major differences in molecular interactions, size and shape, and if

the deviations are positive and large enough partial miscibility may be exhibited at some temperatures within the liquid range. In the field of isotopomer mixtures the effects of difference in isotopic composition is usually a relatively minor contribution to the overall thermodynamics; the title mixtures in this paper fall into this category.

The kinds of isotope effect which have been displayed in mixtures can be classified into the following categories and subcategories:

1. Mixtures in which isotope exchange between the components is important.
2. Mixtures in which hydrogen bonding is an important contribution to the observed thermodynamics, and in which the replacement of protons by deuterons is therefore the key process. This group can be advantageously further subclassified:
   (i) Mixtures in which the pivotal hydrogen bonding occurs between like species of either or both mixture components.
   (ii) Mixtures in which the pivotal hydrogen bonding occurs between the unlike components of the mixture.
3. Mixtures in which there is no isotope effect associated with hydrogen bonding. This class is also further subclassified:
   (i) Nuclidic mixtures in which the only difference between the unlike components is their isotopic content.
   (ii) Mixtures in which hydrogen bonding dominates the observed thermodynamics but in which the isotopic substitution falls on non-hydrogen-bonded sites.
   (iii) Alkane-perfluoroalkane mixtures with which this paper is concerned.

The mixtures discussed here fall into category 3(iii) but to understand their behaviour a brief context-setting review of the behaviour of the other classes, restricted for now to binary mixtures, would seem useful. For simplicity and in keeping with the discussion of the results forming the new material of this paper, we restrict the discussion for the most part to mixtures sufficiently nonideal as to exhibit partial miscibility with liquid-liquid coexistence disappearing in the presence of the coexisting vapour phase at either an upper critical endpoint, UCEP, or a lower critical endpoint, LCEP.

1. Mixtures in which isotope exchange between the components is important.

In mixtures of this kind, e.g. $H_2O + D_2O$, the equilibrium mixture contains more components than the initial mixture. Woermann *et al.* have made a particularly elegant study of hydrogen-deuterium exchange on liquid-liquid phase equilibrium in this kind of mixture.[13] The theory of such mixtures has been successfully developed by Bigeleisen.[14] Since the cause of the isotope effect is in the first instance unrelated to differences in interaction they all fall outside the scope of this paper and are discussed no further.

2. Mixtures in which hydrogen bonding is important

This is a fairly well-tilled field. Seemingly, the earliest work was that of Hall *et al.* [15] on the liquid-liquid phase equilibria of H_2O–phenol and H_2O–nicotine. Somewhat later this was followed by the work of Carlson on the phase equilibria of water-triethylamine with a view to separating D_2O and H_2O.[16] More recently still, Linderström-Lang carried out a comprehensive study of the isotope effects in the thermodynamics of hydrogen-bonded mixtures.[17] The change in critical solution temperature in hydrogen-bonded mixtures can be large, e.g. $T_{UCS}(H_2O–C_6H_5OH)$ is lower by 13.7 K than $T_{UCS}(D_2O–C_6H_5OD)$.[18] As a preface to a detailed account and in order to partially rationalise the effect of replacing the hydrogen-bonded hydrogen by deuterium in such mixtures it is helpful to recall that the energetic outcome of replacing H by D in a conventional hydrogen bond is primarily to decrease the zero-point energy and hence to strengthen the hydrogen bond.[19] We turn now to the two subclasses.

(i) *Mixtures in which the pivotal hydrogen bonding occurs between like species of either or both mixture components*, for example cyclohexane-methanol. In such mixtures one or both components is relatively strongly self-associated through hydrogen bonding and this leads to partial miscibility. Only when the temperature is increased above the threshold of the upper critical solution temperature, T_{UCS}, is sufficient of this aggregation eliminated to allow full miscibility to occur. Mixtures of water with non-hydrogen-bonded diluent substances and of alcohols with alkanes are the classic examples of this kind. Because the deuterium

bond is stronger than the hydrogen bond; isotopic substitution increases the hydrogen-bonding contribution to like component cohesion and so more kinetic energy–and a higher T_{UCS}–is required to bring about complete miscibility. In short, therefore, deuteration lowers the mutual solubility, or, equivalently, makes water a worse solvent, and so raises T_{UCS}. The quantitative effect is expressed by the simple rule: the replacement by D of each H involved in hydrogen bonding increases T_{UCS} by about 1.2 K.[20]

(ii) *Mixtures in which the pivotal hydrogen bonding occurs between the unlike components of the mixture.* Mixtures of this kind rarely exhibit liquid-liquid phase separation from this cause alone since it tends to promote rather than hamper mixing. However, if accompanied by self-hydrogen bonding in one of the components liquid-liquid phase separation can occur; e.g. in mixtures of polyamines or polyethers with water. At low temperatures the unlike hydrogen bonding promotes mixing and complete miscibility is common despite the existence of extensive water self-association. As the temperature rises, both kinds of hydrogen bond are broken but to different extents until above a threshold temperature, known as a lower critical solution temperature, T_{LCS}, the mixing tendency of the unlike hydrogen bonding becomes insufficient to stabilise complete mixing and the mixture separates into a water-rich and a water-poor phase. Most attention in this kind of mixture has been focused on replacing H_2O by D_2O. Using the logic based on the greater strength of the deuterium bond set out above, it might be expected that the outcome of deuteration would be to raise T_{LCS} since more energy is required to break the unlike hydrogen bond. In reality, however, the reverse is usually observed in that T_{LCS} falls and from this it can be deduced that the greater strength of the D_2O-D_2O hydrogen bond, which favours demixing, is dominant. In short, therefore, deuteration again lowers the mutual solubility or makes the water a worse solvent, and so at an LCEP has the effect of *lowering* T_{LCS}.

Apart from polymer-solvent mixtures exhibiting a lower critical endpoint for reasons quite unconnected with these laid out above, many mixtures, certainly all aqueous mixtures, which exhibit an LCEP also exhibit a UCEP unless other kinds of aggregation, such as in aqueous surfactant solutions, intervene or the vapour-liquid coexistence boundary is reached. Mixtures with both an LCEP and a UCEP at a higher temperature are said to exhibit a closed loop; deuteration–usually of the water–in such mixtures reduces the mutual miscibility of the components and therefore lowers T_{LCS} and raises T_{UCS}.

3. Mixtures in which there is no isotope effect associated with hydrogen bonding.

(i) *Nuclidic mixtures in which the components are either simply different isomeric forms of the same element or of substances differing only in the isomeric content.* The study of the thermodynamics of the archetypal nuclidic mixture of this kind–H_2-D_2–was initiated many years ago.[21] A more modern example is the work of Calado *et al.* on the excess functions of CH_4–CD_4.[10]

(ii) *Mixtures in which hydrogen bonding determines the thermodynamics but in which deuteration acts at nonhydrogen bonding centres.* Although there are few examples of mixtures of this kind which exhibit a lower critical endpoint, mixtures exhibiting an upper critical endpoint are much more common, e.g. cyclohexane-methanol.[20] Empirically, it is observed that the outcome of deuteration in such mixtures is to lower T_{UCS} and by lesser amounts per H replaced by D. A common rule states that T_{UCS} drops by around 0.3 K per H replacement.[20,22] These generalisations have been confirmed by Rabinovich and Tsvetkov.[23]

The most persuasive argument to account for isotope effects on the thermodynamics of mixtures free of hydrogen bonding rests on a consideration of the internal part of the partition function, usually neglected in most current molecular theories of liquid mixtures. The general argument has been convincingly made by van Hook and coworkers.[9,24] Its main thrust is that the alteration in the vibration frequency of X-H bonds caused by their transformation into X-D bonds, where X is an atom or molecular fragment, leads to an apparent strengthening of the unlike molecular interaction and hence to an increase in mutual solubility. This would lead to the prediction that deuterating the nonhydrogen-bonded hydrogens of the nonaqueous component of a mixture exhibiting a closed miscibility loop would be to raise T_{LCS} and lower T_{UCS}, the opposite of the effect of replacing H_2O by D_2O; to our knowledge there are no experimental results to check this claim for mixtures exhibiting closed-loop behaviour.

In a rather less persuasive argument treating mixtures like ours in which cyclohexane is replaced by perdeuterocyclohexane, Houessou *et al.* have suggested that since the number density of perdeuterocyclohexane at T = 298.15 K exceeds that of cyclohexane by nearly 0.3% the orbitals in the former

are lower and the polarizability higher than in the undeuterated molecule. These effects they suggest conspire to alter the potential energy of interaction and contribute to the observed changes in the thermodynamics of mixtures containing such molecules which are the subject of this paper.[25]

(iii) *Mixtures of an alkane and a perfluoroalkane*. Mixtures of this kind characteristically exhibit partial miscibility whose cause is now widely attributed, although with little theoretical understanding in terms of its quantum mechanical origin, to a weakness of the unlike molecular interaction compared to that predicted as a geometrical mean of the like interactions of the component as encompassed in the Berthelot rule written in terms of the characteristic energy of interaction ε_{ij} between two molecules i and j as $\varepsilon_{12} = \xi(\varepsilon_{11}\varepsilon_{22})^{0.5}$. For most pairs of unlike nonpolar molecules the correction factor is close to unity but for alkane-perfluoroalkane mixtures ξ is close to 0.9, reflecting a weakness in ε_{12} of around 10%. For mixtures in which one component is polar the same order of unlike weakness is observed but it is false in that the characteristic energy of the polar component includes a polar contribution which is much reduced in the polar-nonpolar interaction. The rule enunciated above for the effect of deuterating nonhydrogen-bonded hydrogens as *reducing* T_{UCS} by about 0.3 K *per* atom when applied to our system would predict a drop of 3.6 K which falls rather short of the 8.5 K actually observed. In this enhanced sensitivity to isotopic substitution, alkane-perfluoroalkane mixtures exhibit another facet of the anomalous thermodynamic behaviour which has attracted so much study over the past forty years. The large magnitude of the effect is partially due to the fact that cyclohexane-perdeuteration in an alkane-perfluoroalkane mixture affects *all* the CH-CF interactions in the mixture rather than only *some* of the segment-segment interactions as in the mixtures used to formulate the 0.3 K rule.

The most obvious explanation of this unexpectedly large isotope effect probably follows the van Hook and Singh argument. However one simple point should be made regarding the interaction of hydrogenous isotopomers. Although the boiling points of nearly all substances go up on deuteration, gas-liquid critical temperatures, T_c, tend to go down. Since boiling points reflect a fairly arbitrary state of vapour pressure equal to one atmosphere and are thus a poorer guide to the strength of intermolecular forces than T_c, these data suggest a weakening of the characteristic energy on deuteration. This is consistent both with the observed greater solubility of deuterated substances in solvents with weaker intermolecular forces and, in turn, with our observations for cyclohexane-perfluorohexane. The argument can be laid out more effectively within the context of the Solubility Parameter Version of the Regular Solution theory to which we now turn.

Solubility parameter and other theoretical treatments

As a guide to the expected thermodynamics of these mixtures appeal can be made to the Solubility Parameter version of the Regular Solution theory of mixtures of Scott and Hildebrand[26] which yields with the Flory-Huggins entropy of mixing the following expression for T_{UCS}:

$$T_{UCS} = 2(\delta_1 - \delta_2)^2[V_1V_2/(V_1^{0.5} + V_2^{0.5})^2]/R, \qquad (2)$$

where δ_1 and V_1 and δ_2 and V_2 are the solubility parameters and molar volumes of components 1 and 2, respectively. The solubility parameters were calculated from the approximate expression:

$$\delta_1 = [(\Delta H_{vap,1} - RT)/V_1]^{0.5}, \qquad (3)$$

where $\Delta H_{vap,1}$ is the molar enthalpy of vaporisation of component 1. The values for the various parameters, all for T = 298.15 K, are listed in Table 2. For consistency the values of ΔH_{vap} were calculated from published vapour pressures[27] using the parameters B and C of the appropriate Antoine equation:

$$\Delta H_{vap} = 2.303RB[T/(t + C)]^2, \qquad (4)$$

where T and t are the temperature in K and °C, respectively. For cyclohexane this procedure produced a ΔH_{vap} acceptably within 1% of that reported by Majer and Svoboda from a careful assessment of enthalpies of vaporisation.[28] It is clear that the effects of perdeuterating cyclohexane are to alter V by no more than 0.3% and δ by no more than 1.2%; these differences are negligible in the present context. Although this theoretical treatment is now regarded as archaic, it is representative of all modern theories in that it takes account of molecular size and volume to some degree. The next elaboration of this primitive theory introduces a factor

ℓ_{12} to take account of the breakdown of the geometric-mean rule for the cross-term δ_{12} inherent in equation (3). In the absence of any guidance of how to calculate this quantity it is pointless to press the theory further. Clearly, however, no current theory of mixtures can readily account for the drop in T_{UCS} observed in cyclohexane-perfluorohexane on perdeuterating the cycloalkane. It may be worth noting, however, that the slightly lower normal boiling point of perdeuterocyclohexane, T_b^o = 78.426°C, indicates slightly weaker intermolecular forces than in cyclohexane, T_b^o = 80.737°C; this is consistent with a slightly lower T_{UCS} for mixtures with the former cycloalkane but scarcely enough to immediately account for the large magnitude of the observed 8.5 K drop in T_{UCS}.

Turning for completeness to the prediction of the critical composition, the expression for the critical mole fraction x_c of perfluorohexane according to the Solubility Parameter version of the Regular Solution theory incorporating a Flory-Huggins entropy of mixing term is given by:

$$[x_c/(1-x_c)] = [V(\text{cyclohexane})/V(\text{perfluorohexane})]^{1.5}. \quad (5)$$

Substituting the values given in Table 2 for the molar volumes leads to a predicted x_c = 0.2825–to be compared to experimental values x_c = 0.3234 for cyclohexane-perfluorohexane and x_c = 0.3195 for perdeuterocyclohexane-perfluorohexane. The predicted critical volume fraction is ϕ_c = 0.4220–to be compared with ϕ_c = 0.4505 for cyclohexane-perfluorohexane and ϕ_c = 0.4620 for perdeuterocyclohexane-perfluorohexane. The experimental x_c exceed the predicted value by 14.3% and the experimental ϕ_c exceed the predicted value by 8%–a smaller margin. The experimental x_c fall closely inside the range predicted by Gilmour, Zwicker, Katz and Scott for an alkane-perfluoroalkane with the $(V_1 - V_2)/(V_1 + V_2)$ ratio of the present mixture.[29] The experimental ϕ_c are also close to the value $\phi_c = 0.428 \pm 0.002$ determined by [12] for a variety of mixtures of isomeric pentanes, hexanes and heptanes with perfluorotributylamine.

5. Conclusions

It seems clear from our results that the isotope effect in cyclohexane-perfluorohexane on changing H to D is more than twice that predicted from previous studies; this will be the object of further study. This result suggests that the usual assumption in reflectivity studies that the surface structure obtained from solutions in a contrast-matched solvent can be taken as identical to that with a pure solvent may bear reexamination. The results on our ternary mixture indicate, in particular, that the ternary tunnel immiscibility gap in the well-defined plane which we have studied is of different topology from the immiscibility gaps of the 'pure' binary mixtures with which it is associated; this casts a warning about arbitrary assumptions about the shape of phase diagrams for ternary mixtures, even those containing two highly similar components. For example, the maximum of the T_{sep} *versus* mixed-solvent composition diagram, whether or not it be regarded as a true critical endpoint, is not a linear function of solvent composition.

References

1 J. Zollweg, *J. Chem. Phys.*, 1971, **55**, 1430.

2 M. T. Lorenzana, E. Jiménez, J. L. Legido, J. Fernández and M. I. Paz-Andrade, *J. Chem. Thermodynamics*, 1993, **25**, 1091.

3 M. Kahlweit, R. Strey, G.Busse, *J. Phys. Chem.*, 1990, **94**, 3881.

4 I. L. Pegg, C. M. Knobler and R. L. Scott, *J. Chem Phys.*, 1990, **92**, 5442.

5 R. L. Scott, *Specialist Periodical Reports of the Chemical Society: Chemical Thermodynamics*, ed. M. L. McGlashan, **2**, Ch. 8, 238, London, 1978.

6 J. C. G. Calado, G. Jancso, J. N. C. Lopez, L. Marko, M. Nunes da Ponte, L. P. N. Rebelo and L. A. K. Staveley, *J. Chem. Phys.*, 1994, **100**, 4582.

7 J. Penfold and R. K. Thomas, *J. Phys.: Condens. Matter*, 1990, **2**, 1369.

8 V. Arroghi, M. L. Fernández and J. S. Higgins, *Science Progress*, 1993/94, **77**, 71.

9 G. Jancso, L. P. N. Rebello and W. A. van Hook, *Chem. Rev.*, 1993, **93**, 2645.

10 J. C. G. Calado, U. K. Deiters, J. N. C. Lopez and L. P. N. Rebello, *Ber. Bunsenges. Phys. Chem.*, 1995, **99**, 721.

11 J. S. Le Guillou and J. Zinn-Justin, *Phys. Rev.*, 1980, **B21**, 3976.

12 M. B. Munson, *J. Phys. Chem.*, 1964, **68**, 796.

13 E. Gulari, B. Chu and D. Woermann, *J. Chem. Phys.*, 1980, **73**, 2480.

14 J. Bigeleisen, *J. Chem. Phys.* , 1977, **67**, 5639 and earlier papers.

15 N. F. Hall, H. R. Wentzel and T. Smith, *J. Am. Chem. Soc.*, 1934, **56**, 1822.

16 C. H. Carlson, *Nuclear Sci. Abs.*, 1956, **10**, 747.

17 C. U. Linderström-Lang, *Acta Chem. Scand.*, 1962, **16**, 1730.

18 E. Schrier, R. J. Loewinger and A. H. Diamond, *J. Phys. Chem.*, 1966, **70**, 586.

19 Y. P. Handa, B. I. Mattingley and D. S. Fenby, *J. Chem. Soc., Faraday Trans.*, 1976, **72**, 1355.

20 W. Schon, D. Woermann and R. Wiechers, *J. Chem. Phys.*, 1986, **85**, 2922.

21 V. N. Grigoriev and N. S. Rudenko, *Zhur. Eksp. Teor. Fiz.*, 1961, **40**, 737.

22 P. Gansen, T. Janssen, W. Schon, D. Woermann and H. Schoenert, *Ber. Bunsenges. Phys. Chem.*, 1980, **84**, 1149.

23 I. B. Rabinovich and V. G. Tsvetkov, *Russ. J. Phys. Chem.*, 1971, **45**, 458.

24 R. R. Singh and W. A. Van Hook, *J. Chem. Phys.*, 1987, **87**, 6097.

25 C. H. Houessou, P. Guenoum, R. Gastand, F. Perrot and D. B. Beysens, *Phys. Rev. A*, 1985, **32**, 1818.

26 *Regular and Related Solutions*, by J. H. Hildebrand, J. M. Prausnitz and R. L. Scott, Van Nostrand Reinhold, New York, 1970, p. 177.

27 *The Vapour Pressures of Pure Substances*, T. Boublík, V. Fried and E. Hála, Elsevier, Amsterdam, 1973.

28 *Enthalpies of Vaporization of Organic Compounds*, V. Majer and V. Svoboda, Chemical Data Series, No 32, ed. H. V. Kehiaian, Blackwells, Oxford, 1985.

29 J. B. Gilmour, J. O. Zwicker, J. Katz and R. L. Scott, *J. Phys. Chem.*, 1967, **71**, 3259.

Table 1 Liquid–liquid phase separation temperatures T_{sep} *vs.* mole fraction x or volume fraction ϕ of C_6F_{14} for various binary or ternary cyclohexane isotopomer + perfluorohexane mixtures

$xc\text{-}C_6H_{12}$–$(1-x)C_6F_{14}$			$xc\text{-}C_6D_{12}$–$(1-x)C_6F_{14}$			$x(0.5c\text{-}C_6D_{12}$–$0.5c\text{-}C_6D_{12})$–$(1-x)C_6F_{14}$		
x	ϕ	T_{sep}/°C	x	ϕ	T_{sep}/°C	x	ϕ	T_{sep}/°C
0.7732	0.8637	35.88	0.8340	0.9035	19.52	0.0615	0.1088	40.51
0.6750	0.7942	53.07	0.6840	0.8014	43.19	0.1072	0.1827	57.36
0.5992	0.7353	60.81	0.5719	0.7134	54.73	0.1812	0.2918	65.84
0.5410	0.6866	66.03	0.4433	0.5974	62.77	0.2708	0.4087	69.30
0.4772	0.6291	69.71	0.3937	0.5475	64.48	0.3044	0.4488	70.67
0.4358	0.5894	71.34	0.3824	0.5357	64.50	0.3443	0.4943	71.41
0.3952	0.5484	72.87	0.3433	0.4934	64.53	0.3901	0.5434	71.52
0.3621	0.5133	73.00	0.2884	0.4303	64.52	0.4418	0.5956	70.92
0.3439	0.4934	72.99	0.2619	0.3981	64.52	0.4676	0.6205	70.74
0.3192	0.4656	72.97	0.2017	0.3201	63.37	0.5406	0.6865	67.23
0.3140	0.4597	72.97	0.1349	0.2251	58.29	0.6794	0.7977	55.73
0.2802	0.4198	72.95	0.0617	0.1092	39.61			
0.2552	0.3891	72.84						
0.2254	0.3510	72.22						
0.1899	0.3034	71.68						
0.1523	0.2503	69.78						
0.1491	0.2457	69.37						
0.1165	0.1968	64.47						
0.0866	0.1498	57.78						
0.0532	0.0946	44.77						

Table 2 Molecular masses M and densities ρ, molar volumes V, polarisabilities α, enthalpies of vaporization ΔH_{vap} and solubility parameters δ at $T = 298.15$ K and polarisabilities α for perfluorohexane, cyclohexane and perdeuterocyclohexane

	M/g mol^{-1}	ρ/g cm^{-3}	V/cm^3 mol^{-1}	α/cm^3 mol^{-1}	ΔH_{vap}/kJ mol^{-1}	δ/J$^{0.5}$ cm$^{-1.5}$
C_6F_{14}	338.05	1.672	202.2	—	32.4	12.2
$c\text{-}C_6H_{12}$	84.16	0.773 54	108.8	6.62	33.3	16.8
$c\text{-}C_6D_{12}$	96.26	0.887 17	108.5	6.55	33.1	16.8

Table 3 Results of fitting the T_{sep} to eqn. (1) for the binary mixtures $c\text{-}C_6H_{12}$–C_6F_{14} and $c\text{-}C_6D_{12}$–C_6F_{14} with $\beta = 0.325$, $\Delta_1 = 0.5$ and $\phi = 0.89$

mixture	T_{UCS}/K	x_c	B_x	C_x	$10^4\ \chi_x^2$	ϕ_c	B_ϕ	C_ϕ	$10^4\ \chi_\phi^2$
$c\text{-}C_6H_{12}$	346.16	0.3234	1.4975	0.7768	2.5	0.4505	1.6790	0.0989	3.5
$c\text{-}C_6D_{12}$	337.69	0.3195	1.5015	0.9060	2.8	0.4620	1.6739	0.0205	4.0

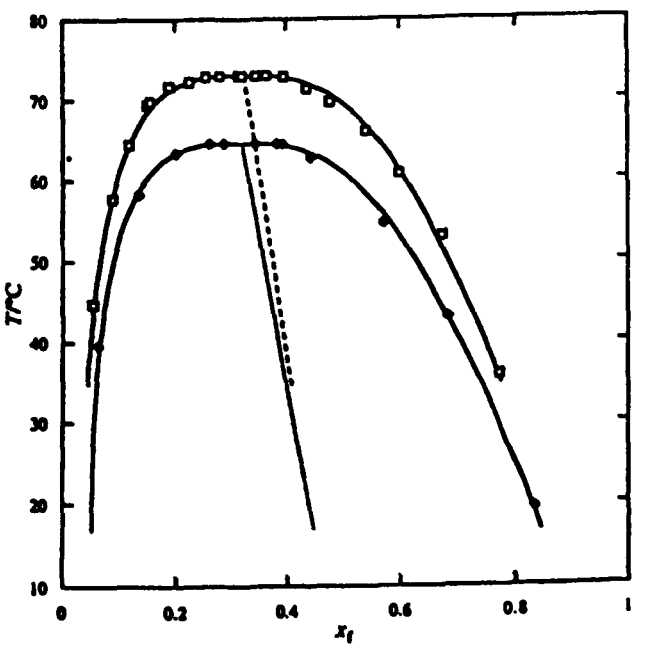

Fig. 1 Liquid–liquid separation temperatures T_{sep} for (□) cyclohexane–perfluorohexane and (◇) perdeuterocyclohexane–perfluorohexane as a function of perfluorohexane mole fraction x_f. The curves and the diameters are drawn according to eqn. (1) with the coefficients shown in Table 3.

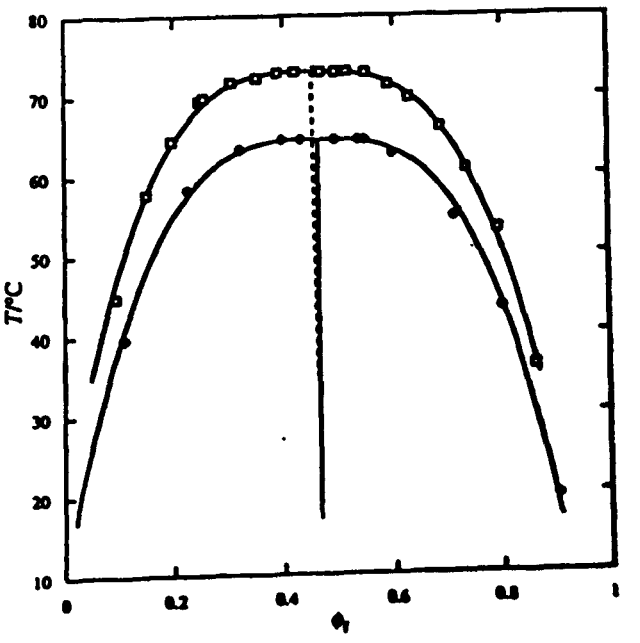

Fig. 2 Liquid–liquid separation temperatures T_{sep} for (□) cyclohexane–perfluorohexane and (◇) perdeuterocyclohexane–perfluorohexane as a function of perfluorohexane volume fraction ϕ_f. The curves and the diameters are drawn according to eqn. (1) with the coefficients shown in Table 3.

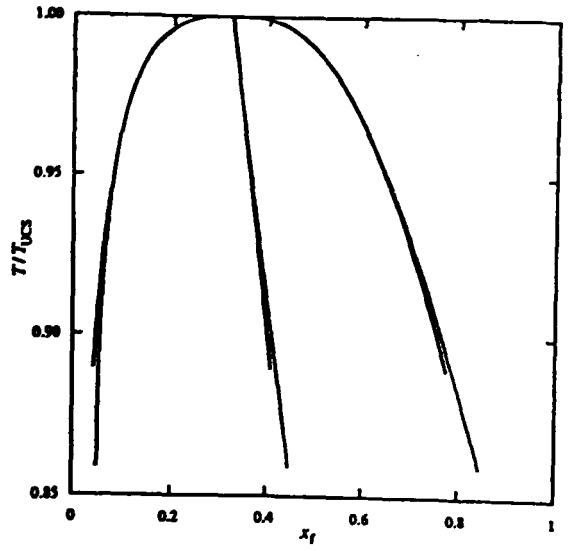

Fig. 3 Reduced liquid–liquid separation temperatures T_{sep}/T_{UCS} for cyclohexane–perfluorohexane (——) and perdeuterocyclohexane–perfluorohexane (···) as a function of perfluorohexane mole fraction x_f. The curves and the diameters are drawn according to eqn. (1) with the coefficients shown in Table 3.

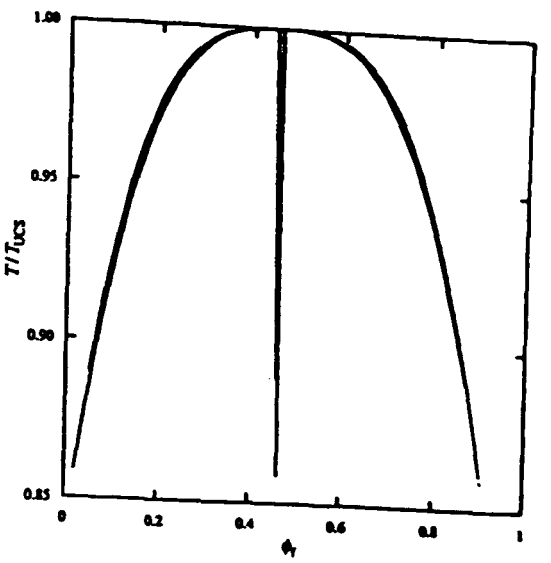

Fig. 4 Reduced liquid–liquid separation temperatures T_{sep}/T_{UCS} for cyclohexane–perfluorohexane (——) and perdeuterocyclohexane–perfluorohexane (···) as a function of perfluorohexane volume fraction ϕ_f. The curves and the diameters are drawn according to eqn. (1) with the coefficients shown in Table 3.

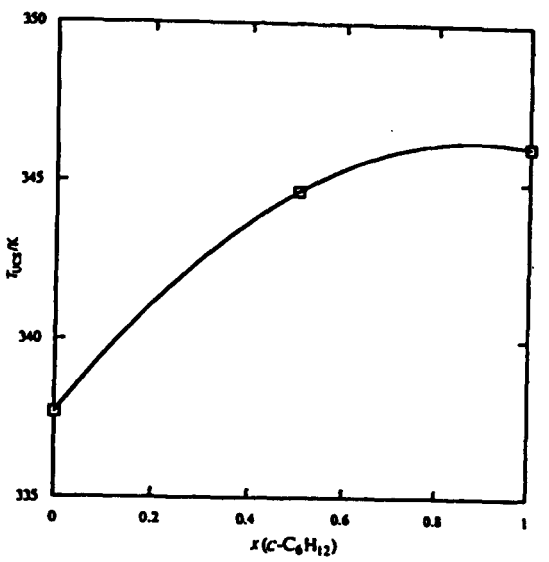

Fig. 5 Upper critical solution temperatures T_{UCS} for cyclohexane–perfluorohexane and perdeuterocyclohexane–perfluorohexane and the maximum phase separation temperature $T_{sep,\,max}$ for the ternary mixture as a function of the cyclohexane mole fraction $x(c\text{-}C_6H_{12})$ in the cyclohexane–perdeuterocyclohexane solvent.

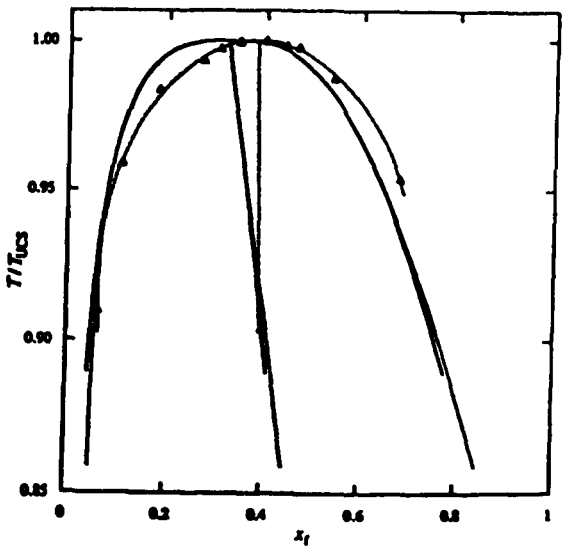

Fig. 6 Reduced liquid–liquid separation temperatures T_{sep}/T_{UCS} for cyclohexane–perfluorohexane (——) and perdeuterocyclohexane–perfluorohexane (···) and for cyclohexane–perdeuterocyclohexane–perfluorohexane with equal volumes of cycloalkane (···Δ···) as a function of perfluorohexane mole fraction x_f. The curves and the diameters for the binary mixtures are drawn according to eqn. (1) with the coefficients shown in Table 3. The analogous lines for the ternary mixture are drawn from similar fits for the purpose of illustration but the coefficients lack the significance attached to those for the binary mixtures and so are not listed.

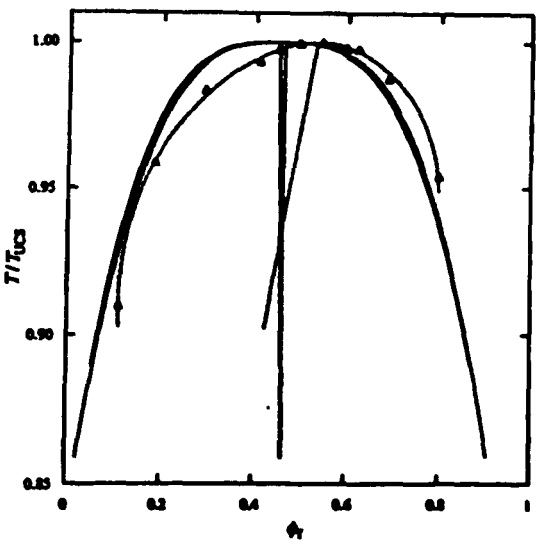

Fig. 7 Reduced liquid–liquid separation temperatures T_{sep}/T_{UCS} for cyclohexane–perfluorohexane (——) and perdeuterocyclohexane–perfluorohexane (···) and for cyclohexane–perdeuterocyclohexane–perfluorohexane with equal volumes of cycloalkane (···Δ···) as a function of perfluorohexane volume fraction ϕ_f. The curves and the diameters for the binary mixtures are drawn according to eqn. (1) with the coefficients shown in Table 3. The analogous lines for the ternary mixture are drawn from similar fits for the purpose of illustration but the coefficients lack the significance attached to those for the binary mixtures and so are not listed.

Thermodynamics of ternary mixtures exhibiting tunnel phase behaviour

Part 2.–*n*-Hexane–*n*-decane–propanenitrile

Patricia J. Clements, Emma Hill and Ian A. McLure*
Department of Chemistry, The University, Sheffield S3 7HF, UK

The shape of the two-liquid-phase coexistence region in the phase prism of the ternary mixture *n*-hexane–*n*-decane–propanenitrile has been determined by measurements of phase-separation temperatures for mixtures in three quasibinary slices each with constant *n*-decane: *n*-hexane volume ratio. These results were used along with the coexistence curve results of Arriaga-Colina, McLure, Clements, and Hill for the binary mixtures *n*-hexane–propanenitrile and *n*-decane–propanenitrile to characterise the topology of the composition-temperature ternary phase diagram. A crude method for the estimation of the tielines for the *n*-decane: *n*-hexane volume ratio = 3:1 quasibinary slice has revealed that they do not lie in the plane of the quasibinary slice. Furthermore, the positions of the tielines change with temperature–tending at higher temperatures to become more parallel to the nearer binary face of the phase diagram.

1. Introduction

This paper is the second in a series dealing with ternary liquid mixtures of the A'–A"–B kind in which the components A' and A" are sufficiently alike in one way or another that the A'–A" binary mixture is essentially ideal and both A' and A" are sufficiently different from B that the A–B binary mixtures exhibit partial miscibility below upper critical solution temperatures T_{UCS}. Ternary mixtures of this kind with A' and A" chosen from the same homologous series are known as pseudo-binary or quasibinary and offer the useful feature that their properties can be 'tuned' by continuously varying the A':A" ratio to meet a particular requirement. As a result, their properties have been have been fairly widely investigated, not least in the study of tricriticality.[1] However, there are other classes of A'–A"–B ternary mixtures in which A' and A", although not homologues, are sufficiently alike that the ternary mixture can still be regarded as quasibinary. Examples of this more limited class of quasibinary mixture are given in this series of reports and they include as A' and A" cyclohexane and perdeuterocyclohexane in our previous paper[2] and *n*-hexane and hexamethyldisiloxane in our next.

Among the most striking of these regularities in behaviour are those in phase relationships. These are conveniently discussed using a three-dimensional (T-ϕ'-ϕ") phase representation–usually employing a right triangular prism–where ϕ' and ϕ" are the compositions, in this report chiefly given as volume fractions, of two of the three components at temperature T. In quasibinary mixtures of the kind studied here, a region of partial miscibility is observed at temperatures below the locus of critical points connecting those of the binary mixtures, T_{UCS}' and T_{UCS}". In the prism representation this region appears as a tunnel extending across the three-component region from the A'–B binary phase diagram to the A"–B binary phase diagram, thus leading to our coining of the term 'tunnel phase behaviour'. Our general purpose is to explore the topology of this tunnel, particularly in ways which take advantage of the comparative simplicity of the (T-ϕ'-ϕ") phase diagram compared to those of ternary diagrams in general. Our motivation is partly the intrinsic interest of this aspect of ternary mixture behaviour but perhaps more important is its bearing on other aspects of ternary behaviour near critical endpoints.

For example, in our first paper we were chiefly concerned with the possible use of cyclohexane–perdeuterocyclohexane as a contrast-matched solvent for neutron reflectivity measurements. Having decided to employ the upper critical solution temperature of these two liquids in binary mixture with perfluorohexane as a convenient guide to the sensitivity of the mixture of cyclohexanes to the isotopomer content and on discovering that there is a substantial isotope effect on the phase diagram of the mixture with perfluorohexane, it seemed natural to determine the broad features and some of the detail of the tunnel part of the phase diagram.

We turn in this paper to another class of quasibinary A'–A"–B mixtures, based on the alkanenitrile–alkane mixtures widely studied in the group.[3] Alkane-alkanenitrile mixtures[4] are usually classed as diluent-strong dipole mixtures and their limited miscibility is associated with the partial disruption of the strong dipolar cohesion in the pure alkanenitrile brought about by the addition of the inert alkane diluent.[5] In these mixtures positive nonideality increases with increasing alkane chain length and decreases rather more sharply, if expressed in terms of T_{UCS}, with increasing alkanenitrile chain length. The properties of the members of the series of mixtures thus can be tuned easily by altering component chain length and so quasibinary mixtures can be devised containing either one alkane and two alkanenitriles of different chain length or two alkanes of different chain length with one alkanenitrile.

Since the properties of the binary mixtures can be more finely tuned in terms of alkane chain length the latter kind of quasibinary mixture was chosen for the present study and the particular mixture chosen was *n*-hexane–*n*-decane–propanenitrile. The binary coexistence curves for *n*-hexane–propanenitrile and *n*-decane–propanenitrile have already been accurately determined by Arriaga Colina *et al.*[6] We were moved to study the phase diagram of the ternary mixture in order to complement measurements of the shear viscosity η near the locus of critical endpoints of the same mixture.[7]

The near-critical behaviour of η for binary mixtures has been reported as a function of temperature for mixtures of critical composition and along both limbs of the liquid-liquid coexistence curve,[8,9,10] and along the critical isotherm.[11] These paths are readily recognised as appropriate for studying criticality in modern terms in binary mixtures. However, it is more difficult to identify in theory the analogous pathway in ternary mixtures and, perhaps, even more difficult in practice to determine it experimentally, certainly not without inordinate expenditure of effort. Nevertheless there have been examples of this kind of study, even for viscosity[12] but not always for simple mixtures.

Quasibinary mixtures exhibiting tunnel phase diagrams offer advantages for straightforward experimental investigation of, say, viscosity, since one can readily determine the viscosity of ternary mixtures formed, in our current terminology, using A'–A"–B mixtures containing A' and A" in fixed proportion, i.e. of quasibinary slices.

A sensible time-economical strategy involves the determination of the viscosity as a function of temperature of a quasibinary slice from above the locus of critical points connecting $T_{UCS'}$ and $T_{UCS"}$ to the two-liquid phase region at lower temperatures in a manner analogous to that for binary mixtures in the studies referenced above. Such investigations of *binary* mixtures carry the simple advantage that at any given temperature the coexisting liquid compositions need not be measured for the purpose of ensuring a well defined approach to the critical endpoint. For *ternary* mixtures this advantage is less marked since, in principle at least, the coexisting compositions should be determined in order to define the approach to the critical endpoint.

The compositions of such mixtures in the one-liquid phase region fall on vertical slices of the (T-ϕ'-$\phi"$) phase diagram that pass through the vertical edge of the phase diagram that represents pure B and in some cases the tielines may fall close to or even on this quasibinary slice. Before assuming that this is the case in any particular mixture and as a guide in choosing mixtures for which it is likely to be true, the following issues entailed in such a procedure need to be addressed.

Among the more important of these issues are the shape and symmetry of the two-phase tunnel, the curvature of the ridge, the location of the tielines, the location of the intersection of the locus of critical points with any particular quasibinary slice and, lastly, the straightforward comparison between the quasibinary slices of the reasonably simple ternary system and the well-documented binary liquid-liquid coexistence

curves of the same mixture near to the locus of critical points. Among other general issues that may need wider investigation are those concerning the renormalisation of the critical indices for ternary mixtures[13] and the appropriate variables for optimising the symmetry, no matter how defined, of the overall phase diagrams and those sections which may be encountered experimentally.

Despite the immense number of ternary mixtures whose phase behaviour has been reported, reckoned in 1971 to be around 4000,[14,15] there has been relatively little systematic work addressing the issues given above. Many of the recent reports deal with the special case of (oil–water–nonionic surfactant) ternary mixtures which form microemulsion phases.[16] Here we are concerned with systems which are simpler both in molecular complexity and in the complexity of the phase diagram.

In phase diagrams containing tunnels of the kind mentioned earlier at temperatures below the lower binary T_{UCS} and in the regions very close to each of the two binary faces showing a miscibility gap, the tielines are closely parallel to the faces of the prism and effectively stem from the B vertex of the isothermal slice of the phase diagram. Tielines for compositions within the tunnel may then be reasonably supposed also to fall on the quasibinary slice at all temperatures and so effectively stack above those below, forming true vertical quasibinary slices projecting from the vertex. However, since the tielines for a partially miscible ternary mixture need not lie, and in practice seem rarely to lie, in the same vertical plane in the triangular prism as the temperature is increased, if the temperature of a mixture with an overall composition falling within the two-phase region is raised, the orientation of the tielines may change. The compositions of the coexisting phases are not then known and a true vertical slice or plane is not being considered.

At temperatures between the binary T_{UCS}' and T_{UCS}'', the two-phase region does not bridge the three-component region but is 'attached' to one face of the prism instead of two. As the tunnel no longer goes right through the prism the tielines may be affected and vertical planes stemming from the vertex may no longer contain the full tielines at the higher temperatures. For these tunnel phase diagrams it is not clear whether the plait points lie at the top of the quasibinary slices projecting from the vertex thus forming a line of plait points along the top of the ridge.

The alternative to the simple situation in which the tielines fall on a quasibinary slice is to determine all the conjugate compositions. It is in part with the aim of avoiding such a tedious measure that the use of tunnel mixtures is willingly embraced in this investigation.

All of the foregoing suggests that the study of A'–A"–B quasibinary mixtures offers advantages for the study of near-critical behaviour in ternary mixtures.

Despite the abundance of information which we should like to garner about the phase diagrams of the title mixture to complement our rheological studies, we are content here to report the outcome of a more modest investigation. Its specific aims were:

1. To determine the liquid-liquid phase-separation temperatures T_{sep} for mixtures of propanenitrile and three alkane stock solutions with the relative volumes at room temperature of *n*-hexane to *n*-decane in the ratios 1:3, 1:1 and 3:1.
2. To attempt to determine if the tielines for these mixtures fall on the corresponding quasibinary slices.
3. To attempt to identify the upper critical solution temperatures for the slices chosen.

2. Experimental

Materials

n-Decane (Aldrich, 99+%), *n*-hexane (Aldrich, 99+%) and propanenitrile (Fluka, >99%) were dried with Molecular Sieves before use.

Procedure

The shape of the two-phase tunnel was determined from measurements of three quasibinary slices in conjunction with the previous results for the two partially miscible true binary mixtures. Stock alkane solutions were weighed out accurately to obtain volume ratios, $V(C_{10}):V(C_6)$ of 1:3, 1:1, and 3:1 and were used to study quasibinary slices by adding propanenitrile. The phase-separation temperatures for samples in sealed Pyrex tubes immersed in a water bath and stirred by means of a glass-coated magnetic follower were

recorded with a calibrated platinum resistance thermometer to a precision of ±0.05 K. Care was taken to ensure that the sample was heated very slowly within *circa* 0.5 K of the phase-separation temperature which was determined visually. Phase-separation temperatures for three compositions close to the critical composition for *n*-hexane–propanenitrile were measured to determine the scaling increment of +0.16 K needed to reconcile the data of Arriaga-Colina *et al.* [6] with our data for this binary slice.

The second part of the investigation involved a crude estimation of the positions of the tielines for the quasibinary slice of $V(C_{10}):V(C_6) = 3:1$. This was undertaken by equilibrating a sample of volume fraction of propanenitrile $\phi = 0.41$ in a cell immersed in a thermostatted water bath and carefully extracting 7-8 portions of the upper phase after thermal and diffusional equilibration. To each weighed portion of extracted upper phase a known mass of propanenitrile was added and the phase-separation temperature of the resulting mixture determined as before. The entire experiment was repeated at three different equilibration temperatures: 8.09, 15.03, and 24.07°C.

If the tielines are in the plane of the ternary slice then the compositions of the coexisting equilibrated phases at each temperature can be determined from the coexistence curve measured previously and the compositions of the samples with added propanenitrile calculated. The temperatures measured for these samples should then agree within a reasonable error margin with those for the same compositions in the coexistence curve. If the separation temperatures do not coincide with the quasibinary coexistence curve then the tielines do not lie in the plane at the chosen temperatures. By considering the overall shape of the tunnel an estimation of the tieline positions can be made. This method of estimating tielines, although not the most accurate, should be sufficient to allow a comparison of the phase-separation temperatures with those already determined. Trial experiments for the binary mixture *n*-decane–propanenitrile showed that the method could be used with reasonable success to explore the orientation of the tielines.

3. Results

The results of the determinations of the liquid-liquid phase-separation temperatures T_{scp} for the three quasibinary slices are given in Table 1. The densities and molar masses used to interconvert measures of composition are listed in Table 2. The T_{scp} *versus* composition results were fitted using CURFIT, the nonlinear least-squares fitting routine of Bevington, [17] to:

$$\phi_{\pm} = \phi_c + C\varepsilon + C_1\varepsilon^{\psi} + C_2\varepsilon^{(\psi+\Delta_1)} \pm 0.5\{B\varepsilon^{\beta} + B_1\varepsilon^{(\beta+\Delta_1)} + B_2\varepsilon^{(\beta+2\Delta_1)} + \dots\} \quad (1)$$

where ϕ is the volume fraction, ϕ_c is the critical volume fraction, $\psi = 0.89$, and $\Delta_1 = 0.5$. The C and B terms are fitting parameters, $\varepsilon = (T_c - T)/T_c$ where T_c is the critical temperature and β is the order-parameter critical exponent and has a value of 0.325 for binary liquid mixtures by *inter alii* Le Guillou and Zinn-Justin[18] and Baker *et alii*.[19] The first set of terms describes the diameter of the curve and the second set forms the order parameter expansion developed by Wegner.[20] The fitting was performed as an exercise in generating smooth curves through the data points and to identify the coordinates of the maxima on the curves–these are listed in Table 3. It was *not* assumed that such points are critical points; the fitting parameters are not quoted but are available. Given that we attached no great significance to their values apart from generating smooth curves, no special care was used to employ the same number of terms in each fit; the slight differences in the shape of the curves may be due to this deliberate neglect.

The experimental T_{sep} points for the three quasibinary slices as a function of the volume fraction of propanenitrile are shown in Fig. 1; the curves are drawn from the outcome of the fitting procedure just described. The results for the quasibinary mixtures and for the constituent partially miscible binary mixtures[6] are shown as fitted curves in Figs. 2 and 3 as functions of the volume fraction and the mole fraction, respectively, of propanenitrile. The points of maximum phase-separation temperature are marked on each curve; in the case of the binary mixtures these are upper critical endpoints.

4. Discussion

General arrangement of the phase diagram

A simple rule for the effect of adding a third component to a partially miscible binary mixture states that the mutual solubility is decreased by addition of a component much more soluble in one of the binary components than the other and increased by the addition of an essentially equally soluble component, i.e. T_{UCS} rises and falls, respectively. This rule applies to the present mixture since T_{UCS} for *n*-hexane-propanenitrile is increased by the addition of *n*-decane which at the lower T_{UCS} is much less soluble in propanenitrile than in *n*-hexane. Similarly, adding the equally miscible *n*-hexane at the higher T_{UCS} for *n*-decane-propanenitrile causes a corresponding *drop* in T_{UCS}.

Quasibinary slices

From Figs. 2 and 3 it can be seen that the quasibinary (T-ϕ) slices, where ϕ is the propanenitrile volume fraction, exhibit simple regularity of shape relatively similar to those for the true binary mixture phase diagrams. The curves are somewhat more symmetrical in volume fraction than in mole fraction.

Fig. 4 shows the maximum temperatures of the curves as a function of decane volume fraction in the *n*-decane–*n*-hexane stock solution. The relationship is all but linear although a statistically significant improvement is obtained using a simple parabola to describe them. The satisfying smoothness of the curve suggests that our measurements bear acceptable precision. The data are well described by expressions of the kind successfully employed to describe real coexistence curves for binary mixtures despite the fact that the maxima of the curves at $T_{sep,max}$ should not be regarded as critical points. This is a little unexpected particularly since no need emerged for renormalised exponents.

The curve-fitting expressions permit an estimate of the composition at the maximum and these are plotted on Fig. 5 as a function of alkane stock solution composition. It is evident that the mole fraction maxima data fall on a much less regular line than do the volume fraction maxima. The results were fitted separately for each composition variable and the difference in regularity may be some small evidence of the 'superiority' of the volume fraction for representing ternary phase diagrams. The scatter also is evidence of the difficulty inherent in obtaining 'critical' compositions from coexistence-curve data even using a well-defined and subjective process of the kind described above. Since the 'critical' composition alters with *n*-decane:*n*-hexane ratio it is apparent that the curves do not form a 'corresponding' set, i.e. they can not be superimposed by representing as reduced 'critical' temperatures, $T_{sep}/T_{sep,max}$ as functions of propanenitrile volume fraction. This is exactly what was found in our earlier study of cyclohexane-perdeuterocyclohexane-perfluorohexane.

Ternary isothermal slices and position of the plait point

The isothermal coexistence curves are shown on Fig. 6. The smooth curves are drawn freehand and not by fitting to an appropriate order-parameter expression. The locus of the maximum phase-separation temperatures is drawn as a full line; it passes through the T_{UCS} of the binaries but it is not coincident with the locus of plait points. Although the maxima of the quasibinary slices should not be regarded as critical or plait points by simple analogy with the maxima of binary coexistence curves, they do have a definable significance on the isothermal coexistence line. This significance is the fact that each isothermal coexistence curve is tangential to the quasibinary slice projection at the maximum temperature point. Accordingly, taking the present diagram as an example, it is clear that all points within the coexistence curve refer to higher phase-separation temperatures than those defining the boundary of the curve itself. Therefore if the plait point does not coincide with the point at $T_{sep,max}$, the quasibinary slice through the plait point must pass through higher temperature regions within the coexistence curve. It follows clearly therefore that in this case, the plait point is not at the maximum in that quasibinary slice (T–ϕ) diagram. Thus we cannot assume that the points of maximum temperature are critical points on the quasibinary slices nor that they are plait points on the isothermal slices. For that reason we refrain from identifying these points as critical points and at the same time are cautious about employing the normal usage of binary mixtures to denominate the coordinates of the maximum on the former as critical temperature and composition.

In order to identify the plait points it would until recently have been deemed necessary to determine the tielines and seek the point at which they collapse to a point. This is the classical time-consuming route to

plait-point identification. The alternative, which we have not so far explored, is to employ the isothermal analogue to our procedure for determining binary coexistence curves and critical point coordinates, i.e. to assume an expression for both the order parameter and for the coexistence curve diameter and then fit all coexistence points, indifferently whether canonical points or not, to an appropriate combined expression in composition. The forms of the analogous curves for isothermal ternary phase diagrams do not appear to have been developed and so we have not thus far pursued this route to establishing the plait point location. Instead we have sought merely to test for coplanarity of the tielines and the quasibinary slices and we now turn to a discussion of the results of our efforts to do so.

Outcome of the tieline mapping

The logic behind our tieline investigation is detailed above. In short, it hangs on the assumption that the tieline is coplanar with a quasibinary slice. If after diluting a known mass of one of the coexisting phases, generated by cooling a mixture of known composition, with a known amount of the B component the coexistence temperature of a known sample coincides with that along the previously known slice 'coexistence' curve then the tieline at the separation sampling temperature is coplanar with the quasibinary slice. If the temperature does not so coincide then the test for coplanarity fails. In the present investigation the separation temperatures were uniformly higher by about one kelvin than expected and thus the test failed. Three conclusions emerge.

The first is that the tielines do not fall on quasibinary slices. Secondly, a simple argument based on the observed increase rather than a decrease quite clearly and unequivocally indicates that at the alkane-rich end of the tieline the mixture contains a higher *n*-decane:*n*-hexane ratio than that of the associated quasibinary slice. It follows therefore since the tieline passes pivotally through the original bulk composition, which coincidentally was in our experiments chosen to be reasonably near the maximum on the quasibinary slice, the other end of the tieline enjoys a lower *n*-decane:*n*-hexane ratio. Thus the tieline is more parallel to the decane-propanenitrile binary edge than to the quasibinary slice. Thirdly, since the discrepancy in temperature between the actual quasibinary slice 'coexistence' curve and the observed dilution curve points is uniform irrespective of the sampling temperature, it appears that the parallelism grows less as the temperature of sampling falls. This is in agreement with naive reasoning which suggests that a given tieline becomes more aligned with quasibinary slices the deeper the tieline lies in the tunnel region, and becomes more parallel to the binary edge the closer it lies to the T_{UCS} of the nearest immiscible binary mixture. These conclusions are illustrated in Fig. 7 which shows the relationship between the orientation of a set of tielines at successively deeper temperatures into the tunnel zone of the phase diagram.

Primitive and rather approximate conservation of mass arguments confirm this general picture, i.e. as the temperature drops the tielines tend to alignment with the quasibinary slices. Thus for the purpose of studying, say, viscosity, the quasibinary slices offer reasonably sensible approximations to coexistence curves but less so towards the maximum.

5. Conclusions

The following conclusions emerge from this investigation:

(1) The ternary phase diagram for the A'-A"-B mixture formed by *n*-hexane–*n*-decane–propanenitrile exhibits straightforward dependence on the *n*-decane:*n*-hexane ratio in quasibinary mixtures, with the maximum temperatures of the quasibinary phase-separation diagrams close to a linear function of that ratio.

(2) The tielines in the three-component region at temperatures well below the locus of critical or plait points tend to become coplanar with the quasibinary slices of fixed *n*-decane:*n*-hexane composition. At temperatures and compositions near the upper critical endpoints of the true binary mixtures they tend to become parallel to the binary edge of the phase diagram.

(3) The plait points do not coincide with the maxima of the quasibinary phase-separation diagrams and so far we have failed to establish the locus of plait points.

1 I. L. Pegg, C. M. Knobler and R. L. Scott, *J. Chem. Phys.*, 1990, **92**, 5442.

2 H. Batchelor, P. J. Clements, I. A. McLure, *J. Chem. Soc. Faraday Trans.*, 1996, **92**, 2255.

3 J.-L. Arriaga-Colina, D. A. Armitage and I. A. McLure, *Fluid Phase Equil.*, in press.

4 I. A. McLure, *Proc. First International Conference on the Thermodynamics of Solutions of Non-Electrolytes*, Santiago de Compostela, 1979.

5 I. A. McLure, A. Trejo Rodriguez, P. A. Ingham and J. F. Steele, *Fluid Phase Equil.*, 1982, **8**, 271.

6 J.-L. Arriaga Colina, I. A. McLure, P. J. Clements and E. Hill, submitted to *Fluid Phase Equil.*

7 P. J. Clements, S. Cooke, I. A. McLure, unpublished measurements.

8 I. A. McLure and I. L. Pegg, *Mol. Phys.*, 1983, **53**, 897.

9 A. O. S. Maczek, M. K. Davies and J. E. C. Jayasuriya, *Ber. Bunsen-Ges. Phys. Chem.*, 1990, **94**, 45.

10 I. A. McLure and P. J. Clements, accepted for publication in *Ber. Bunsen-Ges. Phys. Chem.*

11 A. L. Archer, A. O. S. Maczek and I. A. McLure, unpublished measurements.

12 S. P. Lee and A. J. Purvis, *Chem. Phys.*, 1977, **24**, 191.

13 J. W. Essam and H. Garelick, *Proc. Phys. Soc.*, 1967, **92**, 136.

14 J. Zollweg, *J. Chem. Phys.*, 1971, **55**, 1430.

15 H. Stephen and T. Stephen, (Editors) *Solubilities of Inorganic and Organic Compounds*, Macmillan, New York, 1964, **2**.

16 M. Kahlweit and R. Strey, *Angew. Chem. Int. Ed. Eng.*, 1985, **24**, 654.

17 P. R. Bevington, *Data Reduction and Error Analysis for the Physical Sciences*, McGraw-Hill, New York, 1969.

18 J. C. Le Guillou and J. Zinn-Justin, *Phys. Rev. Lett.*, 1979, **39**, 95.

19 G. A. Baker, B. G. Nickel and D. I. Meiron, *Phys. Rev.*, 1978, **B17**, 1365.

20 F. J. Wegner, *Phys. Rev.*, 1972, **B5**, 4529.

Table 1 Liquid-liquid phase-separation temperatures T_{sep} *vs.* mole fraction x or volume fraction ϕ of propanenitrile for the three quasibinary slices with volume ratios of *n*-decane:*n*-hexane, $V(C_{10}):V(C_6)$, in the *n*-decane-*n*-hexane solvent of 1:3, 1:1, and 3:1.

$V(C_{10}):V(C_6)$ = 1:3			$V(C_{10}):V(C_6)$ = 1:1			$V(C_{10}):V(C_6)$ = 3:1		
x	ϕ	T_{sep}/°C	x	ϕ	T_{sep}/°C	x	ϕ	T_{sep}/°C
0.1839	0.1002	8.16	0.1316	0.0638	3.63	0.1534	0.0685	11.36
0.2455	0.1385	13.20	0.1650	0.0817	10.13	0.2260	0.1060	20.57
0.2829	0.1632	15.37	0.2281	0.1173	16.71	0.2863	0.1400	25.76
0.3351	0.1994	17.18	0.2841	0.1515	20.64	0.3435	0.1751	29.15
0.4015	0.2490	18.52	0.2970	0.1597	21.28	0.3539	0.1818	29.65
0.4389	0.2788	18.90	0.3536	0.1975	23.78	0.4075	0.2182	32.44
0.4833	0.3161	19.22	0.4285	0.2523	25.88	0.4482	0.2479	32.85
0.5113	0.3408	19.27	0.5070	0.3163	26.47	0.5065	0.2940	33.47
0.5316	0.3593	19.30	0.5915	0.3944	26.94	0.5580	0.3387	33.82
0.5606	0.3867	19.33	0.6154	0.4186	27.00	0.6235	0.4019	33.98
0.5665	0.3924	19.32	0.6576	0.4635	26.99	0.6671	0.4485	34.18
0.5943	0.4199	19.44	0.6665	0.4735	26.99	0.6801	0.4632	34.12
0.6011	0.4268	19.41	0.6902	0.5006	26.77	0.7402	0.5362	33.38
0.6032	0.4289	19.41	0.7100	0.5241	26.56	0.7513	0.5508	33.17
0.6222	0.4487	19.31	0.7215	0.5383	26.22	0.7639	0.5676	32.95
0.6481	0.4764	19.13	0.7518	0.5767	25.18	0.8164	0.6434	30.34
0.6773	0.5091	18.51	0.7981	0.6402	22.37	0.8200	0.6490	30.17
0.7066	0.5434	17.95	0.8277	0.6837	19.38	0.8374	0.6764	28.19
0.7443	0.5899	16.25	0.8626	0.7386	14.00	0.8845	0.7566	20.15
0.7918	0.6527	12.57	0.8972	0.7971	6.00	0.9112	0.8063	13.35
0.8341	0.7130	7.08				0.9259	0.8352	7.32

Table 2 Densities ρ, molar masses M, and molar volumes V at T = 298.15 K for *n*-hexane, *n*-decane and propanenitrile

Substance	ρ/g cm^{-3}	M/g mol^{-1}	V/cm^3 mol^{-1}
n-Hexane	0.6549[a]	86.18	131.593
n-Decane	0.7263[b]	142.29	195.911
Propanenitrile	0.7775[c]	55.08	70.842

a American Petroleum Institute, 1953. Project 44.

b R.A. Orwoll and P.J. Flory, *J. Am. Chem. Soc.*, 1967, **89**, 6814.

c R.E. Smith and I.A. McLure, 1978. Unpublished measurements.

Table 3 Maximum phase-separation temperatures $T_{sep,\,max}$ and the corresponding mole fraction x and volume fraction ϕ of propanenitrile in mixtures formed from *n*-decane-*n*-hexane solvent mixtures with volume ratios of *n*-decane:*n*-hexane, $V(C_{10}):V(C_6)$, of 0, 1:3, 1:1, 3:1, and 1. The values were obtained by fitting to equations of the form of eqn. (1).

$V(C_{10}):V(C_6)$	x(propanenitrile)	ϕ(propanenitrile)	$T_{sep,\,max}$ /K	$T_{sep,\,max}$ /°C
0	0.4857	0.3417	284.832	11.682
1:3	0.5594	0.4033	292.485	19.335
1:1	0.6273	0.4313	300.155	27.005
3:1	0.6196	0.4153	307.135	33.985
1	0.6474	0.4084	314.24	41.09

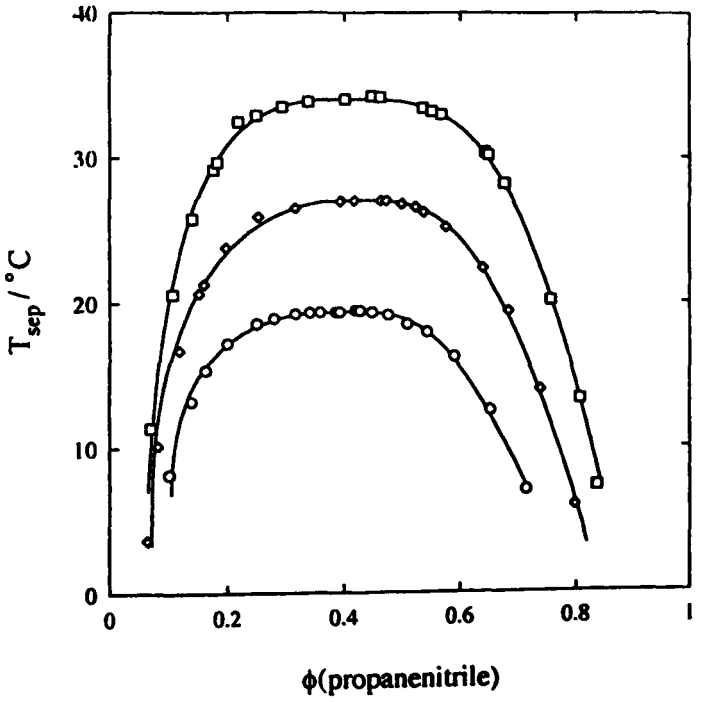

Fig. 1 The experimental phase-separation temperatures T_{sep} for the three quasibinary slices of *n*-hexane–*n*-decane–propanenitrile with volume ratios of *n*-decane:*n*-hexane, $V(C_{10}):V(C_6)$, in the *n*-decane–*n*-hexane solvent of 1:3, 1:1, and 3:1 as a function of propanenitrile volume fraction ϕ. The curves are drawn according to eqn. (1) from top to bottom in diminishing proportion of *n*-decane in the alkane mixture.

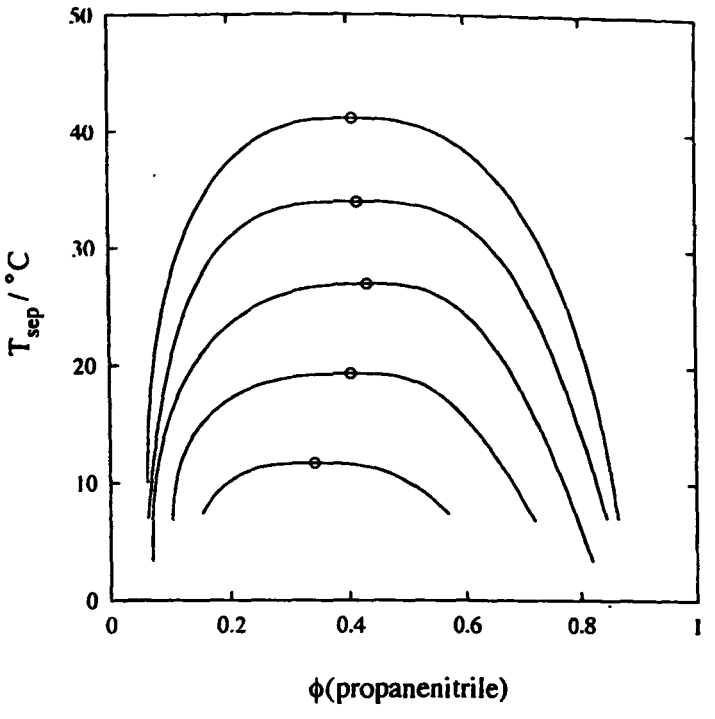

Fig. 2 The phase-separation temperatures T_{sep} for the three quasibinary slices of *n*-hexane–*n*-decane–propanenitrile with volume ratios of *n*-decane:*n*-hexane, $V(C_{10}):V(C_6)$, in the *n*-decane-*n*-hexane solvent of 1:3, 1:1, and 3:1 and the two partially miscible binary coexistence curves for *n*-hexane–propanenitrile and *n*-decane–propanenitrile as a function of the propanenitrile volume fraction ϕ. The curves are drawn from top to bottom in diminishing proportion of *n*-decane in the alkane mixture. The circles represent the maximum temperature $T_{sep,max}$ for each curve.

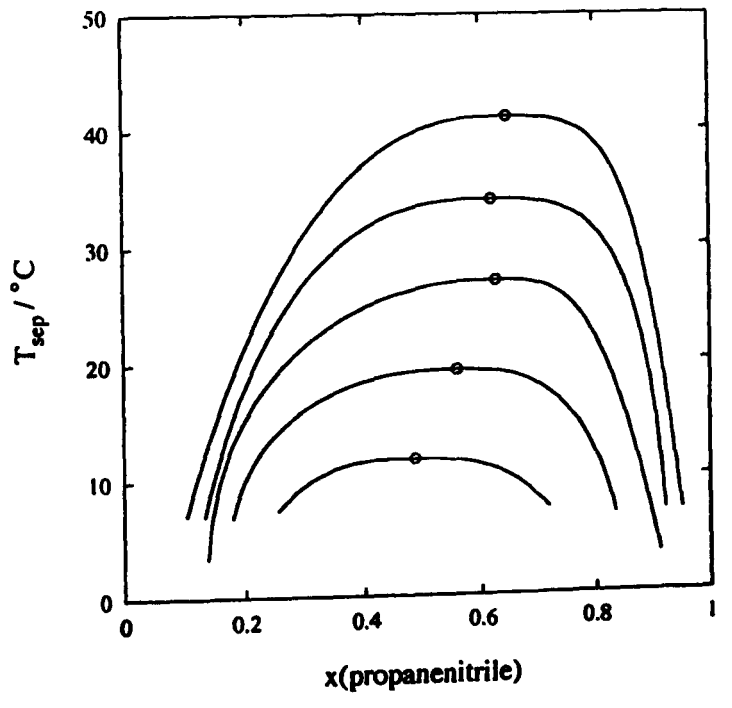

Fig. 3 The phase-separation temperatures T_{sep} for the three quasibinary slices of *n*-hexane–*n*-decane–propanenitrile with volume ratios of *n*-decane:*n*-hexane, $V(C_{10}):V(C_6)$, in the *n*-decane-*n*-hexane solvent of 1:3, 1:1, and 3:1 and the two partially miscible binary coexistence curves for *n*-hexane–propanenitrile and *n*-decane–propanenitrile as a function of propanenitrile mole fraction x. The curves are drawn from top to bottom in diminishing proportion of *n*-decane in the stock alkane mixture. The circles represent the maximum temperature $T_{sep,max}$ for each curve.

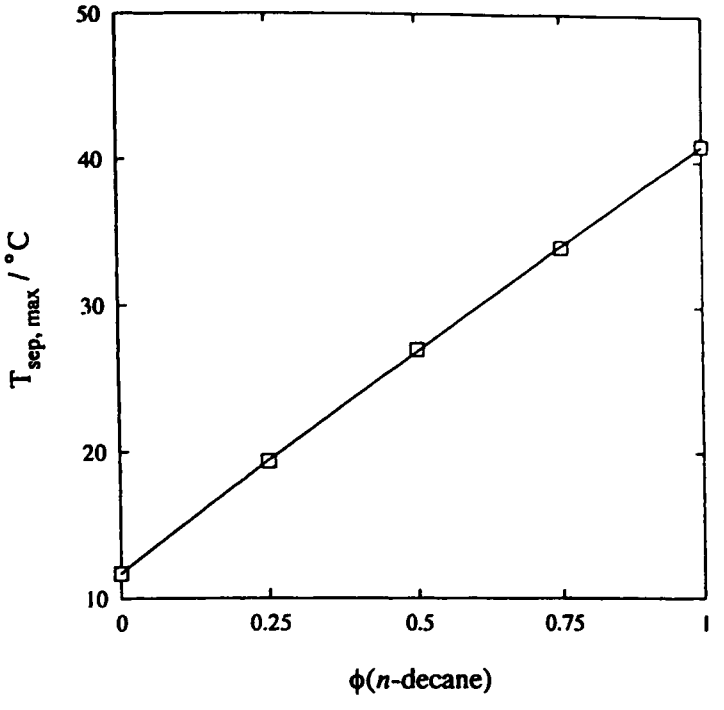

Fig. 4 The maximum phase-separation temperatures $T_{sep,max}$ for *n*-hexane–*n*-decane–propanenitrile as a function of the *n*-decane volume fraction, ϕ(*n*-decane), in the *n*-decane-*n*-hexane stock mixture. The smooth line is a simple parabolic fit through the experimental points.

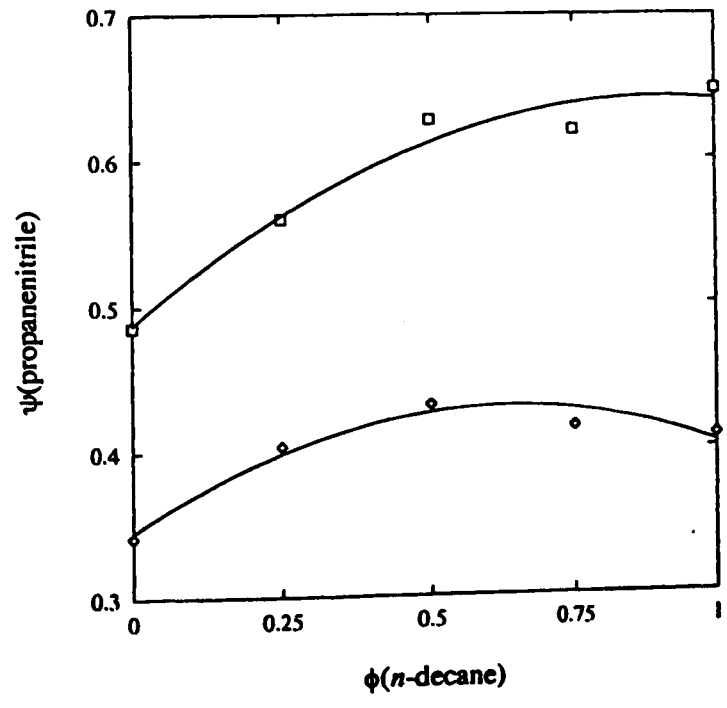

Fig. 5 The compositions ψ corresponding to the maximum phase-separation temperatures $T_{sep,max}$ for *n*-hexane–*n*-decane–propanenitrile as a function of the *n*-decane volume fraction, ϕ(*n*-decane), in the *n*-decane-*n*-hexane stock mixture. The squares are ψ = mole fraction x and the diamonds are ψ = volume fraction ϕ of propanenitrile. The smooth lines are simple parabolic fits through the experimental points.

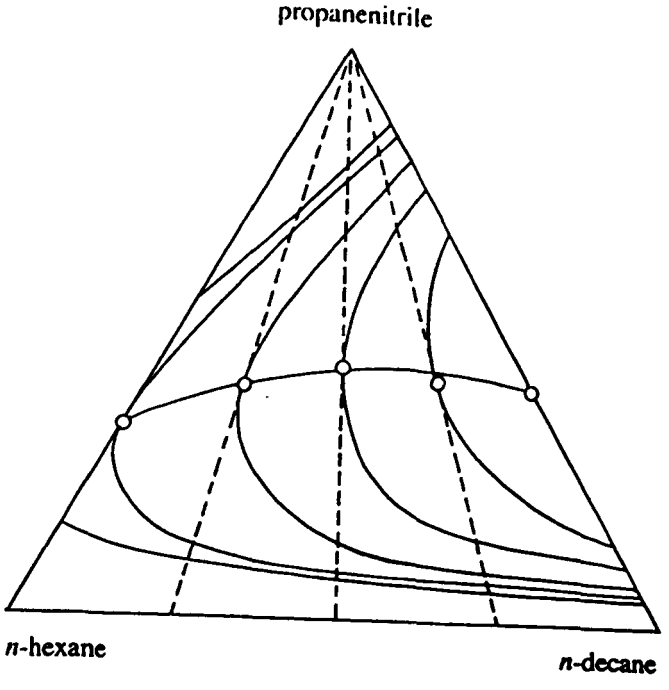

Fig. 6 Triangular phase diagrams for isothermal slices for *n*-hexane–*n*-decane–propanenitrile as a function of the volume fraction ϕ at temperatures 8.09, 11.682, 19.335, 27.005, 33.985, and 41.09°C. The circles represent the compositions at the maximum temperature of either the binary phase diagram or a quasibinary slice, as appropriate.

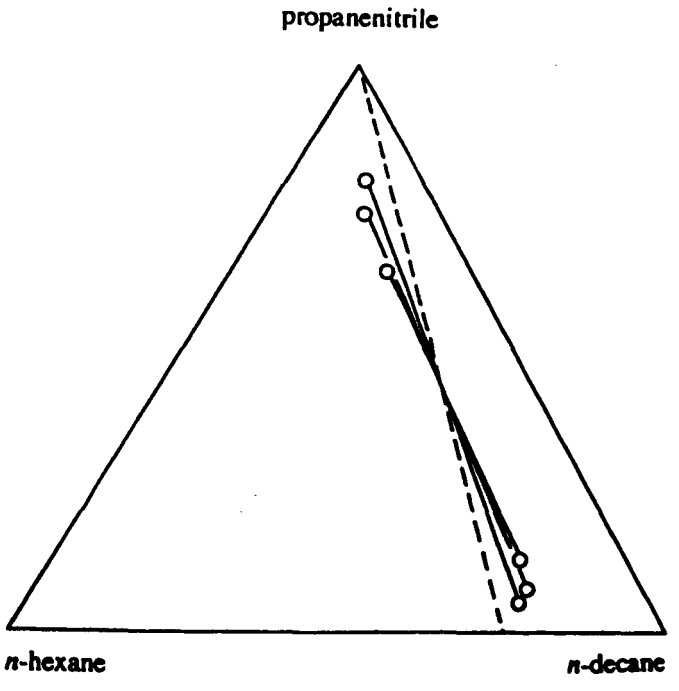

Fig. 7 Illustration on a triangular phase diagram of the relationship between quasibinary slices and the corresponding tielines as a function of temperature in the partially miscible region. The longer the tielines the deeper they lie in the tunnel region of the phase prism; such lines tend to be parallel to the appropriate quasibinary slice. The shorter the tile lines the closer they lie to the upper surface of the tunnel region of the phase prism; such lines tend to be parallel to the appropriate binary face of the phase prism.

Thermodynamics of ternary mixtures exhibiting tunnel phase behaviour

Part 3.–Hexane-hexamethyldisiloxane-perfluorohexane

Patricia J. Clements, Shazia Zafar, Amparo Galindo, George Jackson and Ian A. McLure*
Department of Chemistry, The University, Sheffield, S3 7HF, UK

The phase diagram for the ternary mixture hexane-hexamethyldisiloxane-perfluorohexane has been determined by visual observation of the liquid-liquid phase separation temperatures T_{sep} for the two partially miscible binary mixtures containing perfluorohexane and for three quasibinary temperature-composition slices of volume ratios of hexamethyldisiloxane:hexane of 1:3, 1:1 and 3:1. The upper critical solution temperatures T_{UCS} for the binary mixtures of hexane or hexamethyldisiloxane-perfluorohexane are separated by less than 1 K, 295.76 K and 296.65 K, respectively. For the quasibinary slices, the maximum separation temperatures $T_{sep,max}$ are lower than T_{UCS} for either binary mixture–for the central ternary slice $T_{sep,max}$ = 294.64 K. The projections of the ternary liquid-liquid quasibinary slices map well on to the binary liquid-liquid coexistence curves. A simplified version of the statistical associating fluid theory (SAFT-HS) has been used to predict the phase equilibrium for this system and is in good qualitative agreement with the experimental results. In particular, the decrease in $T_{sep,max}$ for the ternary mixtures is reproduced.

1. Introduction

In the first two parts of this series the phase behaviour of ternary mixtures exhibiting tunnel behaviour due to the chemical similarity of two of the components has been studied. This similarity originated either from isotopomerism,[1] in which two of the components differed only in the complete substitution of H by D atoms or from homologous unbranched alkanes,[2] in which two of the components differed only in chain length. This paper forms the third part of a continuing study of ternary mixtures of this type and reports the results of our measurements and our theoretical description of the liquid-liquid coexistence surface of hexane-hexamethyldisiloxane-perfluorohexane. In this mixture hexane and hexamethyldisiloxane are similar in the sense that their corresponding-states reduction factors T* are almost equal and their pressure reduction factors p* are reasonably similar. Thus hexane and hexamethyldisiloxane, with the same reduced temperature and essentially the same reduced pressure at any actual temperature and pressure, behave in an essentially similar fashion in many theories of mixtures, particularly at low pressure.[3]

Hexamethyldisiloxane $(CH_3)_3Si\text{-}O\text{-}Si(CH_3)_3$ is a member of the series of linear dimethylsiloxanes and is often denoted M_2,[4] where $M = (CH_3)_3Si\text{-}O_{1/2}$. As mentioned above, it is very similar to hexane in many respects, both in pure component properties and in mixtures with, for example, perfluoroalkanes, despite the greater mobility or chain flexibility of hexamethyldisiloxane.[3] For example, the temperature reduction factors T* with respect to octane for M_2 and hexane are very similar–0.903 and 0.901,[5] respectively, although the pressure and volume reduction factors, p* and V*, are rather different, 0.836 and 1, respectively, for the former and 1.252 and 0.774 for the latter. The entropy reduction factors S* illustrate the greater mobility of hexamethyldisiloxane 1.159 compared to 0.857 for hexane. Some of the properties of alkane–dimethylsiloxane mixtures have been described by theories based chiefly on the differences in p* and V*; for example excess volumes[6] and surface tensions.[7] The nonideality of dimethylsiloxane-perfluoroalkane mixtures arises, as does that of alkane-perfluoroalkane mixtures, from the weakness of the unlike interaction energies. This leads to partial miscibility in dimethylsiloxane-perfluoroalkane mixtures, and the upper critical

solution temperatures T_{UCS} for mixtures with perfluorohexane increase with both increasing siloxane chain length, and indeed with increasing perfluoroalkane chain length.[8] By contrast, linear dimethylsiloxane–alkane mixtures are generally almost ideal,[9] and so are completely miscible over wide ranges of temperature and pressure, particularly if the components are of similar size.

2. Experimental

Materials

The hexane and the hexamethyldisiloxane were supplied by Aldrich with stated purities of 99+ mol% and 99.5+ mol%, respectively and were dried with 5 Å Molecular Sieve before use. The perfluorohexane was supplied by Fluorochem with a stated purity of 99 mol%, of which 85% was the normal isomer; in view of the great difficulty of purifying it further it was used as supplied.

Procedure

The shape of the two-phase tunnel was determined from measurements of the liquid-liquid phase separation temperatures T_{sep} of three quasibinary slices and of both partially miscible binary coexistence curves. The quasibinary slices were studied by adding perfluorohexane to stock solutions of volume ratios of hexamethyldisiloxane:hexane, $V(M_2):V(C_6)$, of 1:3, 1:1 and 3:1. The binary and ternary mixtures were made up by mass in sealed vessels containing approximately 2 cm^3 samples immersed in a small water-filled thermostat bath. The temperatures of liquid-liquid phase separation T_{sep} were determined using a calibrated platinum resistance thermometer as the temperature was cycled slowly up and down around the point of phase separation. The mole fraction was determined to ± 0.0001 and T_{sep} to ± 0.01 K although the accuracy is probably no better than ±0.05 K. The T_{sep} of ternary mixtures were more difficult to observe and for them the uncertainty is probably closer to ± 0.1 K.

3. Results

The liquid-liquid separation temperatures T_{sep} for the binary and ternary mixtures of known mole fraction x and volume fraction ϕ are recorded in Tables 1 and 2; throughout the paper the composition variable refers to perfluorohexane. The densities used to calculate ϕ from x are given in Table 3.

The results for the binary mixtures are shown in Figs. 1 and 2. The (T_{sep} + ϕ) results were fitted to expressions of the form:

$$\phi_{\pm} = \phi_C + [C\varepsilon + C_1\varepsilon^{\psi} + C_2\varepsilon^{(\psi + \Delta_1)} + \ldots] \pm {}^1/_2[B\varepsilon^{\beta} + B_1\varepsilon^{(\beta+\Delta_1)} + B_2\varepsilon^{(\beta+2\Delta_1)} + \ldots] \quad (1)$$

where the $\phi_{\pm}$ are compositions on either side of the critical composition ϕ_C, ε is the reduced temperature departure from the critical temperature, i.e., $\varepsilon = |T_{UCS} - T|/T_{UCS}$, the C_i are the diameter amplitudes, ψ is the critical index for the diameter $(\phi_+ + \phi_-)/2$, the B_i are the amplitudes for the order parameter $(\phi_+ - \phi_-)$, β is the order-parameter critical index and Δ_1 is the Wegner gap exponent for the order parameter. The Renormalization Group values for the critical indices were adopted: $\beta = 0.325$, $\psi = 1 - \alpha = 0.89$ and $\Delta_1 = 0.5$.[10] The data were not gathered for the purpose of exploring the finer details of coexistence curve shape, therefore they were of insufficient precision to justify the use of extended-scaling contributions. The fitting was carried out using a pre-optimised value for T_c. The results of the fitting routine are listed in Table 4 where in most entries one more significant figure than can strictly speaking be demonstrably justified is given.

The fitting was also carried out for the quasibinary slices to generate smooth curves through the data points and to identify the maximum temperature $T_{sep,max}$ for each curve and the corresponding mole fraction x and volume fraction ϕ. The results are given in Table 5 along with the critical temperatures and compositions for the two partially miscible binary mixtures.

4. Discussion

Phenomenology

Binary mixtures

In terms of the classification of van Konynenberg and Scott[11] the mixture hexane–hexamethyldisiloxane, which is almost ideal and thus exhibits no partial miscibility, belongs to type I whereas hexane–perfluorohexane and hexamethyldisiloxane–perfluorohexane which do exhibit liquid-liquid immiscibility with a simple gas-liquid critical locus[12] belong to type II.

Fig. 1 shows the liquid-liquid coexistence curve for hexane–perfluorohexane generated from our results. For comparison, the much older results of Bedford and Dunlap[13] are shown. The general agreement between the two sets is reassuring. Our results yield, via the fitting to an expression of the form of eqn. (1), T_{UCS} = 295.76 K and critical mole fraction x_c= 0.3670 which compare well with those reported by Bedford and Dunlap, T_{UCS} = 295.80 K and x_c= 0.370 and by Block, Judd, McLure, Knobler and Scott,[14] T_{UCS} = 295.63 K and x_c = 0.3616. Fig. 2 shows the same information for hexamethyldisiloxane–perfluorohexane and again the curve is drawn using an expression of the form of eqn. (1). The results of McLure, Mokhtari and Bowers[8] fall well on our curve. Our T_{UCS} = 296.65 K and x_c = 0.5103 agree well with those of McLure, Mokhtari and Bowers, T_{UCS} = 297.0 K and x_c = 0.516.

The shape of the hexane-perfluorohexane coexistence curve is significantly different in the mole fraction and volume fraction representations, as is clear from the B and C coefficients in Table 4. The hexamethyldisiloxane–perfluorohexane coexistence curve is essentially the same in either representation because the molar volumes of the components are almost equal. When plotted in the volume fraction representation, the hexane-perfluorohexane and the hexamethyldisiloxane-perfluorohexane coexistence curves are much more alike than in the mole fraction representation, principally in their greater symmetry as judged by the critical volume fractions: ϕ(hexane–perfluorohexane) = 0.4672 and ϕ(hexamethyldisiloxane–perfluorohexane) = 0.4977 and in terms of the critical amplitude rectilinear diameter coefficients C_ϕ which are small. The similarity in shape of the coexistence curves is further evidenced by the similarity of the volume-fraction order-parameter amplitudes B_ϕ = 1.8271 and 1.8491.

Ternary mixtures

The near similarity of T_{UCS} for the two binary mixtures reinforces the notion that, in terms of the thermodynamics of mixtures, hexane and hexamethyldisiloxane can be extremely alike. Little more need be said on that except that following the rule that the addition of a third component roughly equally soluble in both components of a binary mixture close to an upper critical endpoint will depress T_{UCS}, one might expect that T_{UCS} would be lowered on moving into the body of the (T–ϕ_1–ϕ_2) ternary phase diagram. The inevitable consequence is the formation of a col or saddle point on the coexistence surface and that indeed is what is obtained. This point is developed further below.

Turning now to the quasibinary slice results there is a slight conceptual problem, which we have addressed more fully in our recent discussion of the mixture hexane–decane–propanenitrile,[2] namely the propriety of fitting the results to eqn. (1) since in no sense can the maximum in the curve be taken without further, and time-consuming, effort as a critical point. Nevertheless eqn. (1) does meet the need of describing the data and establishing the coordinates at the top of the slice. The results are illustrated on Fig. 3. The first matter of note is the general similarity of the shapes, particularly in mixtures dilute in perfluorohexane. The second is seen rather better on Fig. 4 which shows the maximum temperature on the slices along with T_{UCS} of the binary mixtures. The results fall satisfyingly on a smooth curve, for whose description a simple cubic fit suffices, thus to some extent drawing together and validating the entire data set. The small variation of the highest point along the coexistence surface is striking.

The mole and volume fractions of the maxima, x_{max} and ϕ_{max}, respectively, are displayed as a function of hexamethyldisiloxane volume fraction ϕ(hexamethyldisiloxane) in the hexane–hexamethyldisiloxane stock mixture in Fig. 5. The data fall on smooth curves–almost linear but here simple least-squares fitted parabolas–and so confirm both the precision of our results and the internal consistency of our procedure for estimating from them the coordinates of the maxima. The magnitudes of x_{max} and ϕ_{max} also confirm what by now

scarcely requires confirmation, namely that the volume fractions ϕ_{max} are more constant and closer to 0.5 than are the x_{max}.

Fig. 6 shows isothermal slices on the conventional (T-x'-x") plots where x' and x" are mole fractions of two of the mixture components. The circles indicate the maxima of the quasibinary slices represented by the dashed lines and the smooth line through the circles is intended only as a guide to the eye. From the temperatures of the isothermal slices it is clear that the line passes through a minimum as Fig. 4 shows in a T-ϕ(hexamethyldisiloxane) projection. The occurrence of a tunnel region of coexistence at lower temperatures is apparent as is the narrowing of the coexistence surface in the vicinity of the col. The diagram is displayed in terms of mole fraction since this serves to give a more immediate comparison with the theory which is more naturally couched in mole fraction rather than volume fraction terms.

We turn now to the details of the statistical associating fluid theory (SAFT) used in this work to predict the phase behaviour of hexane-hexamethyldisiloxane-perfluorohexane. Our calculation is carried out at atmospheric pressure. Some of the experimental mixing properties used to determine the parameters in the calculations were measured orthobarically, i.e., in coexistence with the vapour, e.g., notably and obviously the vapour pressures for hexane–hexamethyldisiloxane, while the liquid-liquid coexistence curves presented here were determined for the most part effectively at atmospheric pressure although in closed cells. The results are little different from those which would have been determined orthobarically.

SAFT-HS theory

Background

The SAFT theory used in this work to predict the phase behaviour of mixtures of alkane–dimethylsiloxane–perfluoroalkane mixtures has its roots in the theory of Wertheim for associating molecules with multiple bonding sites.[15,16,17,18,19,20] The theory is based on a graphical expansion of the densities of the free and associated species which can be represented as a simple analytical perturbation theory. Chapman and co-workers[21,22] extended the original theory to mixtures of associating spherical molecules with one bonding site, but phase equilibria was not examined.

The liquid-vapour phase equilibria of model hard-sphere[23] and hard-sphere chain[24] molecules with multiple bonding sites and van der Waals mean-field term interactions have been determined to examine the effect of association on the phase behaviour. In the second paper[24] an accurate equation of state for pure fluids and mixtures of chain molecules formed from tangent hard-sphere segments was obtained within the Wertheim formalism; the expression for the pure fluid is identical to that of Wertheim,[20] but is given in terms of the actual chain length of the molecules instead of the average chain length of the associating system (also see reference (25)). This led to a general expression for the equation of state of mixtures of associating chain molecules with multiple bonding sites, including a van der Waals one-fluid mean-field term. More recently, the phase behaviour of a system which exhibits closed-loop liquid-liquid immiscibility,[26] model water-alkane[27,28] and water-alkanol[29] mixtures, water–alkane mixtures at high pressures,[30] and binary mixtures of hydrogen fluoride with water, difluoromethane and 1,1,1,2-tetrafluoroethane[31] have been examined using such an expression.

We use SAFT-HS to denote this approach since the equation is essentially a simplified prototype of the more sophisticated SAFT equation of state (EOS) which treats the chain as Lennard-Jones (LJ) segments, rather than hard-sphere (HS) segments with van der Waals attractions. The original SAFT EOS for mixtures of associating Lennard-Jones chain molecules incorporates contributions from the molecular cores, the chains, the associating sites and the Lennard-Jones dispersion interactions.[32,33] The theory has been extended to Lennard-Jones and square-well (SW) chains (where the contact values of the distribution function for the LJ and SW monomers are used in the chain contribution instead of the hard-sphere expressions).[34,35,36,37,38,39] A general EOS for chains formed from attractive spherical cores with variable range (SAFT-VR), which offers an accurate representation of the reference system in a simple analytical form, has recently been developed.[40] The Wertheim approach has now been extended to deal with double bonding,[41] ring formation[42,43,44,45] and bond cooperativity.[46]

All of the SAFT EOSs mentioned thus far are based on the first-order perturbation theory of Wertheim. The theory can be extended to second order to account for the dependence of bonding at one site due to bonding at another,[20] but this usually involves the appropriate three-body distribution function. An alternative approach (SAFT-D) has been developed by Ghonasgi and Chapman[47] where dimer-segment terms are included in the chain contribution to deal with the many-body effects in an approximate manner; this has now been applied to SW chains by Tavares et *al.*[48] It should be noted that since SAFT is a molecular based theory, it can be tested directly with computer simulation data: the accuracy of the theory in describing the properties of associating spherical and chain molecules has been reported in a number of studies.[22,23,24,35,49,48,50,51,52,53]

Huang and Radosz have used the SAFT approach to correlate the data for the phase equilibria of over 100 pure components[54] and 60 binary mixtures[55] with great success. Yu and Chen[56] have also used SAFT to examine the liquid-liquid phase equilibria for 41 binary mixtures and eight ternary mixtures using many of the parameters of Huang and Radosz. Other systems which have been examined include ternary systems of alkanes containing ethene and 1-butene,[57] a binary mixture of carbon dioxide and methylnaphthalene,[58] and very recently water-alkane and water-alkanol systems.[59] One should also mention that the approach has also been used to correlate and predict the phase behaviour of polymer solutions (e.g., see ref. (60)).

Here we turn to ternary mixtures with an account of the calculation using the SAFT-HS approach to describe the liquid-liquid phase behaviour of a ternary mixture. As indicated above, one of the constituent binary mixtures belongs to type I and the other two to type II.[11] The objects of the calculation were first to describe the liquid-liquid phase behaviour of the two partially miscible binary mixtures and secondly to describe the upper coexistence surface of the ternary mixture, i.e., the tunnel region of liquid-liquid coexistence. In this paper we are dealing with a trihomologous mixture,[7] i.e., one whose components are drawn from three separate homologous chain-molecule series. It is therefore necessary to specify each homologous series in terms of the equivalent number of segments and their size and interaction strengths.

We therefore open the account with a resumé of the model to be used, followed by the details of the description of the chain structure, the procedure for evaluating the like interaction parameters from the pure component liquids, the assessment of the unlike interaction parameters from the properties of the binary mixtures, some details regarding the implementation of the theory and finally we discuss the outcome.

Model and chain characterisation

We use a simple united-atom chain model wherein chain i is deemed to be formed from m_i hard-sphere segments of equal diameter σ_i bonded tangentially to form a chain (see Fig. 7). In order to examine fluid phase equilibria in such models attractive interactions must also be included. We describe the attractive interactions at the van der Waals mean-field level with an energy parameter α_{ii} associated with each segment; this model is qualitatively similar to that proposed for the alkanes in the original SAFT approach,[32,33,61] but in the latter the segment-segment interactions are described in terms of potentials of the Lennard-Jones form. For convenience in the following account, we denominate the alkane component, here hexane, as chain 1, the perfluoroalkane component, here perfluorohexane, as chain 2, and the dimethylsiloxane, here hexamethyldisiloxane, as chain 3.

We take into account all segment-segment interactions, where, as mentioned above, the segment of the chain is a united atom representation of part of the molecule. A simple empirical relationship between the number of carbon atoms C_1 in the alkyl chain and the number of spherical segments m_1 has been proposed in earlier work:[61,62] $m_1 = 1 + (C_1 - 1)/3$. A value of $m_1 = 1$ thus corresponds to methane, $m_1 = 1 + 1/3$ to ethane, $m_1 = 1 + 2/3$ to propane, $m_1 = 2$ to butane, etc and for hexane $m_1 = 1 + 5/3$. This relationship conforms with the fact that the carbon-carbon bond length in an alkane is about 1/3 of the diameter of the methane molecule. It also gives a reasonable description of the critical pressure and temperature of the homologous series of the alkanes, although it does not reproduce the finer details such as the anomalous progression in the critical pressure from methane to ethane.[30,61,62] For the perfluoroalkane chains, based on similar reasoning, we have $m_2 = 1 + 0.37(C_2 - 1)$, giving for perfluorohexane $m_2 = 2.85$.[62] This reflects the larger perfluoroalkane segment size compared with that of alkanes. For the dimethylsiloxanes we take $m_3 = 1 + 0.5(C_3 - 1)$, where C_3 is the number of silicon atoms along the chain, giving for hexamethyldisiloxane $m_3 = 1.5$. These empirical relationships provide adequate descriptions of the critical properties of all three homologous series.

The great advantage of this approach is that when the diameter and strength of the interactions of the spherical segments are obtained for one member of the homologous series (e.g., hexane) by fitting to its thermodynamic properties, these segment parameters can be used in a transferable way for the other members of the series without further recourse to fitting.[30,62] With the structural element of chain description in place we now seek the various interaction parameters.

Our procedure here followed three stages. The first was to obtain parameters for the pure component fluids, the second to determine the intermolecular parameters for the binary mixtures by comparison of calculations and experimental data, and the third stage was to combine all these data in the calculation for the ternary mixture. Since the ternary is taken as reflecting pairwise interactions only, mixing rules for higher combinations than pairs of molecules need not be invoked. We give details of the procedures later in this work.

Like interaction parameters

For convenience it is useful to define a number of parameters and reduced variables during the calculations of phase equilibria. The volume of a spherical segment of species i of diameter σ_i is denoted by $b_i = \pi \sigma_i^3/6$. The energy of the mean-field interaction is given in terms of the segment volume b_i and the van der Waals constant α_{ii} as $\varepsilon_i = \alpha_{ii}/b_i$. In studying a mixture, the parameters of one of the components can be used to reduce the properties of the other component; in our case we chose species 1 so that, e.g., $\sigma_i^* = \sigma_i/\sigma_1$, $\alpha_{ii}^* = \alpha_{ii}/\alpha_{11}$ etc. The reduced temperature and pressure are defined as $T_i^* = kTb_i/\alpha_{ii} = kT/\varepsilon_i$ and $p_i^* = pb_i^2/\alpha_{ii} = pb_i/\varepsilon_i$, respectively.

Unlike interaction parameters

The only parameters which characterise the mixture are the size and energy interactions between the spherical segments of the alkyl, dimethylsiloxane and perfluoroalkane chains. In our case the corresponding hard-sphere interaction is simply $\sigma_{ij} = (\sigma_i + \sigma_j)/2$ which corresponds to the Lorentz arithmetic-mean mixing rule.[63] This only leaves the three integrated interaction energy parameters of the van der Waals interactions between the three pairs of unlike segments. The use of the geometric-mean mixing rule for the unlike interaction, $\alpha_{ij} = (\alpha_{ii}\alpha_{jj})^{0.5}$, is not adequate for a non-ideal mixture, and the parameter must be obtained by fitting to a property of the mixture.

Details of the implementation

Before we discuss details of the fitting procedure and of the determination of phase equilibria with the SAFT-HS approach it is convenient to summarise the main expressions of the theory. For further details the reader should consult references (24) and (30) for this version of the theory and reference (33) for the original SAFT approach. We give the general equations for mixtures of associating chain molecules formed from hard spherical segments with van der Waals interactions, and then provide the specific equations for the model of interest.

The Helmholtz free energy A for an n-component mixture of associating chain molecules can be separated into various contributions as

$$\frac{A}{NkT} = \frac{A^{ideal}}{NkT} + \frac{A^{hs}}{NkT} + \frac{A^{chain}}{NkT} + \frac{A^{mf}}{NkT}, \qquad (2)$$

where N is the total number of molecules, T is the temperature and k is the Boltzmann constant. The ideal contribution to the free energy is given by [63]

$$\begin{aligned}\frac{A^{ideal}}{NkT} &= \left(\sum_{i=1}^{n} x_i \ln \rho_i \Lambda_i^3\right) - 1, \\ &= x_1 \ln \rho_1 \Lambda_1^3 + x_2 \ln \rho_2 \Lambda_2^3 + x_3 \ln \rho_3 \Lambda_3^3 - 1\end{aligned} \tag{3}$$

The sum is over all species i of the mixture, $x_i = N_i/N$ is the mole fraction, $\rho_i = N_i/V$ the number density, N_i the number of molecules and Λ_i the thermal de Broglie wavelength of species i and V the volume of the system. The expression of Boublík[64] (equivalent to that of Mansoori *et al.* [65]) for a multi-component mixture of hard spheres is used for the reference hard-sphere contribution, i.e,

$$\frac{A^{hs}}{NkT} = \frac{6}{\pi\rho}\left[\left(\frac{\zeta_2^3}{\zeta_3^2} - \zeta_0\right)\ln(1-\zeta_3) + \frac{3\zeta_1\zeta_2}{(1-\zeta_3)} + \frac{\zeta_2^3}{\zeta_3(1-\zeta_3)^2}\right], \tag{4}$$

where $\rho = N/V$ is the total number density of the mixture, the reduced densities ζ_l are defined as

$$\begin{aligned}\zeta_l &= \frac{\pi\rho}{6}\left[\sum_{i=1}^{n} x_i m_i (\sigma_i)^l\right], \\ &= \frac{\pi\rho}{6}\left[x_1 m_1(\sigma_1)^l + x_2 m_2(\sigma_2)^l + x_3 m_3(\sigma_3)^l\right].\end{aligned} \tag{5}$$

ζ_3 is the overall packing fraction of the mixture and m_i is the number and σ_i the diameter of spherical segments of chain i. The monomer hard-sphere contribution is not the only hard-core repulsive contribution to the free energy, as we must also take into account the effect of forming the hard-sphere chains;[24]

$$\begin{aligned}\frac{A^{chain}}{NkT} &= -\sum_{i=1}^{n} x_i (m_i - 1)\ln g^{hs}(\sigma_{ii}) \\ &= -x_1(m_1-1)\ln g^{hs}(\sigma_{11}) - x_2(m_2-1)\ln g^{hs}(\sigma_{22}) - x_3(m_3-1)\ln g^{hs}(\sigma_{33}),\end{aligned} \tag{6}$$

In general, the contact value of the pair radial distribution function for the spherical segments of species i and j in the reference hard-sphere mixture is given by the appropriate Boublík[64] expression as

$$g^{hs}(\sigma_{ij}) = \frac{1}{(1-\zeta_3)} + 3\frac{\sigma_i\sigma_j}{\sigma_i+\sigma_j}\frac{\zeta_2}{(1-\zeta_3)^2} + 2\left(\frac{\sigma_i\sigma_j}{\sigma_i+\sigma_j}\right)^2\frac{\zeta_2^2}{(1-\zeta_3)^3}. \tag{7}$$

Finally, the contribution due to the dispersive attractive interactions is given at the mean-field level in terms of the van der Waals one-fluid theory of mixing.[63]

$$\frac{A^{mf}}{NkT} = -\frac{\rho}{kT}\sum_{i=1}^{n}\sum_{j=1}^{n}\alpha_{ij}x_i x_j m_i m_j,$$

$$= -\frac{\rho}{kT}\left(\alpha_{11}x_1^2m_1^2 + \alpha_{22}x_2^2m_2^2 + \alpha_{33}x_3^2m_3^2\right. \tag{8}$$

$$+ \left. 2\alpha_{12}x_1x_2m_1m_2 + 2\alpha_{13}x_1x_3m_1m_3 + 2\alpha_{23}x_2x_3m_2m_3\right).$$

In this approach we have expressed the mean-field contribution in terms of segment-segment and not molecule-molecule interactions, i.e., α_{11} represents the integrated strength of the hexane–hexane mean-field attraction, α_{12} that for hexane–perfluorohexane, α_{13} that for hexane–hexamethyldisiloxane, α_{22} that for perfluorohexane-perfluorohexane, α_{23} that for perfluorohexane–hexamethyldisiloxane, and α_{33} that for hexamethyldisiloxane-hexamethyldisiloxane segments of the chain. This simple representation together with the relationship between the number of carbon atoms in the alkane and the number of spherical segments allows the phase behaviour of the whole series to be examined with transferable parameters. We re-emphasise that all these parameters, indeed all the interactions considered, are two-body in nature. The calculation of the three-component coexistence surface therefore has been made entirely without any fitting to experimental three-component data. We have, however, checked for and confirmed the absence of immiscibility for the hexane–hexamethyldisiloxane binary mixture.

The other thermodynamic properties can be obtained from the Helmholtz free energy using the standard relationships. For example, the chemical potential of species i is given by μ_i

$$\mu_i = \left(\frac{\partial A}{\partial N_i}\right)_{T,V,N_{j\neq i}} \tag{9}$$

and the compressibility factor by

$$Z = \frac{pV}{NkT} = \sum_i^n\left(x_i\frac{\mu_i}{kT}\right) - \frac{A}{NkT}. \tag{10}$$

These functions are required for a determination of the critical and phase behaviour of the mixture. The gas-liquid and liquid-liquid critical lines can be determined by equating the second and third derivatives of the Gibbs function with respect to the mole fraction to zero. Phase equilibria between phases I and II in mixtures require that the temperature, pressure and chemical potential of each component in each phase are equal, i.e.,

$$T^I = T^{II},\ p^I = p^{II},\ \mu_i{}^I = \mu_i{}^{II} \tag{11}$$

These conditions for phase equilibria are solved numerically using a simplex method.[66] A more detailed description of the techniques are given in a previous paper[27] and in the extensive work of Scott and van Konynenburg.[11]

Determination of the interaction parameters

The parameters characterising the pure components, i.e. σ_i and ε_{ii}, the diameter of the hard sphere segment and the integrated energy of the mean-field interaction of the segment, respectively, were determined by fitting to the experimental critical points of each pure component. These experimental critical points are characterised by T_c = 507.4 K, p_c = 3.04 MPa for hexane,[67] T_c = 448.77 K, p_c = 1.868 MPa for perfluorohexane,[12] and T_c = 518.8 K, p_c = 1.91 MPa for hexamethyldisiloxane.[67] As a result of this fitting the parameters obtained were ε_{11}/k = 3019 K, σ_1 = 3.810 Å for hexane, ε_{22}/k = 2581 K, σ_2 = 4.173 Å for perfluorohexane, and ε_{33}/k = 4260 K, σ_3 = 5.812 Å for hexamethyldisiloxane.

The cross interactions can in principle be determined from any appropriate physical property of the mixture. The assignment of chain segment specification was in this theory normally carried out using gas-liquid critical properties of the components. In that vein therefore, it would seem most sensible to use as a

source of information on the cross terms the gas-liquid critical *locus* for the binary mixture. This has been done successfully for many mixtures, especially of simple substances. However, for mixtures of the more complex molecules under consideration here, the gas-liquid critical locus is rarely known and if it is often with indifferent accuracy. Attention then switches to more accessible data and the choice is often conditioned by the general miscibility of the components.

For partially miscible mixtures, the upper critical solution temperature T_{UCS} is a convenient resource, particularly since we are interested in the liquid region and, more specifically, in the behaviour of the critical point. In any case, this is often the only or at least the most accurately known available information. This is what was done here for hexane–perfluorohexane and hexamethyldisiloxane–perfluorohexane using, as it happens at the start of our calculations and before we had completed measurements on the binary mixtures, the results of Bedford and Dunlap[13] and McLure *et al.*[8] respectively. The resulting parameters are ε_{12}/k = 2511 K ($\alpha_{12}^* = 0.956$) for hexane-perfluorohexane, and ε_{23}/k = 2755 K ($\alpha_{23}^* = 2.05$) for hexamethyldisiloxane-perfluorohexane

For fully miscible mixtures, this procedure is unavailable. Thus in order to determine the unlike interaction parameters for hexane-hexamethyldisiloxane (σ_{13} and ε_{13}) we have examined the gas-liquid coexistence region. More specifically, our parameters were fitted to the isothermal vapour-pressure curves at 303.15 K,[9] yielding ε_{13}/k = 3435 K ($\alpha_{13}^* = 2.29$). It was observed that the SAFT-HS approach produced a slight positive azeotrope if the geometric-mean rule was used to calculate the unlike parameter. In our fitting we have checked that azeotropy is not exhibited. The fitting was very sensitive to the interaction energy parameter and the value used is not too different from that calculated from the geometric-mean rule ($\alpha_{13}^* = 2.24$) which is expected to describe the behaviour of a mixture so close to ideal. The parameters obtained by fitting to experimental data at 303.15 K were further compared with experimental vapour-pressure data at 309.15 K and 315.15 K[9] and with the gas-liquid critical locus for mixtures of composition close to x = 0.5.[67] The parameters proved to be consistent.

Figs. 8 and 9 show the results of the fit to the liquid-liquid critical points of hexane-perfluorohexane and hexamethyldisiloxane-perfluorohexane. Since the theory is a mean field theory, it is not at all unexpected that the shape of the coexistence curve is poorly reproduced. Furthermore, it is unusual for complex theories to reproduce critical compositions well, partly for the same reason, it is no surprise that in this case x_c is not particularly well predicted. However, given the nature of the theory, and the superior need to establish the cross term required to get T_{UCS} the agreement is more than adequate for our purpose. The branches of the coexistence curves in Figs. 8 and 9 do not quite meet due to the difficulty of obtaining convergence of solutions very close to T_{UCS} and an artificial closure was applied. The error so resulting in T_{UCS} is quite unimportant.

For the partially miscible mixtures although both vapour pressures and the gas-liquid critical locus are known for hexane–perfluorohexane they are unknown for hexamethyldisiloxane–perfluorohexane. It was decided therefore in the interest of consistency to follow the path outlined above and resort to the upper critical solution temperatures only.

Outcomes of the application of SAFT theory

Figure 10 shows the tielines at a very low temperature, -60.05°C, well below the range of measurements. They are highly regular and lend confidence to the use of the general theory to define the tielines given the general picture of the coexistence surface thus saving large amounts of experimental effort should the need for tielines arise.

Lastly Fig. 11 shows the phase diagram for a wide range of temperatures. The resemblance to the experimental diagram on Fig. 6 is striking and the more so given the sensitivity of the calculations as just described for fitting the vapour pressure curves for hexane–hexamethyldisiloxane and for the absence of any fitting whatsoever of ternary data. We apply a freehand closure in the immediate vicinity of the line of critical points. The free energy surface close to the plait points in the ternary is very flat and it is difficult to approach the critical point. This is because the system is also very close to the T_{UCS} of the corresponding binary mixtures. Higher precision (quadruple precision) would probably allow us to approach these points more closely.

5. Conclusions

1. The experimental ternary phase diagram confirms the naive expectation of the outcome of mixing a relatively soluble third component with a mixture at its upper critical endpoint, i.e. the critical locus drops to lower temperatures from each partially miscible side of the diagram thus creating a minimum in the locus of plait points about 1 K below the lower T_{UCS} at a mole ratio close to 1.6 in hexane:hexamethyldisiloxane and at a perfluorohexane mole fraction 0.43.

2. The line of maxima in temperature, $T_{sep,max}$ on the ternary triangular diagram cast in mole-fraction terms, although not readily identified as the plait-point locus, is a simple essentially straight line.

3. The theory, based on chain segment numbers and segment volumes and like interactions established from the properties of the pure components and incorporating pairwise unlike interactions obtained from appropriate properties of the three binary mixtures reproduces all the experimental features just listed. In particular, it predicts the depth of the minimum in the plait-point locus of around 1 K but the minimum is rather closer to a mole ratio hexane:hexamethyldisiloxane of 3.7 at a perfluorohexane mole fraction 0.38. Our aim was less to force agreement with experiment, although the degree of agreement just described is gratifying, than to ascertain the ease and qualitative success of extending to ternary mixtures the hard sphere variant of the SAFT theory.

4. Although the experimental determination of tielines across the coexistence liquid-liquid surface is usually a laborious process, the general shape of the surface can be determined as we have illustrated. Fitting that surface using the SAFT theory, which intrinsically determines canonical points and thus tielines, suggests a valuable combined experimental-theoretical approach, particularly using a form of the theory, for example a square-well-based approach (SAFT-VR), which produces binary liquid-liquid coexistence curves with more realistic shape than does the present mean-field approach.

5. Finally, the outcome of the calculations illustrates the success of the SAFT-HS theory in describing the liquid-liquid coexistence surface for hexane-hexamethyldisiloxane-perfluorohexane despite the greater mobility or flexibility of hexamethyldisiloxane over hexane that was mentioned in the introduction, and even more so over the still less flexible perfluorohexane. Furthermore, although there is no doubt some compensation arising from the use of parameters for the binary unlike interactions evaluated within the framework of a mean-field theory, it is interesting that the mean-field theory is an accurate means of relating binary mixture behaviour to ternary mixture behaviour.

References

1 H. K. Batchelor, P. J. Clements and I. A. McLure, *J. Chem. Soc., Faraday Trans.*, 1996, **92**, 2255.

2 P. J. Clements, E. Hill and I. A. McLure, submitted to *J. Chem. Soc., Faraday Trans.*

3 E. Dickinson, I. A. McLure, A. J. Pretty and P. A. Sadler, *Chemical Physics*, 1975, **10**, 17.

4 Nomenclature introduced by D. F. Wilcock, *J. Am. Chem. Soc.*, 1955, **77**, 3427.

5 D. Patterson and J. M. Bardin, *Trans. Faraday Soc.*, 1970, **66**, 321.

6 E. Dickinson and I. A. McLure, *J. Chem. Soc., Faraday Trans. I*, 1974, **70**, 2328.

7 B. Edmonds and I. A. McLure, *J. Chem. Soc, Faraday Trans. I*, 1982, **78**, 3319.

8 I. A. McLure, A. Mokhtari and J. Bowers, 1996, *J. Chem. Soc., Faraday Trans.*, in press.

9 E. Dickinson, I. A. McLure and B. H. Powell, *J. Chem. Soc., Faraday Trans. I*, 1974, **70**, 2321.

10 J. S. Le Guillou and J. Zinn-Justin, *Phys. Rev.*, 1980, **B21**, 3976.

11 R. L. Scott and P. H. van Konynenburg, *Discuss. Faraday Soc.*, 1970, **49**, 87; P. H. van Konynenburg and R. L. Scott, *Philos. Trans. Roy. Soc. London Ser. A*, 1980, **298**, 495.

12 A. E. H. N. Mousa, W. B. Kay and A. Kreglewski, *J. Chem. Thermodyn*, 1972, **4**, 301.

13 R. G. Bedford and R. D. Dunlap, *J. Am. Chem. Soc.*, 1958, **80**, 282.

14 T. E. Block, N. F. Judd, I. A. McLure, C. M. Knobler and R. L. Scott, *J. Phys. Chem.*, 1981, **85**, 3282.

15 M. S. Wertheim, *J. Stat. Phys.*, 1984, **35**, 19.

16 M. S. Wertheim, *J. Stat. Phys.*, 1984, **35**, 35.

17 M. S. Wertheim, *J. Stat. Phys.*, 1986, **42**, 459.

18 M. S. Wertheim, *J. Stat. Phys.*, 1986, **42**, 477.

19 M. S. Wertheim, *J. Chem. Phys.*, 1986, **85**, 2929.

20 M. S. Wertheim, *J. Chem. Phys.*, 1987, **87**, 7323.

21 W. G. Chapman, K. E. Gubbins, C. G. Joslin and C. G. Gray, *Fluid Phase Equil.*, 1986, **29**, 337.

22 C. G. Joslin, C. G. Gray, W. G. Chapman and K. E. Gubbins, *Mol. Phys.*, 1987, **62**, 843.

23 G. Jackson, W. G. Chapman and K. E. Gubbins, *Mol. Phys.*, 1988, **65**, 1.

24 W. G. Chapman, G. Jackson and K. E. Gubbins, *Mol. Phys.*, 1988, **65**, 1057.

25 R. Dickman and C. K. Hall, *J. Chem. Phys.*, 1986, **85**, 4108.

26 G. Jackson, *Mol. Phys.*, 1991, **72**, 1365.

27 D. G. Green and G. Jackson, *J. Chem. Soc., Faraday Trans.*, 1992, **88**, 1395.

28 I. Nezbeda, W. R. Smith and J. Kolafa, *J. Chem. Phys.*, 1994, **100**, 2191.

29 D. G. Green and G. Jackson, *J. Chem. Phys.*, 1992, **97**, 8672.

30 A. Galindo, P. J. Whitehead, G. Jackson and A. N. Burgess, *J. Phys. Chem..*, 1996, **100**, 6781.

31 A. Galindo, P. J. Whitehead, G. Jackson and A. N. Burgess, *J. Phys. Chem.*, submitted for publication.

32 W. G. Chapman, K. E. Gubbins, G. Jackson and M. Radosz, *Fluid Phase Equil.*, 1989, **52**, 31.

33 W. G. Chapman, K. E. Gubbins, G. Jackson and M. Radosz, *Ind. Eng. Chem. Res.*, 1990, **29**, 1709.

34 W. G. Chapman, *J. Chem. Phys.*, 1990, **93**, 4299.

35 D. Ghonasgi and W. G. Chapman, *Mol. Phys.*, 1993, **79**, 291; D. Ghonasgi and W. G. Chapman, *Mol. Phys.*, 1993, **80**, 161.

36 M. Banaszak, Y. C. Chiew and M. Radosz, *Phys. Rev. E*, 1993, **48**, 3760.

37 M. Banaszak, Y. C. Chiew, R. O'Lenick and M. Radosz, *J. Chem. Phys.*, 1994, **100**, 3803.

38 J. K. Johnson, E. A. Müller and Gubbins, K. E., *J. Phys. Chem.*, 1994, **98**, 6413.

39 E. A. Müller, L. F. Vega and K. E. Gubbins, *Mol. Phys.*, 1994, **83**, 1209.

40 A. Gil-Villegas, P. J. Whitehead, A. Galindo, S. J. Mills, G. Jackson and A. N. Burgess, 1996, *J. Chem. Phys.*, submitted for publication.

41 R. P. Sear and G. Jackson, *Mol. Phys.*, 1994, **82**, 1033.

42 R. P. Sear and G. Jackson, *Phys. Rev. E*, 1994, **50**, 386.

43 R. P. Sear and G. Jackson, *Mol. Phys.*, 1996, **87**, 517.

44 D. Ghonasgi, V. Perez and W. G. Chapman, *J. Chem. Phys.*, 1994, **101**, 6880.

45 D. Ghonasgi and W. G. Chapman, *J. Chem. Phys.*, 1995, **102**, 2585.

46 R. P. Sear and G. Jackson, *J. Chem. Phys.*, 1996, in press.

47 D. Ghonasgi and W. G. Chapman, *J. Chem. Phys.*, 1994, **100**, 6633.

48 F. W. Tavares, J. Chang and S. I. Sandler, *Mol. Phys.*, 1995, **86**, 1451.

49 D. Ghonasgi and W. G. Chapman, *J. Chem. Phys.*, 1994, **100**, 6633.

50 I. Nezbeda, J. Kolafa and V. Kalyuzhnyi, *Mol. Phys.*, 1989, **68**, 143.

51 I. Nezbeda and G. A. Iglesias-Silva, *Mol. Phys.*, 1990, **69**, 767.

52 J. K. Johnson and K. E. Gubbins, *Mol. Phys.*, 1992, **77**, 1033.

53 E. A. Müller and K. E. Gubbins, *Mol. Phys.*, 1993, **80**, 957.

54 S. H. Huang and M. Radosz, *Ind. Eng. Chem. Res.*, 1990, **29**, 2284.

55 S. H. Huang and M. Radosz, *Ind. Eng. Chem. Res.*, 1991, **30**, 1994.

56 M.-L. Yu and Y.-P. Chen, *Fluid Phase Equil.*, 1994, **94**, 149.

57 C. J. Greeg, F. P. Stein, S. J. Chen and M. Radosz, *Ind. Eng. Chem. Res.*, 1993, **32**, 1442.

58 C. J. Greeg and M. Radosz, *Fluid Phase Equilibria*, 1993, **86**, 211.

59 T. Kraska and K. E. Gubbins, *Ind. Eng. Chem. Res.*, 1996, submitted for publication.

60 C. Shean-Jer, I. J. Economou, I. G. and M. Radosz, *Macromolecules*, 1992, **25**, 4987.

61 G. Jackson and K. E. Gubbins, *Pure Appl. Chem.*, 1989, **61**, 1021.

62 A. L. Archer, M. D. Amos, G. Jackson and I. A. McLure, *Int. J. Thermophys.*, 1996, **17**, 201.

63 J. S. Rowlinson and F. L. Swinton, *Liquids and Liquid Mixtures*, 3rd Edition, Butterworth Scientific, London, 1982.

64 T. Boublík, *J. Chem. Phys.*, 1970, **53**, 471.

65 G. A. Mansoori, N. F. Carnahan, K. E. Starling and T. W. Leland, *J. Chem. Phys*, 1971, **54**, 1523.

66 W. H. Press, S. A. Teukolsky, W. T. Vetterling and B. P. Flannery, *Numerical Recipes in Fortran*, 1st Edition, Cambridge University Press, 1986.

67 E. Dickinson and I. A. McLure, *J. Chem. Soc., Faraday Trans. I*, 1974, **70**, 2313.

68 R. A. Orwoll and P. J. Flory, *J. Am. Chem. Soc.*, 1967, **89**, 6814, 6822.

69 I. A. McLure, A. J. Pretty and P. A. Sadler, *J. Chem. Eng. Data*, 1977, **22**, 372

70 R. D. Dunlap, C. J. Murphy, Jr. and R. D. Bedford, *J. Am. Chem. Soc.* 1958, **80**, 83.

Table 1 Liquid-liquid phase separation temperatures T_{sep} *vs.* mole fraction x or volume fraction ϕ of perfluorohexane for the binary mixtures of hexane-perfluorohexane and hexamethyldisiloxane-perfluorohexane

(1-x) C_6H_{14}–x C_6F_{14}			(1-x) M_2–x C_6F_{14}		
x	ϕ	T_{sep}/°C	x	ϕ	T_{sep}/°C
0.1111	0.1611	11.18	0.1337	0.1276	3.65
0.1303	0.1871	14.16	0.1569	0.1499	7.78
0.1478	0.2104	16.39	0.1789	0.1711	11.08
0.1704	0.2399	18.86	0.2362	0.2266	17.90
0.2305	0.3152	21.58	0.3574	0.3451	22.58
0.2939	0.3901	22.45	0.4876	0.4741	23.45
0.3199	0.4195	22.52	0.5386	0.5252	23.49
0.3987	0.5047	22.60	0.5624	0.5491	23.38
0.4031	0.5093	22.53	0.5743	0.5611	23.32
0.5022	0.6079	21.79	0.6314	0.6188	22.91
0.6415	0.7333	16.56	0.6637	0.6516	22.42
0.7265	0.8032	10.30	0.6711	0.6591	22.25
0.7644	0.8329	5.90	0.7095	0.6983	21.27
			0.7780	0.7686	17.71
			0.7848	0.7756	17.27
			0.8052	0.7966	15.24
			0.8207	0.8126	13.03
			0.8499	0.8429	7.63
			0.8909	0.8856	2.56

Table 2 Liquid-liquid phase separation temperatures T_{sep} *vs.* mole fraction x or volume fraction ϕ of perfluorohexane for the three quasibinary slices with volume ratios of hexamethyldisiloxane:hexane, $V(M_2):V(C_6)$, in the hexamethyldisiloxane-hexane solvent of 3:1, 1:1 and 1:3

$V(M_2):V(C_6) = 3:1$			$V(M_2):V(C_6) = 1:1$			$V(M_2):V(C_6) = 1:3$		
x	ϕ	T_{sep}/°C	x	ϕ	T_{sep}/°C	x	ϕ	T_{sep}/°C
0.1058	0.1147	1.25	0.1041	0.1261	4.50	0.1217	0.1614	9.76
0.1259	0.1362	5.89	0.1215	0.1466	8.06	0.1361	0.1796	12.08
0.1537	0.1658	10.58	0.1397	0.1678	10.89	0.1673	0.2182	15.73
0.1772	0.1908	13.51	0.1724	0.2055	14.56	0.1973	0.2546	18.34
0.2113	0.2268	16.61	0.1986	0.2354	16.85	0.2358	0.3000	20.10
0.2533	0.2708	19.09	0.2248	0.2648	18.47	0.2377	0.3023	20.24
0.3022	0.3216	20.77	0.2581	0.3017	19.81	0.2724	0.3422	21.05
0.3717	0.3931	21.82	0.2723	0.3173	20.06	0.3128	0.3874	21.53
0.4392	0.4616	22.06	0.2881	0.3345	20.70	0.3210	0.3964	21.54
0.4845	0.5071	22.08	0.3179	0.3666	21.09	0.3777	0.4575	21.67
0.5593	0.5815	21.87	0.3341	0.3839	21.29	0.4147	0.4960	21.82
0.6545	0.6747	20.53	0.3929	0.4456	21.48	0.4239	0.5055	21.71
0.6881	0.7072	19.47	0.4513	0.5053	21.47	0.4615	0.5435	21.61
0.7270	0.7446	17.38	0.4860	0.5401	21.44	0.4633	0.5453	21.58
0.7568	0.7731	16.24	0.5042	0.5581	21.36	0.5271	0.6076	21.08
0.7842	0.7991	13.24	0.5468	0.5998	21.05	0.5713	0.6493	20.09
0.8309	0.8432	7.40	0.5822	0.6338	20.46	0.5720	0.6499	20.06
0.8314	0.8437	7.44	0.6036	0.6541	20.20	0.6289	0.7019	18.20
0.8657	0.8759	1.86	0.6411	0.6893	19.11	0.6402	0.7120	17.97
			0.6805	0.7257	17.53	0.6546	0.7247	16.66
			0.7162	0.7581	15.57	0.6888	0.7546	14.79
			0.7813	0.8161	10.19	0.6922	0.7575	14.42
			0.8228	0.8522	4.83	0.7045	0.7681	13.50
						0.7523	0.8084	9.36

Table 3 Molar masses M and densities ρ at 298.15 K for hexane, hexamethyldisiloxane and perfluorohexane

	M/g mol^{-1}	ρ/g cm^{-3}
C_6H_{14}	86.18	0.655[68]
M_2	162.38	0.761[69]
C_6F_{14}	338.05	1.672[70]

Table 4 Results of fitting the T_{sep} to eqn. (1) for the binary mixtures C_6H_{14}–C_6F_{14} and M_2–C_6F_{14} with $\beta = 0.325$, $\Delta_1 = 0.5$ and $\psi = 0.89$

Mixture	T_{UCS}/K	x_c	B_x	C_x	$10^4\chi_x^2$	ϕ_c	B_ϕ	C_ϕ	$10^4\chi_\phi^2$
C_6H_{14}	295.76	0.3670	1.7228	1.1556	0.96	0.4672	1.8271	0.1965	1.03
M_2	296.65	0.5103	1.8477	-0.0418	2.02	0.4977	1.8491	0.0684	2.05

Table 5 Maximum phase-separation temperatures $T_{sep,max}$ and the corresponding mole fraction x and volume fraction ϕ of perfluorohexane in mixtures formed from hexamethyldisiloxane-hexane solvent mixtures with volume ratios of hexamethyldisiloxane:hexane, $V(M_2):V(C_6)$, of 0, 1:3, 1:1, 3:1 and 1. The values were obtained by fitting to equations of the form of eqn. (1)

$V(M_2):V(C_6)$	x(perfluorohexane)	ϕ(perfluorohexane)	$T_{sep,max}$/°C	$T_{sep,max}$/K
0	0.3700	0.4672	22.61	295.76
1:3	0.3969	0.4745	21.83	294.98
1:1	0.4296	0.4801	21.49	294.64
3:1	0.4719	0.4927	22.09	295.24
1	0.5103	0.4977	23.50	296.65

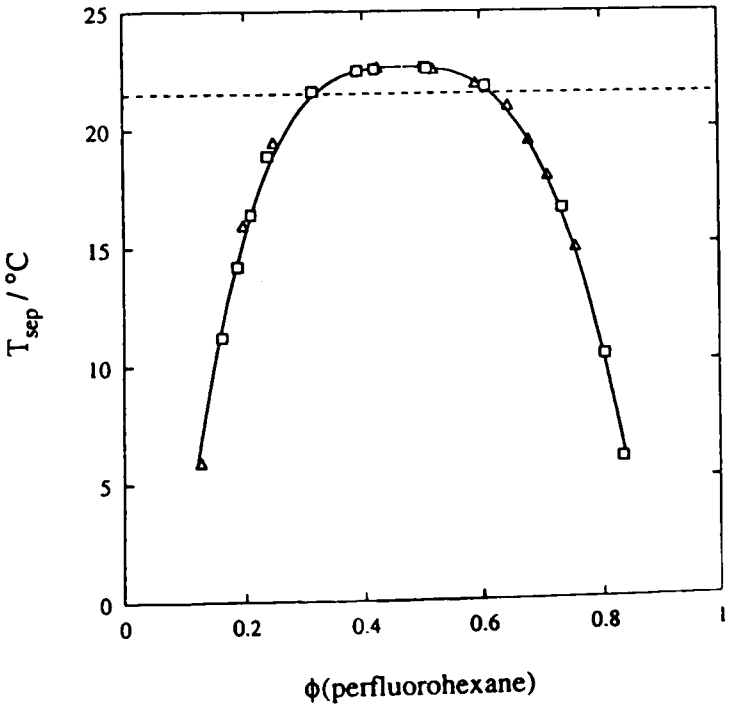

Fig. 1 The experimental phase-separation temperatures T_{sep} for hexane –perfluorohexane as a function of perfluorohexane volume fraction ϕ; our data (□) and those of Bedford and Dunlap (△).[13] The curve is drawn after fitting an expression of the form of eqn. (1) to our data; the coefficients are given in Table 4. The dashed line shows $T_{sep,max}$ for the $V(M_2):V(C_6) = 1:1$ quasibinary slice.

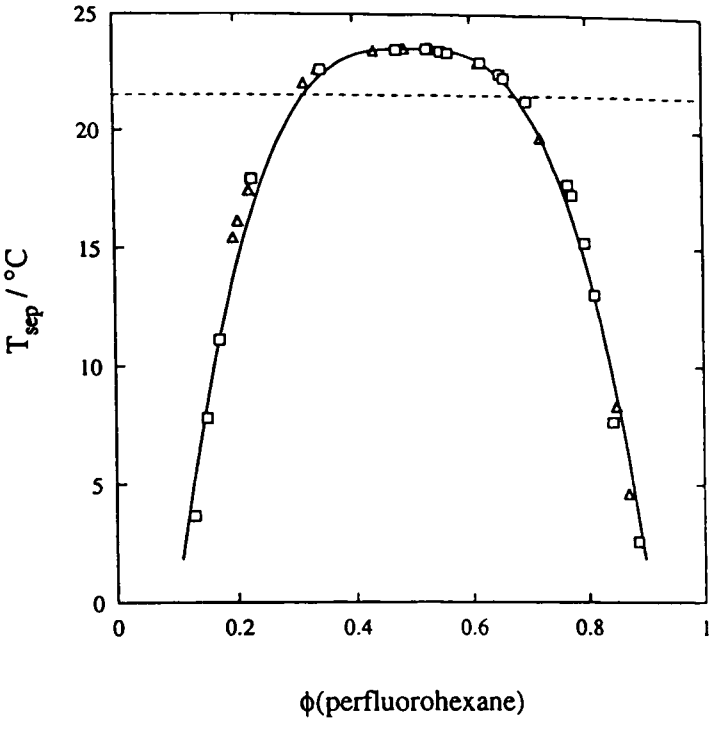

Fig. 2 The experimental phase-separation temperatures T_{sep} for hexamethyldisiloxane–perfluorohexane as a function of perfluorohexane volume fraction ϕ; our data (□) and those of McLure, Mokhtari and Bowers (Δ).[8] The curve is drawn after fitting an expression of the form of eqn. (1) to our data; the coefficients are given in Table 4. The dashed line shows $T_{sep,max}$ for the $V(M_2):V(C_6)$ = 1:1 quasibinary slice.

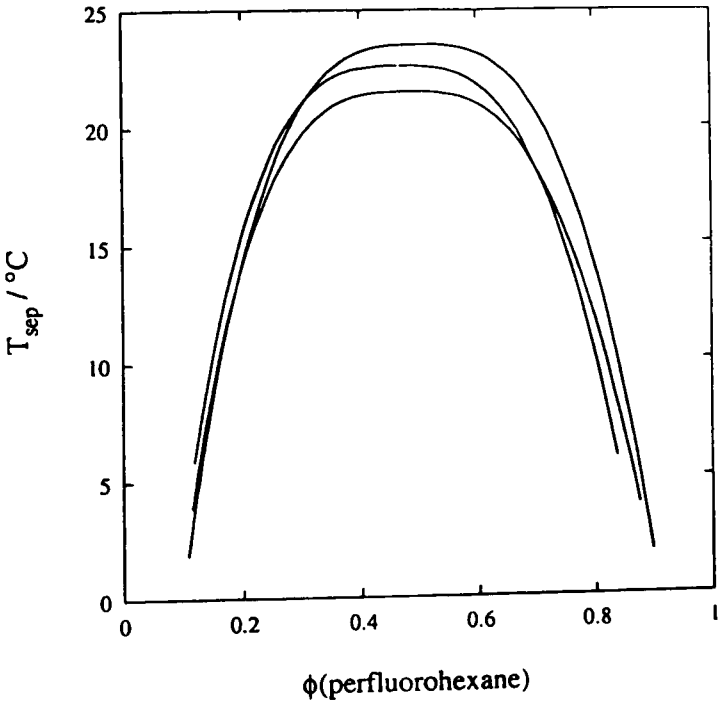

Fig. 3 The phase-separation temperatures T_{sep} for the three quasibinary slices of hexane–hexamethyldisiloxane–perfluorohexane with volume ratios of hexamethyldisiloxane:hexane, $V(M_2):V(C_6)$, of 1:3, 1:1 and 3:1 as a function of perfluorohexane volume fraction ϕ. The curves are obtained by fitting the results to expressions of the form of eqn. (1) taking the maximum temperature on each quasibinary slice, $T_{sep,max}$, in place of T_{UCS}. The curves are drawn from top to bottom with volume ratios $V(M_2):V(C_6)$ of 3:1, 1:3 and 1:1, respectively.

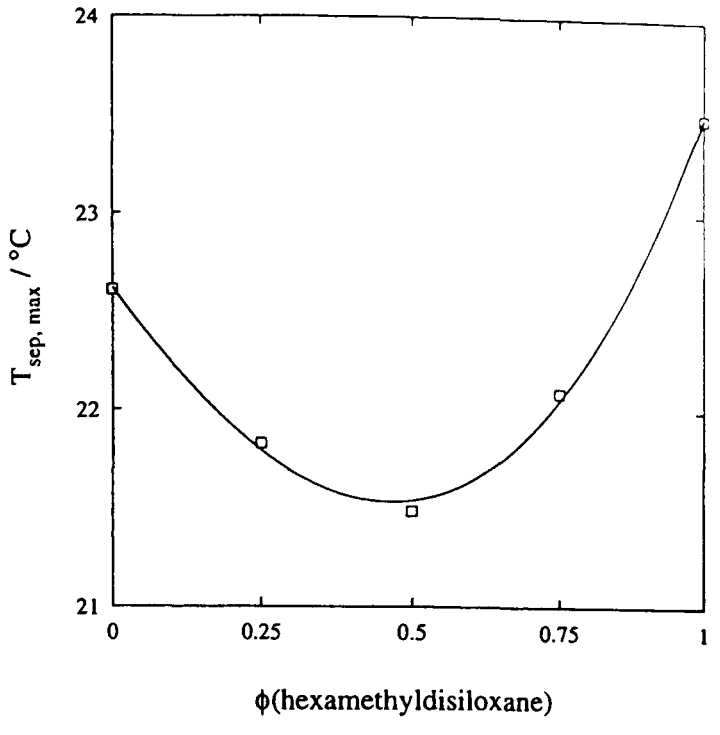

Fig. 4 The maximum phase-separation temperatures $T_{sep,max}$ for hexane–hexamethyldisiloxane–perfluorohexane quasibinary slices as a function of the hexamethyldisiloxane volume fraction, ϕ(hexamethyldisiloxane), in the hexamethyldisiloxane-hexane stock mixture. The smooth line is a simple cubic fit through the experimental points.

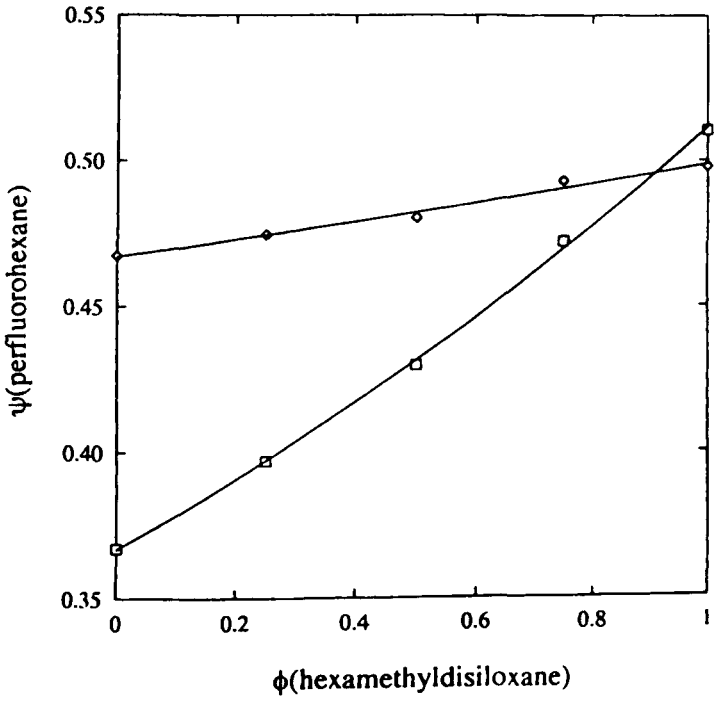

Fig. 5 The compositions ψ corresponding to the maximum phase-separation temperatures $T_{sep,max}$ for hexane–hexamethyldisiloxane–perfluorohexane quasibinary slices as a function of the hexamethyldisiloxane volume fraction, ϕ(hexamethyldisiloxane), in the hexamethyldisiloxane-hexane stock mixture. (□) represent ψ = mole fraction x and (◇) represent ψ = volume fraction ϕ. The smooth lines are simple parabolic fits through the experimental points.

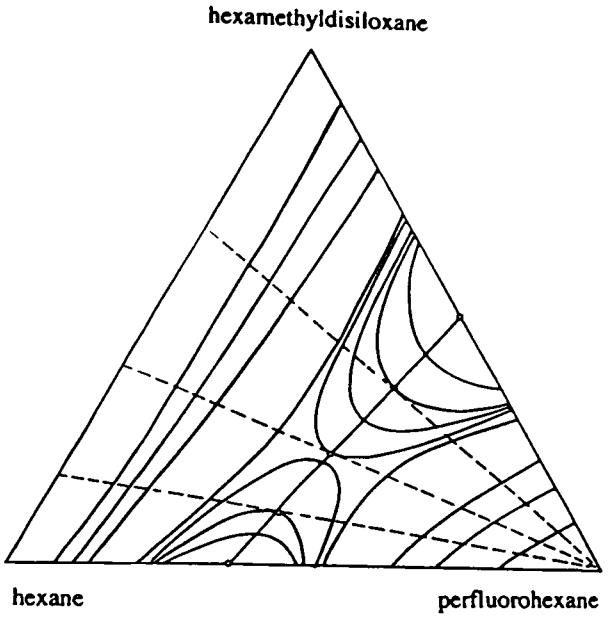

Fig. 6 Triangular phase diagrams for experimentally determined isothermal slices for hexane–hexamethyldisiloxane–perfluorohexane as a function of the mole fraction x at temperatures 0.85, 10.95, 16.05, 21.15, 21.49, 21.83, 22.09, 22.61 and 23.50°C. The dotted lines represent the quasibinary slices with volume ratios $V(M_2):V(C_6)$, of 1:3, 1:1 and 3:1. The circles represent the compositions at the maximum temperature of either the binary phase diagram or a quasibinary slice, as appropriate.

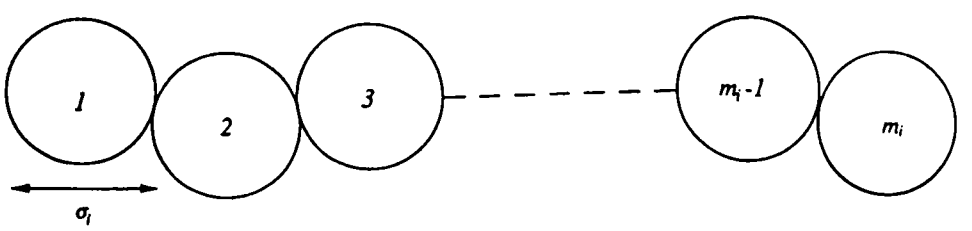

Fig. 7 Molecules modelled as chains of m_i tangent hard spheres of diameter σ_i. A mean-field dispersive interaction is included per spherical segment with an integrated energy of ε_{ii}.

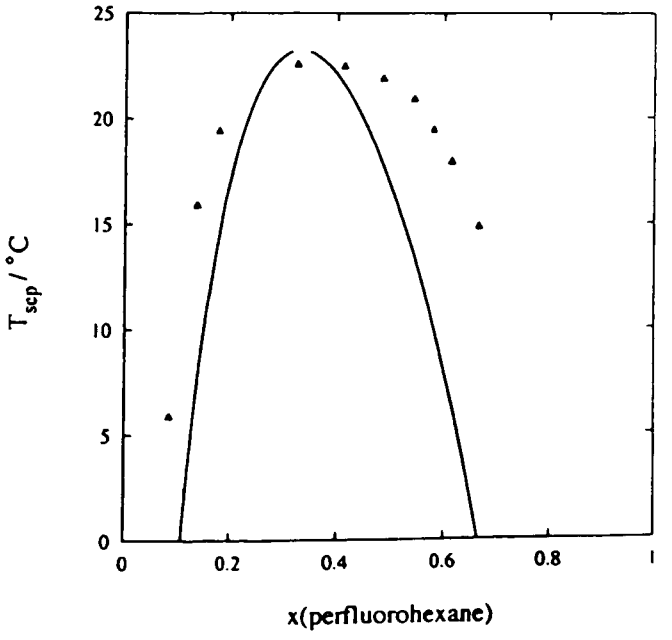

Fig. 8 The experimental phase-separation temperatures T_{sep} for hexane –perfluorohexane as a function of perfluorohexane volume fraction ϕ of Bedford and Dunlap (Δ);[13] these data, as Fig. 1 shows, differ insignificantly from our results and they were in fact used for the fit before our data set was complete. The curve is the theoretical curve drawn as a result of the procedures outlined in the paper. The dotted line indicates a freehand closure across the region in which convergence was difficult.

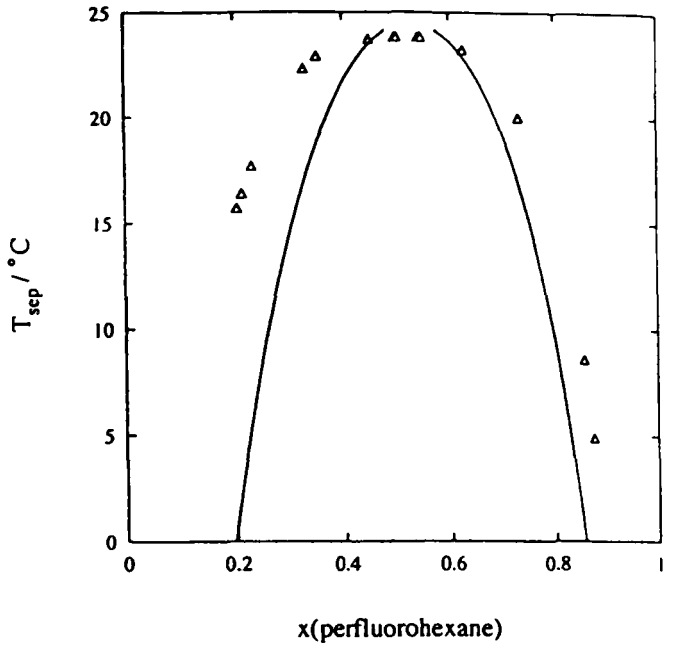

Fig. 9 The experimental phase-separation temperatures T_{sep} for hexamethyldisiloxane–perfluorohexane as a function of perfluorohexane volume fraction ϕ and those of McLure, Mokhtari and Bowers (Δ),[8] these data, as Fig. 2 shows, differ insignificantly from our results and they were in fact used for the fit before our data set was complete. The curve is the theoretical curve drawn as a result of the procedures outlined in the paper. The dotted line indicates a freehand closure across the region in which convergence was difficult.

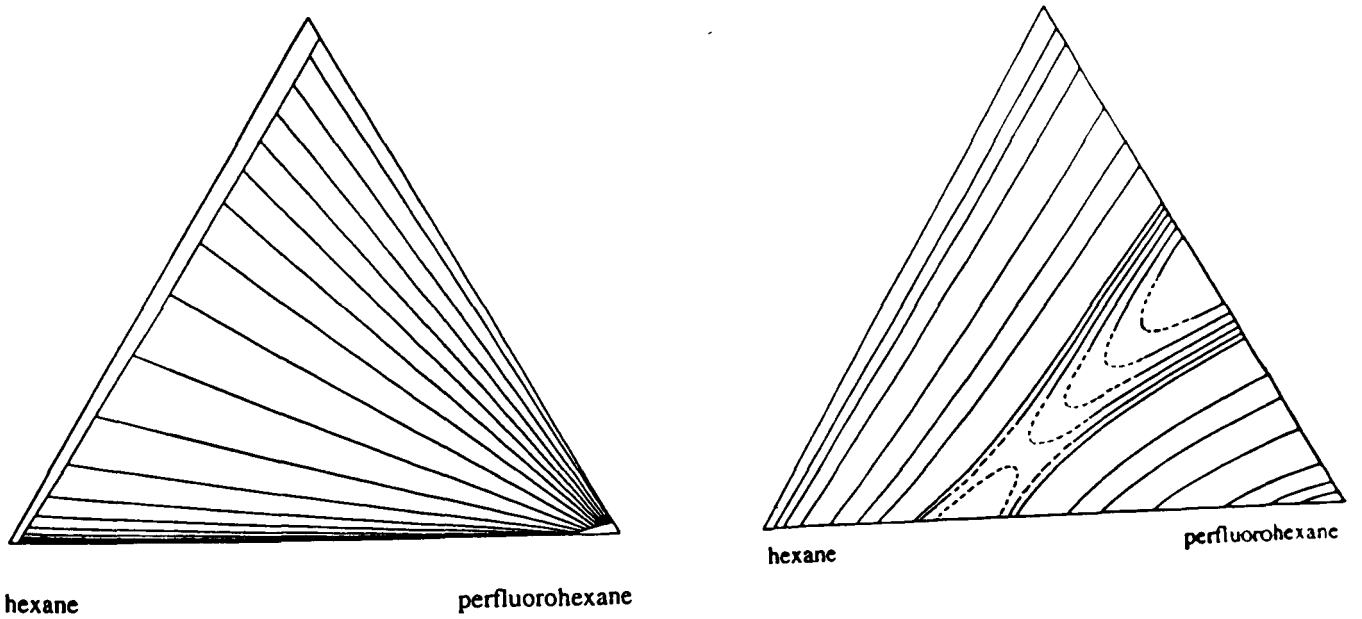

Fig. 10 Isothermal slice at -60.05°C showing the tielines predicted by SAFT-HS theory.

Fig. 11 Triangular phase diagrams predicted using SAFT-HS theory for isothermal slices for hexane–hexamethyldisiloxane–perfluorohexane as a function of the mole fraction x at temperatures -60.05, -39.75, -19.45, 0.85, 10.95, 16.05, 21.15, 21.65, 22.15, 22.65, 23.15 and 23.65°C. The dashed lines represent the extrapolation of the calculated curves in the very small temperature intervals in which convergence was difficult to achieve.

CHAPTER 7: GENERAL CONCLUSIONS

7.1 Overview

7.2 Macroscopic and microscopic viscosities of near-critical mixtures

7.3 Critical-point wetting and critical adsorption

7.4 Ternary mixtures

7.1 Overview

The topics covered in this thesis fall into three basic areas, namely (i) rheological properties of binary mixtures near critical endpoints CEPs, (ii) interfacial properties of binary mixtures near critical endpoints CEPs, and (iii) phase behaviour of simple ternary mixtures. The emphasis is on a comparison between bulk and microscopic behaviour. For example, capillary viscometry has been used to study the bulk macroscopic viscosity, and fluorescence depolarisation of a solute dye has been used to investigate the microscopic viscosity and solvent structure. In addition, evanescent-wave-generated fluorescence spectroscopy has been used to identify the composition of the wetting film at the solid-liquid interface and the wetting transition temperature, and specular neutron reflection has been used to study the detailed molecular liquid structure at the liquid-vapour interface. The general features of the bulk phase behaviour of three ternary mixtures have also been studied both experimentally and theoretically.

Critical points are found in a variety of systems but here we have considered just one type of critical point: liquid-liquid critical points. The studies discussed have involved extending previous work and also applying different or new techniques to a range of systems.

These studies are of two-fold significance in that they contribute both to the development of techniques for the investigation of liquid mixture properties and to the background knowledge on a variety of different mixtures. The information obtained may be of value in other applications. For example, novel techniques for the study of viscosity and fluid flow may be of interest to industry in special circumstances such as close to critical points, and phase equilibria results may be of use in the development of theoretical models. Wetting and surfactancy also have a role in different products and processes, for example in lubrication and foaming. Although much of the current knowledge of liquid mixtures concerns binary mixtures, most commonly encountered fluids have more than two components and the third part of this study has formed a basis for extended work on multicomponent mixtures. The phase behaviour of such systems is usually complex and information on the phase equilibria of simple ternary mixtures is a prerequisite both for studies of various properties in similar mixtures and for phase studies in mixtures of more components such as microemulsions.

The main outcomes of the different areas of study included in this thesis are discussed below.

7.2 Macroscopic and microscopic viscosities of near-critical mixtures

The behaviour of the macroscopic viscosity of binary mixtures near a CEP has been discussed in Chapter 2. Capillary viscometry has been used to study the viscosity of hexane + perfluorohexane along the path of constant critical composition, both for a single-phase mixture above the upper critical solution temperature T_{UCS} and for coexisting phases below T_{UCS}. The expected anomaly at the critical endpoint is observed and is described well by a multiplicative relation between the background and critical parts of the viscosity, with the Renormalisation Group Theory critical exponent $y = 0.04$. The correlation length amplitude $\xi_0 = (5.5\pm1.5)$ Å is higher than values reported from other groups using different techniques.

The behaviour of the macroscopic viscosity near a CEP has been characterised in many studies, although most, as here, have been along the constant composition path. The near-critical viscosity requires further investigation along the isothermal path to confirm experimentally the predicted critical exponent of 0.126. The mathematical descriptions of the viscosity both along the constant composition path, for the single phase and for each coexisting phase, and along the isothermal path need to be reconciled since at the critical point the background terms for each approach must be equal. This is difficult to ensure using different forms of the equation, i.e. multiplicative or additive, along each path. Possible equations to describe the viscosity along the isothermal path remain to be tested.

The near-critical viscosity at a microscopic level has been studied by measuring the rotational correlation times τ_R of fluorescent probes in binary mixtures, in particular in 2-butoxyethanol + H_2O and 2-butoxyethanol + D_2O; the results have been presented in Chapter 3. With one dye, Bodipy, an increase in the product of the rotational correlation time and temperature $\tau_R \cdot T$, taken as a measure of the microviscosity, is observed as the CEP is approached along the constant composition path, but with two other dyes, POPOP and BTBP, a *decrease* in $\tau_R \cdot T$ is observed. The increase observed with Bodipy is the expected behaviour since the macroscopic viscosity exhibits a divergence to infinity at the CEP. However, it seems that for some dyes other effects, such as the structure of the solvent, must play a part.

The microscopic viscosity work described here is, to the best of our knowledge, the first study of its kind on near-critical binary mixtures. During the course of this investigation a large dye probe was found which is suitable for use in our relatively low-viscosity mixtures and yields measurable τ_R values. This work is the initial part of what could be an extensive study of near-critical mixtures at the microscopic level. Suitable dyes in many different mixtures should enable the characterisation of the viscosity and the solvent structure.

7.3 Critical-point wetting and critical adsorption

Critical-point wetting has been studied at the solid-liquid and liquid-vapour interfaces using evanescent-wave-generated fluorescence spectroscopy and specular neutron reflection, respectively. The details of the techniques and the results have been given in Chapters 4 and 5.

At the quartz-liquid interface the techniques investigated to study the wetting transition were steady-state intensity and time-resolved methods, exploiting the shift in the excitation spectrum and the change in the fluorescence lifetime of the dye 1,6-diphenylhexatriene (DPH) in alkanes *versus* perfluoroalkanes. The fluorescence lifetime method was used successfully to study the wetting transition in heptane + perfluorohexane and the wetting transition temperature T_w was identified as 31.5°C, that is 11.5 K below T_{UCS} = 43°C. This is the first time that the fluorescence lifetime method has been used to study a wetting transition.

At the liquid-vapour interface neutron reflectivity measurements have been carried out to study the structure of critical-point wetting layers and the nature of critical adsorption in several mixtures. In hexane + perfluorohexane above T_{UCS} the surface structure is modelled by a subphase enriched in perfluorohexane with respect to the bulk critical composition mixture capped by a monolayer of pure perfluorohexane. As T_{UCS} is approached the subphase becomes increasingly enriched in perfluorohexane and the thickness of the perfluorohexane monolayer increases. This is consistent with our expectations of critical adsorption. Below T_{UCS} a similar model is used comprising a macroscopic perfluorohexane-rich phase with a scattering length density corresponding to that of the bulk lower perfluorohexane-rich phase. Again this phase is capped by a monolayer of pure perfluorohexane and at temperatures further below T_{UCS} this monolayer disappears. The observation of a perfluorohexane-rich layer at the liquid-vapour interface is in agreement with expectations for critical-point wetting.

Slightly more complex interfacial scattering length density profiles are required to describe the surface structure of other perfluoroalkane-containing mixtures. Although methylcyclohexane MCH + perfluoromethylcyclohexane PFMCH mixtures can be modelled in a similar way to hexane + perfluorohexane mixtures, the fitting is very sensitive to the surface and interfilm roughness factors, thus suggesting that the model is not entirely adequate. The surface structure can be more consistently described by a PFMCH-rich subphase capped close to T_{UCS} by three layers of alternating scattering length density with pure PFMCH at the surface. Hexamethyldisiloxane + perfluorohexane cannot be modelled in a similar way to hexane + perfluorohexane, instead requiring a slab model with three or four layers of alternating scattering length density on a subphase of the bulk critical composition above T_{UCS} and of the bulk perfluorohexane-rich phase below T_{UCS}.

The most complex surface structure is observed for 2-butoxyethanol + D_2O. In this mixture measurements were carried out below T_{LCS} and the surface is most successfully modelled by a damped oscillatory scattering length density profile composed of ten layers. This is characterised by a damped amplitude as the bulk mixture is approached, and the D_2O-rich layers decrease in thickness while the 2-butoxyethanol-rich layers increase in thickness with increasing distance from the liquid-vapour interface.

The surface structures identified here from neutron reflectivity measurements fit broadly into the predicted behaviour of critical-point wetting and critical adsorption layers, although the observed structure is more complex than initially expected. These types of mixture deserve further investigation to study the surface in more detail and to compare the features in mixtures for which the intermolecular forces are different kinds.

There are still many issues to be resolved in critical adsorption and critical-point wetting. For example, the wetting transition temperatures at solid-liquid or liquid-vapour interfaces are only known for relatively few systems and interfaces and issues such as the thicknesses of the layers and the order of the transitions remain generally unresolved.

7.4 Ternary mixtures

The studies carried out in this work are on relatively simple ternary mixtures and have been discussed in Chapter 6. Tunnel phase behaviour has been observed for three mixtures in which two of the components are fully miscible over the considered temperature range and both form partially miscible binary mixtures with the third component. These mixtures are (i) cyclohexane + perdeuterocyclohexane + perfluorohexane, (ii) hexane + decane + propanenitrile, and (iii) hexane + hexamethyldisiloxane + perfluorohexane. The phase behaviour of all of these mixtures has been characterised over a range of temperatures close to the two binary T_{UCS} by measuring the phase separation temperatures of mixtures whose compositions fall on quasibinary slices defined by fixed ratios of the two components which are fully miscible.

Mixture (i) is of interest for our neutron reflectivity studies in which deuteration may be used to highlight particular parts of the structure. However, since from this work it is observed that a significant change in T_{UCS} occurs on deuteration it may not be safe to assume that the surface structure of a mixture containing a deuterated component is the same as that of mixture containing the corresponding hydrogenated component. In mixture (i) the maximum phase separation temperature for the central quasibinary slice, in volume fraction terms, is intermediate between the T_{UCS} of the composite binary mixtures but the locus of the line linking the three maximum temperatures is not linear.

Mixture (ii) is composed of two homologous alkanes and the phase behaviour of this mixture is fairly regular. The line linking the binary T_{UCS} and the three maximum phase separation temperatures of the quasibinary slices is almost linear in temperature but some curvature is observed for the composition dependence. This study was

extended to investigate the positions of the tielines and suggests that the tielines do not lie in the plane of the quasibinary slices at all temperatures, but with increasing temperature tend to become more parallel to the nearest binary face of the phase prism. This mixture was selected primarily because the binary T_{UCS} are at convenient temperatures and the shape of the two-phase tunnel was expected to be fairly regular and thus provide a suitable system in which to investigate the tielines and properties such as the viscosity.

Two of the components of mixture (iii), hexane and hexamethyldisiloxane, are similar in many respects both in pure component properties–such as the critical temperature–and in mixtures with, for example, perfluoroalkanes. This latter feature is illustrated by the near-equality within 1 K of the T_{UCS} for hexane + perfluorohexane and hexamethyldisiloxane + perfluorohexane mixtures. The central quasibinary slice has a maximum phase separation temperature approximately 1 K below the lowest T_{UCS} of the binary mixtures. The tunnel thus shows a col or saddle. The phase behaviour of mixture (iii) has also been studied using SAFT-HS theory and this decrease in the maximum temperature in the three-phase region is predicted by the theory.

Experimental phase diagram studies such as these described here are useful for the development of theories of phase equilibria and may also act as models for studies on more complex mixtures such as microemulsions.

ANNEXE A: FLUORESCENCE

A.1 Fluorescence background

The fluorescence process and factors affecting the fluorescence intensity, lifetime and spectra are discussed in this annexe. Fluorescence techniques have been used in Chapter 3 to study the microscopic viscosity of near-critical mixtures and in Chapter 4 to investigate critical-point wetting at the solid-liquid interface.

Fuller descriptions of fluorescence and various influencing factors can be found in the books by Parker (1968) and by Berlman (1965). Other useful sources, particularly for time-resolved fluorescence, include the books by Cundall and Dale (1983) and by Demas (1983).

A.1.1 Mechanism for fluorescence

When a molecule in solution absorbs light it can be promoted to an excited vibrational level of a higher electronic state, as shown in Figure A.1. Some of this energy can then be lost by radiationless processes, such as intermolecular collisions, as the molecule falls to the lowest vibrational level of the upper excited state, and the remaining energy can be emitted as radiation, as the molecule returns to a vibrational level of the ground electronic state. This process is known as *absorption* followed by *fluorescence*.

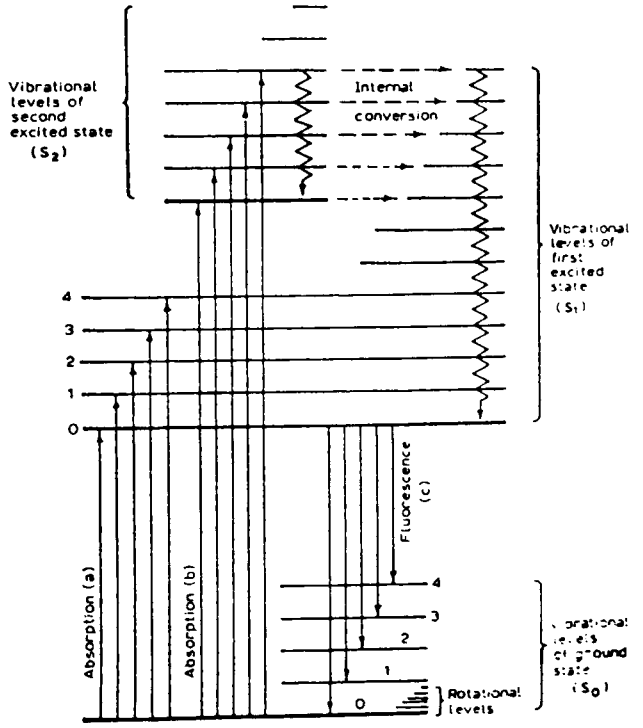

Figure A.1: Energy level diagram showing the transitions giving rise to absorption and fluorescence spectra. (Reproduced from Parker, 1968.)

The radiation emitted is normally of lower frequency than that absorbed, i.e. a shift of the emission to longer wavelengths relative to the absorption is observed and is known as a Stokes shift. The absorption spectrum shows the vibrational spacing of the excited state and the fluorescence emission spectrum displays the vibrational spacing of the ground state. In this simple case the excitation and emission spectra are mirror images, particularly for transitions between the ground and first excited electronic states. This is due to the same transitions occurring in the absorption and the emission spectra and to the similarity in the vibrational spacings of the ground and first excited electronic states.

Light absorption takes place very rapidly, within about 10^{-15} s, and during this time the heavy nuclei of the atoms in the molecule do not appreciably change their positions or momenta. This statement forms the Franck-Condon principle, according to which the most likely absorption or emission transition is taken to be that in which there is no change in nuclear position or momentum during the transition. For a diatomic this is represented on a potential energy-interatomic distance diagram by a vertical transition between the electronic states as shown in Figure A.2. This explains why the intensities of the absorption and emission bands in electronic spectroscopy vary, as some transitions are more likely than others.

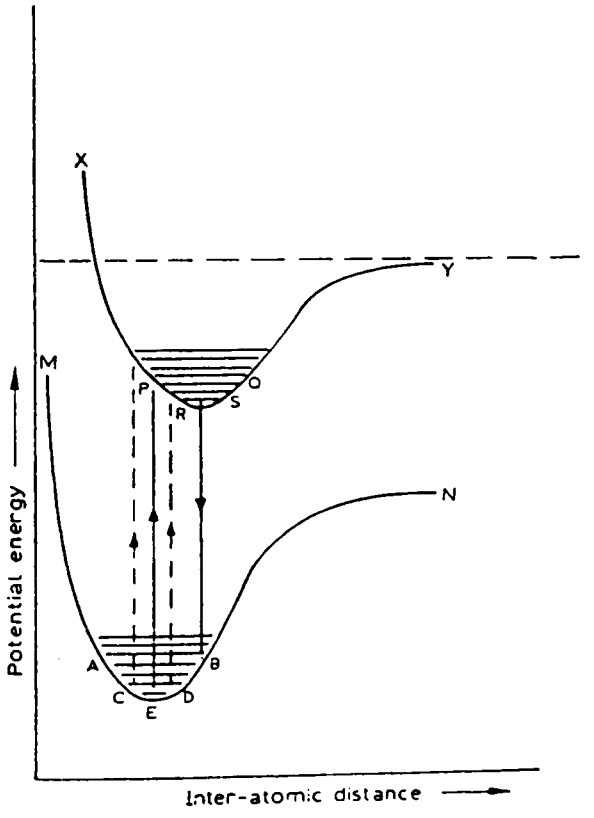

Figure A.2: Potential energy-interatomic distance diagram for a diatomic to illustrate the Franck-Condon principle. (Reproduced from Parker, 1968.)

The (o-o) transition is the lowest frequency transition between the lowest vibrational levels of the ground and first excited state. The bands resulting from these transitions in the absorption and emission spectra may be expected to coincide as the energy gap is the same. However, this is not usually the case due to differing solvation of the species in each state. The excited state is generally more polarisable and thus the degree of solvation is different from that observed for the ground state. Light absorption takes place very quickly and the solvent molecules do not have time to reorient, so the excited state first formed is not the most stable configuration. During the rearrangement of the solvent shell in forming the most stable configurations for the excited species and for the ground state after emission, some energy is lost by radiationless processes and the frequency of the radiation emitted is less than that absorbed. The separation of the (o-o) bands depends on the degrees of solvation for each state and thus varies with the molecule and with the polarity of the solvent.

There is a difference between *absorption* and *excitation* spectra in the way in which they are measured. Absorption spectra are measured by observing which frequencies of radiation are absorbed from the incident radiation as it passes through the sample. Excitation spectra are measured by observing the intensity of the light emitted at a given wavelength as a function of excitation wavelength. The absorption and excitation spectra of a given sample are generally the same but the excitation spectrum may be distorted if the concentration of the solution is too high.

A.1.2 Electronic energy levels and transitions

Fluorescent species are generally unsaturated molecules with extensive π systems. The fluorescence is usually due to π^*-π transitions. Fluorescence can also arise from π^*-n transitions, although these are usually of low probability and may thus have longer lifetimes. Some transitions are forbidden due to considerations such as symmetry, but can be observed due to coupling to a state with an allowed transition or to a slight perturbation in the excited state causing the transition to be partially allowed.

The electronic states are normally numbered in order of increasing energy and are labelled according to their multiplicity, thus singlet states are labelled S_0 (ground state), S_1, S_2...S_n and triplet excited states are labelled T_1, T_2...T_n. The electronic states can also be given a fuller label by including their symmetry, for example ^1A_g and ^1B_u. The A and B labels are group theory symbols for the symmetry of the state. The superscript numbers, 1 in this case, indicate the multiplicity, i.e. singlet states. The g and u subscripts indicate the parity, i.e. the behaviour under inversion. For g states the electronic wavefunction is symmetric under inversion and for u states it is anti-symmetric.

Transitions between states of the same symmetry or the same parity are forbidden. Transitions between states of different multiplicity are spin forbidden, so singlet-singlet transitions are allowed, but singlet-triplet transitions are forbidden. From a consideration of symmetry, parity and multiplicity it can be seen that a ^1A_g-^1B_u transition is allowed.

A.1.3 Fluorescence intensity

The fluorescence intensity is the quantity which is usually studied in an experiment. Steady-state experiments are those in which the total fluorescence intensity due to many excitation processes is measured and the short-time-scale dependence of the fluorescence intensity is not studied. The fluorescence lifetime gives a measure of the decrease in fluorescence intensity with time and this is discussed in the following section.

A.1.4 Fluorescence lifetime

The fluorescence lifetime or decay time is defined as the time taken for the intensity of the fluorescence radiation to fall to a value 1/e of its original maximum value. If n_o molecules are excited to an upper electronic state and the only pathway for return to the ground state is by emission of light, the number of molecules emitting their energy per second, dn/dt, is proportional to the number n of molecules present at a given time:

$$dn/dt = -k_f n \qquad (A.1)$$

where k_f is a first order rate constant for fluorescence emission.
Therefore on integrating:

$$n = n_o e^{-k_f t}. \qquad (A.2)$$

The intensity of the fluorescence decays exponentially. The mean radiative lifetime for fluorescence τ_r is given by:

$$\tau_r = 1/k_f. \qquad (A.3)$$

When $t = \tau_r$, $n = n_o/e$, and the lifetime is thus the time taken for the intensity to fall to 1/e of its original value, as defined above. The observed lifetime is usually less than the calculated radiative lifetime (from expressions involving the integration of the molecular extinction coefficient with respect to wavenumber) due to the competing radiationless processes (Parker, 1968). If τ_r is used to represent the natural lifetime in the absence of any radiationless processes and τ_F the measured decay time or lifetime then:

$$\tau_r = \tau_F/\phi_F \qquad (A.4)$$

where ϕ_F is the fluorescence quantum yield and is the ratio of photons emitted to photons absorbed. Fluorescence lifetimes are generally of the order 10^{-9} s.

A.1.5 Factors which affect the fluorescence

A.1.5.1 Fluorophore substituents

If the structure of a fluorophore is altered by changing the substituents, the positions of the absorption and/or emission bands may be changed. A shift to shorter wavelengths is known as a *hypsochromic* shift and to longer wavelengths as a *bathochromic* shift. If all the hydrogen atoms in benzene are replaced by deuterium atoms a hypsochromic shift is observed in the fluorescence and in the absorption spectra. If alkyl substituents are substituted onto a benzene ring, e.g. to form toluene, a bathochromic shift is generally observed in both the fluorescence and absorption spectra.

A.1.5.2 Solvent

The positions of the fluorescence bands and the structure of the spectrum are affected by the solvent. The polarity of the solvent, reflected in the refractive index and dielectric constant, can have a large effect. Polar *versus* nonpolar solvents can cause changes due to the different dipole moment of many species in the excited state relative to the ground state.

A.1.5.3 Temperature

In general, for most fluorescent species the fluorescence intensity decreases with increasing temperature. At higher temperatures the molecules have greater kinetic energies and more collisions occur providing radiationless pathways for deactivation and thus the intensity of the radiation emitted is lower.

A.1.5.4 Concentration

The relationship between the concentration of an absorbing species and the amount of energy absorbed can be expressed by the Beer-Lambert law:

$$\log_{10}(I_o/I) = \varepsilon c l \qquad (A.5)$$

where $\log_{10}(I_o/I)$ is the optical density or absorbance with I_o the intensity of incident radiation and I the intensity of transmitted radiation, ε is the molar extinction or molar absorption coefficient, c is the concentration and l is the path length of the sample.

If the concentration is too large, so that the absorbance is greater than 0.1, from the above equation it can be shown that the intensity of the transmitted radiation is less than 80%, i.e. more than 20% has been absorbed. If the fluorescence from a sample of high concentration is observed at right angles to the incident beam, as in a fluorescence spectrometer, a significant proportion of the light has been absorbed before it reaches the centre of the cell. Thus the light left to excite the fluorescent species that are detected is less intense, and the fluorescence intensity is therefore lower. The excessive absorption

of the exciting light or of the fluorescence emitted is termed an inner-filter effect. Very low concentrations can be detected by fluorescence means and it is not necessary to use samples of high concentration. Before measuring a fluorescence emission spectrum of a solution it is best to measure the absorption spectrum and dilute the solution until the absorbance is small at the wavelengths to be used for excitation.

Some fluorescent species at high concentrations can form excited dimers called excimers:

$$A^* + A \rightarrow (AA)^*$$
$$(AA)^* \rightarrow A + A + h\nu$$

This occurs for pyrene and a new band is observed at high concentrations due to the fluorescence of the excimer.

A.1.5.5 Dissolved oxygen

The main effect of oxygen as a dissolved species is to provide a radiationless pathway for deexcitation by means of encounters with the fluorescent molecules. This leads to a decrease in the fluorescence intensity and in the fluorescence lifetime. The effect is more pronounced for molecules with long lifetimes as the chance of the radiationless process competing successfully with the radiative emission is greater.

A.1.5.6 Impurities

The emission of the fluorescence usually takes place from the lowest vibrational level of the excited state and thus the shape of the spectrum should be independent of the wavelength of the exciting light if the energy of the exciting light is equal to, or greater than, the energy gap corresponding to the transition. If the emission spectrum changes for excitation at different wavelengths, more than one fluorescent compound is usually present. This may thus indicate the presence of an impurity. An impurity may also show up as an extra decay component in the fluorescence intensity decay profile with time. However, concentration effects can also lead to a second decay component due to the formation of an excimer, as mentioned above.

A.1.6 Rayleigh scattering and the Raman effect

Extra peaks can occur in the fluorescence spectra due to Rayleigh or Raman scattering. When light is passed through a transparent medium some scattering occurs and this is observed even if all dust particles are removed. For incoming light of frequency ν a band is observed in the spectrum at the same wavelength as that of the incoming light which accounts for almost all of the scattered light. This is known as Rayleigh scattering. The light is scattered by particles which are much smaller than the wavelength of light and the intensity of the scattered light is proportional to $1/\lambda^4$. It occurs due to minute regions of fluctuating refractive index in the medium. The secondary waves so generated do not

cancel out exactly so a small proportion of the light is scattered in all directions at the same frequency as the incident radiation.

In addition, bands can be observed on either side of the Rayleigh band and these are due to Raman scattering. The nuclei of the atoms can vibrate with a frequency ν_o and absorb energy as the molecules are excited to higher rotational and vibrational levels, so a band at $(\nu-\nu_o)$, where ν is the frequency of the incident light, may be observed. This is known as Stokes radiation and the radiation is thus scattered with a frequency lower than that of the incident beam. Anti-Stokes radiation can also occur at a higher frequency $(\nu+\nu_o)$. For anti-Stokes radiation the molecule loses energy and so must already have been in an excited vibrational or rotational state; anti-Stokes radiation is thus generally less intense than Stokes radiation. In the Raman effect, light is scattered with a change of wavelength and bands appear at certain frequencies on either side of the Rayleigh band. Raman bands can be identified by exciting at different wavelengths and observing whether the peaks in the spectrum move by a constant amount from the exciting wavelength; no correlation is observed if the extra bands are due to impurities.

References

Berlman, I.B. (1965) *Handbook of Fluorescence Spectra of Aromatic Molecules*, Academic Press, London.

Cundall, R.B.; Dale, R.E. (1983) *Time-Resolved Fluorescence Spectroscopy in Biochemistry and Biology*, Plenum Press, New York.

Demas, J.N. (1983) *Excited State Lifetime Measurements*, Academic Press, London.

Parker, C.A. (1968) *Photoluminescence of Solutions: with Applications to Photochemistry and Analytical Chemistry*, Elsevier, Amsterdam.

APPENDIX: COMPUTER PROGRAMS

Program 1: viscfit

This program was used to fit the viscosity data as discussed in Chapter 2.

```
c Program based on that used by Davies (1988).
c Modified by P. Whitehead, 1996.
c
c this is a programme for fitting viscosities to the usual
c sort of critical-index based near-consolute point expression
c but with the option of incorporating the Oxtoby correction
c for the effect of differing shear viscosity near the consolute
c point.
c
c the following is the function that is being fitted:
c
c    function functn(x,i,a,x1,x2)
c    eps = (x(i) - ain(1))/(ain(1) + 273.15)
c    eps = dabs(eps)
c    tk=x(i)+273.15
c    const=19.499*ain(6)*1.d22
c    xi=dabs(ain(5))*1.d-10*eps**(-.63)
c    elam=(4.*const*xi**3)/(tk*15.)
c    if(elam.lt.0.01)goto 99
c    dlam=0.0214+0.0266*dlog10(elam)+0.0078*(dlog10(elam))**2
c    goto 77
c99  dlam=0.0
c77  functn=ain(2)*1.d-3*dexp(ain(4)*1.d 3/(x(i)+273.15))*eps**ain(3)
c    functn=(1.-dlam)*functn
c
c    note that the temperatures are expressed in degrees celsius.
c
 implicit double precision (a-h,o-z)
     dimension name(10)
     dimension icode(10),icofix(10)
     dimension a(10),deltaa(10),sigmaa(10),ain(10)
     dimension y(120),sigmay(120),x(120),x1(120),x2(120),ndum(120)
     dimension sigx1(120),sigx2(120),sigy(120),sigx(120)
     common /cbl1/ y,ain,icode,nterms
     ctmin=1.d-5
     nitmax=300
     flmax=1.d6
     nexdat=0
800  open(unit=9,file='inp',form='formatted',status='old')
5    write(6,100)
100  format('type: npts,nterms,')
     read(5,*,err=5) npts,nterms
25   write(6,110)
110  format('type: icode,a (from begining)')
     read(5,*,err=25) (icode(i),a(i),i=1,nterms)
     do 10 i=1,10
     ain(i)=0.0
10   continue
35   write(6,120)
120  format('type: nfixps')
     read(5,*,err=35) nfixps
     if(nfixps.eq.0) goto 31
45   write(6,130)
130  format('type: icofix,a')
     read(5,*,err=45) (icofix(i),ain(icofix(i)),i=1,nfixps)
     mode=0
31   if(nexdat.eq.1) goto 32
30   read(9,*) (x(i),y(i),i=1,npts)
c 30  read(9,*) (x(i),y(i),ndum(i),i=1,npts)
32   close(9)
     jsigy=1
     if(jsigy.eq.0) call phisig(sigy,sigx,y,npts)
     write(6,200) npts,nterms,mode,jsigy,nfixps
200  format(5(5x,i5))
     write(6,210)
210  format(1h ,'initial parameters were....')
     write(6,220) (icode(i),a(i),deltaa(i),i=1,nterms)
220  format(3x,' a(',i2,' ) = ',f10.6,' (',f10.6,' )' )
     if(nfixps.eq.0) goto 50
     write(6,240)
240  format(1h ,'fixed parameters were....')
     write(6,250) (icofix(i),ain(icofix(i)),i=1,nfixps)
250  format(3x,' a(',i2,' ) = ',f10.6)
     goto 55
50   write(6,260)
260  format(1h ,'no fixed parameters')
55   continue
     do 40 i=1,nterms
     deltaa(i)=dabs(a(i))/100.
     if(icode(i).eq.1) deltaa(i)=0.001
40   continue
     chisqr=0.
     niter=0
     flamda=0.001
500  niter=niter+1
     chiold=chisqr
     if(mode.ne.0)
    *call varanc(x,i,a,x1,x2,sigx,sigx1,sigx2,sigy,sigmay,npts)
     call curfit(x,y,sigmay,npts,nterms,mode,a,deltaa,x1,x2,sigmaa,
    *flamda,chisqr)
     delchi=(chiold-chisqr)/chisqr
     ctest=dabs(delchi)
     if(ctest.le.ctmin.or.niter.gt.nitmax
    *.or.flamda.gt.flmax) goto 400
     flamda=flamda/10.
     goto 500
400  write(6,230) niter,chisqr,flamda
230  format(/1h ,'niter = ',i2,2x,'chisqr = ',f10.6,2x,
    *'flamda = ',f10.6)
     write(6,270)
270  format(1h ,'fitted parameters are....')
     write(6,280) (icode(i),a(i),sigmaa(i),i=1,nterms)
280  format(3x,' a(',i2,' ) = ',f10.6,' (',f10.6,' )' )
65   write(6,140)
140  format('type: 1=stop,2=call datout,3=another fit')
     read(5,*,err=65) next
     if(next-2) 900,300,600
600  write(6,410)
410  format('type: 1=same data,not 1=new data')
     read(5,*,err=600) nexdat
     if(nexdat.eq.1) goto 5
c    goto 800
     goto 900
300  call datout(x,i,a,sigx,y,sigmay,npts)
     goto 65
900  stop
     end
     subroutine phisig(sigy,sigx,y,npts)
     implicit double precision (a-h,o-z)
     dimension sigy(120),y(120),sigx(120)
     sigmas=0.0009
     sigr=0.0001
     r=0.89
     c=2.0
     sigror=sigr/r
     sigmoc=sigmas/c
     do 10 i=1,npts
     brkt=1.0/y(i)-1.0
     sigwow=sigmoc*(brkt/r+1.0)
     sigy(i)=y(i)*y(i)*dsqrt((sigror*brkt)**2+
    *(sigwow*brkt)**2+(sigwow*r)**2)
10   continue
     return
20   do 30 i=1,npts
     sigy(i)=(1.0d-4)*dsqrt(y(i)-0.965)
     sigx(i)=0.001d0
30   continue
     return
     end
     subroutine datout(x,i,a,sigx,y,sigmay,npts)
     implicit double precision (a-h,o-z)
     dimension x(120),x1(120),y(120),a(10),x2(120),sigmay(120)
    *,sigx(120)
     write(6,10)
     write(6,11)
     sum=0.d0
     do 50 i=1,npts
     if(sigmay(i)) 50,45,50
45   sigmay(i) = 1.d0
50   sum=sum+sigmay(i)
     sigbar=sum/npts
     do 100 i=1,npts
     yy=functn(x,i,a,x1,x2)
     dy=(y(i)-yy)/sigmay(i)
```

```
      write(6,12) x(i),sigx(i),sigmay(i),y(i),yy,dy
  100 continue
      write(6,13) sigbar
      return
   10 format(1h ,2x,'the data used in this fit were...'//)
   11 format(1x,'temp.',8x,'temp.er.',1x,'o.p.er.',4x,'order param.',
     *2x,'calc.o.p.',5x,'deviation'/)
   12 format(d13.6,1x,d8.2,1x,d9.3,1x,2(d13.6,1x),d10.3)
   13 format(2x,' the average standard deviation for this fit was...',
     *d12.6)
      end
      function functn(x,i,a,x1,x2)
      implicit double precision (a-h,o-z)
      dimension y(120)
      dimension x(120), x2(120),x1(120), a(10),ain(10),icode(10)
      common /cbl1/ y,ain,icode,nterms
      do 10 j=1,nterms
      ain(icode(j))=a(j)
   10 continue
      eps = (x(i) - ain(1))/(ain(1) + 273.15)
      eps = dabs(eps)
      tk=x(i)+273.15
      const=19.499*ain(6)*1.d22
      xi=dabs(ain(5))*1.d-10*eps**(-.63)
      elam=(4.*const*xi**3)/(tk*15.)
      if(elam.lt.0.01)goto 99
      dlam=0.0214+0.0266*dlog10(elam)+0.0078*(dlog10(elam))**2
      goto 77
   99 dlam=0.0
   77 functn=ain(2)*1.d-3*dexp(ain(4)*1.d 3/(x(i)+273.15))*eps**ain(3)
      functn=(1.-dlam)*functn
      return
      end
      subroutine curfit (x,y,sigmay,npts,nterms,mode,a,deltaa,x1,x2,
     +                   sigmaa,flamda,chisqr)
      implicit double precision (a-h,o-z)
      dimension x2(120)
      dimension x(120),x1(120),y(120),sigmay(120),a(10),deltaa(10)
      dimension weight(120),alpha(10,10),beta(10),deriv(10)
      dimension array(10,10),b(10),sigmaa(10)
   11 nfree=npts-nterms
      if(nfree) 13,13,20
   13 chisqr=0.
      go to 110
c
c     evaluate weights
c
   20 do 30 i=1,npts
   21 if(mode)22,27,29
   22 if (y(i)) 25,27,23
   23 weight(i)=1./y(i)
      go to 30
   25 weight(i)=1./(-y(i))
      go to 30
   27 weight(i)=1.
      go to 30
   29 weight(i)=1./sigmay(i)**2
   30 continue
c
c     evaluate alpha and beta matrices
c
   31 do 34 j=1,nterms
      beta(j)=0.
      deriv(j)=0.d0
      do 34 k=1,j
   34 alpha(j,k)=0.
   41 do 50 i=1,npts
      call fderiv(x,i,a,deltaa,nterms,deriv,x1,x2)
      w=weight(i)
      yd=y(i)-functn(x,i,a,x1,x2)
      do 46 j=1,nterms
      beta(j)=beta(j)+w*yd*deriv(j)
      sd=w*deriv(j)
      do 46 k=1,j
   46 alpha(j,k)=alpha(j,k)+sd*deriv(k)
   50 continue
   51 do 53 j=1,nterms
      do 53 k=1,j
   53 alpha(k,j)=alpha(j,k)
c
c     evaluate chi square at starting point
c
   60 chisq=0.
   61 do 63 i=1,npts
   62 yfit=functn(x,i,a,x1,x2)
   63 chisq=chisq+weight(i)*(y(i)-yfit)**2
      free=nfree
      chisq1=chisq/free
c
c     invert modified curvature matrix to find new parameters
c
   71 do 74 j=1,nterms
      sd=dsqrt(alpha(j,j))
      do 73 k=1,nterms
   73 array(j,k)=(alpha(j,k)/sd)/dsqrt(alpha(k,k))
   74 array(j,j)=1.0d0+flamda
   80 call matinv(array,nterms,det)
   81 do 84 j=1,nterms
      b(j)=a(j)
      sd=dsqrt(alpha(j,j))
      do 84 k=1,nterms
   84 b(j)=b(j)+beta(k)*(array(j,k)/sd)/dsqrt(alpha(k,k))
c
c     if chi square increases, increase flamda and try again
c
      chisq=0.
   91 do 93 i=1,npts
   92 yfit=functn(x,i,b,x1,x2)
   93 chisq=chisq+weight(i)*(y(i)-yfit)**2
      chisqr=chisq/free
      if (chisq1-chisqr) 95,101,101
   95 flamda=10.*flamda
      if(flamda.le.1.d6) goto 71
      goto 110
c
c     evalute parameters and uncertainties
c
  101 do 103 j=1,nterms
      a(j)=b(j)
  103 sigmaa(j)=dsqrt(array(j,j)/alpha(j,j))
      flamda=flamda/10.d0
  110 continue
      return
      end
      subroutine matinv(array,norder,det)
      implicit double precision (a-h,o-z)
      dimension array(10,10), ik(10), jk(10)
   10 det= 1.
   11 do 100 k=1,norder
c
c      find largest element array(i,j) in rest of matrix
c
      amax=0
   21 do 30 i=k, norder
      do 30 j=k, norder
   23 if (dabs(amax)-dabs(array(i,j))) 24, 24, 30
   24 amax=array(i,j)
      ik(k) = i
      jk(k) = j
   30 continue
c
c      interchange rows and columns to put amax in array(k,k)
c
   31 if (amax) 41, 32, 41
   32 det=0.
      go to 140
   41 i = ik(k)
      if (i-k) 21, 51, 43
   43 do 50 j=1, norder
      save = array(k,j)
      array(k,j) = array(i,j)
   50 array(i,j) = -save
   51 j = jk(k)
      if (j-k) 21, 61, 53
   53 do 60 i=1, norder
      save = array(i,k)
      array(i,k) =array(i,j)
   60 array(i,j) = -save
c
c      accumulate elements of inverse matrix
c
   61 do 70 i=1, norder
      if (i-k) 63, 70, 63
   63 array(i,k) = -array(i,k) / amax
   70 continue
   71 do 80 i=1, norder
      do 80 j=1, norder
      if (i-k) 74, 80, 74
   74 if (j-k) 75, 80, 75
   75 array(i,j) = array(i,j) + array(i,k)*array(k,j)
   80 continue
   81 do 90 j=1, norder
      if (j-k) 83, 90, 83
   83 array(k,j) = array(k,j) / amax
```

```
 90   continue
      array(k,k) =1. / amax
 100  continue
c
c      restore ordering of matrix
c
 101  do 130 l=1,norder
      k=norder-l+1
      j=ik(k)
      if (j-k) 111,111,105
 105  do 110 i=1,norder
      save=array(i,k)
      array(i,k)=-array(i,j)
 110  array(i,j)=save
 111  i=jk(k)
      if (i-k) 130,130,113
 113  do 120 j=1,norder
      save=array(k,j)
      array(k,j)=-array(i,j)
 120  array(i,j)=save
 130  continue
 140  return
      end
      subroutine varanc(x,i,a,x1,x2,sigx,sigx1,sigx2,sigy,sigmay,
     1npts)
      implicit double precision (a-h,o-z)
      dimension x(120),x1(120),x2(120),a(10),sigmay(120),
     1sigx1(120),sigx2(120),sigy(120),sigx(120)
      do 500 i=1,npts
      if(sigx(i).eq.0.d0) go to 100
      x(i)=x(i)+sigx(i)
      yh=functn(x,i,a,x1,x2)
      s2=2.d0*sigx(i)
      x(i)=x(i)-s2
      dydx1=(yh-functn(x,i,a,x1,x2))/s2
      x(i)=x(i)+sigx(i)
 100  continue
      if(sigx1(i).eq.0.d0) go to 200
      x1(i) = x1(i) + sigx1(i)
      yh=functn(x,i,a,x1,x2)
      s2 = 2.d0*sigx1(i)
      x1(i)=x1(i)-s2
      dydx2=(yh-functn(x,i,a,x1,x2))/s2
      x1(i) = x1(i) + sigx1(i)
 200  continue
      if(sigx2(i).eq.0.d0) go to 300
      x2(i) = x2(i) + sigx2(i)
      yh=functn(x,i,a,x1,x2)
      s2 = 2.d0*sigx2(i)
      x2(i)=x2(i)-s2
      dydx3=(yh-functn(x,i,a,x1,x2))/s2
      x2(i) = x2(i) + sigx2(i)
 300  continue
      sigmay(i)=dsqrt(sigy(i)**2+(dydx1*sigx(i))**2+(dydx2*sigx1(i))
     1 **2+(dydx3*sigx2(i))**2)
 500  continue
      return
      end


      subroutine fderiv(x,i,a,deltaa,nterms,deriv,x1,x2)
      implicit double precision (a-h,o-z)
      dimension x2(120)
      dimension x(120),x1(120),a(10),deltaa(10),deriv(10)
 11   do 18 j=1,nterms
      aj=a(j)
      delta=deltaa(j)
      if (delta) 16,18,16
 16   a(j)=aj+delta
      yfit=functn(x,i,a,x1,x2)
      a(j)=aj-delta
      deriv(j)=(yfit-functn(x,i,a,x1,x2))/(2.*delta)
 18   a(j)=aj
      return
      end
```

Program 2: ellipso

This program was used to calculate the factors multiplying the viscosity for an ellipsoid, which were used in the analysis of the microviscosity data presented in Chapter 3.

```
C    ellipso.f - extended Feb93
C    B. Brocklehurst
C
     IMPLICIT CHARACTER*1 (Q)
     CHARACTER*6 FNAME
     DIMENSION XYZ(3),PQR(3),CFAC(3),DIFF(3),YAP(3)
     DIMENSION Y1(1024),Y2(1024),P(1024),DATA(8)
     PARAMETER(PI=3.1415927)
C    Fudge factor for perceived inaccuracy in Perrin integration -
     PARAMETER(FUDG=0.985)
C    This is the Boltzmann factor with units conversion -
     PARAMETER(BOLTZ=1.380622E07)
     PRINT *,' This programme evaluates Perrin integrals and D values'
     PRINT *,' or makes use of the YA parameters, or input D values'
     PRINT *,'  and simulates anisotropy data if required.'
     PRINT *,' For an ellipsoid, mol. dimensions are converted to'
     PRINT *,'  those of an ellipsoid of the same volume.'
C    J. phys. Radium, 1934, 5, 497.
     PRINT *,' Putting in D values - y/n ?'
     READ (5,900) QDF
     IF (QDF.EQ.'Y'.OR.QDF.EQ.'y') THEN
     PRINT *,' Enter Dx, Dy, Dz -'
     READ (5,*) (DIFF(K),K=1,3)
     GO TO 200
     ENDIF
     PRINT *,' Spheroid or ellipsoid (S/E) ?'
     READ (5,900) QSE
     IF (QSE.EQ.'s') QSE='S'
     IF (QSE.NE.'S') THEN
     PRINT *,' Enter the hemi-axes, x, y and z -'
     ELSE
     PRINT *,' NB This section not up-dated .....'
     PRINT *,' Enter the hemi-axes, a, b and b -'
     ENDIF
     READ (5,*) (XYZ(I),I=1,3)
     IF (QSE.NE.'S') THEN
     TR=(6.0/PI)**(1.0/3.0)
     DO I=1,3
     XYZ(I)=XYZ(I)*TR
     ENDDO
     ENDIF
     PRINT *,' Hemi-axes in use (xyz):'
     PRINT *,(XYZ(I),I=1,3)
     IF (QSE.EQ.'S') THEN
     IF (XYZ(1).LT.XYZ(2)) THEN
     PRINT *,' Cannot calculate for this case - sorry.'
     STOP
     ENDIF
     ENDIF
     PRINT *,' Stick (y) or slip (n) calculation ?'
     READ (5,900) QYA
     IF (QYA.EQ.'n'.OR.QYA.EQ.'N') THEN
     PRINT *,' Enter Youngren & Acrivos parameters -'
     READ (5,*) (YAP(I),I=1,3)
     PRINT *,(YAP(I),I=1,3)
     VOL=4.0*PI*XYZ(1)*XYZ(2)*XYZ(3)/3.0
     DO I=1,3
     CFAC(I)=YAP(I)*VOL*6.0
C    ?? Need the factor of 6 but why? Error in Y & A ??
     ENDDO
     PRINT *,'Factors multiplying viscosity are -'
     PRINT *,(CFAC(N),N=1,3)
     ELSE
C    Perrin calculation for sticking ellipsoids -
     DS=(XYZ(1)*XYZ(2)*XYZ(3))**(1.0/3.0)/300.0
     DO I=1,3
     PQR(I)=0.0
     ENDDO
     NI=3
     IF (QSE.EQ.'S') NI=2
     DO N=1,NI
     S=0.0
     DO I=1,30000
     S=S+DS
     GRAND=1.0
     DO J=1,3
     GRAND=GRAND*(XYZ(J)*XYZ(J)+S)
     ENDDO
```

```
      GRAND=(XYZ(N)*XYZ(N)+S)*SQRT(GRAND)
      PQR(N)=PQR(N)+DS/GRAND
      ENDDO
      ENDDO
      IF (QSE.EQ.'S') PQR(3)=PQR(2)
      PRINT *,' Results are :-'
      PRINT *,(PQR(I),I=1,3)
      SUM=PQR(1)+PQR(2)+PQR(3)
      CHEC=2.0/(XYZ(1)*XYZ(2)*XYZ(3))
      PRINT *,' Check sum, which =',SUM
      PRINT *,' should equal 2/xyz =',CHEC
      IF (QSE.EQ.'S') THEN
      TR=SQRT(XYZ(1)*XYZ(1)-XYZ(2)*XYZ(2))
      CS=(XYZ(1)+TR)/XYZ(2)
      CS=2.0*LOG(CS)/TR
      TR=TR*TR
      CP=(CS-2.0/XYZ(1))/TR
      CQ=(2*XYZ(1)/(XYZ(2)**2.0)-CS)/(2.0*TR)
      PRINT *,' Correct values of P and Q are -'
      PRINT *,CP,CQ
      ENDIF
      DO N=1,3
      TR=0.0
      TR1=0.0
      DO K=1,3
      IF (K.NE.N) THEN
      TR=TR+XYZ(K)*XYZ(K)
      TR1=TR1+XYZ(K)*XYZ(K)*PQR(K)
      ENDIF
      ENDDO
      CFAC(N)=16.0*PI*TR/(TR1*3.0)
      ENDDO
      PRINT *,'Factors multiplying viscosity are -'
      PRINT *,(CFAC(N),N=1,3)
      IF (QSE.EQ.'S') THEN
      TR=2.0*XYZ(2)*XYZ(2)
      TR1=2.0*XYZ(2)*XYZ(2)*PQR(2)
      CFAC(1)=16.0*PI*TR/(3.0*TR1)
      TR=XYZ(1)*XYZ(1)+XYZ(3)*XYZ(3)
      TR1=XYZ(1)*XYZ(1)*CP+XYZ(3)*XYZ(3)*CQ
      CFAC(2)=16.0*PI*TR/(3.0*TR1)
      PRINT *,' Correct values are -'
      PRINT *,(CFAC(I),I=1,2)
      ELSE
      PRINT *,' NB fudge factor used = ',FUDG
      DO I=1,3
      CFAC(I)=CFAC(I)*FUDG
      ENDDO
      ENDIF
      ENDIF
C     ******************************************************
C     New section -
C     ******************************************************
      PRINT *,' More calculations -'
      READ (5,900) QMO
      IF (QMO.EQ.'N'.OR.QMO.EQ.'n') STOP
  190 PRINT *,' Enter T / K and eta / kg m-1 s-1'
      READ (5,*) TK,ETA
      PRINT *,' T = ',TK,' eta = ',ETA
      TR=BOLTZ*TK/ETA
      DO I=1,3
      DIFF(I)=TR/CFAC(I)
      ENDDO
  200 PRINT *,' D(x) = ',DIFF(1)
      PRINT *,' D(y) = ',DIFF(2)
      PRINT *,' D(z) = ',DIFF(3)
      PRINT *,' Enter principal axis - 1/2/3'
      READ (5,*) IAX
      IF (IAX.EQ.1) PRINT *,' Principal axis taken to be x'
      IF (IAX.EQ.2) PRINT *,' Principal axis taken to be y'
      IF (IAX.EQ.3) PRINT *,' Principal axis taken to be z'
      PRINT *,' '
      AVD=(DIFF(1)+DIFF(2)+DIFF(3))/3.0
      DPROD=DIFF(1)*DIFF(2)*DIFF(3)
      DEL=0.0
      DO I=1,3
      DEL=DEL+DIFF(I)**2.0-DPROD/DIFF(I)
      ENDDO
      DEL=SQRT(DEL)
      ALPHA=(AVD-DIFF(IAX))/DEL
      BETA1=0.2+0.3*ALPHA
      BETA2=0.2-0.3*ALPHA
      PHI1=1.0E09/(6.0*AVD+2.0*DEL)
      PHI2=1.0E09/(6.0*AVD-2.0*DEL)
      PRINT *,' beta1 = ',BETA1
      PRINT *,' phi1  = ',PHI1
      PRINT *,' beta2 = ',BETA2
      PRINT *,' phi2  = ',PHI2
      IF (QDF.EQ.'Y'.OR.QDF.EQ.'y') THEN
      DXYZ=(DPROD)**(1.0/3.0)
      TAUSPH=1.0E09/(6.0*DXYZ)
      ELSE
      VCHEC=4.0*PI*XYZ(1)*XYZ(2)*XYZ(3)/3.0
      TAUSPH=1.0E09*VCHEC/TR
      ENDIF
      PRINT *,' Check: for sphere - tau = ',TAUSPH
      PRINT *,' Another temperature - y/n ?'
      READ (5,900) QAT
      IF (QAT.EQ.'Y'.OR.QAT.EQ.'y') GO TO 190
      PRINT *,' Simulated data required - y/n ?'
      READ (5,900) QSIM
      IF (QSIM.EQ.'N'.OR.QSIM.EQ.'n') STOP
      PRINT *,' Do you want to convolute with a prompt - y/n?
      READ (5,900) QCON
      IF (QCON.EQ.'Y'.OR.QCON.EQ.'y') THEN
      PRINT *,' Enter file name - nooooo -'
      READ (5,900) FNAME
      OPEN(UNIT=15,FILE=FNAME,STATUS='OLD')
      DO I=1,128
      READ (15,*) ICHAN,(DATA(K),K=1,8)
      DO K=1,8
      P(1025-8*(I-1)-K)=DATA(K)
      ENDDO
      ENDDO
      CLOSE(15)
      PRINT *,' Enter time-scale for prompt -'
      READ (5,*) TS
      STEX=EXP(-TS/PHI1)
      Y1(1)=P(1)
      DO IT=2,1024
      Y1(IT)=Y1(IT-1)*STEX+P(IT)
      ENDDO
      STEX=EXP(-TS/PHI2)
      Y2(1)=P(1)
      DO IT=2,1024
      Y2(IT)=Y2(IT-1)*STEX+P(IT)
      ENDDO
      YMAX=0.0
      DO I=1,1024
      Y1(I)=BETA1*Y1(I)+BETA2*Y2(I)
      IF (Y1(I).GT.YMAX) THEN
      YMAX=Y1(I)
      IPOS=I
      ENDIF
      ENDDO
      DO I=1,1024
      Y1(I)=0.40*Y1(I)/YMAX
      ENDDO
      J=0
      DO I=IPOS,1024
      J=J+1
      Y2(I)=TS*REAL(J)
      ENDDO
      PRINT *,' Time-range of convoluted data: 0 to ',Y2(1024)
      ENDIF
      PRINT *,' Enter file-name for output - xxxxxx'
      READ (5,900) FNAME
      OPEN(UNIT=15,FILE=FNAME,STATUS='NEW')
      PRINT *,' Enter time-range / ns'
      READ (5,*) RANGE
      PRINT *,' Time-range 0 to ',RANGE
      PRINT *,' Enter scale factor (1 for r(0)=0.4) '
      READ (5,*) SCA
      TR=SCA*0.4
      PRINT *,' Scale factor gives r(0) = ',TR
      TD=RANGE/200.0
      IF (QCON.EQ.'Y'.OR.QCON.EQ.'y') THEN
      DO I=IPOS,1024
      Y1(I)=SCA*Y1(I)
      ENDDO
      DO I=IPOS,1024
      IF (Y2(I).LT.RANGE) WRITE (15,901) Y2(I),Y1(I)
      ENDDO
      ELSE
      DO I=1,201
      TR=TD*REAL(I-1)
      ANISO=SCA*(BETA1*EXP(-TR/PHI1)+BETA2*EXP(-TR/PHI2))
      WRITE (15,901) TR,ANISO
      ENDDO
      ENDIF
      STOP
  900 FORMAT(A)
  901 FORMAT(2X,F8.4,2X,F7.5)
      END
```

Program 3: nrfit

This program was used to fit neutron reflectivity data to layer models as discussed in Chapter 5.

```
C     A.N. Burgess, ICI C&P

program nrfit
      IMPLICIT REAL(A-Z)
      INTEGER
I,J,NOPO,SIGN,SHIFT,ITERA,MAXIT,STP,NLAYERI,NREP,NPA
R
      COMMON/SIMS/LAMIN,LAMAX,NREP,NPAR
      COMMON/PARAMS/PARAM(1500),NOPO
      COMMON/REST/RP(1000),QOB(1000)
      COMMON/WHAT/NV,INV(1000),NLAYERI

COMMON/GRAPHS/sob(1000),OB(1000),serr(1000),ERR(1000),CH
ANGE(1500)
      COMMON/FILES/FILE,MAXIT
      COMMON/CHISQD/CHISQ
      CHARACTER*10 NAME(1500)
      COMMON/NAM/NAME,STP
      CHARACTER*9 FILE
      CHARACTER*20 fILENAME
      CHARACTER*60 TITLE(20)
      data name/1500*'        '/
C
C
      NAME(1)='THETA'
      NAME(2)='NBA'
      NAME(3)='DTHETA'
      NAME(4)='NBS'
      NAME(5)='ZBB01'
      NAME(6)='LAYER 1'
      NAME(9)='LAYER 2'
      NAME(12)='LAYER 3'
      NAME(15)='LAYER 4'
      NAME(18)='LAYER 5'
      NAME(21)='LAYER 6'
      NAME(24)='LAYER 7'
      NAME(27)='LAYER 8'
      name(30)='LAYER 9'
      name(33)='LAYER 10'
      name(36)='LAYER 11'
C
C
      PRINT*,''
      PRINT*,''
      PRINT*,''
      WRITE(6,1)
1     FORMAT(TR30,'NEUTRON REFLECTIVITY')
      WRITE(6,2)
2     FORMAT(TR29,'————————————')
      WRITE(6,3)
3     FORMAT(TR33,'CURVE FITTING'/TR32,'————————')
C
      OPEN(UNIT=20,STATUS='OLD',NAME='nrdata.dat')
      READ(20,*)FILENAME
C
      OPEN(UNIT=30,STATUS='OLD',NAME=FILENAME)
      DO I=1,6
      READ(30,9000)TITLE(I)
9000      FORMAT(A70)
      END DO
      READ(30,9005)NOPO
9005      FORMAT(24X,I5)
      DO I=1,2
      READ(30,9000)TITLE(I)
      END DO
      DO I=1,NOPO
      READ(30,*)QOB(I),OB(I),ERR(I)
9010      FORMAT(3(4X,G15.5))
      END DO
C
      CLOSE(UNIT=30)
C
C
C
C
C
      READ(20,*)MAXIT,NLAYERI
      NPAR=7+(nlayeri*3)
      name(npar-1)='SCALE FAC.'
      name(npar)='BKGD'
      NREP=0
      PRINT*,''
      PRINT*,''
      PRINT*,''
      PRINT*,''
      DO I=1,NPAR
      READ(20,*)PARAM(I),CHANGE(I)
      WRITE(6,2000)NAME(I),PARAM(I),CHANGE(I)
      END DO
2000      FORMAT(TR2,A10,'  =',G12.3,TR5,G10.3)
C
C
C
92      CLOSE(UNIT=20)
C
      CALL NRCALC
C
C
C
      npt=nopo-1
      do i=1,nopo
      rp(i)=rp(i)+param(npar)
      sob(i)=ob(i)/param(npar-1)
      serr(i)=err(i)/param(npar-1)
      end do
c
c
      CHIBEST=0.0
      DO I=1,NPt
      CHIBEST=CHIBEST+((sOB(I)-RP(I))/sERR(I))**2
      END DO
      CHIBEST=CHIBEST/NPt
      chisq=chibest
      write(6,2001)chibest
2001      format(/1x,'CHISQ = ',e12.5)
C
C
9997      DO ITERA=1,MAXIT
C
      PRINT*,''
      WRITE(6,5000)ITERA,CHIBEST
5000      FORMAT('  ITERATION = ',I4,TR5,'BEST CHISQ =
',G12.4)
      PRINT*,''
C
      WRITE(6,5010)
5010
FORMAT(1X,'PARAMETER',TR6,'CHANGE',TR5,'VALUE',TR11,'
CHISQ')
      PRINT*,''
      TOT=0
C
      DO I=1,npar
C
      IF(CHANGE(I).EQ.0.) GOTO 1020
      SIGN=1
      SHIFT=0
C
C
1000      PARAM(I)=PARAM(I)+SIGN*CHANGE(I)
c
c     ****************************************
c     check for zero going parameters - optional
c     ****************************************
c
c     IF(PARAM(I).LT.0)THEN
c       PARAM(I)=PARAM(I)-SIGN*CHANGE(I)
c       GOTO 1020
c     END IF
      SHIFT=SHIFT+SIGN

c
      CALL NRCALC
C
      do k=1,nopo
      rp(k)=rp(k)+param(npar)
      sob(k)=ob(k)/param(npar-1)
      serr(k)=err(k)/param(npar-1)
      end do
      CHI=0.0
      DO J=1,NPt
```

```
   CHI=CHI+((sOB(J)-RP(J))/sERR(J))**2
   END DO
   CHI=CHI/NPt
C
   WRITE(6,5020)NAME(I),SHIFT,PARAM(I),CHI
5020    FORMAT(1H ,A10,TR5,I3,TR5,G12.4,TR3,G13.4)
C
   IF((CHIBEST-CHI).GE.0.001)THEN
    CHIBEST=CHI
    IF(ABS(SHIFT).LT.3)GOTO 1000
   ELSE IF(SHIFT.EQ.1)THEN
    SIGN=-1
    SHIFT=0
    PARAM(I)=PARAM(I)+SIGN*CHANGE(I)
    GOTO 1000
   ELSE
    PARAM(I)=PARAM(I)-SIGN*CHANGE(I)
   END IF
C
   IF(SHIFT.NE.-1)TOT=1
C
1020    END DO
C
   PRINT*,''
   DO I=1,NPAR
   WRITE(6,5040)NAME(I),PARAM(I)
5040    FORMAT(1H ,A10,TR2,G12.6)
   END DO
   PRINT*,''
   CHISQ=CHIBEST
   WRITE(6,5050)CHIBEST
5050    FORMAT(1X,'CHISQ = ',G12.4)
   PRINT*,''
C
   IF(TOT.LT.1E-5)GOTO 1010
C
   END DO

C
1010  continue
   CALL NRCALC
C
   do k=1,nopo
   rp(k)=rp(k)+param(npar)
   sob(k)=ob(k)/param(npar-1)
   ser(k)=er(k)/param(npar-1)
   end do
   CHIBEST=0.0
   DO I=1,NPt
   CHIBEST=CHIBEST+((sOB(I)-RP(I))/sERR(I))**2
   END DO
   CHIBEST=CHIBEST/NPt
   CHISQ=CHIBEST
C
   PRINT*,''
   PRINT*,''
C
C
C
   CLOSE(UNIT=20)
C
   open(unit=20,name='nrdata.dat',status='old')
   write(20,1011)filename
1011  FORMAT(A15,13x,'FILE NAME')
   write(20,1012)maxit,nlayeri
1012  format(i3,10x,',',i3,11x,'MAXIT,NL')
   do i=1,npar
   write(20,1013)param(i),change(i),name(i)
1013  FORMAT(e12.5,1x,',',1x,e12.5,1x,'T',a10)
   end do
   close(20)
   open(unit=30,name='nrfit.out',type='unknown')
   do i=1,nopo
   write(30,*)qob(i),rp(i),sob(i),ser(i)
   end do
   close(30)
   STOP 'NRFIT END'
   END
**********************************************************
**************************
*                                        *
*       SUBROUTINE BASED ON LAYER_NEW.FOR CALLED
BY gl1          *
*                                        *
*                                        *
*       CALCS COMPLETE GENERAL MULTILAYER
REFLECTIVITY          *
*                                        *
*             J.PENFOLD  16TH OCTOBER 1987          *
*                                        *
**********************************************************
**************************
*                                        *
   SUBROUTINE NRCALC
   DIMENSION AX(2),CX(2),P(20)
   DIMENSION FLG(500)
   DIMENSION ZBB(500),ZBB1(500)
   DIMENSION A1(2,2),A2(2,2),A3(2,2)
   DIMENSION DN(500),DN1(500),RNBN(500),RNBN1(500)
   DIMENSION RNFN(500),PFN(500),BETAN(500)
   DIMENSION RT(1000),RTP(1000)
   DIMENSION XNIT(50)
   REAL*4 LAMBDA,NBA,NBS
   INTEGER CH1,CH2,NLAYER,NLAYER1,qflag
   COMPLEX*8 AC1,AC2,A1,A2,A3,CI,CR,PFN,AC3
   COMPLEX*8 AC4,RNF,RNF1,BETAN,A22T,A12T
   COMPLEX*8 BTM,BTM1,CBTM,CBTM1,CO
   CHARACTER*40 FNAMEIN,FNAMEOUT
   EQUIVALENCE (AX,AC3)
*
   COMMON/PARAMS/PARAM(1500),NOPO
   COMMON/REST/RP(1000),QOB(1000)
   COMMON/WHAT/NV,INV(1000),NLAYER1
*
   COMMON /CSPEC/
LAMBDA,THETA0,DTHET,DTHETR,K0,PI,TPI,NLAYER
   COMMON /TDATA/
PFN,BETAN,A1,A2,A3,CI,CR,CO,AC1,AC2,AC3,AC4
   COMMON /TDATA1/ RNBN,DN,ZBB,RNFN,FLAG
*
*
    COMMON/SIMS/ LAMIN,LAMAX,NREP,npar
    REAL LAMIN,LAMAX
    qflag=0
    if(qob(1).lt.0.1)qflag=1
*
   DO 10 I=1,NOPO
10     RP(I)=0.00
*
*
*             SET UP SOME CONSTANTS
*
   CX0=0.0
   CX1=1.0
   CI=CMPLX(CX0,CX1)
   CR=CMPLX(CX1,CX0)
   CO=(0.0,0.0)
   PI=ACOS(-1.)
   TPI=2.0*PI
*
*
*    INPUT BASIC CALC AND MODEL PARAMETERS
*
   THETA0=PARAM(1)
   PTHET=PARAM(3)
   NLAYER=NLAYER1
   NBA=PARAM(2)
   NBS=PARAM(4)
   ZBA=PARAM(5)
   ZBA=ZBA**2
   NREP1=NLAYER
   IF(NREP.EQ.0)GOTO 15
   NREP1=NREP
   NFRED=MOD(NLAYER,NREP)
   IF(NFRED.EQ.0)GOTO 15
15     JJ=6
    DO 16 I=1,NREP1
    IF (NREP.EQ.0) THEN
     DN(I+1)=PARAM(JJ)
     RNBN(I+1)=PARAM(JJ+1)
     ZBB(I+1)=PARAM(JJ+2)
     ZBB(I+1)=ZBB(I+1)*ZBB(I+1)
    ELSE
     DN1(I)=PARAM(JJ)
     RNBN1(I)=PARAM(JJ+1)
     ZBB1(I)=PARAM(JJ+2)
    END IF
16     JJ=JJ+3
   IF(NLAYER.EQ.1)GOTO 500
   IF(NREP.EQ.0)GOTO 500
    DO 21 I=2,(NLAYER+1),NREP
     DO 22 J=1,NREP
      K=(I+J-1)
```

```
      RNBN(K)=RNBN1(J)
      DN(K)=DN1(J)
      ZBB(K)=ZBB(J)
22      CONTINUE
21    CONTINUE
500     RNBN(1)=NBA
    RNBN(NLAYER+2)=NBS
    ZBB(1)=ZBA
    ZBB(NLAYER+2)=0.0
    DN(1)=0.0
    DN(NLAYER+2)=0.0
    NLAYER=NLAYER+2
*
*
*   SET UP SOME CONSTANTS
*
*
20    THETA0=THETA0*0.01745
    DTHET=THETA0*PTHET/100.
    DTHET=DTHET/2.35
    DTHETR=DTHET*2.51
    TMAX=THETA0+DTHET*3
    TMIN=THETA0-DTHET*3
    ST0=SIN(THETA0)
    CT0=COS(THETA0)
*
    IF(PTHET.NE.0)GOTO 100
*
*
*   HERE FOR NO RESOLUTION
*
*
    NV=0
    DO 40 J=1,NOPO
     NV=NV+1
     INV(NV)=J
     LAMBDA=QOB(J)
     if(qflag.eq.1)lambda=4.0*pi*st0/qob(j)
    CON=LAMBDA*LAMBDA/TPI
    TL=LAMBDA*LAMBDA
    TLC=78.96/TL
     DO 31 I=1,NLAYER
      RNFN(I)=(1.0-CON*RNBN(I))
31      CONTINUE
     PFN(1)=RNFN(1)*ST0
     DO 32 I=2,NLAYER-1
      RNF=(RNFN(I)**2)*CR
      RNF1=(RNFN(1)**2)*CR
      PFN(I)=CSQRT(RNF-(RNF1*CT0**2))
32      CONTINUE
     RNF=(RNFN(NLAYER)**2)*CR
     RNF1=(RNFN(1)**2)*CR
     PFN(NLAYER)=CSQRT(RNF-(RNF1*CT0**2))
      DO 34 I=2,NLAYER-1
      BETAN(I)=TPI*DN(I)*PFN(I)/LAMBDA
34      CONTINUE
    A1(1,1)=1.0
    A12T=(PFN(1)-PFN(2))/(PFN(1)+PFN(2))
    A1(1,2)=A12T*CEXP(-TLC*ZBB(1)*PFN(1)*PFN(2))
    A1(2,1)=A1(1,2)
    A1(2,2)=1.0
    DO 35 I=2,NLAYER-1
    BTM=BETAN(I)*CI
    BTM1=-BETAN(I)*CI
    IF(CX(2).EQ.0.0) BTM = BETAN(I)*2.0*CI
    CBTM=CEXP(BTM)
    IF(CX(1).EQ.0.0) CBTM1=CEXP(BTM1)
    IF(CX(2).EQ.0.0) CBTM1=1.0*CR
    A2(1,1)=CBTM
    A22T=C0
    IF((PFN(I)+PFN(I+1)).NE.C0)A22T=(PFN(I)-
PFN(I+1))/(PFN(I)+PFN(I+1))
    A22T=A22T*CEXP(-TLC*ZBB(I)*PFN(I)*PFN(I+1))
    A2(1,2)=A22T*CBTM
    A2(2,1)=A22T*CBTM1
    A2(2,2)=CBTM1
*
     CALL MATRIX(A1,A2,A3)
*
    A1(1,1)=A3(1,1)
    A1(1,2)=A3(1,2)
    A1(2,1)=A3(2,1)
    A1(2,2)=A3(2,2)
35    CONTINUE
    AC1=A1(2,1)
    AC2=CONJG(AC1)
    AC3=A1(1,1)
    AC4=CONJG(AC3)
    IF(AX(1).EQ.0.0.AND.AX(2).EQ.0.0)GOTO 400
    RP(J)=(AC1*AC2)/(AC3*AC4)
    GOTO 401
*
400     RP(J)=1.0
    FLG(J)=1.
401     RT(J)=LAMBDA
30    CONTINUE
40    CONTINUE
    GOTO 200
*
*
*   HERE FOR INTEGRATION OVER DELTA THETA
*
*
100     FLAG=0.
    NIT=21
    DT=(TMAX-TMIN)/NIT
    DO 102 I=1,NIT
    XNIT(I)=TMIN+DT*(I-1)
102     CONTINUE
    NIT1=NIT+1
*
    NV=0
    DO 101 J=1,NOPO
     NV=NV+1
     INV(NV)=J
     LAMBDA=QOB(J)
     if(qflag.eq.1)lambda=4.0*pi*st0/qob(j)
    CON=LAMBDA*LAMBDA/TPI
     DO 310 I=1,NLAYER
      RNFN(I)=(1.0-CON*RNBN(I))
310      CONTINUE
     DO 103 II=1,NIT
      X=XNIT(II)
*
      CALL CALCIN(X,F)
*
     RP(J)=RP(J)+F*DT
103      CONTINUE
    IF(FLAG.EQ.1.) FLG(J)=1.0
    FLAG=0.
    RT(J)=LAMBDA
101     CONTINUE
   do i=1,nopo-1
   rp(i)=(rp(i)+rp(i+1))/2.0
   end do
200   return
    END
*                                                     *
*******************************************************
**************************
*                                                     *
*          SUBROUTINE CALCIN, FOR QA02A INTEGRATION
*
*                                                     *
*******************************************************
**************************

    SUBROUTINE CALCIN(X,F)
    DIMENSION
ZBB(500),DN(500),RNBN(500),RNFN(500),PFN(500)
    DIMENSION
BETAN(500),A1(2,2),A2(2,2),A3(2,2),AX(2),CX(2)
    REAL*4 LAMBDA
    COMPLEX*8
AC1,AC2,AC3,AC4,A1,A2,A3,CI,CR,PFN,RNF,RNF1,BETAN,A22
T,A12T
    COMPLEX*8 BTM,BTM1,CBTM,CBTM1,C0
    EQUIVALENCE (AX,AC3),(CX,BTM1)
*
    COMMON /CSPEC/
LAMBDA,THETA0,DTHET,DTHETR,K0,PI,TPI,NLAYER
    COMMON /TDATA/
PFN,BETAN,A1,A2,A3,CI,CR,C0,AC1,AC2,AC3,AC4
    COMMON /TDATA1/ RNBN,DN,ZBB,RNFN,FLAG
*
*
*
    ST0=SIN(X)
    CT0=COS(X)
    TL=LAMBDA*LAMBDA
    TLC=78.96/TL
    PFN(1)=RNFN(1)*ST0
     DO 32 I=2,NLAYER-1
      RNF=(RNFN(I)**2)*CR
```

```
      RNF1=(RNFN(1)**2)*CR
      PFN(I)=CSQRT(RNF-(RNF1*CT0**2))
32    CONTINUE
      RNF=(RNFN(NLAYER)**2)*CR
      RNF1=(RNFN(1)**2)*CR
      PFN(NLAYER)=CSQRT(RNF-(RNF1*CT0**2))
      DO 34 I=2,NLAYER-1
      BETAN(I)=TPI*DN(I)*PFN(I)/LAMBDA
34    CONTINUE
      A1(1,1)=1.0
      A12T=(PFN(1)-PFN(2))/(PFN(1)+PFN(2))
      A1(1,2)=A12T*CEXP(-TLC*ZBB(1)*PFN(1)*PFN(2))
      A1(2,1)=A1(1,2)
      A1(2,2)=1.0
      DO 35 I=2,NLAYER-1
      BTM=BETAN(I)*CI
      BTM1=-BETAN(I)*CI
      IF(CX(2).EQ.0.0) BTM=BETAN(I)*2.0*CI
      CBTM=CEXP(BTM)
      IF(CX(1).EQ.0.0) CBTM1=CEXP(BTM1)
      IF(CX(2).EQ.0.0) CBTM1=1.0*CR
      A2(1,1)=CBTM
      A22T=CO
      IF((PFN(I)+PFN(I+1)).NE.CO)A22T=(PFN(I)-
PFN(I+1))/(PFN(I)+PFN(I+1))
      A22T=A22T*CEXP(-TLC*ZBB(I)*PFN(I)*PFN(I+1))
      A2(1,2)=A22T*CBTM
      A2(2,1)=A22T*CBTM1
      A2(2,2)=CBTM1
*
      CALL MATRIX(A1,A2,A3)
*
      A1(1,1)=A3(1,1)
      A1(1,2)=A3(1,2)
      A1(2,1)=A3(2,1)
      A1(2,2)=A3(2,2)
35    CONTINUE
      AC1=A1(2,1)
      AC2=CONJG(AC1)
      AC3=A1(1,1)
      AC4=CONJG(AC3)
      IF(AX(1).EQ.0.0.AND.AX(2).EQ.0.0) GOTO 400
      ANS=(AC1*AC2)/(AC3*AC4)
      GOTO 401
*
400   ANS=1.0
      FLAG=1
401   GAUSS=(1.0/(DTHETR))*EXP(-0.5*((THETA0-
X)/DTHET)**2)
      F=ANS*GAUSS
      RETURN
      END
*                                                    *
******************************************************
*************************
*                                                    *
*          SUBROUTINE MATRIX - MATRIX
MULTIPLICATION           *
*                                                    *
******************************************************
*************************
*                                                    *
      SUBROUTINE MATRIX(A1,A2,A3)
*                                                    *
      DIMENSION A1(2,2),A2(2,2),A3(2,2)
      COMPLEX*8 A1,A2,A3
*                                                    *
      A3(1,1)=A1(1,1)*A2(1,1)+A1(1,2)*A2(2,1)
      A3(1,2)=A1(1,1)*A2(1,2)+A1(1,2)*A2(2,2)
      A3(2,1)=A1(2,1)*A2(1,1)+A1(2,2)*A2(2,1)
      A3(2,2)=A1(2,1)*A2(1,2)+A1(2,2)*A2(2,2)
      RETURN
      END
*                                                    *
*                                                    *
******************************************************
*************************
```

Program 4: nrmodfit

This program was used to fit neutron reflectivity data to damped oscillatory scattering length density profiles as discussed in Chapter 5.

```
C     A.N. Burgess, ICI C&P

program nrmodfit
      IMPLICIT REAL(A-Z)
      INTEGER
I,J,NOPO,SIGN,SHIFT,ITERA,MAXIT,STP,NLAYERI,NREP,NPA
R
      real modpar(10),delmod(10)
      COMMON/SIMS/LAMIN,LAMAX,NREP,NPAR
      COMMON/PARAMS/PARAM(1500),NOPO
      COMMON/REST/RP(1000),QOB(1000)
      COMMON/WHAT/NV,INV(1000),NLAYERI

COMMON/GRAPHS/sob(1000),OB(1000),ser(1000),ERR(1000),CH
ANGE(1500)
      COMMON/FILES/FILE,MAXIT
      COMMON/CHISQD/CHISQ
      CHARACTER*10 NAME(1500)
      COMMON/NAM/NAME,STP
      CHARACTER*9 FILE
      CHARACTER*20 fILENAME
      CHARACTER*60 TITLE(20)
      data name/1500*'        '/
C
C
      NAME(1)='THETA'
      NAME(2)='NBA'
      NAME(3)='DTHETA'
      NAME(4)='NBS'
      NAME(5)='ZBB01'
      NAME(6)='LAYER 1'
      NAME(9)='LAYER 2'
      NAME(12)='LAYER 3'
      NAME(15)='LAYER 4'
      NAME(18)='LAYER 5'
      NAME(21)='LAYER 6'
      NAME(24)='LAYER 7'
      NAME(27)='LAYER 8'
      name(30)='LAYER 9'
      name(33)='LAYER 10'
      name(36)='LAYER 11'
C
C
      PRINT*,''
      PRINT*,''
      PRINT*,''
      WRITE(6,1)
1     FORMAT(TR30,'NEUTRON REFLECTIVITY')
      WRITE(6,2)
2     FORMAT(TR29,'————————')
      WRITE(6,3)
3     FORMAT(TR33,'CURVE FITTING'/TR32,'————————')
C
      OPEN(UNIT=20,STATUS='OLD',NAME='nrdata.dat')
      READ(20,*)FILENAME
C
      OPEN(UNIT=30,STATUS='OLD',NAME=FILENAME)
      DO I=1,6
      READ(30,9000)TITLE(I)
9000  FORMAT(A70)
      END DO
      READ(30,9005)NOPO
9005  FORMAT(24X,I5)
      DO I=1,2
      READ(30,9000)TITLE(I)
      END DO
      DO I=1,NOPO
      READ(30,*)QOB(I),OB(I),ERR(I)
9010  FORMAT(3(4X,G15.5))
      END DO
C
      CLOSE(UNIT=30)
      open(unit=25,name='nrmod.dat',type='old')
      read(25,*)nmodpar
      do i=1,nmodpar
      read(25,*)modpar(i),delmod(i)
```

```
      end do
      close(25)
C
C
C
C
C
      read(20,*)MAXIT,NLAYERI
      NPAR=7+(nlayeri*3)
      name(npar-1)='SCALE FAC.'
      name(npar)='BKGD'
      NREP=0
      PRINT*,''
      PRINT*,''
      PRINT*,''
      PRINT*,''
      DO I=1,NPAR
      READ(20,*)PARAM(I),CHANGE(I)
      WRITE(6,2000)NAME(I),PARAM(I),CHANGE(I)
      END DO
2000    FORMAT(TR2,A10,'  =',G12.3,TR5,G10.3)
C
C
C
92    CLOSE(UNIT=20)
      nmodpar=nmodpar+1
      modpar(nmodpar)=param(5)
      delmod(nmodpar)=change(5)
      nmodpar=nmodpar+1
      modpar(nmodpar)=param(npar)
      delmod(nmodpar)=change(npar)
C
      call dampcoS(Modpar,nLayerI)
      do i=1,npar
      write(6,2000)name(i),param(i),change(i)
      end dO
      CALL NRCALC
C
C
C
      npt=nopo-1
      do i=1,nopo
      rp(i)=rp(i)+param(npar)
      sob(i)=ob(i)/param(npar-1)
      ser(i)=er(i)/param(npar-1)
      end do
c
c
      CHIBEST=0.0
      DO I=1,NPt
      CHIBEST=CHIBEST+((sOB(I)-RP(I))/sERR(I))**2
      END DO
      CHIBEST=CHIBEST/NPt
      chisq=chibest
      write(6,2001)chibest
2001    format(/1x,'CHISQ = ',e12.5)
C
C
9997    DO ITERA=1,MAXIT
C
      PRINT*,''
      WRITE(6,5000)ITERA,CHIBEST
5000    FORMAT('  ITERATION = ',I4,TR5,'BEST CHISQ =
',G12.4)
      PRINT*,''
C
      WRITE(6,5010)
5010
FORMAT(1X,'PARAMETER',TR6,'CHANGE',TR5,'VALUE',TR11,'
CHISQ')
      PRINT*,''
      TOT=0
C
      DO I=1,nmodpar
C
      IF(delmoD(i).EQ.0.) GOTO 1020
      SIGN=1
      SHIFT=0
C
C
1000    modPAR(I)=moDpaR(I)+SIGN*delmoD(i)
c
      SHIFT=SHIFT+SIGN
c
      call dampcoS(Modpar,nLayerI)
      CALL NRCALC
C
      do k=1,nopo
      rp(k)=rp(k)+param(npar)
      sob(k)=ob(k)/param(npar-1)
      ser(k)=er(k)/param(npar-1)
      end do
      CHI=0.0
      DO J=1,NPt
      CHI=CHI+((sOB(J)-RP(J))/sERR(J))**2
      END DO
      CHI=CHI/NPt
C
      WRITE(6,*)i,SHIFT,modpaR(i),CHI
C
      IF((CHIBEST-CHI).GE.0.001)THEN
       CHIBEST=CHI
       IF(ABS(SHIFT).LT.3)GOTO 1000
      ELSE IF(SHIFT.EQ.1)THEN
       SIGN=-1
       SHIFT=0
       moDpaR(I)=moDpaR(I)+SIGN*delmoD(i)
       GOTO 1000
      ELSE
       moDpaR(I)=moDpaR(I)-SIGN*delmoD(i)
      END IF
C
      IF(SHIFT.NE.-1)TOT=1
C
1020    END DO
C
      PRINT*,''
      DO I=1,NPAR
      WRITE(6,5040)NAME(I),PARAM(I)
5040    FORMAT(1H ,A10,TR2,G12.6)
      END DO
      PRINT*,''
      CHISQ=CHIBEST
      WRITE(6,5050)CHIBEST
5050    FORMAT(1X,'CHISQ = ',G12.4)
      PRINT*,''
C
      IF(TOT.LT.1E-5)GOTO 1010
C
      END DO
C
1010  continue
      call dampcoS(Modpar,nLayerI)
      CALL NRCALC
C
      do k=1,nopo
      rp(k)=rp(k)+param(npar)
      sob(k)=ob(k)/param(npar-1)
      ser(k)=er(k)/param(npar-1)
      end do
      CHIBEST=0.0
      DO I=1,NPt
      CHIBEST=CHIBEST+((sOB(I)-RP(I))/sERR(I))**2
      END DO
      CHIBEST=CHIBEST/NPt
      CHISQ=CHIBEST
C
      PRINT*,''
      PRINT*,''
C
C
C
      CLOSE(UNIT=20)
C
      open(unit=20,name='mrdata.dat',status='old')
      write(20,1011)filename
1011  FORMAT(A15,13x,'FILE NAME')
      write(20,1012)maxit,nlayeri
1012  format(i3,10x,',',i3,11x,'MAXIT,NL')
      do i=1,npar
      write(20,1013)param(i),change(i),name(i)
1013  FORMAT(e12.5,1x,',',1x,e12.5,1x,T,a10)
      end do
      close(20)
      open(unit=25,name='mrmod.dat',status='unknown')
      write(25,*)nmodpaR-2
      do i=1,nmodpar-2
      write(25,*)modpar(i),delmod(i)
      end do
      close(25)
      open(unit=30,name='mfit.out',type='unknown')
      do i=1,nopo
```

```
      write(30,*)qob(i),rp(i),sob(i),ser(i)
      end do
      close(30)
      STOP 'NRFIT END'
      END
*************************************************************
****************************
*                                                           *
*       SUBROUTINE BASED ON LAYER_NEW.FOR CALLED
BY gl1                *
*                                                           *
*                                                           *
*       CALCS COMPLETE GENERAL MULTILAYER
REFLECTIVITY                *
*                                                           *
*             J.PENFOLD  16TH OCTOBER 1987                  *
*                                                           *
*************************************************************
****************************
*                                                           *
      SUBROUTINE NRCALC
      DIMENSION AX(2),CX(2),P(20)
      DIMENSION FLG(500)
      DIMENSION ZBB(500),ZBB1(500)
      DIMENSION A1(2,2),A2(2,2),A3(2,2)
      DIMENSION DN(500),DN1(500),RNBN(500),RNBN1(500)
      DIMENSION RNFN(500),PFN(500),BETAN(500)
      DIMENSION RT(1000),RTP(1000)
      DIMENSION XNIT(50)
      REAL*4 LAMBDA,NBA,NBS
      INTEGER CH1,CH2,NLAYER,NLAYERI,qflag
      COMPLEX*8 AC1,AC2,A1,A2,A3,CI,CR,PFN,AC3
      COMPLEX*8 AC4,RNF,RNF1,BETAN,A22T,A12T
      COMPLEX*8 BTM,BTM1,CBTM,CBTM1,CO
      CHARACTER*40 FNAMEIN,FNAMEOUT
      EQUIVALENCE (AX,AC3)
*
      COMMON/PARAMS/PARAM(1500),NOPO
      COMMON/REST/RP(1000),QOB(1000)
      COMMON/WHAT/NV,INV(1000),NLAYERI
*
      COMMON /CSPEC/
LAMBDA,THETA0,DTHET,DTHETR,K0,PI,TPI,NLAYER
      COMMON /TDATA/
PFN,BETAN,A1,A2,A3,CI,CR,CO,AC1,AC2,AC3,AC4
      COMMON /TDATA1/ RNBN,DN,ZBB,RNFN,FLAG
*
*
       COMMON/SIMS/ LAMIN,LAMAX,NREP,npar
      REAL LAMIN,LAMAX
       qflag=0
       if(qob(1).lt.0.1)qflag=1
*
      DO 10 I=1,NOPO
10      RP(I)=0.00
*
*             SET UP SOME CONSTANTS
*
      CX0=0.0
      CX1=1.0
      CI=CMPLX(CX0,CX1)
      CR=CMPLX(CX1,CX0)
      CO=(0.0,0.0)
      PI=ACOS(-1.)
      TPI=2.0*PI
*
*
*      INPUT BASIC CALC AND MODEL PARAMETERS
*
      THETA0=PARAM(1)
      PTHET=PARAM(3)
      NLAYER=NLAYERI
      NBA=PARAM(2)
      NBS=PARAM(4)
      ZBA=PARAM(5)
      ZBA=ZBA**2
      NREP1=NLAYER
      IF(NREP.EQ.0)GOTO 15
      NREP1=NREP
      NFRED=MOD(NLAYER,NREP)
      IF(NFRED.EQ.0)GOTO 15
15      JJ=6
       DO 16 I=1,NREP1
       IF (NREP.EQ.0) THEN
        DN(I+1)=PARAM(JJ)
        RNBN(I+1)=PARAM(JJ+1)
        ZBB(I+1)=PARAM(JJ+2)
        ZBB(I+1)=ZBB(I+1)*ZBB(I+1)
       ELSE
        DN1(I)=PARAM(JJ)
        RNBN1(I)=PARAM(JJ+1)
        ZBB1(I)=PARAM(JJ+2)
       END IF
16      JJ=JJ+3
      IF(NLAYER.EQ.1)GOTO 500
      IF(NREP.EQ.0)GOTO 500
       DO 21 I=2,(NLAYER+1),NREP
        DO 22 J=1,NREP
         K=(I+J-1)
         RNBN(K)=RNBN1(J)
         DN(K)=DN1(J)
         ZBB(K)=ZBB(J)
22        CONTINUE
21       CONTINUE
500      RNBN(1)=NBA
      RNBN(NLAYER+2)=NBS
      ZBB(1)=ZBA
      ZBB(NLAYER+2)=0.0
      DN(1)=0.0
      DN(NLAYER+2)=0.0
      NLAYER=NLAYER+2
*
*
*       SET UP SOME CONSTANTS
*
*
20      THETA0=THETA0*0.01745
      DTHET=THETA0*PTHET/100.
      DTHET=DTHET/2.35
      DTHETR=DTHET*2.51
      TMAX=THETA0+DTHET*3
      TMIN=THETA0-DTHET*3
      ST0=SIN(THETA0)
      CT0=COS(THETA0)
*
      IF(PTHET.NE.0)GOTO 100
*
*
*       HERE FOR NO RESOLUTION
*
*
      NV=0
      DO 40 J=1,NOPO
       NV=NV+1
       INV(NV)=J
       LAMBDA=QOB(J)
        if(qflag.eq.1)lambda=4.0*pi*st0/qob(j)
       CON=LAMBDA*LAMBDA/TPI
       TL=LAMBDA*LAMBDA
       TLC=78.96/TL
        DO 31 I=1,NLAYER
         RNFN(I)=(1.0-CON*RNBN(I))
31        CONTINUE
        PFN(1)=RNFN(1)*ST0
         DO 32 I=2,NLAYER-1
          RNF=(RNFN(I)**2)*CR
          RNF1=(RNFN(1)**2)*CR
          PFN(I)=CSQRT(RNF-(RNF1*CT0**2))
32        CONTINUE
       RNF=(RNFN(NLAYER)**2)*CR
       RNF1=(RNFN(1)**2)*CR
       PFN(NLAYER)=CSQRT(RNF-(RNF1*CT0**2))
        DO 34 I=2,NLAYER-1
         BETAN(I)=TPI*DN(I)*PFN(I)/LAMBDA
34        CONTINUE
       A1(1,1)=1.0
       A12T=(PFN(1)-PFN(2))/(PFN(1)+PFN(2))
       A1(1,2)=A12T*CEXP(-TLC*ZBB(1)*PFN(1)*PFN(2))
       A1(2,1)=A1(1,2)
       A1(2,2)=1.0
       DO 35 I=2,NLAYER-1
       BTM=BETAN(I)*CI
       BTM1=BETAN(I)*CI
       IF(CX(2).EQ.0.0) BTM = BETAN(I)*2.0*CI
       CBTM=CEXP(BTM)
       IF(CX(1).EQ.0.0) CBTM1=CEXP(BTM1)
       IF(CX(2).EQ.0.0) CBTM1=1.0*CR
       A2(1,1)=CBTM
       A22T=CO
       IF((PFN(I)+PFN(I+1)).NE.CO)A22T=(PFN(I)-
PFN(I+1))/(PFN(I)+PFN(I+1))
       A22T=A22T*CEXP(-TLC*ZBB(I)*PFN(I)*PFN(I+1))
       A2(1,2)=A22T*CBTM
       A2(2,1)=A22T*CBTM1
```

```
      A2(2,2)=CBTM1
*
      CALL MATRIX(A1,A2,A3)
*
      A1(1,1)=A3(1,1)
      A1(1,2)=A3(1,2)
      A1(2,1)=A3(2,1)
      A1(2,2)=A3(2,2)
 35   CONTINUE
      AC1=A1(2,1)
      AC2=CONJG(AC1)
      AC3=A1(1,1)
      AC4=CONJG(AC3)
      IF(AX(1).EQ.0.0.AND.AX(2).EQ.0.0)GOTO 400
      RP(J)=(AC1*AC2)/(AC3*AC4)
      GOTO 401
*
 400  RP(J)=1.0
      FLG(J)=1.
 401  RT(J)=LAMBDA
 30   CONTINUE
 40   CONTINUE
      GOTO 200
*
*
*     HERE FOR INTEGRATION OVER DELTA THETA
*
*
 100  FLAG=0.
      NIT=21
      DT=(TMAX-TMIN)/NIT
      DO 102 I=1,NIT
      XNIT(I)=TMIN+DT*(I-1)
 102  CONTINUE
      NIT1=NIT+1
*
      NV=0
      DO 101 J=1,NOPO
       NV=NV+1
       INV(NV)=J
       LAMBDA=QOB(J)
       if(qflag.eq.1)lambda=4.0*pi*st0/qob(j)
       CON=LAMBDA*LAMBDA/TPI
       DO 310 I=1,NLAYER
        RNFN(I)=(1.0-CON*RNBN(I))
 310   CONTINUE
       DO 103 II=1,NIT
       X=XNIT(II)
*
       CALL CALCIN(X,F)
*
       RP(J)=RP(J)+F*DT
 103   CONTINUE
      IF(FLAG.EQ.1.) FLG(J)=1.0
      FLAG=0.
      RT(J)=LAMBDA
 101  CONTINUE
      do i=1,nopo-1
      rp(i)=(rp(i)+rp(i+1))/2.0
      end do
 200  return
      END
*                                        *
**********************************************************
**************************
*                                        *
*        SUBROUTINE CALCIN, FOR QA02A INTEGRATION
*
*                                        *
**********************************************************
**************************

      SUBROUTINE CALCIN(X,F)
      DIMENSION
ZBB(500),DN(500),RNBN(500),RNFN(500),PFN(500)
      DIMENSION
BETAN(500),A1(2,2),A2(2,2),A3(2,2),AX(2),CX(2)
      REAL*4 LAMBDA
      COMPLEX*8
AC1,AC2,AC3,AC4,A1,A2,A3,CI,CR,PFN,RNF,RNF1,BETAN,A22
T,A12T
      COMPLEX*8 BTM,BTM1,CBTM,CBTM1,CO
      EQUIVALENCE (AX,AC3),(CX,BTM1)
*
      COMMON /CSPEC/
LAMBDA,THETA0,DTHET,DTHETR,K0,PI,TPI,NLAYER
      COMMON /TDATA/
PFN,BETAN,A1,A2,A3,CI,CR,CO,AC1,AC2,AC3,AC4
      COMMON /TDATA1/ RNBN,DN,ZBB,RNFN,FLAG
*
*
*
      ST0=SIN(X)
      CT0=COS(X)
      TL=LAMBDA*LAMBDA
      TLC=78.96/TL
      PFN(1)=RNFN(1)*ST0
       DO 32 I=2,NLAYER-1
        RNF=(RNFN(I)**2)*CR
        RNF1=(RNFN(1)**2)*CR
        PFN(I)=CSQRT(RNF-(RNF1*CT0**2))
 32   CONTINUE
      RNF=(RNFN(NLAYER)**2)*CR
      RNF1=(RNFN(1)**2)*CR
      PFN(NLAYER)=CSQRT(RNF-(RNF1*CT0**2))
       DO 34 I=2,NLAYER-1
       BETAN(I)=TPI*DN(I)*PFN(I)/LAMBDA
 34   CONTINUE
      A1(1,1)=1.0
      A12T=(PFN(1)-PFN(2))/(PFN(1)+PFN(2))
      A1(1,2)=A12T*CEXP(-TLC*ZBB(1)*PFN(1)*PFN(2))
      A1(2,1)=A1(1,2)
      A1(2,2)=1.0
       DO 35 I=2,NLAYER-1
       BTM=BETAN(I)*CI
       BTM1=-BETAN(I)*CI
       IF(CX(2).EQ.0.0) BTM=BETAN(I)*2.0*CI
       CBTM=CEXP(BTM)
       IF(CX(1).EQ.0.0) CBTM1=CEXP(BTM1)
       IF(CX(2).EQ.0.0) CBTM1=1.0*CR
       A2(1,1)=CBTM
       A22T=CO
       IF((PFN(I)+PFN(I+1)).NE.CO)A22T=(PFN(I)-
PFN(I+1))/(PFN(I)+PFN(I+1))
       A22T=A22T*CEXP(-TLC*ZBB(I)*PFN(I)*PFN(I+1))
       A2(1,2)=A22T*CBTM
       A2(2,1)=A22T*CBTM1
       A2(2,2)=CBTM1
*
       CALL MATRIX(A1,A2,A3)
*
       A1(1,1)=A3(1,1)
       A1(1,2)=A3(1,2)
       A1(2,1)=A3(2,1)
       A1(2,2)=A3(2,2)
 35    CONTINUE
      AC1=A1(2,1)
      AC2=CONJG(AC1)
      AC3=A1(1,1)
      AC4=CONJG(AC3)
      IF(AX(1).EQ.0.0.AND.AX(2).EQ.0.0) GOTO 400
      ANS=(AC1*AC2)/(AC3*AC4)
      GOTO 401
*
 400  ANS=1.0
      FLAG=1
 401  GAUSS=(1.0/(DTHETR))*EXP(-0.5*((THETA0-
X)/DTHET)**2)
      F=ANS*GAUSS
      RETURN
      END
*                                        *
**********************************************************
**************************
*                                        *
*        SUBROUTINE MATRIX - MATRIX
MULTIPLICATION
*                                        *
**********************************************************
**************************
*                                        *
      SUBROUTINE MATRIX(A1,A2,A3)
*
      DIMENSION A1(2,2),A2(2,2),A3(2,2)
      COMPLEX*8 A1,A2,A3
*                                        *
      A3(1,1)=A1(1,1)*A2(1,1)+A1(1,2)*A2(2,1)
      A3(1,2)=A1(1,1)*A2(1,2)+A1(1,2)*A2(2,2)
      A3(2,1)=A1(2,1)*A2(1,1)+A1(2,2)*A2(2,1)
      A3(2,2)=A1(2,1)*A2(1,2)+A1(2,2)*A2(2,2)
      RETURN
      END
*
```

```
*                                                    *
******************************************************
**************************
C
    sUbroutine dampcoS(Modpar,nl)
    common/params/param(1500),nopo
    real modpar(1)
    j=5
    param(5)=modpar(7)
    DO i=1,nl,2
    D1=FLOAT(I-1)*modpar(4)
    D2=FLoat(i-1)*modpar(2)
    d3=float(i-1)*modpar(6)
    param(j-1)=modpar(3)*exp(-d1)
    param(j+2)=0.451e-5+(0.635e-5-0.451e-5)*exp(-d2)
    param(j+3)=param(5)
    param(j+4)=modpar(5)*exp(-d3)
    param(j+5)=0.451e-5+(modpar(1)-0.451e-5)*exp(-d2)
    param(j+6)=param(5)
    j=j+6
    end do
    return
    end
```

Program 5: profile

This program was used to calculate neutron scattering length density profiles normal to the interface as a function of distance z through the interface as discussed in Chapter 5.

```
    program PROFILE

c This program is based on that written by Archie Eaglesham at ICI
c C&P
c to calculate the scattering length density as a function of distance
c through a multilayer system, taking into account surface roughness.

c set up array and character dimensions
c
    dimension rho(500), dlay(500), sigma(500)
    dimension zcoord(1000),drho(1000),rint(1000),rscat(1000)
    dimension rhoint(1000)
c     character*1 ans1,ans2,ans3
    character*20 file_in


c Input scattering length densities, thicknesses, and rougnesses.

c     WRITE(6,100)
c100     FORMAT('ENTER PARAMETER FILENAME')
c     READ(5,'(a)')file_in
c     OPEN(UNIT=3,FILE=file_in,STATUS='OLD')
    WRITE(6,110)
110     FORMAT('ENTER NUMBER OF LAYERS')
    READ(5,*) n
    WRITE(6,120)
120     FORMAT('ENTER SUBSTRATE Nb')
    READ(5,*) rho(1)
    nflag=0
    if(rho(1).lt.0.0)nflag=1
    rholim=rho(1)
    WRITE(6,130)
130     FORMAT('ENTER THE SUBSTRATE ROUGHNESS')
    READ(5,*) sigma(2)
    sigma(2)=sigma(2)**2
    WRITE(6,140)
140     FORMAT('ENTER ZMIN AND ZMAX FOR
CALCULATION')
    READ(5,*) zmin,zmax
c
    DO 10 I=1,n
    WRITE(6,150) I
150     FORMAT('ENTER d, Nb, zb FOR LAYER (layer next to sub.
first)',X,I1)
    READ(5,*) dlay(I+1), rho(I+1), sigma(I+2)
    IF(rho(I+1).LT.0.0)nflag=1
    IF(rho(I+1).GT.rholim)rholim=rho(I+1)
    sigma(I+2)=sigma(I+2)**2
10     CONTINUE
c
c Set up some constants
c
    dlay(1)=0.0
    dlay(n+2)=0.0
    sigma(1)=0.0
    rho(n+2)=0.0
    pi=4.0*atan(1.0)
    tpi=2.0*pi
    mstep=1000
    dz=(zmax-zmin)/mstep
c
c mstep defines the step size for the trapezoidal integration of
c     d(rho)/dz
c
c calculate d(rho)/dz
c
    DO 20 J=1,mstep
    z=zmin+J*dz
    drhodz=0.0
c
    dl=0.0
c
    DO 30 I=1,n+1
    dl=dl+dlay(I)
    deltarho=rho(I+1)-rho(I)
    prefac1=sqrt(tpi*sigma(I+1))
    prefac2=2*sigma(I+1)
    top=(z-dl)**2
    top=-1.0*top
    sum=deltarho/prefac1
    temp=top/prefac2
    if(temp.LT.-10.0)then
    sum=0.0
    else
    sum=sum*exp(temp)
    endif
    drhodz=drhodz+sum
30     continue
c
c some scaling..
c
c
    zcoord(J)=z
    if(drhoz.GE.0.0)then
    rint(J)=drhodz*dz
    drho(J)=100.0*drhodz
    else
    rint(J)=drhodz*dz
    drho(J)=100.0*drhodz
    endif
c
20     continue
c
c
c calculate rho(z)
c
    temp=rho(1)
    DO 40 I=1,mstep
    temp=temp+rint(I)
    rscat(I)=temp
40     continue
c
c calculate integral of rho(z)
c
    temp20=0.0
    DO 50 I=1,mstep
    rhoint(I)=(rscat(I)*dz)+temp20
    temp20=rhoint(I)
50     continue
    open(unit=9,file='data.dat', status='unknown')
    DO 60 I=1,mstep,10
    write(9,*) zcoord(I),rscat(I),rhoint(I)
60     continue
    write(6,502)
502     format('the results are in data.dat file')
    close(unit=9)
c
stop
    end
```

Program 6: tempcfit5

This program was used to analyse experimental coexistence curve data as discussed in Chapter 6.

```
program tempcfit5
C                                Modified 1 July 1993
C                                George Jackson
C   CCFIT - Analysis of coexistence curve data
C
C   This program can be compiled by,
C   COMPILE program-name -GHOST -APPLIB -DEV device-
number
C   ("program-name" must end with ".FTN")
C   (a suitable device-number for plotting results is CC1012).
C   It can be executed by,
C   EXECUTE program-name -PLOT plotfile-name
C   (This opens the file "plotfile-name" to receive graphical output.)
C   The graph can then be produced by,
C   SPOOL plotfile-name -PLOT
C   (Note: Only one graph can be produced on each execution.)
C
C        X    = Array of independent variable data
C        Y    = Array of dependent variable data
C        SIGX  = Standard deviation of X
C        SIGY  = Standard deviation of Y
C        SIGMAY = Standard deviation propagated to Y (total)
C        NPTS  = Number of data pairs
C        NTERMS = Number of parameters to be optimized
C        NFIXPS = Number of parameters to be fixed
C        A    = Array of parameters (ordered as input)
C        ICODE  = Array of floating parameter identities in FUNCTN
segment
C        ICOFIX = Array of fixed parameter identities in FUNCTN
segment
C        AIN   = Array of parameters reordered to match FUNCTN
segment
C        SIGMAA = Array of standard deviations of parameters in A
C        MODE  = Determines weighting factor:
C             +1  WEIGHT(I)=1/SIGMAY(I)**2
C              0  WEIGHT(I)=1
C             -1  WEIGHT(I)=1/Y(I)
C        JSIGY  = Set to zero to employ PHISIG
C
    IMPLICIT DOUBLE PRECISION (A-H,O-Z)
    INTEGER*2 S18,S10,S1
    character*30 fname
    DIMENSION
A(10),DELTAA(10),SIGMAA(10),AIN(10),ICODE(10),ICOFIX(10)
    DIMENSION Y(120),SIGMAY(120),X(120)
   &,SIGY(120),SIGX(120),DEV(120),DELTAT(120)
    COMMON /CBL1/Y,AIN,ICODE,NTERMS
    COMMON /CBL2/A,NPTS
    DATA S18/18/,S10/10/,S1/1/
    do 1492 i=1,10
    a(i)=0.0D00
    icode(i)=0.0D00
    icofix(i)=0.0D00
    deltaa(i)=0.0D00
    sigmaa(i)=0.0D00
1492 continue
    CTMIN=1.0D-5
    NITMAX=300
    FLMAX=1.0D6
    NEXDAT=0
800 write(6,*) ' enter filename'
    read(5,1112) fname
    write(6,1112) ' File: '//fname
1112 format(a)
    continue
5   WRITE(6,100)
100 FORMAT(' TYPE: NPTS,NTERMS,MODE,JSIGY')
    READ(5,*,ERR=5) NPTS,NTERMS,MODE,JSIGY
25  WRITE(6,110)
110 FORMAT(' TYPE: ICODE,A (FROM BEGINING)')
    READ(5,*,ERR=25) (ICODE(I),A(I),I=1,NTERMS)
    DO 10 I=1,10
    AIN(I)=0.0D00
10  CONTINUE
35  WRITE(6,120)
120 FORMAT(' TYPE: NFIXPS')
    READ(5,*,ERR=35) NFIXPS
    IF(NFIXPS.EQ.0) GOTO 31
45  WRITE(6,130)
130 FORMAT(' TYPE: ICOFIX,A')
    READ(5,*,ERR=45) (ICOFIX(I),AIN(ICOFIX(I)),I=1,NFIXPS)
31  IF(NEXDAT.EQ.1) GOTO 32
    open (unit=55,file=fname,status='old')
30  READ(55,*) (X(I),Y(I),SIGX(I),SIGY(I),I=1,NPTS)
    close(55)
32  continue
    IF(JSIGY.EQ.0) CALL PHISIG(SIGY,SIGX,Y,NPTS)
    WRITE(6,200) NPTS,NTERMS,MODE,JSIGY,NFIXPS
200 FORMAT(5(5X,I5))
    WRITE(6,210)
210 FORMAT(1H ,'INITIAL PARAMETERS WERE...')
    WRITE(6,220) (ICODE(I),A(I),DELTAA(I),I=1,NTERMS)
220 FORMAT(3X,' A(',I2,') = ',F10.6,' (',F10.6,')')
    IF(NFIXPS.EQ.0) GOTO 50
    WRITE(6,240)
240 FORMAT(1H ,'FIXED PARAMETERS WERE...')
    WRITE(6,250) (ICOFIX(I),AIN(ICOFIX(I)),I=1,NFIXPS)
250 FORMAT(3X,' A(',I2,') = ',F10.6)
    GOTO 55
50  WRITE(6,260)
260 FORMAT(1H ,'NO FIXED PARAMETERS')
55  CONTINUE
    DO 40 I=1,NTERMS
    DELTAA(I)=DABS(A(I))/100.0D00
    IF(ICODE(I).EQ.1) DELTAA(I)=0.001D00
40  CONTINUE
    CHISQR=0.0D00
    NITER=0
    FLAMDA=0.001D00
500 NITER=NITER+1
    CHIOLD=CHISQR
    IF(MODE.NE.0) CALL
VARANC(X,I,A,SIGX,SIGY,SIGMAY,NPTS)
    CALL
CURFIT(X,Y,SIGMAY,NPTS,NTERMS,MODE,A,DELTAA,SIGM
AA,
   &FLAMDA,CHISQR)
    DELCHI=(CHIOLD-CHISQR)/CHISQR
    CTEST=DABS(DELCHI)
    IF(CTEST.LE.CTMIN.OR.NITER.GT.NITMAX
   &.OR.FLAMDA.GT.FLMAX) GOTO 400
    FLAMDA=FLAMDA/10.0D00
    GOTO 500
400 WRITE(6,230) NITER,CHISQR,FLAMDA
230 FORMAT(/1H ,'NITER = ',I2,2X,'CHISQR = ',F10.6,2X,
   &'FLAMDA = ',F10.6)
    dysq=0.0D00
    do 103 i=1,npts
    yy=functn(x,i,a)
    dy=y(i)-yy
    dysq=dysq+dy*dy
103 continue
    sigbar=dsqrt(dysq)/dfloat(npts)
    write(6,*) 'std=',sigbar
    WRITE(6,270)
270 FORMAT(1H ,'FITTED PARAMETERS ARE....')
    WRITE(6,280) (ICODE(I),A(I),SIGMAA(I),I=1,NTERMS)
280 FORMAT(3X,' A(',I2,') = ',F10.6,' (',F10.6,')')
65  WRITE(6,140)
140 FORMAT(' TYPE: 1=STOP,2=CALL DATOUT,3=ANOTHER
FIT'
   &,',4=PLOT DEVIATIONS,5=PLOT RESULTS')
    READ(5,*,ERR=65) NEXT
    IF (NEXT.EQ.4) GOTO 310
    IF (NEXT.EQ.5) GOTO 315
    IF (NEXT.EQ.1) GOTO 900
    IF (NEXT.EQ.2) GOTO 300
    IF (NEXT.EQ.3) GOTO 600
315 AIN1=AIN(1)
    CALL DPLOTR(X,Y,NPTS,AIN1)
    GOTO 65
310 DO 320 I=1,NPTS
    DEV(I)=(Y(I)-FUNCTN(X,I,A))/1.0D00
    DELTAT(I)=DABS(X(I)-AIN(1))
320 CONTINUE
    CALL DPLOT(DELTAT,DEV,NPTS)
    GOTO 65
600 WRITE(6,410)
410 FORMAT(' TYPE: 1=SAME DATA,2=NEW DATA')
    READ(5,*,ERR=600) NEXDAT
```

```
      IF(NEXDAT.EQ.1) GOTO 5
      GOTO 800
  300 CALL DATOUT(X,I,A,SIGX,Y,SIGMAY,NPTS)
      GOTO 65
  900 STOP
      END
C
C   PHISIG - Calculates error in volume fraction
C          SIGMAS = Experimental weighing error (g)
C          SIGR   = Error in pure component densities (g/cc)
C          R      = Ratio of pure component densities
C          C      = Volume of sample (cc)
C
      SUBROUTINE PHISIG(SIGY,SIGX,Y,NPTS)
      IMPLICIT DOUBLE PRECISION (A-H,O-Z)
      DIMENSION SIGY(120),Y(120),SIGX(120)
      SIGMAS=0.0009D00
      SIGR=0.0001D00
      R=0.89D00
      C=2.0D00
  100 WRITE(6,110)
  110 FORMAT(' TYPE: 1=AC/HEX, 2=BXL/AQ')
      READ(5,*,ERR=100)ISYS
      IF(ISYS.EQ.2)GOTO 120
      SIGMAS=0.0005D00
      SIGR=0.0001D00
      R=0.98D00
      C=1.4D00
  120 SIGROR=SIGR/R
      SIGMOC=SIGMAS/C
      DO 10 I=1,NPTS
      BRKT=1.0D00/Y(I)-1.0D00
      SIGWOW=SIGMOC*(BRKT/R+1.0D00)
      SIGY(I)=Y(I)*Y(I)*DSQRT((SIGROR*BRKT)**2.0D00+
     *(SIGWOW*BRKT)**2.0D00+(SIGWOW*R)**2.0D00)
   10 CONTINUE
      RETURN
      END
C
C   DATOUT - Outputs data, errors, YY and deviations
C          YY   = Calculated value of function at X(I)
C          DY   = Deviation at X(I)
C
      SUBROUTINE DATOUT(X,I,A,SIGX,Y,SIGMAY,NPTS)
      IMPLICIT DOUBLE PRECISION (A-H,O-Z)
      DIMENSION X(120),Y(120),A(10),SIGMAY(120),SIGX(120)
      WRITE(6,10)
      WRITE(6,11)
      SUM=0.0D00
      DO 50 I=1,NPTS
      IF (nint(SIGMAY(I)).EQ.0) SIGMAY(I) = 1.0D00
      SUM=SUM+SIGMAY(I)
   50 continue
      SIGBAR=SUM/dfloat(NPTS)+SIGX(I)
C     Redundant old section above. SIGX not needed but in list.
      DYSQ=0.0D00
      DO 100 I=1,NPTS
      YY=FUNCTN(X,I,A)
      DY=100.0*(Y(I)-YY)/Y(I)
      DYSQ=DYSQ+DY*DY
      WRITE(6,12) X(I),Y(I),YY,DY
  100 CONTINUE
      SIGBAR=DSQRT(DYSQ)/dfloat(NPTS)
      WRITE(6,13) SIGBAR
   10 FORMAT(1H ,2X,'THE DATA USED IN THIS FIT
     WERE...'//)
   11 FORMAT(6X,'X',10X,'Y.OBS',9X,'Y.CALC',4X,'%
     DEVIATION'/)
   12 FORMAT(3(G13.5,1X),G10.3)
   13 FORMAT(2X,' THE RMS % DEVIATION FOR THIS FIT
     WAS...',G12.6)
      RETURN
      END
C
C   FUNCTN - Calculates value of fitting function for given set of A
     at X(I)
C
      FUNCTION FUNCTN(X,I,A)
      IMPLICIT DOUBLE PRECISION (A-H,O-Z)
      DIMENSION Y(120),X(120), A(10),AIN(10),ICODE(10)
      COMMON/CBL1/Y,AIN,ICODE,NTERMS
      DO 10 J=1,NTERMS
      AIN(ICODE(J))=A(J)
   10 CONTINUE
      EPS = (X(I) - AIN(1))/AIN(1)
      EPS = DABS(EPS)
      SIGN=0.5D00
      IF(Y(I).LT.AIN(2)) SIGN=-0.5D00

      FUNCTN=AIN(2)+AIN(8)*EPS**(0.89D00)+AIN(5)*EPS+AIN(9)
     *EPS**1.39D00

     *+SIGN*(AIN(4)*EPS**AIN(3)+AIN(6)*EPS**(AIN(3)+0.5D00)

     *+AIN(10)*EPS**(AIN(3)+1.0D00)+AIN(7)*EPS**(AIN(3)+1.5D0
     0))
      RETURN
      END
C
C   CURFIT - See Bevington
C
      SUBROUTINE CURFIT
     (X,Y,SIGMAY,NPTS,NTERMS,MODE,A,DELTAA,
     *SIGMAA,FLAMDA,CHISQR)
      IMPLICIT DOUBLE PRECISION (A-H,O-Z)
      DIMENSION
     X(120),Y(120),SIGMAY(120),A(10),DELTAA(10)
      DIMENSION
     WEIGHT(120),ALPHA(10,10),BETA(10),DERIV(10),
     *ARRAY(10,10),B(10),SIGMAA(10)
      save
   11 NFREE=NPTS-NTERMS
      IF(NFREE.gt.0) goto 20
   13 CHISQR=0.0D00
      GO TO 110
C
C   EVALUATE WEIGHTS
C
   20 DO 30 I=1,NPTS
   21 IF(MODE.lt.0) goto 22
      if (mode.eq.0) goto 27
      if (mode.gt.0) goto 29
   22 IF (Y(I).lt.0.0d00) goto 25
      if (y(i).eq.0.0d00) goto 27
      if (y(i).gt.0.0d00) goto 23
   23 WEIGHT(I)=1.0D00/Y(I)
      GO TO 30
   25 WEIGHT(I)=1.0D00/(-Y(I))
      GO TO 30
   27 WEIGHT(I)=1.0D00
      GO TO 30
   29 WEIGHT(I)=1.0D00/SIGMAY(I)**2.0D00
   30 CONTINUE
C
C   EVALUATE ALPHA AND BETA MATRICES
C
   31 DO 34 J=1,NTERMS
      BETA(J)=0.0D00
      DERIV(J)=0.0D00
      DO 134 K=1,J
      ALPHA(J,K)=0.0D00
  134 continue
   34 continue
   41 DO 50 I=1,NPTS
      CALL FDERIV(X,I,A,DELTAA,NTERMS,DERIV)
      W=WEIGHT(I)
      YD=Y(I)-FUNCTN(X,I,A)
      DO 46 J=1,NTERMS
      BETA(J)=BETA(J)+W*YD*DERIV(J)
      SD=W*DERIV(J)
      DO 146 K=1,J
      ALPHA(J,K)=ALPHA(J,K)+SD*DERIV(K)
  146 continue
   46 continue
   50 CONTINUE
   51 DO 53 J=1,NTERMS
      DO 153 K=1,J
      ALPHA(K,J)=ALPHA(J,K)
  153 continue
   53 continue
C
C   EVALUATE CHI SQUARE AT STARTING POINT
C
   60 CHISQ=0.0D00
   61 DO 63 I=1,NPTS
   62 YFIT=FUNCTN(X,I,A)
      CHISQ=CHISQ+WEIGHT(I)*(Y(I)-YFIT)**2.0D00
   63 continue
      FREE=dfloat(NFREE)
      CHISQ1=CHISQ/FREE
C
C   INVERT MODIFIED CURVATURE MATRIX TO FIND NEW
     PARAMETERS
C
```

```
 71  DO 74 J=1,NTERMS
     SD=DSQRT(ALPHA(J,J))
     DO 73 K=1,NTERMS
     ARRAY(J,K)=(ALPHA(J,K)/SD)/DSQRT(ALPHA(K,K))
 73  continue
     ARRAY(J,J)=1.0D0+FLAMDA
 74  continue
 80  CALL MATINV(ARRAY,NTERMS,DET)
 81  DO 84 J=1,NTERMS
     B(J)=A(J)
     SD=DSQRT(ALPHA(J,J))
     DO 184 K=1,NTERMS
     B(J)=B(J)+BETA(K)*(ARRAY(J,K)/SD)/DSQRT(ALPHA(K,K))
184  continue
 84  continue
C
C    IF CHI SQUARE INCREASES, INCREASE FLAMDA AND
TRY AGAIN
C
     CHISQ=0.0D00
 91  DO 93 I=1,NPTS
 92  YFIT=FUNCTN(X,I,B)
 93  CHISQ=CHISQ+WEIGHT(I)*(Y(I)-YFIT)**2.0D00
     CHISQR=CHISQ/FREE
     IF ((CHISQ1-CHISQR).ge.0.0d00) goto 101
 95  FLAMDA=10.0D00*FLAMDA
     IF(FLAMDA.LE.1.0D6) GOTO 71
     GOTO 110
C
C    EVALUTE PARAMETERS AND UNCERTAINTIES
C
101  DO 103 J=1,NTERMS
     A(J)=B(J)
103  SIGMAA(J)=DSQRT(ARRAY(J,J)/ALPHA(J,J))
     FLAMDA=FLAMDA/10.0D00
110  CONTINUE
     RETURN
     END
C
C    MATINV - See Bevington
C
     SUBROUTINE MATINV(ARRAY,NORDER,DET)
     IMPLICIT DOUBLE PRECISION (A-H,O-Z)
     DIMENSION ARRAY(10,10), IK(10), JK(10)
     save
 10  DET= 1.0D00
 11  DO 100 K=1,NORDER
C
C      FIND LARGEST ELEMENT ARRAY(I,J) IN REST OF
MATRIX
C
     AMAX=0.0D00
 21  DO 30 I=K, NORDER
     DO 1130 J=K, NORDER
 23  IF ((DABS(AMAX)-DABS(ARRAY(I,J))).gt.0.0d00) goto 1130
 24  AMAX=ARRAY(I,J)
     IK(K) = I
     JK(K) = J
1130 CONTINUE
 30  CONTINUE
C
 61  DO 70 I=1, NORDER
     if ((i-k).eq.0) goto 70
 63  ARRAY(I,K) = -ARRAY(I,K) / AMAX
 70  CONTINUE
 71  DO 80 I=1, NORDER
     DO 180 J=1, NORDER
     if ((i-k).eq.0) goto 180
 74  if ((j-k).eq.0) goto 180
 75  ARRAY(I,J) = ARRAY(I,J) + ARRAY(I,K)*ARRAY(K,J)
180  CONTINUE
 80  CONTINUE
 81  DO 90 J=1, NORDER
     if ((j-k).eq.0) goto 90
 83  ARRAY(K,J) = ARRAY(K,J) / AMAX
 90  CONTINUE
     ARRAY(K,K) =1.0D00/ AMAX
100  CONTINUE
C
C      RESTORE ORDERING OF MATRIX
C
101  DO 130 L=1,NORDER
     K=NORDER-L+1
     J=IK(K)
     if ((j-k).le.0) goto 111
105  DO 110 I=1,NORDER
     xSAVE=ARRAY(I,K)
     ARRAY(I,K)=-ARRAY(I,J)
110  ARRAY(I,J)=xSAVE
111  I=JK(K)
     if ((i-k).le.0) goto 130
113  DO 120 J=1,NORDER
     xSAVE=ARRAY(K,J)
     ARRAY(K,J)=-ARRAY(I,J)
120  ARRAY(I,J)=xSAVE
130  CONTINUE
140  RETURN
     END
C
C    VARANC - Accumulates error in X and Y in an error, SIGMAY,
in the
C          dependent variable, Y, only
C
     SUBROUTINE VARANC(X,I,A,SIGX,SIGY,SIGMAY,NPTS)
     IMPLICIT DOUBLE PRECISION (A-H,O-Z)
     DIMENSION
X(120),A(10),SIGMAY(120),SIGY(120),SIGX(120)
     save
     DO 500 I=1,NPTS
     IF(SIGX(I).EQ.0.0D00) GO TO 100
     X(I)=X(I)+SIGX(I)
     YH=FUNCTN(X,I,A)
     S2=2.0D00*SIGX(I)
     X(I)=X(I)-S2
     DYDX1=(YH-FUNCTN(X,I,A))/S2
     X(I)=X(I)+SIGX(I)
100  CONTINUE

SIGMAY(I)=DSQRT(SIGY(I)**2.0D00+(DYDX1*SIGX(I))**2.0D
00)
500  CONTINUE
```

```
*+AIN(5)+1.39D00*AIN(9)*EPS**0.39D00)+SIGN*(AIN(4)*AIN(
3)*EPS
   ***(AIN(3)-1.0D00)+AIN(6)*(AIN(3)+0.5D00)*EPS**(AIN(3)-
0.5D00)
   *+AIN(10)*(AIN(3)+1.0D00)

**EPS**AIN(3)+AIN(7)*(AIN(3)+1.5D00)*EPS**(AIN(3)+0.5)))/
AIN(1)
    else if (I.eq.2) then
2   D=1.0D00
    else if (I.eq.3) then
3
D=SIGN*DLOG(EPS)*(AIN(4)*EPS**AIN(3)+AIN(6)*EPS**(AI
N(3)+0.5D00)

*+AIN(10)*EPS**(AIN(3)+1.0D00)+AIN(7)*EPS**(AIN(3)+1.5D0
0))
    else if (I.eq.4) then
4   D=SIGN*EPS**AIN(3)
    else if (I.eq.5) then
5   D=EPS
    else if (I.eq.6) then
6   D=SIGN*EPS**(AIN(3)+0.5D00)
    else if (I.eq.7) then
7   D=SIGN*EPS**(AIN(3)+1.5D00)
    else if (I.eq.8) then
8   D=EPS**(1-0.11D00)
    else if (I.eq.9) then
9   D=EPS**1.39D00
    else if (I.eq.10) then
10  D=SIGN*EPS**(AIN(3)+1.0D00)
    end if
50  DERIV(J)=D
30  CONTINUE
    RETURN
    END
C
C   DPLOT - Produces a plot of deviations against ABS(T-Tc)
C
    SUBROUTINE DPLOT(X,Y,NPTS)
    RETURN
    END
C
C       FUNCTION FPLOT
C     This function converts the double precision
C   value of FUNCTN into single precision, suitable
C   for plottting.
C
    FUNCTION FPLOT(F)
    RETURN
    END
C         SUBROUTINE DPLOTR
C     This subroutine plots the experimental points
C   and the curve obtained from the function. The sign
C   of the function must be changed to plot the upper
C   portion of the curve so the function exists in two
C   forms, FUNCTN and FUNCTS.
C
    SUBROUTINE DPLOTR(X,Y,NPTS,AIN1)
    RETURN
    END
C
C     FUNCTION FPLOTS
C     This is equivalent to FPLOT except it calls the function
C   FUNCTS which has the sign reversed.
C
    FUNCTION FPLOTS(F)
    RETURN
    END
C
C     FUNCTION FUNCTS
C     This is equivalent to FUNCTN except the sign is
C   reversed, and so it allows the top of the graph to be plotted.
C
    FUNCTION FUNCTS(X,I,A)
    RETURN
    END
```

References

[The bracketed references are included for completeness but were not readily available.]

Aizpiri, A.G.; Monroy, F.; del Campo, C.; Rubio, R.G.; Pena, M.D. (1992) *Chem. Phys.*, 165, 31-39. 'Range of simple scaling and critical amplitudes near a LCST. The 2-butoxyethanol + water system.'

Alford, P.C.; Palmer, T.F. (1982) *Chem. Phys. Lett.*, 86, 248-253. 'Fluorescence of DPH derivatives. Evidence for emission from S_2 and S_1 excited states.'

Alford, P.C.; Palmer, T.F. (1983) *J. Chem. Soc. Faraday Trans. 2*, 79, 433-447 (and 1708-1710 - *corrigenda*). 'Photophysics of derivatives of all-*trans*-1,6-diphenyl-1,3,5-hexatriene (DPH).'

Alford, P.C.; Palmer, T.F. (1986) *Chem. Phys. Lett.*, 127, 19-25. 'Fluorescence of derivatives of all-*trans*-1,6-diphenyl-1,3,5-hexatriene.'

Allen, M.T.; Whitten, D.G. (1989) *Chem. Rev.*, 89, 1691-1702. 'The photophysics and photochemistry of α,ω-diphenylpolyene singlet states.'

Aratono, M.; Kahlweit, M. (1991) *J. Chem. Phys.*, 95, 8578-8583 (and *J. Chem. Phys.*, 97, 5932 - erratum). 'Wetting in water-oil-nonionic amphiphile mixtures.'

Archer, A.L. (1995) Ph.D. Thesis, University of Sheffield. 'Alkane + perfluoroalkane mixtures: A theoretical and experimental study of near-critical phase equilibria, thermodynamics, and transport properties.'

Archer, A.L.; Amos, M.D.; Jackson, G.; McLure, I.A. (1996) *Int. J. Thermophys.*, 17, 201-211. 'The theoretical prediction of the critical points of alkanes, perfluoroalkanes, and their mixtures using Bonded Hard Sphere (BHS) theory.'

Arrighi, V.; Fernandez, M.L.; Higgins, J.S. (1993/94) *Sci. Prog.*, 77, 71-90. 'Looking' at polymers with neutrons.'

Atkins, P.W. (1982) *Physical Chemistry*, 2nd ed., Oxford University Press, Oxford.

Axelrod, D.; Burghardt, T.P.; Thompson, N.L. (1984) *Ann. Rev. Biophys. Bioeng.*, 13, 247-268. 'Total internal reflection fluorescence.'

Baaken, C.; Belkoura, L.; Fusenig, S.; Müller-Kirschbaum, Th.; Woermann, D. (1990) *Ber. Bunsenges. Phys. Chem.*, 94, 150-158. 'Study of the system 2-butoxyethanol/water in the vicinity of its lower critical point: measurements of light scattering and ultrasonic absorption.'

Bansal, V.K.; Shah, D.O. (1977) In *Micellization, Solubilization and Microemulsions*, Vol. 1, Ed. Mittal, K.L., Plenum Press, New York. 'Micellar solutions for improved oil recovery.'

Barlow, D.J.; Ma, G.; Lawrence, M.J.; Webster, J.R.P.; Penfold, J. (1995) *Langmuir*, 11, 3737-3741. 'Neutron reflectance studies of a novel nonionic surfactant and molecular modeling of the surfactant vesicles.'

Barr, G. (1931) *A Monograph of Viscometry*, Oxford University Press, London.

Bartoli, F.J.; Litovitz, T.A. (1972) *J. Chem. Phys.*, 56, 413-425. 'Raman scattering: orientational motions in liquids.'

Bates, T.W.; Stockmayer, W.H. (1968) *Macromolecules* 1, 12-17. 'Conformational energies of perfluoroalkanes. II. Dipole moments of $H(CF_2)_nH$.'

Beaglehole, D. (1980) *J. Chem. Phys.*, 73, 3366-3371. 'Adsorption at the liquid-vapor interface of a binary liquid mixture.'

Bedford, R.G.; Dunlap, R.D. (1958) *J. Am. Chem. Soc.*, 80, 282-285. 'Solubilities and volume changes attending mixing for the system: perfluoro-*n*-hexane-*n*-hexane.'

Bell, M.A.; Crystall, B.; Rumbles, G.; Porter, G.; Klug, D.R. (1994) *Chem. Phys. Lett.*, 221, 15-22. 'The influence of a solid/liquid interface on the fluorescence kinetics of the triphenylmethane dye malachite green.'

Bellocq, A.M.; Biais, J.; Clin, B.; Gelot, A.; Lalanne, P.; Lemanceau, B. (1980) *J. Colloid Interface Sci.*, 74, 311-321. 'Three-dimensional phase diagram of the brine-toluene-butanol-sodium dodecyl sulfate system.'

Ben-Amotz, D.; Drake, J.M. (1988) *J. Chem. Phys.*, 89, 1019-1029. 'The solute size effect in rotational diffusion experiments: a test of microscopic friction theories.'

Ben-Amotz, D.; Scott, T.W. (1987) *J. Chem. Phys.*, 87, 3739-3748. 'Microscopic frictional forces on molecular motion in liquids. Picosecond rotational diffusion in alkanes and alcohols.'

Benavides, A.L. (1996) Private communication.

Bennes, R.; Douillard, J.M.; Privat, M.; Tenebre, L. (1985) *J. Phys. Chem.*, 89, 1822-1825. 'An ellipsometric study of the liquid-vapor interface of a binary system near its lower consolute solution temperature: water–2-butoxyethanol.'

Berg, R.F.; Moldover, M.R. (1988) *J. Chem. Phys.*, 89, 3694-3704. 'Critical exponent for the viscosity of four binary liquids.'

Berlman, I.B. (1965) *Handbook of Fluorescence Spectra of Aromatic Molecules*, Academic Press, London.

Bevington, P.R. (1969) *Data Reduction and Error Analysis for the Physical Sciences*, McGraw-Hill, New York.

Beysens, D. (1989) In *Liquides aux Interfaces/Liquids at Interfaces*, Elsevier, New York. 'Study of wetting and adsorption phenomena at fluid and fluid mixture interfaces.'

Beysens, D.; Leibler, S. (1982) *J. Physique Lett.*, 43, L133-L136. 'Observation of an anomalous adsorption in a critical binary mixture.'

Bhattacharjee, J.K.; Ferrell, R.A. (1983) *Phys. Rev. A*, 28, 2363-2369. 'Critical viscosity exponent for a classical fluid.'

Binks, B.P.; Fletcher, P.D.I.; Sager, W.F.C.; Thompson, R.L. (1995) *Langmuir*, 11, 977-983. 'Adsorption of semifluorinated alkanes at hydrocarbon-air surfaces'

Binks, B.P.; Fletcher, P.D.I.; Thompson, R.L. (1996) *Ber. Bunsenges. Phys. Chem.*, 100, 232-236. 'Surfactant properties of semifluorinated alkanes in hydrocarbon and fluorocarbon solvents.'

Birdi, K.S. (1977) In *Micellization, Solubilization and Microemulsions*, Vol. 1, Ed. Mittal, K.L., Plenum Press, New York. 'Thermodynamics of micelle formation.'

Birks, J.B. (1978) *Chem. Phys. Lett.*, 54, 430-434. 'Horizontal radiationless transitions.'

Birks, J.B.; Birch, D.J.S. (1975) *Chem. Phys. Lett.*, 31, 608-610. 'The fluorescence of diphenyl- and retinol-polyenes.'

Birks, J.B.; Tripathi, G.N.R.; Lumb, M.D. (1978) *Chem. Phys.*, 33, 185-194. 'The fluorescence of all-*trans* diphenyl polyenes.'

Bisht, P.B.; Fukuda, K.; Hirayama, S. (1996) *Chem. Phys. Lett.*, 258, 71-79. 'Ripple structures in the fluorescence spectra of N,N'-bis(2,5-di-tert-butylphenyl)-3,4:9,10-perylenebis(dicarboximide) (DBPI) in spherical micrometer-sized polystyrene beads.'

Block, T.E.; Judd, N.F.; McLure, I.A.; Knobler, C.M.; Scott, R.L. (1981) *J. Phys. Chem.*, 85, 3282-3290. 'Excess volumes in the critical solution region.'

Bondi, A. (1964) *J. Phys. Chem.*, 68, 441-451. 'Van der Waals volumes and radii.'

Bonkhoff, K.; Hirtz, A.; Findenegg, G.H. (1991) *Physica A*, 172, 174-199. 'Interfacial tensions in the three-phase region of nonionic surfactant + water + alkane systems: critical point effects and aggregation behaviour.'

Bonn, D.; Wegdam, G.H.; Kellay, H.; Nieuwenhuizen, Th.M. (1992) *Europhys. Lett.*, 20, 235-239. 'Molecular layering on a fluid substrate.'

Bonn, D.; Kellay, H.; Wegdam, G.H. (1993) *J. Chem. Phys.*, 99, 7115-7123. 'Wetting and layering in critical binary fluid mixtures.'

Bonn, D.; Kellay, H.; Meunier, J. (1994) *Ber. Bunsenges. Phys. Chem.*, 98, 399-402. 'Experimental observation of prewetting in a binary liquid mixture.'

Bowers, J. (1995) Ph.D. Thesis, University of Sheffield. 'An exploration of wetting and adsorption behaviour near a critical endpoint.'

Bowers, J. (1996a) Unpublished results.

Bowers, J. (1996b) Postdoctoral research report, University of Sheffield.

Bowers, J.; McLure, I.A.; Whitfield, R.; Burgess, A.N.; Eaglesham, A. (1996a) *Langmuir*, in press. 'Surface composition studies on *n*-hexane + perfluoro-*n*-hexane by specular neutron reflection.'

Bowers, J.; Burgess, A.N.; Clements, P.J.; McLure, I.A.; Steitz, R.; Findenegg, G.H. (1996b) In preparation for *Phys. Rev. E*, Rapid Communications. 'Neutron reflectivity measurements from the free surface of $C_4E_1 + D_2O$.'

Bowers, J.; McLure, I.A.; Clements, P.J. (1996c) *Physica A*, in press. 'Wetting near consolute points by evanescent-wave-generated fluorescence spectroscopy. 3. Fluorescence lifetimes: *n*-heptane + perfluoro-*n*-hexane at the upper critical endpoint.'

Brocklehurst, B. (1987) *Chemistry in Britain*, 23, 853-856. 'Time-resolved luminescence using synchrotron radiation.'

Brunet, J.; Gubbins, K.E. (1969) *Trans. Faraday Soc.*, 65, 1255-1266. 'Viscosity of binary liquid mixtures near the critical mixing point.'

Burstyn, H.C.; Sengers, J.V. (1982) *Phys. Rev. A*, 25, 448-465. 'Decay rate of critical concentration fluctuations in a binary liquid.'

Byrne, J. (1994) *Neutrons, Nuclei and Matter: An Exploration of the Physics of Slow Neutrons*, Institute of Physics Publishing, Bristol.

Cahn, J.W. (1977) *J. Chem. Phys.*, 66, 3667-3672. 'Critical point wetting.'

Caldararu, H.; Caragheorgheopol, A.; Vasilescu, M.; Dragutan, H.; Lemmetyinen, H. (1994) *J. Phys. Chem.*, 98, 5320-5331. 'Structure of the polar core in reverse micelles of nonionic poly(oxyethylene) surfactants, as studied by spin probe and fluorescence probe techniques.'

Calmettes, P. (1977) *Phys. Rev. Lett.*, 39, 1151-1154. 'Critical transport properties of fluids.'

Calmettes, P. (1979) *J. Physique Lett.*, 40, L535-L538. 'Universal ratios of critical amplitudes for the shear viscosity.'

Cannon, M.R.; Manning, R.E.; Bell, J.D. (1960) *Analytical Chem.*, 32, 355-358. 'Viscosity measurement. The kinetic energy correction and a new viscometer.'

Cazabat, A.M.; Langevin, D.; Meunier, J.; Pouchelon, A. (1982a) *Adv. Colloid Interface Sci.*, 16, 175-199. 'Critical behaviour in microemulsions.'

Cazabat, A.M.; Langevin, D.; Meunier, J.; Pouchelon, A. (1982b) *J. Physique-Lett.*, 43, L89-L95. 'Critical behaviour in microemulsions.'

Cazabat, A.M.; Langevin, D.; Sorba, O. (1982c) *J. Physique-Lett.*, 43, L505-L511. 'Anomalous viscosity of microemulsions near a critical point.'

Cehelnik, E.D.; Cundall, R.B.; Lockwood, J.R.; Palmer, T.F. (1974) *Chem. Phys. Lett.*, 27, 586-588. '1,6-Diphenyl-1,3,5-hexatriene as a fluorescence standard.'

Cehelnik, E.D.; Cundall, R.B.; Lockwood, J.R.; Palmer, T.F. (1975) *J. Phys. Chem.*, 79, 1369-1376. 'Solvent and temperature effects on the fluorescence of all-*trans*-1,6-diphenyl-1,3,5-hexatriene.'

Chen, L.-J., Jeng, J.-F.; Robert, M.; Shukla, K.P. (1990) *Phys. Rev. A*, 42, 4716-4723. 'Experimental study of interfacial phase transitions in three-component surfactant systems.'

Chen, L.J.; Yan, W.J.; Hsu, M.C.; Tyan, D.L. (1994) *J. Phys. Chem.*, 98, 1910-1917. 'Wetting transitions at liquid-liquid interfaces in three-component water + oil + nonionic surfactant systems.'

Chittofrati, A.; Lenti, D.; Sanguineti, A.; Visca, M.; Gambi, C.; Senatra, D.; Zhen, Z. (1989a) *Colloids and Surfaces*, 41, 45-49. 'Perfluorinated surfactants at the perfluoropolyether-water interface.'

Chittofrati, A.; Lenti, D.; Sanguineti, A.; Visca, M.; Gambi, C.M.C.; Senatra, D.; Zhou, Z. (1989b) *Prog. Colloid Polymer Sci.*, 79, 218-225. 'Perfluoropolyether microemulsions.'

Clements, P.J.; Bowers, J.; Brocklehurst, B.; McLure, I.A. (1995) *Mol. Phys.*, 86, 873-878. 'The near-critical microscopic viscosity of binary liquid mixtures: 2-butoxyethanol + water at the lower critical endpoint.'

Cohn, R.H.; Jacobs, D.T. (1984) *J. Chem. Phys.*, 80, 856-859. 'Acetone impurity effects on the binary fluid mixture methanol-cyclohexane.'

Copp, J.L.; Everett, D.H. (1953) *Faraday Soc. Discus.*, 15, 174-188. 'Thermodynamics of binary mixtures containing amines.'

Cox, H.L.; Cretcher, L.H. (1926) *J. Am. Chem. Soc.*, 48, 451-453. 'The influence of temperature on the reciprocal solubility of the mono-alkyl ethers of ethylene glycol and water.'

Crowley, T.L.; Lee, E.M.; Simister, E.A.; Thomas, R.K.; Penfold, J.; Rennie, A.R. (1991) *Colloids and Surfaces*, 52, 85-106. 'The application of neutron reflection to the study of layers adsorbed at liquid interfaces.'

Dahlmann, U.; Schneider, G.M. (1989) *J. Chem. Thermodynamics*, 21, 997-1004. '(Liquid + liquid) phase equilibria and critical curves of (ethanol + dodecane or tetradecane or hexadecane or 2,2,4,4,6,8,8,-heptamethylnonane) from 0.1 MPa to 120.0 MPa.'

D'Arrigo, G.; Teixeira, J. (1990) *J. Chem. Soc. Faraday Trans.*, 86, 1503-1509. 'Small-angle neutron scattering study of D_2O-alcohol solutions.'

D'Arrigo, G.; Mistura, L.; Tartaglia, P. (1977) *J. Chem. Phys.*, 66, 80-84. 'Concentration and temperature dependence of viscosity in the critical mixing region of aniline-cyclohexane.'

Edmonds, B.; McLure, I.A. (1982) *J. Chem. Soc. Faraday Trans. I*, 78, 3319-3329. Thermodynamics of *n*-alkane + dimethylsiloxane mixtures. Part 4. Surface tensions.'

[Einstein, A. (1905) *Ann. Phys., Ser. 4*, 17, 549.]

[Einstein, A. (1906) *Ann. Phys., Ser. 4*, 19, 371.]

Elizalde, F.; Gracia, J.; Costas, M. (1988) *J. Phys. Chem.*, 92, 3565-3568. 'Effect of aggregates in bulk and surface properties. Surface tension, foam stability, and heat capacities for 2-butoxyethanol + water.'

Ellis, C.M. (1967) *J. Chem. Education*, 44, 405-407. 'The 2-butoxyethanol-water system. Critical solution temperatures and salting-out effects.'

Eustaquio-Rincón, R.; Trejo, A. (1994) *J. Chem. Soc. Faraday Trans.*, 90, 113-120. 'Thermodynamics of liquid binary (alkanenitrile-alkane) mixtures. Part 1. Experimental excess molar volume at 298.15 K and its interpretation with the Prigogine-Flory-Patterson theory.'

Evans, B.; Chan, M. (1996) *Physics World*, 49 (APR), 48-52. 'To wet or not to wet?'

Evans, R.; Henderson, J.R.; Hoyle, D.C.; Parry, A.O.; Sabeur, Z.A. (1993) *Mol. Phys.*, 80, 755-775. 'Asymptotic decay of liquid structure: oscillatory liquid-vapour density profiles and the Fisher-Widom line.'

Evans, R.; Leote de Carvalho, R.J.F.; Henderson, J.R.; Hoyle, D.C. (1994) *J. Chem. Phys.*, 100, 591-603. 'Asymptotic decay of correlations in liquids and their mixtures.'

Fattinger, Ch. (1987) Ph.D. Thesis, Swiss Federal Institute of Technology, Zürich. 'Laser induced luminescence of molecules near interfaces.'

Fattinger, Ch.; Honegger, F.; Lukosz, W. (1986a) *Helv. Phys. Acta,* 59, 1079-1084. 'Evanescent-wave-induced luminescence as a probe for adsorption of dye molecules at a liquid-solid interface.'

Fattinger, Ch.; Honegger, F.; Lukosz, W. (1986b) *Phys. Rev. Lett.*, 57, 2536-2539. 'Dendritic solidification in narrow gaps and surface-pressure-induced wetting transition.'

Fattinger, Ch.; Togni, G.; Lukosz, W. (1987) *Surf. Sci.*, 189/190, 405-410. 'Wetting in narrow gaps and capillaries: Temperature and surface-pressure-induced wetting transitions.'

Fenby, D.V.; Kooner, Z.S.; Khurma, J.R. (1981) *Fluid Phase Equil.*, 7, 327-338. 'Deuterium isotope effects in liquid-liquid phase diagrams: A review.'

Fernández, J.; McLure, I.A. (1996) *J. Chem. Thermodynamics*, in press.

Fisher, M.E.; de Gennes, P.G. (1978) *C.R. Acad. Sci. Paris, Ser. B*, 287, 207-209. 'Physique des colloïdes. Phénomènes aux parois dans un mélange binaire critique.'

Fixman, M. (1962) *J. Chem. Phys.*, 36, 310-318. 'Viscosity of critical mixtures.'

Ford, W.E.; Kamat, P.V. (1987) *J. Phys. Chem.*, 91, 6373-6380. 'Photchemistry of 3,4,9,10-perylenetetracarboxylic dianhydride dyes. 3. Singlet and triplet excited-state properties of the bis(2,5-di-*tert*-butylphenyl)imide derivative.'

Fowkes, F.M. (1967) In *Solvent Properties of Surfactant Solutions*, Ed. Shinoda, K., Marcel Dekker, New York. 'The interactions of polar molecules, micelles, and polymers in nonaqueous media.'

Francis, A.W. (1951) *J. Phys. Chem.*, 56, 510-513. 'Structural colours in emulsions.'

Francis, A.W. (1953) *Ind. Eng. Chem.*, 45, 2789-2792. 'Isopycnics and twin density lines. Systems with two liquid phases.'

D'Arrigo, G.; Mallamace, F.; Micali, N.; Paparelli, A.; Vasi, C. (1991a) *Phys. Rev. A*, 44, 2578-2587. 'Molecular aggregations in water-2-butoxyethanol mixtures by ultrasonic and Brillouin light-scattering measurements.'

D'Arrigo, G.; Teixeira, J.; Giordano, R.; Mallamace, F. (1991b) *J. Chem. Phys.*, 95, 2732-2737. 'A small-angle neutron scattering study of 2-butoxyethanol/D_2O solutions.'

Davies, M.K. (1988) Ph.D. Thesis, University of Sheffield. 'Transport properties near the upper critical solution temperature of a binary liquid mixture.'

De Backer, S.; Dutt, G.B.; Ameloot, M.; De Schryver, F.C.; Mullen, K.; Holtrup, F. (1996) *J. Phys. Chem.*, 100, 512-518. 'Fluorescence anisotropy of 2,5,8,11-tetra-*tert*-butylperylene and 2,5,10,13-tetra-*tert*-butylterrylene in alkanes and alcohols.'

De Gennes, P.G. (1981) *J. Physique Lett.*, 42, L377-L379. 'Some effects of long range forces on interfacial phenomena.'

Demas, J.N. (1983) *Excited State Lifetime Measurements*, Academic Press, London.

D'Evelyn, M.P.; Rice, S.A. (1983) *J. Chem. Phys.*, 78, 5081-5095. 'A study of the liquid-vapor interface of mercury: computer simulation results.'

Dickinson, E.; McLure, I.A. (1974a) *J. Chem. Soc. Faraday Trans. I*, 70, 2313-2320. 'Thermodynamics of *n*-alkane + dimethylsiloxane mixtures. Part 1. Gas-liquid critical temperatures and pressures.'

Dickinson, E.; McLure, I.A. (1974b) *J. Chem. Soc. Faraday Trans. I*, 70, 2328-2337. 'Thermodynamics of *n*-alkane + dimethylsiloxane mixtures. Part 3. Excess volume.'

Dickinson, E.; McLure, I.A.; Powell, B.H. (1974) *J. Chem. Soc. Faraday Trans. I*, 70, 2321-2327. 'Thermodynamics of *n*-alkane + dimethylsiloxane mixtures. Part 2. Vapour pressures and enthalpies of mixing.'

Dietrich, S. (1988) In *Phase Transitions and Critical Phenomena*, Vol. 12, Ed. Domb, C.; Lebowitz, J.L., Academic Press, London. 'Wetting phenomena.'

Dietrich, S.; Schick, M. (1986) *Phys. Rev. B*, 33, 4952-4968. 'Order of wetting transitions.'

Dote, J.L.; Kivelson, D.; Schwartz, R.N. (1981) *J. Phys. Chem.*, 85, 2169-2180. 'A molecular quasi-hydrodynamic free-space model for molecular rotational relaxation in liquids.'

Dunlap, R.D.; Murphy, C.J.; Bedford, R.G. (1958) *J. Am. Chem. Soc.*, 80, 83-85. 'Some physical properties of perfluoro-*n*-hexane.'

Dunlap, R.D.; Bedford, R.G.; Woodbrey, J.C.; Furrow, S.D. (1959) *J. Am. Chem. Soc.*, 81, 2927-2930. 'Liquid-vapour equilibrium for the system: perfluoro-*n*-hexane-*n*-hexane.'

Dutt, G.B.; Doraiswamy, S. (1992) *J. Chem. Phys.*, 96, 2475-2491. 'Picosecond reorientational dynamics of polar dye probes in binary aqueous mixtures.'

Dyke, D.E.L.; Rowlinson, J.S.; Thacker, R. (1959) *Trans. Faraday Soc.*, 55, 903-910. 'The physical properties of some fluorine compounds and their solutions. Part 4. - Solutions in hydrocarbons.'

Eaglesham, A.; Herrington, T.M. (1995) *J. Colloid Interface Sci.*, 171, 1-7. 'A neutron reflectivity study of spread monolayers of eicosanoic acid, valinomycin, and their equimolar mixture.'

Ebner, C.; Saam, W.F. (1977) *Phys. Rev. Lett.*, 38, 1486-1489. 'New phase-transition phenomena in thin argon films.'

Edmonds, B.; McLure, I.A. (1982) *J. Chem. Soc. Faraday Trans. I*, 78, 3319-3329. 'Thermodynamics of *n*-alkane + dimethylsiloxane mixtures. Part 4. Surface tensions.'

[Einstein, A. (1905) *Ann. Phys., Ser. 4*, 17, 549.]

[Einstein, A. (1906) *Ann. Phys., Ser. 4*, 19, 371.]

Elizalde, F.; Gracia, J.; Costas, M. (1988) *J. Phys. Chem.*, 92, 3565-3568. 'Effect of aggregates in bulk and surface properties. Surface tension, foam stability, and heat capacities for 2-butoxyethanol + water.'

Ellis, C.M. (1967) *J. Chem. Education*, 44, 405-407. 'The 2-butoxyethanol-water system. Critical solution temperatures and salting-out effects.'

Eustaquio-Rincón, R.; Trejo, A. (1994) *J. Chem. Soc. Faraday Trans.*, 90, 113-120. 'Thermodynamics of liquid binary (alkanenitrile-alkane) mixtures. Part 1. Experimental excess molar volume at 298.15 K and its interpretation with the Prigogine-Flory-Patterson theory.'

Evans, B.; Chan, M. (1996) *Physics World*, 49 (APR), 48-52. 'To wet or not to wet?'

Evans, R.; Henderson, J.R.; Hoyle, D.C.; Parry, A.O.; Sabeur, Z.A. (1993) *Mol. Phys.*, 80, 755-775. 'Asymptotic decay of liquid structure: oscillatory liquid-vapour density profiles and the Fisher-Widom line.'

Evans, R.; Leote de Carvalho, R.J.F.; Henderson, J.R.; Hoyle, D.C. (1994) *J. Chem. Phys.*, 100, 591-603. 'Asymptotic decay of correlations in liquids and their mixtures.'

Fattinger, Ch. (1987) Ph.D. Thesis, Swiss Federal Institute of Technology, Zürich. 'Laser induced luminescence of molecules near interfaces.'

Fattinger, Ch.; Honegger, F.; Lukosz, W. (1986a) *Helv. Phys. Acta,* 59, 1079-1084. 'Evanescent-wave-induced luminescence as a probe for adsorption of dye molecules at a liquid-solid interface.'

Fattinger, Ch.; Honegger, F.; Lukosz, W. (1986b) *Phys. Rev. Lett.*, 57, 2536-2539. 'Dendritic solidification in narrow gaps and surface-pressure-induced wetting transition.'

Fattinger, Ch.; Togni, G.; Lukosz, W. (1987) *Surf. Sci.*, 189/190, 405-410. 'Wetting in narrow gaps and capillaries: Temperature and surface-pressure-induced wetting transitions.'

Fenby, D.V.; Kooner, Z.S.; Khurma, J.R. (1981) *Fluid Phase Equil.*, 7, 327-338. 'Deuterium isotope effects in liquid-liquid phase diagrams: A review.'

Fernández, J.; McLure, I.A. (1996) *J. Chem. Thermodynamics*, in press.

Fisher, M.E.; de Gennes, P.G. (1978) *C.R. Acad. Sci. Paris, Ser. B*, 287, 207-209. 'Physique des colloïdes. Phénomènes aux parois dans un mélange binaire critique.'

Fixman, M. (1962) *J. Chem. Phys.*, 36, 310-318. 'Viscosity of critical mixtures.'

Ford, W.E.; Kamat, P.V. (1987) *J. Phys. Chem.*, 91, 6373-6380. 'Photchemistry of 3,4,9,10-perylenetetracarboxylic dianhydride dyes. 3. Singlet and triplet excited-state properties of the bis(2,5-di-*tert*-butylphenyl)imide derivative.'

Fowkes, F.M. (1967) In *Solvent Properties of Surfactant Solutions*, Ed. Shinoda, K., Marcel Dekker, New York. 'The interactions of polar molecules, micelles, and polymers in nonaqueous media.'

Francis, A.W. (1951) *J. Phys. Chem.*, 56, 510-513. 'Structural colours in emulsions.'

Francis, A.W. (1953) *Ind. Eng. Chem.*, 45, 2789-2792. 'Isopycnics and twin density lines. Systems with two liquid phases.'

French, H.T.; Richards, A.; Stokes, R.H. (1979) *J. Chem. Thermodynamics*, 11, 671-686. 'Thermodynamics of the partially miscible system ethanol + hexadecane.'

Friedländer, J. (1901) *Z. Physik. Chem.*, 38, 385-440. 'Über merkwürdige Erscheinungen in der Umgebung des kritischen Punktes teilweise mischbarer Flüssigkeiten.'

Fusenig, St.; Woermann, D. (1993) *Ber. Bunsenges. Phys. Chem.*, 97, 577-582. 'Static light scattering experiments with 2-butoxyethanol/water mixtures of near critical composition in the vicinity of the lower critical point.'

Gaines, G.L. (1991) *Langmuir*, 7, 3054-3056. 'Surface activity of semifluorinated alkanes - $F(CF_2)_m(CH_2)_nH$.'

Garisto, F.; Kapral, R. (1976) *Phys. Rev. A*, 14, 884-885. 'Vertex corrections to the shear viscosity critical exponent.'

[Gierer, A.; Wirtz, K. (1953) *Z. Naturforsch.*, A8, 532.]

Gilmour, J.B.; Zwicker, J.O.; Katz, J.; Scott, R.L. (1967) *J. Phys. Chem.*, 71, 3259-3270. 'Fluorocarbon solutions at low temperatures. V. The liquid mixtures C_2H_6 + C_2F_6, C_3H_8 + C_2F_6, CH_4 + C_3F_8, C_2H_6 + C_3F_8, C_3H_8 + C_3F_8, *n*-C_4H_{10} + C_3F_8, *i*-C_4H_{10} + C_3F_8, C_3H_8 + *n*-C_4F_{10}, *n*-C_6H_{14} + *n*-C_4F_{10}, *n*-C_7H_{16} + *n*-C_4F_{10}, *n*-C_9H_{20} + *n*-C_4F_{10}, and *n*-$C_{10}H_{22}$ + *n*-C_4F_{10}.'

Glasstone, S. (1940) *Text-book of Physical Chemistry*, Macmillan, London.

Gonçalves, F.A.; Kestin, J.; Sengers, J.V. (1991) *Int. J. Thermophys.*, 12, 1013-1028. 'Surface-tension effects in suspended-level capillary viscometers.'

Gradzielski, M.; Langevin, D.; Magid, L.; Strey, R. (1995) *J. Phys. Chem.*, 99, 13232-13238. 'Small-angle neutron scattering from diffuse interfaces. 2. Polydisperse shells in water-*n*-alkane-$C_{10}E_4$ microemulsions.'

Grätzel, M.; Thomas, J.K. (1973) *J. Am. Chem. Soc.*, 95, 6885-6889. 'On the dynamics of pyrene fluorescence quenching in aqueous ionic micellar systems. Factors affecting the permeability of micelles.'

Gray, P.; Holland, S.; Maczek, A.O.S. (1970) *Trans. Faraday Soc.*, 66, 107-126. 'Thermal conductivities of binary mixtures of organic vapours and inert diluents.'

Greef, R. (1990) In *Surface Analysis Techniques and Applications*, Ed. Neagle, W.; Randell, D.R., The Royal Society of Chemistry, Cambridge. 'Ellipsometry - A versatile tool in surface analysis.'

Green, D.G. (1992) Ph.D. Thesis, University of Sheffield. 'Theory and simulation of phase equilibria and critical behaviour in aqueous solutions of chain molecules and other model mixtures.'

Greer, S.C.; Moldover, M.R. (1981) *Ann. Rev. Phys. Chem.*, 32, 233-265. 'Thermodynamic anomalies at critical points of fluids.'

Gross, U.; Papke, G.; Rüdiger, S. (1993) *J. Fluorine Chem.* 61, 11-16. 'Fluorocarbons as blood substitutes: critical solution temperatures of some perfluorocarbons and their mixtures.'

Grunberg, L.; Nissan, A.H. (1949) *Nature*, 164, 799-800. 'Mixture law for viscosity.'

Guest, D.; Langevin, D. (1986) *J. Colloid Interface Sci.*, 112, 208-220. 'Light scattering study of a multiphase microemulsion system.'

Habib, S.; Gruner, K. (1988) *Rev. Sci. Instrum.*, 59, 2290-2293. 'Automatic capillary viscometer for fluids with variable opacity.'

Ham, J.S. (1953) *J. Chem. Phys.*, 21, 756-758. 'A new electronic state in benzene.'

Hamai, S.; Tamai, N.; Masuhara, H. (1995) *J. Phys. Chem.*, 99, 4980-4985. 'Excimer formation of pyrene in a solid/polymer solution interface layer. A time-resolved total internal reflection fluorescence study.'

[Hao, H. (1991) Ph.D. Thesis, University of Maryland.]

Hardy, R.C. (1963) *NBS Viscometer Calibrating Liquids and Capillary Tube Viscometers*, Monograph 55, Washington DC.

Hariharan, A.; Harris, J.G. (1994) *J. Chem. Phys.*, 101, 4156-4165. 'Structure and thermodynamics of the liquid-vapour interface of fluorocarbons and semifluorinated alkane diblocks: A molecular dynamics study.'

Haslam, A.J. (1992) B.Sc. Project Report, University of Sheffield. 'Viscosity anomalies in a binary liquid mixture near a consolute point.'

Heady, R.B.; Cahn, J.W. (1973) *J. Chem. Phys.*, 58, 896-910. 'Experimental test of classical nucleation theory in a liquid-liquid miscibility gap system.'

Heavens, O.S. (1955) *Optical Properties of Thin Films*, Butterworth, London.

Heidel, B.; Findenegg, G.H. (1984) *J. Phys. Chem.*, 88, 6575-6579. 'Ellipsometric study of the surface of a binary liquid mixture near a critical solution point.'

Heidel, B.; Findenegg, G.H. (1987) *J. Chem. Phys.*, 87, 706-713. 'Ellipsometric study of critical adsorption at the surface of a polymer solution: Evidence for a slowly decaying interfacial profile.'

Hickman, J.B. (1955) *J. Am. Chem. Soc.*, 77, 6154-6156. 'Solubility of isomeric hexanes in perfluoroheptane.'

Hicks, C.P.; Hurle, R.L.; Toczylkin, L.S.; Young, C.L. (1978) *Aust. J. Chem.*, 31, 19-25. 'Upper critical solution temperatures of hydrocarbon + fluorocarbon mixtures.'

Hildebrand, J.H.; Scott, R.L. (1950) *Ann. Rev. Phys. Chem.*, 1, 75-92. 'Solutions of nonelectrolytes.'

Hildebrand, J.H.; Fisher, B.B.; Benesi, H.A. (1950) *J. Am. Chem. Soc.*, 72, 4348-4351. 'Solubility of perfluoro-*n*-heptane with benzene, carbon tetrachloride, chloroform, *n*-heptane and 2,2,4-trimethylpentane.'

Hildebrand, J.H.; Prausnitz, J.M.; Scott, R.L. (1970) *Regular and Related Solutions*, Van Nostrand Reinhold, New York.

Hirtz, A.; Bonkhoff, K.; Findenegg, G.H. (1993) *Adv. Colloid Interface Sci.*, 44, 241-281. 'Optical studies of liquid interfaces in amphiphilic systems: How wetting and adsorption are modified by surfactant aggregation.'

Hohenburg, P.C.; Halperin, B.I. (1977) *Rev. Modern Phys.*, 49, 435-479. 'Theory of dynamic critical phenomena.'

Höpken, J.; Möller, M. (1992) *Macromolecules*, 25, 2482-2489. 'On the morphology of (perfluoroalkyl)alkanes.'

Houessou, C.; Guenoun, P.; Gastaud, R.; Perrot, F.; Beysens, D. (1985) *Phys. Rev. A*, 32, 1818-1833. 'Critical behaviour of the binary fluids cyclohexane-methanol, deuterated cyclohexane-methanol and of their isodensity mixture: Application to microgravity simulations and wetting phenomena.'

Hu, C.-M.; Zwanzig, R. (1974) *J. Chem. Phys.*, 60, 4354-4357. 'Rotational friction coefficients for spheroids with the slipping boundary condition.'

Huang, Z.; Schlossman, M.L.; Acero, A.A.; Lei, N.; Zhang, Z.; Rice, S.A. (1995) *Abs. Papers Am. Chem. Soc.*, 210, p128-COLL. 'Structural studies of semifluorinated hydrocarbon monolayers at the air/water interface.'

Huang, Z.; Acero, A.A.; Lei, N.; Rice, S.A.; Zhang, Z.; Schlossman, M.L. (1996) *J. Chem. Soc. Faraday Trans.*, 92, 545-552. 'Structural studies of semifluorinated hydrocarbon monolayers at the air/water interface.'

Hudson, B.S.; Kohler, B.E. (1973) *J. Chem. Phys.*, 59, 4984-5002. 'Polyene spectroscopy: The lowest energy excited singlet state of diphenyloctatetraene and other linear polyenes.'

Huheey, J.E. (1983) *Inorganic Chemistry, Principles of Structure and Reactivity*, 3rd ed., Harper and Row, New York.

Hunter, R.J. (1987) *Foundations of Colloid Science*, Oxford University Press, Oxford.

Hurle, R.L.; Toczylkin, L.; Young, C.L. (1977) *J. Chem. Soc. Faraday Trans. 2*, 73, 618-622. 'Theoretical prediction of phase behaviour at high temperatures and pressures for non-polar mixtures. Part 3. Comparison with upper critical solution temperatures for perfluoromethylcyclohexane + hydrocarbons.'

Hutchinson, E.; Shinoda, K. (1967) In *Solvent Properties of Surfactant Solutions*, Ed. Shinoda, K., Marcel Dekker, New York. 'An outline of the solvent properties of surfactant solutions.'

Ito, N.; Saito, K.; Kato, T.; Fujiyama, T. (1981) *Bull. Chem. Soc. Japan*, 54, 991-997. 'Observation of mutual diffusion coefficients and cooperative motions in binary solutions of t-butyl alcohol-water and 2-butoxyethanol-water.'

Ito, N.; Fujiyama, T.; Udagawa, Y. (1983) *Bull. Chem. Soc. Japan*, 56, 379-385. 'A study of local structure formation in binary solutions of 2-butoxyethanol and water by Rayleigh scattering and Raman spectra.'

Itoh, T.; Kohler, B.E. (1987) *J. Phys. Chem.*, 91, 1760-1764. 'Dual fluorescence of diphenylpolyenes.'

Izumi, Y.; Dondos, A.; Picot, C.; Benoit, H. (1981) *J. Physique*, 42, 353-358. 'Shear viscosity measurements in the binary mixture butyl cellosolve-water near its upper and lower critical consolute points.'

Jobe, D.J.; Verrall, R.E. (1990) *Langmuir* 6, 1750-1757. 'Polarised fluorescence emission measurements in mixtures of 2-butoxyethanol, cetyltrimethylammonium bromide, and water.'

Jobe, D.J.; Verrall, R.E.; Palepu, R.; Reinsborough, V.C. (1988) *J. Phys. Chem.*, 92, 3582-3586. 'Fluorescence and conductometric studies of potassium 2-(p-toluidinyl)-naphthalene-6-sulfonate/cyclodextrin/surfactant systems.'

Jones, R.A.L.; Norton, L.J.; Kramer, E.J.; Bates, F.S.; Wiltzius, P. (1991) *Phys. Rev. Lett.*, 66, 1326-1329. 'Surface-directed spinodal decomposition.'

Kahlweit, M. (1982) *J. Colloid Interface Sci.*, 90, 197-202. 'The phase behaviour of systems of the type H_2O-oil-nonionic surfactant-electrolyte.'

Kahlweit, M. (1988) *Science*, 240, 617-621. 'Microemulsions.'

Kahlweit, M.; Busse, G. (1989) *J. Chem. Phys.*, 91, 1339-1344. 'Wetting in mixtures of water, nonionic amphiphiles, and nonpolar solvents.'

Kahlweit, M.; Strey, R. (1985) *Angew. Chem. Int. Ed. Engl.*, 24, 654-668. 'Phase behaviour of ternary systems of the type H_2O-oil-nonionic amphiphile (microemulsions).'

Kahlweit, M.; Lessner, E.; Strey, R. (1983) *J. Phys. Chem.*, 87, 5032-5040. 'Influence of the properties of the oil and the surfactant on the phase behaviour of systems of the type water-oil-nonionic surfactant.'

Kahlweit, M.; Strey, R.; Busse, G. (1990) *J. Phys. Chem.*, 94, 3881-3894. 'Microemulsions: a qualitative thermodynamic approach.'

Karolin J.; Johansson, L.B.-A.; Strandberg, L.; Ny, T. (1994) *J. Am. Chem. Soc.*, 116, 7801-7806. 'Fluorescence and absorption spectroscopic properties of dipyrromethene boron difluoride (BODIPY) derivatives in liquids, lipid membranes, and proteins.'

Kato, S.; Jobe, D.; Rao, N.P.; Ho, C.H.; Verrall, R.E. (1986) *J. Phys. Chem.*, 90, 4167-4174. 'Ultrasonic relaxation studies of 2-butoxyethanol-water and 2-butoxyethanol-water-cetyltrimethylammonium bromide solutions as a function of composition.'

Kawasaki, K. (1966) *Phys. Rev., Series 2*, 150, 291-306. 'Correlation-function approach to the transport coefficients near the critical point. I. '

Kawasaki, K. (1969) *Phys. Lett.*, 30A, 325-326. 'Decay rate of concentration fluctuation of a binary mixture in the non-hydrodynamical regime.'

Kawasaki, K. (1970a) *Annales Phys.*, 61, 1-56. 'Kinetic equations and time correlation functions of critical fluctuations.'

Kawasaki, K. (1970b) *Phys. Rev. A*, 1, 1750-1757. 'Sound attenuation and dispersion near the liquid-gas critical point.'

Kell, G.S. (1975) *J. Chem. Eng. Data*, 20, 97-105. 'Density, thermal expansivity, and compressibility of liquid water from 0° to 150°C: Correlations and tables for atmospheric pressure and saturation reviewed and expressed on 1968 temperature scale.'

Kertes, A.S. (1977) In *Micellization, Solubilization and Microemulsions,* Vol. 1, Ed. Mittal, K.L., Plenum Press, New York. 'Aggregation of surfactants in hydrocarbons. Incompatibility of the critical micelle concentration concept with experimental data.'

Kestin, J.; Whitelaw, J.H.; Zien, T.F. (1964) *Physica*, 30, 161-181. 'The viscosity of carbon dioxide in the neighbourhood of the critical point.'

Kestin, J.; Sokolov, M.; Wakeham, W. (1973) *Applied Sci. Res.*, 27, 241-264. 'Theory of capillary viscometers.'

Kilpatrick, P.K.; Gorman, C.A.; Davis, H.T.; Scriven, L.E.; Miller, W.G. (1986) *J. Phys. Chem.*, 90, 5292-5299. 'Patterns of phase behaviour in ternary ethoxylated alcohol-*n*-alkane-water mixtures.'

Kivelson, D.; Madden, P.A. (1980) *Ann. Rev. Phys. Chem.*, 31, 523-558. 'Light scattering studies of molecular liquids.'

Knecht, B.; Woermann, D. (1995) *Ber. Bunsenges. Phys. Chem.*, 99, 1067-1069. 'Composition dependence of the liquid/air interfacial tension of 2-butoxyethanol/water mixtures at temperatures below the lower critical temperature.'

Koester, L.; Yelon, W.B. (1982) *Compilation of Neutron Scattering Lengths*, Netherlands Energy Research Foundation, Petten.

Koga, Y. (1992) *J. Phys. Chem.*, 96, 10466-10468. 'Transition of mixing scheme in the water-rich region of aqueous 2-butoxyethanol: partial molar volumes and their derivatives.'

Koga, Y.; Siu, W.W.Y.; Wong, T.Y.H. (1990) *J. Phys. Chem.*, 94, 3879-3881. 'Transition of short- to medium-range order in aqueous solution of 2-butoxyethanol.'

Kohler, B.E.; Itoh, T. (1988) *J. Phys. Chem.*, 92, 5120-5122. 'Fluorescence from the 1^1B_u state of diphenylhexatriene: Inversion of the 1^1B_u and 2^1A_g levels in CS_2.'

Kowert, B.A.; Higgins, E.J.; Mariencheck, W.I.; Stemmler, T.L.; Kantorovich, V. (1996) *J. Phys. Chem.*, 100, 11211-11217. 'Electron spin resonance studies of reorientational motion in glass-forming liquids.'

Kwon, O'D.; Beaglehole, D.; Webb, W.W.; Widom, B.; Schmidt, J.W.; Cahn, J.W.; Moldover, M.R.; Stephenson, B. (1982) *Phys. Rev. Lett.*, 48, 185-188. 'Thickness of the liquid-vapor wetting layer.'

Lakowicz, J.R. and Maliwal, B.P. (1985) *Biophys. Chem.*, 21, 61-78. 'Construction and performance of a variable-frequency phase-modulation fluorometer.'

Langevin, D. (1987) In *Microemulsions: Structure and Dynamics*, Ed. Friberg, S.E.; Bothorel, P., CRC Press, Boca Raton, Florida. 'Low interfacial tensions in microemulsion systems.'

Langevin, D. (1988) *Acc. Chem. Res.*, 21, 255-260. 'Microemulsions.'

Langevin, D. (1996) *Ber. Bunsenges. Phys. Chem.*, 100, 336-343. 'Optical methods for studying microemulsions and microemulsion interfaces.'

Law, B.M. (1994) *Ber. Bunsenges. Phys. Chem.*, 98, 472-477. 'Surface amplitude ratios and nucleated wetting near a critical end point.'

Lee, S.P.; Purvis, A.J. (1977) *Chem. Phys.*, 24, 191-199. 'The nonlinear shear gradient effect on the shear viscosity of a ternary system near a plait point.'

Lee, D.D.; Chen, S.H.; Majkrzak, C.F.; Satija, S.K. (1995) *Phys. Rev. E*, 52, R29-R32. 'Bulk and surface correlations in a microemulsion.'

Le Guillou, J.C.; Zinn-Justin, J. (1977) *Phys. Rev. Lett.*, 39, 95-98. 'Critical exponents for the *n*-vector model in three dimensions from field theory.'

Leister, H.M.; Allegra, J.C.; Allen, G.F. (1969) *J. Chem. Phys.*, 51, 3701-3708. 'Tracer diffusion and shear viscosity in the liquid-liquid critical region.'

Lekner, J. (1987) *Theory of Reflection*, Martinus Nijhoff, Dordrecht.

Lekner, J. (1991) *Physica B*, 173, 99-111. 'Reflection theory and the analysis of neutron reflection data.'

Lenk, R. (1986) *Fluctuations, Diffusion and Spin Relaxation*, Elsevier, Amsterdam.

Lindman, B.; Wennerström, H. (1980) In *Micelles*, Springer-Verlag, New York. 'Micelles. Amphiphile aggregation in aqueous solution.'

Liu, A.J.; Fisher, M.E. (1989) *Phys. Rev. A*, 40, 7202-7221. 'Universal critical adsorption profile from optical experiments.'

Lobo, L.Q.; Staveley, L.A.K. (1981) *J. Chem. Eng. Data*, 26, 404-407. 'Thermodynamic properties of liquid carbon tetrafluoride.'

Lombardo, D.; Mallamace, F.; Micali, N.; D'Arrigo, G. (1994) *Phys. Rev. E*, 49, 1430-1438. 'Dynamic critical phenomena in water-butoxyethanol mixtures studied by viscosity and light-scattering measurements.'

Lo Nostro, P.; Chen, S.-H. (1993) *J. Phys. Chem.*, 97, 6535-6540. 'Aggregation of a semifluorinated *n*-alkane in perfluorooctane.'

Lo Nostro, P. (1995) *Adv. Colloid Interface Sci.*, 56, 245-287. 'Phase separation properties of fluorocarbons, hydrocarbons and their copolymers.'

Lo Nostro, P.; Ku, C.Y.; Chen, S.-H.; Lin, J.-S. (1995) *J. Phys. Chem.*, 99, 10858-10864. 'Effect of a semifluorinated copolymer on the phase separation of a fluorocarbon/hydrocarbon mixture.'

Lopez-Delgado, R.; Tramer, A.; Munro, I.H. (1974) *Chem. Phys.*, 5, 72-83. 'A new pulsed light source for lifetime studies and time resolved spectroscopy: The synchrotron radiation from an electron storage ring.'

Lu, J.R.; Simister, E.A.; Lee, E.M.; Thomas, R.K.; Rennie, A.R.; Penfold, J. (1992) *Langmuir*, 8, 1837-1844. 'Direct determination by neutron reflection of the penetration of water into surfactant layers at the air/water interface.'

Lu, J.R.; Marrocco, A.; Su, T.J.; Thomas, R.K.; Penfold, J. (1993a) *J. Colloid Interface Sci.*, 158, 303-316. 'Adsorption of dodecyl sulfate surfactants with monovalent metal counterions at the air-water interface studied by neutron reflection and surface tension.'

Lu, J.R.; Li, Z.X.; Su, T.J.; Thomas, R.K.; Penfold, J. (1993b) *Langmuir*, 9, 2408-2416. 'Structure of adsorbed layers of ethylene glycol monododecyl ether surfactants with one, two, and four ethylene oxide groups, as determined by neutron reflection.'

Lu, J.R.; Hromadova, M.; Thomas, R.K.; Penfold, J. (1993c) *Langmuir*, 9, 2417-2425. 'Neutron reflection from triethylene glycol monododecyl ether adsorbed at the air-liquid interface: The variation of the hydrocarbon chain distribution with surface concentration.'

Lu, J.R.; Simister, E.A.; Thomas, R.K.; Penfold, J. (1993d) *J. Phys. Chem.*, 97, 13907-13913. 'Structure of the surface of a surfactant solution above the critical micelle concentration.'

Luettmer-Strathmann, J.; Sengers, J.V.; Olchowy, G.A. (1995) *J. Chem. Phys.*, 103, 7482-7501. 'Non-asymptotic critical behavior of the transport properties of fluids.'

Lukosz, W. (1979) *J. Opt. Soc. Am.*, 69, 1495-1503. 'Light emission by magnetic and electric dipoles close to a plane dielectric interface. III. Radiation patterns of dipoles with arbitrary orientation.'

Lukosz, W. (1981) *J. Opt. Soc. Am.*, 71, 744-754. 'Light emission by multipole sources in thin layers. I. Radiation patterns of electric and magnetic dipoles.'

Maczek, A.O.S.; Davies, M.K.; Jayasuriya, J.E.C. (1990) *Ber. Bunsenges. Phys. Chem.*, 94, 425-428. 'Amplitude ratios for viscosity & thermal conductivity anomalies near a UCST.'

Magnussen, O.M.; Ocko, B.M.; Regan, M.J.; Penanen, K.; Pershan, P.S.; Deutsch, M. (1995) *Phys. Rev. Lett.*, 74, 4444-4447. 'X-ray reflectivity measurements of surface layering in liquid mercury.'

Maiti, N.C.; Mazumdar, S.; Periasamy, N. (1995) *J. Phys. Chem.*, 99, 10708-10715. 'Dynamics of porphyrin molecules in micelles. Picosecond time-resolved fluorescence anisotropy studies.'

Majer, V.; Svoboda, V. (1985) *Enthalpies of Vaporization of Organic Compounds*, Chemical Data Series, No. 32, Ed. Kehiaian, H.V., Blackwells, Oxford.

Mallamace, F.; Micali, N.; D'Arrigo, G. (1991) *Phys. Rev. A*, 44, 6652-6658. 'Dynamical effects of supramolecular aggregates in water-butoxyethanol mixtures studied by viscosity measurements.'

Marsh, D. (1989) In *Biological Magnetic Resonance, Vol. 8, Spin Labelling*, Ed. Berliner, L.J.; Reuben, J., Plenum Press, New York.

Marsh, D.; Horváth, L.I. (1989) In *Advanced EPR. Applications in Biology and Biochemistry*, Ed. Hoff, A.J., Elsevier, Amsterdam.

Mathis, G.; Leempoel, P.; Ravey, J.-C.; Selve, C.; Delpuech, J.-J. (1984) *J. Am. Chem. Soc.*, 106, 6162-6171. 'A novel class of nonionic microemulsions: Fluorocarbons in aqueous solutions of fluorinated poly(oxyethylene) surfactants.'

McLure, I.A. (1979) In proceedings of '*I Conferencia Internacional de Termodinamica de Disolucion de no Electrolitos*', *Santiago de Compostela*. 'Thermodynamics of *n*-alkanenitrile + *n*-alkane mixtures.'

McLure, I.A.; Clements, P.J. (1996) Submitted for publication in *Surface Sci. Lett.* 'Wetting in narrow gaps and capillaries: Temperature- and surface-pressure-induced wetting transitions. A comment.'

McLure, I.A.; Mokhtari, A. (1982) *J. Solution Chem.*, 11, 27-44. 'Thermodynamics of solutions of iodine and perfluorocarbons in cycloalkanes.'

McLure, I.A.; Neville, J.F. (1977) *J. Chem. Thermodynamics*, 9, 957-961. 'An analysis of the gas-liquid critical properties of the dimethylsiloxanes establishing tetramethylsilane as the forerunner of the series.'

McLure, I.A.; Trejo Rodriguez, A. (1980) *J. Chem. Thermodynamics*, 12, 745-751. 'Excess functions for (*n*-alkanenitrile + *n*-alkane) liquid mixtures. I. Excess volumes at 303.15 K for propanenitrile, *n*-butanenitrile, and *n*-hexanenitrile with some C_5 to C_{14} *n*-alkanes.'

McLure, I.A.; Trejo Rodriguez, A. (1982) *J. Chem. Thermodynamics*, 14, 439-445. 'Excess functions for (*n*-alkanenitrile + *n*-alkane) liquid mixtures. 2. Excess enthalpies at 298.15 K for propanenitrile and *n*-butanenitrile with some C_5 to C_{14} *n*-alkanes.'

McLure, I.A.; Williamson, A.-M. (1996) *Physica A*, in press. 'Wetting near consolute points by evanescent-wave-generated fluorescence spectroscopy. 1. Differential solubility: 2,6-lutidine + water at the lower critical endpoint.'

McLure, I.A.; Edmonds, B.; Lal, M. (1973) *Nature (Phys. Sci.)*, 241, 71. 'Extremes in surface tension of fluorocarbon + hydrocarbon mixtures.'

McLure, I.A.; Pretty, A.J.; Sadler, P.A. (1977) *J. Chem. Eng. Data*, 22, 372-376. 'Specific volumes, thermal pressure coefficients, and derived quantities of five dimethylsiloxane oligomers from 25 to 140°C.'

McLure, I.A.; Trejo Rodriguez, A.; Ingham, P.A.; Steele, J.F. (1982) *Fluid Phase Equil.*, 8, 271-284. 'Phase equilibria for binary *n*-alkanenitrile-*n*-alkane mixtures. I. Upper liquid-liquid coexistence temperatures for ethanenitrile, propanenitrile, and *n*-butanenitrile with some C_5-C_{18} *n*-alkanes.'

McLure, I.A.; Soares, V.A.M.; Williamson, A.M. (1993) *Langmuir*, 9, 2190-2201. 'Total Surface Segregation. A fresh look at the Gibbs adsorption isotherm for binary liquid mixtures.'

McLure, I.A.; Arriaga-Colina, J.L.; Armitage, D.A. (1994) *Fluid Phase Equil.*, in press. 'Phase equilibria for binary *n*-alkanenitrile-*n*-alkane mixtures. III. Vapour-liquid phase equilibria for propanenitrile with C_5-C_8 *n*-alkanes.'

McLure, I.A.; Mokhtari, A.; Bowers, J. (1996) *J. Chem. Soc. Faraday Trans.*, in press. 'Thermodynamics of linear dimethylsiloxane + perfluoroalkane mixtures. 1. Liquid/liquid coexistence curves for hexamethyldisiloxane, octamethyltrisiloxane, or decamethyltetrasiloxane + tetradecafluorohexane near the upper critical endpoint.'

Mertsch, R.; Wolf, B.A. (1994) *Ber. Bunsenges. Phys. Chem.*, 98, 1275-1280. 'On the significance of molecular surfaces and thermodynamic interactions for the excess viscosities of liquid mixtures.'

Michael, D.; Benjamin, I. (1995) *J. Phys. Chem.*, 99, 16810-16813. 'Proposed experimental probe of the liquid/liquid interface structure: Molecular dynamics of charge transfer at the water/octanol interface.'

Mills, D.M. (1984) *Physics Today*, 37 (APR), 22-30. 'Time-resolution experiments using x-ray synchrotron radiation.'

[Mohamadi, F.; Richards, N.G.J.; Guida, W.C.; Liskamp, R.; Lipton, M.; Caufield, C.; Chang, G.; Hendrickson, T.; Still, W.C. (1990) *J. Comput. Chem.*, 11, 440.]

Moldover, M.R.; Cahn, J.W. (1980) *Science*, 207, 1073-1075. 'An interface phase transition: Complete to partial wetting.'

Munro, I.H.; Shaw, D.; Jones, G.R.; Martin, M.M. (1985) *Anal. Inst.*, 14, 465-482. 'Time resolved fluorescence spectroscopy with synchrotron radiation.'

Munson, M.S.B. (1964) *J. Phys. Chem.*, 68, 796-801. 'Solutions of fluorochemicals and hydrocarbons.'

Myers, D.B.; Smith, R.A.; Katz, J.; Scott, R.L. (1966) *J. Phys. Chem.*, 70, 3341-3343. 'The effect of pressure on liquid miscibility.'

Naldrett, S.N.; Maass, O. (1940) *Can. J. Res.*, 18B, 322-332. 'The viscosity of carbon dioxide in the critical region.'

Naumann, C.; Brumm, T.; Rennie, A.R.; Penfold, J.; Bayerl, T.M. (1995) *Langmuir*, 11, 3948-3952. 'Hydration of DPPC monolayers at the air/water interface and its modulation by the nonionic surfactant $C_{12}E_4$: A neutron reflection study.'

Némethy, G.; Scheraga, H.A. (1964) *J. Chem. Phys.*, 41, 680-689. 'Structure of water and hydrophobic bonding in proteins. IV. The thermodynamic properties of liquid deuterium oxide.'

Newton, I. (1704) Original work reproduced in *Opticks*, Dover Publications, New York, 1952.

Nicholson, J.D.; Doherty, J.V.; Clarke, J.H.R. (1982) In *Microemulsions*, Ed. Robb, I.D., Plenum Press, New York. 'Dynamic light scattering from water microemulsions in organic media.'

Nieuwoudt, J.C.; Sengers, J.V. (1989) *J. Chem. Phys.*, 90, 457-462. 'A reevaluation of the viscosity exponent for binary mixtures near the consolute point.'

Nivaggioli, T.; Tsao, B.; Alexandridis, P.; Hatton, T.A. (1995) *Langmuir*, 11, 119-126. 'Microviscosity in pluronic and tetronic poly(ethylene oxide)-poly(propylene oxide) block copolymer micelles.'

Ohta, T. (1977) *J. Phys. C: Solid State Phys.*, 10, 791-793. 'Multiplicative renormalization of the anomalous shear viscosity in classical liquids.'

Oxtoby, D.W. (1975) *J. Chem. Phys.*, 62, 1463-1468. 'Nonlinear effects in the shear viscosity of fluids near the critical point.'

Papoutsi, D.; Bekiari, V.; Stathatos, E.; Lianos, P. (1995) *Langmuir*, 11, 4355-4360. 'Molecular diffusion and fluorescence energy-transfer studies in thin surfactant films.'

Parker, C.A. (1968) *Photoluminescence of Solutions: with Applications to Photochemistry and Analytical Chemistry*, Elsevier, Amsterdam.

Parsonage, N.G.; Scott, R.L. (1962) *J. Chem. Phys.*, 37, 304-306. 'Contribution of octopole-octopole interactions to the excess properties of mixtures of tetrahedral molecules.'

Pegg, I.L. (1982) Ph.D. Thesis, University of Sheffield. 'Interfaces in near-critical binary liquid mixtures; a classical and light-scattering study.'

Pegg, I.L.; McLure, I.A. (1984) *Mol. Phys.*, 53, 897-916. 'Shear viscosity through the consolute point for three binary liquid mixtures.'

Penfold, J. (1988) Rutherford internal report, RAL-88-088. 'The adaptation of methods in multilayer optics for the calculation of specular neutron reflection.'

Penfold, J. (1991) *Physica B*, 173, 1-10. 'Instrumentation for neutron reflectivity.'

Penfold, J.; Thomas, R.K. (1990) *J. Phys.: Condens. Matter*, 2, 1369-1412. 'The application of the specular reflection of neutrons to the study of surfaces and interfaces.'

Penfold, J.; Ward, R.C.; Williams, W.G. (1987) *J. Phys. E*, 20, 1411-1417. 'A time-of-flight neutron reflectometer for surface and interfacial studies.'

Perl, R.; Ferrell, R.A. (1972a) *Phys. Rev. Lett.*, 29, 51-54. 'Critical viscosity and diffusion in the binary-liquid phase transition.'

Perl, R.; Ferrell, R.A. (1972b) *Phys. Rev. A*, 6, 2358-2369. 'Decoupled-mode theory of critical viscosity and diffusion in the binary-liquid phase transition.'

Perrin, F. (1934) *J. Physique Radium*, 5, 497-511. 'Mouvement Brownien d'un ellipsoide (I). Dispersion diélectrique pour des molécules ellipsoidales.'

Perron, G.; De Lisi, R.; Davidson, I.; Genereux, S.; Desnoyers, J.E. (1981) *J. Colloid Interface Sci.*, 79, 432-442. 'On the use of thermodynamic transfer functions for the study of the effect of additives on micellisation: Volumes and heat capacities of sodium octanoate systems.'

Petrula, J.R.; Strauss, H.L.; Lao, K.Q.-H.; Pecora, R. (1978) *J. Chem. Phys.*, 68, 623-627. 'Depolarized scattering at a binary liquid critical point.'

Phillies, G.D.J.; Chappell, P.J.; Kivelson, D. (1978) *J. Chem. Phys.*, 68, 4031-4033. 'Evidence against a strong critical anomaly in the depolarized Rayleigh line of nitrobenzene:*n*-hexane.'

Pohl, D.W.; Goldburg, W.I. (1982) *Phys. Rev. Lett.*, 48, 1111-1114. 'Wetting transition in lutidine-water mixtures.'

Pouchelon, A.; Meunier, J.; Langevin, D.; Cazabat, A.M. (1980a) *J. Physique-Lett.*, 41, L239-L242. 'Light scattering from oil-water interfaces: measurements of low interfacial tensions.'

Pouchelon, A.; Meunier, J.; Langevin, D.; Chatenay, D.; Cazabat, A.M. (1980b) *Chem. Phys. Lett.*, 76, 277-281. 'Low interfacial tensions in three-phase systems obtained with oil-water-surfactant mixtures.'

Pownall, H.J.; Smith, L.C. (1973) *J. Am. Chem. Soc.*, 95, 3136-3140. 'Viscosity of the hydrocarbon region of micelles. Measurement by excimer fluorescence.'

Pozharskaya, G.I.; Kasapova, N.L.; Skripov, V.P.; Kolpakov, Yu.D. (1984) *J. Chem. Therm.*, 16, 267-272. 'The spinodal approximation by the method of scattering of light in (*n*-hexane + *n*-tetradecafluorohexane).'

Prigogine, I.; Defay, R. (1954) *Chemical Thermodynamics*, translated by Everett, D.H., Longmans Green and Co., London.

Rabolt, J.F.; Russell, T.P.; Twieg, R.J. (1984) *Macromolecules*, 17, 2786-2794. 'Structural studies of semifluorinated *n*-alkanes. 1. Synthesis and characterisation of $F(CF_2)_n(CH_2)_mH$ in the solid state.'

Rademacher, A.; Märkle, S.; Langhals, H. (1982) *Chem. Ber.*, 115, 2927-2934. 'Lösliche perylen-fluoreszenzfarbstoffe mit hoher photostabilität.'

Ravi, R.; Ben-Amotz, D. (1994) *Chem. Phys.*, 183, 385-392. 'Translational and rotational dynamics in liquids. Comparison of experiment, kinetic theory and hydrodynamics.'

Reed, T.M., III; Taylor, T.E. (1959) *J. Phys. Chem.*, 63, 58-67. 'Viscosities of liquid mixtures.'

Ren, Y.; Schoichet, M.S.; McCarthy, T.J.; Stidham, H.D.; Hsu, S.L. (1995) *Macromolecules*, 28, 358-364. 'Spectroscopic characterisation of polymer adsorption at the air-solution interface.'

Reynolds, O. (1883) *Phil. Trans. Royal Soc.*, 174, 935-982. 'An experimental investigation of the circumstances which determine whether the motion of water shall be direct or sinuous, and of the law of resistance in parallel channels.'

Richardson, R.M.; Roser, S.J. (1991) *Langmuir*, 7, 1458-1467. 'Neutron reflection studies of spread monolayers of docosanoic acid and pentadecanoic acid on water.'

Robert, M.; Shukla, K.P. (1992) *Fluid Phase Equil.*, 79, 241-253. 'Experimental study of wetting properties of three-component surfactant systems.'

Rondelez, F.; Ausserre, D.; Hervet, H. (1987) *Ann. Rev. Phys. Chem.*, 38, 317-347. 'Experimental studies of polymer concentration profiles at solid-liquid and liquid-gas interfaces by optical and x-ray evanescent wave techniques.'

Roser, S.J.; Felici, R.; Eaglesham, A. (1994) *Langmuir*, 10, 3853-3856. 'Energy dispersive X-ray reflection from a liquid-liquid interface.'

Rowlinson, J.S.; Swinton, F.L. (1982) *Liquids and Liquid Mixtures*, 3rd ed., Butterworth, London.

Rowlinson, J.S.; Widom, B. (1982) *Molecular Theory of Capillarity*, Oxford University Press, Oxford.

Roy, M.; Doraiswamy, S. (1993) *J. Chem. Phys.*, 98, 3213-3223. 'Rotational dynamics of nonpolar solutes in different solvents: Comparative evaluation of the hydrodynamic and quasihydrodynamic models.'

Saito, H.; Nishiwaki, K.; Handa, T.; Ito, S.; Miyajima, K. (1995) *Langmuir,* 11, 3742-3747. 'Comparative study of fluorescence anisotropy in surface monolayers of emulsions and bilayers of vesicles.'

Saroja, G.; Samanta, A. (1995) *Chem. Phys. Lett.*, 246, 506-512. 'Polarity of the micelle-water interface as seen by 4-aminophthalimide, a solvent sensitive fluorescence probe.'

[Scarpa, O. (1903) *Nuovo Cimento*, 6, 277.]

Schmidt, J.W. (1986) *J. Chem. Phys.*, 85, 3631-3635. 'A stabilized vapor liquid interface in deuterated cyclohexane-methanol mixtures.'

Schmidt, J.W. (1990) *Phys. Rev. A*, 41, 885-890. 'Universal adsorption at the vapor-liquid interface near the consolute point.'

Schmidt, J.W.; Moldover, M.R. (1983a) *Annals. NY Acad. Sci.*, 404, 350. 'Studies of thin films in binary fluid mixtures using ellipsometry.'

Schmidt, J.W.; Moldover, M.R. (1983b) *J. Chem. Phys.*, 79, 379-387. 'First-order wetting transition at a liquid-vapor interface.'

Schmidt, J.W.; Moldover, M.R. (1985) *J. Chem. Phys.*, 83, 1829-1834. 'The liquid-vapor interface of a binary liquid mixture near the consolute point.'

Schmitz, J.; Belkoura, L.; Woermann, D. (1994) *Annalen der Physik*, 3, 1-12. 'Light scattering and small angle neutron scattering experiments with an aggregating binary liquid mixture of critical composition.'

Schmitz, J.; Belkoura, L.; Woermann, D. (1995) *Ber. Bunsenges. Phys. Chem.*, 99, 848-852. 'Concentration fluctuations in the vicinity of the liquid/liquid coexistence curve of a binary mixture with a lower critical point.'

Schneider, G. (1963) *Z. Phys. Chem.*, 37, 333-352. 'Druckeinfluss auf die entmischung flüssiger systeme, I. Geschlossene mischungslücken bis 5000 bar.'

Schneider, G.M. (1978) In *Specialist Periodical Reports, Chemical Thermodynamics*, Vol. 2, The Chemical Society, London. 'High pressure phase diagrams and critical properties of fluid mixtures.'

Schön, W.; Wiechers, R.; Woermann, D. (1986) *J. Chem. Phys.*, 85, 2922-2928. 'Deuterium isotope effects in binary critical mixtures.'

Schulz, J. (1996) Private communication.

Scott, R.L. (1948) *J. Am. Chem. Soc.*, 70, 4090-4093. 'The solubility of fluorocarbons.'

Scott, R.L. (1978) In *Specialist Periodical Reports, Chemical Thermodynamics*, Vol. 2, The Chemical Society, London. 'Critical exponents for binary fluid mixtures.'

Scriven, L.E. (1977) In *Micellization, Solubilization and Microemulsions,* Vol. 2, Ed. Mittal, K.L., Plenum Press, New York. 'Equilibrium bicontinuous structures.'

Sears, V.F. (1989) *An Introduction to the Theory of Neutron Optical Phenomena and their Applications*, Oxford University Press, Oxford.

[Sengers, J.V. (1971) In *Proc. Int. School Enrico Fermi, Course L1, Critical Phenomena*, Ed. Green, M.S., Academic Press, New York.]

Sengers, J.V. (1973) In *AIP Conference Proceedings, No. 11, Transport Phenomena*, Ed. Kestin, J., Am. Inst. Phys., New York. 'Transport properties of gases and binary liquids near the critical state.'

Sengers, J.V. (1985) *Int. J. Thermophys.*, 6, 203-232. 'Transport properties of fluids near critical points.'

Sengers, J.V. (1993) Private communication.

Shinitzky, M.; Dianoux, A.C.; Gitler, C.; Weber, G. (1971) *Biochemistry*, 10, 2106-2113. 'Microviscosity and order in the hydrocarbon region of micelles and membranes determined with fluorescent probes. I. Synthetic micelles.'

Shinoda, K. (1967) In *Solvent Properties of Surfactant Solutions*, Ed. Shinoda, K., Marcel Dekker, New York. 'Solvent properties of nonionic surfactants in aqueous solutions.'

Siggia, E.D.; Halperin, B.I.; Hohenberg, P.C. (1976) *Phys. Rev. B*, 13, 2110-2123. 'Renormalization-group treatment of the critical dynamics of the binary-fluid and gas-liquid transitions.'

Simon, M.; Knobler, C.M. (1971) *J. Chem. Thermodynamics*, 3, 657-662. 'The excess Gibbs energy of liquid CH_4+CF_4 at 98K.'

Simon, M.; Fannin, A.A.; Knobler, C.M. (1972) *Ber. Bunsenges. Phys. Chem.*, 76, 321-324. 'Thermodynamic properties of the system CH_4-CF_4 in the neighbourhood of the upper critical solution temperature.'

Simons, J.H.; Dunlap, R.D. (1950) *J. Chem. Phys.*, 18, 335-346. 'The properties of *n*-pentforane and its mixtures with *n*-pentane.'

Simons, J.H.; Mausteller, J.W. (1952) *J. Chem. Phys.*, 20, 1516-1519. 'The properties of *n*-butforane and its mixtures with *n*-butane.'

Sluis, D.; D'Evelyn, M.P.; Rice, S.A. (1983) *J. Chem. Phys.*, 78, 1611-1613. 'Experimental and theoretical studies of the density profile in the liquid-vapor interface of Cs.'

Smit, B.; Hilbers, P.A.J.; Esselink, K.; Rupert, L.A.M.; van Os, N.M.; Schlijper, A.G. (1990) *Nature*, 348, 624-625. 'Computer simulations of a water/oil interface in the presence of micelles.'

Smit, B.; Hilbers, P.A.J.; Esselink, K.; Rupert, L.A.M.; van Os, N.M.; Schlijper, A.G. (1991) *J. Phys. Chem.*, 95, 6361-6368. 'Structure of a water/oil interface in the presence of micelles: A computer simulation study.'

Snyder, R.B.; Eckert, C.A. (1973) *J. Chem. Eng. Data*, 18, 282-285. 'Effect of third component on liquid-liquid critical point.'

Song, K.; Twieg, R.J.; Rabolt, J.F. (1990) *Macromolecules*, 23, 3712-3714. 'Low-temperature crystal-crystal phase transitions in triblock semifluorinated *n*-alkanes.'

Steele, W.A. (1976) *Adv. Chem. Phys.*, 34, 1-104. 'The rotation of molecules in dense phases.'

Steitz, R.; Braun, Ch.; Lang, P.; Findenegg, G.H. (1996) Unpublished measurements.

Stigter, D. (1967) *J. Colloid Interface Sci.*, 23, 379-388. 'On density, hydration, shape, and charge of micelles of sodium dodecyl sulfate and dodecyl ammonium chloride.'

Strumpf, H.J.; Collings, A.F.; Pings, C.J. (1974) *J. Chem. Phys.*, 60, 3109-3123. 'Viscosity of xenon and ethane in the critical region.'

Sullivan, D.E. (1981) *J. Chem. Phys.*, 74, 2604-2615. 'Surface tension and contact angle of a liquid-solid interface.'

Swinney, H.L.; Henry, D.L. (1973) *Phys. Rev. A*, 8, 2586-2617. 'Dynamics of fluids near the critical point: decay rate of order-parameter fluctuations.'

Szydlowski, J. (1994) *J. Molec. Structure*, 321, 101-113. 'Isotope effects on phase equilibria in hydrogen bonded systems, especially vapor pressure and miscibility isotope effects.'

Tanford, C. (1972) *J. Phys. Chem.*, 76, 3020-3024. 'Micelle shape and size.'

Tanford, C. (1977) In *Micellization, Solubilization and Microemulsions*, Vol. 1, Ed. Mittal, K.L., Plenum Press, New York. 'Thermodynamics of micellization of simple amphiphiles in aqueous media.'

Tarazona, P.; Telo da Gama, M.M.; Evans, R. (1983) *Mol. Phys.*, 49, 283-300. 'Wetting transitions at fluid-fluid interfaces. I. The order of the transition.'

Teletzke, G.F.; Scriven, L.E.; Davis, H.T. (1982) *J. Chem. Phys.*, 77, 5794-5798. 'Wetting transitions: First order or second order?'

Teletzke, G.F.; Scriven, L.E.; Davis, H.T. (1983) *J. Chem. Phys.*, 78, 1431-1439. 'Wetting transitions. II. First order or second order?'

Telo da Gama, M.M.; Evans, R. (1983) *Mol. Phys.*, 48, 251-266. 'The structure and surface tension of the liquid-vapour interface near the upper critical endpoint of a binary mixture of Lennard-Jones fluids. II. The three phase region and the Cahn wetting transition.'

Teubner, M.; Strey, R. (1987) *J. Chem. Phys.*, 87, 3195-3200. 'Origin of the scattering peak in microemulsions.'

Toxvaerd, S.; Stecki, J. (1995) *J. Chem. Phys.*, 102, 7163-7168. 'Density profiles at a planar liquid-liquid interface.'

Trejo Rodriguez, A.; McLure, I.A. (1983) *Fluid Phase Equil.*, 12, 297-305. 'Phase equilibria for binary *n*-alkanenitrile-*n*-alkane mixtures. II. Gas-liquid pressure-temperature-composition critical loci for ethanenitrile with C_4-C_{11} *n*-alkanes.'

Tsai, B.C.; McIntyre, D. (1974) *J. Chem. Phys.*, 60, 937-945. 'Shear viscosity of nitroethane-3-methylpentane in the critical region.'

Turberg, M.P.; Brady, J.E. (1988) *J. Am. Chem. Soc.*, 110, 7797-7801. 'Semifluorinated hydrocarbons: primitive surfactant molecules.'

Twieg, R.J.; Russell, T.P.; Siemens, R.; Rabolt, J.F. (1985) *Macromolecules*, 18, 1361-1362. 'Observation of a "gel" phase in binary mixtures of semifluorinated *n*-alkanes with hydrocarbon liquids.'

Ubbelohde, L. (1936) *J. Inst. Petrol.*, 19, 376-420. 'The simplest and most accurate viscometer, and other instruments with suspended level.'

Van Konynenburg, P.H.; Scott, R.L. (1980) *Phil. Trans. Royal Soc.*, 298, 495-540. 'Critical lines and phase equilibria in binary van der Waals mixtures.'

Van Wazer, J.R.; Lyons, J.W.; Kim, K.Y.; Colwell, R.E. (1963) *Viscosity and Flow Measurement*, Interscience, New York.

Wakeham, W.A.; Nagashima, A.; Sengers, J.V., Eds. (1991) *Measurement of the Transport Properties of Fluids, Experimental Thermodynamics*, Vol. III, IUPAC Chemical Data Series No. 37, Blackwell Scientific, Oxford.

Walker, J.S.; Vause, C.A. (1987) *Sci. Am.*, 256, 90-97. 'Reappearing phases.'

Ware, W.R.; Andre, J.C. (1983) In *Time-Resolved Fluorescence Spectroscopy in Biochemistry and Biology*, Ed. Cundall, R.B.; Dale, R.E., Plenum Press, New York.

Waterson, S.D.; Semmens, J.; Young, C.L. (1980) *Aust. J. Chem.*, 33, 1987-1992. 'Upper critical solution temperatures of perfluoro-*n*-hexane + alkane, sulphur hexafluoride + siloxane and perfluoropropane + siloxane mixtures.'

Weast, R.C. (1974) *Handbook of Chemistry and Physics*, 55th ed., Chemical Rubber Company, Cleveland.

Wegner, F.J. (1972) *Phys. Rev. B*, 5, 4529-4536. 'Corrections to scaling laws.'

Westh, P.; Koga, Y. (1996) *J. Phys. Chem.*, 100, 433-438. 'Intermolecular interactions in 2-butoxyethanol-DMSO-H_2O.'

Whitfield, R. (1996) Ph.D. Thesis, University of Sheffield. 'A study of the non-critical interfaces of (perfluoroalkane + alkane) mixtures close to their upper critical solution temperature.'

Widom, B. (1977) *J. Chem. Phys.*, 67, 872-880. 'Noncritical interface near a critical endpoint.'

Widom, B. (1978) *J. Chem. Phys.*, 68, 3878-3883. 'Structure of the $\alpha\gamma$ interface.'

Williams, A.M.; Jiang, Y.; Ben-Amotz, D. (1994) *Chem. Phys.*, 180, 119-129. 'Molecular reorientation dynamics and microscopic friction in liquids.'

Williamson, A.M. (1990) Ph.D. Thesis, University of Sheffield. 'Classical and optical studies of adsorption and wetting in binary liquid mixtures near consolute points.'

Williamson, A.-M.; McLure, I.A. (1996) *Physica A*, in press. 'Wetting near consolute points by evanescent-wave-generated fluorescence spectroscopy. 2. Selective

excitation: methylcyclohexane + perfluoromethylcyclohexane at the upper critical endpoint.'

Wilson, K.G. (1971a) *Phys. Rev. B*, 4, 3174-3183. 'Renormalization group and critical phenomena. I. Renormalization group and the Kadanoff scaling picture.'

Wilson, K.G. (1971b) *Phys. Rev. B*, 4, 3184-3205. 'Renormalization group and critical phenomena. II. Phase-space cell analysis of critical behaviour.'

Wilson, K.G. (1979) *Sci. Am.*, 241 (AUG), 140-157. 'Problems in physics with many scales of length.'

Windsor, C.G. (1981) *Pulsed Neutron Scattering*, Taylor & Francis, London.

Wirth, M.J.; Chou, S.-H. (1991) *J. Phys. Chem.*, 95, 1786-1789. 'Behaviour of the rotational diffusion tensor of tetracene under subslip conditions.'

Wurz, U.; Grubie, M.; Woermann, D. (1992) *Ber. Bunsenges. Phys. Chem.*, 96, 1460-1463. 'The specific heat of butoxyethanol/water critical mixtures.'

Yekta, A.; Duhamel, J.; Brochard, P.; Adiwidjaja, H.; Winnik, M.A. (1993) *Macromolecules*, 26, 1829-1836. 'A fluorescent probe study of micelle-like cluster formation in aqueous solutions of hydrophobically modified poly(ethylene oxide).'

Youngren, G.K.; Acrivos, A. (1975) *J. Chem. Phys.*, 63, 3846-3848. 'Rotational friction coefficients for ellipsoids and chemical molecules with the slip boundary condition.'

Zielesny, A.; Schmitz, J.; Limberg, S.; Aizpiri, A.G.; Fusenig, S.; Woermann, D. (1994) *Int. J. Thermophys.*, 15, 67-94. 'Viscosity and diffusivity of a binary liquid mixture of critical composition - study of the system 2-butoxyethanol water.

Zwanzig, R. (1978) *J. Chem. Phys.*, 68, 4325-4327. 'Rotational friction coefficients of a bumpy cylinder with slipping and sticking boundary conditions.'